

**Final Report:**

**Examination of the Influence of California Regional Particulate Air Quality Study  
Fog Episodes on Aerosol Formation and Removal**

**by**

**Jeffrey L., Collett, Jr., Pierre Herckes, Hui Chang, and Taehyoung Lee  
Atmospheric Science Department  
Colorado State University  
Fort Collins, CO 80523**

**and**

**Spyros N. Pandis and Kathleen Fahey  
Department of Chemical Engineering  
Carnegie Mellon University  
Pittsburgh, PA 15213**

**Submitted to:**

**San Joaquin Valleywide Air Pollution Study Agency**

**January 13, 2005**

## **DISCLAIMER**

The statements and conclusions in this report are those of the Contractor and not necessarily those of the California Air Resources Board, the San Joaquin Valleywide Air Pollution Study Agency, or its Policy Committee, their employees or their members. The mention of commercial products, their source, or their use in connection with material reported herein is not to be construed as actual or implied endorsement of such products.

## **ACKNOWLEDGMENTS**

We are grateful to D. Sherman, J. Reilly, and G. Kang for assistance with the CRPAQS fog field campaign. We are especially grateful to C. McDade for excellent logistical support and to K. Magliano and J. Watson for useful discussions. Partial support for this work was provided by grants from the National Science Foundation (ATM-9980540 and ATM-0222607).

## EXECUTIVE SUMMARY

Fogs are comprised of tiny water droplets, typically ranging in size from several micrometers to several tens of micrometers. These drops form by water vapor condensation onto aerosol nuclei known as cloud condensation nuclei (CCN). Water soluble constituents in the CCN determine the initial composition of the fog. Fog drop composition is further influenced by dissolution of soluble gases and aqueous phase chemical reactions (see Figure E-1). While much has been learned about fog interactions with key inorganic aerosol species (e.g., ammonium sulfate and nitrate), it is only in

recent years that investigators have begun examining interactions between fogs and carbonaceous aerosols and volatile organic compounds.

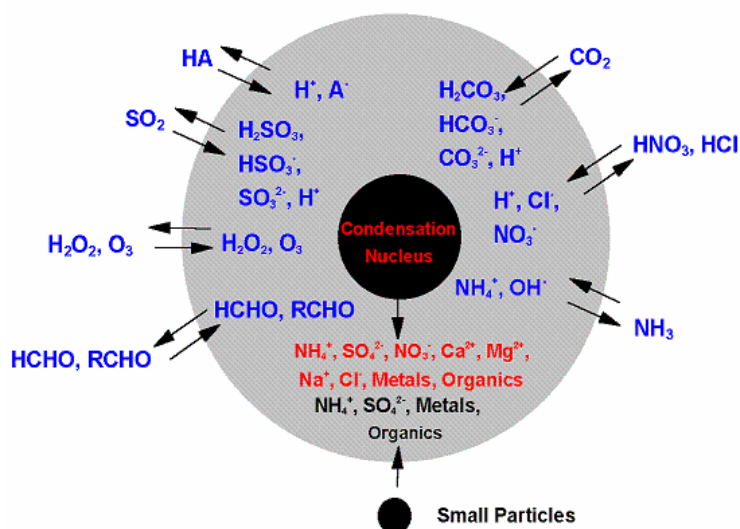


Figure ES-1. Simple illustration of particle and gas scavenging processes that influence the composition of a fog drop.

During the winter persistent high pressure over the Great Basin creates a strong subsidence inversion over California's Central Valley, with a base typically a few hundred meters off the valley floor and below the surrounding mountain ridges (Holets et al., 1981). With the help of the mountains, this strong inversion forms a lid over the air basin, trapping cool, moist air within the valley. Subsiding air results in clear skies, providing excellent conditions for strong radiative cooling at night and, if sufficient moisture is present, the formation of dense, widespread radiation fogs.

Fogs have two important, competing effects on aerosol populations:

- New aerosol mass formation through gas scavenging and chemical reaction in the droplets leading to non-volatile species (e.g. conversion of SO<sub>2</sub> to sulfate) that remain in the particle phase after droplet evaporation
- Aerosol scavenging followed by deposition through droplet settling and/or impaction

The relative importance of these two processes depends on the environment in which the fog forms: meteorological conditions, number and composition of aerosol particles, gas phase chemical composition, etc.... The net effect of a fog on atmospheric aerosol concentrations may change during a fog event; oxidation could be more important at the beginning of the fog event when reactant concentrations are higher, while deposition rates may increase over time with the growth of fog droplets.

Previous studies of sulfur oxidation in San Joaquin Valley (SJV) fogs have shown that dissolved sulfur dioxide can react rapidly, either being oxidized to sulfate or reacting with carbonyl compounds to form hydroxyalkylsulfonic acids. Variations in fog drop composition with size are known to influence the rates of chemical reactions as well (e.g., Reilly et al., 2001).

Deposition due to fog drop sedimentation or impaction has been known to be an important removal process for atmospheric pollutants for a long time (Waldman, 1986). Some studies have tried to assess the deposition fluxes by fog in the SJV by modeling (Lillis et al., 1999) or by measurements (Collett et al., 2001). Relatively few measurements exist, however, regarding atmospheric removal of fog solutes by drop deposition or how drop-size dependent fog composition affects removal rates for various chemical species.

While much is now known about the inorganic composition of SJV fogwater, little is known about the scavenging and removal of carbonaceous aerosol by these fogs. Despite measurement of high total organic carbon (TOC) concentrations (e.g., during IMS95), the composition of the organic species making up this TOC is largely unknown in the SJV and elsewhere. Although the net effect of SJV fog episodes is expected to be to reduce



atmospheric loadings of carbonaceous aerosol, the magnitude of this removal was unknown prior to CRPAQS.

In order to improve our understanding of the role fogs play in influencing aerosol concentrations in California's Central Valley, Colorado State University made measurements of the chemical and physical properties of fogs at several valley locations during the CRPAQS winter intensive. These observations subsequently formed the basis for a data analysis effort aimed at better characterizing fog composition and interactions between CRPAQS fogs and pollution levels, especially fine particles. Our approach to the study and key study results are summarized here. More detailed information is available in the full project report which follows this summary.

#### ES-1. Approach

Colorado State University conducted measurements of fog properties, both physical and chemical, at several Valley sites as part of the CRPAQS winter intensive. Measurements began in mid-December and extended through early February. The most extensive measurements were made at the Angiola core site, where we made both ground and tower-based measurements of fog composition. Additional measurements at this site were made of the fog drop size distribution, fog liquid water content (LWC), fog deposition, and drop size-resolved fog composition. Core site measurements were complemented by additional fog occurrence and fog composition measurements at three satellite sites: Helm, Bakersfield, and McKittrick.

Several fog episodes were successfully sampled in December, January, and early February. In sum, more than 200 fog samples were collected from a variety of fog collector types. Measurements of the composition of collected fog samples included characterization of a wide range of inorganic and organic solutes. Deposition measurements included determination of fog borne fluxes of several major ion species as well as total organic carbon (TOC).

CRPAQS fog observations were explored in the data analysis phase of the project in order to improve our understanding of the interactions between CRPAQS fogs and airborne fine particles and soluble trace gases. Particular emphasis was placed on examining how these fogs process organic pollutants and how variations in fog composition across the fog drop size spectrum influence both particle deposition and production of new particle mass. Results from this and other recent SJV fog campaigns were also compared to observations made in the early 1980s, to ascertain whether significant changes in fog composition have occurred over this twenty year period.

In order to test the ability of current fog models to accurately simulate the chemical and physical properties of fogs, as well as the influence of radiation fogs on particle scavenging and removal, observations from the CRPAQS fog study were compared to a numerical simulation of a CRPAQS fog episode using the Carnegie Mellon University fog model. Particular attention was paid to the ability of the model to accurately capture key features of the fogs, including fog LWC, bulk and drop size-resolved fog composition, and deposition fluxes of fog borne solutes. The ability of a more heavily parameterized, and computationally practical, version of the model to accurately capture key features was also examined.

## ES-2. Major Conclusions

The fog measurement campaign and subsequent data analysis phase produced a number of significant findings. These include the following major observations and conclusions:

- Several fog episodes were characterized during CRPAQS. Most of the fog episodes were relatively shallow and featured very large droplets. Rarely did the top of the fog layer reach even 100 m, in contrast to much deeper fogs observed during IMS95 and other studies in the San Joaquin Valley (SJV). The very large drops formed during CRPAQS probably result from strong radiative cooling directly from the drops themselves, through the shallow fog layer, driving rapid condensational growth. These large drops settle from the fog relatively quickly,

enhancing the ability of the fogs to rapidly remove scavenged airborne particulate matter.

- The chemical composition of the fogs during CRPAQS was dominated by nitrogen species, with important contributions also from organic compounds and sulfate. Ammonium and nitrate were the most abundant individual compounds; nitrite and sulfate were also found to be present at significant concentrations as were several organic compounds, including formate, acetate, and formaldehyde. Abundant gas phase ammonia absorbed by fog drops helps keep the fog pH relatively high, with pH values typically well above 6. Material present in fog drops is derived from a combination of aerosol particle scavenging, gas absorption, and aqueous phase reactions.
- Comparison of Bakersfield fog composition measurements in CRPAQS and other recent SJV fog studies with measurements made in the 1980s reveals a statistically significant decrease in fog concentrations of sulfate and an increase in fog pH. These changes are consistent with intervening declines in SO<sub>2</sub> emissions in the southern SJV, which would translate into less production of sulfate and greater availability of ammonia to raise fog pH.
- Comparison of fog composition during CRPAQS at Bakersfield, Angiola, and Helm reveals that Angiola and Helm, both rural sites, have generally similar compositions. Urban Bakersfield fog contained greater concentrations of sulfate and nitrite.
- The high pH droplets present in CRPAQS fogs make them effective atmospheric reactors for dissolved sulfur dioxide. Both oxidation to sulfate and reaction with dissolved formaldehyde to produce hydroxymethanesulfonic acid (HMS) are important reaction pathways. Numerical simulations using a single drop fog chemistry model reveal the importance of considering effects of mass transport limitations on aqueous sulfur chemistry in the large fog drops observed in CRPAQS fogs. Measurement of HMS in individual aerosol particles in the SJV, as suggested by the group of Kim Prather, should provide an effective way for monitoring the fraction of ambient particles that have undergone fog processing.

- Previous studies have documented the important role SJV fogs play in cleansing the atmosphere via particle scavenging followed by drop deposition. The importance of this mechanism was again observed during CRPAQS, with fog deposition fluxes capable of reducing boundary layer fine particle concentrations of major species (e.g., nitrate and ammonium) at a rate on the order of  $1 \mu\text{g}/\text{m}^3$  hr. The fogs are also effective at scavenging and removing sulfate, but this removal is often offset by similar rates of sulfate production via aqueous phase oxidation of sulfur dioxide.
- Preferential enrichment of major ion species in small fog drops reduces most species' deposition velocities below the deposition velocity for fog water. Nitrite, which was often enriched in large fog drops, exhibited deposition velocities higher than fog water. Accounting for drop size-dependent species concentrations is essential to accurately modeling rates of pollutant deposition in SJV fogs.
- Results obtained during CRPAQS also indicate the important role that SJV fogs play in scavenging and deposition of organic carbon. SJV fogs contain a rich mix of organic compounds, with major constituents including formaldehyde, formate, and acetate. Many larger organic molecules are also observed, including both polar and non-polar compounds. Approximately 25% of the fog organic carbon, on average, is present as undissolved, suspended material in the droplets. As much as half of the fog organic matter may be comprised of high molecular weight compounds, with molecular masses exceeding several hundred Daltons. Future studies are needed to better characterize this high molecular weight material and determine whether it comes mainly from aerosol scavenging or is produced by aqueous phase reactions of lower molecular weight precursors.
- The wide variety of organic compounds observed in the fogs indicates that carbonaceous aerosol particles from many source types undergo active fog processing. Observations of fog scavenging of organic and elemental carbon also indicate the importance of fog processing of carbonaceous aerosol species. Organic carbon was observed to be more actively processed by CRPAQS fogs

than elemental carbon. Differences were also observed between the efficiency of CRPAQS fogs in scavenging different types of fine particle organic carbon.

Wood smoke particles were scavenged more efficiently and particles containing polycyclic aromatic hydrocarbons (PAH) less efficiently than fine particle OC as a whole. CRPAQS fogs were also observed to efficiently scavenge and remove the pesticide Diazinon. Together, these observations suggest that fogs may be more effective cleansing the boundary layer of OC from some source types than others, a topic deserving further attention in future studies.

- Deposition fluxes of organic carbon in fog water were significant, yielding atmospheric removal rates on the order of  $66 \mu\text{gC}/\text{m}^2 \text{ hr}$ . Because some of the fog burden of organic carbon is comprised of soluble, volatile organic compounds (VOC), a portion of the deposited carbon may be released back to the atmosphere when deposited fog water evaporates following a fog episode.
- Comparisons of fine particle organic carbon concentrations before and after fog episodes also suggests that aqueous phase reactions of dissolved VOCs may be important in producing new, secondary organic aerosol matter. Much more work is needed to examine this hypothesis in future investigations.
- Measurements of the stability of carbonyl compounds in actual fog water reveal the importance of stabilizing these species as soon as possible following sample collection. Analysis of field-stabilized samples collected in Fresno fog episodes after CRPAQS reveal significant contributions of several carbonyl and dicarbonyl compounds to SJV fog organic carbon burdens. Glyoxal and methylglyoxal, in particular, were observed at substantial concentrations nearly equivalent to formaldehyde.
- The CMU fog model, a 14-section size-resolved fog model with explicit fog microphysics, was used to simulate a CRPAQS fog episode and was able to predict the liquid water evolution, bulk aqueous-phase concentration measurements, drop size-resolved trends, and deposition fluxes for a number of species in close agreement with observed values. The predicted evolution of the distribution of aerosol species like sulfate, nitrate, ammonium, and chloride

indicated significant differences over the course of fog processing. Different size-dependent processes controlled the size-distribution development at different stages of fog processing. Early in processing, the dissolution of soluble gases and rapid aqueous phase reactions control the development of the size distribution. At later times, the effects of deposition begin to dominate, and push the peak of the distribution towards smaller diameters. Model predictions of the evolution of most key species approached bulk aqueous-phase concentration measurements. During the early stages of the fog, the behavior of species originating partially in the gas phase ( $\text{NO}_3^-$ ,  $\text{SO}_4^{2-}$ ) was heavily influenced by dissolution into the droplets and rapid aqueous phase reactions. Following these initial peaks in aqueous phase concentrations, deposition began to dominate, and the species were gradually depleted from the fog layer.

- In an effort to test the accuracy of a computationally less expensive Variable Size Resolution Model (VSRM), sulfate concentrations predicted by the highly size resolved fog model were compared with the VSRM (Fahey and Pandis, 2001). While the VSRM approached the sulfate predictions of the dynamic fog model when the size dependent deposition is given as an input, the model failed to predict a similar evolution when using a simplified deposition calculation published for another fog. This indicates that it might be worthwhile to ascertain the appropriate deposition dependence before running the VSRM for lengthy fog applications.

While the CRPAQS fog study and subsequent data analysis have greatly aided our understanding of the importance of fog processing of both inorganic and organic aerosol species, a significant need remains to continue studies of this type. In particular, our understanding of the production and removal of fine particle organic carbon remains in its infancy. Much more work is needed to elucidate the relative efficiencies with which fogs scavenge and deposit carbonaceous particles from different source types and to determine the extent of secondary organic aerosol formation occurring via aqueous phase

reaction pathways that convert soluble VOCs to nonvolatile products that are released back to the aerosol when a fog evaporates.

## **Table of Contents**

Executive Summary .....	iii
List of Figures .....	xiv
List of Tables .....	xxii
Chapter 1. Introduction .....	1-1
1.1 Fog formation and maintenance.....	1-1
1.2 Aerosol activation .....	1-2
1.3 Aerosol scavenging, removal and production in fogs.....	1-6
1.4 Fog scavenging of gases and secondary aerosol production .....	1-8
1.5 Aqueous phase reactions of organics.....	1-15
1.6 Solute deposition in fogs.....	1-16
1.7 Issues of drop size-dependent fog composition .....	1-17
1.8 Net effects of fogs on pollutant concentrations .....	1-18
1.9 Investigating the chemistry of fog formation and dissipation in California's Central Valley .....	1-18
1.10 Open questions and study objectives .....	1-26
Chapter 2. Experimental description.....	2-1
2.1 Sampling sites and times.....	2-1
2.2 Sampling .....	2-2
2.3 Sample handling and chemical analysis .....	2-13
2.4 Quality control .....	2-21
2.5 Instrumental quality control.....	2-26
Chapter 3. Overview of fog episodes and fog composition.....	3-1
3.1 Summary of fog sampling.....	3-1
3.2 Weather conditions .....	3-2
3.3 Drop size distribution and evolution.....	3-6
3.4 Bulk fog composition.....	3-10
3.5 Drop size dependent fog composition.....	3-19
3.6 Fog observations at the satellite sites.....	3-29
3.7 Fog observations on the Angiola tower .....	3-43
3.8 Changes in SJV fog composition over two decades .....	3-52



Chapter 4. Organic composition of CRPAQS fogs and interactions with carbonaceous aerosols .....	4-1
4.1 Overview.....	4-1
4.2 Determination of carbonyl compounds by HPLC .....	4-4
4.3 Functional group characterization of organic compounds in fog water .....	4-30
4.4 CRPAQS fog interactions with elemental and organic carbon.....	4-34
4.5 CRPAQS fog interactions with organic aerosols.....	4-39
Chapter 5. Aerosol processing and removal by CRPAQS fogs.....	5-1
5.1 Overview.....	5-1
5.2 Results and discussion .....	5-4
5.3 Sulfur dioxide reaction in fog drops .....	5-25
5.4 Overall effects of fog on atmospheric species concentrations.....	5-42
Chapter 6. Modeling the influence of size-dependent droplet composition on pollutant processing by San Joaquin Valley fogs .....	6-1
6.1 Introduction.....	6-1
6.2. Model description .....	6-3
6.3. Available measurements during the fog episode .....	6-5
6.4. Results.....	6-6
6.5 Comparison with the VSRM.....	6-18
6.6 Conclusions.....	6-21
Chapter 7. Summary and conclusions.....	7-1
Bibliography .....	8-1
Appendix A. The CSU optical fog detector.....	A-1
Appendix B. Organic matter in central California radiation fogs.....	B-1
Appendix C. On the use of anion exchange chromatography for the characterization of water soluble organic carbon .....	C-1
Appendix D. On the drop-size dependence of organic acid and formaldehyde concentrations in fog.....	D-1

## **List of Figures**

Figure 1-1. Köhler curves for NaCl and (NH <sub>4</sub> ) <sub>2</sub> SO <sub>4</sub> particles for various dry particle diameters .....	1-3
Figure 1-2. Simplified chemistry of a cloud/fog drop. ....	1-8
Figure 1-3. Rate of S(IV) oxidation by O <sub>3</sub> in the aqueous phase under conditions typical of a Los Angeles atmosphere, with SO <sub>2</sub> =20 ppb and O <sub>3</sub> =50 ppb.....	1-13
Figure 1-4. Oxidation rates of the three S(IV) oxidation pathways, along with the rate of HMS formation for typical conditions in central California fogs.....	1-15
Figure 1-5. Terrain map of California Central Valley area. The red dot on the map indicates the approximate location of the main CRPAQS Angiola sampling site.....	1-19
Figure 1-6. Measured composition in a typical bulk fog sample collected at Fresno during IMS95. ....	1-20
Figure 2-1. Photo of the Angiola field laboratory, where collected fog samples were processed.....	2-1
Figure 2-2. Angiola sampling site overview on a foggy day.....	2-2
Figure 2-3. Gerber Scientific Particulate Volume Monitor (model PVM-100).....	2-3
Figure 2-4. CSU optical fog detector.....	2-3
Figure 2-5. Caltech Active Strand Cloud Collector (CASCC).....	2-4
Figure 2-6. Fan revolution speed and air velocity measured for the CASCC as a function of applied fan voltage.....	2-5
Figure 2-7. Corrected air speed and revolution speed vs voltage on the stainless steel CASCC .....	2-6
Figure 2-8. An all-plastic size-fractionating CASCC (sf-CASCC) mounted on site. ....	2-7
Figure 2-9. Corrected air velocity and revolution speed vs voltage for the sf-CASCC. .	2-7
Figure 2-10. Corrected air velocity and revolution speed vs voltage for the ss-sf-CASCC.....	2-8
Figure 2-11. The CSU 5-stage collector .....	2-8
Figure 2-12. CSASP-100-HV optical probe .....	2-9
Figure 2-13. Two deposition plates deployed during CRPAQS.....	2-11
Figure 2-14. Two balances set up to record deposition fluxes to a bare metal and an artificial grass surface. ....	2-12
Figure 2-15. Gas phase measurements of total soluble hydroperoxides by continuous monitor.....	2-13
Figure 2-16. A Microorifice Uniform Deposit Impactor (MOUDI). ....	2-13
Figure 2-17. Schematic describing fog sample fractionation for OC measurements. ...	2-19

Figure 2-18. HP 1050 HPLC system. ....	2-21
Figure 3-1. Fog LWC timeline measured at Angiola during the period 12/13/00 – 2/3/01. ....	3-4
Figure 3-2. Effective diameter and LWC measured by PVM on 12/17 & 12/18/00. ....	3-5
Figure 3-3. Effective diameter and LWC on 12/18 & 12/19/00. ....	3-5
Figure 3-4. Effective diameter and LWC on 01/21/00. ....	3-5
Figure 3-5. Effective diameter and LWC on 1/25/00 (top panel) and 02/01/00 (lower panel).....	3-6
Figure 3-6. Comparison between effective diameters obtained from the PVM and the CSASP on 12/17 & 12/18/00.....	3-7
Figure 3-7. Comparison of effective diameter from the PVM and CSASP for the fog event on 12/17 & 12/18/00. ....	3-8
Figure 3-8. Comparison of LWC obtained by PVM and CSASP for the fog event on 12/17 & 12/18/00. ....	3-9
Figure 3-9. Drop size distribution evolution with time on 12/17 & 12/18/00. ....	3-10
Figure 3-10. Timelines of three ion concentrations and pH in CASCC fog samples. ....	3-11
Figure 3-11. Timelines of three major ions, nitrite and pH in CASCC fog samples during the 12/17/00&12/18/00 fog event. ....	3-11
Figure 3-12. Timelines of three major ions, nitrite and pH in CASCC samples during the 12/18/00&12/19/00 fog event. ....	3-12
Figure 3-13. Timelines of three major ions, nitrite and pH in CASCC samples on 01/17/01. ....	3-12
Figure 3-14. Timelines of three major ions, nitrite and pH in CASCC samples on 01/21/01. ....	3-12
Figure 3-15. Timelines of three major ions, nitrite and pH in CASCC samples on 01/25/01. ....	3-13
Figure 3-16. Timelines of three major ions, nitrite and pH in CASCC samples on 01/31/01. ....	3-13
Figure 3- 17. Ammonium concentrations vs. total concentration of nitrate, sulfate and nitrite for all fog events.....	3-13
Figure 3-18. Timelines of formate, acetate, TOC and HCHO concentrations for all fog events. ....	3-14
Figure 3-19 Timelines of formate, acetate, TOC and HCHO in CASCC samples in the 12/17&12/18/00 fog event. ....	3-15
Figure 3-20. Timelines of formate, acetate, TOC and HCHO in CASCC samples on 01/17/01. ....	3-15
Figure 3-21. Measured composition for Angiola fog episodes	

during winter 2000/2001 .....	3-18
Figure 3-22. Total cation concentrations vs. total anion concentrations. ....	3-19
Figure 3-23. Large vs. small drop pH for all fog events of CRPAQS. ....	3-21
Figure 3-24. Large vs. small drop $\text{Cl}^-$ concentrations .....	3-21
Figure 3-25. Large vs. small drop $\text{NO}_3^-$ concentrations.....	3-21
Figure 3-26. Large vs. small drop $\text{SO}_4^{2-}$ concentrations .....	3-22
Figure 3-27. Large vs. small drop $\text{Na}^+$ concentrations .....	3-22
Figure 3-28. Large vs. small drop $\text{NH}_4^+$ concentrations .....	3-22
Figure 3-29. Large vs. small drop $\text{K}^+$ concentrations .....	3-23
Figure 3-31. Large vs. small drop $\text{Ca}^{2+}$ concentrations .....	3-23
Figure 3-30. Large vs. small drop $\text{Mg}^{2+}$ concentrations .....	3-23
Figure 3-32. Large vs. small drop total Fe concentrations .....	3-24
Figure 3-33. Large vs. small drop total Mn concentrations.....	3-24
Figure 3-34. Large vs. small drop $\text{NO}_2^-$ concentrations.....	3-24
Figure 3-35. Large vs. small drop HCHO concentrations .....	3-25
Figure 3-36. Large vs. small drop TOC concentrations.....	3-25
Figure 3-37. Large vs. small drop formate concentrations .....	3-25
Figure 3-38. Large vs. small drop acetate concentrations .....	3-26
Figure 3-39. Large vs. small drop propionate concentrations .....	3-26
Figure 3-40. Large vs. small drop oxalate concentrations.....	3-26
Figure 3-41. pH value vs. theoretical Dp50 of the 5-stage collector .....	3-27
Figure 3-42. Major ion concentrations vs. theoretical Dp50 of 5-stage collector on day 01/17/01 .....	3-28
Figure 3-43. Major ion concentrations vs. theoretical Dp50 of 5-stage collector on day 12/19/00 .....	3-28
Figure 3-44. Major ion concentrations vs. theoretical Dp50 of 5-stage collector on day 01/31/01 .....	3-28
Figure 3-45. Remote site automated fog sampling set-up .....	3-30
Figure 3-46. Set-up at the Helm site .....	3-31
Figure 3-47. Sampling set-up in McKittrick.....	3-34
Figure 3-48. Sampling set-up in Bakersfield .....	3-35
Figure 3-49. Angiola LWC and fog sampling times for the night of January 31 <sup>st</sup> .....	3-36
Figure 3-50. Average ion concentrations in Bakersfield and Angiola fog during the Jan. 31st event .....	3-38

Figure 3-51. Evolution of fog concentrations in Angiola and Helm from 12/17-12/19/00 .....	3-39
Figure 3-52. LWC and sampling times for the night of January 10 <sup>th</sup> .....	3-40
Figure 3-53. Evolution of fog concentrations in Angiola and Helm on the morning of 1/10 .....	3-40
Figure 3-54. Average fog composition ( $\mu\text{eq/l}$ ) observed at three sites during CRPAQS.....	3-41
Figure 3-55a. Average major ion concentrations for Helm, Bakersfield and Angiola fog samples.....	3-42
Figure 3-55b. Average minor ion concentrations and pH for Helm, Bakersfield and Angiola fog samples .....	3-43
Figure 3-56. Observation tower at the Angiola site.....	3-44
Figure 3-57. Experimental platform for fog sampling.....	3-45
Figure 3-58. LWC evolution ( $\text{mg/m}^3$ ) on January 21st 2001.....	3-47
Figure 3-59a. Evolution of concentrations of fog samples sampled at tower level 0 (3m) and level 2 (23m) during the morning hours of January 21st 2001 .....	3-48
Figure 3-59b. Evolution of concentrations of samples sampled at tower level 0 (3m, blue) and level 2 (23m, green) during the morning hours of January 21st 2001 .....	3-49
Figure 3-60. Profiles of average tower fog concentrations on January 21 <sup>st</sup> .....	3-50
Figure 3-61. Vertical profiles of average (vol weighted) fog concentrations on January 21 <sup>st</sup> .....	3-51
Figure 3-62. pH of fog samples collected in Bakersfield in the period 1982-2001 .....	3-53
Figure 3-63. Sulfate concentrations ( $\mu\text{N}$ ) observed in Bakersfield fogs in the period 1982-2001.....	3-54
Figure 3-64. Nitrate concentrations ( $\mu\text{N}$ ) observed in Bakersfield fogs in the period 1982-2001.....	3-54
Figure 4-1. Average fractions of TOC and DOC in CRPAQS fog samples.....	4-1
Figure 4-2. Molecular weight analysis of DOC for six fog water samples .....	4-2
Figure 4-3. Mass fractions of CRPAQS fog DOC comprised by several key low MW species.....	4-3
Figure 4-4. 2-D and 3-D views of an example chromatogram showing retention times and wavelength dependent absorption for several carbonyls in a standard.....	4-10
Figure 4-5. Several example carbonyl calibration curves.....	4-11
Figure 4-6. Carbonyl stability test in a real fog water matrix.....	4-20
Figure 4-7. Comparison of pH between large and small Fresno fog drops .....	4-22

Figure 4-8. Typical composition of carbonaceous material comprising the total dissolved organic carbon (DOC) content observed for several Fresno radiation fog samples .....	4-26
Figure 4-9. Concentrations of HCHO measured by the HPLC method and fluorescence in large and small drop samples collected with the ss-sf-CASCC in Fresno radiation fogs on Jan 10-Jan 11, 2004.....	4-27
Figure 4-10. Concentrations of acetaldehyde measured by the HPLC method in large and small drop samples collected with the ss-sf-CASCC in Fresno radiation fogs on Jan 10-Jan 11, 2004 .....	4-27
Figure 4-11. Concentrations of acrolein and acetone measured by the HPLC method in large and small drop samples collected with the ss-sf-CASCC in Fresno radiation fogs on Jan 10-Jan 11, 2004.....	4-28
Figure 4-12. Concentrations of isovaleraldehyde measured by the HPLC method in large and small drop samples collected with the ss-sf-CASCC in Fresno radiation fogs on Jan 10-Jan 11, 2004.....	4-28
Figure 4-13. Concentrations of glyoxal measured by the HPLC method in large and small drop samples collected with the ss-sf-CASCC in Fresno radiation fogs on Jan 10-Jan 11, 2004.....	4-29
Figure 4-14. Concentrations of methylglyoxal measured by the HPLC method in large and small drop samples collected with the ss-sf-CASCC in Fresno radiation fogs on Jan 10-Jan 11, 2004.....	4-29
Figure 4-15. HPLC chromatograms of fog water. The three fractions defined in the test (FR1, FR2 FR3) are indicated by the horizontal bars above the chromatogram. The peak due to nitrate is also evidenced. (taken from Decesari et al. (2000))......	4-30
Figure 4-16. HPLC chromatogram of one CRPAQS fog sample from 12/17/00.....	4-31
Figure 4-17. HPLC chromatogram of CRPAQS fog sample AGCC03101.....	4-32
Figure 4-18. HPLC chromatogram of CRPAQS fog sample AGPCL03101.....	4-32
Figure 4-19. HPLC chromatogram of CRPAQS fog sample AGPCL03102.....	4-33
Figure 4-20. HPLC chromatogram of CRPAQS fog sample AGPCL03103.....	4-33
Figure 4-21. LWC, TC and OC/EC ratio for the period December 14 to December 21, 2000.....	4-34
Figure 4-22. LWC, TC and OC/EC ratio for January 14 to January 20, 2001 .....	4-35
Figure 4-23. LWC, TC and OC/EC ratio for January 24 to January 26, 2001 .....	4-35
Figure 4-24. LWC, TC and OC/EC ratio for January 30 to February 2, 2001 .....	4-36
Figure 4-25. EC vs OC concentrations from continuous measurements at Angiola .....	4-38
Figure 4-26. Short term DRI filter EC vs OC data for IOP days at Angiola.....	4-39
Figure 4-27. Evolution of fog LWC and ratio of particulate concentrations of levoglucosan to OC at Angiola during the period 12/14 to 12/21/00 .....	4-41

Figure 4-28. Evolution of fog LWC and ratio of particulate concentrations of levoglucosan to OC at Angiola during the period 1/14 to 1/20/01 .....	4-41
Figure 4-29. Evolution of LWC and ratio of particulate concentrations of levoglucosan to OC at Angiola during the period 1/24 to 1/27/01 .....	4-42
Figure 4-30. Evolution of fog LWC and ratio of particulate concentrations of levoglucosan to OC at Angiola during the period 1/29 to 2/3/01 .....	4-43
Figure 4-31. Evolution of LWC and ratio of particulate concentrations of pyrene to OC, at the beginning of the CRPAQS fog study .....	4-44
Figure 4-32. Evolution of fog LWC and ratio of particulate concentrations of anthracenedione to OC at Angiola during the beginning of the CRPAQS fog study ....	4-44
Figure 4-33. Evolution of fog LWC, particle phase Diazinon concentration and ratio of Diazinon to OC at Angiola towards the end of the CRPAQS fog study .....	4-45
Figure 5-1. Comparison of fog water masses collected by two deposition plates .....	5-5
Figure 5-2. Comparison of fog water fluxes collected by two deposition plates .....	5-5
Figure 5-3. Comparison of $\text{Cl}^-$ concentrations in fog water collected by two deposition plates .....	5-5
Figure 5-4. Comparison of $\text{Cl}^-$ fluxes collected by two deposition plates .....	5-6
Figure 5-5. Comparison of $\text{NO}_3^-$ concentrations in fog water collected by two deposition plates .....	5-6
Figure 5-6. Comparison of $\text{NO}_3^-$ fluxes collected by two deposition plates .....	5-6
Figure 5-7. Comparison of $\text{SO}_4^{2-}$ concentrations in fog water collected by two deposition plates .....	5-7
Figure 5-8. Comparison of $\text{SO}_4^{2-}$ fluxes collected by two deposition plates .....	5-7
Figure 5-9. Comparison of $\text{Na}^+$ concentrations in fog water collected by two deposition plates .....	5-7
Figure 5-10. Comparison of $\text{Na}^+$ fluxes collected by two deposition plates .....	5-8
Figure 5-11. Comparison of $\text{NH}_4^+$ concentrations in fog water collected by two deposition plates .....	5-8
Figure 5-12. Comparison of $\text{NH}_4^+$ fluxes collected by two deposition plates .....	5-8
Figure 5-13. Comparison of $\text{K}^+$ concentrations in fog water collected by two deposition plates .....	5-9
Figure 5-14. Comparison of $\text{K}^+$ fluxes collected by two deposition plates .....	5-9
Figure 5-15. Comparison of $\text{Mg}^{2+}$ concentrations in fog water collected by two deposition plates .....	5-9
Figure 5-16. Comparison of $\text{Mg}^{2+}$ fluxes collected by two deposition plates .....	5-10
Figure 5-17. Comparison of $\text{Ca}^{2+}$ concentrations in fog water collected by two deposition plates .....	5-10

Figure 5-18. Comparison of $\text{Ca}^{2+}$ fluxes collected by two deposition plates .....	5-10
Figure 5-19. Comparison of $\text{NO}_2^-$ concentrations in fog water collected by two deposition plates .....	5-11
Figure 5-20. Comparison of $\text{NO}_2^-$ fluxes collected by two deposition plates.....	5-11
Figure 5-21. Comparison of TOC concentrations in fog water collected by two deposition plates .....	5-11
Figure 5-22. Comparison of TOC flux collected by two deposition plates.....	5-12
Figure 5-23. Area normalized balance reading on 12/18/00. Temperature and wind speed trendlines are also presented for reference.....	5-14
Figure 5-24. Comparison of 10 minute average water fluxes on two balances on 12/18/00 .....	5-16
Figure 5-25. Comparison of 10 minute average water fluxes on two balances on 12/19/00 .....	5-16
Figure 5-26 Comparison of 10 minute average water fluxes on two balances on 01/15/01 .....	5-16
Figure 5-27. Comparison of 10 minute average water fluxes on two balances on 01/17/01 .....	5-17
Figure 5-28. Comparison of 10 min average water fluxes on two balances on 01/21/01 .....	5-17
Figure 5-29. Comparison of 10 minute average water fluxes on two balances on 01/25/01 .....	5-17
Figure 5-30. Comparison of 10 min average water fluxes on two balances on 01/31/01 .....	5-18
Figure 5-31. Deposition velocities of fogwater, TOC, $\text{NH}_4^+$ , $\text{SO}_4^{2-}$ , $\text{NO}_3^-$ and $\text{NO}_2^-$ ....	5-22
Figure 5-32. Deposition velocities of fogwater, $\text{Cl}^-$ , $\text{Na}^+$ , $\text{K}^+$ , $\text{Mg}^{2+}$ and $\text{Ca}^{2+}$ .....	5-23
Figure 5-34. Fog drop size distributions (large vs. small drop concentrations from the sf-CASCC or ss-sf-CASCC) of $\text{NH}_4^+$ , $\text{SO}_4^{2-}$ , $\text{NO}_3^-$ , TOC, $\text{NO}_2^-$ and $\text{Ca}^{2+}$ .....	5-24
Figure 5-35. Deposition velocity vs. small/large drop concentration ratio for fog samples collected in the 12/18/00 fog event. Each point represents one species (from left to right $\text{NO}_2^-$ , $\text{NH}_4^+$ , $\text{SO}_4^{2-}$ and $\text{NO}_3^-$ ). .....	5-25
Figure 5-35. S(IV) sinks as calculated by the aqueous phase chemistry model for both the large (upper panel) and small (lower panel) drop fractions from the sf-CASCC .....	5-36
Figure 5-36. Sensitivity test of the rate of HMS formation to changes in the HCHO concentration.....	5-37
Figure 5-37. Sensitivity test of rate of the $\text{H}_2\text{O}_2$ -S(IV) oxidation pathway to $\text{H}_2\text{O}_2$ concentrations .....	5-38
Figure 5-38. Sensitivity test of the rate of the $\text{O}_3$ -S(IV) oxidation pathway to $\text{O}_3$ concentrations .....	5-38



Figure 5-39. Theoretical rates of ozone and hydrogen peroxide oxidation of S(IV) and HMS formation averaged for all the large drop and small drop fog samples.....	5-40
Figure 5-40. Comparison of HMS formation modeled rates and theoretical rates.....	5-41
Figure 5-41. Comparison of ozone oxidation modeled rates and theoretical rates.....	5-41
Figure 5-42. Theoretical and model rate comparison to large/small ratios for all fog sample periods .....	5-42
Figure 5-43. Timelines of deposition removal rates of four major ions in the 12/17/00 - 12/18/00 fog event .....	5-44
Figure 6-1. Predicted and observed liquid water content for the simulated fog event. The initial time corresponds to 6:00 p.m. on December 18, 2000 .....	6-7
Figure 6-2. Evolution of diameters for the 14 modeled sections.....	6-8
Figure 6-3. Predicted size distributions for sulfate, ammonium, nitrate and chloride....	6-9
Figure 6-4. Predicted and observed (a) sulfate, (b) nitrate, (c) ammonium, (d) chloride, (e) calcium, (f) manganese, (g) sodium, and (h) iron concentrations in the fog droplets (sections 8-14).....	6-11
Figure 6-5. Comparison of predicted and observed size-resolved aqueous-phase concentrations of (a) ammonium, (b) sulfate, (c) chloride, (d) nitrate, (e) calcium, and (f) sodium.....	6-14
Figure 6-6. Predicted and observed depositional fluxes for (a) ammonium, (b) chloride, (c) sulfate, (d) nitrate, (e) calcium, and (f) sodium in $\text{neq/m}^2/\text{min}$ . One deposition sample was collected from 5:15 to 7:35 a.m. on December 19, 2000 .....	6-16
Figure 6-7. Average depositional flux for (a) sulfate, (b) nitrate, (c) ammonium, (d) chloride, (e) calcium, and (f) sodium for different diameter ranges.....	6-17
Figure 6-8. Total sulfate predictions for the 14-section dynamic fog model and the VSRM .....	6-19
Figure 6-9. The final size distributions of sulfate predicted by the VSRM and dynamic fog model .....	6-20
Figure 6-10. Predicted sulfate concentrations for the VSRM and the dynamic fog model (a) using the equation for depositional flux as a function of liquid water content derived by Pandis et al., 1990b and (b) reducing by 60% the depositional flux used in Figure 10a .....	6-21

## **List of Tables**

Table 2-1. Calibration table of the CSASP during the CRPAQS study .....	2-9
Table 2-2. Aliquot preservation protocol. ....	2-15
Table 2-3. RSD, MDL and sample concentration summaries for CRPAQS fog ions....	2-23
Table 2-4. Statistical analysis for organic acids.....	2-24
Table 2-5. Statistical analysis for S(IV), HCHO, H <sub>2</sub> O <sub>2</sub> , Fe <sup>2+</sup> , Mn <sup>2+</sup> , TOC and DOC...	2-25
Table 2-6. Statistical analysis for MOUDI samples.....	2-25
Table 2-7. Summary of collector flow rates and size cuts. ....	2-26
Table 3-1. Summary of collected fog samples in Angiola by collector type. ....	3-3
Table 3-2. Summary of weather conditions during fog events. ....	3-3
Table 3-3. Volume-weighted average solute concentrations in all fog events. ....	3-16
Table 3-4 Summary of bulk fog sample composition.....	3-17
Table 3-5. Overview of satellite site fog sampling during CRPAQS.....	3-29
Table 3-6. Overview of collected samples at Helm .....	3-31
Table 3-7. Chemical composition of samples collected in Helm.....	3-32
Table 3-8. Correlation matrix for Helm fog components.....	3-33
Table 3-9. Chemical composition of the fog sample collected in Bakersfield .....	3-35
Table 3-10. Composition of Al-CASCC2 samples collected at the Angiola site.....	3-36
Table 3-11. Overview of tower fog experiments .....	3-46
Table 3-12. Available Bakersfield fog composition data sets used for temporal trend analysis.....	3-53
Table 3-13. Comparison of Bakersfield fog water concentrations in samples collected in the 1980s and the period 1990-2001 .....	3-55
Table 4-1. Required reagents for carbonyl and dicarbonyl analysis. ....	4-6
Table 4-2. Chemical structures of key carbonyls and dicarbonyls .....	4-8
Table 4-3. Carbonyl and dicarbonyl concentrations in blanks.....	4-12
Table 4-4. Minimum detection limits of carbonyls.....	4-12
Table 4-5. DNPH recrystallization results .....	4-14
Table 4-6. Precision of carbonyl analyses.....	4-15
Table 4-7. Accuracy for carbonyls analysis .....	4-16
Table 4-8. Concentrations of artificial fog water parallel samples .....	4-17
Table 4-9. Comparison of concentrations of artificial fog water samples .....	4-18

Table 4-10. Stability test in a real fog water matrix.....	4-19
Table 4-11. Carbonyl and dicarbonyl concentrations of CRPAQS fog samples.....	4-23
Table 4-12. Sampling information and concentrations of detectable carbonyls and dicarbonyls in Fresno fog samples.....	4-24
Table 4-13. Summary of Fresno bulk organic fog sample composition .....	4-25
Table 4-14. Observed scavenging efficiencies.....	4-38
Table 5-1. Deposited fog water mass, ion and TOC concentrations observed on the two deposition plates.....	5-2
Table 5-2. Fog water, ion and TOC fluxes derived from the two deposition plates .....	5-3
Table 5-3. Summary of observed deposition fluxes in CRPAQS fogs .....	5-12
Table 5-4. Relative standard deviations of deposited fog concentrations and fluxes derived from two deposition plates.....	5-13
Table 5-5. Linear regression analysis of water flux vs. fog LWC and effective diameter for CRPAQS.....	5-19
Table 5-6. Average deposition velocities of all species to two deposition plates .....	5-20
Table 5-7. Typical ranges of deposition velocities and relative standard deviations .....	5-22
Table 5-8 Parameters and initial conditions in the model.....	5-30
Table 5-9. Model input parameters used for fog events at the Angiola main site.....	5-31
Table 5-10. Partition function, Q, and rates for S(IV) oxidation by hydrogen peroxide and ozone and HMS formation.....	5-34
Table 5-11. Theoretical S(IV) oxidation rate and HMS formation rate for all fog samples .....	5-39
Table 5-12. Deposition removal rates of each species for all fog events.....	5-43
Table 5-13. Total mass removal of species by fog episodes during CRPAQS.....	5-44
Table 5-14. Estimated reduction in ground level ambient concentrations by fog episodes during CRPAQS assuming a 100 m fog depth.....	5-45
Table 6-1. Gas phase and aerosol inputs for the simulation of the fog event at Angiola, California on December 18-19, 2000.....	6-6

## Chapter 1

### Introduction

#### 1.1 Fog formation and maintenance

Fog is a layer-type cloud that makes contact with the ground. It is comprised of tiny water droplets, typically ranging in size from several micrometers to several tens of micrometers. These drops form by water vapor condensing onto aerosol nuclei. As atmospheric relative humidity surpasses one hundred percent, some aerosol particles (known as cloud condensation nuclei or CCN) are activated to form fog droplets through the process of heterogeneous nucleation. The first particles to activate tend to be larger in size and contain a high fraction of soluble material. As the supersaturation in the air mass continues to rise, additional particles can also activate to form drops. Activation of new drops will continue until the peak supersaturation is reached. At this point depletion of water vapor due to condensational drop growth prevents the supersaturation from climbing higher. A fog droplet with a diameter of  $\sim 25\mu\text{m}$  settles under the influence of gravity at about 5cm per second. At this rate most droplets in a fog layer would reach the ground in a few hours. Maintaining a fog beyond several hours, therefore, requires a replenishment of droplets.

There are four main types of fog: radiation fog, frontal fog, advection fog and ice or snow fog corresponding to the primary three mechanisms for fog formation:

- (1) cool the air to below its dew point temperature. Fog produced by strong radiative cooling of the earth's surface is called "radiation fog" since radiation and conduction are the primary means for cooling stable nighttime air near the ground. Formation of radiation fog requires calm winds and clear skies. Clear skies promote effective radiative cooling of the surface which, in turn, cools the air layer adjacent to the ground. The presence of modest to strong winds inhibits cooling of the surface air layer due to promotion of vertical mixing. As a radiation fog develops, the upper reaches of the fog layer itself cool by radiation to a clear sky, leading to cooling of overlying air parcels and entrainment. This process occurs throughout the night, if conditions are favorable, leading to a deepening fog layer. Cooling of an air parcel to form fog also occurs in advection fog. Advection fog occurs when warm, moist air moves over a colder surface that cools the overlying air parcel to its dew point resulting in fog formation.
- (2) "Ice or snow fog" forms when a very cold air parcel reaches its saturation conditions with respect to ice as a result of adding a small amount of water vapor.
- (3) "Frontal fog" typically forms on the colder side of a front. Steady stratiform precipitation transfers water in the form of precipitation to the subcloud layer where it evaporates, sometimes producing a saturated air parcel and forming frontal fog.

Once fog forms, it is maintained by newly formed water droplets. If the air cannot at least maintain its degree of saturation either by continual cooling or by evaporation and mixing of vapor into the air, the fog will begin to dissipate. There are three important mechanisms for fog dissipation: (1) the sizes of fog droplets increase so that they become heavy and settle to the ground (possibly as a light drizzle); (2) the air is heated and fog evaporates; and (3) cooler saturated air near the surface mixes with the warmer unsaturated air above.

## 1.2 Aerosol activation

Fog is more likely to form in an environment with large CCN concentrations characterized by a low activation critical supersaturation. Köhler theory is used to

compute the equilibrium vapor pressure over a solution droplet. It defines the critical diameter at which a droplet is activated and begins to grow spontaneously by water vapor uptake. It also describes the equilibrium growth of aerosol particles in terms of their size, chemical composition and corresponding concentrations in the droplets. The Köhler equation can be written as

$$s = 1 + \frac{2\sigma_s M_w}{RT\rho_w r} - \frac{3M_w \Phi_s}{4\pi\rho_s r^3} \quad (1-1)$$

where  $s$  is the equilibrium saturation ratio of water vapor above a drop surface,  $M_w$  is the molecular weight of the solute,  $\rho_w$  is the density of water,  $\sigma_s$  is the droplet surface tension,  $r$  is the droplet radius,  $\Phi_s$  is the osmotic coefficient of the aqueous solution,  $R$  is the gas constant and  $T$  is absolute temperature.

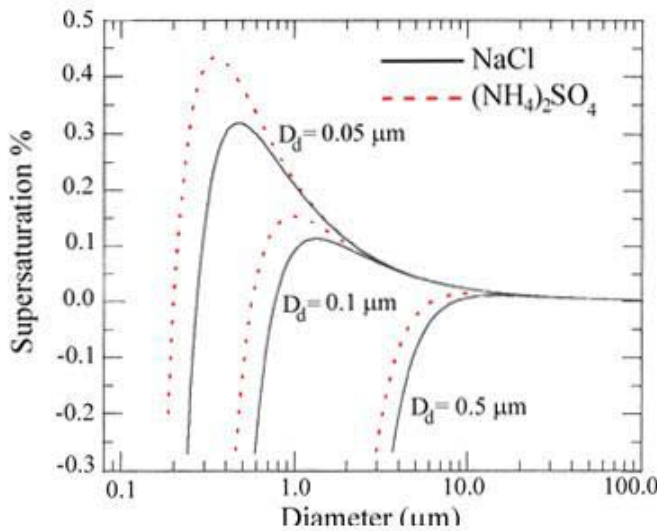


Figure 1-1. Köhler curves for NaCl and  $(\text{NH}_4)_2\text{SO}_4$  particles for various dry particle diameters (Hanel, 1976).

Figure 1-1 shows Köhler curves for NaCl and  $(\text{NH}_4)_2\text{SO}_4$  particles for various dry particle diameters (Hanel, 1976). As the environmental humidity increases, a solution drop “grows” up the left side of the curve. This portion of the curve describes a stable equilibrium: droplets which deviate slightly in size from the equilibrium value tend to be returned to that equilibrium size by evaporation or condensation. A particle in stable equilibrium is called a haze droplet. The peak values of  $S$  on a Köhler curve is known as

the critical supersaturation; the corresponding diameter or radius is termed the critical diameter or critical radius. Once a droplet has crossed this critical size, it is said to be activated and begins to grow unstably by spontaneous addition of water vapor. The larger the drop grows, the lower the equilibrium saturation value and, hence, the lower the ambient supersaturation needs to be to continue to promote droplet growth. The portion of the curve to the right of the critical size represents a situation of unstable equilibrium. An activated droplet in the unstable equilibrium regime is called a fog or cloud drop.

The shape of a Köhler curve is determined by a competition between multiple effects. The second term on the right hand side of the Köhler equation, the Kelvin term, includes the influence of surface tension within the Kelvin effect, that is, the increase of the water vapor pressure due to the curvature of the droplet surface. The third term, the Raoult term, defines the equilibrium vapor pressure reduction due to dissolved solute in the Raoult effect.

Although Köhler theory has long been applied to growth and activation of droplets formed on inorganic salt particles, many atmospheric particles contain both water soluble (inorganic ions and some organics) and insoluble substances (dust, elemental carbon, etc...). Köhler theory readily explains the behavior of water soluble particles in the atmosphere. Kulmala et al. (1997) discuss some of the factors that complicate the typical interpretation of Köhler theory as applied to inorganic salt particles. Effects are illustrated for the inclusion of an insoluble or slightly soluble core and for uptake of highly soluble nitric acid. All of these cases suggest possible changes in the critical activation size and critical supersaturation.

In terms of organic compounds, which represent an important part of the aerosol water soluble fraction, some researchers have examined Köhler theory with hypothesized organic components and concentrations. Some surfactants can change the surface characteristics of droplets, which is important to the activation of aerosol particles to form cloud condensation nuclei (Decesari et al., 2000; Mircea et al., 2002). Shulman et al. (1996) measured solubilities and surface tensions for difunctional organic acids (malonic

acid, glutaric acid, succinic acid, oxalic acid, adipic acid, phthalic acid, and cis-pinonic acid) in various concentrations of  $(\text{NH}_4)_2\text{SO}_4$  and  $\text{NH}_4\text{HSO}_4$  aqueous solutions. These experiments simulate the growth of cloud droplets nucleating on sulfate aerosols. Model results using these data indicate that the organic compounds affect cloud droplet growth by two mechanisms: (1) by gradual dissolution in the growing (diluting) droplet, which affects the shape of the Köhler growth curve, and (2) by reducing the droplet surface tension which decreases the critical supersaturation. Recently, several investigators (Laaksonen et al., 1998; Facchini et al., 1999a; Facchini et al., 1999b; Hitzenger et al., 2002; Mircea et al., 2002) used a modified Köhler equation and variable surface tension values derived from field data to demonstrate that organic compounds with surface active properties will decrease the surface tension of droplets, and will highly increase CCN number concentrations. However, a similar method was used by Li et al. (1998) and they concluded that “Reduction in critical supersaturation caused by the reduction in  $\sigma$  (Kelvin effect) associated with the surfactant is dominated by the increase in  $S_c$  with the decreasing number of moles of solute in the droplet (Raoult effect) as surfactant displaces NaCl solute mass”. The different conclusions were questioned and discussed in the literature (Rodhe, 1999; Facchini et al., 2001; Rood et al., 2001). The major difference appears to result from the fact that they used different organic compounds in the models. The influence of organic compounds on aerosol hygroscopicity in general is also receiving increasing attention. Saxena et al. (1995) found that aggregate hygroscopic properties of inorganic particles are altered substantially when organics are also present, and alterations can be positive or negative. For non-urban location, organics appeared to enhance water absorption by inorganics; for urban locations, the net effect of organics was to diminish water absorption by the inorganics. Certainly, however, the effects in any individual case will require more knowledge than we presently have about the organic compounds present in atmospheric aerosols.

Understanding the influence of organics on fog drop activation requires improved information about the organic composition of particles that are actively scavenged by fogs via nucleation. Because there are hundreds, perhaps thousands, of individual organic compounds present in fog drops (not all of which extract in a single solvent or elute



through a gas chromatograph), it may be more effective initially to focus on characterizing the types/families of compounds that are present and considering their ability to modify drop surface tension. Without such knowledge, it is very difficult to accurately predict the effects of organics on drop activation. Many current efforts to do so make unrealistic assumptions about the composition of organics involved. A frequent inaccurate assumption is that dicarboxylic acids dominate organic carbon in aerosol particles and fog drops.

Overall, Köhler theory can work to predict activation of soluble inorganic and organic species when composition is simple and well described (Raymond et al., 2002). An extension to treat more complex mixtures containing many low-solubility (higher molecular weight) organic species is necessary due to their abundance in fog water (Herckes et al., 2002b).

### 1.3 Aerosol scavenging, removal and production in fogs

Over the last 20 years, it has become increasingly evident that clouds and fogs play an important role as processors of aerosol particles and trace gases (Waldman et al., 1983; Jacob et al., 1984; Fuzzi, 1988; Dlugi, 1989; Collett et al., 1990; Cereceda et al., 1991; Fuzzi et al., 1994; Collett et al., 1999b;). Fogs comprise a complex multiphase system. Fogs act both as reactors for the production of new chemical species and as a pathway for particle and trace gas removal, mainly via wet deposition and direct deposition of fog drops to the ground or to vegetation.

There are mainly three mechanisms for aerosol scavenging by fog. The dominant mechanisms vary depending on the size of the particle. For Aitken particles ( $r < 0.1\mu\text{m}$ ), the primary scavenging process is Brownian diffusion. For accumulation mode particles ( $0.1\mu\text{m} < r < 1.0\mu\text{m}$ ), the primary scavenging process is nucleation (as described above). For even larger particles, collision between aerosol particles and fog droplets (scavenging by impaction and interception, hydrodynamic capture) is typically more effective.

Particles with diameters bigger than 10  $\mu\text{m}$  tend to settle on the ground near their emission source. Particles with diameters less than 0.1  $\mu\text{m}$  also tend to have short lifetimes in the atmosphere and aids in their dry deposition, due to their rapid diffusion and coagulation, which leads to larger sizes. Accumulation mode particles, by contrast, have rather long lifetimes in the atmosphere (on the order of several days) and thus can be transported long distances. These long lifetimes can be shortened considerably by interactions with precipitating clouds or, in some environments, with radiation fogs. Removal of accumulation mode aerosol particles from the atmosphere is of keen interest because of the important roles they play in impacting radiative transfer (with implications for climate and visibility) and human respiratory health.

Munger et al. (1983a) proposed a cyclical relationship between the occurrence of smog and fog, which was termed a “smog-fog-smog” cycle. A polluted atmosphere with a high aerosol concentration assists the formation of late night and early morning fog, which appears to enhance smog production, visibility reduction, and aerosol concentration levels during the following day. Several investigators, however, have also recognized that long-lived fogs can actually help cleanse the atmosphere by nucleation scavenging of particles followed by fog drop settling to the surface. Jacob et al. (1984) were among the first to propose that enhanced aerosol deposition in fog layers efficiently limits pollutant buildup during air stagnation episodes.

Fogs can produce additional aerosol material by uptake of soluble gases that react in the droplets to form non-volatile products. When the fog evaporates, this new non-volatile solute is left behind as part of the residual aerosol. The classic example of fog production of aerosol mass is uptake of sulfur dioxide followed by its oxidation to sulfate. Since the reaction time of sulfur oxidation in drops is several minutes to hours, the typical lifetime of fog is sufficient for the production of significant sulfate (Pandis et al., 1992). Although sulfate production has received the most attention, there are other aqueous phase reactions that can also lead to secondary aerosol production. These include reactions that produce low volatility organic compounds. The production of non-volatile material in fog drops leads to the release from dissipating fogs of aerosol particles that may be larger and more

soluble than the CCN on which the drops originally formed. The new aerosol particles are likely to be more effective CCN than their precursors.

#### 1.4 Fog scavenging of gases and secondary aerosol production

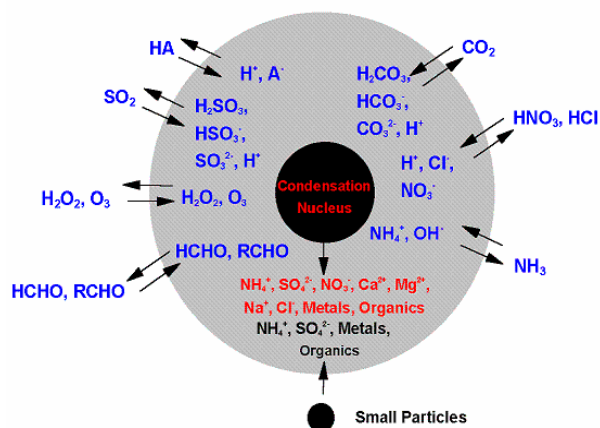


Figure 1-2. Simplified chemistry of a cloud/fog drop.

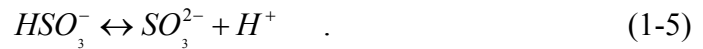
The fundamental scavenging role of water droplets is widely recognized and interactions for some species have been investigated (Chameides et al., 1983; Calvert et al., 1985; Jacob, 1986; Laj et al., 1997). As shown in Figure 1-2, chemical species of interest include  $\text{SO}_2$ ,  $\text{CO}_2$ , nitrogen compounds ( $\text{NO}$ ,  $\text{NO}_2$ ,  $\text{HNO}_3$ ,  $\text{NH}_3$ ), oxidants ( $\text{H}_2\text{O}_2$ , organic peroxides, and  $\text{O}_3$ ), and a large variety of organic compounds (formaldehyde and other low molecular weight aldehydes, small carboxylic acids, phenols, etc.). Many of these soluble gases play an important role in determining fog/cloud pH. In remote environments, for example, pH is determined largely by uptake of carbon dioxide along with formic and acetic acids. In more polluted environments uptake of gaseous acids (e.g.,  $\text{HNO}_3$ ) and bases ( $\text{NH}_3$ ) exert significant control on drop composition and acidity.

Soluble gases dissolving into fog drops sometimes undergo significant reaction to form non-volatile products, a topic introduced above. Uptake of gas phase oxidants can be an important aspect of these reactions as well.  $\text{O}_3$  and  $\text{H}_2\text{O}_2$ , for example, can act as important oxidants for dissolved sulfur dioxide.  $\text{HCHO}$  is of interest because it can react with sulfur dioxide to form hydroxymethanesulfonate (HMS) at high pH (Boyce et al., 1984; Munger et al., 1986).

Gas uptake by fog drops includes four major steps: transport through the gas phase to the drop surface, transport across the gas-liquid interface, transport within the aqueous phase, and chemical reaction (e.g., ionization) in the drop (Daum et al., 1984). The partitioning of a gas into fog droplets depends on its solubility. Henry's law describes the equilibrium solubility:

$$[A(aq)] = H_A p_A \quad (1-2)$$

where  $p_A$  is the partial pressure of species A in the gas phase (unit: atm); and  $[A(aq)]$  is the aqueous phase concentration of A in equilibrium with  $p_A$  (unit: mol L<sup>-1</sup>).  $H_A$  is the Henry's law equilibrium constant (unit: mol L<sup>-1</sup> atm<sup>-1</sup>), which depends on temperature. Solubility typically increases as temperature declines. Henry's law as written above only describes the physical solubility. For some gases such as SO<sub>2</sub>, ionization in the aqueous phase is important and enhances the solubility:



Using the equations above we can derive  $H_A^*$ , an "effective" Henry's Law constant, for SO<sub>2</sub> which includes the enhanced solubility due to ionization:

$$H_{SO_2}^* = H_{SO_2} \left( 1 + \frac{K_1}{[H^+]} + \frac{K_1 K_2}{[H^+]^2} \right) \quad (1-6)$$

where  $K_1$  and  $K_2$  are the acid dissociation constants corresponding to reactions (1-4) and (1-5) above, respectively. Note that  $H_{SO_2}^*$  depends on the pH of the solution. The solubility increases as pH increases. Thus the effect of ionization in solution is to increase

the effective solubility. Other important gases that have enhanced solubility due to ionization include carbon dioxide, nitric acid, ammonia, and carboxylic acids.

The solubility of HCHO in fog drops is also enhanced in solution by the formation of a gem diol:



The effective Henry's law coefficient for the total dissolved formaldehyde  $H_{HCHO}^*$  is:

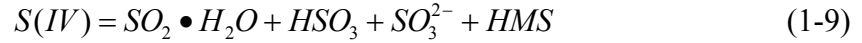
$$H_{HCHO}^* = H_{HCHO}(1 + K_{HCHO}) \cong H_{HCHO}K_{HCHO} \quad . \quad (1-8)$$

$K_{HCHO}$  is rather large at 298K, suggesting that hydration is essentially complete and that practically all dissolved formaldehyde will exist in its gem diol form.

Gas-to-particle conversion of chemical species in the atmosphere generates secondary aerosol matter. As mentioned above fog drops can serve as micro-reactors to convert primary pollutants, such as gas phase SO<sub>2</sub>, to secondary aerosol species such as sulfates (Seinfeld et al., 1998). Aqueous phase production of secondary aerosol requires the following combination of processes: dissolution of soluble gases in fog drops and subsequent reaction in the droplets to form new non-volatile species.

Many chemical species incorporated in water droplets can react in the aqueous phase (Fuzzi, 1995). Considerable attention has been focused on the aqueous oxidation of dissolved sulfur dioxide to sulfate because sulfate comprises a significant fraction of the atmospheric aerosol and contributes significantly to issues such as acid deposition, visibility degradation, and climate forcing. Aerosol sulfates comprise about 5 to 20 percent of the total suspended particulate matter in urban air (Wark et al., 1998). Outside urban areas this fraction can grow even higher.

Oxidation of sulfur in the atmosphere can occur both in the gas and in the aqueous phases. Aqueous phase oxidation is of special interest because it occurs much more rapidly than gas phase oxidation. Because dissolved SO<sub>2</sub> can have different forms in solution, the oxidation state (+4) is used to represent all the forms:

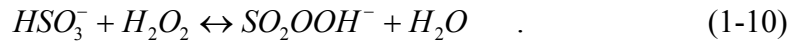


and the final oxidized state (+6) of sulfate, bisulfate, or sulfuric acid is referred to as S(VI).

Several sulfur oxidation mechanisms occur in the aqueous phase (Seinfeld and Pandis, 1998), their importance depending on the drop pH and the availability of oxidants and catalysts. Three important pathways are oxidation by hydrogen peroxide, oxidation by ozone, and oxidation by oxygen (auto-oxidation) catalyzed by Fe(III) and Mn(II).

#### 1.4.1 S(IV) oxidation by hydrogen peroxide (H<sub>2</sub>O<sub>2</sub>)

The oxidation of S(IV) by hydrogen peroxide is typically considered the major pathway in acidic environments. H<sub>2</sub>O<sub>2</sub> in the gas phase can easily dissolve into cloud or fog droplets due to its high solubility. According to (McArdle et al., 1983), the reaction proceeds via a nucleophilic attack of hydrogen peroxide on bisulfite as the principal reactive S(IV) species:



The peroxymonosulfurous acid formed reacts with a proton to produce sulfuric acid:



The latter reaction becomes faster if the aqueous phase gets more acidic. Hoffmann et al., (1985) suggest the following reaction rate expression:

$$\frac{d[SO_4^{2-}]}{dt} = \frac{k[H^+][H_2O_2][HSO_3^-]}{1 + K[H^+]} \quad (1-12)$$

where  $k=7.5 \times 10^7 \text{ M}^{-1}\text{s}^{-1}$  and  $K=13 \text{ M}^{-1}$  at 298K. A lack of pH dependence for  $\text{pH} > 2$  in the overall rate expression results from the fact that the concentration of  $\text{HSO}_3^-$  declines at lower pH, due to a decrease in  $\text{HSO}_2^*$  and a shift in speciation from  $\text{HSO}_3^-$  to  $\text{H}_2\text{SO}_3$ , offsetting the influence of  $\text{H}^+$  on the rate of reaction (1-11).

Organic peroxides have also been proposed as potential aqueous S(IV) oxidants. For example, hydroxymethyl hydroperoxide ( $\text{HOCH}_2\text{OOH}$ ) may be important in S(IV) oxidation, depending on the relative amount compared to  $\text{H}_2\text{O}_2$  (Zhou et al., 1992). Generally, however, concentrations and solubilities of organic hydroperoxides are thought to be low enough that they are of only minor importance as S(IV) oxidants.

S(IV) oxidation by hydrogen peroxide is viewed as the most effective reaction at low pH values. This pathway can be detectable in the cloud or fog through a decrease of gas phase  $\text{SO}_2$  and  $\text{H}_2\text{O}_2$  or an increase of S(VI) in the aqueous phase (Husain, 1989).

#### 1.4.2 S(IV) oxidation by ozone ( $\text{O}_3$ )

Ozone reacts very slowly with  $\text{SO}_2$  in the gas phase where the OH radical is the dominant oxidant. However, the aqueous phase oxidation of S(IV) by ozone can be rapid and can even dominate aqueous phase sulfate production when drop pH is high or hydrogen peroxide is depleted. This reaction can simply be written as:



This reaction can be considered as nucleophilic attack by S(IV) species on  $\text{O}_3$ , Hoffmann (1986) found that this oxidation process can be treated in terms of individual reactions of the various forms of S(IV):  $\text{SO}_2 \cdot \text{H}_2\text{O}$ ,  $\text{HSO}_3^-$  and  $\text{SO}_3^{2-}$  each can react with

ozone separately with a unique mechanism and rate constant. The total oxidation rate can be written as:

$$-\frac{dS(IV)}{dt} = (k_0\alpha_0 + k_1\alpha_1 + k_2\alpha_2)[S(IV)][O_3] \quad (1-14)$$

where  $\alpha_0$ ,  $\alpha_1$  and  $\alpha_2$  are the fractions of free S(IV) present as  $SO_2 \cdot H_2O$ ,  $HSO_3^-$  and  $SO_3^{2-}$ , respectively, and  $k_0$ ,  $k_1$  and  $k_2$  are rate constants.

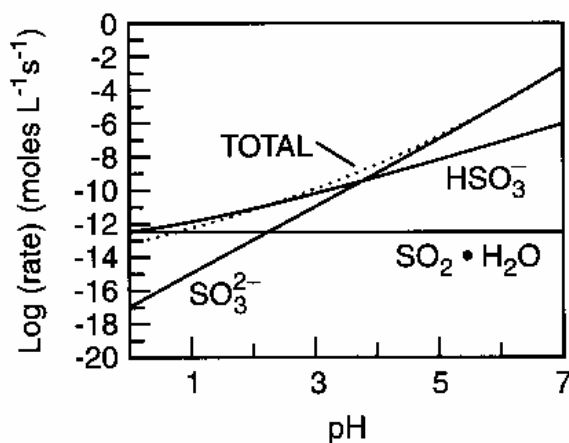


Figure 1-3. Rate of S(IV) oxidation by  $O_3$  in the aqueous phase under conditions typical of a Los Angeles atmosphere, with  $SO_2=20$  ppb and  $O_3=50$  ppb (adapted from Hoffmann, 1986).

Existing experimental kinetic and mechanistic data suggest that this reaction has a complex pH dependence (Maahs, 1983; Martin, 1984; Penkett et al., 1979). Figure 1-3 shows the pH dependence of the rate of total reaction and of individual reactions by the three sulfur species. Because the effective solubility of sulfur dioxide increase with pH and because sulfite is oxidized much more rapidly than bisulfite, which is oxidized more rapidly than sulfurous acid, the reaction rate of sulfate production by this pathway increase strongly with increasing pH. Therefore, S(IV) oxidation by ozone is most important at high pH.

#### 1.4.3 S(IV) oxidation by oxygen ( $O_2$ )

S(IV) oxidation by oxygen is very slow except in the presence of catalysts such as Fe(III) and Mn(II). Synergistic effects were found for the catalysis when Fe(III) and Mn(II) co-exist in the aqueous phase (Martin, 1994). In fog water these two trace metal ions can



be relatively abundant because they are common aerosol components often coming from earth crust erosion. The catalyzed auto-oxidation mechanism and its kinetics are very complex. Even though several researchers have reported rate expressions, no common form has been accepted. The reaction rate is sensitive to various factors such as pH, ionic strength and concentrations of all species. Generally, we know that the catalyzed reaction is most likely to be important when pH is about neutral, in the range of about 6-7. Although an accurate measurement of the iron and manganese oxidation states is difficult in the field, an upper bound to S(IV) oxidation by oxygen can be determined by using the total Fe and Mn concentrations. In general, since S(IV) oxidation by oxygen is only significant when pH value is near neutral, i.e., in the range of 6~7, and at this pH range, formation of HMS and S(IV) oxidation by ozone can be even faster, metal catalyzed S(IV) oxidation typically doesn't play a large role in overall sulfate production in fogs (Rao et al., 1998).

#### 1.4.4 Reaction of dissolved SO<sub>2</sub> with HCHO

Field studies have found that total S(IV) concentrations in fog water are sometimes much higher than Henry's law predicts, because HSO<sub>3</sub><sup>-</sup> and SO<sub>3</sub><sup>2-</sup> in fog can react with dissolved aldehydes. The most important reaction is with formaldehyde, to produce hydroxymethanesulfonic acid, HOCH<sub>2</sub>SO<sub>3</sub>H (HMS) (Boyce et al., 1984):



The product of the first reaction HOCH<sub>2</sub>SO<sub>3</sub><sup>-</sup> is HMSA, anion of HMS. HMSA can dissociate further to form <sup>-</sup>OCH<sub>2</sub>SO<sub>3</sub><sup>-</sup>, though the second dissociation is weak.

Formation of HMS is favored at high pH. It is accordingly an important additional sink for sulfur dioxide in high pH drops. An interesting feature of HMS chemistry is that the high pH condition favored for its production is not good for its preservation. Munger et al. (1986) found that if the fog pH is initially high but decreases due to formation of S(VI) by oxidation processes, HMS will be produced and maintained in fog water.

Oxidation by OH radical is probably the major sink of HMS in daytime fog (Jacob, 1986; Pandis et al., 1989b). The lifetime of HMS is about 1 hour to 10 hours. Therefore, in high pH fogs with abundant HCHO, measured S(IV) will be mostly comprised of HMS, not  $\text{HSO}_3^-$  or  $\text{SO}_3^{2-}$  (Rao et al., 1998).

#### 1.4.5 The overall fate of S(IV)

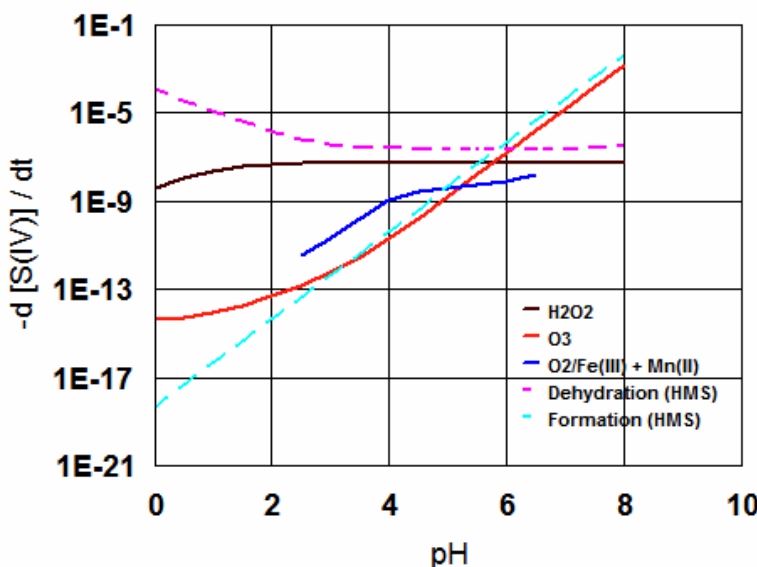


Figure 1-4. Oxidation rates of the three S(IV) oxidation pathways, along with the rate of HMS formation for typical conditions in central California fogs.

Figure 1-4 shows the oxidation rates of the three S(IV) oxidation pathways described above along with the rate of HMS formation for typical conditions in central California fogs. The oxidation of S(IV) by hydrogen peroxide is important and is typically considered the major pathway in most environments, where pH is below 5-6. Oxidation by ozone is important at high pH where it competes with HMS formation for  $\text{SO}_2$  taken up from the gas phase. S(IV) oxidation via oxygen is too slow to be an important contributor to the fate of dissolved  $\text{SO}_2$ .

#### 1.5 Aqueous phase reactions of organics

A variety of aqueous phase reactions also exist that involve organic compounds. In fact, it is possible that a significant portion of secondary organic aerosol (SOA) formation takes place in cloud and fog droplets (Facchini et al., 1992; Blando et al., 2000). Aumont et al.

(2000) proposed that high carboxylic acid concentrations in cloud water samples cannot be explained by a gas-phase source, which suggests that besides aerosol and gas scavenging, VOC oxidation in cloud and fog water are also important for carboxylic acid formation. Aqueous phase oxidation processes can enhance the solubility of organic aerosol by introducing polar functional groups into the molecular structure (e.g., mono- and dicarboxylic acids, aldehydes, alcohols, ketones and organic peroxides, which are fairly abundant in fog water (Facchini et al., 1999a; Blando et al., 2000). Blando et al. (2000) summarize evidence that cloud and fog processes produce fine organic particulate matter in the atmosphere and could be important contributors to SOA formation, although the contribution of this formation pathway should be further investigated. Specific compounds identified as potential precursors include aldehydes (e.g., formaldehyde, acetaldehyde and propionaldehyde), acetone, alcohols (e.g., methanol, ethanol, 2-propanol and phenol), monocarboxylic acids, and organic peroxides. Carboxylic acids (e.g. diacids), glyoxal, esters, organosulfur compounds, polyols, amines and amino acids are potential products of cloud and fog processing.

Most of the research to date on aqueous phase SOA formation has been theoretical in nature and rather speculative. The importance of aqueous phase oxidation remains unclear and cannot yet be fully assessed. Further research is certainly required.

## 1.6 Solute deposition in fogs

As mentioned earlier fog drop deposition can be an important mechanism for removing pollutants from the atmosphere. Deposition mechanisms for fog droplets include inertial impaction, interception and sedimentation (Burkhard et al., 2000; Eugster et al., 2001; Wrzesinsky et al., 2001). Sedimentation is the dominant mechanism for radiation fogs in locations with low wind speeds and low surface roughness. Impaction and interception are important for capture of drops by vegetation such as montane forest canopies. In some areas fog/cloud drop deposition can significantly enhance total wet deposition to terrestrial ecosystems. Collett et al. (2001) found that key solute (e.g., nitrate, sulfate and ammonium) deposition velocities in radiation fogs range from approximately 1 to 10 cm s<sup>-1</sup>. These

values are much higher than deposition velocities for accumulation mode aerosol particles, suggesting fogs are important contributors to cleansing of the atmosphere. Lillis et al. (1999) evaluated fog effects on the production and removal of particulate matter in a polluted fog layer and found that aerosol and gas scavenging and drop deposition can significantly reduce atmospheric nitrate and ammonium concentrations while removal of sulfate was roughly offset by aqueous phase sulfate production. Little attention has been paid to the effectiveness of fogs in removal of carbonaceous aerosols.

### 1.7 Issues of drop size-dependent fog composition

One topic receiving increased concern in recent years is the variation of solute concentrations across the fog drop size spectrum. A variety of factors can contribute to this variation, including the size-dependent composition of CCN, faster dilution of small droplets by condensational growth, and faster uptake of soluble gases by smaller fog drops. Initial differences in fog drop composition with drop size can be further enhanced by differing rates of aqueous phase reactions (due to the reaction rate dependence on reactant concentrations). A number of experimental studies revealed that fog drop composition can vary with drop size and point out several implications of these variations (Noone et al., 1988; Heintzenberg et al., 1989; Munger et al., 1989b; Ogren et al., 1989; Pandis et al., 1990; Collett et al., 1993; Collett et al., 1994a; Collett et al., 1995; Demoz et al., 1995; Bator et al., 1997; Collett et al., 1998; Rao et al., 1998; Hoag et al., 1999a; Xu et al., 1999; Herckes et al., 2001; Reilly et al., 2001; Moore et al., 2002; Straub et al., 2002;). Studies in radiation fogs often reveal that small drops are more acidic than large drops and also contain higher concentrations of key solutes. The differences in drop composition are believed to give rise to drop size-dependent rates of sulfate production (e.g., Gurciullo et al., 1997; Rattigan et al., 2001; Reilly et al., 2001). Because drop sedimentation is a strong function of drop size, size-dependent fog drop composition can also give rise to enhanced deposition velocities for species enriched in large fog drops and reduced deposition velocities for species enriched in small drops. Hoag et al. (1999a) point out the importance of simulating drop size-dependent fog composition for accurately predicting effects of fogs on pollutant removal.

## 1.8 Net effects of fogs on pollutant concentrations

Fog constitutes a multiphase atmospheric system; gaseous species, particulate matter and liquid droplets coexist. The net effect of fogs on aerosol and gas concentrations can be described as follows:

- Fog formation occurs by condensation of water vapor onto atmospheric aerosol particles when the temperature reaches its dew point. Which aerosol particles activate depends on the peak supersaturation and aerosol characteristics.
- After fog forms fog drops scavenge gases and unactivated aerosol particles, and heterogeneous chemical reactions occur within fog drops to form new species.
- Some fog droplets are removed by deposition onto the ground or vegetation, acting as a vector for removal of scavenged material.
- Modified aerosol particles containing new secondary aerosol components are generated when drops evaporate during fog dissipation.

## 1.9 Investigating the chemistry of fog formation and dissipation in California's Central Valley

The two regions of the world where fog chemistry has been most extensively studied are the Po Valley of northern Italy and California's Central Valley. Because my research focuses on California fog chemistry, I review here some of the history of fog studies in this region and summarize key findings from this earlier work.

### 1.9.1 Terrain and weather conditions in the valley

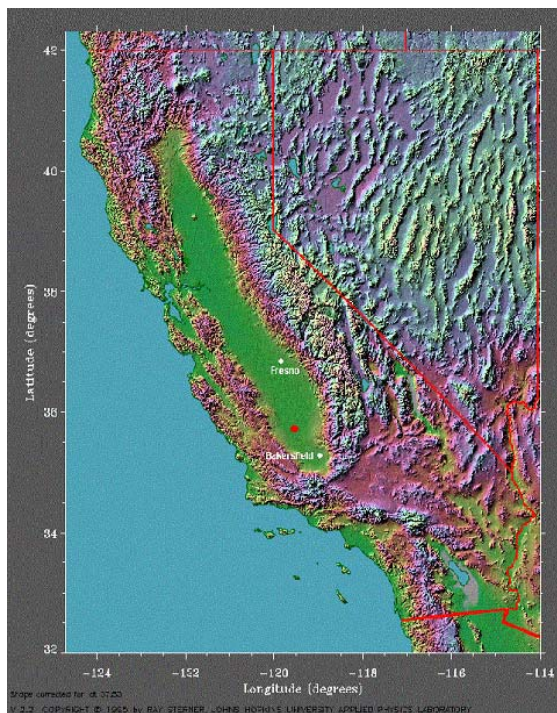


Figure 1-5. Terrain map of California Central Valley area. The red dot on the map indicates the approximate location of the main CRPAQS Angiola sampling site.

Figure 1-5 shows the California Central Valley, which lies between the Coastal Range and the Sierra Nevada range. During the winter time, high pressure over the Great Basin, known as the Great Basin High, creates a strong subsidence inversion over the valley with a base typically a few hundred meters off the valley floor and

below the surrounding mountain ridges (Holets et al., 1981). With the help of the mountains, this strong inversion forms a lid over the air basin, trapping the cool, moist air within the valley. Tracer studies have documented a lack of ventilation in the valley during these prolonged episodes (Reible, 1982; Jacob et al., 1987). The subsiding air over the valley results in clear skies providing excellent conditions for strong radiative cooling at night and, if sufficient moisture is present, the formation of dense, widespread radiation fogs.

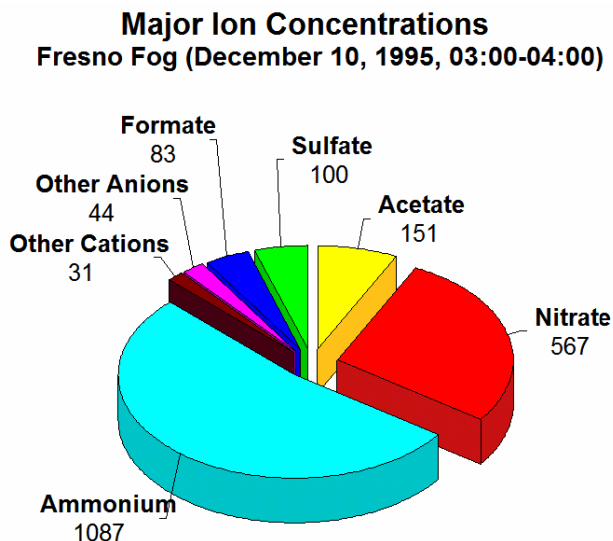
Holets et al. (1981) summarized the meteorological data in the Central Valley typical of fog episodes: surface temperature is about 2°C, the lapse rate inside the fog layer is between the dry and moist adiabatic lapse rates, wind speeds are less than 1 m s<sup>-1</sup>, and the mean fog layer thickness is approximately 300m. Some different patterns of fog episodes have been observed in the valley (Jacob et al., 1986a; Welch et al., 1986; Lee, 1987;). Welch et al. (1986) concluded that fogs in the San Joaquin Valley (SJV), the southern section of the Central Valley, have relatively constant thickness throughout the valley. Lee (1987) found distinct fog layers existed in the valley by using satellite imagery from the

Geostationary Orbiting Earth Satellite (GOES). Jacob et al. (1986a) observed two types of mixing height diurnal patterns.

Due to the persistence of the Great Basin High, the Central Valley often experiences extended periods of stagnation and associated degradation of air quality during the winter. As mentioned above, these stagnation episodes are frequently accompanied by nightly fog formation, with fogs forming anytime after 6PM and often lasting into the late morning (episodes can last up to 18 hours or more). These frequent, long lasting, dense fog events yield low visibilities and can result in major traffic accidents.

### 1.9.2 Fog composition

Studies of the chemical composition of Central Valley fogs began in the early 1980s. Munger et al. (1983b) measured the pH of fog water and the concentrations of major ions in Oildale (near Bakersfield) and three sites in the Los Angeles air basin. Several studies (Munger et al., 1983a; Waldman et al., 1983; Hoffmann, 1984) showed that fog chemistry is strongly related to the composition of the air mass in which it forms. Jacob et al. (1986a) found that fogwater acidity in the SJV is determined largely by the relative abundances of local acidic ( $\text{SO}_2$ ,  $\text{NO}_x$ ) and alkaline ( $\text{NH}_3$ ) emissions, and that fogs formed in areas of high alkalinity tend to be rather basic (pH greater than 5.6, the value expected from equilibrium with atmospheric carbon dioxide). Jacob et al. (1986a,b) also found that



sufficient ammonia was available everywhere in the valley, except near the western edge, to neutralize the acidity of fog water.

Figure 1-6. Measured composition in a typical bulk fog sample collected at Fresno during IMS95. All concentrations are listed in  $\mu\text{N}$ . (Collett et al., 1999b)

Jacob et al. (1984) pointed out that the major inorganic ions in fog water in the Central Valley are ammonium, nitrate and sulfate and that their aqueous-phase concentrations varied depending on the fog growth stage. Later studies (Collett et al., 1994a; Collett et al., 1994b; Rao et al., 1995; Rao et al., 1998) also found that the pH is relatively basic and ammonium and nitrate are major contributors to fog composition, with smaller inputs from sulfate, formaldehyde, and HMS. Figure 1-6 shows a typical fog sample composition measured in Fresno during the 1995 Integrated Monitoring Study (IMS95) (Collett et al., 1999b). These typical 1995 concentrations of most species are comparable to those measured more than a decade earlier (Jacob et al., 1984; Jacob et al., 1986a; Munger et al., 1989a). However, sulfate and S(IV) were present at much lower concentrations than in the period 1982-1984. These declines appear to reflect intervening decreases in valley SO<sub>2</sub> emissions. In addition the IMS95 measurements revealed that two carboxylic acids, formic and acetic acid, comprise a significant part of the fog ion content. Acetate concentrations were typically higher than formate concentrations and also higher than sulfate concentrations (Collett et al., 1999b).

### 1.9.3 Sulfur reactions

One key focus of past Central Valley fog studies was to examine S(IV) oxidation processes. We now know that S(IV) can be oxidized by H<sub>2</sub>O<sub>2</sub>, ozone, and O<sub>2</sub> catalyzed by metals (Fe and Mn), or can react with HCHO to form HMS. Pandis et al. (1989b) proposed that the oxidation of S(IV) by H<sub>2</sub>O<sub>2</sub>, O<sub>2</sub> catalyzed by metals (Fe and Mn), OH and NO<sub>2</sub> were the main pathways for the aqueous-phase production of sulfate.

S(IV) oxidation by hydrogen peroxide (H<sub>2</sub>O<sub>2</sub>) is viewed as the most effective reaction at low pH. Pandis et al. (1989b) found that H<sub>2</sub>O<sub>2</sub> was present in significant amounts above the fog layers in Bakersfield, and new H<sub>2</sub>O<sub>2</sub> is entrained into the fog layer and is available for the S(IV) oxidation; after the depletion of H<sub>2</sub>O<sub>2</sub>, metal (Fe and Mn) catalyzed oxidation was predicted to be the major sulfate production pathway. The concentrations of



metals (Fe and Mn) have been reported (Munger et al., 1983a; Jacob et al., 1984; Erel et al., 1993) to vary between valley sampling sites. Later studies (e.g., Hoag et al., 1999; Reilly et al., 2000) indicated that ozone and hydrogen peroxide were the dominant oxidants for S(IV) in Central Valley fogs but that these oxidation pathways compete with HMS formation for available dissolved sulfur dioxide.

Beginning in the 1980s, Munger et al. (1984) measured HCHO concentrations and discovered that the formation of S(IV)-aldehyde adducts represents an important sink for dissolved SO<sub>2</sub> in the high pH valley fogs. Munger et al. (1986) also measured HMS formation in valley fogs and found that HMS comprised the major fraction of S(IV). Because HMS formation is even faster than S(IV) oxidation at high pH, it competes with S(IV) oxidation for the fate of dissolved SO<sub>2</sub> (Collett et al., 1994a; Collett et al., 1994b; Rao et al., 1995; Rao et al., 1998). Reilly et al. (2000) showed that mass transport limitations, combined with the fast rate of HMS formation, strongly limited the amount of S(IV) oxidation, particularly in large fog drops. Subsequent work by the group of Kim Prather (Silva et al., 1999; Whiteaker et al., 2003), using a single particle aerosol mass spectrometer, has demonstrated the importance of HMS formation in aerosol particles processed by high pH Central Valley fogs.

#### 1.9.4 Size dependent composition

A number of studies have examined the drop size-dependent composition of Central Valley fogs (Collett et al., 1994a; Rao et al., 1995; Bator et al., 1997; Rao et al., 1998; Collett et al., 1999; Hoag et al., 1999; Reilly et al., 2000; Moore et al., 2004). These studies revealed significant differences between the composition of small and large fog drops. Smaller fog drops were observed to have lower pH than large drops and to contain higher concentrations of ammonium, nitrate and sulfate. Patterns of size-dependence were more variable for metals while nitrite has been observed to be enriched in higher pH, large drops. Moore et al. (2004a,b) demonstrated that the composition variability observable with a 5-stage cloud impactor was even larger than observed with earlier 2- and 3-stage collectors.

Because of the pH and metals concentration differences with drop size, S(IV) oxidation reactions may proceed at different reaction rates in small and large drops. As pointed out above, however, competing reactions (especially HMS formation) and finite rates of mass transport of reactants into large fog drops also influence droplet size-dependent oxidation rates (Reilly et al., 2000). Studies have also shown that in alkaline environments, where ozone is an important aqueous S(IV) oxidant, variations in pH among a droplet population can result in faster rates of sulfate production than are expected based on average fog drop properties (Collett et al., 1999a; Hoag et al., 1999b), due to the non-linear dependence of the oxidation rate on the  $H^+$  concentration. Rates of HMS formation have also been found to vary with drop size (Rao et al., 1995), given the dependence of the HMS formation rate on pH.

#### 1.9.5 Fog deposition and net effects of Central Valley fogs on aerosol populations

Deposition processes in Central Valley fogs have been of increasing interest due to the influence they may exert on pollution buildup during winter stagnation episodes. Jacob et al. (1984) suggested that enhanced aerosol deposition in fogs efficiently limits pollutant accumulation during stagnation episodes. Waldman et al. (1987) suggested that sulfate deposition in fog drops was fast enough to balance aqueous phase sulfate production, thus preventing sulfate levels from rising during extended fog episodes. Pandis et al. (1989a) modeled one radiation fog episode and found that a fog episode can reduce aerosol concentrations effectively. Lillis et al. (1999) used the Carnegie Mellon University bulk fog chemistry model to simulate the fog effect on ground based concentration of sulfate, nitrate and ammonium; they proposed that a typical SJV fog episode will remove micrograms per square meter of sulfate, nitrate and ammonium.

Recent studies have indicated that the drop size-dependence of Central Valley fog composition can also influence deposition rates of fog solutes. Preferential enrichment of species in small fog drops decreases deposition velocities (Collett et al., 1998; Hoag et al., 1999a; Collett et al., 2001). Deposition plates have been used to measure the deposition

fluxes and velocities of fog-borne ions (Collett et al., 2001), revealing that deposition velocities for species enriched in small fog drops are smaller than the fog water deposition velocity and that the ordering of deposition velocities (ammonium > sulfate > nitrate) appears to reflect how strongly they are enriched in small drops. Moore et al. (2003) took this a step further by showing that nitrite in Davis fogs, which is enriched in large fog drops, has a deposition velocity much higher than the other solutes and typically even higher than fog water. Hoag et al. (1999a) used a drop size-resolved version of the Carnegie Mellon University fog chemistry model to reproduce observations of fog composition and deposition in the IMS95 study and revealed more detail about changes in deposition velocities at different fog stages. The model predicted a low deposition velocity for nitrate, a result of its enrichment in smaller drops. Sulfate had a slightly higher deposition velocity. Ammonium had the highest event average deposition velocity; because of the high fog pH, ammonia is still available in the gas phase even after several hours of fog and can dissolve into larger fog droplets with higher settling velocities.

The aerosol scavenging efficiency of a fog determines which preexisting aerosol particles can be processed by the fog. Munger et al. (1990) suggested that aerosol scavenging ratios in urban fogs range from 10% to 90%. Hoag et al. (1999a) suggested that particles smaller than 1.1  $\mu\text{m}$  (at 95% RH) were not affected by the fog. Size-dependent aerosol scavenging efficiencies by fogs have the potential to differentially affect fog-processed aerosol size distributions. Illustrating this, Moore et al. (2004) examined aerosol size distributions before and after fog episodes in Davis, California and found evidence of large particle removal and build up of smaller particles.

Through this series of studies, the net effect of Central Valley fogs on aerosol concentrations has begun to clarify. Short fog episodes generally allow sufficient time for aqueous sulfate production but do not provide sufficient time for appreciable pollutant removal by fog drop deposition. As fog episodes lengthen, sulfate production, which is concentrated during the first hours of an event, becomes less important relative to pollutant deposition, which occurs at a significant rate throughout the entire fog episode. As mentioned earlier, Central Valley fog simulations by Lillis et al. (1999) suggest that the

main effect of fogs on aerosol populations is removal for nitrate and ammonium while sulfate removal is approximately balanced by new sulfate production. Little is known, however, about the influence of fogs on carbonaceous aerosols.

#### 1.9.6 Organics in Central Valley fogs

Fog/cloud processing of carbonaceous aerosol particles has been of increasing interest over the past several years (Capel et al., 1990; Erel et al., 1993; Luttke et al., 1997; Luttke et al., 1997; Facchini et al., 1999a; Facchini et al., 1999b; Decesari et al., 2000; Facchini et al., 2000; Limbeck et al., 2000; Fuzzi et al., 2001;). Studies in California Central Valley fogs have shown that organic carbon comprises a significant fraction of the total solute loading (Collett et al., 1999; Herckes et al., 2002). Major individual organic species in these fogs include formate, acetate and formaldehyde (Munger et al., 1989; Erel et al., 1993; Rao et al., 1995; Collett et al., 1999). Work by the group of Anastasio in Davis fogs (Anastasio et al., 2000; Anastasio et al., 2001; McGregor et al., 2001; Zhang et al., 2001) has also illustrated that organic nitrogen compounds are present in significant concentrations and that photochemical reactions involving these species can be relatively fast. Measurements by Collett et al. (1990) in clouds intercepting the Sierra Nevada downwind of the Central Valley reveal significant concentrations of dicarbonyl compounds, including glyoxal and methyl glyoxal. The speciation of much of the organic carbon in Central Valley fogs (and in other clouds and fogs, too), however, remains unknown.

In addition to contributing significantly to fog solute loading, some of the low molecular weight organic compounds show interesting drop size-dependence or exert interesting effects on fog chemistry. Rao et al. (1995) found that formaldehyde concentrations were generally higher in small drops than in large drops. These observations contradicted expectations that mass transport of HCHO into the drops should be fast enough to maintain gas-liquid equilibrium in the presence of drop growth or formaldehyde hydration in solution and that equilibrium concentrations of HCHO should not vary with drop size. Martin et al. (1991) proposed that for urban areas formate could

reduce the rate of the Fe(III) catalyzed oxidation by as much as a factor of 10 in the high pH regime. Collett et al. (1999b) found that bicarbonate, ammonium, formate and acetate can provide the droplet with acid-buffering capacity to slow the anticipated rapid pH drop due to oxidation of S(IV) by ozone in the high pH environment. Additional buffering from unidentified compounds (possibly including humic like substances) has a similar effect. Numerical simulation of this effect (Collett et al., 1999b) indicated a significant impact on aqueous phase sulfate production by the pH sensitive ozone pathway, with drop pH remaining 0.3 – 0.7 pH units higher and sulfate production increasing by 50%.

While spatial variability in inorganic fog solute concentrations in the Central Valley is generally modest, greater differences between urban and rural fog chemistry were observed for organic species, including acetic acid and formaldehyde. Collett et al. (1999b) found that acetate tends to be more concentrated at the urban sites, consistent with contributions from combustion and a shorter atmospheric lifetime. Measurements also show that fog concentrations of formaldehyde and total organic carbon (TOC) are more concentrated in urban sites.

So far we know little about fog processing of organic aerosol particles and trace gases. Numerous organic compounds, including various alkanes, polycyclic aromatic hydrocarbons (PAH) and alkanolic acids were found in Davis (California) fog water samples (Herckes et al., 2002a) where ~30% of the total dissolved organic matter and about 2/3 of the low molecular weight fraction (MW<500 Da) has been identified. Numerous compounds were present in both the dissolved and insoluble phases, indicating a need to include both phases in studies of scavenging behavior. The presence in fog drops of organic markers for wood smoke, vehicle exhaust, and other carbonaceous aerosol sources suggest that fogs play an important role as processors of many types of carbonaceous particles.

## 1.10 Open questions and study objectives

### 1.10.1 Major findings to date in Central Valley fogs:

- A fair body of data is available concerning inorganic and low molecular weight organic species concentrations in Central Valley fogs. Nitrate, ammonium, nitrite, acetate, formate, and formaldehyde are major contributors to the fog composition.
- These fogs often have high ammonium concentrations yielding a high pH.
- Formaldehyde reacts with dissolved  $\text{SO}_2$  in fogs stabilizing it as HMS and reducing the amount of sulfate formed. This reaction is favored under the basic conditions often observed.
- The fogs contain a large amount of organic carbon; however, the speciation of most of this carbon is unknown.
- Significant chemical composition differences have been found among droplets of different size. These differences impact fog processing of valley aerosols.
- Fog chemistry models (especially the Caltech/CMU model) have been used to predict Central Valley fog composition and to examine aerosol processing by these fogs. Model predictions, which compare reasonably well with observations, indicate that considering drop size-dependent fog composition is important to accurately predicting solute deposition velocities and aqueous phase sulfate production.

1.10.2 Remaining needs for improving our understanding of Central Valley fogs, their composition, and their influence on aerosol populations:

- More observations are needed of the drop size distributions and liquid water contents of Central Valley fogs. These have seldom been measured well in previous studies, making it more difficult to understand fog evolution and drop deposition.
- More information is needed with regard to the drop size-dependence of solute concentrations. In particular, there is a need to look in more detail at organic carbon and nitrite, which have received little prior attention.
- More observations of fog solute deposition fluxes and deposition velocities are needed to evaluate the role of these fogs as atmospheric cleansers and to better constrain model simulations. Deposition observations are needed for all major solutes, but there is a particularly strong need to quantify organic carbon deposition in fogs.

- More information is needed about the large fraction of fog solute loadings comprised of organic species.

### 1.10.3 Primary study objectives

The main objective of this study was to make measurements of the physical and chemical characteristics of fogs during CRPAQS and use these observations to promote an increased understanding of the effects SJV fogs exert on valley air pollution levels. In particular, we attempted to:

- Make real observations of fog composition and microphysics during the California Regional Particulate Air Quality Study (CRPAQS).
- Better characterize the size-dependent composition of Central Valley fogs, including better resolution of the size-dependence and more observations of organic carbon.
- Characterize deposition fluxes of inorganic and organic fog solutes. Attempt to explain observed differences in solute deposition velocities using measured drop size-dependent solute concentrations. Examine how fog-related solute removal fluxes vary with fog episode duration.
- Examine the capacity of the atmosphere for new aerosol mass formation, via aqueous S(IV) oxidation and HMS formation, during fog episodes. Such information is a key component for understanding net effects of the fog episodes on boundary layer sulfate concentrations.
- Develop new methods for speciation of fog organics. Better characterize the organic composition and organic species' concentrations. Examine interactions between fog drops and carbonaceous aerosols.
- Evaluate the ability of the Carnegie Mellon University fog model to accurately simulate the physics and chemistry of CRPAQS fogs, with particular emphasis on the model's ability to accurately simulate drop size-dependent fog composition and its influence on aerosol processing.

Study methodology and results are outlined in the next 5 chapters, plus a conclusions chapter, and in four appendices that contain draft or published journal articles.



## Chapter 2

### Experimental description

#### 2.1 Sampling sites and times

Fog sampling was conducted in California's Central Valley in winter 2000/2001 as part of the winter intensive for the California Regional PM<sub>2.5</sub> Air Quality Study (CRPAQS). A typical fog sampling period was from 1 to 2 hours. At the end of each sampling period, fog samples were retrieved from collectors, weighed and measured for pH in a small field laboratory in a trailer (Figure 2-1). Some sample aliquots were made for further analysis of total organic carbon (TOC), dissolved organic carbon (DOC), formaldehyde, organic acids, S(IV), H<sub>2</sub>O<sub>2</sub>, trace metals (Fe and Mn), and additional organic species. Samples were then refrigerated and sent to the laboratory for later analysis. Following sample analysis and completion of QA/QC procedures, sample information was submitted to the CRPAQS database.



Figure 2-1. Photo of the Angiola field laboratory, where collected fog samples were processed.

##### 2.1.1 Angiola sampling site



Figure 2-2. Angiola sampling site overview on a foggy day.

Fog samples were collected during CRPAQS at one core site (Angiola, see Fig. 2-2) and three satellite sites. The Angiola core site is located in the center of the San Joaquin Valley ( $35^{\circ}35'N$ ,  $119^{\circ}32'W$ , 60m above sea level), surrounded by a large area of agricultural farmland. The site was enclosed by a wire fence, where cloud collectors and other instruments were set up. The ground-based fog collectors were spaced about 15 to 20m apart to avoid influencing each other. Additional collectors were mounted on the CRPAQS sampling tower, as described in more detail later. Additional automated fog sampling systems were deployed at three satellite sites: Helm, Bakersfield, and McKittrick. As described below, fog samples were collected at Helm and Bakersfield, but no fog was observed at McKittrick during the period equipment was deployed there.

## 2.2 Sampling

This section outlines the sampling and analytical methods used in the field experiments and the laboratory. Some of the analysis methods are included in the Standard Operating Procedures written for the 1995 Integrated Monitoring Study (IMS95).

Field measurements included ground-based observations of bulk (all sites) and size-resolved (Angiola only) fog composition, vertical profiles of fog presence and composition (Angiola only), and fog deposition fluxes of water and major ions

(Angiola only).

### 2.2.1 Fog liquid water content measurements

A Gerber Scientific Particulate Volume Monitor (model PVM-100) (Figure 2-3) was used to provide continuous measurements of liquid water content (LWC) at Angiola. LWC measurements provide a record of fog presence and fog density. When the LWC reaches a certain value (usually taken as  $75\text{mg/m}^3$ ) for a period of 15 minutes, the data acquisition system was set to page a site operator. PVM calibrations (both of LWC and particle surface area (PSA)) were regularly performed using a manufacturer supplied disk.

A newly designed CSU optical fog detector (OFD) was also used (Emert, 2001; Carrillo et al., 2004; Fig. 2-4) on the ground at all sites. The ground-based OFD was co-located with the PVM-100 to provide a basis of assessing whether the optical sensor data can be used to determine fog presence and thickness. OFDs were also deployed at three levels of the 100 m Angiola tower to activate tower-based fog collectors.



Figure 2-3. Gerber Scientific Particulate Volume Monitor (model PVM-100).

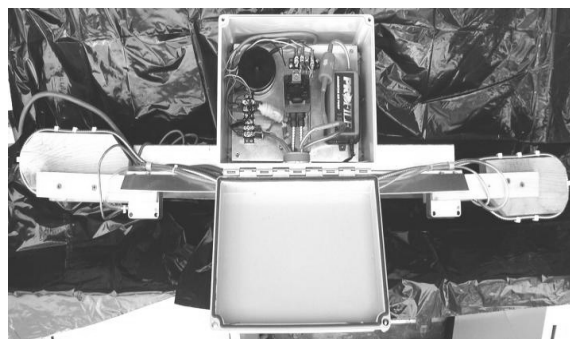


Figure 2-4. CSU optical fog detector.

### 2.2.2 Bulk fog collection

On the ground we set up a Caltech Active Strand Cloud Collector (CASCC) (Figure 2-5) (Demos, et al., 1996), which was used to collect bulk fog samples. It employs a fan to draw air across six rows of 508  $\mu\text{m}$  Teflon strands. The fog drops are collected based on their inertia. Drops with too much inertia to follow the fluid streamline around the strands impact. The collected droplets run down the strands and are collected into a polyethylene collection bottle.

The collector flow rate and cut size are influenced by fan revolution speed, which determines the air velocity through the collector. Under different applied DC voltages, the fan will rotate at different speeds and draw air through the collector at different velocities. Because fog drops are collected based on their inertia, altering the sampling velocity will change the collector efficiency curves. Corrections for flow rate are needed to determine modified flow rates and cut sizes as a function of applied fan voltage.

Figure 2-6 shows the CASCC average velocity measurement results made at CSU following the field experiment. These values were determined using a hot wire anemometer, corrected for standard conditions, in a cross section of the CASCC. The data indicate that the fan revolution speed and average velocity through the collector are linear functions of applied fan voltage. Theoretically, the 50% cut size of the CASCC is 3.5  $\mu\text{m}$  at a flow rate of 8.5 m/s (Demos, et al., 1996). Based on the voltage we used in CRPAQS study (10.6V for CASCC), we observe an average velocity of approximately 9.9m/s, producing a 50% cut size still at about 3.5  $\mu\text{m}$  (size cut doesn't change much with velocity for this system).



Figure 2-5. Caltech Active Strand Cloud Collector (CASCC).

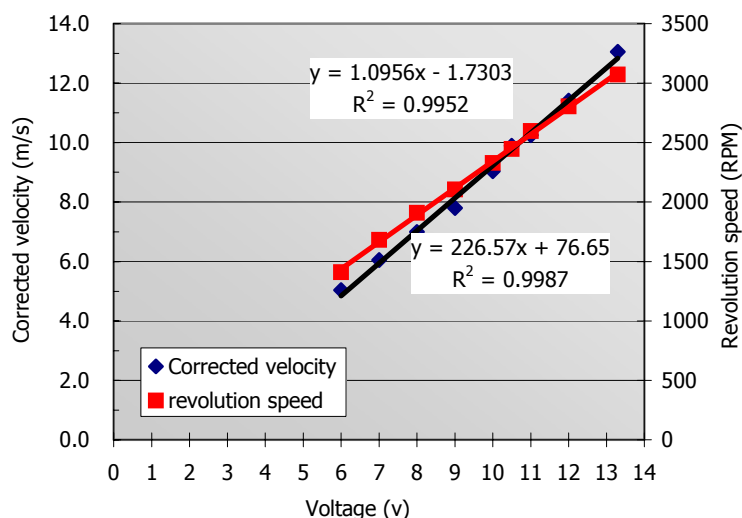


Figure 2-6. Fan revolution speed and air velocity measured for the CASCC as a function of applied fan voltage. "Corrected" means the flow rate has been corrected due to air pressure difference at different altitude.

A Caltech Heated Rod Cloud Collector (CHRCC) (Demos, et al., 1996) was also used in some fog events when air temperatures fell below freezing. The collection mechanism of the CHRCC is the same as the CASCC, except that the CHRCC use hollow stainless steel rods as impaction surfaces. Each rod contains nichrome wire encased in a Teflon sleeve. This permits internal heating of the rods by passage of a current through the nichrome wire. During CRPAQS when supercooled drops froze on CHRCC collection surfaces, the CHRCC was turned off at about 15 minute sampling intervals, then heating was turned on for an appropriate time (usually about 15 seconds) to let the frozen rime melt and flow into the sampling bottle. Frequent heating can prevent significant ice from accumulating on the rods; rime accumulation can change the diameter of the collection rods and their cut size. Turning off the fan while heating and heating for a very short period both minimize potential sample evaporation from the rods.

A bulk stainless steel CASCC (ss-CASCC) (Herckes et al., 2002) was used to collect fog for analysis of total organic carbon (TOC) and individual organic species by Gas Chromatography / Mass Spectrometry (GC/MS). The structure of the ss-CASCC is similar to the CASCC, except the ss-CASCC uses stainless steel walls, stainless steel strands, a stainless steel trough and sampling tube, and glass sample bottles. Figure 2-7 shows the ss-CASCC sampling velocity as a function of applied fan voltage. The data are similar to the CASCC results shown above, consistent with

their design similarities. Based on CRPAQS fan voltages, the sampling velocity and size cut for the ss-CASCC are approximately 9.9 m/s and 3.5 $\mu$ m, respectively.

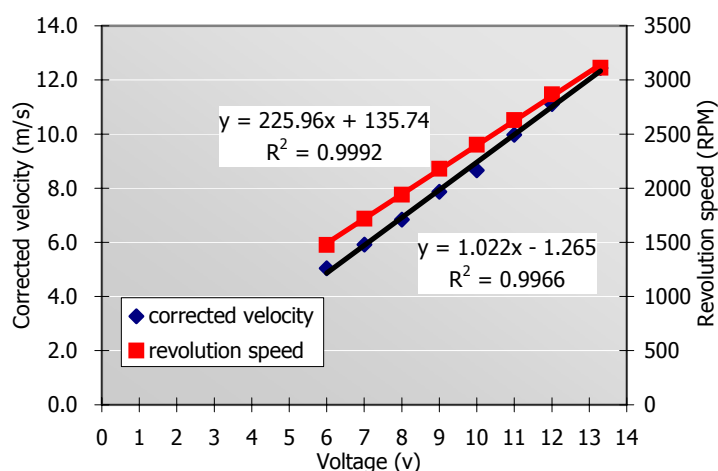


Figure 2-7. Corrected air speed and revolution speed vs voltage on the stainless steel CASCC (ss-CASCC). "Corrected" means the flow rate has been corrected due to air pressure difference at different altitude.

The CASCC, CHRCC and ss-CASCC collectors were used to collect sequential fog samples at time intervals between 1 and 2 hours throughout each fog event.

### 2.2.3 Size-resolved fog composition

An all-plastic size-fractionating CASCC (sf-CASCC) (Figure 2-8) (Demoz, et al., 1996), was used to collect and analyze drop size-resolved fog samples. The sf-CASCC is similar to the CASCC but has an extra inlet stage (4 rows of eight 12.7 mm diameter Teflon rods) before the 6 rows of 508  $\mu$ m strands. Theoretically, it draws the droplets through the sampler at a velocity of 6.7 m/s and has a total flow rate of 19 m<sup>3</sup>/min; and theoretical 50% cut sizes for the two stages of the sf-CASCC have been estimated as 4 $\mu$ m and 23 $\mu$ m. Similar to bulk fog samples, sample weight and pH were measured on site, and preserved aliquots were made for some species.

As with the CASCC some fan voltage corrections needed to be applied to calculate the real flow rate and cut size. Figure 2-9 shows the velocity-voltage relationship measured for the sf-CASCC. The fan voltage used in CRPAQS was 11.1v, corresponding to a 7.5 m/s average sampling velocity. The size cut for the second stage doesn't change much due to this velocity decrease, remaining about 3.5  $\mu$ m, but the size cut for the first stage changes to about 21  $\mu$ m.



Figure 2-8. An all-plastic size-fractionating CASCC (sf-CASCC) mounted on site. The first stage, second stage, sampling bottle and fan parts can clearly be seen.

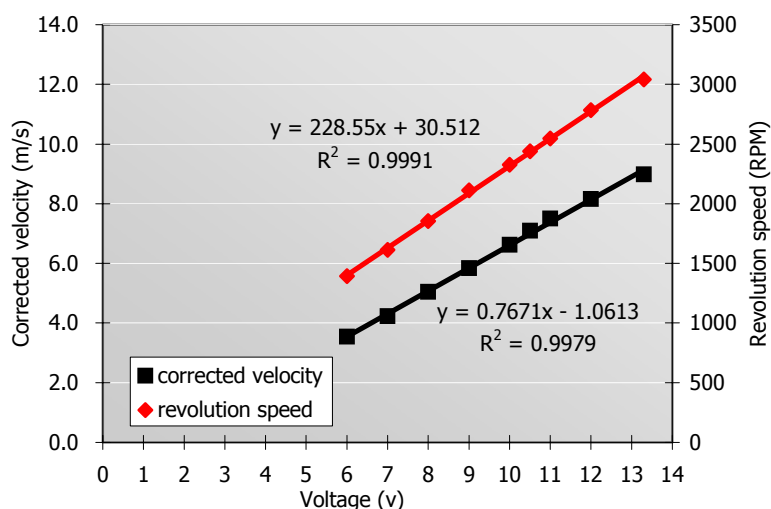


Figure 2-9. Corrected air velocity and revolution speed vs voltage for the sf-CASCC. "Corrected" means the flow rate has been corrected due to air pressure difference at different altitude.

A two-stage stainless steel size-fractionating CASCC (ss-sf-CASCC) was used to collect samples for organic analysis. The principle of this collector is the same as the sf-CASCC, but it is twice as large in width and uses two fans side to permit greater sample collection. The data from this collector were used to examine how TOC concentrations vary between large and small fog drops. Figure 2-10 shows the relationship between fan voltage and average sample velocity for the ss-sf-CASCC. The operational sample velocity in the field was 8.2 m/s with 50% size cuts of 19  $\mu\text{m}$  for the first stage and 3.5  $\mu\text{m}$  for the second stage.



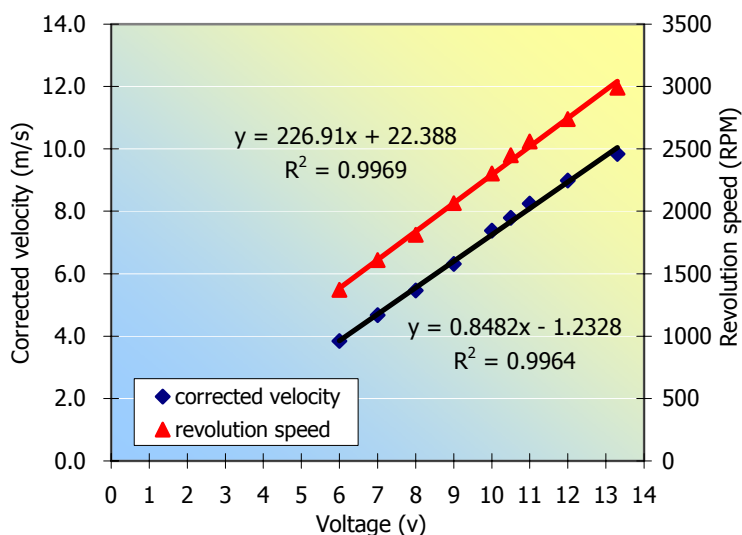


Figure 2-10. Corrected air velocity and revolution speed vs voltage for the ss-sf-CASCC. "Corrected" means the flow rate has been corrected due to air pressure difference at different altitude.

Samples from the CSU 5-stage collector (Figure 2-11) (Moore et al., 2002; Straub et al., 2002) provided detailed information on how major ions concentrations and fog pH vary across the drop size spectrum. The 5-stage collector is a cascade impactor that consists of five stages, with stage size cuts ranging from 5 to 30 $\mu$ m theoretically (30, 25, 15, 10 and 4  $\mu$ m for stage-1 to stage-5). Lab and model evaluations of the collector performance (Straub et al., 2002) show that the collector works approximately as designed, although there is some overlap between drop sizes collected in the first two stages.

As seen from Figure 2-11, the collector is mounted at 45° to the horizontal to help collected water drain toward polyethylene sample vials mounted on one end of each stage. At the end of sampling period, a set of clean rubber spatulas is used to remove the remaining water from each stage.



Figure 2-11. The CSU 5-stage collector shown deployed in an earlier cloud campaign at Whiteface Mtn, NY. Photo by K. Moore.



## 2.2.4 Size distribution of fog droplets



Figure 2-12. CSASP-100-HV optical probe.

Size distributions of fog drops were measured by a Particle Measurement Systems Classical Scattering Active Spectrometer (CSASP) CSASP-100-HV optical probe (Figure 2-12). We set the CSASP to use 20 bins to measure fog drops from  $5\mu\text{m}$  to  $47\mu\text{m}$  diameter. The CSASP can provide information on how fog drop size distribution changes with time, with sampling intervals as short as one second.

Table 2-1. Calibration table of the CSASP during the CRPAQS study

Date	Bead Diameter ( $\mu\text{m}$ )	Reading (Ave Drop Dia) ( $\mu\text{m}$ )	Dia from conversion table ( $\mu\text{m}$ )
23 Dec 2000	$10 \pm 1.0$	8.33	9.5-10
	$20 \pm 1.4$	15.83	19-19.5
	$30 \pm 2.0$	23.97	29.5-30
	Zero Reading	7.26 (average for 78 seconds)	
19 Jan 2001	$10 \pm 1.0$	13.81	16-16.5
	$20 \pm 1.4$	19.49	24-24.5
	$30 \pm 2.0$	23.65	29-29.5
	Zero Reading	5.45 (average for 67 seconds)	

The CSASP calibration was checked by DMT during the probe's upgrade. It was subsequently checked, using monodisperse glass beads, twice during the CRPAQS

study. Table 2-1 shows the CSASP calibration table for CRPAQS. Comparing the expected diameters from the conversion table with true bead diameters, the calibration was good on Dec 23<sup>rd</sup> 2000, but somewhat further off on Jan 19<sup>th</sup> 2001.

Another frequently used drop size distribution measurement instrument is the Forward Scattering Spectrometer Probe (FSSP), which use the same principles as CSASP but is non-aspirated. Both PVM-100 and FSSP were used in some experiments (Fuzzi et al., 1992, Wobrock et al. 1994, Choulaton et al. 1997; Fuzzi et al., 1998), and measurements of LWC from the PVM-100 were compared to LWC measurements from a FSSP-100. CSASP measurements were only found in limited experiments (e.g., Pinnick et al., 1979). Therefore, most of the discussions about problems with drop size distribution measurement here are based on the literature discussion of the FSSP, but also include CSASP characteristics in CRPAQS studies, and many of the issues are common to both instruments.

During CRPAQS we found that the effective diameters ( $D_{\text{eff}}$ ) measured by the CSASP agreed well with PVM measurements of the same parameter; however, the CSASP tended to substantially overestimate the LWC relative to the PVM. Two factors possibly contributing to this difference are:

- A possible bias in PVM LWC for large drop sizes: the response of the PVM is known to drop off for drop sizes larger than about 40  $\mu\text{m}$  diameter (Gerber et al., 1991), although Wendisch et al. (1998) report individual PVM units may show a negative LWC bias at a lower threshold. Therefore, the PVM in CRPAQS may underestimate LWC when there is high LWC comprised by fog with large fog drops.
- A possible bias in CSASP LWC: Gerber et al. (1999) demonstrate that flow focusing and concentration of droplets in the sensing volume of an FSSP can lead to a significant overestimate of LWC. We conducted a simple computational fluid dynamics simulation of droplet focusing in the CSASP by using the commercial Fluent model. Our results suggest that the inlet of the CSASP also acts as a droplet concentrator, artificially enhancing the concentrations of large droplets sensed by the probe and producing an overestimation of LWC. It's also possible that the sensing volume in our CSASP is not accurately defined.

Due to the difficulty of finding comparable and reproducible conditions in ground-based field measurements, no general agreed explanations of the discrepancy between the measurements of these two instruments exists. Since the average diameter of fog droplets in CRPAQS was of the order of 25  $\mu\text{m}$ , PVM measured LWC should be accurate enough. Based on the analysis above, the CSASP drop size distributions were normalized to PVM LWC.

#### 2.2.5 Fog deposition

Fog deposition measurements were carried out by using two deposition plates (Figure 2-13) and two recording balance systems (Figure 2-14). The deposition plates are made of Teflon and have been tested in Davis California radiation fogs (Collett et al., 2001; Moore et al., 2004b). Two square Teflon deposition plates (0.30m<sup>2</sup>) were used to assess possible sample contamination. Samples were typically collected at 2 hr intervals to match other cloud composition measurement periods or to provide sufficient sample (>10 ml) for composition analysis.



Figure 2-13. Two deposition plates deployed during CRPAQS. The plastic sheeting beneath the plates was used to eliminate possible contamination from the ground.

Collected fog water was scraped from the interior of the plate and transferred to a polyethylene sample bottle. Right after collection, samples were weighed and aliquots were taken for measurements of ion concentrations and Total Organic Carbon (TOC).



Figure 2-14. Two balances set up to record deposition fluxes to a bare metal and an artificial grass surface.

In addition to the Teflon deposition plates, we operated an automated deposition flux monitoring system previously tested at Davis (Collett et al., 2001). This system consists of two recording balances (PB3002-S, Mettler Toledo, Switzerland) that record the mass flux of water with a time resolution of 1Hz. The difference between these two balances was that a rectangular ( $0.029 \text{ m}^2$ ) artificial grass surface was put on one of the two balances to examine surface roughness effects on deposition, while the other balance used its own round bare metal weighing pan ( $0.024 \text{ m}^2$ ) as the sampling surface. The data were averaged to 10 minute intervals to evaluate the possible difference between these two surfaces, and then averaged to 20 minute intervals.

#### 2.2.6 Gas phase measurements

Gas phase measurements of total soluble hydroperoxides at Angiola were measured using a continuous monitor based on the method of Lazrus et al. (1986) at 10 minute intervals (Figure 2-15). Soluble hydroperoxides (including hydrogen peroxide and soluble organic peroxides) were captured from the air into solution where they are reacted to produce a fluorescent dimer, the concentration of which is measured by an on-line fluorimeter. Although the instrument responds to both hydrogen peroxide and soluble organic hydroperoxides, this mixture is strongly dominated by hydrogen peroxide in most cases, including IMS95 measurements in the SJV.



Figure 2-15. Gas phase measurements of total soluble hydroperoxides by continuous monitor.

### 2.2.7 Size-resolved aerosol composition

A Microorifice Uniform Deposit Impactor (MOUDI) was used to sample pre- and post-fog size-resolved aerosol (Figure 2-16). The MOUDI has 8 impaction stages and one afterfilter. The working flow rate was 30 lpm, set by monitoring the calibrated pressure drop through the instrument and verified by use of a dry gas meter. The MOUDI was operated over a time period of eight to fourteen hours depending on the status of pre-/post-fog measurements.



Figure 2-16. A Microorifice Uniform Deposit Impactor (MOUDI).

### 2.3 Sample handling and chemical analysis

During each fog event collected fog samples were immediately brought to a small field lab (Figure 2-1). Samples were first weighed together with the bottle to get net sample weight (sample bottles had been weighed before putting onto the collectors).

Then samples were aliquotted for subsequent chemical analysis in our lab at CSU. Table 2-2 lists the species aliquots prepared in the field and the amount of added preservation solutions for each species. pH measurement had the highest priority for all the samples, then ion chromatography (IC) analysis. For other species, the priority depends on the sample type and collector used. For example, metal analysis had higher priority for the 5-stage collector, while TOC/ DOC aliquots usually had higher priority for stainless steel collector samples. Table 2-2 also lists the sample amount needed/desired for each species. Large and small refer to the sample volume required. Available sample volumes determine how much sample can be used to make aliquots, and what analysis can be done for each sample. In cases where sample volume was limited, small volume aliquot procedures were available for some aliquots. These generally use only 100 µl sample (amount of preservation solutions are also changed proportionately to sample volume).

Table 2-2. Aliquot preservation protocol.

Aliquot*	Sample amount	Preferred vial	9.7% HNO <sub>3</sub> Solution	S(IV) Preservative Solution	Catalase Solution	H <sub>2</sub> O <sub>2</sub> Conditioning Reagent	H <sub>2</sub> O <sub>2</sub> Flurescent Reagent	HCHO preservative solution	Chloroform
pH	40 µl	0.5 ml micro centrifuge tube							
IC	500 µl	Plastic IC vial (lid w/septum)							
<b>Metals:</b>									
<b>Large</b>	1 ml	1.2 ml cryovial	100 µl						
<b>Small</b>	100 µl	plastic IC vial	10 µl						
<b>H2O2:</b>									
<b>Large</b>	1 ml	1.5 ml glass vial				200 µl	200 µl		
<b>Small</b>	100 µl	glass insert vial				20 µl	20 µl		
<b>S(IV):</b>									
<b>Large</b>	1 ml	1.5 ml glass vial		100 µl	100 µl				
<b>Small</b>	100 µl	glass insert vial		10 µl	10 µl				
<b>HCHO:</b>									
<b>Large</b>	1 ml	1.5 ml glass vial						100 µl	
<b>Small</b>	100 µl	glass insert vial						10 µl	
<b>TOC/DOC</b>	5~15 ml	Glass vial							
<b>Organic acid</b>	500 µl	Glass vial							20 µl

\*large (small) means how much the sample amount would be if the amount of water of a sample is sufficient (unsufficient).

### 2.3.1 Sample weight

A sample bottle was replaced at defined intervals, usually 1 or 2 hours depending on LWC. The sample weight (volume) was obtained by subtracting the empty bottle weight from the weight of the bottle with sample.

### 2.3.2 pH measurements

The pH of samples was measured on site with an Orion Model 290A or 250A pH meter and a Microelectrodes, Inc. Model MI-710 pH combination electrode, calibrated with pH 4 and 7 standards. A periodic calibration check was made to assure the calibration accuracy.

### 2.3.3 Ion concentrations

Sample aliquots were prepared for major ion analysis by pipetting 500  $\mu$ l of sample into a polypropylene auto-sampler vial. The vial was sealed with a Teflon-lined septum and lid.

Inorganic anion ( $\text{NO}_3^-$ ,  $\text{NO}_2^-$ ,  $\text{SO}_4^{2-}$ , and  $\text{Cl}^-$ ) concentrations were determined by using a Dionex DX-500 ion chromatograph equipped with an AS3500 auto-sampler, an AG4A-SC guard column, AS4A-SC separation column, suppressed by Dionex Anion Self-Regenerating Suppressor (ASRS), and detected by conductivity detection. Separation was achieved using a 1.8 mM  $\text{Na}_2\text{CO}_3$ /1.7 mM  $\text{NaHCO}_3$  eluent at a flow rate of 2.0 ml/min.

Inorganic cation ( $\text{Na}^+$ ,  $\text{NH}_4^+$ ,  $\text{K}^+$ ,  $\text{Mg}^{2+}$  and  $\text{Ca}^{2+}$ ) concentrations were determined using a second DX-500 ion chromatograph equipped with an AS3500 auto-sampler, CG-12 and CS-12 guard and separation columns, suppressed by a Dionex Cation Self-Regenerating Suppressor (CSRS) and detected by conductivity detection. Separation was achieved by using a 20 mM methanesulfonic acid eluent at a flow rate of 1.0 ml/min.



Both IC systems were calibrated daily using a series of lab-prepared ion standards. Calibration accuracy was monitored by injection of independent, NIST traceable standards. Calibration stability during each day's analysis was monitored by periodic injection of a standard solution.

#### 2.3.4 Metals

Samples were analyzed for Fe and Mn using a Varian Model 640Z Graphite Furnace Atomic Absorption Spectrometer (GFAAS) with Zeeman background correction. If the sample concentration is too high, either a manual or an automatic dilution was used. Modified (optimized by Katharine Moore) varian-recommended analytical procedures (in GFAAS operation manuals) were used to determine Fe and Mn in the fog water. Aliquots were prepared in the field for trace metal analysis by acidification to near pH 1 with trace metal grade nitric acid. Adding nitric acid stabilizes the samples by minimizing precipitation and wall adsorption.

#### 2.3.5 S(IV)

Since S(IV) in fogwater can be oxidized by  $\text{H}_2\text{O}_2$ ,  $\text{O}_3$  and  $\text{O}_2$  in the presence of transition metals, samples were stabilized by adding buffered HCHO to complex S(IV) in the solution to form hydroxymethanesulfonate (HMS) (Dasgupta et al., 1980), and by adding of catalase to destroy any hydrogen peroxide in the sample. Treated samples were analyzed on a Hach DR/4000 visible spectrophotometer by the pararosaniline method (Dasgupta, 1981). This technique provides a measurement of total S(IV), namely dissolved sulfur dioxide, bisulfite, and sulfite (together comprising "free" S(IV)) plus any HMS present before preservation of the sample.

#### 2.3.6 Formaldehyde

Formaldehyde can form stable HMS in the presence of bisulfite. Formaldehyde was preserved by adding HCHO preservation solution containing bisulfite on site (20 mM

NaOH, 10 mM CDTA, 3 mM NaHSO<sub>3</sub>). Samples were then analyzed by fluorescence spectrophotometer (Dong et al., 1987). This method measured the free formaldehyde and any HMS in the solution before preservation.

#### 2.3.7 H<sub>2</sub>O<sub>2</sub> (aq)

Aqueous phase H<sub>2</sub>O<sub>2</sub> in the fog samples was stabilized by adding p-hydroxyphenylacetic acid (POHPA) solution in the field to form a dimer, then measured using a Shimadzu RF-1501 spectrophotometer (Lazrus et al., 1985; Rao et al., 1997). Generally, this method measures not only the free/inorganic H<sub>2</sub>O<sub>2</sub> in the solution, but also organic peroxide. Because organic peroxide is typically not important and generally represents less than 1% of the aqueous peroxide concentration (Seinfeld et al., 1998), this measurement closely approximates the hydrogen peroxide concentration in the solution.

#### 2.3.8 Organic Acids

Aliquots for later analysis of organic acids were prepared by addition of a small volume of chloroform, which acts as a biocide. C1-C3 carboxylic acids were analyzed using the anion Dionex IC. The organic acid column in this analysis was a Dionex AS-11 separation column with an AG-11 guard column. Separation was achieved using a 0.5 mM NaOH eluent at a flow rate of 2.0 ml/min. The IC was calibrated daily using a series of lab-prepared standards. Calibration stability during each day's analysis was monitored by periodic injection of a standard solution.

Figure 2-17 describes sample fractionation methods. Immediately after sampling, aliquots were prepared for measurement of pH and TOC. Remaining sample was later filtered through baked quartz filters (Pall Gellman Pallflex Tissuquartz) in order to make a distinction between the dissolved phase (dissolved organic carbon, DOC) and the insoluble phase of the fog water. Then Ultrafiltration was used to separate organic matter as an approximate function of molecular weight and TOC content of each fraction was measured. Detail sample preparation and measurement were described below.

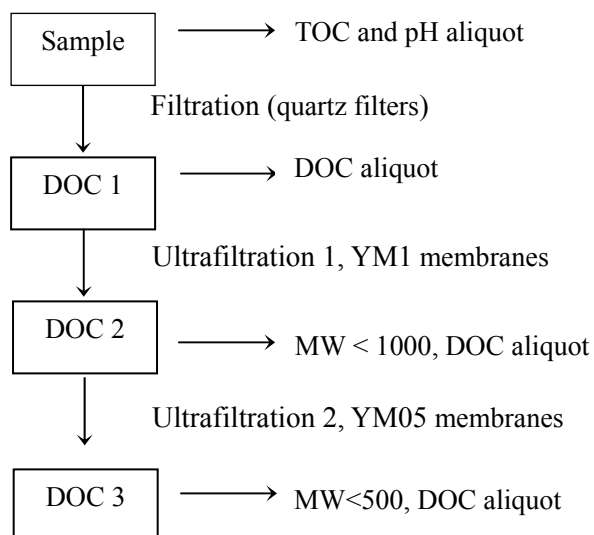


Figure 2-17. Schematic describing fog sample fractionation for OC measurements.

### 2.3.9 TOC/DOC and GC/MS analysis

Sample aliquots for total organic carbon (TOC) analysis were prepared by pipetting 5-20 ml of sample, depending on available sample, into a pre-baked glass vial and sealing with a Teflon-lined cap. TOC was measured using a Shimadzu TOC-5000A analyzer. The instrument vaporizes and oxidizes the sample on a platinum catalyst in a 680°C furnace, followed by infrared measurement of the evolved carbon dioxide. This yields a measurement of total carbon (TC) (elemental carbon theoretically is not included). A second measurement determining sample carbonate (inorganic carbon, IC) measures evolved carbon dioxide following sample acidification. TOC is determined as TC minus IC.

Additional sample was filtered through baked quartz filters (Pall Gelman Pallflex Tissuquartz) to make a distinction between the dissolved phase (dissolved organic carbon, DOC) and the insoluble phase of the fog water (“dissolved” refers to the filtrate and “insoluble” to the material retained on the filter).

The filter and filtrate were spiked with deuterated compounds used as internal standards for trace organic compound quantification. The filter samples were extracted three times with 25 ml of dichloromethane (DCM). Samples of 100–200 ml of filtrate, depending on available sample, were extracted three times with 25 ml of DCM after adjusting the sample pH to 1 and sample salinity to 50 g/l by adding NaCl. The DCM from the liquid/liquid extraction was dried over Na<sub>2</sub>SO<sub>4</sub>. DCM extracts were concentrated to 0.25 ml using a vacuum centrifuge and/or nitrogen blowdown prior to analysis. A first fraction of the concentrated extract was injected directly into an HP 6890/5973 Gas Chromatography coupled to Mass Spectrometry (GC-MS) for analysis. A second fraction was derivatized with diazomethane to transform organic acids to their methylester analogs prior to analysis. Greater detail about this methodology is provided by Herckes et al. (2002).

#### 2.3.10 Ultrafiltration

Ultrafiltration was used to separate organic matter as an approximate function of molecular weight and the TOC content of each fraction was measured. The experimental set up for the ultrafiltration procedure was adapted from Likens et al. (1983). Physical separation of DOC into molecular size ranges was completed in a pressurized and stirred ultrafiltration cell (Amicon model 8050), using the following MILLIPORE ultrafiltration membranes: YM1 (nominal size cut of 1000 Daltons) and YC05 (nominal size cut of 500 Daltons).

#### 2.3.11 Carbonyl and functional group analysis

An HPLC method was used for determining concentrations of carbonyl and dicarbonyl compounds in the fog samples. A second HPLC method was used to characterize the split of fog DOC among different functional group classes. Details of the sampling and preservation methods and analysis are described later. For the carbonyl analysis, Angiola fog samples were derivatized in our lab in Fort Collins more than a year after collection, after data analysis funding was obtained to support these measurements. Figure 2-18

shows the HPLC system we used, including solvent module, helium degasser / sparger, thermostatted column compartment, binary pump, diode array detector, and autosampler.



Figure 2-18. HP 1050 HPLC system.

## 2.4 Quality Control

Several procedures were used to ensure the integrity of each fog measurement, including calibrating instruments, cleaning collectors before each event, taking blanks, and analyzing replicate samples.

Individual instrument calibration was carried out at a certain time based on the instrument's maintenance requirement. Calibration of the PVM and CSASP was discussed above. Before the setup in the field, the collectors were first taken apart to thoroughly clean them with Triton-X100, and then rinse with deionized (DI) water. After mounting the collectors (except 5-stage collector), all the fog collectors were cleaned before each event. Some DI water was sprayed directly into the collectors using clean spray bottles and collected water served as a collector blank. This is to simulate the real process of fog droplet collection, since the sprayed water droplets follow approximately the same paths as the samples collected. A separate DI blank was taken from the DI water bottle used for spraying.

Uncertainties and minimum detection limits (MDL) were calculated for each species measured through all the fog episodes. For CRPAQS samples, although the field campaign lasted for about two months, all the samples from different fog episodes were stored in the refrigerator and the laboratory measurements for most species were done at the same time. Therefore, only one precision estimate (relative standard deviation, RSD) and one MDL are calculated for each species.

During each fog event, for every 3~4 samples, a sample was chosen to make two identical sets of aliquots known as duplicates. Duplicates were used to test the consistency of making and analyzing sample aliquots. Sample replicates, replicate analyses of one sample aliquot in the lab, capture analytical measurement precision only.

Precision uncertainties were calculated and reported as RSD in percent. The RSD was calculated using duplicate sample pairs, or using analytical standard replicates if it was impossible to use sample replicates. The formula to calculate RSD is as follows:

$$RSD = \frac{\left[ \left( \frac{1}{M} \right) \times \sum_{j=1}^M (\sigma_j)^2 \right]^{\frac{1}{2}}}{\bar{x}} \times 100\% \quad (2-1)$$

and the value for  $\sigma_j$  is calculated as in Equation (2-2)

$$\sigma_j = \frac{|x_1 - x_2|}{\sqrt{2}} \quad (2-2)$$

where  $M$  represents the number of pairs of replicates used,  $\sigma_j$  is the standard deviation of each analysis pair and  $\bar{x}$  is the average of all replicates.

To determine the minimum detection limit, blank samples analyzed for each species

were used. The minimum detection limit  $\Delta x_{\min}$  is:

$$x_{\min} - x_b = \Delta x_{\min} \geq ts_b \sqrt{\frac{N_1 + N_b}{N_1 N_b}} \quad (2-3)$$

where  $t$  is the value given at the 95% confidence level for the appropriate number of degrees of freedom,  $s_b$  is the blank standard deviation,  $N_1$  is the number of sample measurements (for single analysis,  $N_1 = 1$ ), and  $N_b$  is the number of analyzed blanks. The subscript  $b$  refers to the blank determination.

#### 2.4.1 Ion concentrations

Table 2-3. RSD, MDL and sample concentration summaries for CRPAQS fog ions.

		Cl <sup>-</sup>	NO <sub>3</sub> <sup>-</sup>	NO <sub>2</sub> <sup>-</sup>	SO <sub>4</sub> <sup>2-</sup>	Na <sup>+</sup>	NH <sub>4</sub> <sup>+</sup>	K <sup>+</sup>	Mg <sup>2+</sup>	Ca <sup>2+</sup>
MDL (95% CL) (μN)		8.0	18.2	4.3	6.5	12.1	27.9	1.3	1.8	4.1
RSD (%)		4.7	3.6	4.6	7.6	7.3	5.5	21.2	9.0	7.4
# of sample pair		66	66	66	66	55	55	55	55	55
Sample concentrati on (μN)	Minimum	8.7	36.6	3.2	8.7	0.1	0.0	0.8	4.3	4.3
	Maximum	168.1	3547.0	321.2	1463.4	243.6	4492.1	80.1	78.1	116.3
	Mean	31.9	626.2	44.5	146.5	30.9	1104.4	12.4	9.8	28.2

Table 2-3 lists the statistical analysis for ions, including Cl<sup>-</sup>, NO<sub>3</sub><sup>-</sup>, NO<sub>2</sub><sup>-</sup>, SO<sub>4</sub><sup>2-</sup>, Na<sup>+</sup>, NH<sub>4</sub><sup>+</sup>, K<sup>+</sup>, Mg<sup>2+</sup> and Ca<sup>2+</sup>. The MDL were calculated from blank measurements for all the samples from all the collectors except the 5-stage collector. The RSD were calculated from sample replicates. K<sup>+</sup> has a relatively higher RSD because its peak in the chromatogram is near the peak of NH<sub>4</sub><sup>+</sup>, leading to greater interference when the concentration of NH<sub>4</sub><sup>+</sup> is high. The RSD of the remaining ions are all well below 10%. These results are consistent with or better than past studies at Whiteface Mountain and

Davis (Reilly, 2000). The MDL results are higher than at Whiteface Mountain and Davis, but still in a reasonable range because the MDL are all far below the sample means, except for sodium.

#### 2.4.2 Organic acids

Table 2-4 shows the statistical analyses for organic acids. The RSD were calculated from sample replicates, and the MDL were calculated from standard measurement because the blanks of some species did not exhibit any detectable peaks. We can see that the RSD are all less than 10%, quite reasonable for organic acid analysis. MDL of acetate, formate and oxalate are smaller than sample means respectively, while for propionate, glutarate, succinate and malonate, their MDL are larger than measured sample means.

Table 2-4. Statistical analysis for organic acids.

	Acetate	Propionate	Formate	Oxalate	Glutarate	Succinic	Malonate
MDL (95% CL) ( $\mu\text{N}$ )	4.1	3.7	4.2	3.2	5.6	5.8	5.0
RSD (%)	3.8	3.8	2.4	2.8	4.6	4.8	5.4
# of sample pair	10	10	10	10	10	10	10
Minimum	1.4	0.0	6.7	5.5	0.0	0.0	0.0
Sample concentration ( $\mu\text{N}$ )							
Maximum	197.2	11.5	121.6	44.0	6.9	10.8	26.5
Mean	44.7	3.2	40.1	12.3	1.0	2.3	2.1

\* MDL was calculated by replicate standard analyses

#### 2.4.3 S(IV), HCHO, H<sub>2</sub>O<sub>2</sub>, metal (Fe, Mn), TOC and DOC

Table 2-5 lists the statistical analysis results for S(IV), HCHO, H<sub>2</sub>O<sub>2</sub>, metals (Fe, Mn), TOC and DOC. MDL and RSD were obtained from blanks and sample replicates, except S(IV), which were calculated from standard analyses. Comparing the RSD and MDL of S(IV), HCHO, H<sub>2</sub>O<sub>2</sub> and metals with earlier results at Whiteface Mountain and Davis



(Reilly, 2000), there is little difference between them. The RSD of iron is smaller here, only 4.1% compared with 11.1% in Whiteface Mountain and Davis.

Table 2-5. Statistical analysis for S(IV), HCHO, H<sub>2</sub>O<sub>2</sub>, Fe<sup>2+</sup>, Mn<sup>2+</sup>, TOC and DOC.

	S(IV) (μM)	HCHO (μM)	H <sub>2</sub> O <sub>2</sub> (μM)	Fe <sup>2+</sup> (μg/l)	Mn <sup>2+</sup> (μg/l)	TOC (ppmC)	DOC (ppmC)
MDL (95% CL) (μN)	1.5	3.3	0.07	6.9	0.3	0.5	0.2
RSD (%)	6.7	7.1	6.6	4.1	2.7	2.1	5.7
# of sample pair	10	14	7	60	60	17	7
Minimum	3.9*	5.4	0.8	12.4	0.8	0.3	3.9
Sample concentration Maximum	5.9*	50.8	18.8	478.6	29.9	17.4	7.7
Mean	5.1*	21.9	4.6	121.2	6.9	9.3	6.4

\* min, max and mean are for standard.

#### 2.4.4 MOUDI

Table 2-6. Statistical analysis for MOUDI samples.

	Na <sup>+</sup>	NH <sub>4</sub> <sup>+</sup>	K <sup>+</sup>	Mg <sup>2+</sup>	Ca <sup>2+</sup>	Cl <sup>-</sup>	NO <sub>3</sub> <sup>-</sup>	SO <sub>4</sub> <sup>2-</sup>
MDL (95% CL) * (ng/m <sup>3</sup> )	8.0	1.4	1.2	5.1	12.3	8.2	6.6	4.0
RSD (%)	5.3	2.6	4.5	2.2	3.8	9.6	13	6.0
# of sample pair	6	6	6	6	6	5	5	4
Mean (μg/m <sup>3</sup> )	1.42	19.1	0.99	4.45	4.33	0.55	28.0	3.87

\* MDLs were calculated from BRAVO data.

Table 2-6 shows the statistical data for MOUDI samples. Compared with BRAVO (Big Bend Regional Aerosol and Visibility Observational study) data (Lee, 2002; Lee et al.,

2004), the RSD of  $\text{NO}_3^-$  is a little higher, 13% vs. 5.9%, but still in a reasonable range. No reliable MDL values were obtained for the MOUDI due to the limited numbers of sample blanks in this study. MOUDI MDL values from the BRAVO study are included in Table 2-6 for information.

## 2.5 Instrumental quality control

This section summarizes the instrumental quality control and some uncertainties with the instruments. The instrumental quality control includes correct calibration of instruments, collector efficiency measurements, and corresponding cut size measurement.

### 2.5.1 Flow rate measurements

As stated before the most important factor for the fog collectors impacting accuracy of sampling velocity and cut size is the fan voltage. The fan law determines that the revolution speed of a DC-powered fan has a linear relation to the air flow velocity, and also has a linear relation to the voltage exerted on the fan. Therefore, the voltage is critical in determining the operation characteristics of collectors. Demoz et al. (1996) proposed that the flow rates in the Caltech collectors are assumed to be accurate to within  $\pm 5\%$  of design values if the correct voltage is applied to the fans. A summary of flow rate and size cut info for collectors is shown in Table 2-7.

Table 2-7. Summary of collector flow rates and size cuts.

	Voltage (V)		Air Velocity (m/s)		Size Cut ( $\mu\text{m}$ )	
	Design	CRPAQS	Design	CRPAQS	Design	CRPAQS
CASCC	13.3	10.6	8.5	9.9	3.5	3.5
ss-CASCC	13.3	10.6	8.5	9.6	3.5	3.5
sf-CASCC	13.3	11.1	6.7	7.5	23(1 <sup>st</sup> stage)	21(1 <sup>st</sup> stage)
					4(2 <sup>nd</sup> stage)	3.5 (2 <sup>nd</sup> stage)

ss-sf- CASCC	13.3	11.0	6.7	8.2	23(1 <sup>st</sup> stage) 4(2 <sup>nd</sup> stage)	19(1 <sup>st</sup> stage) 3.5 (2 <sup>nd</sup> stage)
-----------------	------	------	-----	-----	---	--

---

Variation in voltage on the fan will change the flow rate dramatically, but modest variations in flow rate do not change the droplet collection efficiency and size cut very much.

## Chapter 3

### Overview of fog episodes and fog composition

#### 3.1 Summary of fog sampling

During the study (winter 2000/2001), we encountered several fog events and successfully collected over two hundred fog samples. The measurements and analysis include weather conditions, physical size distributions, and chemical analysis of over ten species in gas and aqueous phases. In this chapter, these data will be presented and discussed. There were some short fog events and they were insufficient for fog collection since the duration was not long enough to collect enough sample. There were also some freezing fog events during which the temperatures were under zero Celsius degree, which would made fog water freeze on the sampling strands and rods, making it impossible to collect and causing some serious deflection of size distributions.

Table 3-1 summarizes collected fog samples in Angiola by collector type. Overall, the sampled fog events are as follows:

- Dec 17/18 (day 352)

A very good fog event with typical weather conditions of radiation fog, it started at 22:15pm and finished at 12:00 noon the next day. This event yielded a total of 66 samples, from different collectors and time periods.

- Dec 18/19 (day 353)

This fog event started at 23:00pm, then lifted but came back again at 1:20am until 7:30am in the morning. 25 samples were collected.

- Jan 6<sup>th</sup>

We collected one fog sample from 6:00am to 8:00am by using CHRCC since temperatures were below freezing.

- Jan 10<sup>th</sup>

A total of 6 samples were collected from 6:15am to 7:55am.

- Jan 15<sup>th</sup>

19 samples were collected from 23:30 pm to 3:00am.

- Jan 17<sup>th</sup>

A freezing fog event lasted from 12:00pm to 7:00am, 20 samples were collected.

- Jan 21<sup>st</sup>

Total of 25 samples were collected form 6:00am to 9:00am.

- Jan 25<sup>th</sup>

A patchy fog event. The fog event lasted from 3:30am until 8:00am, with interruptions of low LWC. 16 samples were collected.

- Jan 31<sup>st</sup>

A short fog event from 4:00am until 9:30am. 25 samples were collected.

- Feb 1<sup>st</sup>

A patchy fog event lasted from 1:00am to 5:20am. 16 samples were collected.

### 3.2 Weather conditions

Table 3-2 shows a summary of three basic weather parameters of all fog events: average wind speed, average temperature and average relative humidity. As we can see, the average temperatures of these fog events were above zero degrees, except Jan 06 and Jan 17, whose average temperatures were below or close to zero degree. The wind speeds were all less than 2m/s, consistent with the calm wind required for radiation fogs. These were the typical weather conditions for radiation fogs.

Table 3-1. Summary of collected fog samples in Angiola by collector type.

Date	CASCC	Sf CASCC	Heated CASCC	Dep Plates	ss CASCC	Sf ss CASCC	5-state collector	Tower Level 0	Tower Level 1	Tower Level 2	Tower Level 3	Total
Dec 17, 2000	13	11		6	8	12		12	4			66
Dec 18, 2000	4	3		1	2	3	1	3	8			25
Jan 06, 2001			1									1
Jan 10, 2001	2		2			2						6
Jan 15, 2001	1	1	1	1	1	1						6
Jan 17, 2001	3	3	4	4	4	1	1					20
Jan 21, 2001	3	3	3	2	1	1		4	3	5	5	25
Jan 25, 2001	3	2	3	2	2	2		2				16
Jan 31, 2001	4	3		2	2	2	1	5	6			25
Feb 01, 2001	2	2		1	2	2		3	4			16
<b>Total</b>	<b>35</b>	<b>28</b>	<b>14</b>	<b>19</b>	<b>22</b>	<b>24</b>	<b>3</b>	<b>29</b>	<b>25</b>	<b>5</b>	<b>5</b>	<b>206</b>

Multiple fraction from the same fractionating collector have been counted as one sample

Table 3-2. Summary of weather conditions during fog events.

Date	Wind Speed (m/s)	Temperature (°C)	Relative Humidity (%)
Dec 17, 2000	0.4	5.1	97
Dec 18, 2000	0.7	2.7	97
Jan 06, 2001	0.8	-1.7	85
Jan 10, 2001	1.5	1.7	95
Jan 15, 2001	1.0	2.6	89
Jan 17, 2001	0.7	0.2	92
Jan 21, 2001	1.9	3.0	94
Jan 25, 2001	0.5	2.9	94
Jan 31, 2001	0.8	4.9	94
Feb 01, 2001	1.1	2.0	92

For each fog event, the PVM recorded LWC ( $\text{mg/m}^3$ ) and the total surface area of all drops ( $S$ , unit:  $\text{cm}^2/\text{m}^3$ ). We can calculate the effective diameter ( $D_{\text{eff}}$ , unit:  $\mu\text{m}$ ) from these

data. The equation is as follows:

$$D_{eff} = 60 \times \frac{LWC}{S} \quad (3-1)$$

Figure 3-1 shows a timeline of fog LWC for the entire measurement period. Fog episodes were seen throughout much of the period, including those successfully sampled as outlined above. Some events in late December were not successfully sampled due to unanticipated freezing of supercooled drops on collector surfaces. Changes in sampling protocol were made in January to also permit some sampling of freezing fog episodes.

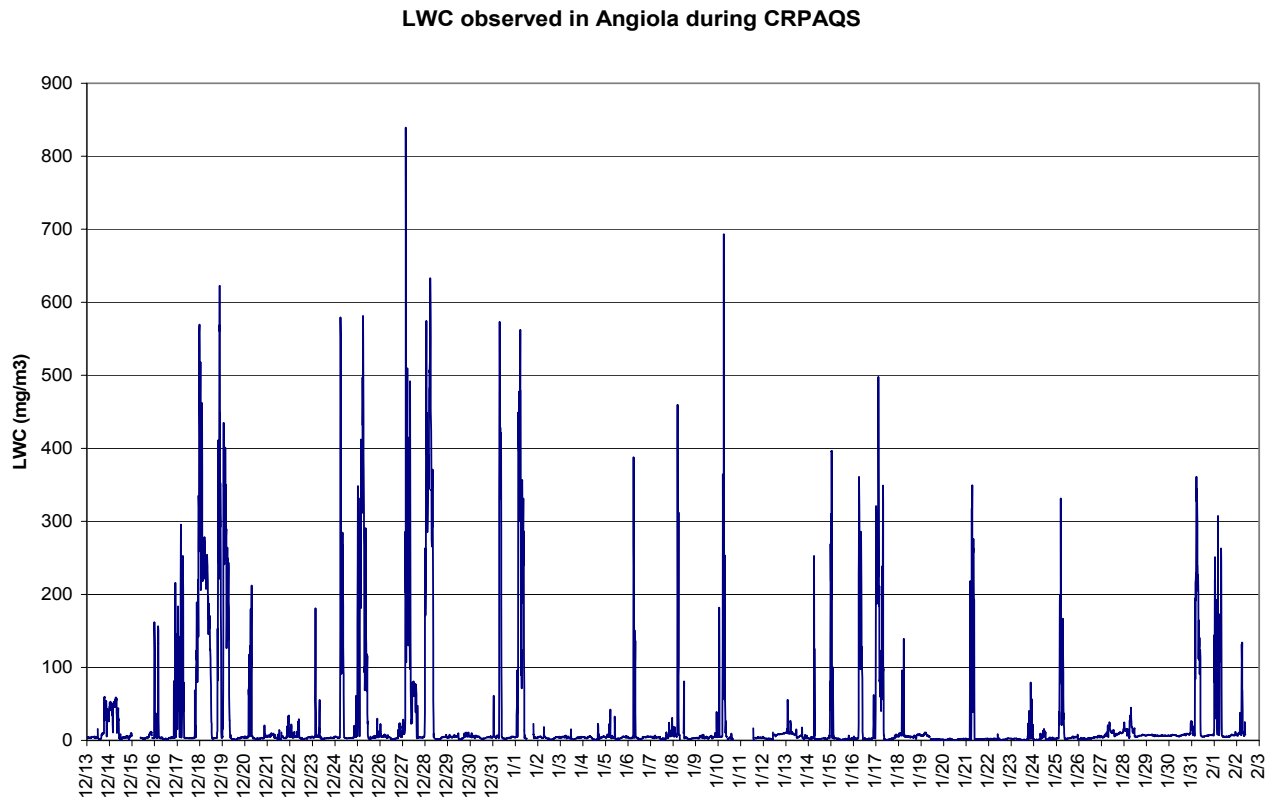


Figure 3-1. Fog LWC timeline measured at Angiola during the period 12/13/00 – 2/3/01.

Figures 3-2 to 3-5 show effective diameter ( $D_{eff}$ ) and LWC profiles of the sampled fog events.

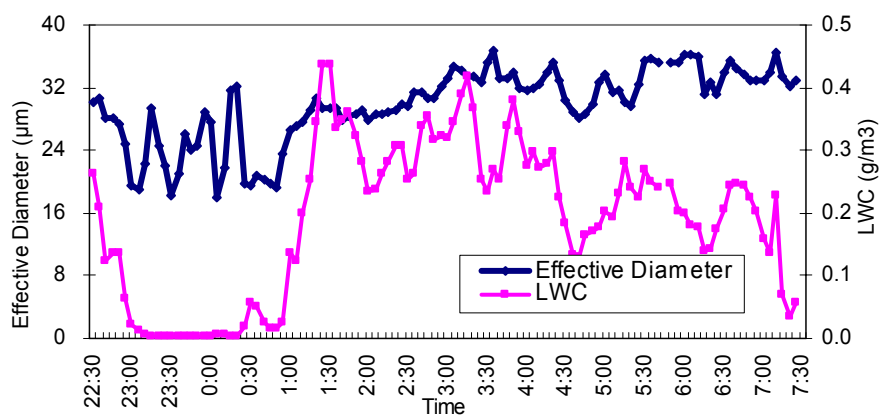


Figure 3-2. Effective diameter and LWC measured by PVM on 12/17 & 12/18/00.

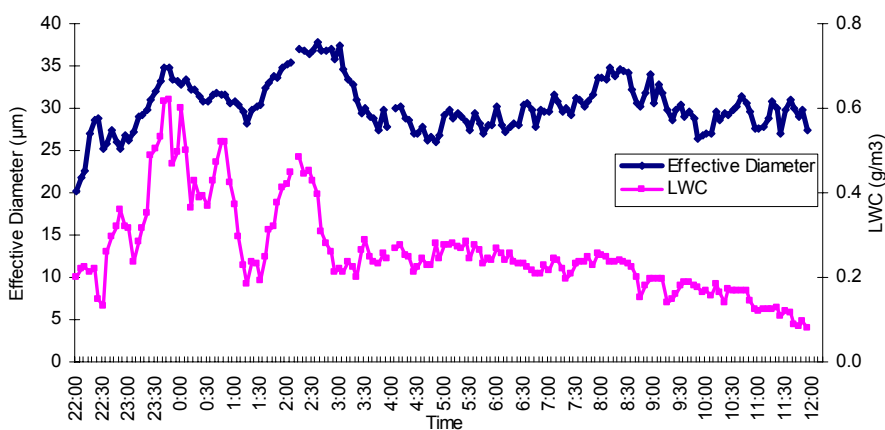


Figure 3-3. Effective diameter and LWC on 12/18 & 12/19/00.

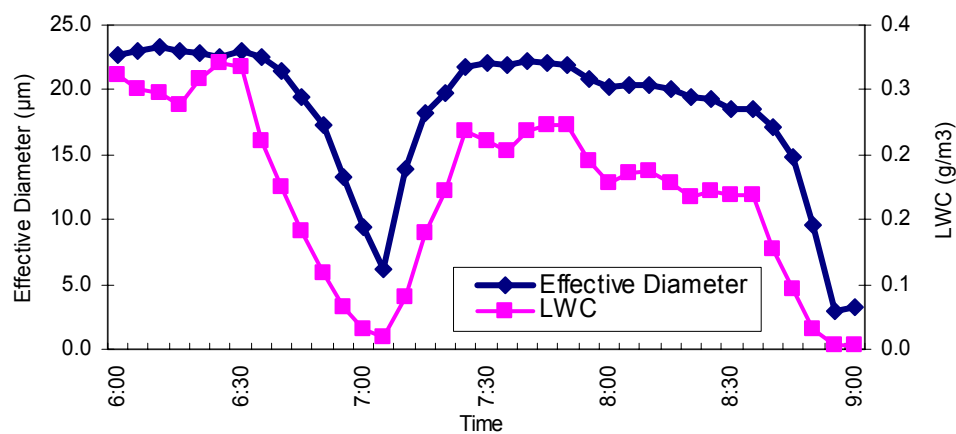


Figure 3-4. Effective diameter and LWC on 01/21/00.



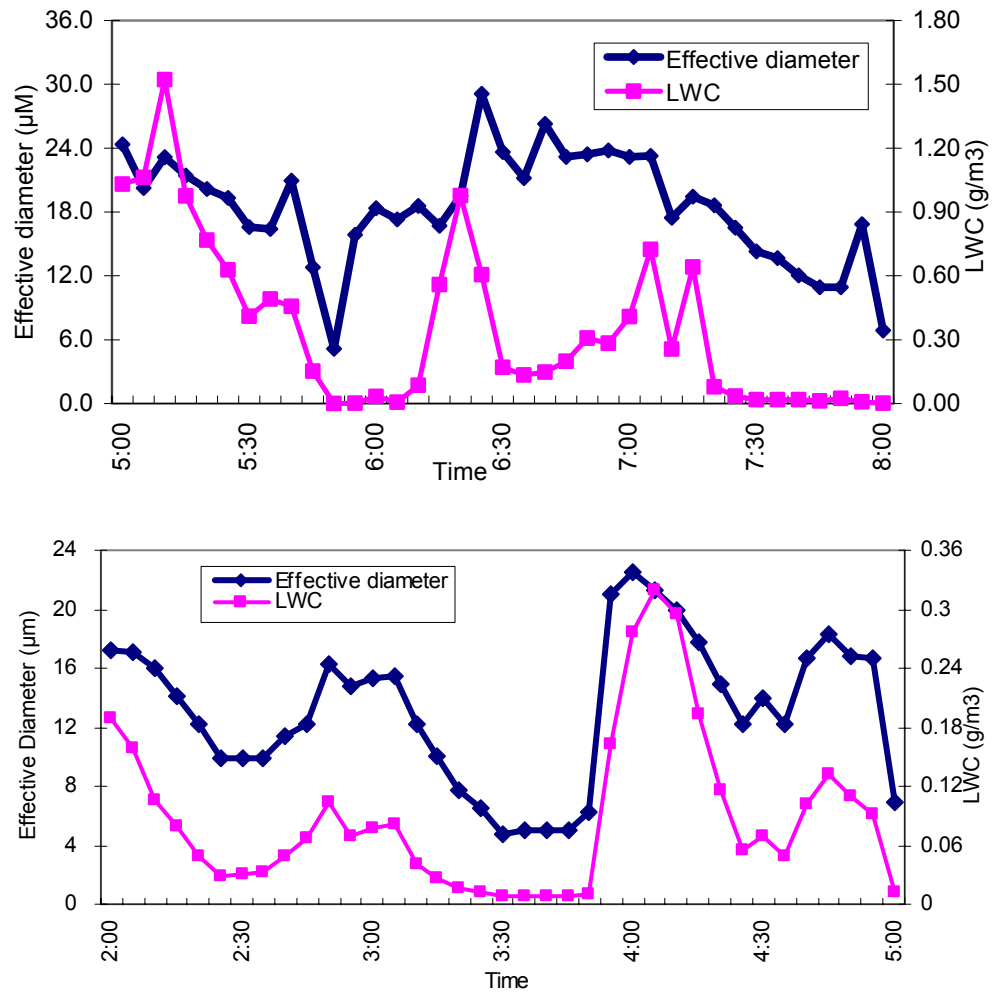


Figure 3-5. Effective diameter and LWC on 1/25/00 (top panel) and 02/01/00 (lower panel).

### 3.3 Drop size distribution and evolution

The CSASP was used to measure the fog drop size distribution and its evolution in 20 bins, ranging from 5  $\mu\text{m}$  to 47  $\mu\text{m}$ . CSASP measures the distribution at one second interval and data are saved in files for further treatment.

#### 3.3.1 Comparison between CSASP and PVM

Data from both the PVM and CSASP can be used to determine LWC and effective

diameter. As stated in chapter two, the intercomparisons are sometimes acceptable, but large differences in ground-based LWC measurements made with the CSASP and PVM have also been observed (Wendisch 1998; Gerber et al., 1999). Therefore, an intercomparison of the data is necessary.

The PVM reports LWC and particle surface area in two channels. The CSASP reports absolute numbers of drops of each diameter and total sampling volume of air, then number concentrations of fog droplets in each diameter range can be calculated by dividing absolute numbers of drops by total sampling volume of air.

Figure 3-6 shows a timeline comparison of effective diameters of a fog event obtained from PVM and CSASP on 12/17 & 12/18/00. The trend of these two timelines of effective diameter was similar, while we can see that PVM reported larger effective diameters than CSASP. Figure 3-7 provides a detailed view of the comparison between these two effective diameters.

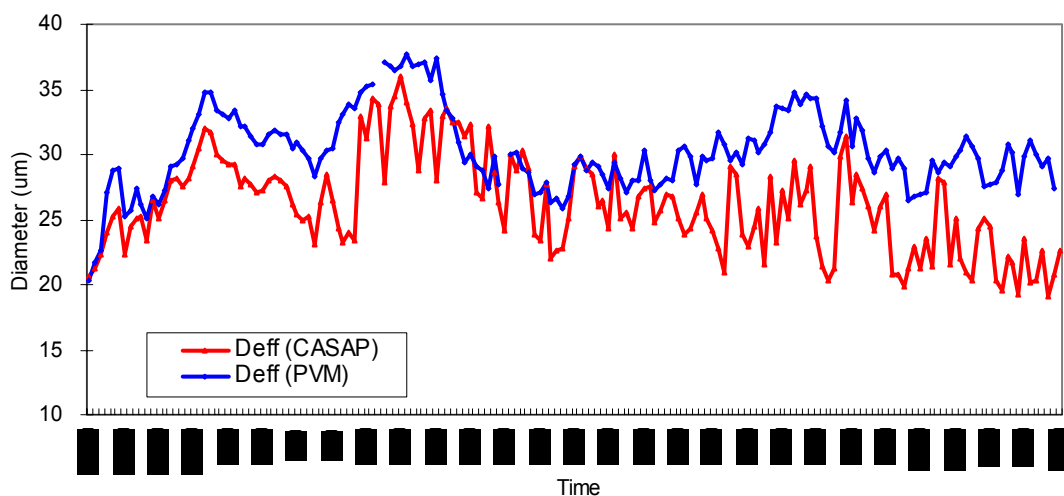


Figure 3-6. Comparison between effective diameters obtained from the PVM and the CSASP on 12/17 & 12/18/00.

Figure 3-8 shows the LWC obtained from the PVM and CSASP. We can see that LWC measurements showed a large difference. The CSASP reported much higher LWC than PVM. In order to understand why the CSASP tends to report higher LWC than PVM while size distribution measurements are consistent with PVM, we used a 2-D computational fluid dynamics model to simulate this process. The CSASP is an active instrument. It uses a fan to make the air go through a horn-like tube, which acts like a flow regulator, then it uses a laser to measure the droplet size distribution at the center of the tube. Gerber et al. (1999) found that the inlet of CSASP can act as a "flow accelerator." If bigger droplets are focused to the center of sampling tube, the CSASP could strongly overestimate LWC.

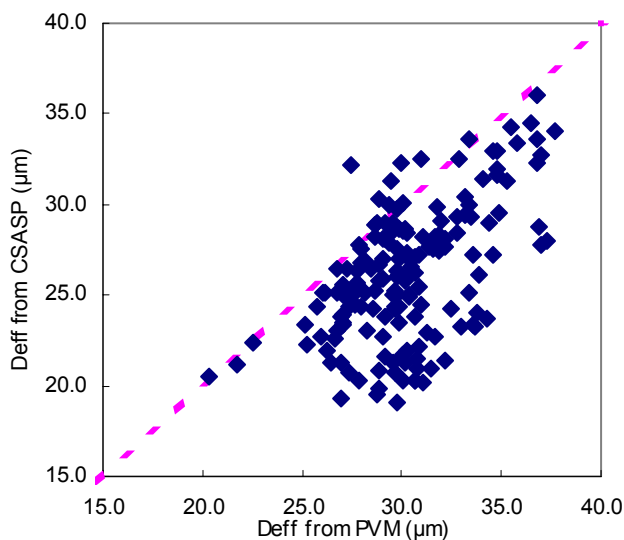


Figure 3-7. Comparison of effective diameter from the PVM and CSASP for the fog event on 12/17 & 12/18/00.

Overall for the CRPAQS study, the CSASP data cannot reliably be used to calculate LWC, but the shape of the size distribution is still somewhat useful. Therefore, we used PVM LWC data to normalize the integrated CSASP volume distribution.

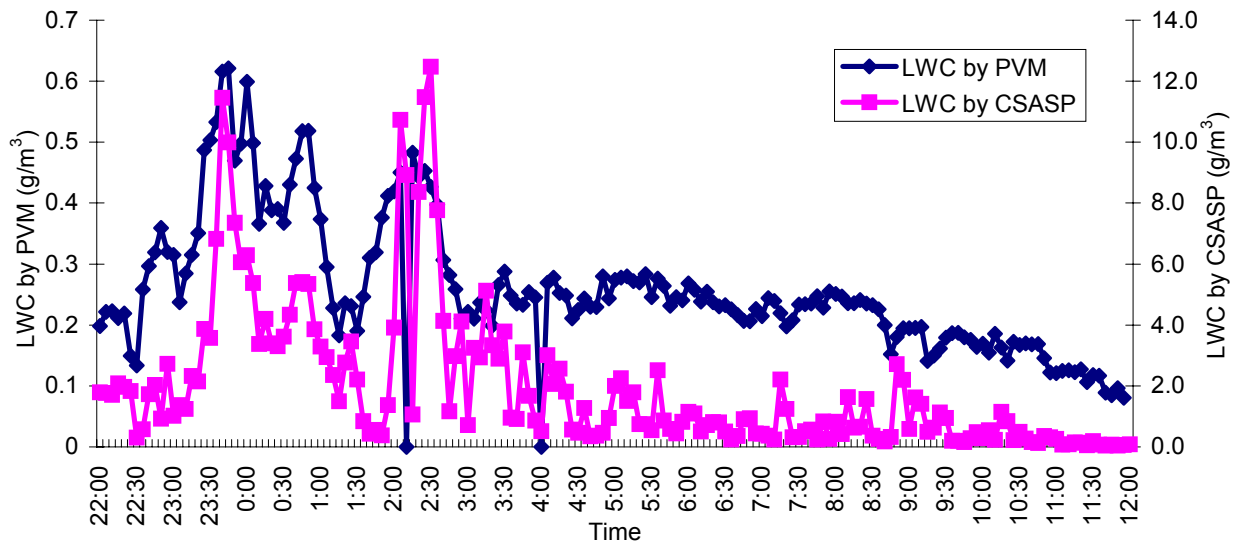


Figure 3-8. Comparison of LWC obtained by PVM and CSASP for the fog event on 12/17 & 12/18/00.

Figure 3-9 shows the fog drop size distribution evolution ( $dN/d\log D_p$ ) with time on 12/18/00. The x axis is the time, averaged to one hour interval to have a simple but better view of the evolution of the size distribution. The y axis is the diameter ranges of the bins, from 5  $\mu\text{m}$  to 47  $\mu\text{m}$ . z axis is the number concentration.

This fog event started at 22:15pm, but we started the CSASP at around 12:00am after receiving the fog paging notification from the PVM and traveling to the site. After about two hours from the beginning of the fog event, fog droplets have a high number concentration with a monodisperse distribution, and the center of the peak was larger than 25  $\mu\text{m}$ . With time passing by, the center of the peak shifted to the left with larger number concentration in smaller diameter range. This is interesting and probably reflects preferential loss of large fog drops by sedimentation. Note that the absolute number concentration decreases from the original distribution, suggesting that fog drops were depositing to the ground by wet deposition. After the first several hours, which was the fog developing stage, smaller aerosol particles probably began to activate to form fog drops,

thus having larger number concentrations of smaller drops than larger drops(a tail on the plots).

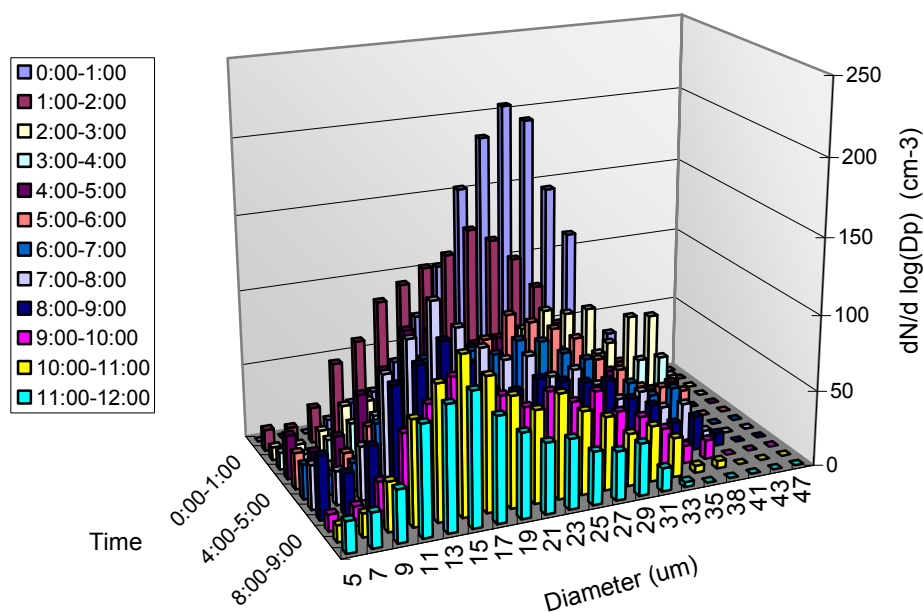


Figure 3-9. Drop size distribution evolution with time on 12/17 & 12/18/00.

### 3.4 Bulk fog composition

In this section we address the composition of “bulk” CRPAQS fog samples. Bulk samples are those where all fog drop sizes are collected into a single sample for analysis.

#### 3.4.1 Components and concentrations

##### 3.4.1.1 Major inorganic ions and pH

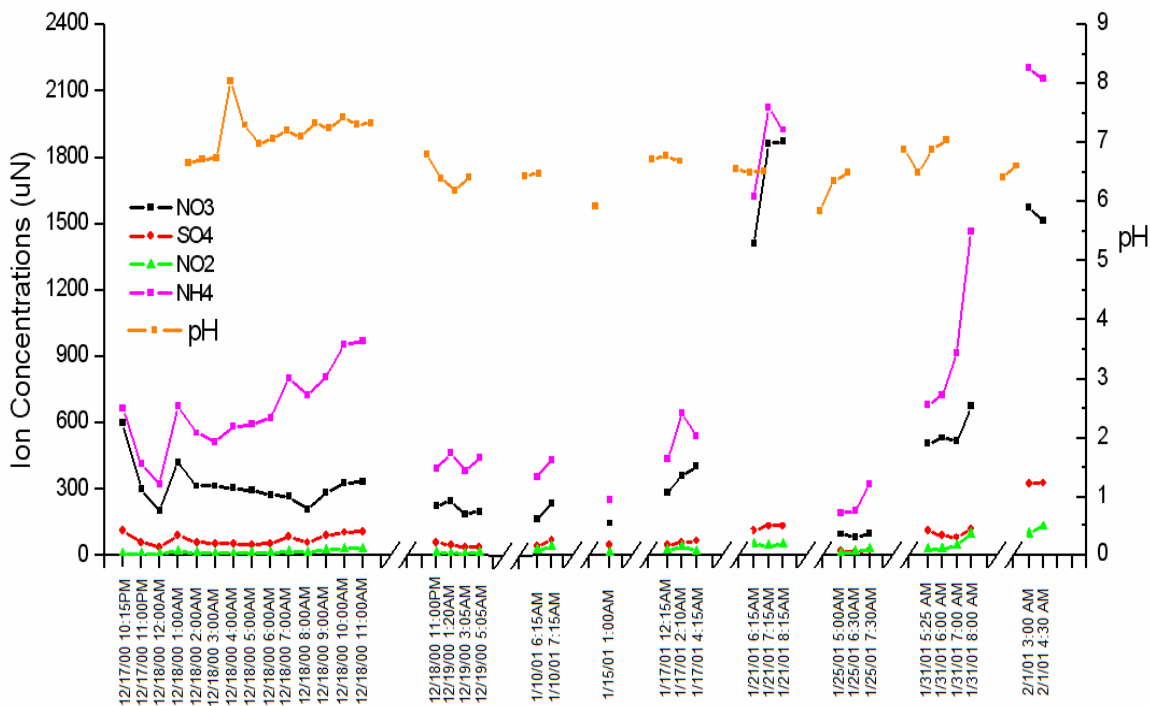


Figure 3-10. Timelines of three ion concentrations and pH in CASCC fog samples.

From past studies including IMS95, we know that major inorganic ions in SJV fogs include ammonium, sulfate and nitrate. Figure 3-10 shows the timelines of pH value, these three major inorganic ions and nitrite concentrations for all the fog events in CASCC bulk fog samples. Figures 3-11 to Figure 3-16 show detailed timelines of species concentrations in the sampling periods with more than two samples.

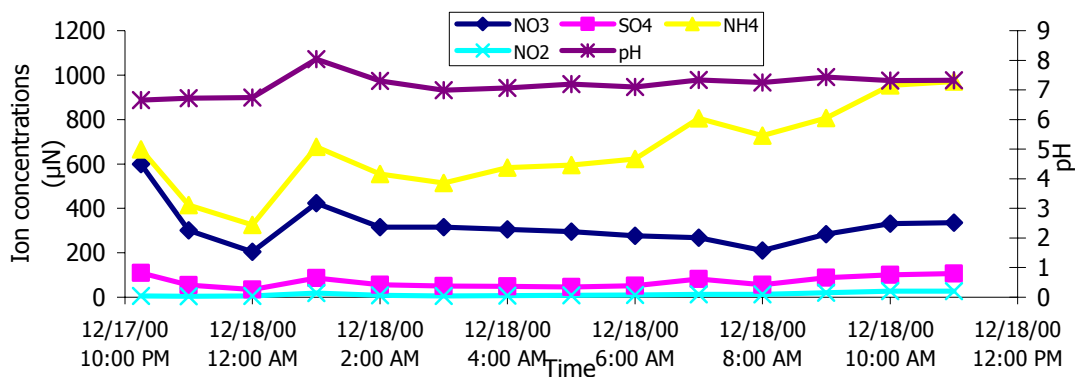


Figure 3-11. Timelines of three major ions, nitrite and pH in CASCC fog samples during the 12/17/00&12/18/00 fog event.

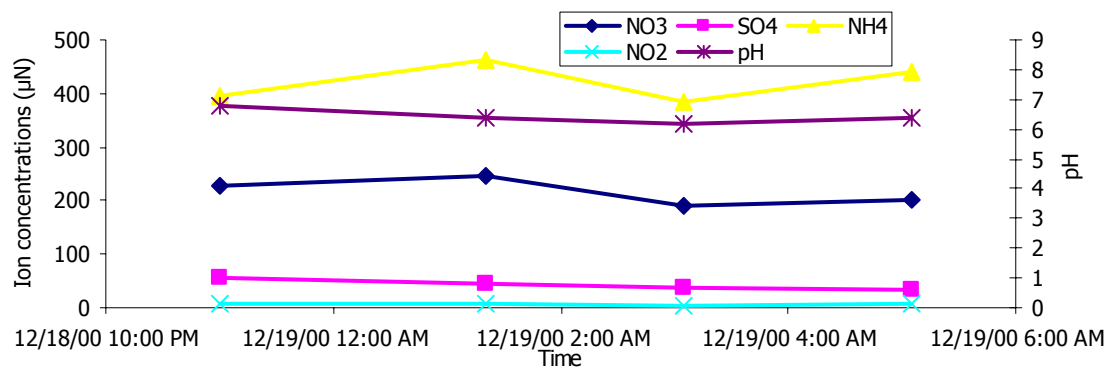


Figure 3-12. Timelines of three major ions, nitrite and pH in CASCC samples during the 12/18/00&12/19/00 fog event.

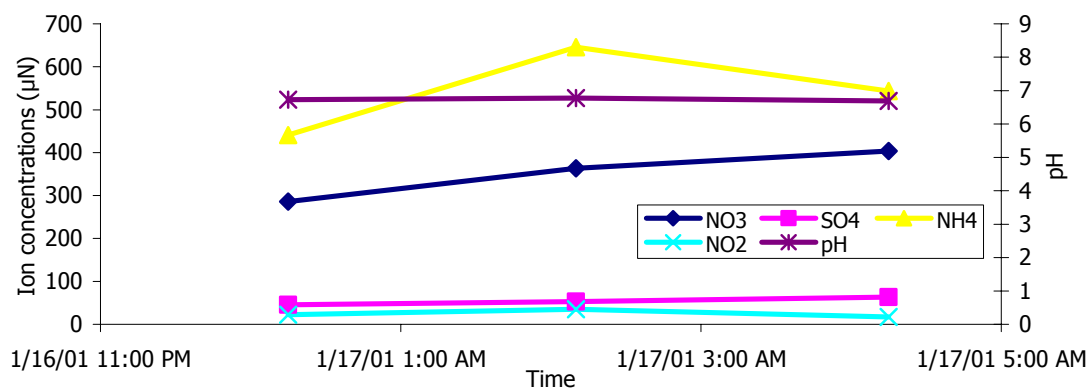


Figure 3-13. Timelines of three major ions, nitrite and pH in CASCC samples on 01/17/01.

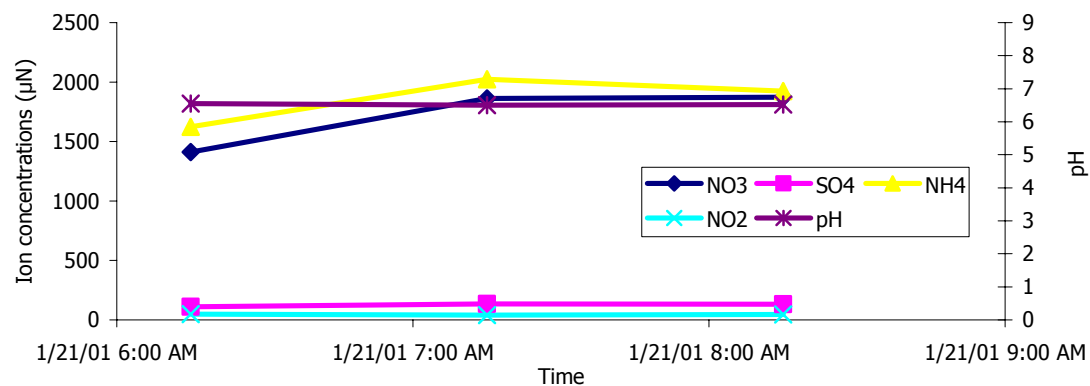


Figure 3-14. Timelines of three major ions, nitrite and pH in CASCC samples on 01/21/01.

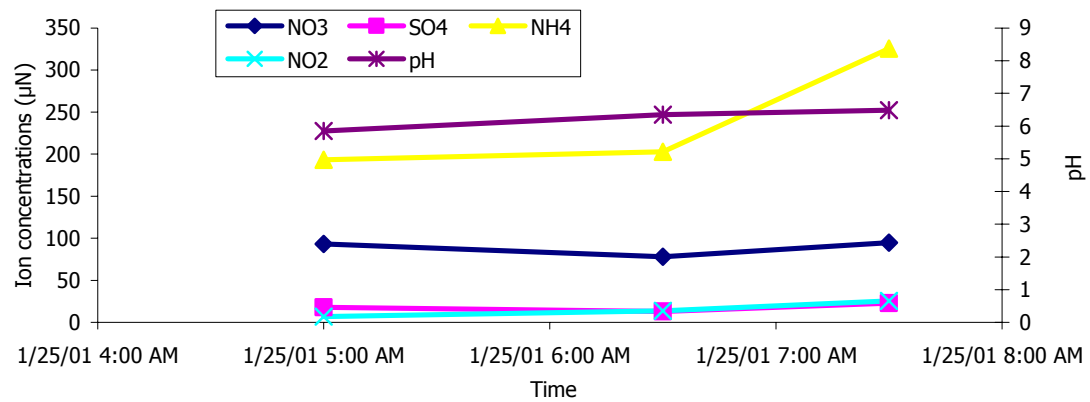


Figure 3-15. Timelines of three major ions, nitrite and pH in CASC samples on 01/25/01.

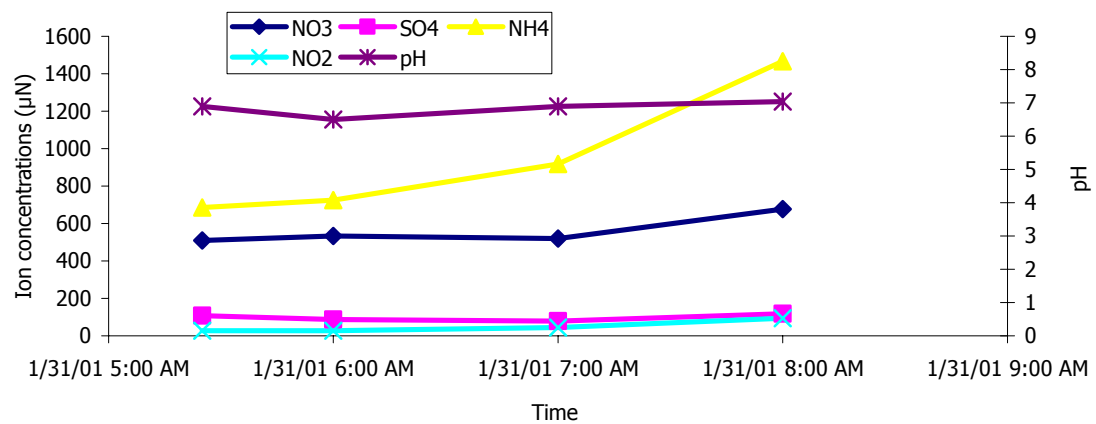


Figure 3-16. Timelines of three major ions, nitrite and pH in CASC samples on 01/31/01.

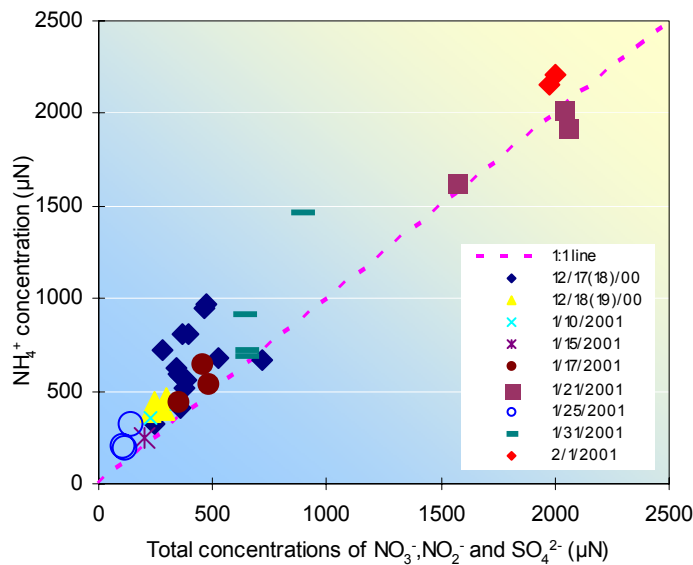


Figure 3- 17. Ammonium concentrations vs. total concentration of nitrate, sulfate and nitrite for all fog events.



The fog collected during CRPAQS was relatively alkaline, with the range of pH in the samples from 6.0 to 8.02, averaging 6.78. To understand this trend, we can take a look at the timelines of ammonium, nitrate and sulfate plotted in Figure 3-10, and also in Figure 3-17, which shows the ammonium concentration against total concentrations of nitrate, sulfate and nitrite. We can see that there were large amounts of ammonium in the fog drops, more than sufficient to neutralize the acid species and make the fog samples alkaline.

### 3.4.1.2 Organics

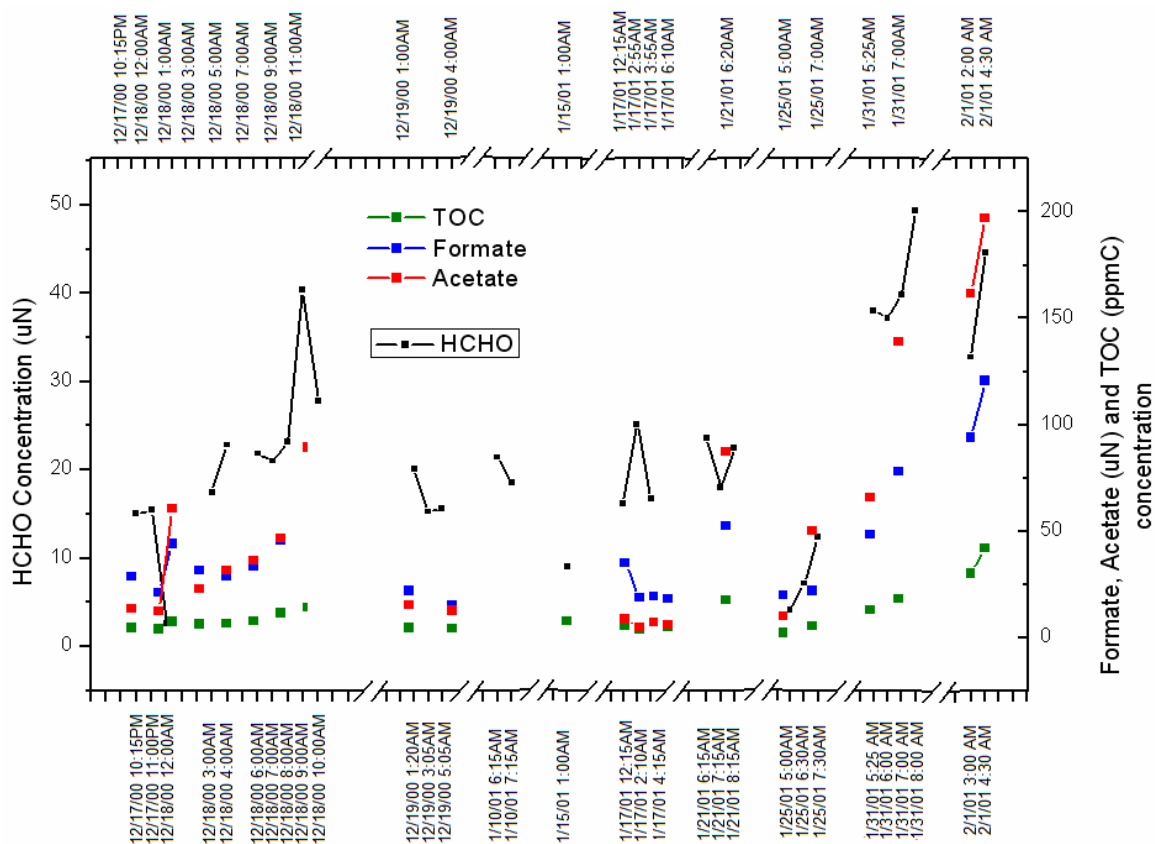


Figure 3-18. Timelines of formate, acetate, TOC and HCHO concentrations for all fog events. The HCHO concentration is from the CASCC; other species are from the ss-CASCC.

Previous studies showed that formate and acetate are two dominant organic acid anions in high pH SJV fog drops. Formaldehyde is one of the dominant species in fog water as well. Figure 3-18 shows timelines of formaldehyde, formate, acetate and total organic carbon (TOC) concentrations in CRPAQS bulk fog samples. Figures 3-19 and 3-20 show detailed timelines for the 12/17&18/00 and 01/17/01 fog events.

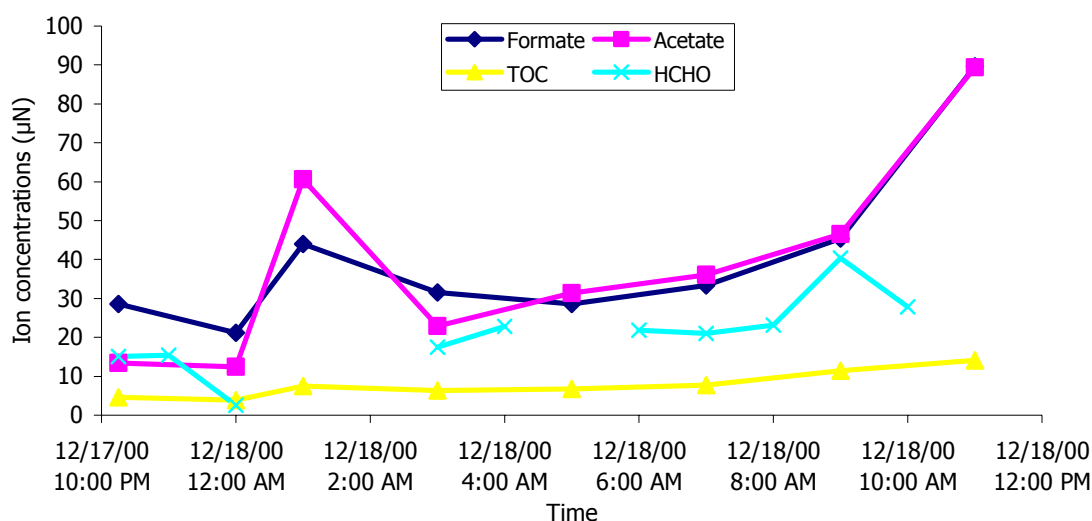


Figure 3-19 Timelines of formate, acetate, TOC and HCHO in CASCC samples in the 12/17&12/18/00 fog event.

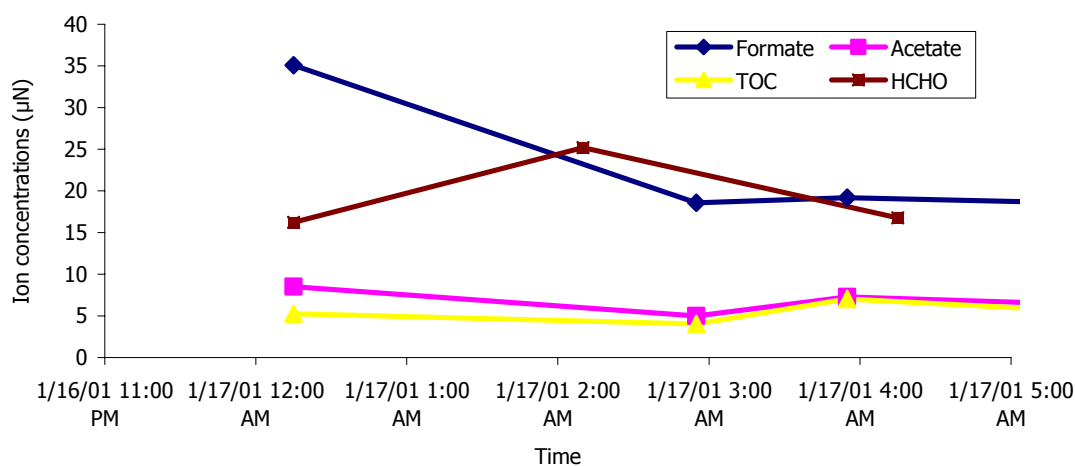


Figure 3-20. Timelines of formate, acetate, TOC and HCHO in CASCC samples on 01/17/01.

Formaldehyde concentrations range from 2.6  $\mu\text{N}$  to 49.3  $\mu\text{N}$ , averaging 22.4  $\mu\text{N}$ ; formate concentrations range from 14.9  $\mu\text{N}$  to 120.7  $\mu\text{N}$ , averaging 42.2  $\mu\text{N}$ ; acetate concentrations range from 5.0  $\mu\text{N}$  to 197.8  $\mu\text{N}$ , averaging 51.4  $\mu\text{N}$ . TOC concentrations range from 2.3 ppmC to 41.9 ppmC, averaging 10.4 ppmC.

### 3.4.2 Average fog solute concentrations

Table 3-3. Volume-weighted average solute concentrations in all fog events.

Date	[NO <sub>3</sub> <sup>-</sup> ] ( $\mu\text{N}$ )	[SO <sub>4</sub> <sup>2-</sup> ] ( $\mu\text{N}$ )	[NO <sub>2</sub> ] ( $\mu\text{N}$ )	[NH <sub>4</sub> <sup>+</sup> ] ( $\mu\text{N}$ )	[Formate] ( $\mu\text{N}$ )	[Acetate] ( $\mu\text{N}$ )	[Pyruvate] ( $\mu\text{N}$ )	[Oxalate] ( $\mu\text{N}$ )	TOC (ppmC)
12/18/00	308.0	62.5	9.9	597.5	33.7	32.6	0.0	7.0	6.6
12/19/00	210.6	38.2	6.3	426.2	19.0	14.3	0.0	6.6	4.4
1/10/01	181.3	43.4	--	374.7	--	--	--	--	--
1/15/01	145.9	44.5	--	250.7	--	--	--	--	--
1/17/01	348.1	54.6	6.6	499.1	23.0	6.7	0.0	7.3	5.1
1/21/01	1731.3	126.2	46.7	1879.8	52.6	87.2	0.0	11.4	17.7
1/25/01	85.7	15.9	15.6	214.3	20.7	24.3	0.0	1.2	3.3
1/31/01	555.7	97.6	53.8	922.3	64.6	106.2	0.0	8.4	15.9
2/1/01	1537.4	329.4	111.6	2173.0	103.6	174.4	0.2	21.5	34.4
Total Average	567.1	90.3	35.8	815.3	45.3	63.7	0.0	9.1	12.5

Date	[Na <sup>+</sup> ] ( $\mu\text{N}$ )	[Cl <sup>-</sup> ] ( $\mu\text{N}$ )	[K <sup>+</sup> ] ( $\mu\text{N}$ )	[Mg <sup>2+</sup> ] ( $\mu\text{N}$ )	[Ca <sup>2+</sup> ] ( $\mu\text{N}$ )	Total [Fe] ( $\mu\text{g/l}$ )	Total [Mn] ( $\mu\text{g/l}$ )	H <sub>2</sub> O <sub>2</sub> (ppbV)	S(IV) ( $\mu\text{M}$ )	HCHO ( $\mu\text{N}$ )
12/18/00	3.6	15.4	3.9	6.9	21.0	215.0	5.3	0.2	1.3	12.9
12/19/00	4.5	11.3	3.4	5.7	10.2	153.8	9.4	0.02	1.5	16.8
1/10/01	9.1	12.1	5.8	4.6	10.4	105.5	4.7	0.1	5.9	20.8
1/15/01	10.6	17.7	3.2	4.4	5.8	16.9	0.9	0.01	--	9.1
1/17/01	3.1	15.7	5.3	4.8	12.3	50.7	2.5	0.2	3.2	16.8
1/21/01	4.8	19.0	11.8	5.9	15.2	168.1	7.2	0.0	5.2	20.8
1/25/01	14.9	20.0	2.3	5.6	7.2	50.1	2.9	0.1	0.4	6.7
1/31/01	9.3	21.5	5.8	5.3	7.1	64.2	3.2	0.1	3.0	40.7
2/1/01	16.8	39.5	17.2	8.1	32.5	325.6	16.0	N/A	4.9	40.4
Total Average	8.5	19.1	6.5	5.7	13.5	127.8	5.8	0.1	3.2	20.6

-- means the concentrations were below detection limits or not detected

Table 3-3 lists the volume-weighted average concentrations of major ions and species for all the CRPAQS Angiola fog events. The concentrations of species for each fog episode were normalized by the sample weight of all samples (CASCC fog samples were

used to calculate the concentrations of inorganic species, while ss-CASCC samples were used to calculate the concentrations of organic species), then CRPAQS study average concentrations of species were obtained by averaging the mass weighted concentration over all the fog events.

Table 3-4 Summary of bulk fog sample composition

Species	Number of samples	Concentration Range	Median
pH (pH units)	36	5.85-8.04	6.73
Cl <sup>-</sup> (μN)	36	10.5-39.8	16.3
NO <sub>3</sub> <sup>-</sup> (μN)	36	78.1-1872.1	303.5
NO <sub>2</sub> <sup>-</sup> (μN)	36	4.7-131.9	17.7
SO <sub>4</sub> <sup>2-</sup> (μN)	36	12.9-329.5	56.5
Formate (μN)	22	14.9-120.7	31.6
Acetate (μN)	22	5.0-197.2	31.4
Propionate (μN)	22	ND <sup>a</sup> -10.4	1.7
Pyruvate (μN)	22	ND-0.7	0.7
Oxalate (μN)	22	3.2-24.9	7.2
Na <sup>+</sup> (μN)	36	0.13-22.5	5.8
K <sup>+</sup> (μN)	36	1.9-18.6	4.3
NH <sub>4</sub> <sup>+</sup> (μN)	36	193.2-2203.7	608.3
Mg <sup>2+</sup> (μN)	36	4.2-24.8	5.3
Ca <sup>2+</sup> (μN)	36	5.6-101.5	10.7
HCHO (μM)	36	2.6-49.3	21
Fe (μg l <sup>-1</sup> )	24	16.9-341.9	77.5
Mn (μg l <sup>-1</sup> )	24	0.9-16.5	4.1
TOC (ppmC)	22	2.3-41.9	6.9

ND<sup>a</sup> Not detected- the response was below the detection limit for this species.

Similar to Table 3-3, Table 3-4 shows the concentration ranges of all measured species in bulk fog samples collected at Angiola. It shows that species with the highest concentrations include ammonium, nitrate, sulfate, nitrite, formate, acetate and formaldehyde.

Based on Table 3-3, Figure 3-21 shows a pie diagram of average sample composition for the SJV fogs. The dominant species measured were ammonium, nitrate, nitrite, sulfate, formate, and acetate, consistent with previous studies in the SJV (e.g., Collett et al., 1999). The ammonium concentration is comparable with the average measured in fog samples collected in the 1995 Integrated Monitoring Study (IMS95), 815  $\mu\text{N}$  vs. 1087  $\mu\text{N}$ . The average nitrate concentration is about six times higher than the sulfate concentration, also consistent with IMS95 observations.

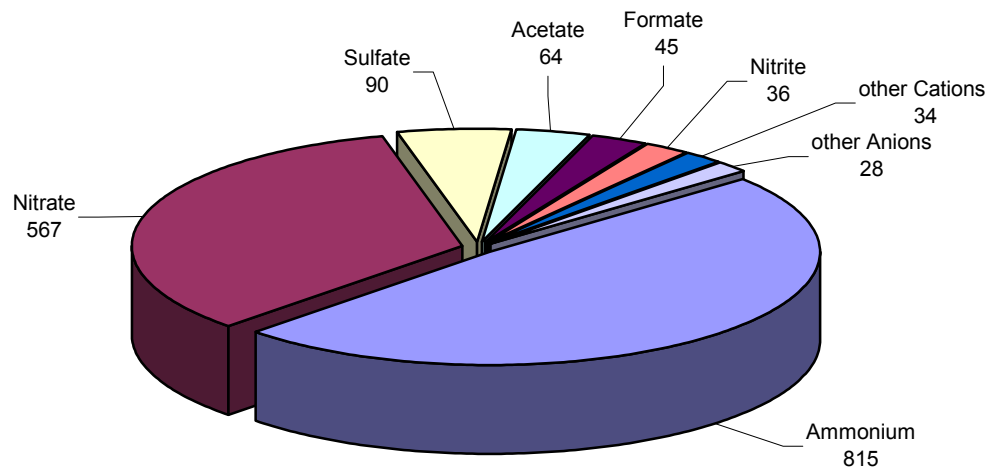


Figure 3-21. Measured composition for Angiola fog episodes during winter 2000/2001. All concentrations are listed as  $\mu\text{N}$ . Other cations include sodium, potassium, calcium, magnesium and  $\text{H}^+$ . Other anions include chloride, propionate, pyruvate and oxalate.

From Table 3-3 and Figure 3-21, we can roughly calculate the charge balance for each episode and the total balance for all CRPAQS fog events. A liquid solution should be electrically neutral, with the positive and negative charged ions balanced. For our fog samples, the electrical balance equation is roughly as follows (concentration unit:  $\mu\text{N}$ ):

$$[\text{H}^+] + [\text{NH}_4^+] = [\text{OH}^-] + [\text{NO}_3^-] + [\text{SO}_4^{2-}] + [\text{NO}_2^-] + [\text{Formate}] + [\text{Acetate}] \quad (3-2)$$

Because formate and acetate are weak organic acids (formic acid  $pK_a=3.75$ ; acetic acid  $pK_a = 4.75$ ), they will not be fully ionized at a lower pH environment. For our samples since the pH value ranges from 6.0 to 8.02, averaging 6.78, the portion of unionized form of formate and acetate is very small thus can be ignored in the charge balance equation.

Taking account of the major anions (nitrate, sulfate, nitrite, formate, acetate) and major cations (ammonium and hydrogen concentrations), Figure 3-22 shows a comparison of total major cation concentrations vs. total major anion concentrations in the fog water. Total cation concentrations were slightly higher than total anion concentrations, possibly because other anions, such as higher molecular weight organic acids and bicarbonate, were not counted in the equation. Overall, cation concentrations were only about 8% higher than anion concentrations. Typically a charge balance within 10% is assumed to be quite good for fog composition measurements, even when all species are quantified.

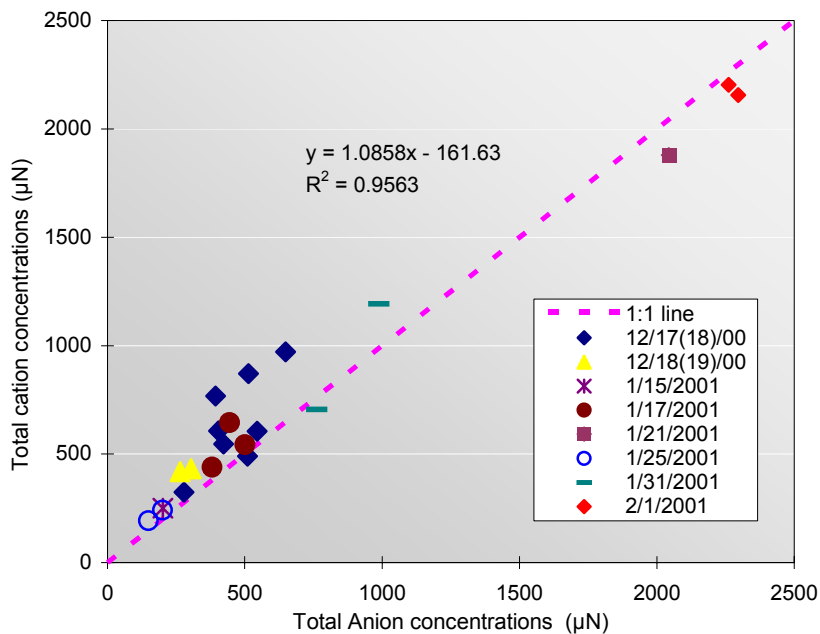


Figure 3-22. Total cation concentrations vs. total anion concentrations.

### 3.5 Drop size dependent fog composition

### 3.5.1 pH and inorganic species

Figures 3-23 to Figure 3-34 plot the large vs. small drop pH and concentrations of inorganic species including  $\text{Cl}^-$ ,  $\text{NO}_3^-$ ,  $\text{SO}_4^{2-}$ ,  $\text{NH}_4^+$ ,  $\text{Na}^+$ ,  $\text{K}^+$ ,  $\text{Mg}^{2+}$ ,  $\text{Ca}^{2+}$ , Fe, Mn and  $\text{NO}_2^-$  for all fog events. Samples were collected with 2-stage sf-CASCC. Figures 3-35 to Figure 3-40 show the large vs. small drop concentrations of organic species including HCHO, TOC, formate, acetate, propionate and oxalate for all fog events. Samples for organic analysis were collected by the ss-sf-CASCC. Different fog events are shown as different colors. An error bar is plotted based on the analytical RSD of each species reported in chapter two.

From Figure 3-10, the timeline of pH values in the fog events, we know that pH values were a little bit alkaline (relative to equilibrium with atmospheric  $\text{CO}_2$ , which is about pH 5.6), and unlike previous SJV fog studies (e.g., Moore et al., 2004a,b) in an urban area, our pH values of large and small droplets didn't show much difference.

For inorganic species, significant chemical concentration differences were seen between large and small drop fractions. Chloride, ammonium, sulfate, nitrate, potassium, manganese, calcium and TOC were all enriched in smaller drops; total Fe and Mn showed no preference of enrichment; nitrite was enriched in larger drops. This size dependence is consistent with patterns observed previously in SJV fogs (Collett et al., 1999).

For organic species, formic acid showed a weak trend of enrichment in small drops. Formic acid enriched in small drops in most samples, but enrichment is seen in large drops in some samples as well. Acetic acid shows the same trend as formic acid. Additional analysis of the size-dependence of these low molecular weight carboxylic acids was conducted and has been published (Ervens et al., 2003, included as Appendix D).

Propionate didn't show any preferred size distribution. It is almost evenly distributed along the 1:1 line with no significant enrichment in large and small drops. Oxalate is the only di-acid that we measured, and shows very strong enrichment in small drops.

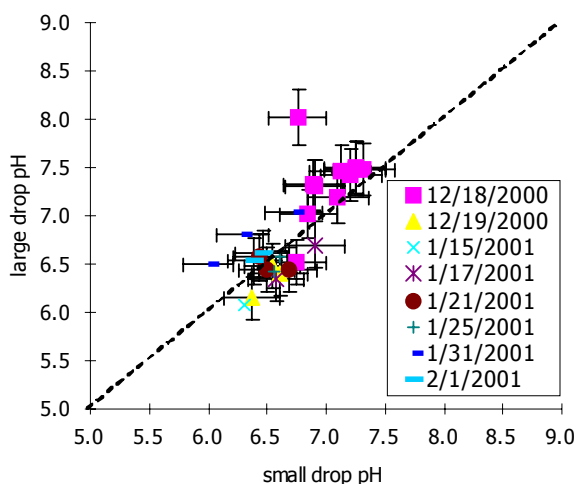


Figure 3-23. Large vs. small drop pH for all fog events of CRPAQS. Error bars represent analytical RSD listed in chapter two.

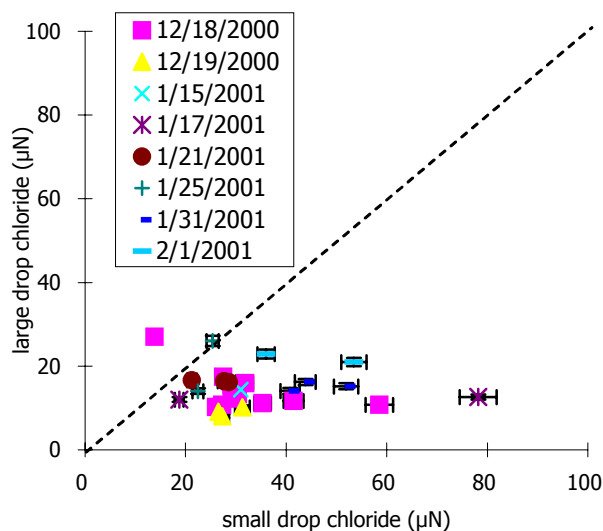


Figure 3-24. Large vs. small drop  $\text{Cl}^-$  concentrations for all fog events of CRPAQS. Error bars represent analytical RSD listed in chapter two.

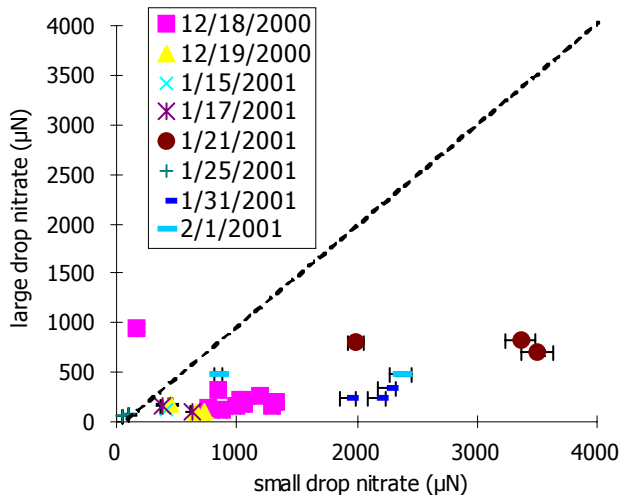


Figure 3-25. Large vs. small drop  $\text{NO}_3^-$  concentrations for all fog events of CRPAQS. Error bars represent analytical RSD listed in chapter two.



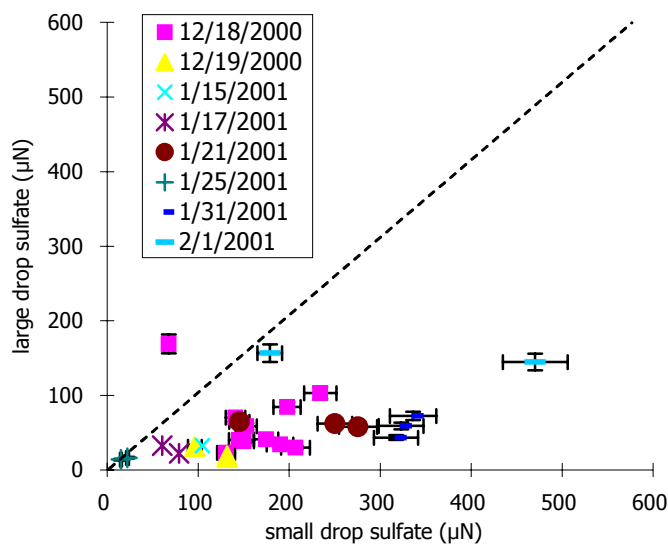


Figure 3-26. Large vs. small drop  $\text{SO}_4^{2-}$  concentrations for all fog events of CRPAQS. Error bars represent analytical RSD listed in chapter two.

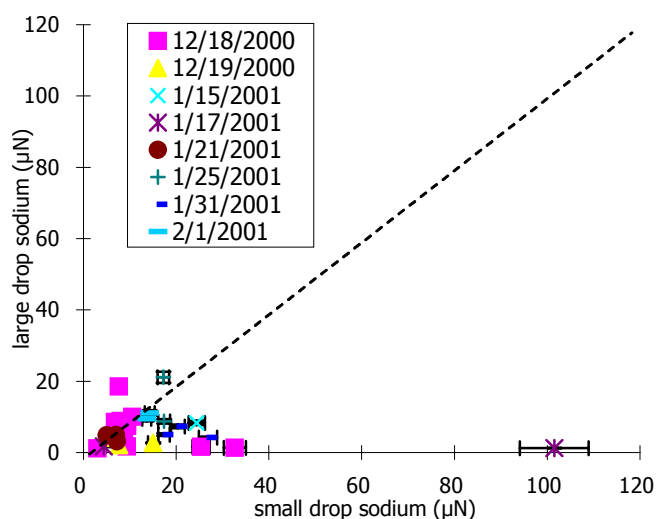


Figure 3-27. Large vs. small drop  $\text{Na}^+$  concentrations for all fog events of CRPAQS. Error bars represent analytical RSD listed in chapter two.

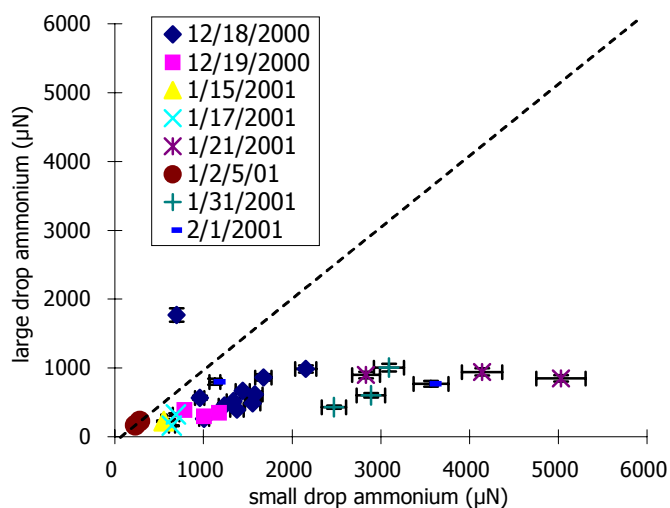


Figure 3-28. Large vs. small drop  $\text{NH}_4^+$  concentrations for all fog events of CRPAQS. Error bars represent analytical RSD listed in chapter two.

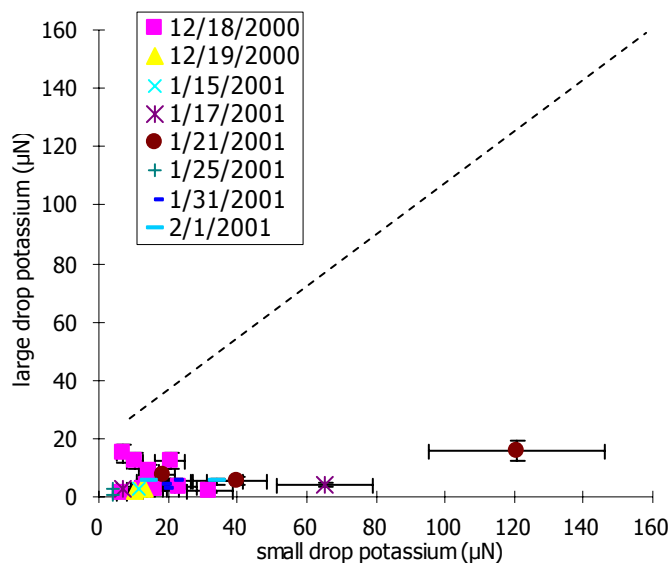


Figure 3-29. Large vs. small drop  $\text{K}^+$  concentrations for all fog events of CRPAQS. Error bars represent analytical RSD listed in chapter two.

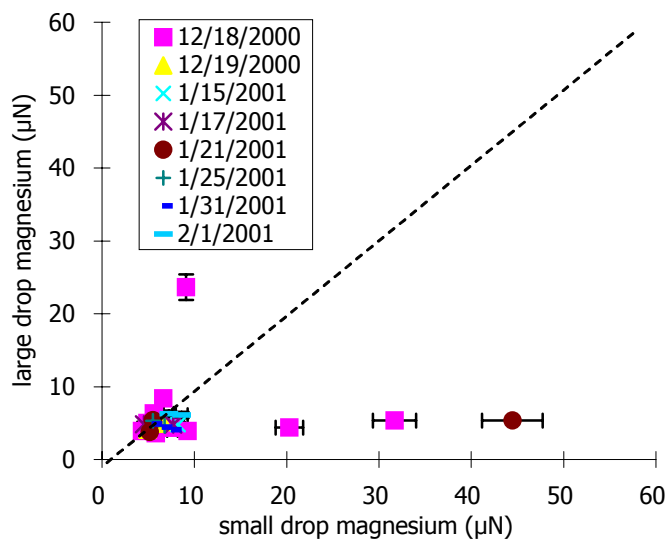


Figure 3-30. Large vs. small drop  $\text{Mg}^{2+}$  concentrations for all fog events of CRPAQS. Error bars represent analytical RSD listed in chapter two.

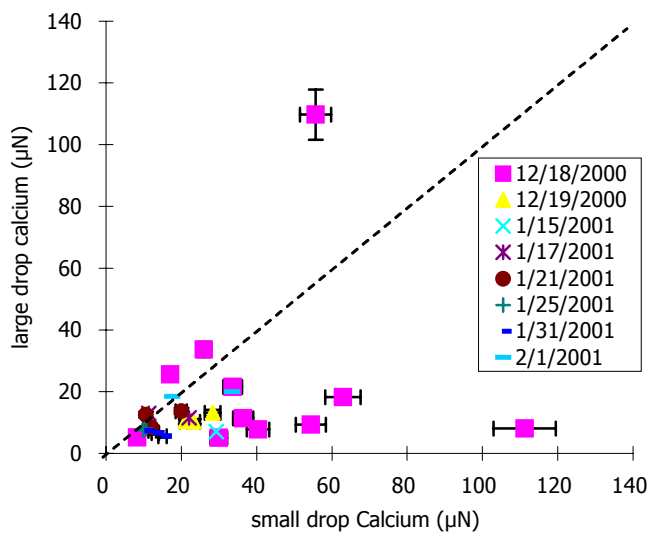


Figure 3-31. Large vs. small drop  $\text{Ca}^{2+}$  concentrations for all fog events of CRPAQS. Error bars represent analytical RSD listed in chapter two.

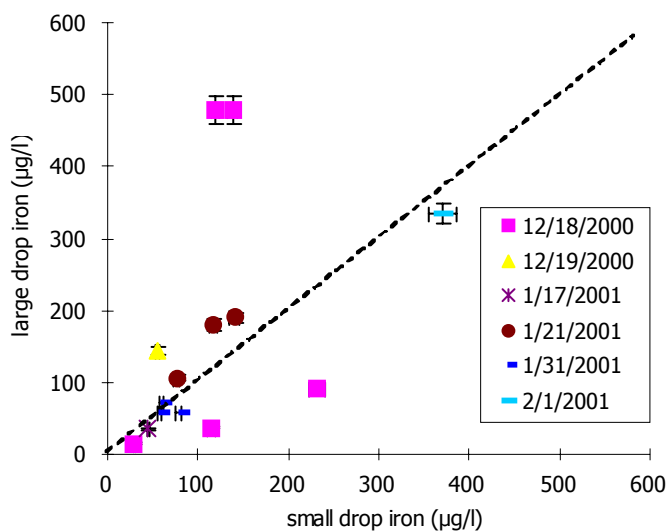


Figure 3-32. Large vs. small drop total Fe concentrations for all fog events of CRPAQS. Error bars represent analytical RSD listed in chapter two.

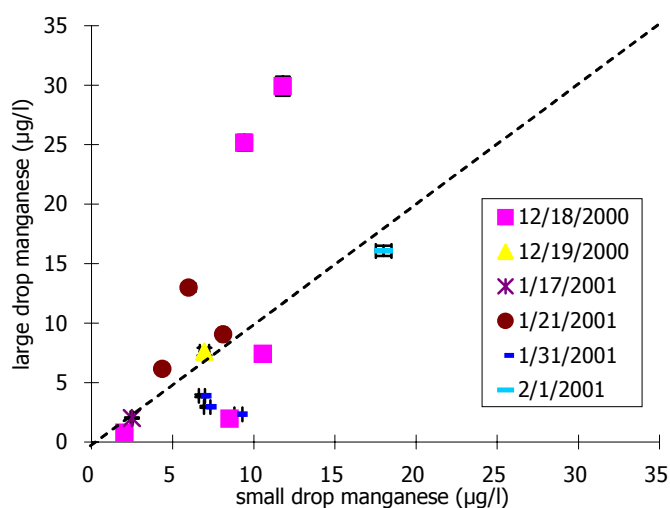


Figure 3-33. Large vs. small drop total Mn concentrations for all fog events of CRPAQS. Error bars represent analytical RSD listed in chapter two.

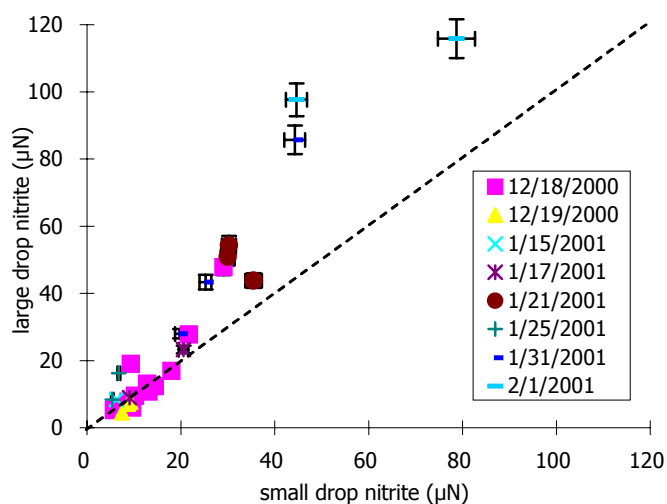


Figure 3-34. Large vs. small drop  $\text{NO}_2^-$  concentrations for all fog events of CRPAQS. Error bars represent analytical RSD listed in chapter two.

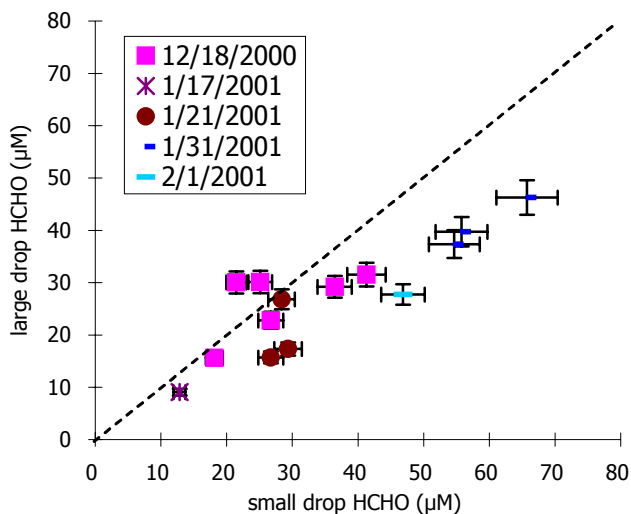


Figure 3-35. Large vs. small drop HCHO concentrations for all fog events of CRPAQS. Error bars represent analytical RSD listed in chapter two.

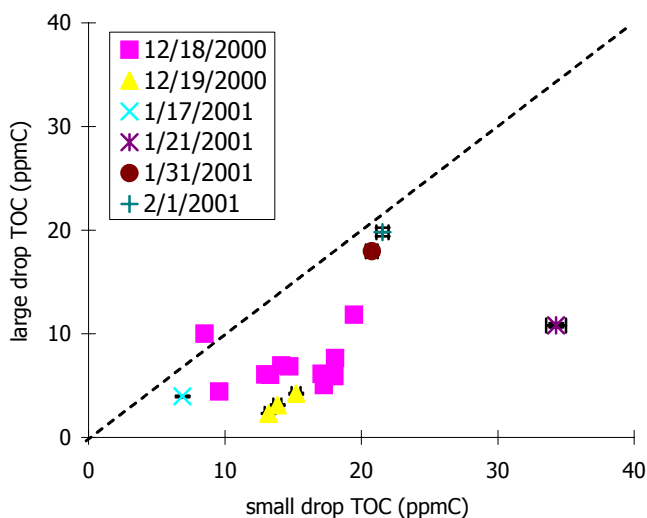


Figure 3-36. Large vs. small drop TOC concentrations for all fog events of CRPAQS. Error bars represent analytical RSD listed in chapter two.

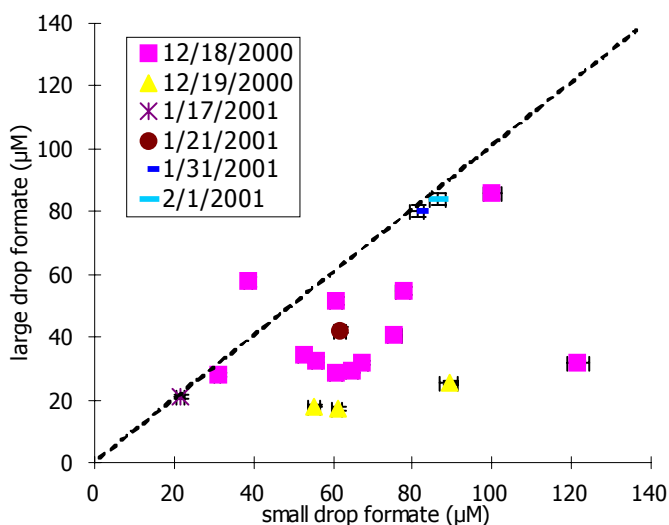


Figure 3-37. Large vs. small drop formate concentrations for all fog events of CRPAQS. Error bars represent analytical RSD listed in chapter two.

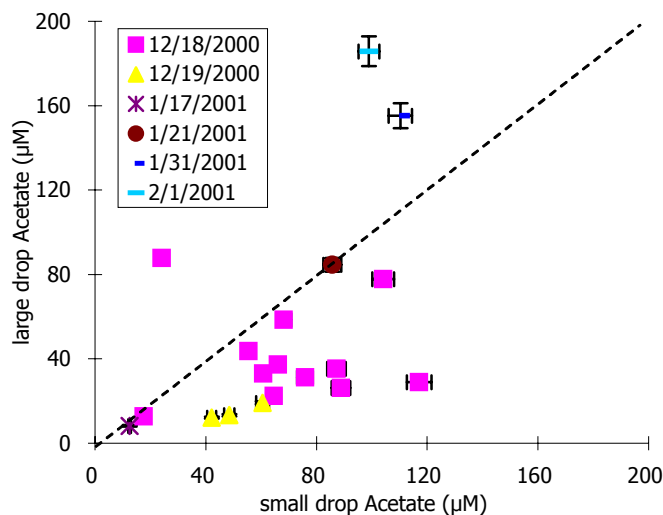


Figure 3-38. Large vs. small drop acetate concentrations for all fog events of CRPAQS. Error bars represent analytical RSD listed in chapter two.

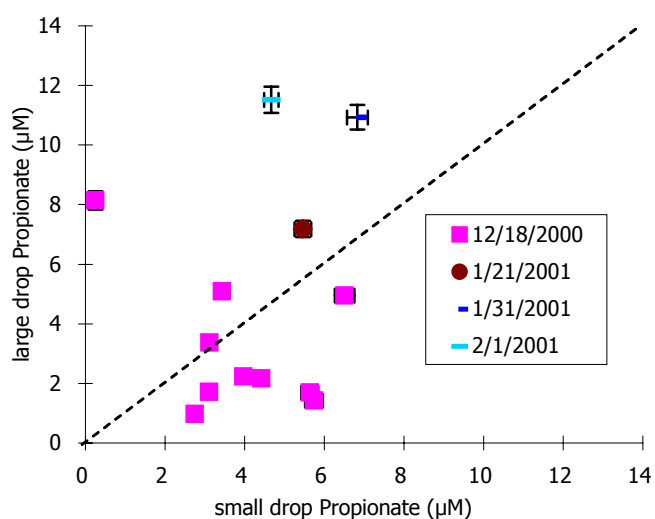


Figure 3-39. Large vs. small drop propionate concentrations for all fog events of CRPAQS. Error bars represent analytical RSD listed in chapter two.

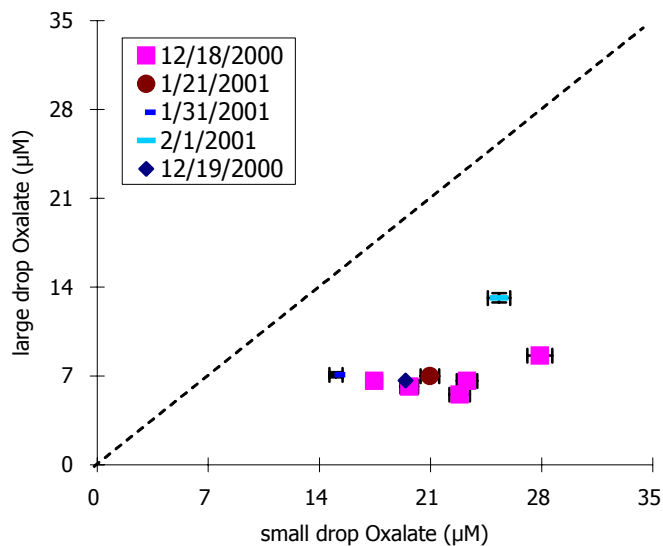


Figure 3-40. Large vs. small drop oxalate concentrations for all fog events of CRPAQS. Error bars represent analytical RSD listed in chapter two.

### 3.5.2 Size distributions from the CSU 5-stage collector

The CSU 5-stage collector was used to get more detailed size distribution information of fog drop composition. Figure 3-41 shows the pH value size distribution from the 5 stage collector for samples collected in the events of 12/18&12/19/00, 01/17/01 and 01/31/01 respectively. The pH values ranges from 6.32 to 7.11, averaging 6.7 for these three events, consistent with bulk fog samples pH values. For fog events 12/19/00 and 1/31/01, we don't see a significant difference of pH with drop size; for the fog event on 1/17/2001, the pH value appears slightly higher in intermediate sized drops. Figures 3-42 to 3-44 show ammonium nitrate, nitrite and sulfate concentrations for the same three fog events. Ammonium and nitrate concentrations showed very strong size dependence; sulfate also exhibited a large composition difference between large and small drops. Nitrite showed less size dependence than the other three ions, consistent with the results from the 2 stage sf-CASCC.

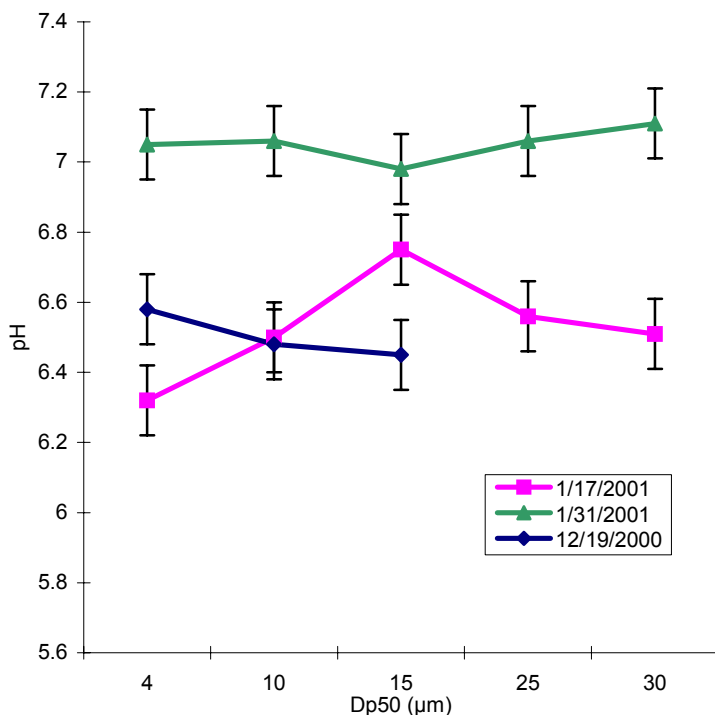


Figure 3-41. pH value vs. theoretical  $Dp_{50}$  of the 5-stage collector.

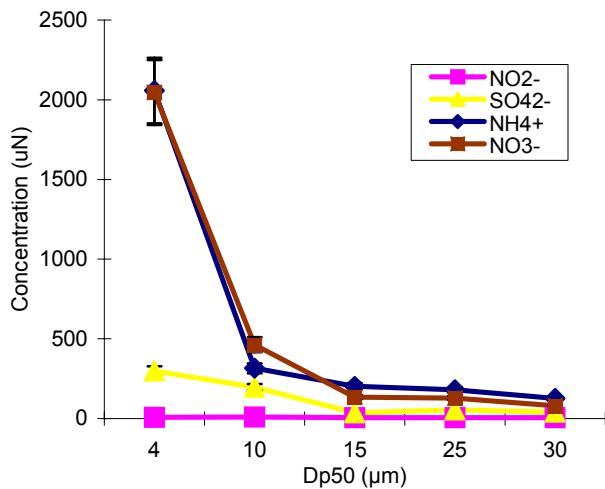


Figure 3-42. Major ion concentrations vs. theoretical  $Dp_{50}$  of 5-stage collector on day 01/17/01.

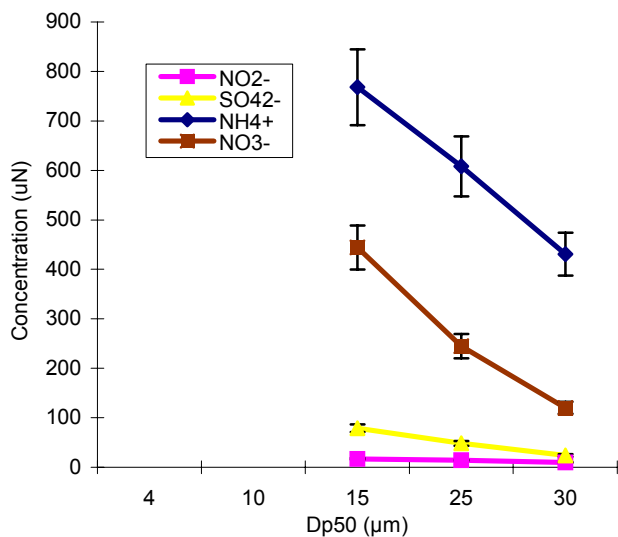


Figure 3-43. Major ion concentrations vs. theoretical  $Dp_{50}$  of 5-stage collector on day 12/19/00.

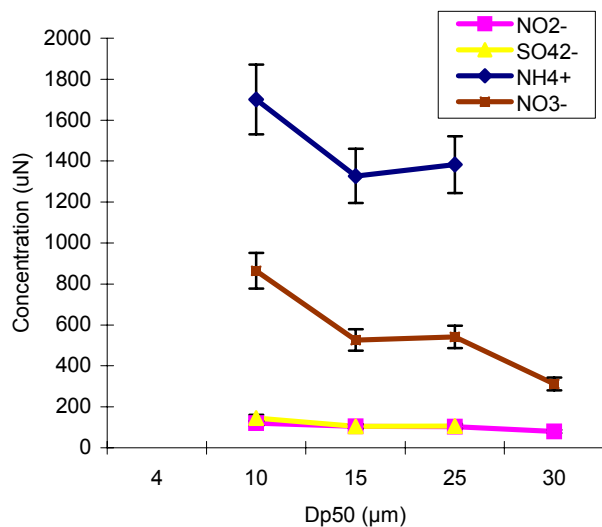


Figure 3-44. Major ion concentrations vs. theoretical  $Dp_{50}$  of 5-stage collector on day 01/31/01.

### 3.6 Fog observations at the satellite sites

During the 2000/2001 CRPAQS fog project, CSU collected fog samples at 4 locations in the San Joaquin Valley. The core sampling site for the fog study was located close to the town of Angiola (N35°35',W119°32', 60 m asl); satellite collection sites have been established in Bakersfield (N35°21',W119°3', 119 m asl), close to the town of Helm (N36°5',W120°10', 55 m asl), and in McKittrick. The Angiola, McKittrick and Helm sites had agricultural background characteristics, whereas the Bakersfield site was located in the center of town, on the parking lot of a small shopping mall.

The sampling sites have been chosen during a visit in fall of 2000. The satellite sites have been chosen because of their distribution across the valley and based on logistics (protected area, power and phone availability). The sites of Bakersfield and McKittrick in the southern valley were selected, in part, to provide a comparison with fog studies at those locations in prior years. The site of Helm was the most convenient in a rural location in the northern part of the San Joaquin Valley.

Table 3-5. Overview of satellite site fog sampling during CRPAQS

Location	Collector	Active period	Number of samples
Helm	CASCC2	12/5/00-1/31/01	6
Bakersfield	CASCC2	1/18/00-1/31/01	1
McKittrick	CASCC2	12/6/00-1/18/01	0

The three remotes sites were each equipped with an automated fogwater collection system comprised of a Caltech Active Strand Cloudwater Collector version 2, known as a



CASCC2 (Demos et al., 1996), a CSU optical fog detector (CSU-OFD), a relative humidity sensor, a temperature sensor and a Campbell datalogger (Figure 3-45). A detailed Standard Operating Procedure (SOP) was prepared by CSU in advance of the CRPAQS winter intensive for operation of these new fog collection systems. The OFD was developed in part with support from CRPAQS. Appendix A provides a complete description of the OFD and its evaluation in SJV fogs and other environments. Table 3-5 gives an overview of the monitoring dates and number of event samples collected for each satellite location (and for Angiola as a comparison). The most fog was observed at Helm.

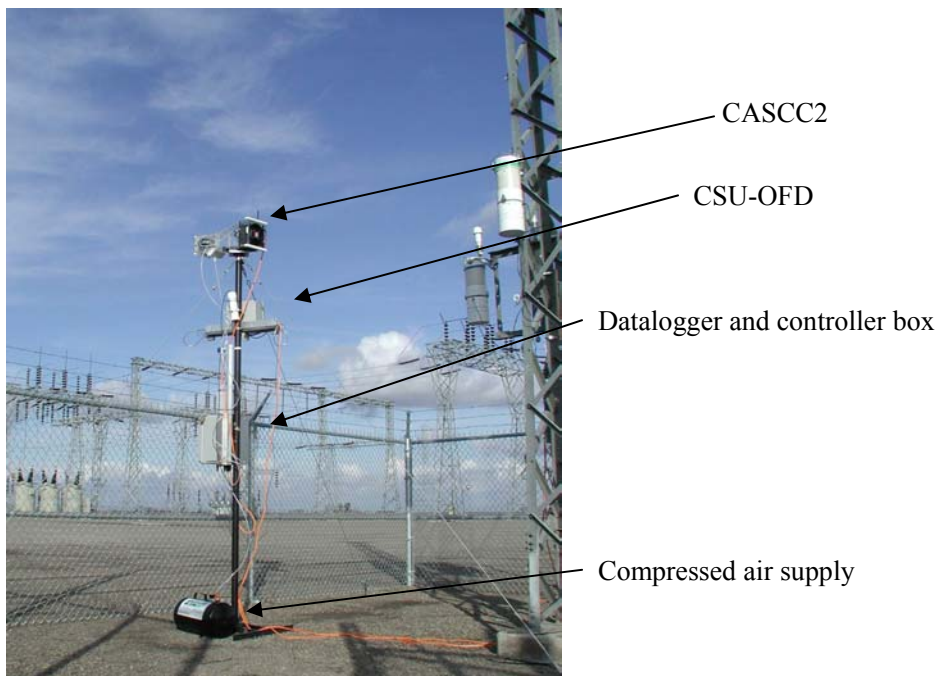


Figure 3-45. Remote site automated fog sampling set-up.

### 3.6.1. Helm

The Helm site was operational from December 5<sup>th</sup> 2000 until January 31<sup>st</sup> 2001. It was collocated with an electrical installation and had a standard set-up (figure 3-46). At this

site no phone line was available so the automated fogwater collector was not equipped with a modem. Sample retrieval and maintenance were performed at regular intervals. During the study period, 6 event samples were collected. Table 3-6 gives an overview of the selected samples.



**Figure 3-46.** Set-up at the Helm site, left: sampling system, right: location

**Table 3-6.** Overview of collected samples at Helm

Date	Sampling		Duration (min)	Volume (ml)
	Start	End		
12/17/00	2:30	9:35	425	284
12/19/00	4:55	6:00	65	37.5
12/31/00	8:55	9:45	50	27.9
01/01/01	2:40	4:00	80	98.2
01/02/01	5:40	9:15	215	90
01/10/01	5:00	7:05	125	12

**Table 3-7.** Chemical composition of samples collected in Helm

	pH	Cl <sup>-</sup> μeq/L	NO <sub>3</sub> <sup>-</sup> μeq/L	NO <sub>2</sub> <sup>-</sup> μeq/L	SO <sub>4</sub> <sup>2-</sup> μeq/L	Na <sup>+</sup> μeq/L	NH <sub>4</sub> <sup>+</sup> μeq/L	K <sup>+</sup> μeq/L	Mg <sup>2+</sup> μeq/L	Ca <sup>2+</sup> μeq/L	TOC mgC/L
12/17/00	6.43	15.4	363	14.1	87	6	646	5.1	5.4	7.6	6.96
12/19/00	6.74	47	335	27.8	1411	10.8	1789	15.6	10.1	15.5	7.90
12/31/00	6.9	12.2	773	24.2	71	3.66	1105	5.2	5.3	6.2	11
01/01/01	6.95	17.4	898	25.7	71	2.84	1195	5.2	5.7	6.2	16.7
01/02/01	7.03	13	1110	14.4	91	3.65	1597	6.8	4.8	5	16.3
01/10/01	6.7	13.7	222	34.1	45	8.01	445	9.3	6.7	9.1	9.14
	pH	Cl <sup>-</sup>	NO <sub>3</sub> <sup>-</sup>	NO <sub>2</sub> <sup>-</sup>	SO <sub>4</sub> <sup>2-</sup>	Na <sup>+</sup>	NH <sub>4</sub> <sup>+</sup>	K <sup>+</sup>	Mg <sup>2+</sup>	Ca <sup>2+</sup>	TOC
min	6.43	12.2	222	14.1	45	2.8	445	5.1	4.8	5	6.96
max	7.03	47	1110	34.1	1411	13.7	1789	15.6	10.1	15.5	16.7
median	6.82	14.6	568	25	79	4.8	1150	6.1	5.6	6.9	10.1
average	6.79	19.8	617	23.6	296	6.8	1129	7.9	6.3	8.2	11.3

The results of the chemical composition are given in table 3-7. The major ions are ammonium and nitrate and the pH is rather high (6.8 on average). These results are consistent with prior observations in the San Joaquin Valley. What is rather surprising is the second event (12/19/00), which shows a very high concentration of sulfates, atypical for this site and much higher than in other samples. We don't have a clear explanation for this observation. Another striking observation is the very high Cl/Na ratio. This ratio averages 3.6(1.7-6.1) and is consistently higher than the sea salt ratio of 1.13. This may indicate a source of chloride other than sea salt. We have nevertheless to be cautious as sodium and chloride concentrations are close to their detection limits.

Table 3-8 shows a species concentration correlation matrix for major ions in Helm fog samples. A detailed interpretation is difficult due to the small number of samples. It is nevertheless interesting that TOC, acidity and nitrogen species are not well correlated to anything.  $\text{Cl}^-$  is not correlated to  $\text{Na}^+$ , which seems to confirm the observation of their ratios that  $\text{Cl}^-$  has a different source. The correlation of Mg and Ca with  $\text{SO}_4^{2-}$  is difficult to interpret and could be due simply to covariance with LWC. The correlation of  $\text{Mg}^{2+}$ ,  $\text{Ca}^{2+}$  and  $\text{K}^+$  might be the result of a common soil origin.

Table 3-8. Correlation matrix for Helm fog components (in bold, significant at 99%)

	H+	Cl-	NO <sub>2</sub> -	NO <sub>3</sub> -	SO <sub>4</sub> =	Na+	NH <sub>4</sub> +	K+	Mg <sup>++</sup>	Ca <sup>++</sup>	TOC
H+	<b>1</b>										
Cl-	0.038	<b>1</b>									
NO <sub>2</sub> -	-0.242	0.333	<b>1</b>								
NO <sub>3</sub> -	-0.693	-0.388	-0.495	<b>1</b>							
SO <sub>4</sub> =	0.009	<b>0.990</b>	0.306	-0.368	<b>1</b>						
Na+	0.378	0.765	0.492	-0.821	0.774	<b>1</b>					
NH <sub>4</sub> +	-0.557	0.598	-0.152	0.483	0.633	0.063	<b>1</b>				
K+	-0.043	0.895	0.530	-0.500	0.915	0.892	0.457	<b>1</b>			
Mg <sup>++</sup>	0.074	<b>0.951</b>	0.571	-0.586	<b>0.940</b>	0.887	0.388	<b>0.955</b>	<b>1</b>		
Ca <sup>++</sup>	0.223	<b>0.928</b>	0.515	-0.685	<b>0.923</b>	<b>0.937</b>	0.296	<b>0.937</b>	<b>0.986</b>	<b>1</b>	
TOC	-0.773	-0.362	-0.201	0.900	-0.384	-0.742	0.372	-0.412	-0.483	-0.617	<b>1</b>

### 3.6.2 McKittrick

The site of McKittrick was equipped with a fog sampling system from December 6<sup>th</sup> to January 18<sup>th</sup> (figure 3-47). During this period no fog event occurred at this site. The site was dismantled on January 18<sup>th</sup> as the equipment was moved to the Bakersfield site because this site where fog was more likely. The absence of fog at McKittrick was

somewhat unexpected because the location was chosen to compare results with a previous study, which took place in this location (Jacob et al., 1986).



Figure 3-47. Sampling set-up in McKittrick -- left: sampler, right: location

### **3.6.3. Bakersfield**

The Bakersfield site was first installed on December 10<sup>th</sup>. Unfortunately numerous problems related to the sampling equipment, more specifically, the data logger and control unit prevented correct operation. Therefore on January 18, the fully functional sampler from McKittrick was moved to Bakersfield (figure 3-48). We experienced only one single fog event on the morning of January 31<sup>st</sup>. The composition of this sample is reported in Table 3-9. The site was dismantled on January 31<sup>st</sup>.



Figure 3-48. Sampling set-up in Bakersfield. Right: sampler, left: location

Table 3-9. Chemical composition of the fog sample collected in Bakersfield

Sample	pH	Cl <sup>-</sup>	NO <sub>3</sub> <sup>-</sup>	NO <sub>2</sub> <sup>-</sup>	SO <sub>4</sub> <sup>2-</sup>	Na <sup>+</sup>	NH <sub>4</sub> <sup>+</sup>	K <sup>+</sup>	Mg <sup>2+</sup>	Ca <sup>2+</sup>	TOC
-----μN-----											mgC/L
3101	6.61	36.7	446	315	872	29.98	1716	20.8	11.3	41.85	26.65

#### 3.6.4. Angiola

As part of operations at Angiola, we operated an OFD and a ground-based aluminum version of the CASCC2 to provide a fog composition comparison between Angiola and the three satellite fog sampling sites. The ground instrumentation was operational from December 10<sup>th</sup> 2000 to February 2<sup>nd</sup> 2001. A total of 27 samples were collected with the Al-CASCC2 at Angiola. Table 3-10 provides an overview of the sample composition.

Table 3-10. Composition of AI-CASCC2 samples collected at the Angiola site

	pH	Cl <sup>-</sup>	NO <sub>3</sub> <sup>-</sup>	NO <sub>2</sub> <sup>-</sup>	SO <sub>4</sub> <sup>2-</sup>	Na <sup>+</sup>	NH <sub>4</sub> <sup>+</sup>	K <sup>+</sup>	Mg <sup>2+</sup>	Ca <sup>2+</sup>	TOC
		-----μN-----									mgC/L
number	26	27	27	27	27	27	27	27	27	27	
Min	6.42	12.7	198	5.82	92.7	3.75	4315	3.8	5.7	7.3	
Max	8.05	59.5	2007	142	432	32	3238	70	39	91.8	
Median	6.96	22.9	509	27.8	190	12.4	998	7	8.2	19.4	
Average	7.0	25.6	802	40.6	201.3	13.6	1336	12.7	10.2	24.8	

### 3.6.5 Spatial variability in fog composition across the Valley

#### 3.6.5.1. Simultaneous observations

##### *Event of January 31, 2001*

On January 31<sup>st</sup>, we observed fog simultaneously at the Angiola and Bakersfield sites. And samples were collected over similar periods at the two locations. Figure 3-49 illustrates the Angiola LWC timeline along with the fog sampling periods at Angiola (with the CASCC and AI-CASCC2) and at Bakersfield (with the CASCC2).

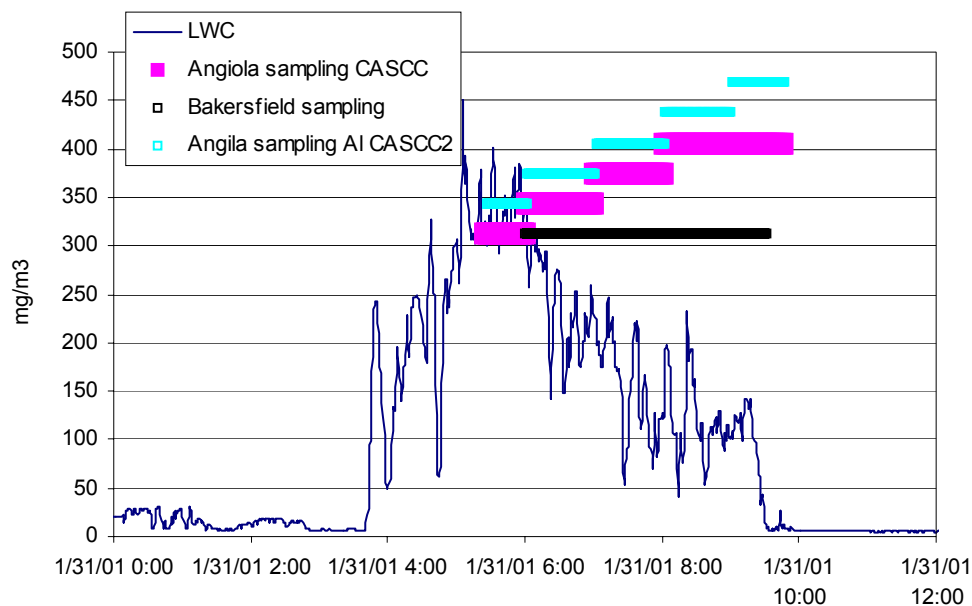


Figure 3-49. Angiola LWC and fog sampling times for the night of January 31<sup>st</sup>.

In figure 3-50, we compare the volume weighted average fog compositions of Angiola with Bakersfield. In figure 7 we plotted the major parameters time resolved on both sites. We observe similar concentrations for nitrate at the Angiola and Bakersfield site but higher concentrations for ammonium, sulfate and nitrite at the Bakersfield site. The higher concentrations of ammonium and sulfate may come from higher concentrations of ammonium sulfate aerosol at the urban location closer to oil recovery and refining operations in the southern SJV. For nitrite, higher concentrations of precursor species at the urban site may be responsible for the observation. The pH is slightly lower at the Bakersfield site but all minor ion concentrations are higher at this site. Finally the TOC observed in Bakersfield (not plotted, 26.7 ppmC) is also higher than in Angiola (15.9ppmC on average (CASCC)). No LWC data is available from Bakersfield, so it is not possible to say for sure whether LWC differences between the two sites are responsible for some of the observed concentration differences. Lower fogwater collection rates at Bakersfield during this event, however, are suggestive of a lower LWC and, hence, less dilution of fog condensation nuclei.



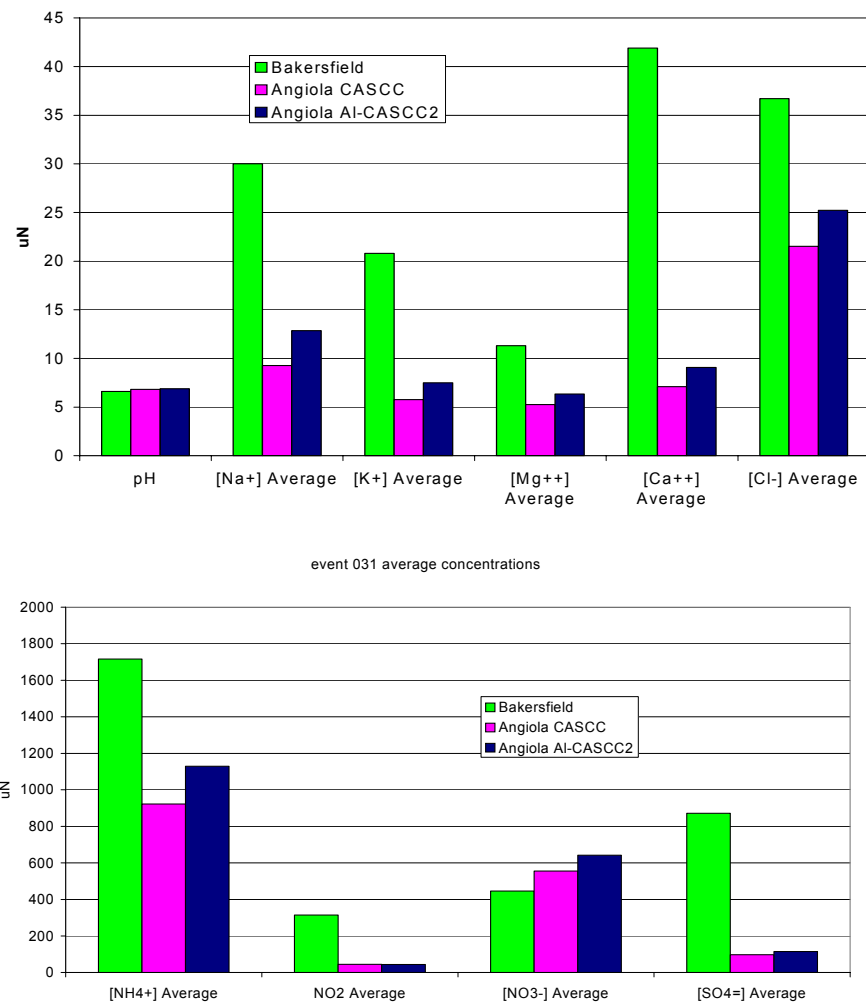


Figure 3-50. Average ion concentrations in Bakersfield and Angiola fog during the Jan. 31st event.

### *Events of December 17-19, 2000*

During the period December 17 – 19 we observed fog events at Helm and Angiola. Compositions of the fog samples collected at the two sites during this period are shown in Fig. 3-51. Concentrations at both sites are fairly similar, with the exception of ammonium and sulfate, which are somewhat higher on the morning of 12/19 at Helm.

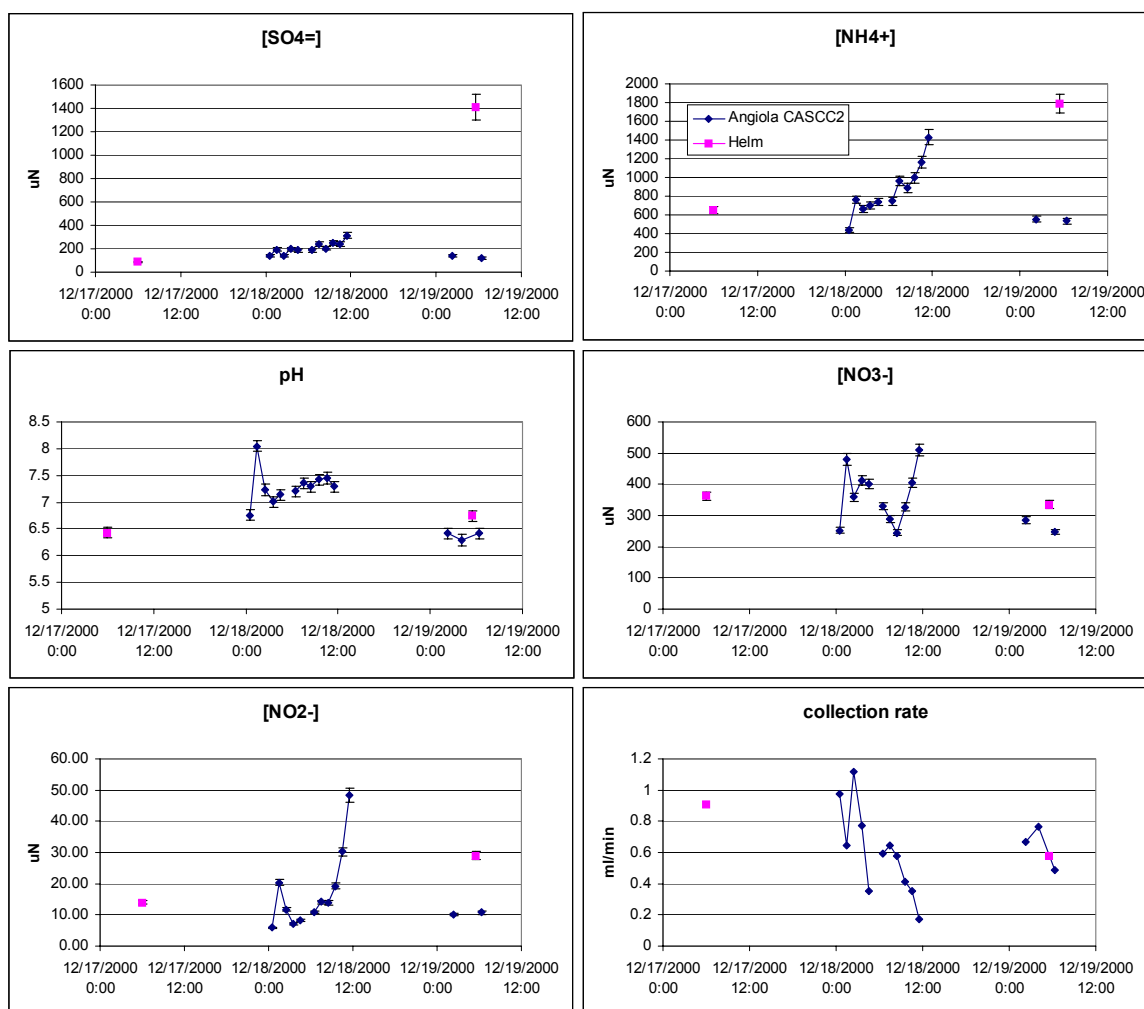


Figure 3-51. Evolution of fog concentrations in Angiola and Helm from 12/17-12/19/00.

### *Event of January 10<sup>th</sup> 2001*

On January 10<sup>th</sup> 2001, a very short fog event was observed simultaneously in Angiola and Helm. Fig. 3-52 depicts the Angiola LWC timeline and the collection periods at both sites. Fig. 3-53 compares the fog composition at both sites. The composition of samples was very similar, despite a lower fog collection rate (and presumably LWC) at Helm.

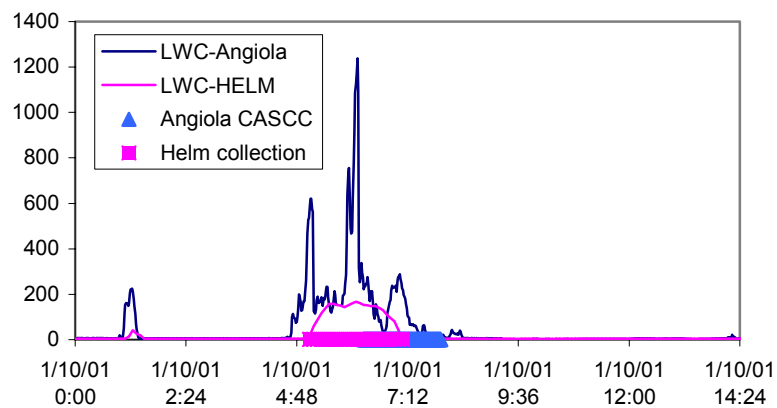


Figure 3-52. LWC and sampling times for the night of January 10<sup>th</sup>.

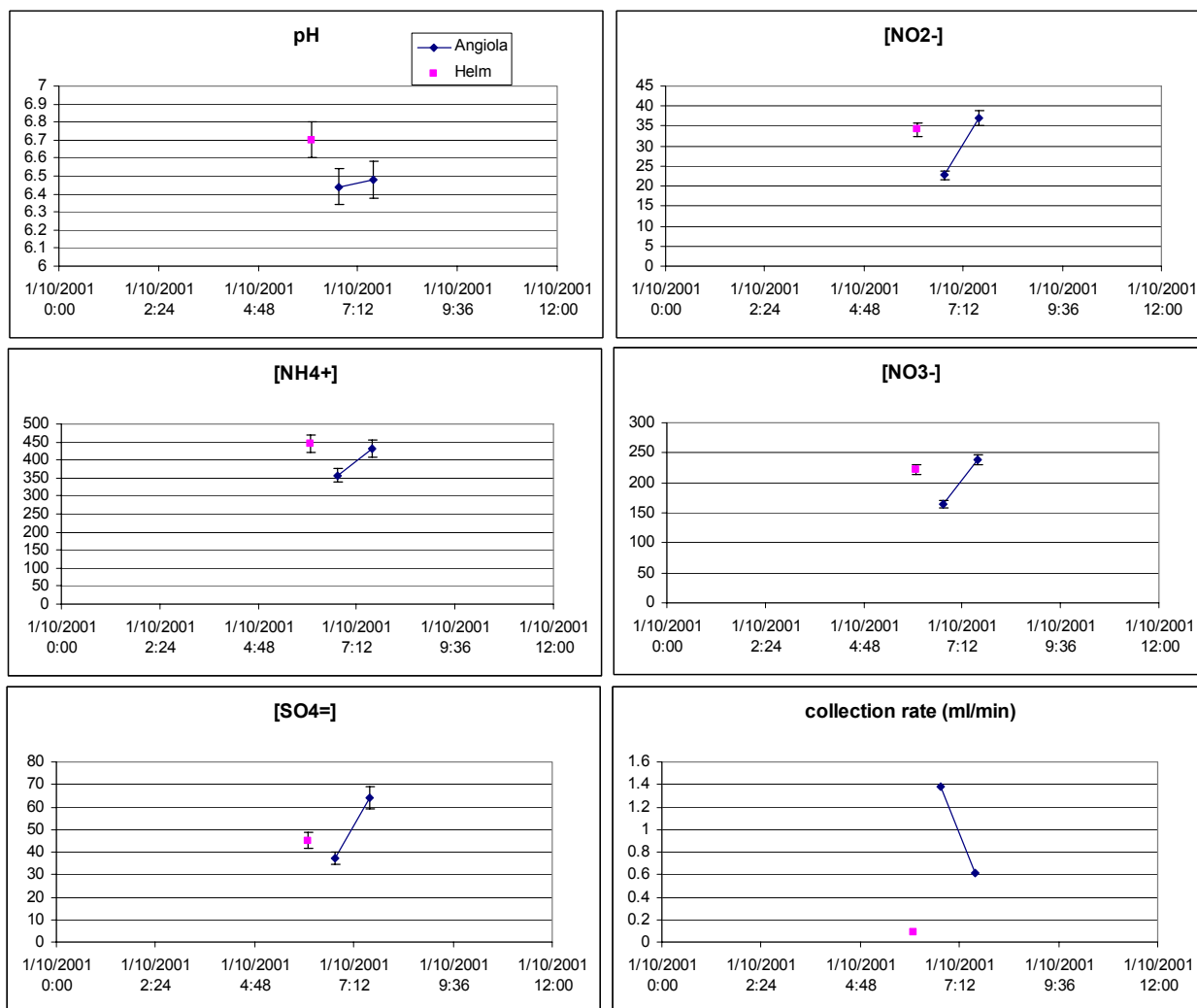


Figure 3-53. Evolution of fog concentrations in Angiola and Helm on the morning of 1/10.

### 3.6.5.2 Overall observations

Figure 3-54 compares the volume weighted average fog water composition (based on  $\mu\text{eq/L}$ ) at Angiola, Helm, and Bakersfield during the CRPAQS study.

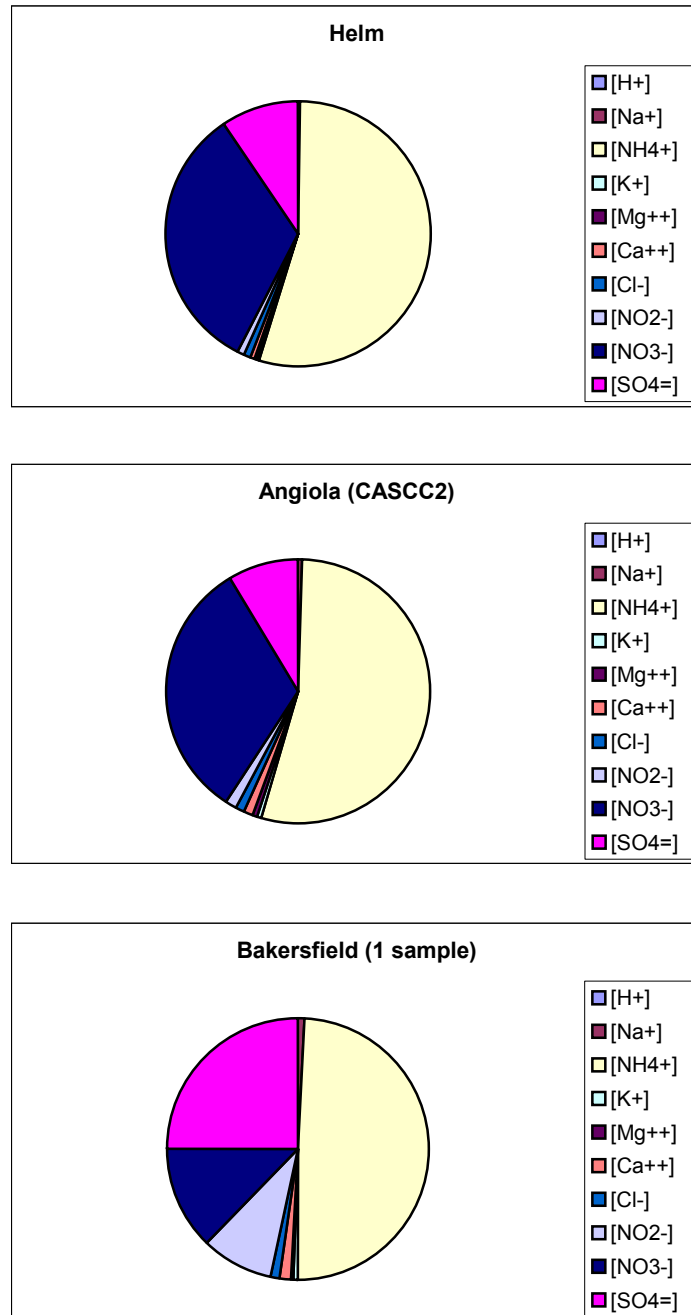


Figure 3-54. Average fog composition ( $\mu\text{eq/l}$ ) observed at three sites during CRPAQS.

We observe that ammonium is the most abundant component at all 3 sites, as reported previously for the San Joaquin Valley (e.g. Collett et al., 1999). At the rural locations, nitrate is the second most important and sulfate accounts for only 10% of the ionic composition, while nitrite concentrations are small. At the urban site, by contrast, sulfate is the second most abundant ion and nitrate and nitrite concentrations are of similar importance. Previous observations showed that fog sulfate concentrations in the Bakersfield area are higher than in other locations in the San Joaquin Valley, likely due to increased sulfur dioxide emissions associated with oil recovery and refining in the southern SJV.

Figure 3-55 compares the average fog water ion concentrations measured at all three sites during CRPAQS. The fogwater chemistry at all sites is nitrogen dominated with ammonium being the dominant species. At the more remote sites, nitrate is the second most abundant species. Sulfate is most important in Bakersfield. At this urban site, nitrite shows also higher concentrations. The pH at all 3 sites is very similar (6.6-6.9 on average) and elevated due to high ammonia concentrations in the valley.

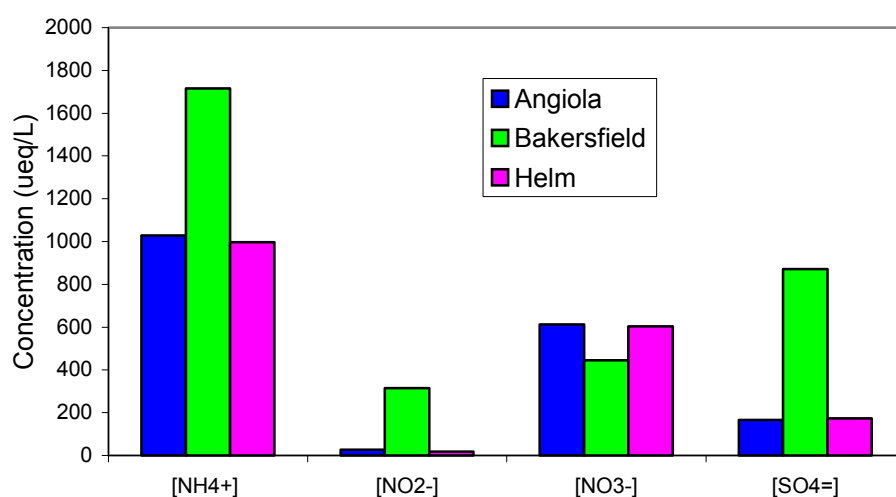


Figure 3-55a. Average major ion concentrations for Helm, Bakersfield and Angiola fog samples.

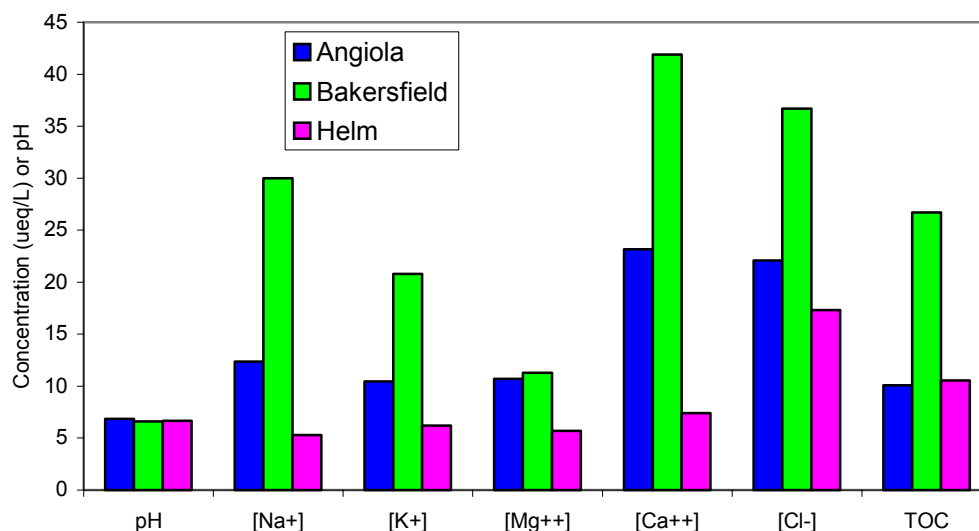


Figure 3-55b. Average minor ion concentrations and pH for Helm, Bakersfield and Angiola fog samples.

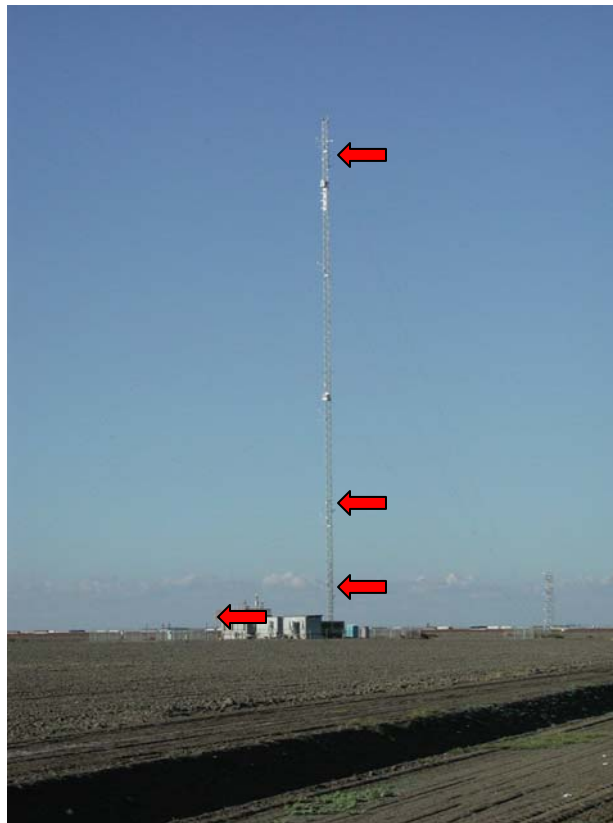
### 3.7. Fog observations on the Angiola tower

During the CRPAQS study experiments were carried out on a 100m tower to study vertical profiles of liquid water content and chemical composition of radiation fogs at the main study site in Angiola. The observation tower (Figure 3-56) at the Angiola site was equipped at 3 different levels (8m, 23m and 91m) with experimental platforms (Figure 3-57) containing:

- CSU-OFD, Optical Fog Detector (see Appendix A) to detect the presence of fog and to give a semi-quantitative measurement of Liquid Water Content LWC. The CSU-OFD's are new instruments in development. The Particle Volume Monitors (PVM) were too expensive (~25,000\$/PVM) and too heavy to deploy on the tower as originally planned.
- A data logger to log the measurements of the CSU-OFD and to control the fog collection by the fog sampler and sampling carousel.
- An aluminum version of the Caltech Active Cloudwater Collector (Al-CASCC2)

- A sampling carousel containing 10 sampling bottles, allowing the collection of 10 hourly samples

In addition a setup (AI-CASCC2, CSU-OFD, PVM), deployed on the ground on 3 m poles, collocated with other ground instruments, completed the instrumentation for vertical profiles.



**Figure 3-56.** Observation tower at the Angiola site with the 4 observation platforms at 3m, 8m, 23m and 91m.

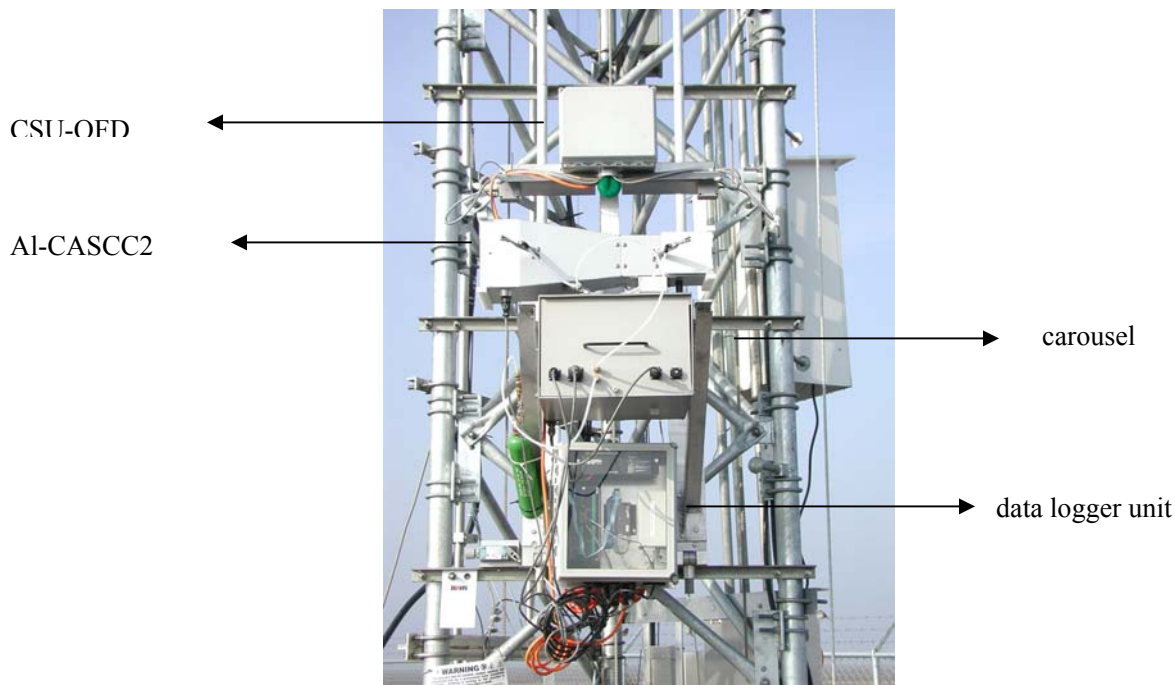


Figure 3-57. Experimental platform for fog sampling.

The experiments were operated from December 10<sup>th</sup> 2000 to February 2<sup>nd</sup> 2001. Although the set-up experienced some technical problems, due to malfunctioning data logger control modules and occasional power failures at the tower levels, a large number of LWC data could be collected. Table 3-11 gives an overview of the various collected events. In addition fog water samples were collected on 3 out of 4 levels. Unfortunately the fog experienced at the site was frequently confined to a shallow layer near the ground and only during one event (January 21<sup>st</sup> 2001) were samples collected at the middle level of the tower (23m). The confinement of the fog to lower altitudes was visually confirmed by the field operators. Results are described here only for the Jan. 21<sup>st</sup> event since that event permitted the only real look at vertical variations in fog composition.



Table 3-11. Overview of tower fog experiments with status of the CSU-OFD and number of fog samples collected at different levels.

Date		3m	8m	23m	91m
December 17/18 <sup>th</sup>		D 11	D 4	M -	D -
December 18/19 <sup>th</sup>		D 3	D 8	M -	N -
January 6 <sup>th</sup>	Freezing	D -	D -	N -	N -
January 16 <sup>th</sup>		D* -	D -	M -	M -
January 16/17 <sup>th</sup>	Freezing	D -	M -	D -	M -
January 21 <sup>st</sup>		D 4	M 3	D 4	N X
January 25 <sup>th</sup>		D* 2	M -	D -	N -
January 31 <sup>st</sup>		D 5	M 5	M -	M -
February 1 <sup>st</sup>		D 4	M 4	M -	M -

*D-fog detected, M- data missing, N- fog not detected, D\* detected by PVM*

*X-samples retrieved but not validated due to equipment malfunction.*

On the morning of January 21<sup>st</sup>, we observed some fog formation and dissipation at the ground level in the morning hours (Figure 3-58). The event is detected by both PVM and CSU-OFD on the ground. The PVM and the CSU-OFD on level 2 track very well suggesting that the dissipation occurs through all the layer up to 23m. Unfortunately no data are available on level 1. There was no fog detected on level 3 suggesting a fog layer of less than 91 m.

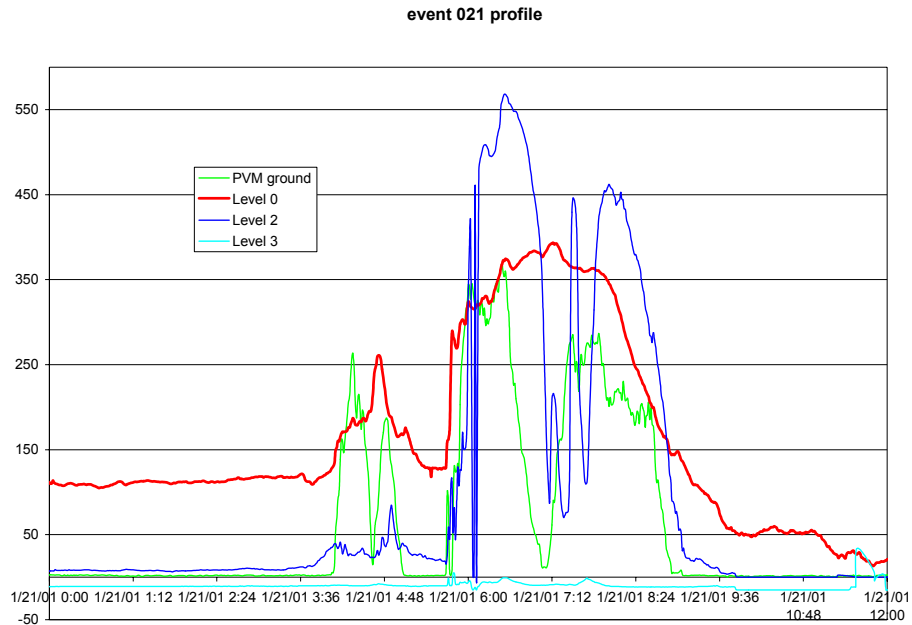


Figure 3-58. LWC evolution ( $\text{mg}/\text{m}^3$ ) on January 21<sup>st</sup> 2001. Levels 0, 2 and 3 LWC values were estimated based upon OFD response.

Samples were retrieved from levels 0, 1, and 2. Level 1 was working but the OFD data were not logged by the data logger so it is not possible to retrace exactly when the fog was sampled at this level. Time series of fog composition for levels 0 and 2 are presented in figure 3-59. The higher level shows generally higher concentrations, consistent with lower collected samples volumes (lower LWC). There is no significant difference in pH between the different levels. Ammonium, nitrate and sulfate show similar variations with time. Na, Cl, Mg and Ca concentrations seem to converge over time.

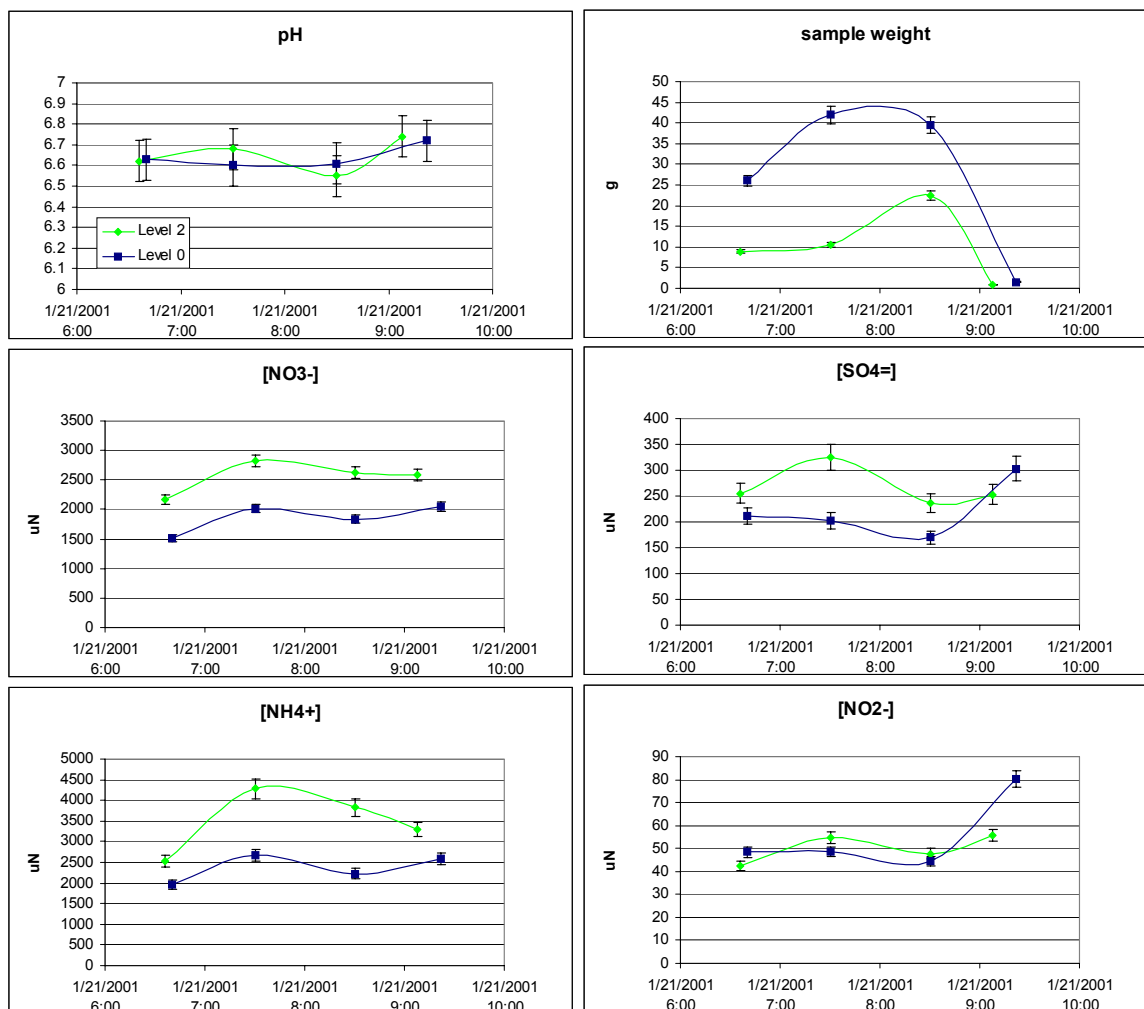


Figure 3-59a. Evolution of concentrations of fog samples sampled at tower level 0 (3m) and level 2 (23m) during the morning hours of January 21<sup>st</sup> 2001.

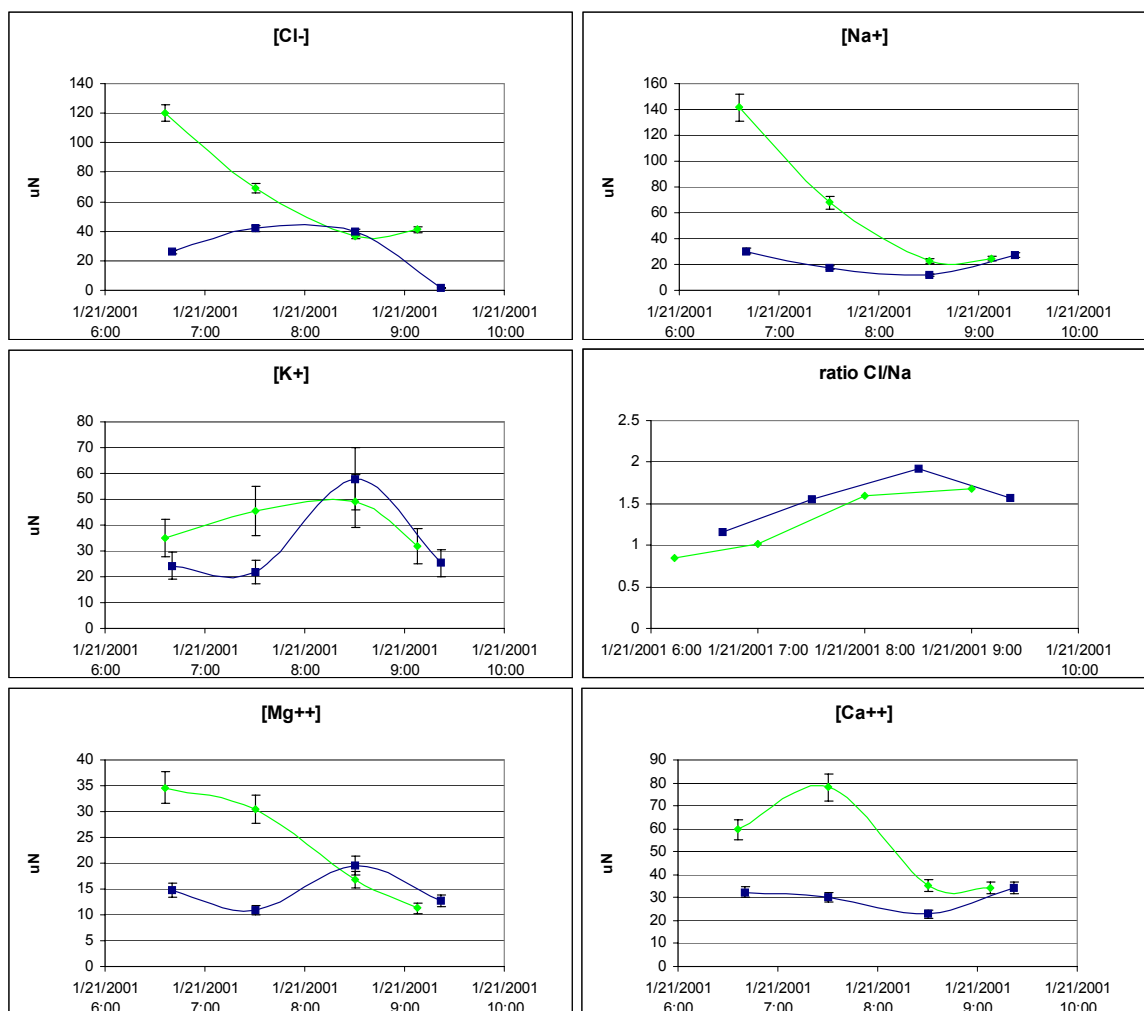


Figure 3-59b. Evolution of concentrations of samples sampled at tower level 0 (3m, blue) and level 2 (23m, green) during the morning hours of January 21<sup>st</sup> 2001.

Figures 3-60 and 3-61 present the average fog concentrations (volume weighted) observed at the 3 lower measurement levels of the tower. This includes level 1, for which no sample time information was available but for which the collected samples derive from the same event. We observe that there is no significant variation in pH with height. For the major ions ( $\text{NO}_3^-$ ,  $\text{SO}_4^{2-}$  and  $\text{NH}_4^+$ ), the highest level shows slightly higher concentrations than the lower levels. There is little difference in the lower levels (3m and 8m). For the minor ions, we observe also higher concentrations in the higher level 21m.

This may simply be related to a lower LWC at the higher level; the average collection rate is only about 10 ml/h on this level compared to 20 and 25 ml/h on the other levels. Finally for the minor ions it is interesting to see that there may be slightly higher concentrations in more terragenic species ( $\text{Mg}^{2+}$ ,  $\text{Ca}^{2+}$  and  $\text{K}^{+}$ ) close to the ground, whereas  $\text{Na}^{+}$  and  $\text{Cl}^{-}$  don't show this pattern.

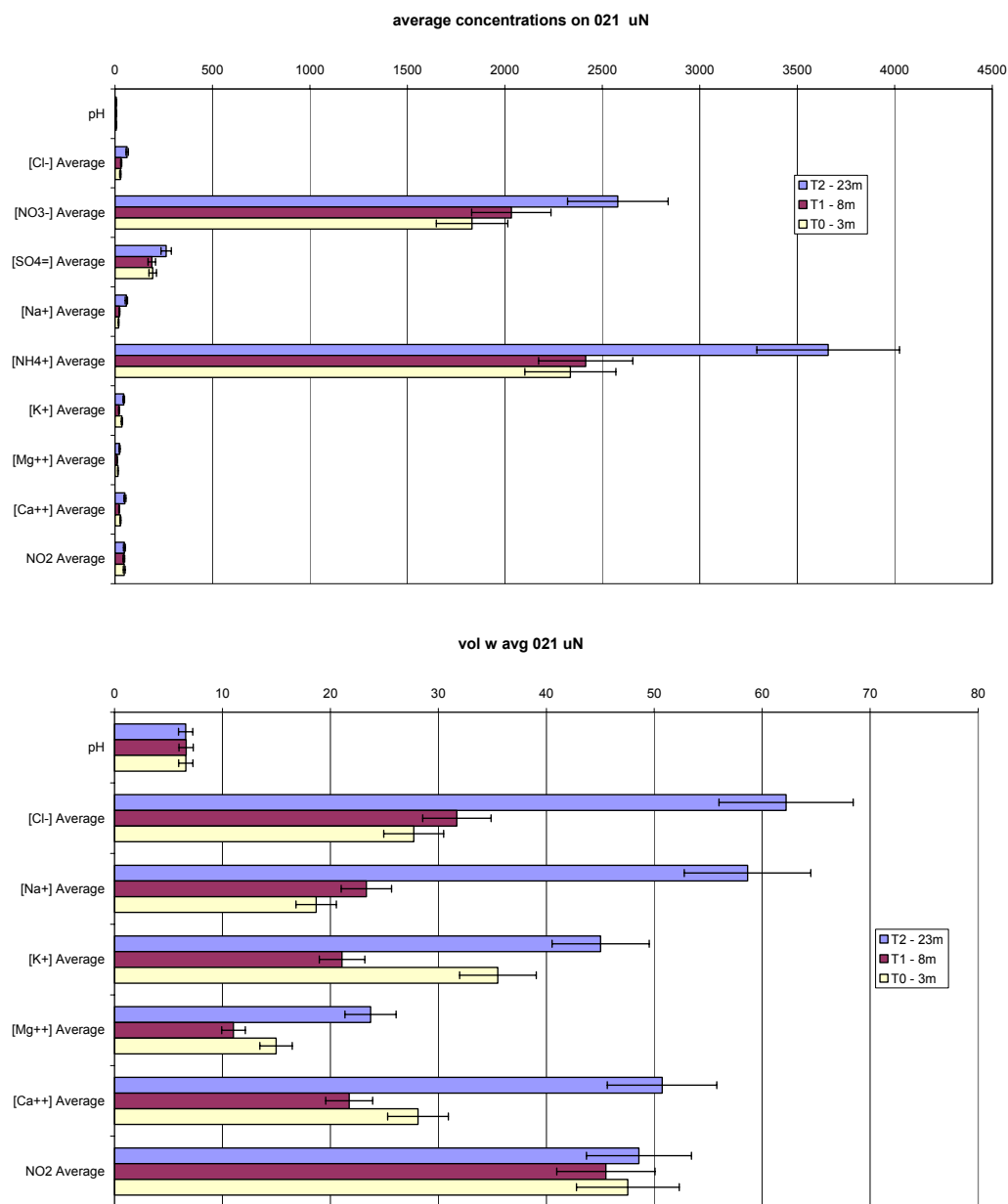


Figure 3-60. Profiles of average tower fog concentrations on January 21<sup>st</sup>. Error bars represent  $\pm 10\%$ .

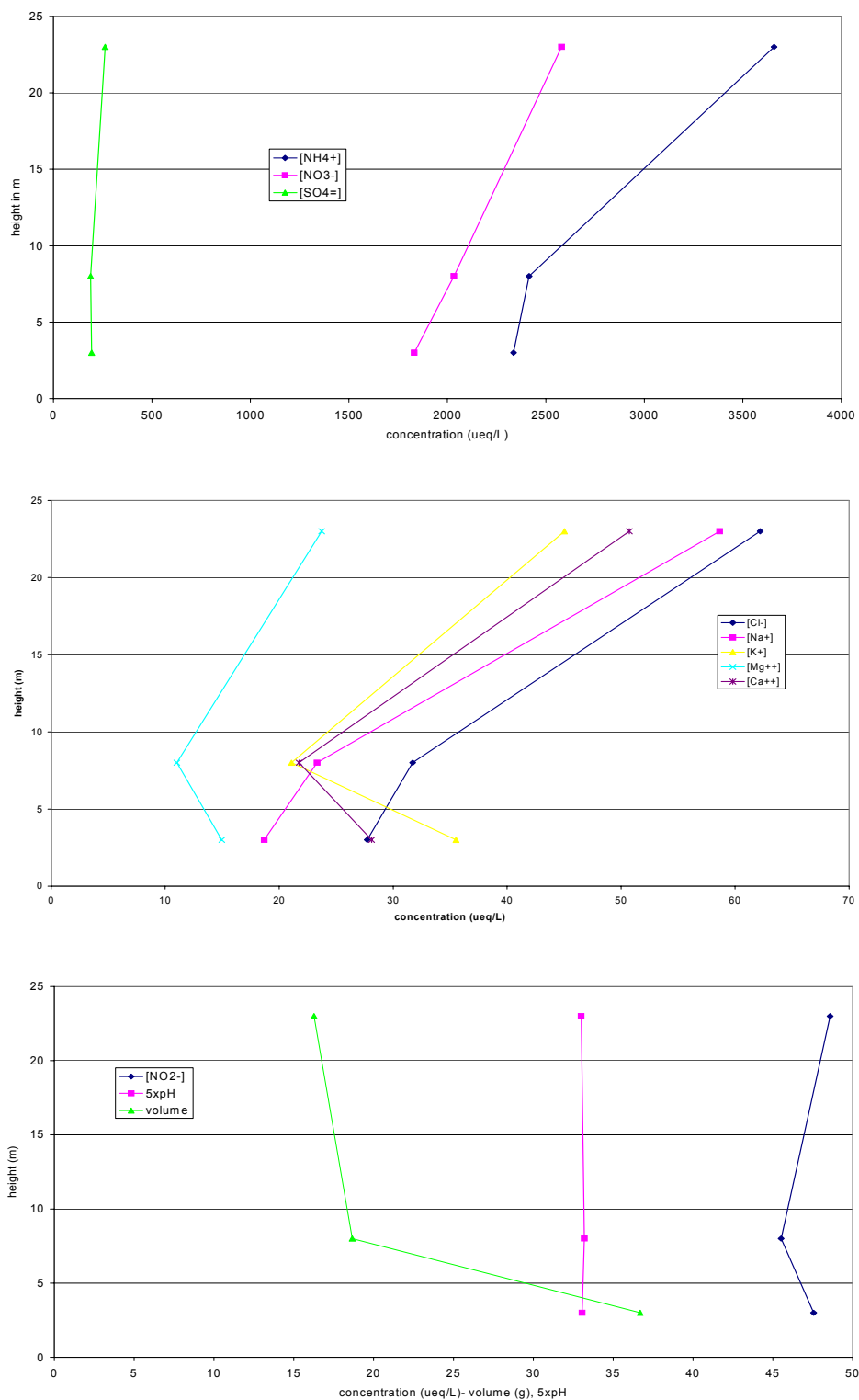


Figure 3-61. Vertical profiles of average (vol weighted) fog concentrations on January 21<sup>st</sup>.

Overall, the tower experiments gave some valuable insights in the vertical structure of CRPAQS radiation fogs:

- Radiation fogs at the Angiola site during the CRPAQS study were frequently confined to a shallow layer close to the ground (<25m). This was likely a special condition of our sampling site, rather than a general pattern of SJV fog events as previous studies showed much deeper layers (e.g. (Collett et al., 1999)). The small vertical extent of these fogs probably led to effective radiative cooling directly from the fog drops themselves, leading to production of large drops (and high fog LWC) near the surface). As discussed in Chapter 5, the formation of large drops resulted in high sedimentation velocities.
- The Colorado State University Optical Dog Detector (CSU-OFD) proved to be a useful tool for detecting fog on the tower. The collected sample volumes as well as collection rates decrease with altitude suggesting a higher LWC close to the ground and then a decrease with altitude.
- We could not observe any significant variation in pH with altitude. The acidity appears to be constant throughout the fog layer. This is consistent with previous observations in deeper fog layers made during IMS 95 at the Candelabra Tower.
- Major ion concentrations increased with altitude in the fog layer. The observed difference is barely significant between the lower levels (3m and 8m), but higher at the 23m level. A similar observation is made for minor ions (Na, Cl, Mg, Ca,...). This might be the result of the apparent decrease of LWC with altitude as LWC and ion concentrations often show an anticorrelation (Elbert et al., 2000; Moller et al., 1996).

### 3.8 Changes in SJV fog composition over two decades

Fogwater composition has been studied periodically in California's San Joaquin Valley since the early 1980's, beginning with the research of the group of Michael Hoffmann at Caltech and extending through IMS95 and CRPAQS. Due to changes in measurement locations, it is somewhat difficult to look at possible time trends in SJV fog composition. The best available dataset can be assembled for the city of Bakersfield, where studies have been conducted at least since winter 1982/83 through IMS95 and CRPAQS. Table 3-12 gives an overview of the available datasets.

Table 3-12. Available Bakersfield fog composition data sets used for temporal trend analysis

Period	Source
12/1982-1/1984	D. Jacob, Caltech Ph.D. thesis
12/1984-1/1985	J. Waldman, Caltech Ph.D. thesis
1993	Collett group
1994	Collett group
1995	Collett group IMS 95
2001	Collett group CRPAQS

Figures 3-62, 3-63 and 3-64 highlight observations of fog composition from these datasets for pH, sulfate, and nitrate.

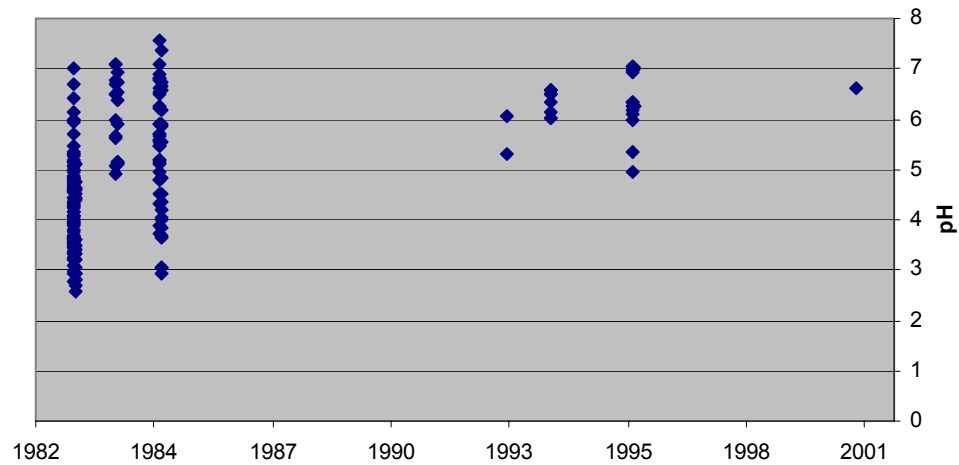


Figure 3-62. pH of fog samples collected in Bakersfield in the period 1982-2001.



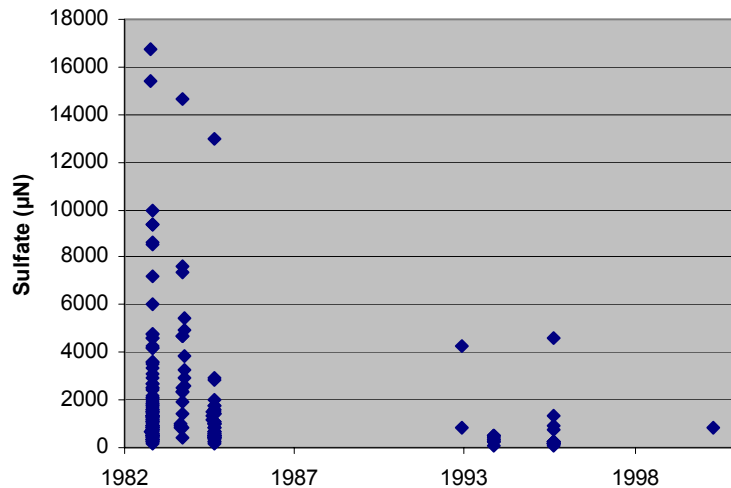


Figure 3-63. Sulfate concentrations ( $\mu\text{N}$ ) observed in Bakersfield fogs in the period 1982-2001.

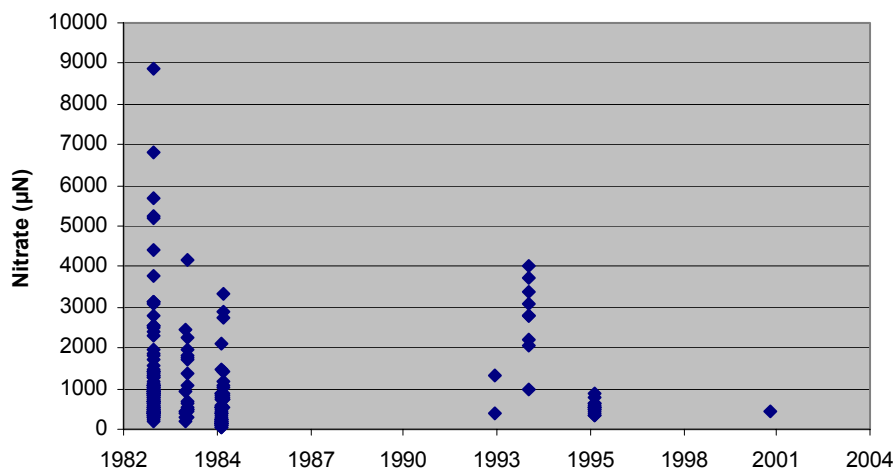


Figure 3-64. Nitrate concentrations ( $\mu\text{N}$ ) observed in Bakersfield fogs in the period 1982-2001.

From Figures 3-62 to 3-64 we see a large number of samples have been collected in Bakersfield. The analysis of any time trend is complicated by several issues:

- fog samples are only collected during short time intervals in winter of a few selected years
- sample locations in Bakersfield vary somewhat over time
- the frequency of fog during the IMS95 and CRPAQS campaigns was much lower at Bakersfield than in studies conducted in the early 1980s.

Keeping these limitations in mind, a 2-sample Student T-test was used to examine if the

average concentrations of fog components in the 80s differ significantly from observations in the 1990s, including CRPAQS. Results are presented in Table 3-13.

Table 3-13. Comparison of Bakersfield fog water concentrations in samples collected in the 1980s and the period 1990-2001.

variable	N	80s		N	1990-2001		P-value
		mean	stdev		mean	stdev	
<b>pH</b>	<b>185</b>	<b>4.8</b>	<b>1.21</b>	<b>26</b>	<b>6.3</b>	<b>0.522</b>	<b>0.000</b>
Na <sup>+</sup> (μN)	177	70	279	26	23.6	25.7	0.034
K <sup>+</sup> (μN)	141	33	104	26	25.2	13.3	0.377
NH <sub>4</sub> <sup>+</sup> (μN)	185	2903	3509	26	2966	2206	0.900
<b>Ca<sup>2+</sup> (μN)</b>	<b>177</b>	<b>239</b>	<b>615</b>	<b>24</b>	<b>49.3</b>	<b>61</b>	<b>0.000</b>
<b>Mg<sup>2+</sup> (μN)</b>	<b>178</b>	<b>30.6</b>	<b>77.3</b>	<b>24</b>	<b>7.93</b>	<b>5.48</b>	<b>0.000</b>
Cl <sup>-</sup> (μN)	153	174	481	26	69.3	92.1	0.016
NO <sub>3</sub> <sup>-</sup> (μN)	185	1350	3248	26	1337	1209	0.969
<b>SO<sub>4</sub><sup>2-</sup> (μN)</b>	<b>185</b>	<b>2031</b>	<b>2693</b>	<b>26</b>	<b>720</b>	<b>1147</b>	<b>0.000</b>
HCHO (μM)	145	167	116	14	121	101	0.130
Fe (μg/l)	119	708	1413	13	463	196	0.084
Mn (μg/l)	117	99	470	11	18.1	12.2	0.065

Bold – significantly different mean at 99% confidence level (alpha=P <0.01)

Results of these tests suggest that for pH, Ca, Mg and sulfate the mean concentrations in the 90s differ significantly from the 80s. The change in sulfate concentrations may reflect decreases in emissions of SO<sub>2</sub> in the southern SJV since the early 1980s. As sulfate concentrations decrease it is expected that pH values will rise, as also observed here. Changes in Ca<sup>2+</sup> and Mg<sup>2+</sup> concentrations are more difficult to explain and may reflect differences in measurement approaches. In the 1980s the Caltech group measured these species by atomic absorption spectrometry (AAS) while the later measurements were completed by ion chromatography. The higher concentrations measured by AAS might represent additional, insoluble forms of Mg and Ca in the samples. The apparent change in Ca and Mg concentrations might also reflect inclusion of many low volume (and presumably low LWC) samples in the 1980s data set. These

might be especially influenced by some collection of dust. If we volume weight the samples and repeat the comparison of averages from the two periods, significant changes (99% confidence level) are seen only for sulfate (decreases by more than a factor of two) and pH (increases by 1.3 pH units).

## Chapter 4

### Organic composition of CRPAQS fogs and interactions with carbonaceous aerosols

#### 4.1 Overview

This chapter focuses on observations of the organic composition of Central California radiation fogs, on improvement of techniques for characterizing organic species concentrations, and on issues related to organic aerosol and trace gas processing by these fogs.

##### 4.1.1 TOC and DOC

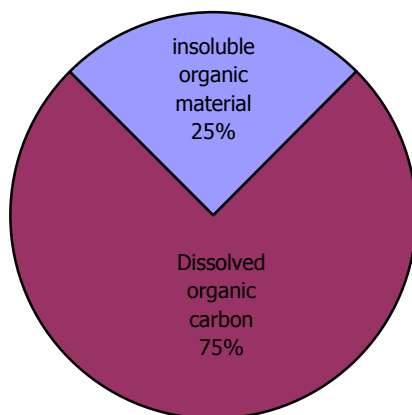


Figure 4-1. Average fractions of TOC and DOC in CRPAQS fog samples.

Figure 4-1 shows the average split between total and dissolved organic carbon for CRPAQS fog samples. Results are shown for bulk fog samples collected with the ss-CASCC. It can be seen that an average of 75% of the organic material is dissolved, as operationally defined by the fraction of organic carbon in fog samples which

passed through a quartz fiber filter. The results indicate that insoluble matter is an important part of the organic carbon burden of the CRPAQS fog drops and should not be ignored. A more detailed breakdown by sample is shown by Herckes et al. (2002), attached as Appendix B. This finding should caution those who routinely filter fog and cloud samples, looking only at the soluble fraction, as it is clear that a significant amount of insoluble carbon is also being processed by the fog. The insoluble fraction probably contains a wide variety of organic material, perhaps including a significant amount of biological material (Bauer et al., 2002).

#### 4.1.2 MW analysis of DOC

Molecular weight (MW) analyses of DOC in six fog samples were performed using ultrafiltration, which allows the classification of dissolved organic matter in different molecular weight classes. Results of the technique give an approximate idea of the molecular weight distribution of the DOC, but should not be over-interpreted as molecular structure, in addition to molecule size, influences the observed partitioning.

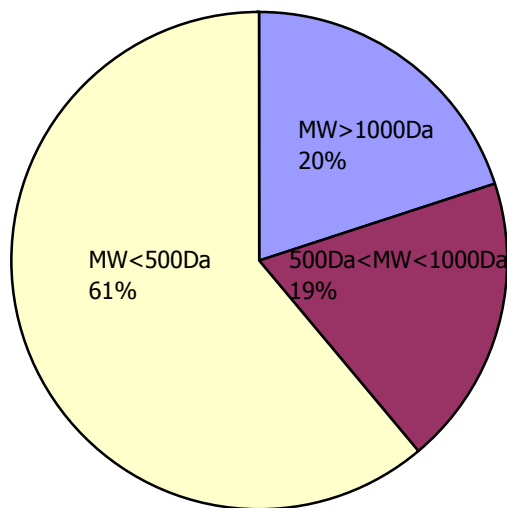


Figure 4-2. Molecular weight analysis of DOC for six fog water samples.

Figure 4-2 shows the average molecular weight distribution as a pie diagram. On average approximately 61% of the DOC is comprised of organic compounds with MW less than 500Da. The remaining 39% of the DOC is approximately evenly split between

compounds with MW between 500Da and 1000Da and compounds with MW > 1000Da. The presence of this large amount of high molecular weight material, reported in greater detail by Herckes et al. (2002) (see Appendix B), came as something of a surprise and necessitates a change in future approaches to characterizing the organic speciation of fog organics.

#### 4.1.3 DOC composition

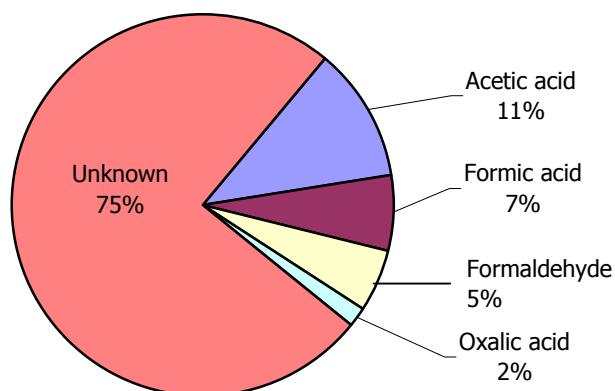


Figure 4-3. Mass fractions of CRPAQS fog DOC comprised by several key low MW species.

Past studies have found that several low molecular weight organic compounds can comprise a significant fraction of the organic burden in clouds and fogs. Figure 4-3 shows the average contributions of acetic acid, formic acid, oxalic acid, and formaldehyde to CRPAQS fog DOC. On a carbon mass basis, acetic acid is the dominant compound, comprising on average 11% of the fog DOC. Formic acid (7%), and formaldehyde (5%) follow in importance. Oxalic acid, the simplest dicarboxylic acid, makes up only 2%, on average, of the fog DOC. The relatively small contribution by oxalic acid stands in contrast to traditional use of dicarboxylic acids as model compounds for organic aerosol interactions with clouds and fogs. Together, the four compounds depicted here comprise only about one-fourth of the fog DOC, but make up nearly half of the DOC with MW < 500 Da. The importance of these four compounds is consistent with earlier observations of the organic speciation of SJV fogs.

Clearly there remains a significant fraction of fog borne organics that need to be

identified, even in the lower MW range. One class of compounds worth investigating is carbonyls and dicarbonyls. Collett et al. (1990) found that glyoxal and methyl glyoxal, two simple dicarbonyl compounds, had significant concentrations in clouds intercepting the slopes of the Sierra Nevada downwind of the Central Valley. Certainly, then, it seems worthwhile measuring concentrations of these compounds in the valley fogs. Also, functional group analysis, proposed by others to characterize water soluble organic compounds (WSOC) in fogs and aerosols, will help us better understand the profiles and abundance of soluble organic matter in fog water.

Measurement of carbonyl compounds is challenging because of their trace concentrations and interferences arising from other pollutants in fog water. Carbonyl compounds are directly emitted from a variety of sources including automotive, stationary source, and other industrial emissions, as well as from natural biogenic sources. Secondary production via atmospheric oxidation of other volatile organic compounds (VOC) can also be important sources. A review of atmospheric hydrocarbon oxidation mechanisms reveals many that are initiated by hydroxyl radical attack and eventually result in production of a variety of carbonyl and dicarbonyl compounds. Carbonyls themselves are also quite reactive and exert an important influence on  $\text{NO}_x$  and ozone chemistry in the troposphere (Fung et al., 1981; Seinfeld et al., 1998; Finlayson-Pitts et al., 2000). Problems previously identified in measurement of atmospheric carbonyls and dicarbonyls include 1) incomplete collection of carbonyls, 2) loss of carbonyl compounds by physical processes, vaporization, or by reactions with other pollutants in fog water, and 3) variable blanks resulting from contamination of reagents and/or sampling equipment.

## 4.2 Determination of carbonyl compounds by HPLC

### 4.2.1 Overview

In order to more fully characterize organic compound processing by CRPAQS fogs, CSU requested additional resources in the data analysis phase to adapt an existing analytical method for aqueous carbonyls compounds and make measurements of fog

carbonyls. Carbonyl compounds in fog samples were measured using a revised version of U.S. EPA Method 8315(A). It provides procedures for the determination of free carbonyl and dicarbonyl compounds in solid and liquid (aqueous) samples by derivatization with 2,4-dinitrophenylhydrazine (DNPH), and application of high performance liquid chromatography (HPLC) with ultraviolet (UV) detection.

Derivatization of carbonyl compounds by the DNPH method is based on the acid-catalyzed derivatization of carbonyls by nucleophilic addition of DNPH to a C=O bond, followed by 1,2-elimination of water to form 2,4-dinitrophenylhydrazone. (The DNPH-hydrazones formed during sample derivatization are non-volatile).

The yellow to deep-orange colored DNPH-hydrazones have UV absorption maxima in the 360-375 nm range (for carbonyls) and near 430nm (for dicarbonyls), and can be analyzed by a high performance liquid chromatography (HPLC) method coupled with UV absorbance detection.

The water soluble low molecular weight (C<sub>1</sub>-C<sub>7</sub>) carbonyl compounds that can be quantified by this approach include formaldehyde, acetaldehyde, acrolein, acetone, propionaldehyde, crotonaldehyde, butyraldehyde, benzaldehyde, isovaleraldehyde, valeraldehyde, tolualdehyde, hexaldehyde, glyoxal and methyl glyoxal.

#### 4.2.2 Instruments and reagents

##### 4.2.2.1 HPLC conditions

HPLC operating conditions were adjusted to optimize chromatographic conditions for our particular analytical needs.

- Column: C18, 25 cm x 4.6 mm , 5 µm particle size. Supelco
- Mobile Phase Gradient: 50/50 acetonitrile/water (v/v), hold for 20 min. 50/50 acetonitrile/water to 95% acetonitrile in 15 min, 95% acetonitrile for 5 min.



Total is 40 minutes plus 6 minutes flush time.

- Temperature: 40.0°C
- Flow Rate: 1.5 ml/min
- Detector: Ultraviolet absorption, monitored at 360 nm for mono-carbonyls, 430nm for dicarbonyls (Glyoxal and Methyl Glyoxal)
- Injection Volume: 20µl

#### 4.2.2.2 Reagents

Table 4-1 shows the reagents used for carbonyls analysis. Standards are expected to be stable for about 6 weeks. All standards should be checked frequently for signs of degradation or evaporation. The lowest standard concentration should be at or just above the minimum detection limits when low concentration samples are anticipated. The other concentrations of the calibration curve should correspond to the expected range of concentrations in target samples.

Table 4-1. Required reagents for carbonyl and dicarbonyl analysis.

Methylene chloride	CH <sub>2</sub> Cl <sub>2</sub> - HPLC grade or equivalent, Fisher Scientific
Acetonitrile	CH <sub>3</sub> CN - HPLC grade or equivalent. Fisher Scientific
Sodium hydroxide solutions	NaOH, 6M,
Hydrochloric acid	HCl, 6M, J.T.Baker
Sodium sulfate	Na <sub>2</sub> SO <sub>4</sub> - granular, anhydrous. Chempure
Citric acid	C <sub>6</sub> H <sub>8</sub> O <sub>7</sub> , 1.0 M solution, Fisher Scientific
Sodium citrate	C <sub>6</sub> H <sub>5</sub> Na <sub>3</sub> O <sub>7</sub> ·2H <sub>2</sub> O, 1.0 M trisodium salt dihydrate solution. Fisher Scientific
Citrate buffer	1 M, pH 3.0 - Prepare by adding 80ml of 1 M citric acid solution to 20 ml of 1 M sodium citrate solution. Mix thoroughly. Adjust pH with NaOH or HCl as needed. Fisher Scientific
DNPH	2,4-Dinitrophenylhydrazine, [2,4-(O <sub>2</sub> N) <sub>2</sub> C <sub>6</sub> H <sub>3</sub> ]NHNH <sub>2</sub> (DNPH), 70% in organic-free reagent water (w/w), Sigma. Add 428.7mg recrystallized 70% (w/w) DNPH solution in 100ml of acetonitrile to make a 3.00mg/ml solution.
Aldehyde stock standard	Commercial product: TO11/IP6A Carbonyl-DNPH Mix, Supelco Company, including 15 aldehyde compounds. Part#

	47284-U. Analytical concentrations are 15µg/ml.
Calibration standards	A minimum of 5 concentrations (range from 0.02µg/ml to 0.45µg/ml of carbonyls) in acetonitrile from the stock standard. Store all standard solutions at 4°C in a glass vial with a PTFE-lined cap, leaving minimum headspace, and in the dark.

#### 4.2.3 Procedures

Glassware must be scrupulously cleaned. Glassware should be rinsed as soon as possible after use with the last solvent used. This should be followed by detergent washing with hot water and rinses with DI water. After washing, the glassware should then be drained, dried, and heated in a laboratory oven at 450°C for two to three hours before reuse. Solvent rinses with acetonitrile may be substituted for the oven heating. After drying and cooling, glassware should be stored in a clean environment to prevent accumulation of dust or other contaminants.

NOTE: Do not rinse glassware with acetone or methanol. These solvents react with DNPH to form interferences.

- a. A measured volume of fog water sample (usually 20 ml or less, depending on the amount of real sample) is buffered to pH=3 and derivatized with 2,4-dinitrophenylhydrazine (DNPH): Transfer sample into reaction vessel, add 4 ml of citrate buffer and adjust the pH to  $3.0 \pm 0.1$  with 6M HCl or 6M NaOH. Add 6 ml of DNPH reagent, seal the container, and place on a heated (40°C), stirring plate for about 2 hours. Adjust the agitation to produce a gentle swirling of the reaction solution.
- b. The derivatized compound is serially extracted three times with methylene chloride. Serially extract the solution with three 20 ml portions of methylene chloride using a 125 ml or 250 ml separatory funnel. Combine the methylene chloride layers in a flask and add ~5.0 grams of anhydrous sodium sulfate. Swirl contents to complete the extract drying process.

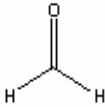
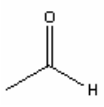
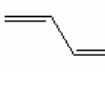
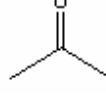
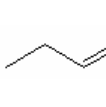
- c. The methylene chloride extracts are concentrated. Pour the extract into the evaporator flask, being careful to minimize transfer of sodium sulfate granules. Wash the flask with 3~4 ml of methylene chloride three times and combine wash to the evaporator flask to complete quantitative transfer.
- d. Exchange with acetonitrile prior to HPLC analysis. Concentrate the extract to a final volume of ~1ml, and exchange the solvent to acetonitrile prior to analysis.



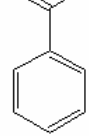

#### 4.2.3 HPLC method results

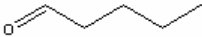
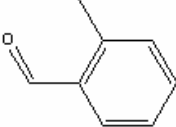
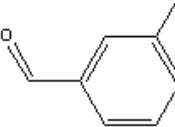
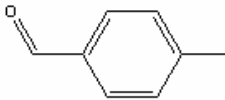
##### 5.2.4.1 Chemical structures of carbonyls and dicarbonyls


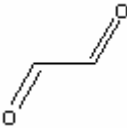
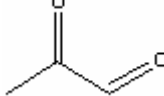
Numerous carbonyl and dicarbonyl compounds can be analyzed by this method. Table 4-2 lists several compounds analyzed in this study, along with their chemical structures.

Table 4-2. Chemical structures of key carbonyls and dicarbonyls.

Name	Formaldehyde	Acetaldehyde	Acrolein	Acetone	Propionaldehyde
Formula	HCHO	C <sub>2</sub> H <sub>4</sub> O	C <sub>3</sub> H <sub>4</sub> O	C <sub>3</sub> H <sub>6</sub> O	C <sub>3</sub> H <sub>6</sub> O
Molecular weight	30.0262	44.053	56.064	58.0798	58.0798
Structure					

Name	Crotonaldehyde	Butyraldehyde	Benzaldehyde	Isovaleraldehyde
Formula	C <sub>4</sub> H <sub>6</sub> O	C <sub>4</sub> H <sub>8</sub> O	C <sub>7</sub> H <sub>6</sub> O	C <sub>5</sub> H <sub>10</sub> O
Molecular weight	70.0908	72.1066	106.1238	86.1334
Structure				

Name	Valeraldehyde	o-Tolualdehyde	m-Tolualdehyde	p-Tolualdehyde
Formula	C <sub>5</sub> H <sub>10</sub> O	C <sub>8</sub> H <sub>8</sub> O		
Molecular weight	86.1334	120.1506		
Structure				

Name	Hexaldehyde	Glyoxal	Methyl glyoxal
Formula	C <sub>6</sub> H <sub>12</sub> O	C <sub>2</sub> H <sub>2</sub> O <sub>2</sub>	C <sub>3</sub> H <sub>4</sub> O <sub>2</sub>
Molecular Weight	100.1602	58.0366	72.0634
Structure			

#### 4.2.3.2 Example chromatograms

Figure 4-4 depicts 2-D and 3-D views of one example chromatogram showing retention times of several carbonyls in an analyzed standard. From left to right, the peaks in the 2D chromatogram are formaldehyde, acetaldehyde, acrolein+acetone, propionaldehyde, crotonaldehyde, butyraldehyde, benzaldehyde, isovaleraldehyde, valeraldehyde, o-tolualdehyde, and m-tolualdehyde (including p-tolualdehyde which co-elutes). The analytical separation occurs over approximately 30 minutes. During our testing of the method we were unable to separate acrolein and acetone, which co-elute as indicated. Even strong changes to the separation method resulted in little improvement in the separation of these two compounds, Therefore, all results presented below consider these two compounds together.

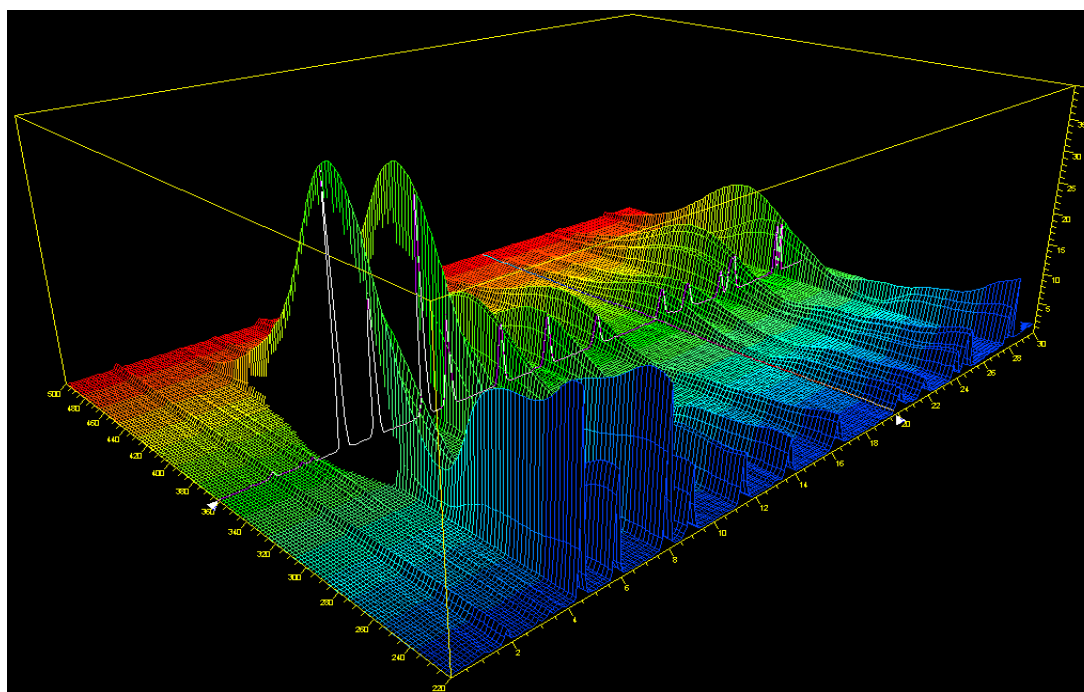
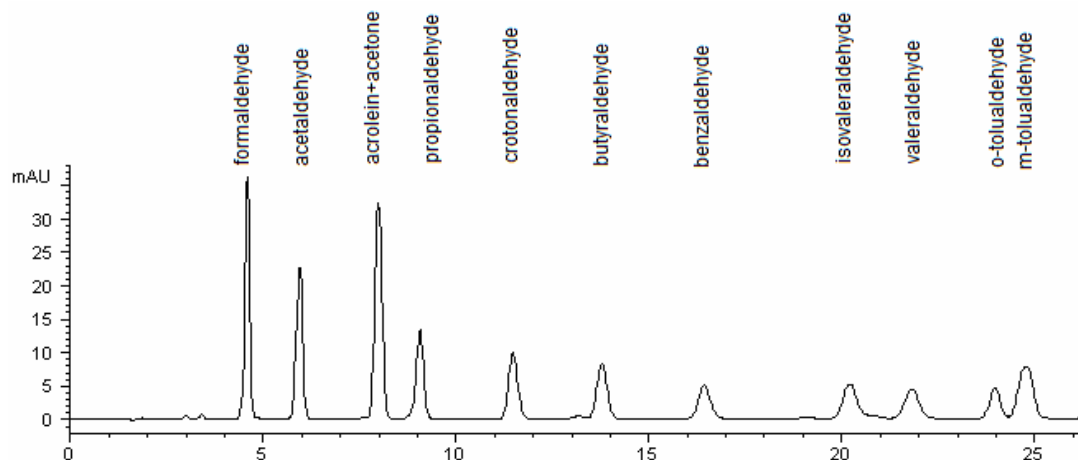


Figure 4-4. 2-D and 3-D views of an example chromatogram showing retention times and wavelength dependent absorption for several carbonyls in a standard.

In the 3-D chromatogram view, the x axis indicates retention time, the y axis indicates the detection wavelength (from 220 nm to 500 nm), and the z-axis indicates the measured absorbance. The white curve bisecting the figure at 360nm is the 2-D view of the chromatogram discussed above. It is clear that 360 nm is close to the absorption maximum for many of the carbonyls, while several of the more complex carbonyls tend to absorb most strongly at longer wavelengths.

#### 4.2.3.3 Carbonyl calibration results

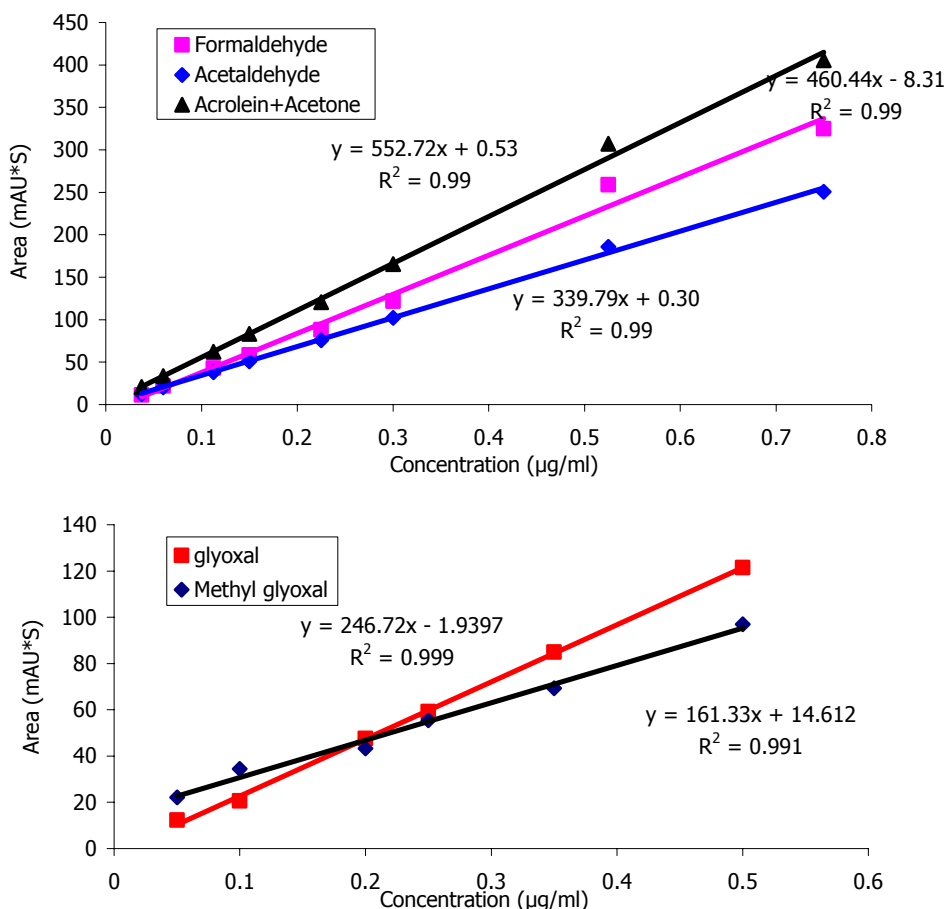


Figure 4-5. Several example carbonyl calibration curves. Calibration curves of formaldehyde, acetaldehyde, acrolein+acetone were based on standards analyzed on 01/25/04 with absorbance monitored at 360 nm. Glyoxal and methyl glyoxal calibration curves were constructed on the same date, but absorbance of these compounds was monitored at 430 nm.

Method calibration curves were constructed based on injection of dilute standards prepared from a commercial stock standard containing DNPH-derivatized carbonyls. During each measurement period, standard solutions were made freshly from this stock solution. In order to make the standards consistent with samples, DNPH was also added to these standards which were treated the same way as samples.

Dicarbonyls analyzed in the work include glyoxal and methyl glyoxal. There is no commercial DNPH-derivatized standard available for either compound. Therefore, stock calibration solutions were manually made by adding proper amounts of glyoxal and methyl glyoxal into DI water and derivatizing. All the calibration standards for dicarbonyls were derivatized by DNPH and treated the same way as samples.

Figure 4-5 shows the calibration results for three abundant aldehydes as well as for glyoxal and methyl glyoxal. The calibration results for the other compounds reported here exhibit a similar linear relation between concentration and absorption.

#### 4.2.3.4 Blank and Minimum Detection Limit (MDL)

Table 4-3. Carbonyl and dicarbonyl concentrations in blanks (20 ml DI water).

<u>Species</u>	Concentration (µg/ml)					
	BLK1	BLK2	BLK3	BLK4	BLK5	BLK6
Formaldehyde	0.01	0.01	0.02	0.01	0.01	0.01
Acetaldehyde	0.01	0.01	--	--	--	--
Acrolein+Acetone	0.02	0.01	0.02	0.02	0.02	0.02
Propionaldehyde	--	--	--	--	--	--
Crotonaldehyde	--	--	--	--	--	--
Butyraldehyde	--	--	--	--	--	--
Benzaldehyde	--	--	--	--	--	--
Isovaleraldehyde	--	--	--	--	--	--
Valeraldehyde	--	--	--	--	--	--
o-Tolualdehyde	--	--	--	--	--	--
m-Tolualdehyde	--	--	--	--	--	--
Glyoxal	--	--	--	--	--	--
Methyl Glyoxal	--	--	--	--	--	--

-- means the compound was not detected

Table 4-4. Minimum detection limits of carbonyls based on replicate low level (0.015 µg/ml) standard analyses

<u>Species</u>	Concentration (µg/ml)									<i>Published MDL</i>
	A*	B	C	D	E	F	G	H	<b>MDL</b>	

Formaldehyde	0.023	0.021	0.021	0.021	0.021	0.024	0.022	0.021	0.025	0.02
Acetaldehyde	0.013	0.012	0.012	0.012	0.012	0.012	0.012	0.011	0.013	0.11
Acrolein+Acetone	0.011	0.011	0.011	0.011	0.011	0.012	0.011	0.011	0.013	--
Propionaldehyde	0.011	0.011	0.010	0.011	0.011	0.012	0.010	0.011	0.012	0.008
Crotonaldehyde	0.013	0.012	0.013	0.013	0.012	0.013	0.013	0.014	0.015	0.006
Butyraldehyde	0.014	0.013	0.012	0.013	0.014	0.013	0.013	0.013	0.015	0.008
Benzaldehyde	0.010	0.012	0.009	0.010	0.012	0.007	0.011	0.009	0.014	--
Isovaleraldehyde	0.014	0.012	0.012	0.014	0.013	0.012	0.013	0.011	0.015	--
Valeraldehyde	0.011	0.010	0.009	0.011	0.013	0.010	0.009	0.010	0.013	--
o-Tolualdehyde	0.009	0.010	0.011	0.014	0.012	0.012	0.011	0.010	0.015	--
m-Tolualdehyde	0.011	0.011	0.010	0.011	0.011	0.012	0.011	0.010	0.012	--

\* A to H are parallel replicate samples

Table 4-3 shows the carbonyl and dicarbonyl concentrations measured in six blanks (20 ml organic-free DI water). Since many compounds were not detected in these blanks, method detection limits were calculated by replicate analyses of a low concentration standard. Table 4-4 lists the MDL determined for each species, based on analyzing eight replicate samples (A to H). The minimum detection limits are comparable to published MDLs in EPA method 8315A, with some carbonyl MDLs slightly exceeding the published MDLs. The MDL for a specific sample may differ from the listed value, depending upon interferences from the sample matrix and the volume of sample used in the procedure. In the EPA method 8315A, the MDLs were obtained using 100 ml DI water, while 20 ml samples were used in our methods (we use 20 ml instead of 100 ml to be consistent with our 20 ml fog water samples – larger volumes are hard to obtain and dedicate just for this analysis). Generally, using larger sample volumes will lower the detection limits. Therefore, slightly higher MDLs in our results are very reasonable.

The concentrations of most carbonyls and dicarbonyls in the blanks are below the Minimum Detection Limit. For formaldehyde, acetaldehyde, and acrolein+acetone, the concentrations are also very low.

#### 4.2.3.5 DNPH Recrystallization

Formaldehyde contamination of the DNPH reagent is frequently encountered due to its



widespread occurrence in the environment. In order to ensure acceptable results, the DNPH reagent must be purified by multiple recrystallizations in HPLC-grade acetonitrile. Recrystallization is accomplished, at 40-60°C, by slow evaporation of the solvent to maximize crystal size. The purified DNPH crystals are stored under HPLC-grade acetonitrile. Impurity levels of carbonyl compounds in the DNPH are determined prior to sample analysis and should be less than 25 µg/ml. Detailed DNPH recrystallization procedures can be found in EPA method 8315A.

Table 4-5. DNPH recrystallization results.

Species	Original concentration (µg/ml)	First recrystallization (µg/ml)	Second recrystallization (µg/ml)
Formaldehyde	0.02	---*	---
Acetaldehyde	0.08	0.15	0.01
Acrolein+Acetone	2.15	0.53	0.03
Propionaldehyde	0.01	---	---
Crotonaldehyde	---	---	---
Butyraldehyde	---	---	---
Benzaldehyde	---	---	---
Isovaleraldehyde	---	---	---
Valeraldehyde	---	---	---
o-Tolualdehyde	---	---	---
m-Tolualdehyde	---	---	---
Glyoxal	---	---	---
Methyl Glyoxal	---	---	---

--- the compound is not detected

Table 4-5 shows the results of blank tests using original and recrystallized (once and two times respectively) 2,4-dinitrophenylhydrazine (DNPH). We can see that after the first recrystallization the concentrations of detectable compounds have already dropped to below 25 µg/l, but are still higher than blank concentrations listed in Table 4-3. After a second recrystallization the concentrationa are below or comparable to the blanks listed in Table 4-3.

#### 4.2.3.6 HPLC Uncertainty (RSD)

Table 4-6. Precision of carbonyl analyses based on replicate standards (0.15µg/ml).

Species	Concentration of Standard (µg/ml)					RSD (%)
	1st*	2nd	3rd	4th	5th	
Formaldehyde	0.16	0.16	0.18	0.17	0.16	4
Acetaldehyde	0.16	0.16	0.16	0.16	0.16	2
Acrolein+Acetone	0.16	0.16	0.16	0.16	0.16	2
Propionaldehyde	0.15	0.16	0.16	0.16	0.16	2
Crotonaldehyde	0.16	0.16	0.16	0.16	0.15	2
Butyraldehyde	0.16	0.16	0.16	0.16	0.16	2
Benzaldehyde	0.15	0.15	0.15	0.16	0.15	2
Isovaleraldehyde	0.15	0.15	0.16	0.15	0.16	2
Valeraldehyde	0.15	0.16	0.16	0.15	0.16	2
o-Tolualdehyde	0.15	0.15	0.16	0.16	0.16	3
m-Tolualdehyde	0.15	0.15	0.16	0.16	0.16	2

\* 1<sup>st</sup> to 5<sup>th</sup> are replicate analyses.

Table 4-6 shows the precision of carbonyl measurements for a standard solution (carbonyl concentrations: 0.15 µg/ml), which was prepared by diluting 100 µl aldehyde stock standard solution into 10 ml. This sample was measured 5 times repeatedly by HPLC to test method precision. All the uncertainties are smaller than 5% (relative standard deviation, RSD).

#### 4.2.3.7 Standard Accuracy

In order to test if this method has good/stable recovery ratios (efficiencies) for each compound, parallel samples (STD1 to STD4) were made from the stock standard solution, which contained identical concentration (about 0.11 µg/ml) of DNPH derivatized carbonyls. These were processed by the same method as fog water samples. Table 4-7 shows the measured sample concentrations and measurement accuracy of each species. Some species, such as formaldehyde, have greater error due to widespread occurrence in the environment leading to contamination during processing.

Table 4-7. Accuracy for carbonyls analysis.

Species	Concentration( $\mu\text{g/ml}$ )					Theoretical value	Error
	STD1*	STD2	STD3	STD4	Average	( $\mu\text{g/ml}$ )	(%)
Formaldehyde	0.13	0.14	0.14	0.13	0.14	0.11	+21
Acetaldehyde	0.13	0.12	0.12	0.12	0.12	0.11	+9
Acrolein+aceton	0.10	0.10	0.10	0.09	0.10	0.11	-11
Propionaldehyde	0.11	0.12	0.11	0.11	0.11	0.11	-0.4
Crotonaldehyde	0.10	0.10	0.10	0.10	0.10	0.11	-12
Butyraldehyde	0.09	0.09	0.09	0.09	0.09	0.11	-18
Benzaldehyde	0.09	0.08	0.09	0.08	0.09	0.11	-23
Isovaleraldehyde	0.09	0.09	0.09	0.09	0.09	0.11	-20
Valeraldehyde	0.11	0.11	0.11	0.11	0.11	0.11	-3
o-Tolualdehyde	0.11	0.11	0.11	0.11	0.11	0.11	-2
m-Tolualdehyde	0.11	0.11	0.11	0.11	0.11	0.11	-2

\* STD1 to STD4 were replicate analyses.

#### 4.2.3.8 Artificial fog water samples

Artificial fog water samples were used to test the derivatization process with DNPH. These samples yield an overview of the validity of the method. A one liter stock artificial fog water solution was made, by adding known amounts of formaldehyde, acetone and benzaldehyde, and kept in the refrigerator. The theoretical concentrations in the stock solution are 11  $\mu\text{g/ml}$  formaldehyde and 20  $\mu\text{g/ml}$  each for acetone and benzaldehyde. The theoretical concentration of formaldehyde was obtained by fluorescence measurement (Dong et al., 1987). Formaldehyde can form a stable compound, HMS, in the presence of bisulfite. HMS can later be decomposed to formaldehyde to be analyzed. After decomposition, formaldehyde is reacted with 2,4-pentanedione and ammonia to quantitatively form a yellow product, diacetyldihydrolutidine (DDL), which is measured by fluorescence. With excess 2,4-pentanedione and ammonia, the amount of DDL produced equals the amount of formaldehyde present in solution. Therefore, the formaldehyde concentration can be determined from the amount of DDL. Theoretical concentrations of acetone and benzaldehyde were calculated based on the amount added to the solution.

Sample solution was made freshly each time before reaction by adding 1ml stock solution into a 100ml volumetric flask and diluting with DI water.

Table 4-8. Concentrations of artificial fog water parallel samples.

Species	Concentration (µg/ml)						Theoretical concentration* (µg/ml)
	Artifog -1	Artifog -2	Artifog -3	Artifog -4	Artifog -5	Artifog -6 Average	
Formaldehyde	0.11	0.10	0.11	0.10	0.13	0.12	0.11
Acetone	0.06	0.08	0.07	0.09	0.06	0.08	0.20
Benzaldehyde	0.20	0.18	0.20	0.19	0.20	0.20	0.20

\*formaldehyde theoretical concentration were measured by RF-1501 spectrofluorotometer; Acetone and benzaldehyde theoretical concentrations were calculated based on the amount added to the solution.

Table 4-8 shows the concentrations of six artificial fog sample replicates analyzed in parallel. We can see that for formaldehyde and benzaldehyde, the theoretical concentration and measured concentration fit very well. But for acetone, the measured concentration is much smaller than the calculated concentration. This reflects the significant volatility of acetone resulting in loss from the prepared solution. A similar loss phenomena was observed for formaldehyde. The target concentration was supposed to be 0.20 µg/ml when I made the artificial fog water solution by weighing the formaldehyde added to the solution, while the real/theoretical concentration measured by a fluorescence method was only 0.11 µg/ml.

#### 4.2.3.9 Stability of samples

Concentrations of carbonyls in stored, unpreserved CRPAQS fog water samples (collected in winter 2000/2001 and analyzed in summer 2003) were found to be very low. Formaldehyde concentrations in some samples were even close to DI water blank values, inconsistent with large amounts of formaldehyde measured by a fluorescence technique (see Chapter 2) in preserved fog water aliquots soon after the samples had been collected. The loss of aldehydes can be explained by chemical instability of aldehydes in fog water,

volatilization, microbial degradation, etc. Therefore, a stability test is extremely important for determining appropriate sample collection, preservation, and handling processes. If the compounds of interest are not stable, we then have to treat samples on site immediately after collection and/or send them back to the lab as soon as possible for analysis.

Two kinds of solutions were made to compare carbonyl stability. One is artificial fog water samples, with DI water as the base matrix, adding appropriate amounts of carbonyl and dicarbonyl compounds; the other uses a real fog water base matrix.

Table 4-9. Comparison of concentrations of artificial fog water samples.

Species	Concentration (µg/ml)						Theoretical concentration (µg/ml)*
	Artifog-1 (03/22/03)	Artifog-2 (03/22/03)	Artifog-1 (05/23/03)	Artifog-2 (05/23/03)	Artifog-7 (05/22/03)	Artifog-8 (05/22/03)	
Formaldehyde	0.11	0.10	0.11	0.11	0.10	0.11	0.11
Acetone	0.06	0.08	0.06	0.08	0.06	0.05	0.20
Benzaldehyde	0.20	0.18	0.20	0.20	0.20	0.19	0.20

\*formaldehyde theoretical concentration were measured by RF-1501 spectrofluorometer; Acetone and benzaldehyde theoretical concentrations were calculated based on the amount added to the solution.

Table 4-9 lists the concentrations of four parallel artificial fog water samples prepared using a DI water base matrix. Two samples (artifog-1 and artifog-2) were made and analyzed on 03/22/03, then re-analyzed on 05/23/03. The other two samples (artifog-7 and artifog-8) were freshly made on 05/22/03. We can see that there is no significant difference among them. For the first two samples (artifog-1 and artifog-2), we can conclude that after derivatization with DNPH, it is stable for two months, which is long enough for the samples to be transferred back to the lab and be analyzed. Comparing the first two parallel samples (artifog-1 and artifog-2) with the second parallel samples (artifog-7 and artifog-8), we can also conclude that the artificial fog samples were also stable without derivatization (the next table will show that real fog matrix were not stable in similar conditions). This is probably because the matrix of the artificial fog water is DI water, and nothing in the solutions like microorganisms can react with aldehydes and degrade the solutions.

Table 4-10. Stability test in a real fog water matrix.

Species	9/15/03 (µg/ml)	9/18/03 (µg/ml)	9/22/03 (µg/ml)	9/29/03 (µg/ml)	10/7/03 (µg/ml)	10/15/03 (µg/ml)
Acetone	0.33	0.32	0.29	0.25	0.27	0.32
Benzaldehyde	1.11	0.72	0.53	<0.02	<0.02	<0.02
Glyoxal	0.94	0.83	0.84	0.71	0.67	0.59
Methyl Glyoxal	1.19	1.06	0.84	0.47	0.25	0.07

Table 4-10 shows stability results for two carbonyl and two dicarbonyl compounds prepared and analyzed in an authentic fog water matrix (archived California Central Valley fog samples). Figure 4-6 shows the data in Table 4-10. We can see that even though the samples prepared with a DI water base matrix were stable, the samples with a real fog water base matrix were not. The concentrations of carbonyls except acetone began dropping within a few days. After one month, all the carbonyls except acetone and glyoxal were gone from the samples. Our results confirm that it is necessary to derivatize samples on site because carbonyls in fog water sample will degrade fast, but our results shows that derivatized samples are stable for at least two months and do not need to be analyzed within 3 days. In a subsequent, NSF-sponsored Fresno fog campaign, fog samples were derivatized on site, then transfer back to main lab in Fort Collins at the end of the whole fog campaign (Jan 13<sup>th</sup> 2004), and analyzed from Jan 21<sup>st</sup> to 26<sup>th</sup>, 2004.

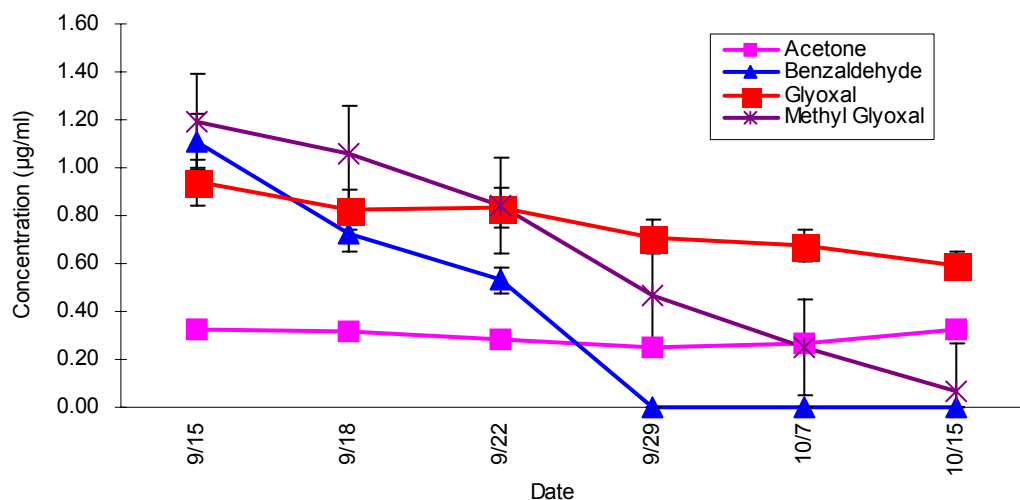


Figure 4-6. Carbonyl stability test in a real fog water matrix.

#### 4.2.3 California SJV fog water samples carbonyl analysis

Nineteen CRPAQS fog water samples have been analyzed by the method above. Analyses were completed in Sept 2003. These samples were collected during the Angiola CRPAQS campaign by CASC and sf-CASC collectors, and include twelve samples of one fog event from 12/17/2000 night to 12/18/2000 noon, four samples of large fog droplets from the same fog event, and three samples from a fog event on 12/19/2000. Table 4-11 shows the concentrations of detectable carbonyl and dicarbonyl compounds. For most of the samples except AGCC35201 (first Angiola ground sample, collected by CASC collector on 12/17/08), the concentrations of carbonyls and dicarbonyls are very low. For example, based on the formaldehyde analysis by spectrophotometer, the average concentration of Formaldehyde in California Angiola fog samples is 20.6 µN, while the concentrations of formaldehyde in these nineteen fog water samples are all less than 1 µM. These samples were stored in the refrigerator for over two years. Stability test conducted as part of this work show that the samples will degrade very fast (less than one month to reach detection limit) if not derivatized on site. This strongly suggests that the samples have been significantly degraded during the long storage time, and most of the original carbonyls and dicarbonyls were lost. For sample AGCC35201, there are still fairly large concentrations of glyoxal and methyl glyoxal in it.

#### 4.2.3 Fresno fog water analysis

Twenty one fog water samples collected during an NSF-sponsored Fresno fog campaign in 2003/04 were analyzed. Although these samples were not part of the CRPAQS study, their collection in the CRPAQS domain makes them relevant to understanding SJV fog processing of organic constituents. Therefore, we include a brief discussion of our findings for these samples here. The samples were collected by ss-CASCC and ss-sf-CASCC at a site on the Fresno State University campus. Samples were derivatized on-site first then transferred back to CSU for analysis. Analyses were finished about ten days after the campaign (From Jan 21<sup>st</sup> to 26<sup>th</sup>, 2004). These samples were collected during three fog events:

- 12/31/03- 01/01/04  
A fog event lasted from 3:52am to 6:30am, one sample was collected (FSC36401).
- 01/10/04- 01/11/04  
A fog event lasted from 9:30pm to 11:40am next day. Four bulk fog water (FSC01001, 01002, 01003, 01004), four large fog drop samples (FSCL01001, 01002, 01003, 01004) and three small fog drop samples (FSCS01001, 01002, 01003) were collected.
- 01/11/04- 01/12/04  
A fog event lasted from 6:00pm to 10:00am next day. Three bulk fog water samples (FSC01101, 01102, 01103), three large fog droplets samples (FSCL01101, 01102, 01103) and three small fog droplets samples (FSCS01101, 01102, 01103) were collected.

Table 4-12 shows the sampling information including date, time, sample weight, pH and concentrations of detectable carbonyls and dicarbonyls. Two dicarbonyls we are interested in were found in the bulk fog samples, but not all carbonyls we looked for were found. Formaldehyde, acetaldehyde, acrolein+acetone, isovaleraldehyde, glyoxal and methyl glyoxal had larger concentrations than butyraldehyde, o-tolualdehyde and,



m-tolualdehyde.

#### 4.2.3.1 Fresno fog sample pH and pH size distribution

From Table 4-12, we can see that for Fresno bulk fog water samples, the pH ranged from 6.58 to 7.23, averaging 6.90, similar to Angiola CRPAQS fog samples and previous SJV fog studies. Again, as we recall, the unique characteristic of California San Joaquin valley fogs is that fog water contains large inputs of ammonia which is the main factor making the fogs alkaline.

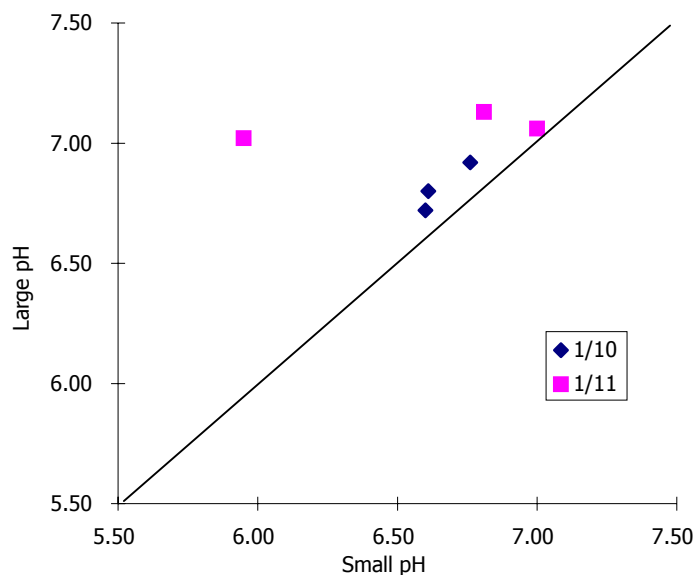


Figure 4-7. Comparison of pH between large and small Fresno fog drops.

Figure 4-7 plots the pH values in large and small fog droplets according to Table 4-12. All the data points are above the 1:1 line, implying that pH in small drops is lower than in large drops. The first pair of size fractionated samples (FSCL01101 and FSCS01101) of the fog event on 01/11/04, shows a large difference (5.95 small vs. 7.02 large). This result contrasts with the other samples examined here and with most Angiola CRPAQS fog samples.

Table 4-11. Carbonyl and dicarbonyl concentrations of CRPAQS fog samples.

Samples	Sample Start Date	Sample Start Time	Sample End Time	Formaldehyde (μM)	Acetaldehyde (μM)	Acrolein+ acetone (μM)	Crotonaldehyde (μM)	Glyoxal (μM)	Methyl Glyoxal (μM)
AGCC35201*	12/17/2000	10:15 PM	11:00 PM	0.86	0.41	0.34	--**	25.42	14.76
AGCC35202	12/17/2000	11:00 PM	12:00 AM	0.47	0.62	0.63	--	--	0.73
AGCC35303	12/18/2000	12:00 AM	1:00 AM	0.56	--	0.19	--	--	--
AGCC35204	12/18/2000	1:00 AM	2:00 AM	0.45	0.51	0.60	--	--	1.00
AGCC35206	12/18/2000	3:00 AM	4:00 AM	0.53	0.59	0.54	--	--	0.77
AGCC35207	12/18/2000	4:00 AM	5:00 AM	0.66	0.59	0.76	--	--	0.91
AGCC35208	12/18/2000	5:00 AM	6:00 AM	0.60	0.54	0.66	--	--	0.75
AGCC35209	12/18/2000	6:00 AM	7:00 AM	0.51	0.59	0.68	--	--	1.04
AGCC35210	12/18/2000	7:00 AM	8:00 AM	0.52	0.57	0.57	--	--	0.79
AGCC35211	12/18/2000	8:00 AM	9:00 AM	0.54	0.92	0.35	--	--	0.14
AGCC35212	12/18/2000	9:00 AM	10:00 AM	0.51	0.56	0.70	--	--	0.90
AGCC35213	12/18/2000	10:00 AM	11:00 AM	0.54	0.63	0.55	--	--	1.20
AGPCL35201	12/18/2000	12:00 AM	1:00 AM	0.95	0.58	0.17	0.64	--	0.50
AGPCL35205	12/18/2000	4:00 AM	6:00 AM	0.84	1.22	0.32	0.88	0.13	4.76
AGPCL35207	12/18/2000	7:00 AM	8:00 AM	0.81	0.58	0.20	0.45	0.12	0.81
AGPCL35208	12/18/2000	8:00 AM	9:00 AM	0.60	1.03	0.37	--	--	0.14
AGCC35302	12/19/2000	1:20 AM	3:00 AM	0.78	0.55	0.17	--	--	0.42
AGCC35303	12/19/2000	3:05 AM	5:05 AM	0.73	0.49	0.19	--	0.09	0.37
AGCC35304	12/19/2000	5:05 AM	7:35 AM	0.74	0.54	0.19	0.36	0.11	0.59

\*Sample nomenclature: AG: Angiola ground; CC: plastic CASCC collector; PCL: plastic sf-CASCC collector

352: 12/17/00; 353: 12/18/00; The last two digits are sample sequence.

\*\*-- means the concentration is below detection limit.

Table 4-12. Sampling information and concentrations of detectable carbonyls and dicarbonyls in Fresno fog samples.

4-24	Sample Name	Sample Start Date	Sample Start Time	Sample End Time	Sample Weight (g)	pH	Formaldehyde (μM)	Acetaldehyde (μM)	Acrolein +acetone (μM)	Butyraldehyde (μM)	Isovaleraldehyde (μM)	o-Tolualdehyde (μM)	m-Tolualdehyde (μM)	Gloxyal (μM)	Methyl Glyoxal (μM)
	FSC36401*	12/31/03	3:52 AM	6:30 AM	73.3	6.63	24.59	4.18	1.71	--**	2.76	--	0.10	8.81	10.73
	FSC01001	1/10/04	9:30 PM	11:37 PM	255.38	6.71	13.47	3.64	1.10	--	1.82	--	0.07	9.64	9.63
	FSC01002	1/10/04	11:38 PM	2:00 AM	238.04	6.58	17.40	5.42	1.62	--	3.34	--	0.14	26.65	16.59
	FSC01003	1/10/04	2:00 AM	9:30 AM	760.10	6.89	16.76	2.83	1.05	--	1.16	--	0.05	5.19	5.87
	FSC01004	1/11/04	9:30 AM	11:40 AM	96.9	7.1	24.08	3.51	2.45	--	1.83	--	0.10	12.33	12.53
	FSC01101	1/11/04	6:00 PM	1:00 AM	183.7	6.91	38.16	5.49	4.60	--	5.75	--	0.28	28.02	24.60
	FSC01102	1/11/04	1:00 AM	7:00 AM	213.15	7.18	28.21	3.34	3.03	--	1.81	--	0.08	10.82	8.94
	FSC01103	1/11/04	7:00 AM	10:00 AM	83.5	7.23	36.69	3.87	2.13	--	1.97	--	0.09	11.29	10.00
	FSCL01001	1/10/04	9:30 PM	1:30 AM	849.17	6.72	18.27	3.18	0.87	--	1.96	--	0.04	6.32	9.81
	FSCL01002	1/10/04	1:30 AM	5:30 AM	897.42	6.8	18.62	2.88	0.94	--	1.15	--	0.05	4.18	6.83
	FSCL01003	1/10/04	5:30 AM	9:30 AM	759.40	6.92	16.20	2.61	0.75	--	0.94	--	0.04	3.26	4.77
	FSCL01004	1/11/04	9:30 AM	11:40 AM	215.2	7.05	20.04	2.50	2.54	--	1.42	--	0.09	8.21	11.33
	FSCL01101	1/11/04	6:00 PM	1:00 AM	559.75	7.02	40.80	3.32	2.70	--	3.55	--	0.14	15.86	19.39
	FSCL01102	1/11/20	1:00 AM	7:05 AM	574.42	7.13	21.21	1.86	1.03	--	1.11	--	0.04	4.23	4.42
	FSCL01103	1/11/04	7:05 AM	10:05 AM	264.37	7.06	36.51	2.36	2.21	--	1.55	--	0.08	7.40	9.16
	FSCS01001	1/10/04	9:30 PM	1:30 AM	65.01	6.6	21.84	3.03	1.13	--	2.96	0.31	0.11	10.11	14.18
	FSCS01002	1/10/04	1:30 AM	5:30 AM	81.11	6.61	17.25	4.25	1.33	--	2.69	--	0.10	17.36	11.01
	FSCS01003	1/10/04	5:30 AM	9:30 AM	100.12	6.76	14.33	3.25	1.26	--	1.83	--	0.07	12.19	7.43
	FSCS01101	1/11/04	6:00 PM	1:00 AM	44.1	5.95	30.72	9.22	5.86	3.16	9.83	--	0.39	79.19	36.91
	FSCS01102	1/11/04	1:00 AM	7:05 AM	65.66	6.81	27.73	9.28	4.94	2.04	6.32	--	0.24	53.15	23.94
	FSCS01103	1/11/04	7:05 AM	10:05 AM	32.01	7	27.98	6.16	2.98	--	3.14	--	0.12	27.25	13.60

\*Sample nomenclature: F: Fresno; SC: ss-CASCC collector; SCL: large cut-size fraction of ss-sf-CASCC collector; SCS: small cut-size fraction of ss-sf-CASCC collector; 364, 010, 011: 352: 12/30/00, 01/10/04, 01/11/04; The last two digits are sample sequence.

\*\*-- means the concentration is below detection limit.

#### 4.2.3.2 Fresno bulk fog sample carbonyl and dicarbonyl concentrations

Formaldehyde concentrations in the Fresno fogs ranged from 13.5  $\mu\text{M}$  to 38.2  $\mu\text{M}$ , averaging 24.9  $\mu\text{M}$ . Formaldehyde is a highly soluble gas, because of its gem-diol formation in water, and is often abundant in urban atmospheres. It is directly emitted from combustion sources and produced via photochemical oxidation of many hydrocarbons. The background level of gas phase formaldehyde is reported to be in the range of 0.4-2 ppb, while in urban areas the value can be up to 10 times higher (Munger et al., 1984).

Table 4-13 shows the summary of pH and bulk organic fog sample composition. Acetaldehyde concentrations range from 2.8  $\mu\text{M}$  to 5.5  $\mu\text{M}$ , averaging 4.0  $\mu\text{M}$ ; acrolein+acetone ranges from 1.0  $\mu\text{M}$  to 4.6  $\mu\text{M}$ , averaging 2.2  $\mu\text{M}$ ; isovaleraldehyde ranges from 1.2  $\mu\text{M}$  to 5.8  $\mu\text{M}$ , averaging 2.6  $\mu\text{M}$ ; concentrations of m-tolualdehyde were smaller than other carbonyls, but still above the blanks.

Table 4-13. Summary of Fresno bulk organic fog sample composition.

Species	Number of samples	Concentration Range	Median
pH (pH units)	8	6.58-7.23	6.90
Formaldehyde ( $\mu\text{M}$ )	8	13.47-38.16	24.92
Acetaldehyde ( $\mu\text{M}$ )	8	2.83-5.49	4.04
acrolein+acetone ( $\mu\text{M}$ )	8	1.04-4.60	2.21
Isovaleraldehyde ( $\mu\text{M}$ )	8	1.16-5.75	2.55
Glyoxal ( $\mu\text{M}$ )	8	5.19-28.02	14.10
methyl glyoxal ( $\mu\text{M}$ )	8	5.87-24.60	12.36
m-tolualdehyde ( $\mu\text{M}$ )	8	0.04-0.28	0.11

Two dicarbonyls had higher concentrations than all carbonyls except formaldehyde. Glyoxal concentrations range from 5.2  $\mu\text{M}$  to 28.0  $\mu\text{M}$ , averaging 14.1  $\mu\text{M}$ . Methyl glyoxal concentrations range from 5.9  $\mu\text{M}$  to 24.6  $\mu\text{M}$ , averaging 12.4  $\mu\text{M}$ . These relatively high concentrations indicate the importance of considering dicarbonyls when looking at carbonyl concentrations or the general makeup of fog DOC.

#### 4.2.3.3 Fresno bulk fog sample composition

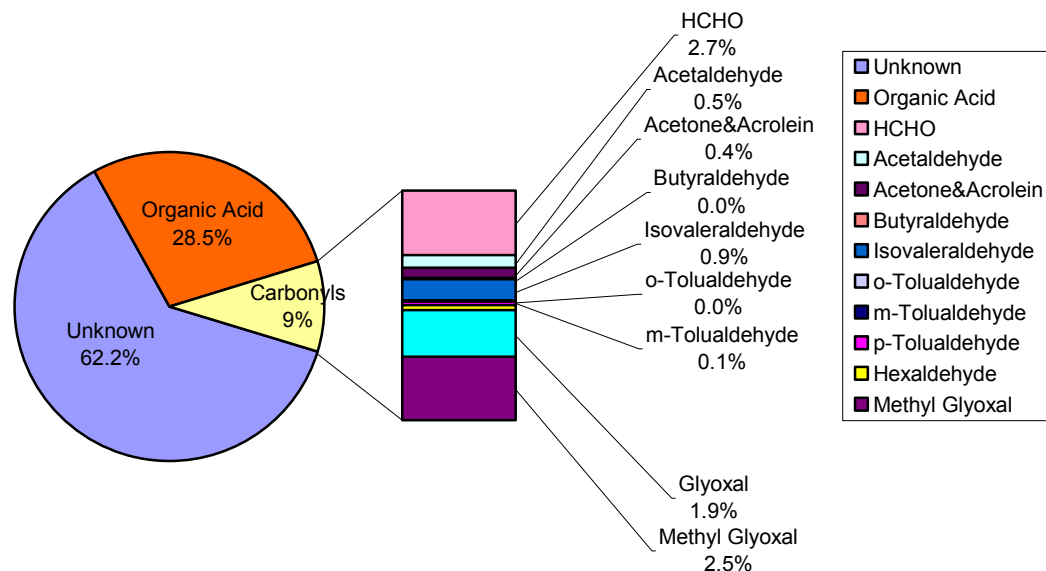


Figure 4-8. Typical composition of carbonaceous material comprising the total dissolved organic carbon (DOC) content observed for several Fresno radiation fog samples.

Figure 4-8 shows the average/typical composition of organic material comprising the total DOC in the Fresno fog samples. Organic acids (including formate, acetate, propionate, pyruvate, glutarate, succinate, malonate and oxalate) comprise 28.5% of the total DOC, while carbonyls comprise 9% of the total DOC. Among the carbonyls, formaldehyde, glyoxal and methyl glyoxal are the most abundant carbonyls in fog samples, comprising together an average of 7.1% of total DOC in the fog samples.

#### 4.2.3.4 Species size distribution of Fresno fog samples

Figures 4-9 to 4-17 shows the size distributions of carbonyls and dicarbonyls. HCHO didn't show a strong size dependence; it was approximately evenly distributed between small and large drops. Other carbonyls and dicarbonyls were more or less all enriched in small drops.

Figure 4-9. Concentrations of HCHO measured by the HPLC method and fluorescence in large and small drop samples collected with the ss-sf-CASCC in Fresno radiation fogs on Jan 10-Jan 11, 2004.

Formaldehyde didn't show large differences between large and small drops. HCHO in drops is largely taken up from the gas phase and similar

partitioning to small and large drops is expected if equilibrium is attained. Most of the available HCHO remains in the gas phase inside typical fogs and clouds (Seinfeld et al., 1998).

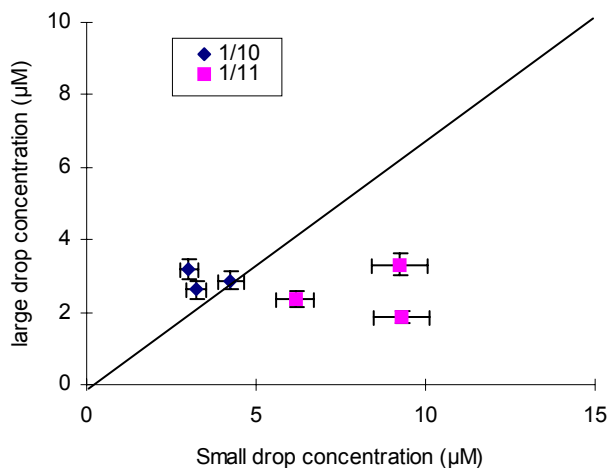
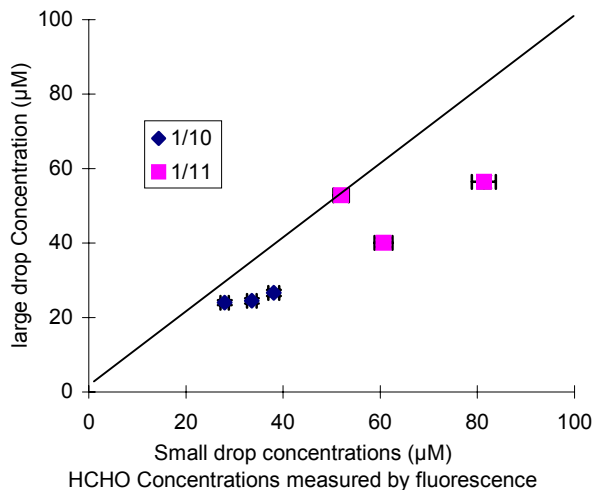


Figure 4-10. Concentrations of acetaldehyde measured by the HPLC method in large and small drop samples collected with the ss-sf-CASCC in Fresno radiation fogs on Jan 10-Jan 11, 2004.

Typical sources of acetaldehyde include emissions from combustion processes such as motor vehicles, incomplete combustion in fireplaces, industry, etc. In California, photochemical oxidation is the largest source - as high as 41 to 67 percent of acetaldehyde concentrations in the ambient air (Seinfeld et al., 1998). Acetaldehyde exists in the atmosphere in the gas phase. From Figure 4-10 we see a tendency for acetaldehyde to be enriched in smaller fog drops in the Jan. 11<sup>th</sup> samples but little size-dependence for the Jan. 10<sup>th</sup> samples.

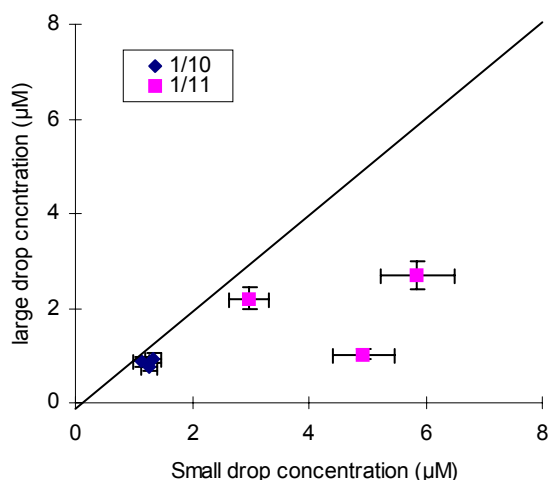


Figure 4-11. Concentrations of acrolein and acetone measured by the HPLC method in large and small drop samples collected with the ss-sf-CASCC in Fresno radiation fogs on Jan 10-Jan 11, 2004.

Acrolein can be formed from the breakdown of certain pollutants, such as heterogeneously catalyzed gas-phase oxidation of propene. Acrolein can also be from burning tobacco, or from burning gasoline. Acetone is the simplest representative of the ketones. The major source of acetone is from industrial emission where it is produced or used. Acetone is also found in plants, forest etc. As illustrated in Figure 4-11, acrolein and acetone also appear to be enriched in smaller fog drops on Jan. 11<sup>th</sup> but not on the 10<sup>th</sup>.

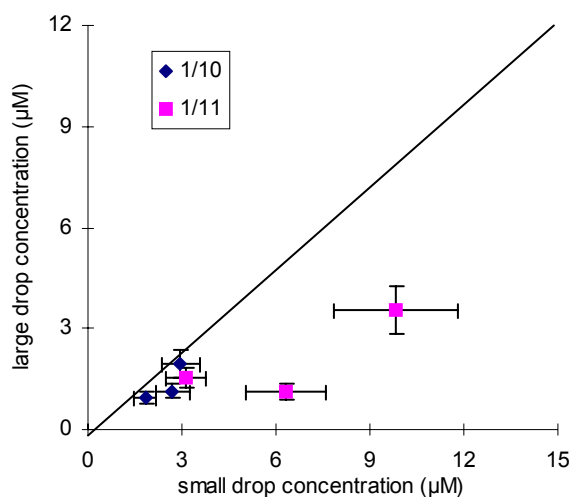


Figure 4-12. Concentrations of isovaleraldehyde measured by the HPLC method in large and small drop samples collected with the ss-sf-CASCC in Fresno radiation fogs on Jan 10-Jan 11, 2004.

Isovaleraldehyde was enriched in small drops collected on Jan. 11<sup>th</sup> as seen from Figure 4-12. It is a compound with an apple-like odor which can be derived from natural sources such as honey or the rain forest. It also comes from industrial emissions, such as those

associated with the food and fragrance industry, and contributes to the aromatic qualities of coffee.

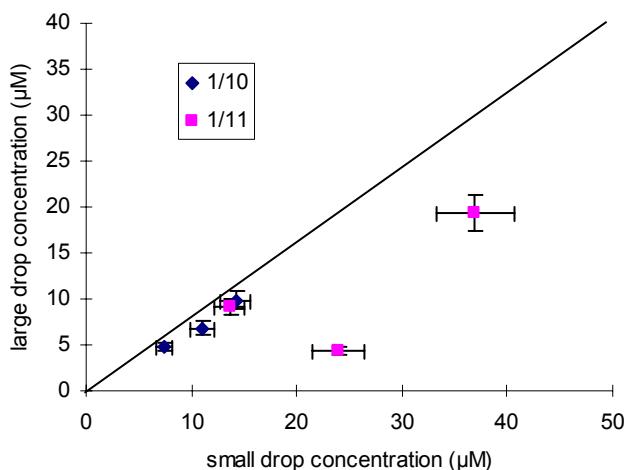


Figure 4-13. Concentrations of glyoxal measured by the HPLC method in large and small drop samples collected with the ss-sf-CASCC in Fresno radiation fogs on Jan 10-Jan 11, 2004.

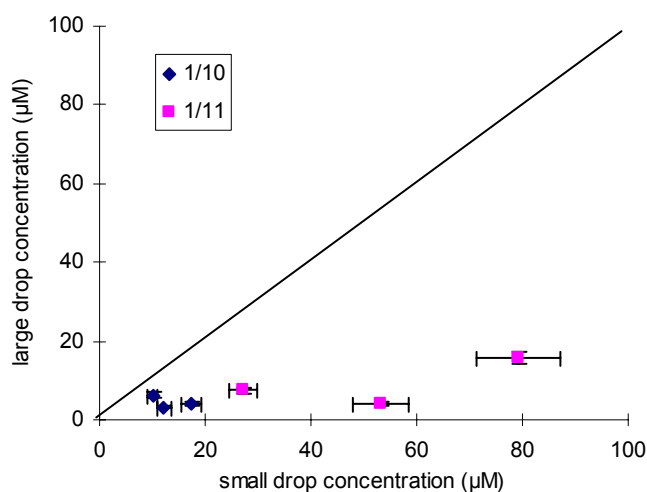


Figure 4-14. Concentrations of methylglyoxal measured by the HPLC method in large and small drop samples collected with the ss-sf-CASCC in Fresno radiation fogs on Jan 10-Jan 11, 2004.

Glyoxal and methyl glyoxal are present in tobacco smoke and are also products of ring opening reactions of PAHs. For example, toluene and other aromatics, after reaction with hydroxyl radical and oxygen in the environment, will generate ring-fragmentation products including glyoxal and methyl glyoxal (Seinfeld et al., 1998). Also some  $\alpha,\beta$ -unsaturated carbonyls, for example, acrolein, can react with ozone and OH radical, and ultimately give rise to  $\alpha$ -dicarbonyls such as glyoxal and methyl glyoxal. Figure 4-13 and 4-14 show that glyoxal and methyl glyoxal are somewhat enriched in smaller drops with generally greater enrichment for methylglyoxal. This strong enrichment in small drops mirrors patterns often seen in SJV fogs for TOC and inorganic solutes and suggests



these species are probably associated with scavenged particles. Recent studies also suggest that glyoxal may be an important aqueous phase reaction product.

#### 4.3 Functional group characterization of organic compounds in fog water.

Several investigations (e.g., Gundel et al., 1994; Saxena et al., 1996; Suzuki et al., 1998; Facchini et al., 1999; Zappoli et al., 1999; Blando et al., 2000; Decesari et al., 2000) have found that mono-, di-, and polyfunctional carboxylic acids are important contributors to water soluble organic carbon in fogs and aerosol particles. Here we utilize a different HPLC method to provide a functional group separation of organic acids. The method was first described by Fuzzi et al. (2001). It is designed to separate organic compounds in aqueous samples into several compound classes by separation on an HPLC ion exchange column with UV detection.

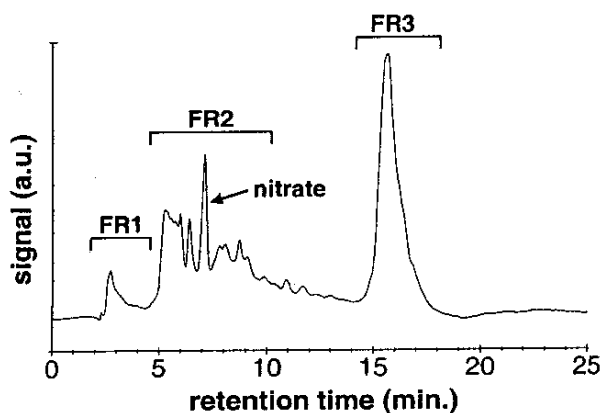


Figure 4-15. HPLC chromatograms of fog water. The three fractions defined in the test (FR1, FR2 FR3) are indicated by the horizontal bars above the chromatogram. The peak due to nitrate is also evidenced. (taken from Decesari et al. (2000)).

This method uses gradient elution by increasing the ionic strength of the eluent buffer solution to separate the WSOC in fog water. Uncharged (neutral) compounds are expected to elute the quickest because the separation method relies on ion exchange. One expects compounds with a greater number of charges (e.g., poly-functional carboxylic acids) to bind more strongly and elute later. Figure 4-15 illustrates a typical chromatogram obtained by application of this method to a fog from the Po Valley, Italy. Three fractions are identified, which the method originators typically classify as FR1 (neutral/basic compounds), FR2 (mono- and dicarboxylic acids) and FR3 (polycarboxylic acids).

This method provides a complementary way to investigate the form of the carbonaceous fraction (water-soluble organic compounds, WSOC) in fog water and was used to examine additional characteristics of organic matter in selected CRPAQS fog samples as part of our CRPAQS data analysis project. This work was completed in lieu of CRPAQS fog sample phenols analysis originally planned as it was felt to be more useful and because of likely phenol degradation during sample storage. A complete description of the method and some of its limitations is included in a journal article currently in press (Chang et al., 2005), which we include as Appendix C.

Several Angiola fog samples were analyzed by the HPLC DEAE method in Oct 2003. In many of these samples, little response was observed, probably reflecting compound degradation during the long storage period. Figure 4-16 shows a representative spectrum for sample AGCC35204, the fourth fog sample collected on 12/17/00 by a CASC collector. The peak at 6.8 min apparently is nitrate. The remainder of the chromatogram is not much different from analyzed blank samples.

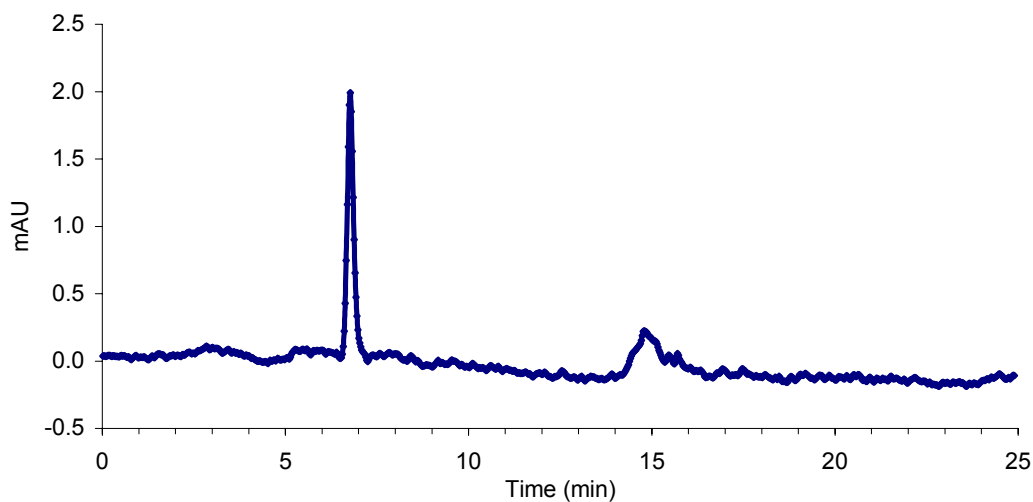


Figure 4-16. HPLC chromatogram of one CRPAQS fog sample from 12/17/00.

Four samples were found to be different from the other samples (AGCC03101, AGPCL03101, AGPCL03102 and AGPCL03103). These are bulk and large drop fog samples from a Jan 31<sup>st</sup> fog event. They all show multiple peaks with strong absorptions in

the UV. Figures 4-17 to 4-20 shows the results for these four samples.

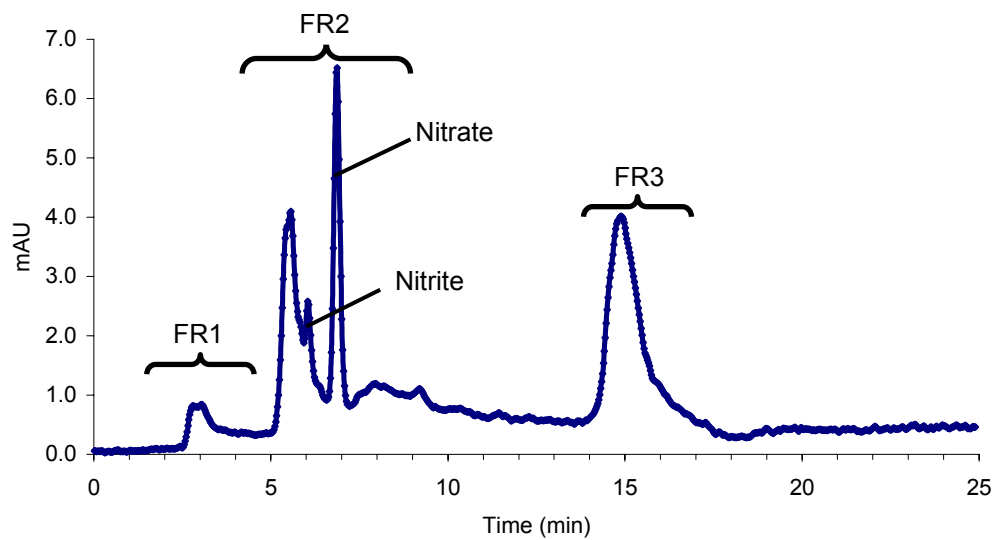


Figure 4-17. HPLC chromatogram of CRPAQS fog sample AGCC03101.

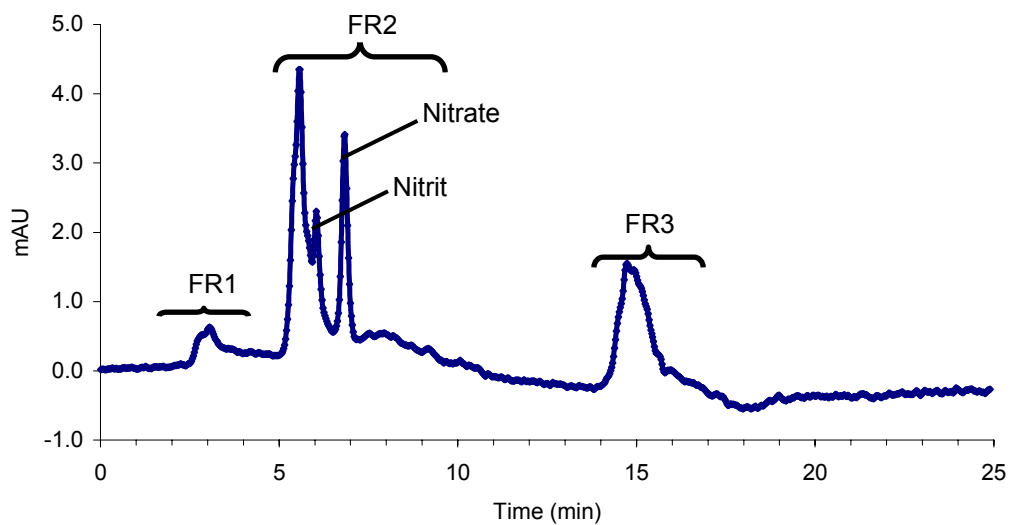


Figure 4-18. HPLC chromatogram of CRPAQS fog sample AGPCL03101.

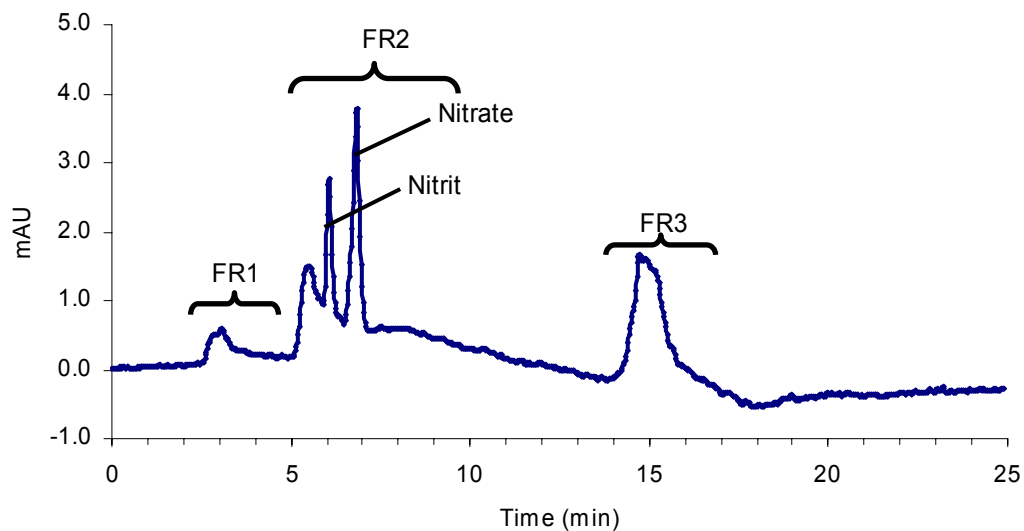


Figure 4-19. HPLC chromatogram of CRPAQS fog sample AGPCL03102.

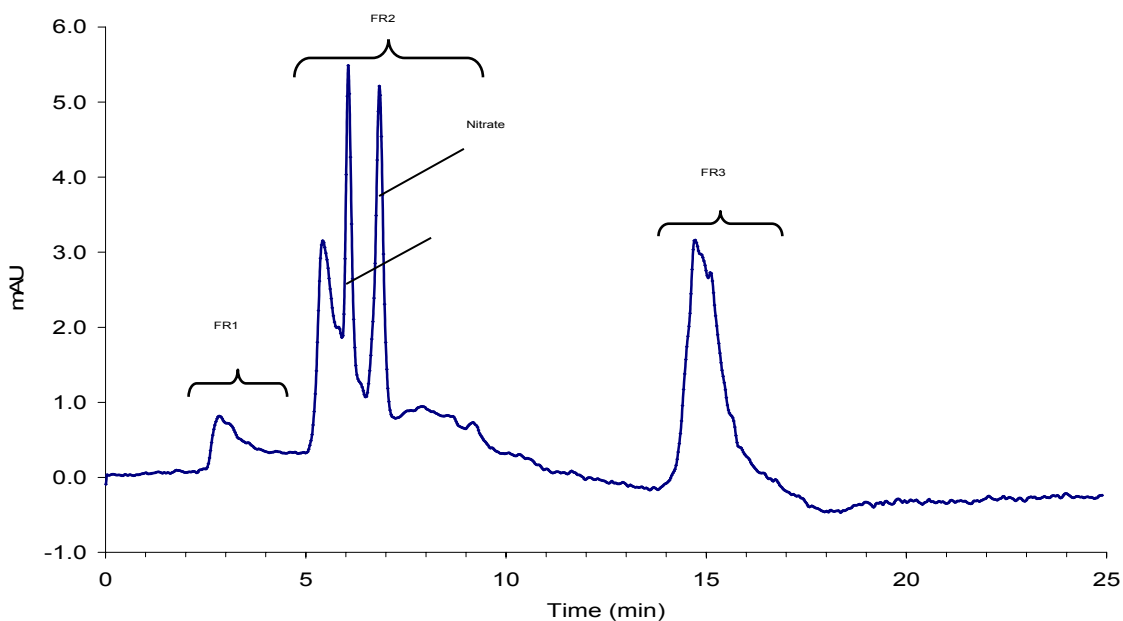


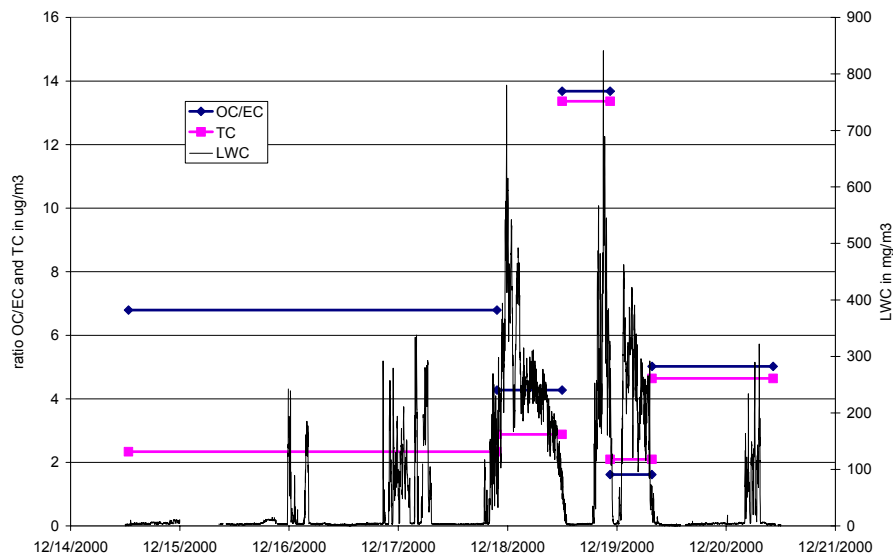
Figure 4-20. HPLC chromatogram of CRPAQS fog sample AGPCL03103.

These four chromatograms are very similar to the example shown by Fuzzi et al. (2000) for Po Valley fog. We can clearly see the nitrite and nitrate peaks, and three organic fractions as well. The prominence of FR3 suggests an important contribution to the fog organic burden from polyfunctional organic compounds, perhaps reflecting some of the

high molecular weight material measured above by ultrafiltration.

#### 4.4 CRPAQS fog interactions with elemental and organic carbon

One of the goals of the study was to investigate the effect of SJV fogs on particulate organic matter. Therefore at Angiola we collected pre- and post-fog aerosol samples as well as samples of interstitial (between the fog drops/non-scavenged) aerosol during fog episodes. A selected subset of samples was analyzed by an outside laboratory (Sunset Laboratories) for total (TC), organic (OC) and elemental carbon (EC). The results are presented in figures 4-21 to 4-24, together with the fog Liquid Water Content (LWC), which is indicative of the presence and density of fog. During fog events the TC concentrations and OC/EC ratios correspond to interstitial particles, collected downstream of a fog collector.



**Figure 4-21.** LWC, TC and OC/EC ratio for the period December 14 to December 21, 2000.

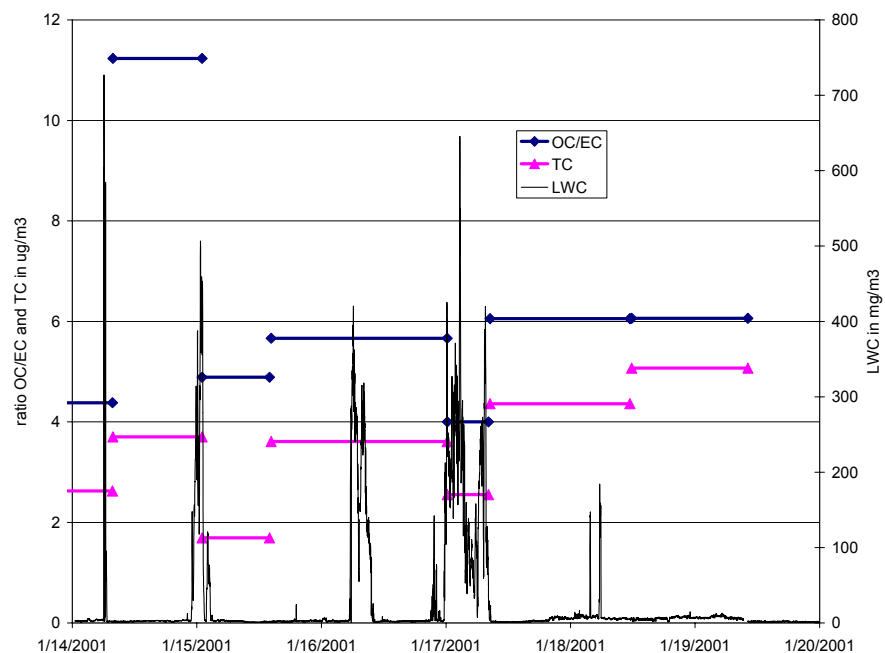


Figure 4-22. LWC, TC and OC/EC ratio for the period January 14 to January 20, 2001.

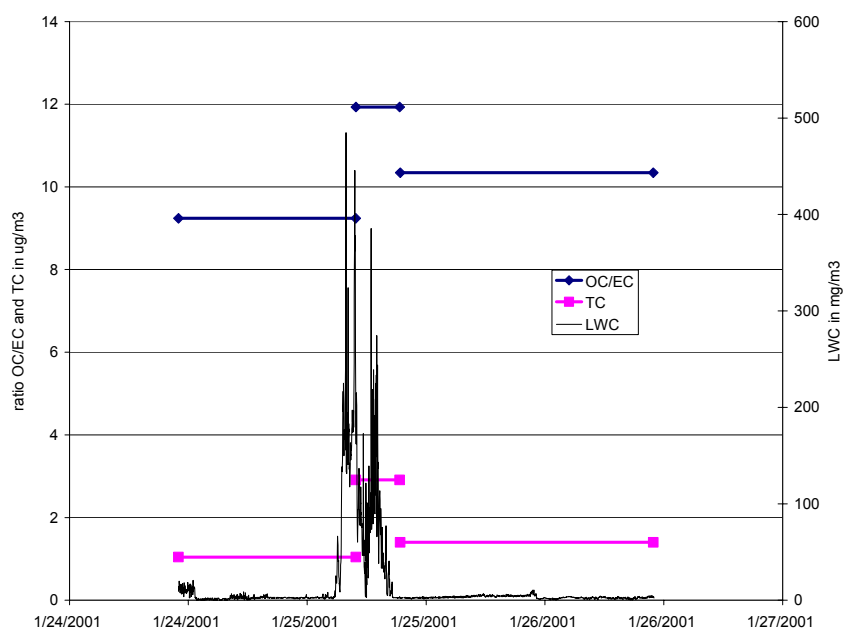


Figure 4-23. LWC, TC and OC/EC ratio for the period January 24 to January 26, 2001.

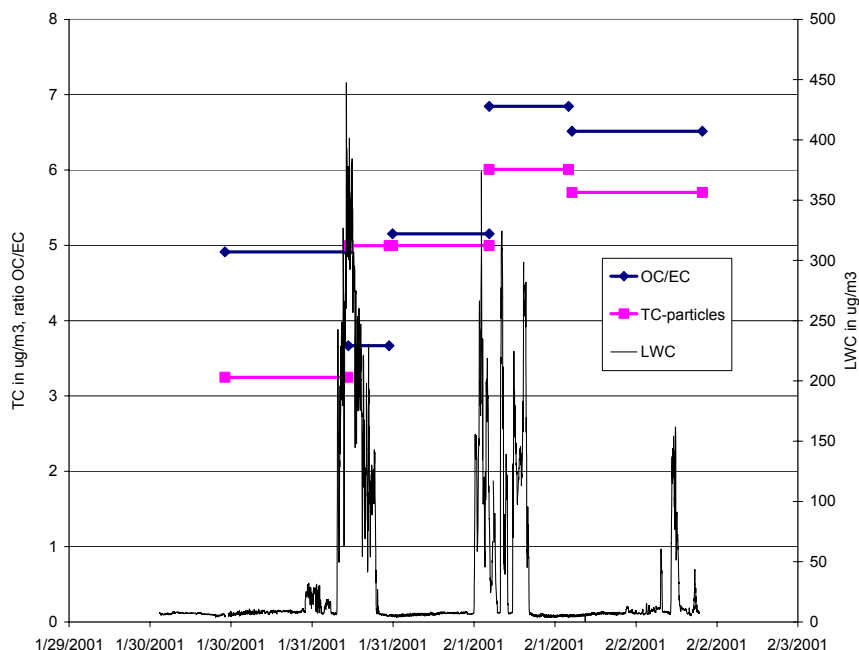


Figure 4-24. LWC, TC and OC/EC ratio for the period January 30 to February 2, 2001.

As evidenced in the plots, it is difficult to schedule short-term aerosol measurements to correspond exactly to the desired periods before, during, and after fog especially given the rather unpredictable nature of fog onset and dissipation. Interpreting differences between pre- and post-fog samples as fog scavenging and definition of aerosol carbon is also challenging as the depth of the boundary layer typically grows with onset of the fog, entraining material of unknown concentration and composition from above.

The observations suggest that a significant part of the organic carbon (OC) gets scavenged; elemental carbon (EC) is less efficiently scavenged than OC resulting in decreased OC/EC ratios in the interstitial samples. This is particularly obvious on December 18<sup>th</sup> and 19<sup>th</sup>, January 17<sup>th</sup> and January 31<sup>st</sup>. In all of these cases the ratio OC/EC decreased in the interstitial sample compared to pre-fog conditions and increased again after the fog dissipated, drying out the droplets which become particles again. On January 15<sup>th</sup> the fog event was too short to be well represented in sampling. The same is true for January 25<sup>th</sup> where the interstitial sample does not contain the beginning of the fog event but only the end part, hence it is not really representative. Finally, on February 1<sup>st</sup> the fog

dissipated and reformed several times, preventing us from differentiating clearly between interstitial and ambient particle concentrations. Overall we are confident that the results show that organic carbon gets scavenged preferentially vs. elemental carbon. Similar results have been observed in clouds forming in the Austrian Alps.

Concerning total particulate carbon scavenging, the observations indicate that for most samples the interstitial total carbon (TC) is less than the pre-fog carbon consistent with a portion of the fine particle TC being scavenged by fog drops. This is also consistent with the high concentrations of total organic carbon (TOC) observed in the fogwater, although one must keep in mind that fog TOC represents a mix of scavenged particulate OC and gaseous volatile organic compounds (e.g., acetic acid, formic acid, and formaldehyde). In some periods, the TC does not decrease as expected. This may reflect changes occurring in atmospheric composition during the sampling periods and/or effects of entrainment from above the boundary layer during fog growth. Interestingly, post-fog concentrations of particles are often higher than pre-fog concentrations raising a question as to whether aqueous reactions in the fog drops might transform soluble VOCs into lower volatility secondary organic aerosol (SOA) species, analogous to aqueous phase transformation of gaseous sulfur dioxide to particulate sulfate. Although transformations of this type have been discussed in the literature (e.g., Blando and Turpin, 2000), the organic chemistry of the atmospheric aqueous phase is largely unknown and the importance of aqueous phase SOA production is primarily a topic of speculation at present. Significant aqueous SOA production has not been clearly documented in any field experiment, in part because of the difficulty of adequately characterizing such a complex, multiphase system. Measurements during CRPAQS are also inadequate to do more than speculate whether the presence of the fogs contributed to SOA formation or whether changes in particulate TC concentrations resulted from other mechanisms such as advection or entrainment.

We tentatively calculated OC, EC, and TC scavenging efficiencies for all fog events where data were available. The results are given in Table 4-14 for three events where fog scavenging appeared to dominate concentration changes (i.e., TC was observed to decrease upon fog formation). Scavenging efficiencies for OC were calculated to vary between 33 and 90%. Scavenging efficiencies for EC were much lower, ranging from 5 to 12%.



Table 4-14. Observed scavenging efficiencies

Date	$\eta_{OC}$	$\eta_{EC}$	$\eta_{TC}$
19-Dec	0.90	0.12	0.84
15-Jan	0.59	0.05	0.54
17-Jan	0.33	0.06	0.29

As described above, the ability to make fog scavenging measurements of this type is limited in part by concentration changes that can occur during the long sampling intervals needed for the filter-based sampling. We hoped to minimize this problem by making use of semi-continuous measurements of OC and EC made independently at Angiola during CRPAQS. Examination of this data set, however, revealed several problems. Figure 4-25 illustrates that CRPAQS continuous OC/EC measurements indicate the presence of similar amounts of OC and EC. This finding seems unlikely and the reported concentrations are inconsistent with the values we measured on our filter samples. The continuous data also show a spurious shift in values after a certain date. Consequently, we opted not to rely on these data for examining fog effects on particulate carbon.

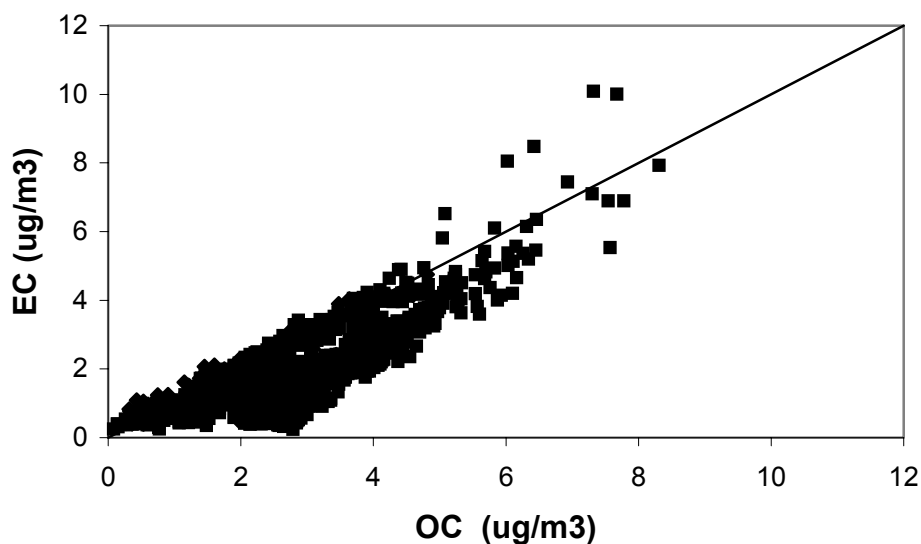


Figure 4-25. EC vs OC concentrations from continuous measurements at Angiola.

A different particulate carbon data set available at the Angola site is from DRI, obtained by thermal optical reflectance method measurements of filter samples. This data is available for ~5 hour filter samples on intensive operation days. Examining relevant periods of data, it appears that EC vs OC shows a steeper slope for samples collected during fog periods compared to samples collected during fog free periods (figure 4-26). This would suggest again that OC gets scavenged preferentially compared to EC (the fog drops are generally too large to penetrate the PM<sub>2.5</sub> inlet of the aerosol sampler). Nevertheless the data are quite scattered and a possible artifact may derive from the fact that non fog periods are mainly during the daytime while fog periods are during night time. Hence a diurnal variation in OC/EC ratios could bias the results.

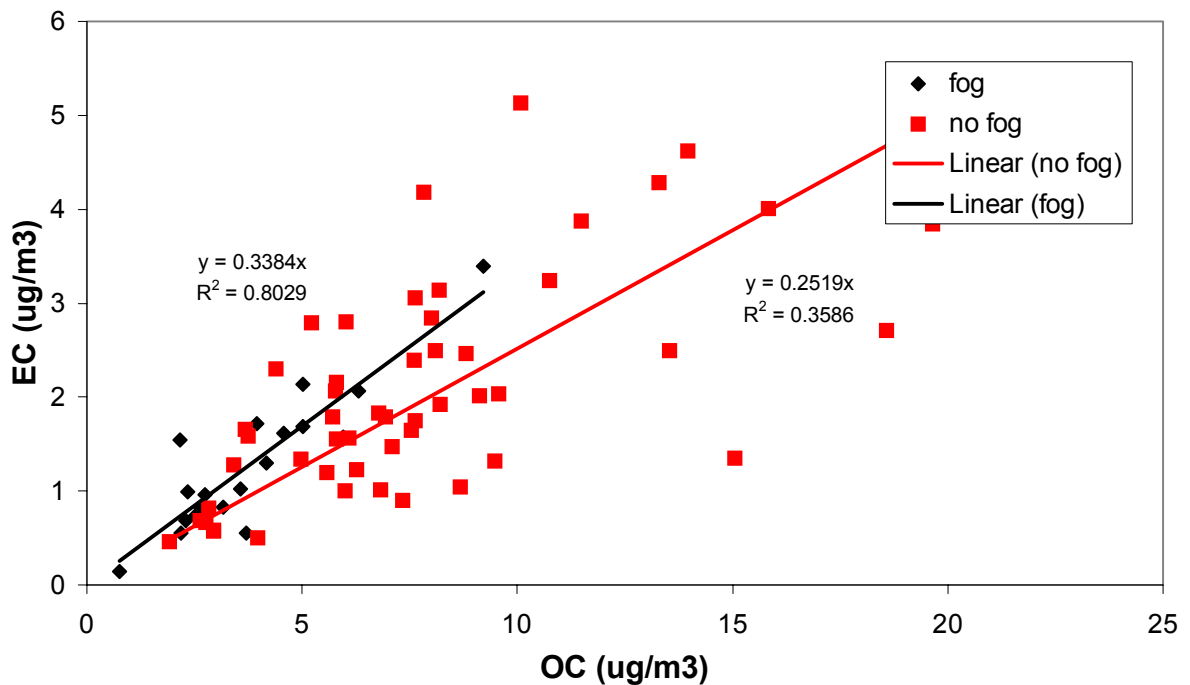


Figure 4-26. Short term DRI filter EC vs OC data for IOP days at Angiola.

#### 4.5 CRPAQS fog interactions with organic aerosols

In addition to organic and elemental carbon scavenging we looked at scavenging of individual organic species (X) and their variation compared to organic carbon (X/OC). Evaluation of the results shows some of the same limitations observed for carbon

scavenging: long sampling times and varying degrees of mismatch between sample periods and fog occurrence. These shortcomings limit the definitiveness of the results. Furthermore, for individual trace organic species, concentrations in the relatively short duration interstitial samples are often close to or below detection limit. With these limitations in mind, we discuss here scavenging results for several individual organic compounds or compound families.

#### **4.5.1 Levoglucosan**

Figures 4-27 to 4-30 show the variation of levoglucosan concentrations throughout different CRPAQS fog events. Levoglucosan is a compound commonly used as a tracer for wood smoke as it is emitted into the atmosphere by combustion of cellulose. In the first events of the study (see Fig. 4-27), it appears that levoglucosan concentrations decrease strongly in the particulate phase during fog events. These decreases are even larger than particulate OC concentration decreases, suggesting that carbonaceous particles in wood smoke are scavenged preferentially over other organic carbon particle types. This is not terribly surprising, given the more polar nature and higher degree of water solubility of levoglucosan and other wood combustion products. In the post-fog and interstitial aerosol samples on 12/18 and 12/19, in fact, levoglucosan/OC ratios approach zero, suggesting strong scavenging and deposition of wood smoke particles by the fog. A higher levoglucosan/OC ratio following the 12/19 fog event may reflect transport of fresh or non-fog-processed aerosol to Angiola during this longer sampling period.

During a second fog episode, on the night of 1/16-17 (figure 4-28) the situation is similar with a lower ratio during the fog event than prior to the fog event, suggesting again preferential scavenging. The levoglucosan/OC ratio again climbs following the event. Although this may reflect transport of fresh or unprocessed wood smoke aerosol, no evidence is available to support or refute this hypothesis. During all of the periods examined, we see considerable variability in the fraction of OC accounted for by levoglucosan. This is not surprising given the apparent strong influence of the fog on wood smoke particles, but it is interesting given that levoglucosan is certainly a major, if

not the most abundant organic species in the fine particles, accounting for up to 3% of the organic carbon.

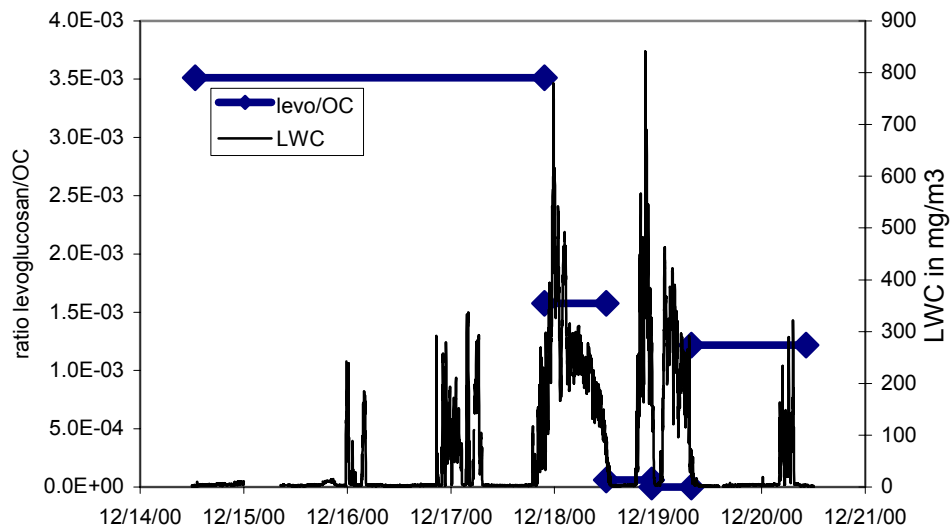


Figure 4-27. Evolution of fog LWC and ratio of particulate concentrations of levoglucosan to OC at Angiola during the period 12/14 to 12/21/00.

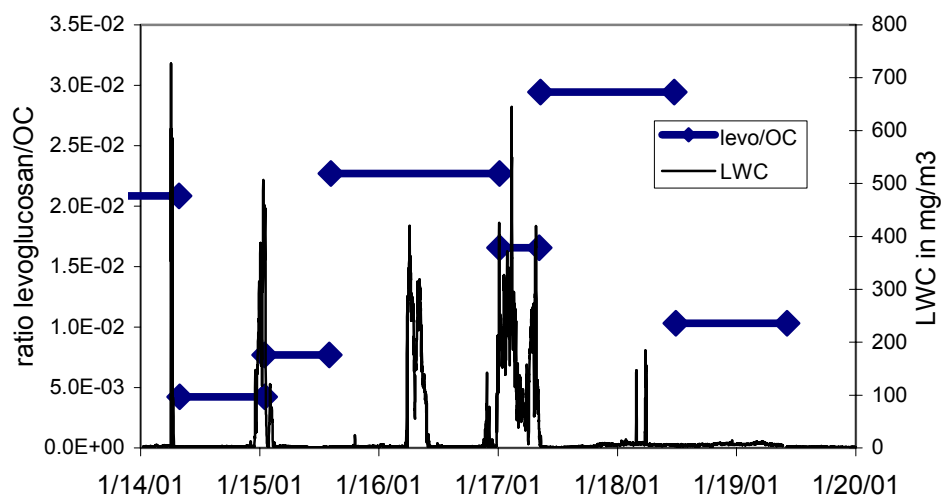


Figure 4-28. Evolution of fog LWC and ratio of particulate concentrations of levoglucosan to OC at Angiola during the period 1/14 to 1/20/01.

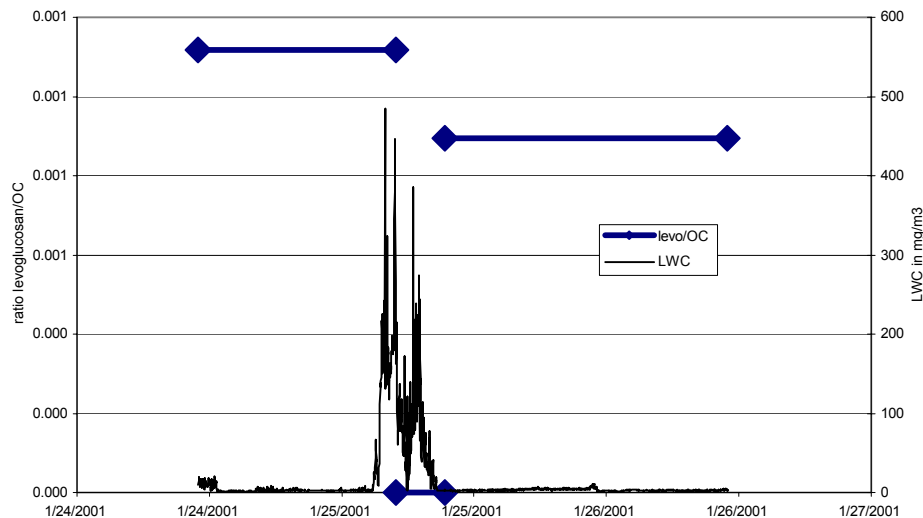


Figure 4-29. Evolution of LWC and ratio of particulate concentrations of levoglucosan to OC at Angiola during the period 1/24 to 1/27/01.

Figure 4-29 shows a fog event towards the end of January in a period where levoglucosan concentrations were rather low. During this time, in the interstitial aerosol sample, levoglucosan was not even detected. Hence, we see the same phenomenon as in the two previous periods where levoglucosan is scavenged preferentially compared to total fine particle OC. The levoglucosan/OC ratio again climbs following the fog, but this time does not exceed the pre-fog concentration.

All the fog events discussed up to now suggest that wood smoke particles are scavenged preferentially relative to the remainder of the fine particle organic carbon. One other period of fog/scavenging data is available in late January/early February. In this period, however, sampling periods are not very well matched with fog occurrence and dissipation, making it difficult to interpret aerosol-fog interactions.

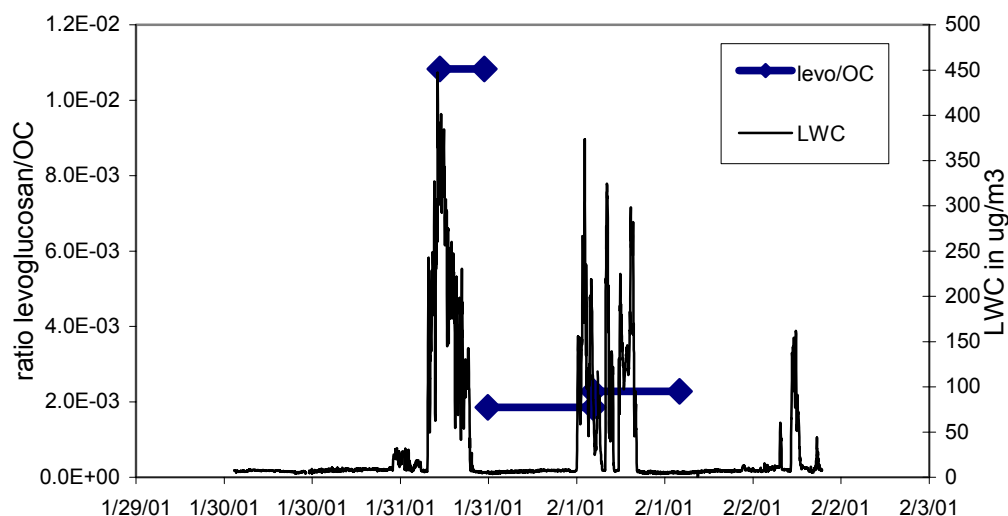


Figure 4-30. Evolution of fog LWC and ratio of particulate concentrations of levoglucosan to OC at Angiola during the period 1/29 to 2/3/01.

Overall it appears that levoglucosan, and by extension wood smoke, is scavenged preferentially by CRPAQS fogs over other organic carbon particle types. This results sometimes in a decrease in importance of wood smoke in the ambient carbonaceous matter after a fog event. Interpretation of the data is complicated, however, by the relatively long sampling periods needed to ensure adequate filter mass loadings of levoglucosan and the difficulty in matching filter sampling periods precisely with fog onset and dissipation over a multi-week study. Techniques currently in development in our laboratory for more rapid levoglucosan measurement promise to improve our ability to examine wood smoke scavenging by fog in future studies.

#### 4.5.2 Polycyclic Aromatic Hydrocarbons (PAH)

In addition to levoglucosan, we followed the evolution of selected PAH in a few fog episodes. Additional problems arise in this case due to the low concentrations of these species which are often close to or below detection limits in short duration samples. While the data are not entirely clear cut, they tend to show that PAH, very nonpolar and insoluble molecules, like pyrene (Figure 4-31), are scavenged less efficiently than OC as a whole resulting in higher pyrene/OC ratios in the interstitial aerosol compared to the ambient aerosol before and after a fog event.

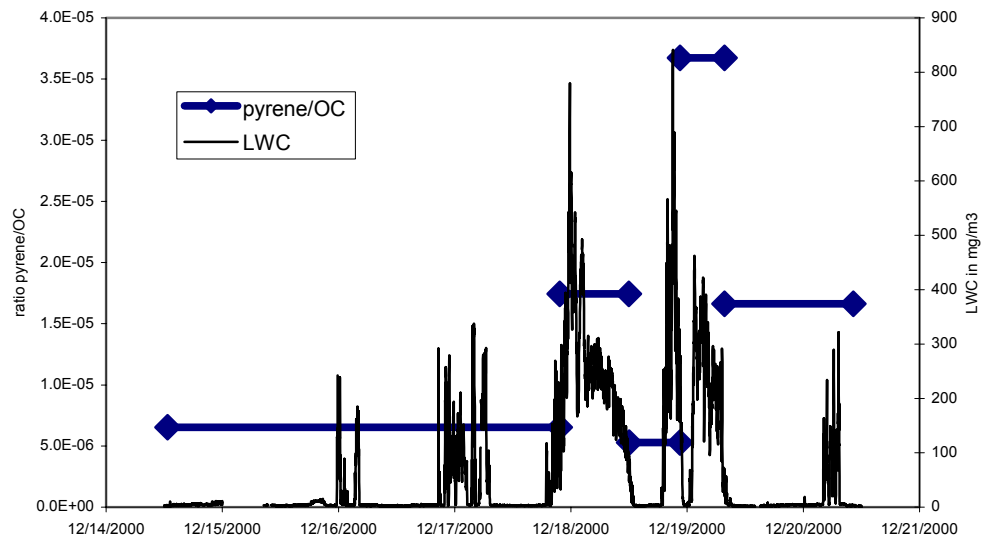


Figure 4-31. Evolution of LWC and ratio of particulate concentrations of pyrene to OC, at the beginning of the CRPAQS fog study.

On the other hand oxy-PAH, including anthracenedione (Figure 4-32), show lower species/OC ratios in the interstitial aerosol than in the ambient aerosol before or after fog. Anthracenedione was in fact not detected in the interstitial aerosol; assuming a concentration equal to its detection limit would still imply a sharp decrease in anthracenedione/OC ratios during fog.

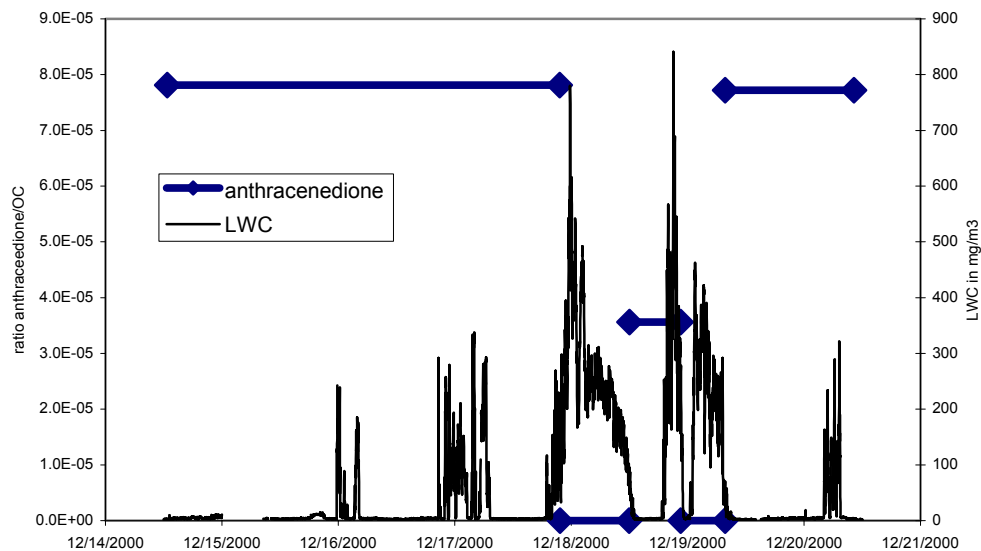


Figure 4-32. Evolution of fog LWC and ratio of particulate concentrations of anthracenedione to OC at Angiola during the beginning of the CRPAQS fog study.

### 4.5.3 Pesticides

We finally look at the variability of a particle bound pesticide (Diazinon) in foggy CRPAQS periods. Figure 4-33 shows the variability in concentrations and in the ratio of the pesticide to OC. While the pesticide is always detected in non-fog periods, it was never detected in the interstitial particles. Diazinon was observed to be a dominant species in the fog droplets themselves, consistent with effective fog scavenging of this species from the atmosphere. This strong interaction suggests the occurrence of fog may provide an effective pathway for removing Diazinon from the atmosphere. We take up the topic of fog deposition in the next chapter.

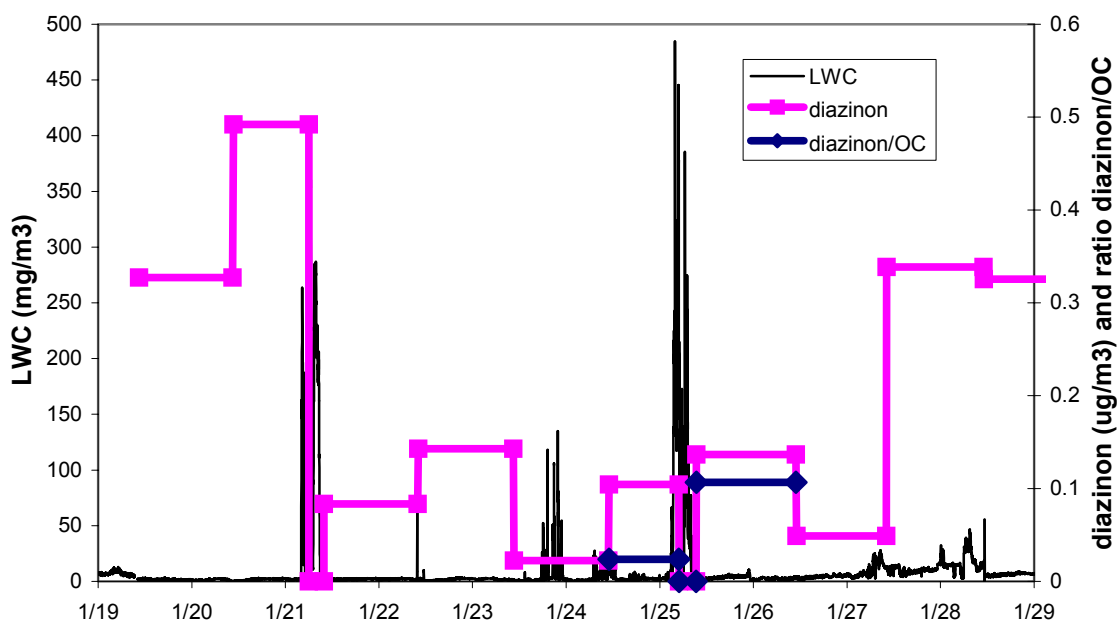


Figure 4-33. Evolution of fog LWC, particle phase Diazinon concentration and ratio of Diazinon to OC at Angiola towards the end of the CRPAQS fog study.



## Chapter 5

### Aerosol processing and removal by CRPAQS fogs

#### 5.1 Overview

Fog scavenging of both particles and soluble gases followed by deposition of fog droplets can be an important wet removal process of air pollutants and other atmospheric species (Collett et al., 2001; Moore et al., 2004). Sedimentation dominates drop removal in low wind speed radiation fogs over smooth surfaces (Dollard et al., 1983; Fitzjarrald et al., 1986; Eugster et al., 2001), while impaction and interception can be quite important for capture of fog drops by forest canopies and grasslands (Eugster et al., 2001; Wrzesinsky et al., 2001). Formal studies show that enhanced aerosol deposition in fogs efficiently limits pollutant accumulation during stagnation episodes; this limitation and even reductions have been attributed, at least in part, to removal of scavenged aerosols by deposition of fog drops (Jacob et al., 1984; Jacob et al., 1986; Waldman et al., 1987; Forkel et al., 1990; Pandis et al., 1992; Lillis et al., 1999).

In order to evaluate the role SJV radiation fogs played in pollutant removal during the CRPAQS study, several deposition measurements were made. The purposes of this study were to (1) evaluate the suitability and consistency of simple fog deposition measurement methods, (2) observe and evaluate the impacts of different underlying surfaces, (3) characterize individual species deposition fluxes and velocities, and (4) examine the relationship between deposition velocity of an individual chemical species and its distribution across the fog drop size spectrum. We discuss the findings of these measurements here. The measurement methods were previously described in Chapter 2.

Table 5-1. Deposited fog water mass, ion and TOC concentrations observed on the two deposition plates

Sample Start Date	Sample Start Time	Sample End Time	Fog water (g)		Cl <sup>-</sup> (μN)		NO <sub>3</sub> <sup>-</sup> (μN)		NO <sub>2</sub> <sup>-</sup> (μN)		SO <sub>4</sub> <sup>2-</sup> (μN)		Na <sup>+</sup> (μN)		NH <sub>4</sub> <sup>+</sup> (μN)		K <sup>+</sup> (μN)		Mg <sup>2+</sup> (μN)		Ca <sup>2+</sup> (μN)		TOC (ppmC)	
			Dplate 1	Dplate 2	Dplate 1	Dplate 2	Dplate 1	Dplate 2	Dplate 1	Dplate 2	Dplate 1	Dplate 2	Dplate 1	Dplate 2	Dplate 1	Dplate 2	Dplate 1	Dplate 2	Dplate 1	Dplate 2	Dplate 1	Dplate 2	Dplate 1	Dplate 2
12/17/2000	11:00 PM	1:00 AM	9.28	8.39	--	17.2	--	167	--	8.81	--	35.1	--	8.52	--	452	--	5.68	--	6.51	--	35.7	4.31	--
12/18/2000	1:00 AM	3:10 AM	17.4	16.8	18.4	17.3	176	169	11.5	11.8	40.8	38.9	10.0	10.0	485	502	8.24	8.04	8.83	9.64	48.9	60.2	4.79	4.25
12/18/2000	3:10 AM	6:10 AM	33.1	--	15.5	13.7	158	160	8.55	9.20	31.4	32.6	4.96	3.82	520	526	6.12	4.71	5.98	6.38	18.8	29.1	3.18	--
12/18/2000	6:10 AM	8:15 AM	19.5	19.2	20.1	20.5	129	138	11.3	13.0	63.1	66.6	23.4	22.7	759	768	5.18	5.11	6.20	5.55	20.7	23.9	3.65	3.84
12/18/2000	8:15 AM	10:00 AM	8.90	8.10	39.5	33.3	154	160	17.9	18.3	84.3	89.4	45.2	30.6	891	902	21.8	9.44	8.34	8.06	36.6	44.5	5.85	5.79
12/18/2000	10:00 AM	12:00 PM	1.00	1.80	77.3	68.6	520	470	90.6	82.8	351	340	175	155	1859	1701	62.6	51.5	42.0	60.8	38.6	36.0	27.3	--
12/19/2000*	5:15 AM	7:35 AM	7.70	4.60	15.8	14.2	80.1	81.0	11.3	11.9	20.4	19.8	13.8	12.2	439	422	7.41	6.49	5.59	6.19	24.1	17.6	2.81	--
1/15/2001	1:00 AM	3:00 AM	5.10	5.30	18.7	23.3	45.8	49.7	11.1	9.65	12.4	13.7	13.7	14.2	231	223	9.01	8.69	5.43	4.85	13.2	18.7	3.67	4.91
1/17/2001	12:15 AM	2:00 AM	3.80	4.90	22.3	28.4	100	114	44.3	45.6	21.8	30.5	14.0	19.7	380	534	12.3	20.6	5.86	8.14	31.8	46.4	7.81	--
1/17/2001	2:00 AM	3:55 AM	8.00	7.70	14.4	19.5	80.3	83.8	33.9	35.5	19.4	21.0	4.20	11.0	335	374	5.68	10.2	4.97	5.27	14.8	20.2	5.15	6.59
1/17/2001	4:00 AM	6:00 AM	5.70	5.50	15.4	16.7	54.7	59.0	51.4	54.0	18.8	21.6	7.11	8.57	295	313	6.32	7.05	5.63	5.42	19.6	21.3	5.16	6.21
1/17/2001	6:00 AM	8:00 AM	7.40	6.90	18.8	19.4	63.0	69.1	55.9	61.2	20.6	23.2	9.99	10.2	316	313	8.08	6.19	5.65	5.54	16.7	16.6	--	--
1/21/2001	6:15 AM	7:15 AM	2.70	2.70	22.0	25.3	463	423	51.4	46.1	50.3	40.9	27.7	20.5	889	731	22.9	19.3	8.68	6.04	25.8	26.3	9.12	--
1/21/2001	7:15 AM	9:15 AM	7.00	7.20	24.6	16.8	365	352	61.8	56.6	61.2	56.5	30.1	16.8	786	703	17.0	8.88	10.1	7.65	42.9	40.7	11.9	11.0
1/25/2001	5:00 AM	6:00 AM	2.80	1.90	56.4	67.0	26.6	36.1	8.69	13.2	11.5	22.1	46.4	69.1	152	262	15.6	27.4	6.74	10.6	62.1	66.2	7.22	--
1/25/2001	6:00 AM	7:30 AM	2.90	2.70	54.5	63.6	37.1	40.4	18.3	19.6	13.9	18.3	41.6	50.5	250	259	6.55	10.8	6.87	7.58	14.0	25.7	6.67	--
1/31/2001	5:15 AM	7:00 AM	12.6	14.1	27.0	24.0	220	210	37.2	37.5	55.5	61.6	24.0	23.2	575	581	9.19	6.61	5.01	7.91	40.5	42.6	9.33	10.9
1/31/2001	7:00 AM	9:05 AM	3.30	2.90	28.8	30.0	450	459	129	135	108	115	38.9	37.0	1370	1301	16.8	16.4	7.64	6.88	27.8	31.0	23.5	20.9
2/1/2001	2:15 AM	3:55 AM	5.00	--	28.4	--	92.5	--	51.4	--	44.4	--	23.8	--	335	--	12.1	--	6.24	--	30.0	--	6.77	--

TOC, total organic carbon; Dplate, Deposition plate; μN, micronormal; ppmC, parts per million carbon by mass

\* There was a problem on the second deposition plate, so only the data from the first plate is used

Table 5-2. Fog water, ion and TOC fluxes derived from the two deposition plates.

Sample Start Date	Sample Start Time	Sample End Time	Fog water (g/m2/min)		Cl- (neq/m2/min)		NO3- (neq/m2/min)		NO2- (neq/m2/min)		SO42- (neq/m2/min)		Na+ (neq/m2/min)		NH4+ (neq/m2/min)		K+ (neq/m2/min)		Mg2+ (neq/m2/min)		Ca2+ (neq/m2/min)		TOC (µgC/m2/min)	
			Dplate 1	Dplate 2	Dplate 1	Dplate 2	Dplate 1	Dplate 2	Dplate 1	Dplate 2	Dplate 1	Dplate 2	Dplate 1	Dplate 2	Dplate 1	Dplate 2	Dplate 1	Dplate 2	Dplate 1	Dplate 2	Dplate 1	Dplate 2	Dplate 1	Dplate 2
12/17/2000	11:00 PM	1:00 AM	0.26	0.23	--	4.02	--	38.9	--	2.05	--	8.18	--	1.99	--	105	--	1.32	--	1.52	--	8.32	1.11	--
12/18/2000	1:00 AM	3:10 AM	0.45	0.43	8.19	7.45	78.7	72.9	5.14	5.08	18.2	16.8	4.48	4.31	216	216	3.68	3.46	3.94	4.15	21.8	25.9	2.14	1.83
12/18/2000	3:10 AM	6:10 AM	0.61	--	9.49	--	97.0	--	5.24	--	19.2	--	3.04	--	319	--	3.75	--	3.67	--	11.5	--	1.95	--
12/18/2000	6:10 AM	8:15 AM	0.52	0.51	10.5	10.5	67.1	70.4	5.89	6.65	32.8	34.1	12.2	11.6	395	393	2.69	2.62	3.22	2.84	10.8	12.2	1.90	1.97
12/18/2000	8:15 AM	10:00 AM	0.28	0.26	11.2	8.57	43.6	41.2	5.05	4.71	23.8	23.0	12.8	7.88	252	232	6.16	2.43	2.36	2.07	10.3	11.4	1.65	1.49
12/18/2000	10:00 AM	12:00 PM	0.03	0.05	2.15	3.43	14.4	23.5	2.52	4.14	9.76	17.0	4.85	7.76	51.6	85.1	1.74	2.57	1.17	3.04	1.07	1.80	0.76	--
12/19/2000	5:15 AM	7:35 AM	0.12	--	2.89	--	14.7	--	2.07	--	3.74	--	2.54	--	80.5	--	1.36	--	1.02	--	4.42	--	0.52	--
1/15/2001	1:00 AM	3:00 AM	0.14	0.15	2.65	3.43	6.49	7.32	1.57	1.42	1.76	2.02	1.94	2.09	32.8	32.9	1.28	1.28	0.77	0.71	1.87	2.75	0.52	0.72
1/17/2001	12:15 AM	2:00 AM	0.12	0.16	2.69	4.42	12.1	17.7	5.35	7.09	2.63	4.75	1.69	3.06	45.8	83.1	1.49	3.20	0.71	1.27	3.77	7.21	0.94	--
1/17/2001	2:00 AM	3:55 AM	0.25	0.24	3.65	4.78	20.4	20.5	8.60	8.68	4.92	5.12	1.07	2.70	85.2	91.3	1.44	2.49	1.26	1.29	3.76	4.94	1.31	1.61
1/17/2001	4:00 AM	6:00 AM	0.16	0.15	2.44	2.55	8.66	9.01	8.14	8.25	2.98	3.30	1.13	1.31	46.7	47.8	1.00	1.08	0.89	0.83	3.06	3.26	0.82	0.95
1/17/2001	6:00 AM	8:00 AM	0.21	0.19	3.86	3.72	12.9	13.2	11.5	11.7	4.23	4.44	2.05	1.95	65.0	59.9	1.66	1.19	1.16	1.06	3.43	3.19	--	--
1/21/2001	6:15 AM	7:15 AM	0.15	0.15	3.30	3.80	69.5	63.5	7.71	6.91	7.55	6.14	4.16	3.08	133	110	3.43	2.89	1.30	0.91	3.86	3.95	1.37	--
1/21/2001	7:15 AM	9:15 AM	0.19	0.20	4.78	3.35	71.0	70.5	12.0	11.3	11.9	11.3	5.85	3.37	153	141	3.30	1.78	1.96	1.53	8.35	8.14	2.32	2.20
1/25/2001	5:00 AM	6:00 AM	0.16	0.11	8.78	7.07	4.14	3.81	1.35	1.39	1.79	2.33	7.22	7.30	23.6	27.6	2.43	2.89	1.05	1.11	9.66	6.99	1.12	--
1/25/2001	6:00 AM	7:30 AM	0.11	0.10	5.85	6.36	3.98	4.04	1.96	1.96	1.49	1.83	4.47	5.05	26.9	25.9	0.70	1.08	0.74	0.76	1.47	2.57	0.72	--
1/31/2001	5:15 AM	7:00 AM	0.40	0.45	10.8	10.7	88.1	94.0	14.9	16.8	22.2	27.6	9.60	10.4	230	260	3.68	2.96	2.00	3.54	16.2	19.1	3.73	4.87
1/31/2001	7:00 AM	9:05 AM	0.09	0.08	2.53	2.32	39.6	35.5	11.3	10.4	9.48	8.91	3.42	2.86	121	101	1.47	1.27	0.67	0.53	2.45	2.40	2.07	1.61
2/1/2001	2:15 AM	3:55 AM	0.17	--	4.73	--	15.4	--	8.56	--	7.40	--	3.96	--	55.9	--	2.02	--	1.04	--	5.00	--	1.13	--

TOC, total organic carbon; Dplate, deposition plate;

neq/m2/min, nanoequivalents per square meter per minute; µgC/m2/min, microgram carbon per square meter per minute

\* There was a problem on the second deposition plate, so only the flux from the first plate is used

In addition to this removal mechanism, fog scavenges preexisting gases and aerosol particles and can increase the amount of particulate matter through chemical reactions in the aqueous phase. One of the most important reactions is the oxidation of aqueous free S(IV) into sulfuric acid. In order to study the new particle production in fogs via S(IV) oxidation, an aqueous chemical model was used to obtain the sulfate production rates with drop size. This model also includes S(IV) reaction to form hydroxymethanesulfonate (HMS) which was observed during CRPAQS by the Prather group to be a useful marker of aerosol processing by fogs..

## 5.2 Results and Discussion

### 5.2.1 Ion concentrations and flux calculations from deposition plates

Teflon deposition plates were used to measure deposition fluxes of fog water and fog solutes in several CRPAQS fog episodes. Table 5-1 lists the sampling date and time of each fog event and concentrations of major ions and total organic carbon (TOC) measured in deposited fog water collected by two deposition plates operated side-by-side. Table 5-2 lists the fluxes of water, TOC and ions, including  $\text{Cl}^-$ ,  $\text{NO}_3^-$ ,  $\text{SO}_4^{2-}$ ,  $\text{Na}^+$ ,  $\text{NH}_4^+$ ,  $\text{Mg}^{2+}$ ,  $\text{K}^+$ ,  $\text{Ca}^{2+}$  and  $\text{NO}_2^-$ . Figures 5-1 to 5-22 provide a comparison of water mass, solute concentrations and species fluxes observed on the replicate deposition plates. The results reveal that the two deposition plates agree well. Correlation coefficients ( $R^2$ ) between the two plates for fluxes of water,  $\text{NO}_3^-$ ,  $\text{SO}_4^{2-}$ ,  $\text{NH}_4^+$ ,  $\text{Ca}^{2+}$ ,  $\text{NO}_2^-$  and TOC are higher than 0.9 (not shown in figures); while correlation coefficients for fluxes of  $\text{Cl}^-$ ,  $\text{Na}^+$ ,  $\text{Mg}^{2+}$  and  $\text{K}^+$  are less than 0.9, probably because the concentrations of these four ions were relatively low, and they could more easily be affected by contamination from nearby dust or during sample handling.

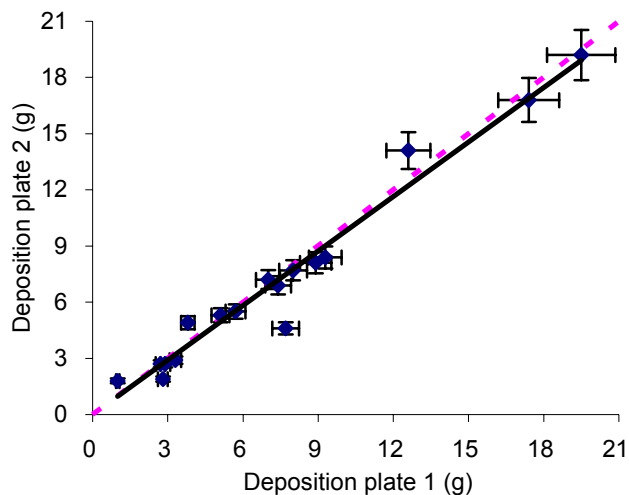


Figure 5-1. Comparison of fog water masses collected by two deposition plates. The solid line is a data trendline; the dashed line is the 1:1 line. Error bars represent the pooled standard deviation of replicate samples from 2 collocated deposition plates.

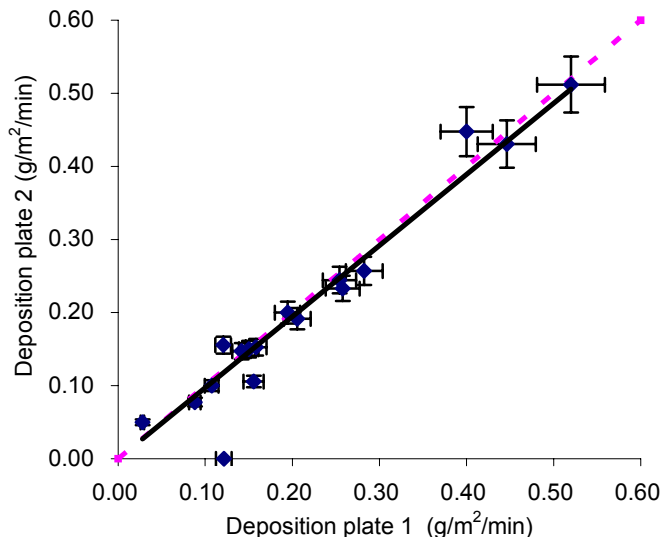


Figure 5-2. Comparison of fog water fluxes collected by two deposition plates. The solid line is a data trendline; The dashed line is the 1:1 line. Error bars represent the pooled standard deviation of replicate samples from two collocated deposition plates.

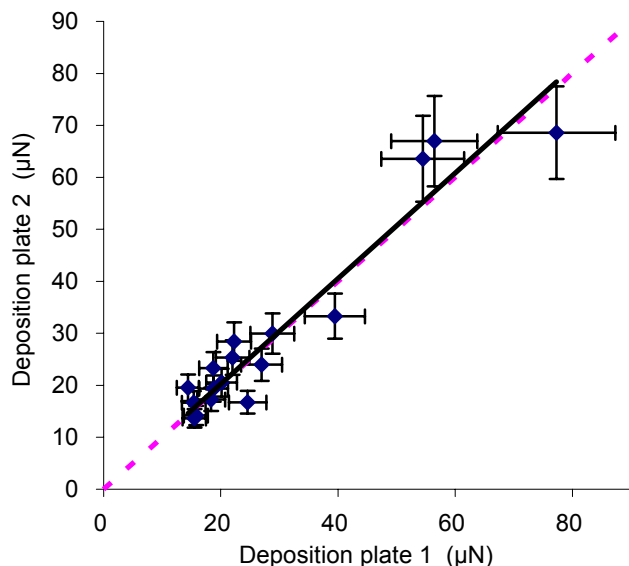


Figure 5-3. Comparison of  $\text{Cl}^-$  concentrations in fog water collected by two deposition plates. The solid line is a data trendline; the dashed line is the 1:1 line. Error bars represent the pooled standard deviation of replicate samples from 2 collocated deposition plates.

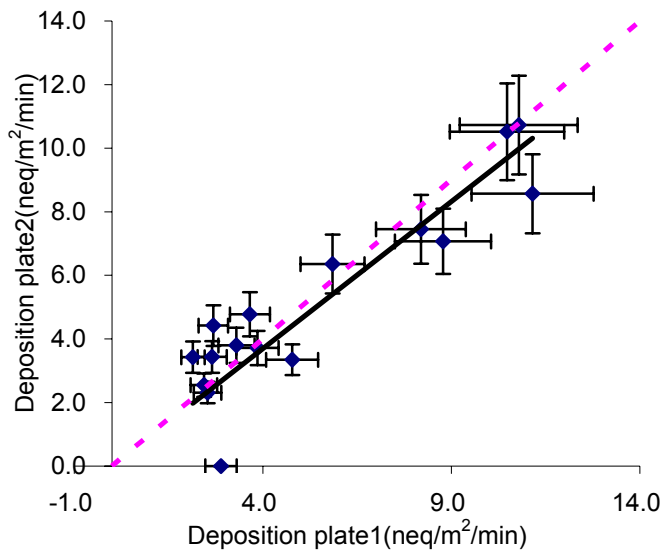


Figure 5-4. Comparison of  $\text{Cl}^-$  fluxes collected by two deposition plates. The solid line is a data trendline; the dashed line is the 1:1 line. Error bars represent the pooled standard deviation of replicate samples from 2 collocated deposition plates.

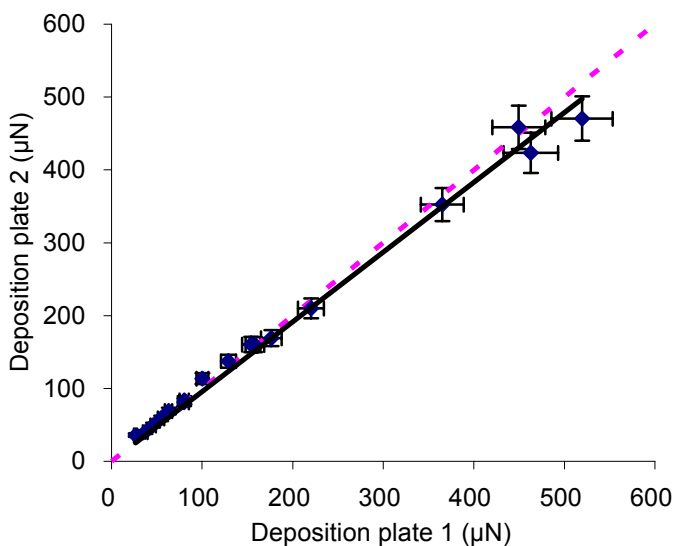


Figure 5-5. Comparison of  $\text{NO}_3^-$  concentrations in fog water collected by two deposition plates. The solid line is a data trendline; the dashed line is the 1:1 line. Error bars represent the pooled standard deviation of replicate samples from 2 collocated deposition plates.

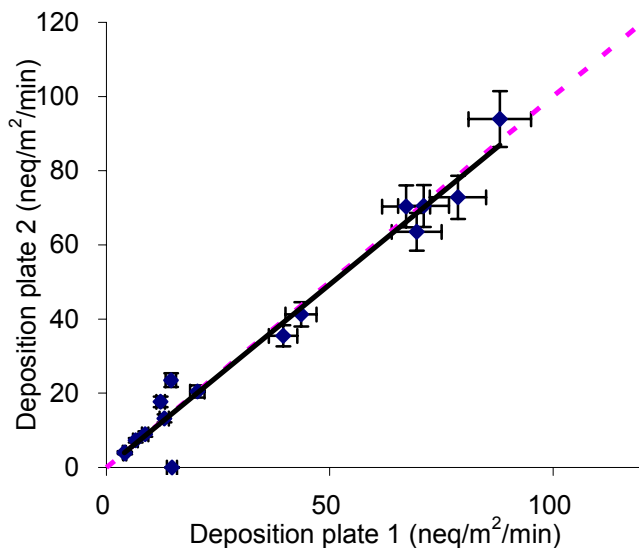


Figure 5-6. Comparison of  $\text{NO}_3^-$  fluxes collected by two deposition plates. The solid line is a data trendline; the dashed line is the 1:1 line. Error bars represent the pooled standard deviation of replicate samples from 2 collocated deposition plates.

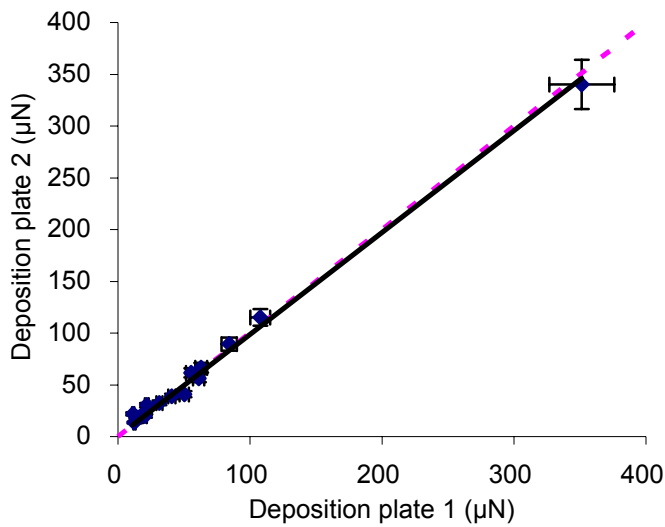


Figure 5-7. Comparison of  $\text{SO}_4^{2-}$  concentrations in fog water collected by two deposition plates. The solid line is a data trendline; the dashed line is the 1:1 line. Error bars represent the pooled standard deviation of replicate samples from 2 collocated deposition plates.

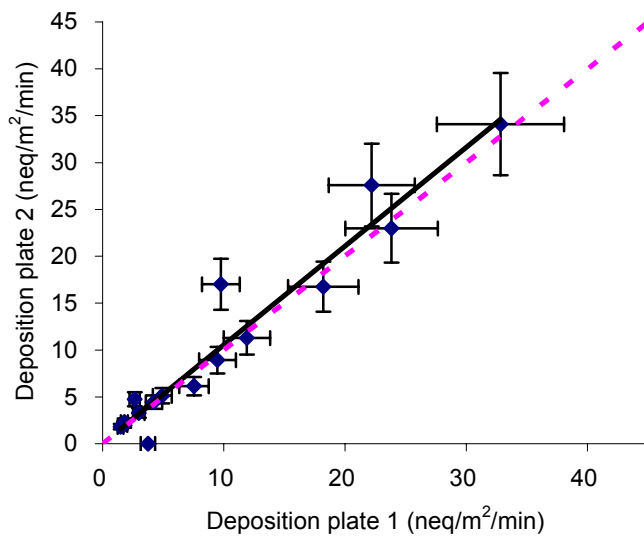


Figure 5-8. Comparison of  $\text{SO}_4^{2-}$  fluxes collected by two deposition plates. The solid line is a data trendline; the dashed line is the 1:1 line. Error bars represent the pooled standard deviation of replicate samples from 2 collocated deposition plates.

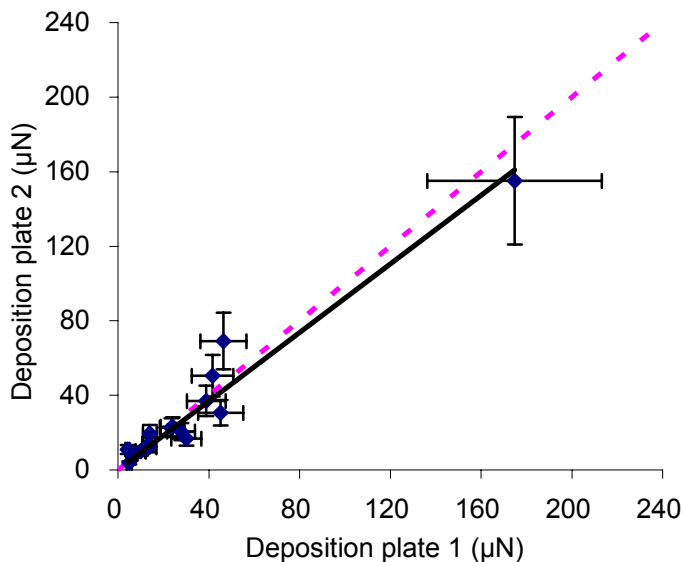


Figure 5-9. Comparison of  $\text{Na}^+$  concentrations in fog water collected by two deposition plates. The solid line is a data trendline; the dashed line is the 1:1 line. Error bars represent the pooled standard deviation of replicate samples from 2 collocated deposition plates.

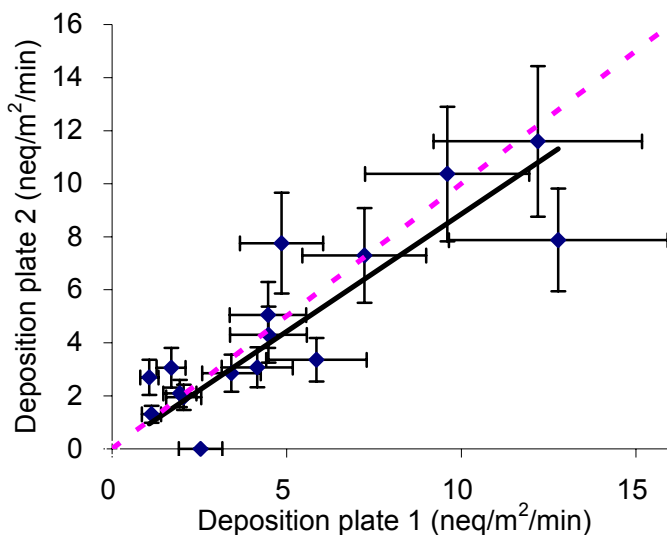


Figure 5-10. Comparison of Na<sup>+</sup> fluxes collected by two deposition plates. The solid line is a data trendline; the dashed line is the 1:1 line. Error bars represent the pooled standard deviation of replicate samples from 2 collocated deposition plates.

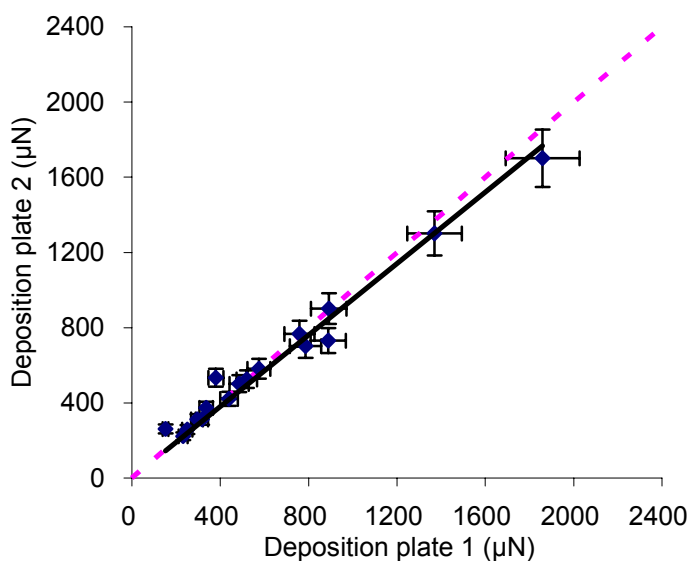


Figure 5-11. Comparison of NH<sub>4</sub><sup>+</sup> concentrations in fog water collected by two deposition plates. The solid line is a data trendline; the dashed line is the 1:1 line. Error bars represent the pooled standard deviation of replicate samples from 2 collocated deposition plates.

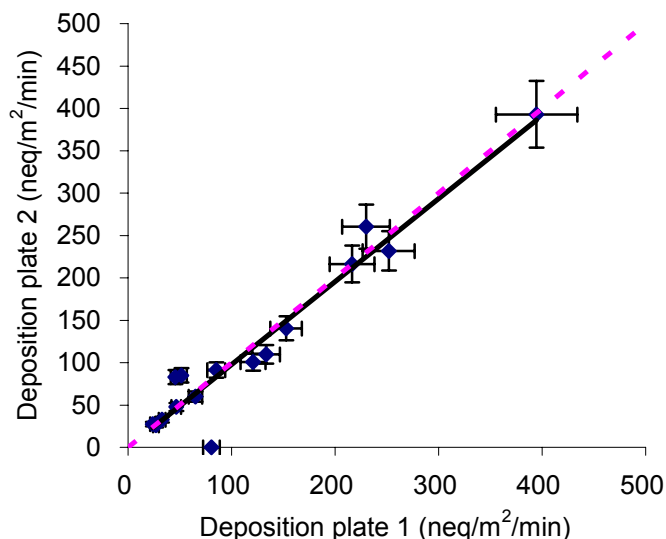


Figure 5-12. Comparison of NH<sub>4</sub><sup>+</sup> fluxes collected by two deposition plates. The solid line is a data trendline; The dashed line is the 1:1 line. Error bars represent the pooled standard deviation of replicate samples from 2 collocated deposition plates.



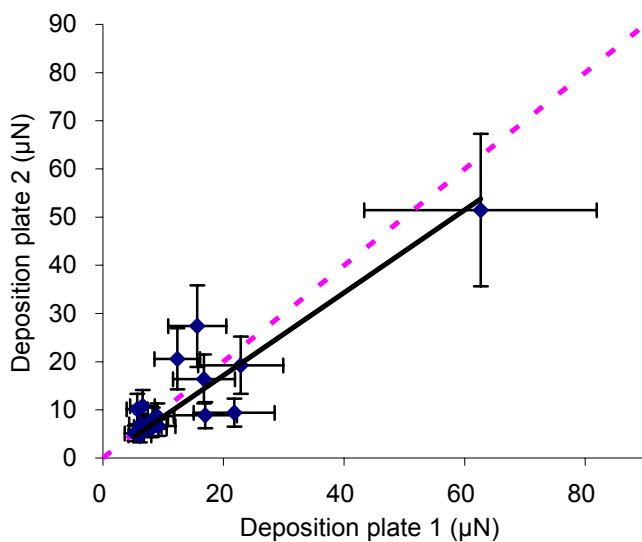


Figure 5-13. Comparison of  $K^+$  concentrations in fog water collected by two deposition plates. The solid line is a data trendline; the dashed line is the 1:1 line. Error bars represent the pooled standard deviation of replicate samples from 2 collocated deposition plates.

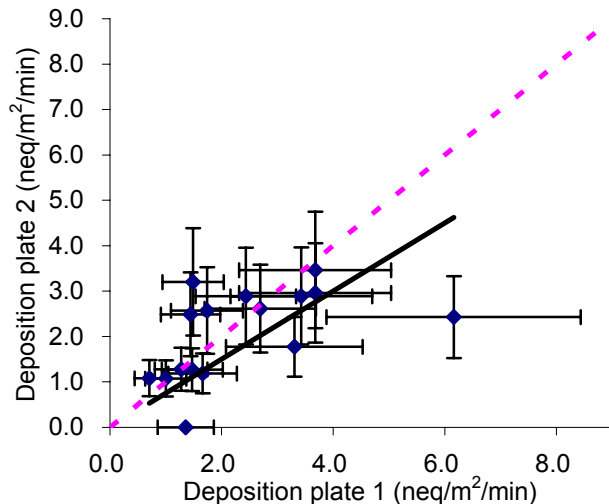


Figure 5-14. Comparison of  $K^+$  fluxes collected by two deposition plates. The solid line is a data trendline; The dashed line is the 1:1 line. Error bars represent the pooled standard deviation of replicate samples from 2 collocated deposition plates.

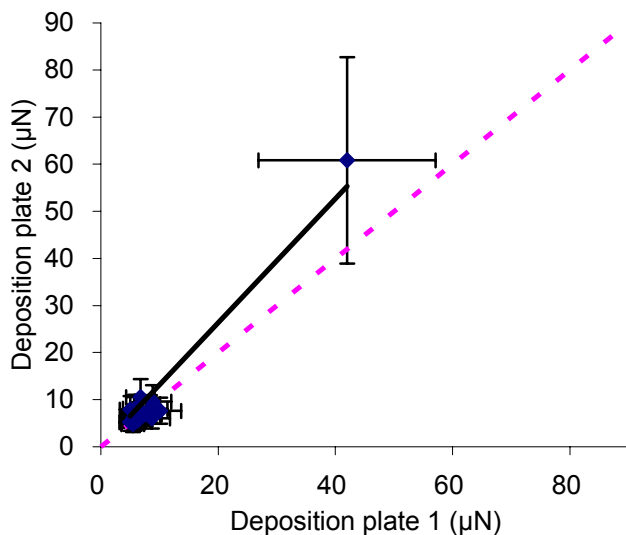


Figure 5-15. Comparison of  $Mg^{2+}$  concentrations in fog water collected by two deposition plates. The solid line is a data trendline; the dashed line is the 1:1 line. Error bars represent the pooled standard deviation of replicate samples from 2 collocated deposition plates.

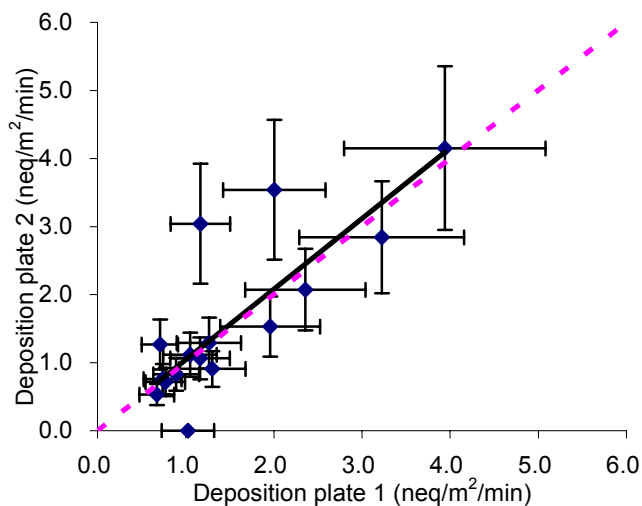


Figure 5-16. Comparison of  $\text{Mg}^{2+}$  fluxes collected by two deposition plates. The solid line is a data trendline; the dashed line is the 1:1 line. Error bars represent the pooled standard deviation of replicate samples from 2 collocated deposition plates.

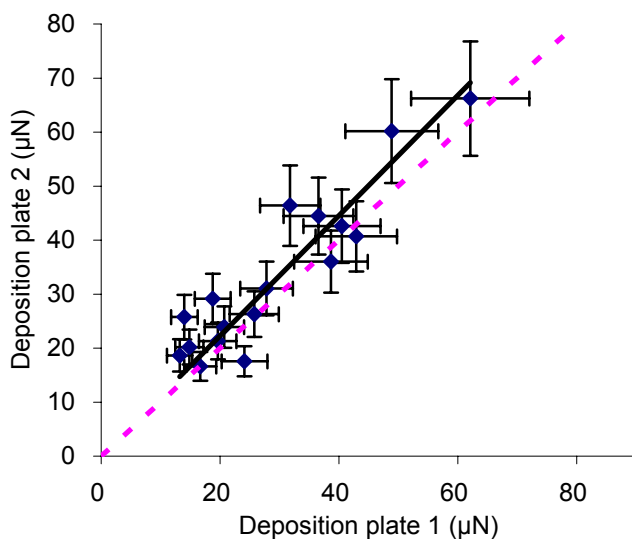


Figure 5-17. Comparison of  $\text{Ca}^{2+}$  concentrations in fog water collected by two deposition plates. The solid line is a data trendline; the dashed line is the 1:1 line. Error bars represent the pooled standard deviation of replicate samples from 2 collocated deposition plates.

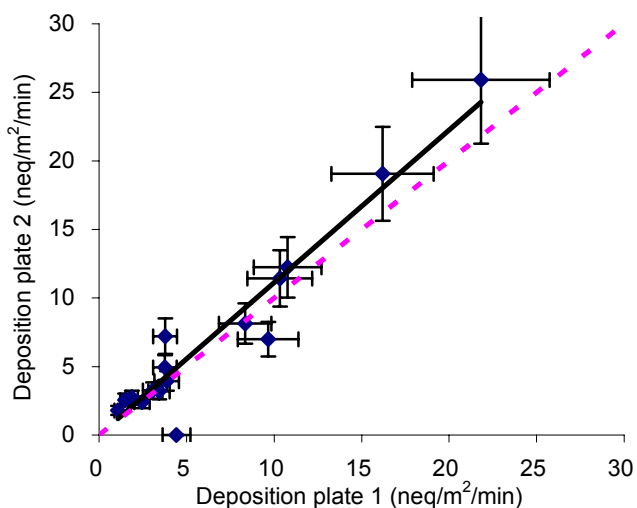


Figure 5-18. Comparison of  $\text{Ca}^{2+}$  fluxes collected by two deposition plates. The solid line is a data trendline; the dashed line is the 1:1 line. Error bars represent the pooled standard deviation of replicate samples from 2 collocated deposition plates.

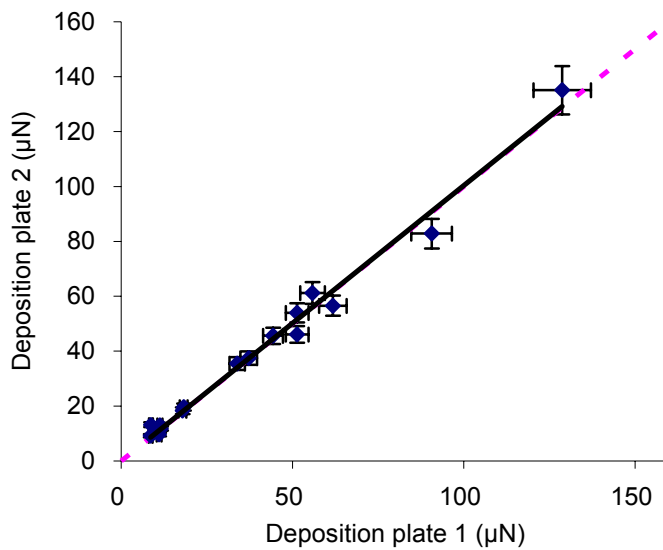


Figure 5-19. Comparison of  $\text{NO}_2^-$  concentrations in fog water collected by two deposition plates. The solid line is a data trendline; the dashed line is the 1:1 line. Error bars represent the pooled standard deviation of replicate samples from 2 collocated deposition plates.

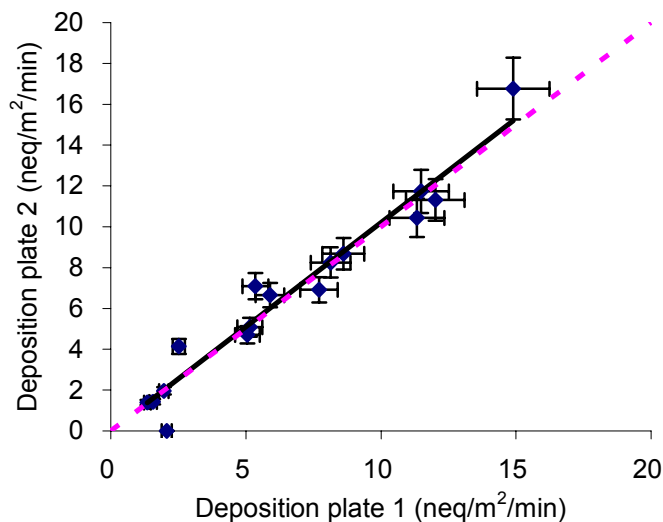


Figure 5-20. Comparison of  $\text{NO}_2^-$  fluxes collected by two deposition plates. The solid line is a data trendline; the dashed line is the 1:1 line. Error bars represent the pooled standard deviation of replicate samples from 2 collocated deposition plates.

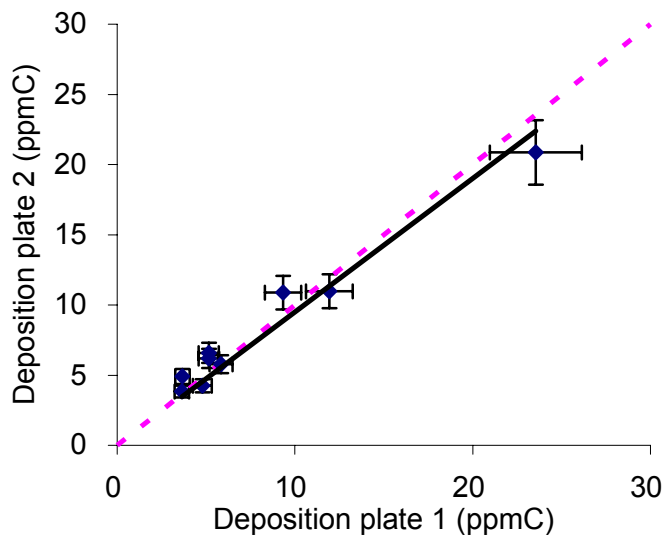


Figure 5-21. Comparison of TOC concentrations in fog water collected by two deposition plates. The solid line is a data trendline; the dashed line is the 1:1 line. Error bars represent the pooled standard deviation of replicate samples from 2 collocated deposition plates.

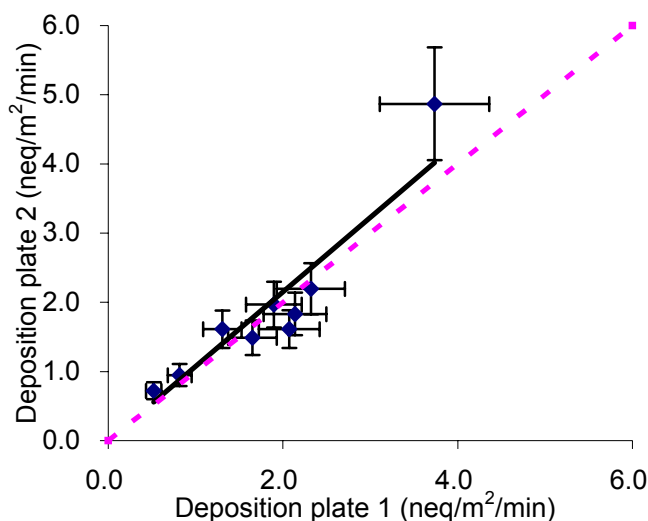


Figure 5-22. Comparison of TOC fluxes collected by two deposition plates. The solid line is a data trendline; The dashed line is the 1:1 line. Error bars represent the pooled standard deviation of replicate samples from 2 collocated deposition plates.

Table 5-3. Summary of observed deposition fluxes in CRPAQS fogs.

<i>(Solute)</i>		<i>Minimum</i>	<i>Maximum</i>	<i>Average</i>
H <sub>2</sub> O	(g/m <sup>2</sup> /min)	0.03	0.61	0.22
Cl <sup>-</sup>	(neq/m <sup>2</sup> /min)	2.15	11.2	5.50
NO <sub>3</sub> <sup>-</sup>	(neq/m <sup>2</sup> /min)	3.81	97.0	36.9
NO <sub>2</sub> <sup>-</sup>	(neq/m <sup>2</sup> /min)	1.35	16.8	6.69
SO <sub>4</sub> <sup>2-</sup>	(neq/m <sup>2</sup> /min)	1.49	34.1	10.7
Na <sup>+</sup>	(neq/m <sup>2</sup> /min)	1.07	12.8	4.80
NH <sub>4</sub> <sup>+</sup>	(neq/m <sup>2</sup> /min)	23.6	395	128
K <sup>+</sup>	(neq/m <sup>2</sup> /min)	0.70	6.16	2.29
Mg <sup>2+</sup>	(neq/m <sup>2</sup> /min)	0.53	4.15	1.65
Ca <sup>2+</sup>	(neq/m <sup>2</sup> /min)	1.07	25.9	7.26
TOC	(µgC/m <sup>2</sup> /min)	0.52	4.87	1.60

g/m<sup>2</sup>/min, gram per square meter per minute; neq/m<sup>2</sup>/min, nanoequivalents per square meter per minute; µgC/m<sup>2</sup>/min, microgram carbon per square meter per minute.

A summary of the range of water and ion fluxes is shown in Table 5-3. Fog water flux rates averaged 0.22 g/m<sup>2</sup>/min during the seven fog episodes. Flux rates for nitrate and ammonium were the highest among the chemical species, averaging 36.9 neq/m<sup>2</sup>/min and 128 neq/m<sup>2</sup>/min, respectively. Sulfate flux rates averaged only 10.7 neq/m<sup>2</sup>/min. Compared with results from an earlier study in Davis, California (Collett et al., 2001), in

which the mean fluxes of nitrate, ammonium and sulfate were 71.4 neq/m<sup>2</sup>/min, 140.1 neq/m<sup>2</sup>/min and 9.5 neq/m<sup>2</sup>/min, the average fluxes of sulfate and ammonium are similar, but the Angiola CRPAQS nitrate flux is only about one half the Davis value. These results could reflect spatial variability in the large valley (Collett et al., 2001).

Table 5-4 lists the precision estimates of concentration and flux measurements, by species, as determined from the replicate deposition plate measurements. The results indicate that the deposition plates provided relatively precise measurements for major fog solute species, with relative standard deviation of 6.5-11.3% for water mass, sulfate, nitrate, nitrite, ammonium and TOC concentrations and 7.5-16.9% for measurements of water, sulfate, nitrate, nitrite, ammonium and TOC fluxes. Precision decreases somewhat for trace species.

Table 5-4. Relative standard deviations of deposited fog concentrations and fluxes derived from two deposition plates.

Solute	RSD of Concentration (%)	RSD of Flux (%)
Water	6.6	7.5
Cl <sup>-</sup>	13.0	14.5
NO <sub>3</sub> <sup>-</sup>	6.6	8.0
NO <sub>2</sub> <sup>-</sup>	6.5	9.0
SO <sub>4</sub> <sup>2-</sup>	7.2	16.4
Na <sup>+</sup>	21.4	24.5
NH <sub>4</sub> <sup>+</sup>	9.2	10.2
K <sup>+</sup>	13.4	37.4
Mg <sup>2+</sup>	35.9	29.3
Ca <sup>2+</sup>	15.6	18.1
TOC	11.3	16.9

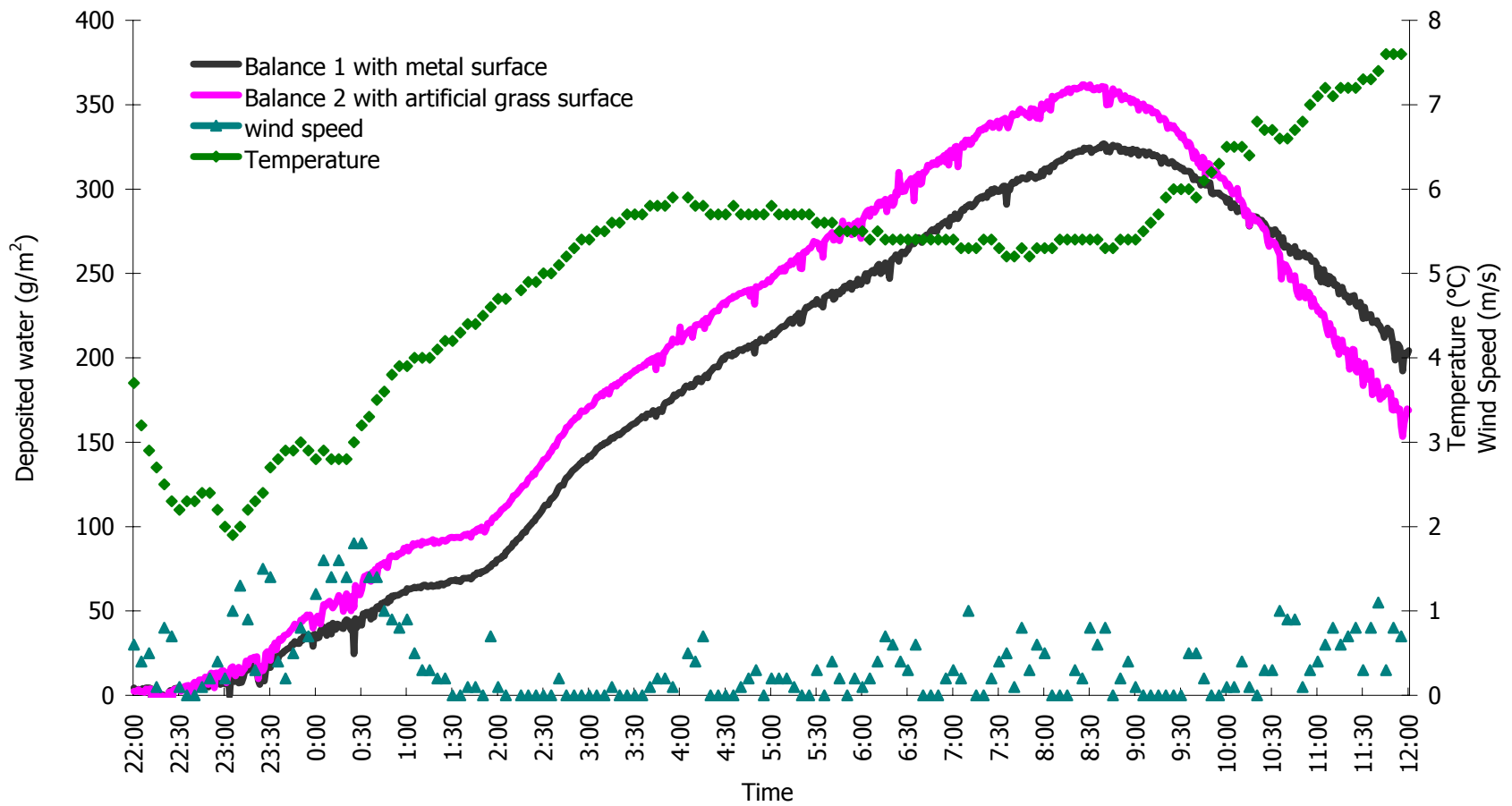


Figure 5-23. Area normalized balance reading on 12/18/00. Temperature and wind speed trendlines are also presented for reference.

### 5.2.2 Water fluxes derived from the balances

Figure 5-23 shows the temperature and wind speed profile and the accumulating water mass on two balances during one fog event (day 352, 12/17/00 22:00 to 12/18/00 12:00). The data were normalized by balance collection area so that we are able to compare them directly. The peaks on the water mass curves possibly represent turbulence effects on balance readings. The results show that the accumulation of water was higher on a balance with an artificial grass deposition surface than on one with a bare metal surface. The results also show that after sunrise, evaporation from the balances becomes significant. Evaporation eventually dominates the change in accumulated mass as the two balances show a net mass loss after about 8:00. Note the rate of loss is higher from the artificial grass surface than from the bare metal surface. A similar post-sunrise loss of water was reported by Collett et al. (2001).

Figure 5-24 to Figure 5-30 compare 10-minute average water fluxes on the two balances in the rest of the fog episodes. Data are included only for periods prior to 07:30 am, in order to avoid the post-sunrise evaporation effect. Data points above the 1:1 line indicate that the water flux on the grass surface is higher than on the metal surface, and vice versa. The results again indicate that the water fluxes tend to be somewhat higher on the grass surface. If we combine data from all the fog events together and regress deposition flux to the grass surface against deposition flux to the metal surface, we find that the enhancement in grass surface deposition averages approximately 5%. Enhanced deposition to the grass surface likely results from an increase in turbulent deposition to this rougher surface.

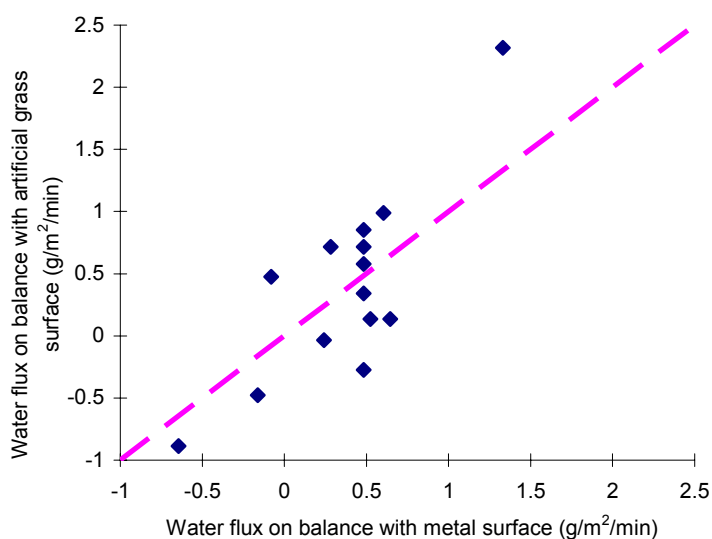


Figure 5-24. Comparison of 10 minute average water fluxes on two balances on 12/18/00. The dashed line is the 1:1 line.

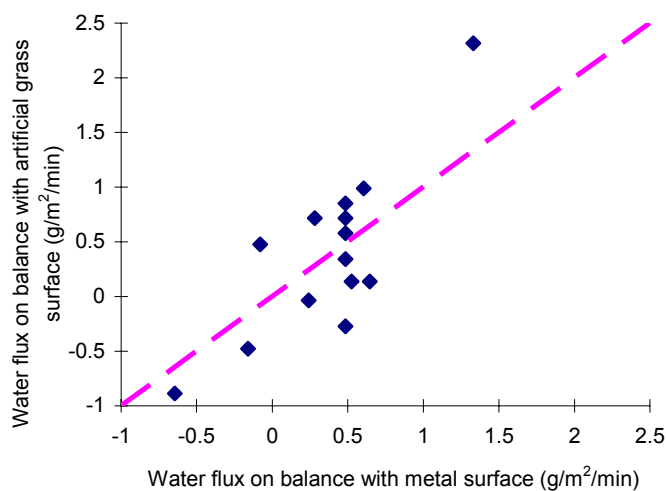


Figure 5-25. Comparison of 10 minute average water fluxes on two balances on 12/19/00. The dashed line is the 1:1 line.

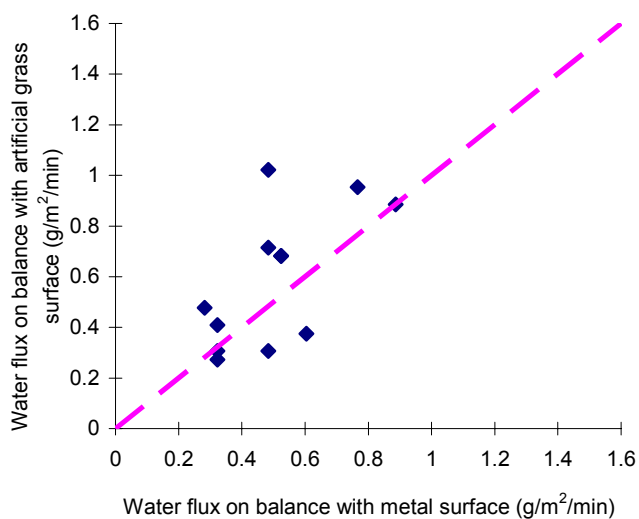


Figure 5-26 Comparison of 10 minute average water fluxes on two balances on 01/15/01. The dashed line is the 1:1 line.



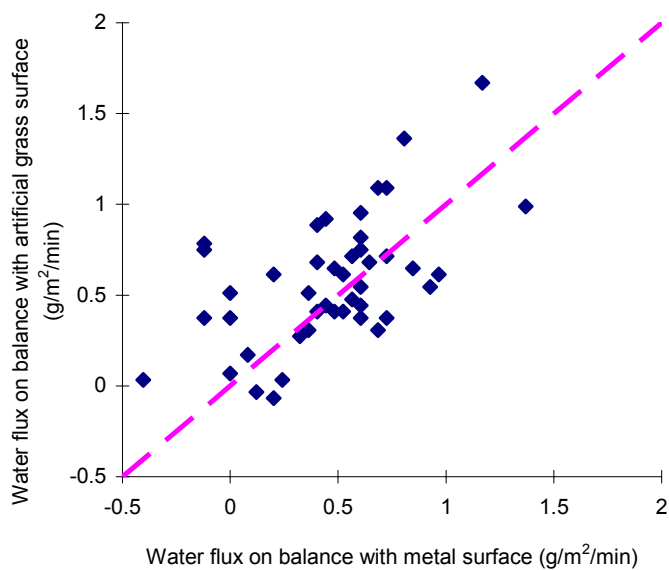


Figure 5-27. Comparison of 10 minute average water fluxes on two balances on 01/17/01. The dashed line is the 1:1 line.

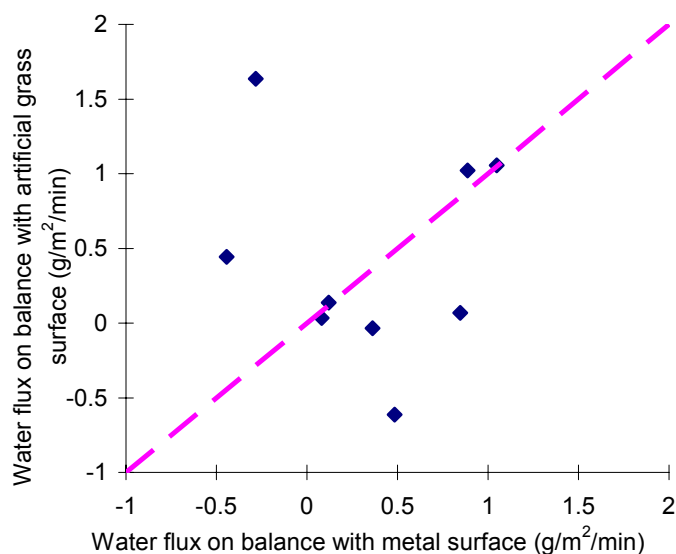


Figure 5-28. Comparison of 10 min average water fluxes on two balances on 01/21/01. The dashed line is the 1:1 line.

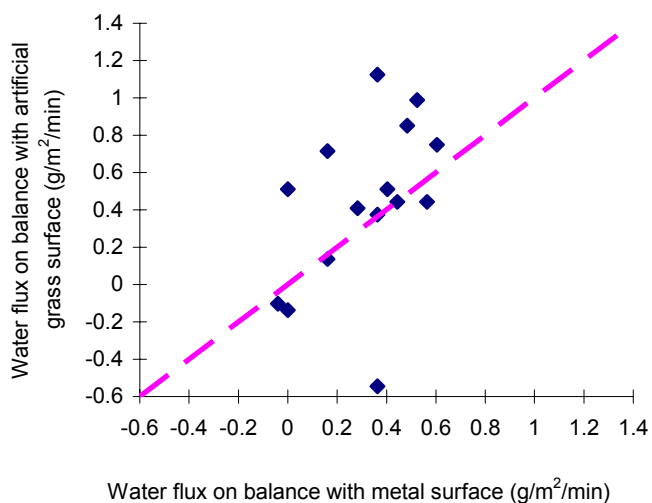


Figure 5-29. Comparison of 10 minute average water fluxes on two balances on 01/25/01. The dashed line is the 1:1 line.

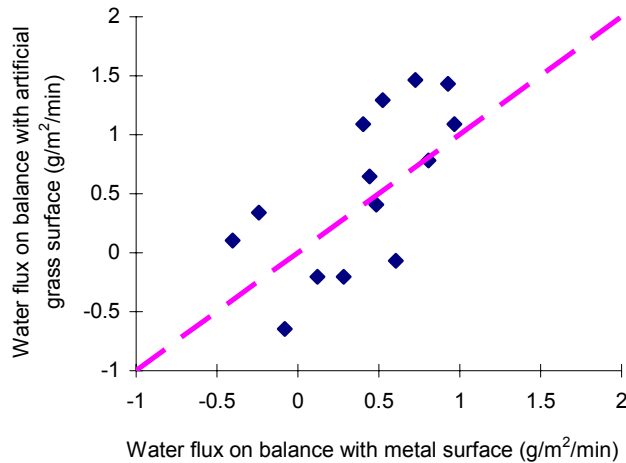


Figure 5-30. Comparison of 10 min average water fluxes on two balances on 01/31/01. The dashed line is the 1:1 line.

### 5.2.3 Comparison of water fluxes to plates and balances and flux variation with fog liquid water content and effective diameter

Fog liquid water content (LWC, with unit  $\text{mg/m}^3$ ) was measured using a Gerber Scientific Particulate Volume Monitor (Model PVM-100) that was calibrated using a manufacturer supplied disk. The PVM also measures particle surface area ( $\text{cm}^2/\text{m}^3$ ) and reports drop effective diameter ( $\mu\text{m}$ ). PVM data were recorded at 1-minute intervals. Figure 5-31 shows 20-minute average water fluxes derived from the two balances along with fog LWC and effective diameter ( $D_{\text{eff}}$ ), obtained from the PVM. Data from the two balances agree with each other reasonably well. Before sunrise, when PVM-LWC or effective diameter rose, so did the water fluxes measured by the two balances. When the temperature went higher, the fog started to evaporate; water fluxes to the two balances started to go down and showed negative values indicating net water evaporation from the deposition collection surface. Meanwhile, effective diameter and LWC didn't change dramatically, but slowly, consistent with the fog being maintained by evaporating deposited fog water on the ground.

It is apparent that fog LWC can affect fog water deposition fluxes as it is a measure of the airborne concentration of fog water. Since droplet settling velocities increase strongly as a function of drop diameter, we also expect to see some dependence of fog deposition

velocities in this low wind speed environment on effective diameter. In order to look at whether variations in fog LWC and effective diameter can explain the temporal variability in fog water flux rates, we performed a linear regression utilizing the simple, linear model:

$$Y = \alpha LWC + \beta D_{eff} + \gamma \quad (5-1)$$

where  $\alpha$  and  $\beta$  are regression coefficients and  $\gamma$  is a constant. The units of LWC,  $D_{eff}$  are gram per cubic meter and micrometer, respectively.

Table 5-5. Linear regression analysis of water flux vs. fog LWC and effective diameter for CRPAQS.

Model	R	R <sup>2</sup>	Adjusted R <sup>2</sup>	Std. Error of the estimate	
Summary	0.629*	0.395	0.364	0.506	
<hr style="border-top: 1px dashed black;"/>					
	Unstandardized Coefficients		Standardized Coefficients		
Coefficients	B	Std. Error	Beta	t	Sig.
Constant	-1.377	0.893		-1.542	0.131
LWC	3.462	0.849	0.575	4.077	0.000
D <sub>eff</sub>	2.294×10 <sup>-2</sup>	0.032	0.101	0.716	0.478

\*Predictors: Constant,  $D_{eff}$  and LWC

Equation (5-1) was solved by linear regression analysis using averaged 20-minute average water fluxes to two balances in the 12/17/00 fog event. 42 data points were used in the regression. Table 5-5 shows the linear regression results. The unstandardized coefficients and constant are 3.462, 0.023 and -1.377 respectively, so the equation is

$$Y = 3.462 LWC + 0.023 D_{eff} - 1.377$$

The correlation coefficient ( $R^2$ ) of the regression analysis is 0.4, indicating that only ~ 40% of the observed flux variability is explained by the linear model. The absence of greater explanatory power for this model could be the result of several factors. First, the assumption that drop deposition occurs solely by sedimentation is not completely accurate, as some turbulent deposition certainly occurs. Second, LWC and effective diameter are measured at ~ 3 m above the surface while deposition is measured at the ground. Third, the model is flawed in that LWC and effective diameter are not truly independent variables and the dependence of deposition velocity on effective diameter is not truly a linear function. Nevertheless, the fact that this simple, linear model shows some dependence of deposition flux on LWC and  $D_{\text{eff}}$  is reassuring.

#### 5.2.4 Deposition velocities

Table 5-6. Average deposition velocities of all species to two deposition plates.

Samples	Water (cm/s)	Cl <sup>-</sup> (cm/s)	NO <sub>3</sub> <sup>-</sup> (cm/s)	NO <sub>2</sub> <sup>-</sup> (cm/s)	SO <sub>4</sub> <sup>2-</sup> (cm/s)	Na <sup>+</sup> (cm/s)	NH <sub>4</sub> <sup>+</sup> (cm/s)	K <sup>+</sup> (cm/s)	Mg <sup>2+</sup> (cm/s)	Ca <sup>2+</sup> (cm/s)	TOC (cm/s)
12/17/00-01	0.9	1.1	0.6	1.4	0.7	9.1	1.1	2.4	1.3	5.2	1.0
12/18/00-02	2.3	2.5	1.1	2.1	1.3	3.3	1.9	2.9	1.5	2.0	1.4
12/18/00-03	4.1	4.5	2.1	4.8	2.6	--*	3.7	8.6	4.7	6.8	2.0
12/18/00-04	3.7	4.7	1.8	3.9	3.6	10.1	4.0	5.2	4.5	6.6	1.9
12/18/00-05	2.4	6.0	1.5	2.7	2.9	--	2.8	9.4	3.9	7.7	1.5
12/18/00-06	0.5	2.2	0.7	1.5	1.6	13.2	0.9	3.8	3.6	0.6	0.8
12/19/00-01	1.0	2.2	0.6	4.2	2.0	0.9	3.9	1.5	3.0	1.4	1.0
1/15/01-01	3.4	4.0	1.1	3.8	1.0	4.5	3.1	9.3	3.9	9.4	1.9
1/17/01-01	0.9	1.7	0.4	1.9	0.6	10.2	1.0	3.8	1.4	3.2	1.2
1/17/01-02	1.7	2.0	0.4	1.7	0.6	10.2	0.9	2.6	1.8	2.6	2.4
1/17/01-03	3.1	2.8	0.4	--	1.0	5.2	1.7	3.2	3.6	4.8	2.5
1/17/01-04	1.7	2.6	0.7	--	1.2	6.9	2.5	3.9	1.8	2.1	--
1/21/01-01	1.4	2.1	0.4	1.7	0.6	13.2	0.7	3.1	2.4	3.5	0.7
1/21/01-02	2.0	2.1	0.4	2.7	0.9	8.7	0.8	2.4	2.4	4.9	1.3
1/25/01-01	3.0	--	1.0	4.7	2.6	16.6	3.0	--	4.5	--	--
1/25/01-02	1.6	4.2	0.8	2.2	2.0	4.4	2.0	6.8	2.1	5.2	2.1
1/31/01-01	2.5	2.8	1.0	3.5	1.5	5.9	2.1	4.8	3.2	--	2.0
1/31/01-02	1.0	1.4	0.8	2.4	1.1	4.6	1.1	2.1	1.4	3.9	1.2

2/1/01-01	6.0	4.3	0.4	3.3	0.8	11.1	0.9	5.0	5.3	5.9	1.4
-----------	-----	-----	-----	-----	-----	------	-----	-----	-----	-----	-----

--\* : not detected or sample not available

Deposition velocities were determined for fog water, fog ions and TOC. The deposition velocity was calculated according to the following equation:

$$v_i = \frac{Flux_i}{LWC \times Concentration_i} \quad (5-2)$$

where  $v_i$  is the deposition velocity of species  $i$ ,  $Flux_i$  is the measured flux of species  $i$  to the deposition plates,  $LWC$  is the fog liquid water content measured by the PVM and  $Concentration_i$  is the aqueous concentration of species  $i$  in the simultaneously collected fog samples, which were collected by the Caltech Active Strand Cloudwater Collector (CASCC) for ion analysis and by the stainless steel CASCC (ss-CASCC) for TOC analysis.

Table 5-6 shows the overall computed deposition velocities of fog water and solute species in the study fog events. Table 5-7 presents the typical ranges of deposition velocities and the measurement precision (RSD) for each species determined from the replicate plate measurements. Fog water deposition velocities ranged from 0.5-6.0 cm/s, averaging 2.3 cm/s, comparable to previous observations in central California radiation fogs (Collett et al., 2001), which range from 1 cm/s to more than 10 cm/s. The TOC deposition velocity ranged from 0.7-2.5 cm/s, averaging 1.5 cm/s, which is similar to or smaller than the fog water deposition velocity. We can see that average deposition velocity trend is  $NO_2^- > \text{water} > NH_4^+ > TOC \sim SO_4^{2-} > NO_3^-$ . Figure 5-31 and 5-32 show the deposition velocities of these species for each fog event. The species dependent trend in average deposition velocities for each fog events is also  $NO_2^- > \text{water} > NH_4^+ > TOC \sim SO_4^{2-} > NO_3^-$ .

Table 5-7. Typical ranges of deposition velocities and relative standard deviations.

Solute	Deposition velocity (cm/s)				RSD (%)
	Minimum	Maximum	Median	Average	
NO <sub>3</sub> <sup>-</sup>	0.4	2.1	0.7	0.9	8.1
SO <sub>4</sub> <sup>2-</sup>	0.6	3.6	1.1	1.5	11.1
TOC	0.7	2.5	1.4	1.5	16.9
NH <sub>4</sub> <sup>+</sup>	0.7	4.0	1.7	1.9	10.4
Water	0.5	6.0	2.0	2.3	7.6
NO <sub>2</sub> <sup>-</sup>	1.4	4.8	2.4	2.7	9.2
Mg <sup>2+</sup>	1.3	5.3	2.4	2.9	29.7
Cl <sup>-</sup>	1.1	6.0	2.5	3.0	14.8
K <sup>+</sup>	2.1	9.4	3.8	4.6	37.9
Ca <sup>2+</sup>	0.6	9.4	4.8	4.6	18.3
Na <sup>+</sup>	3.3	16.6	8.7	8.3	24.9

RSD, relative standard deviation, which is calculated from replicate samples of two collocated deposition plates.

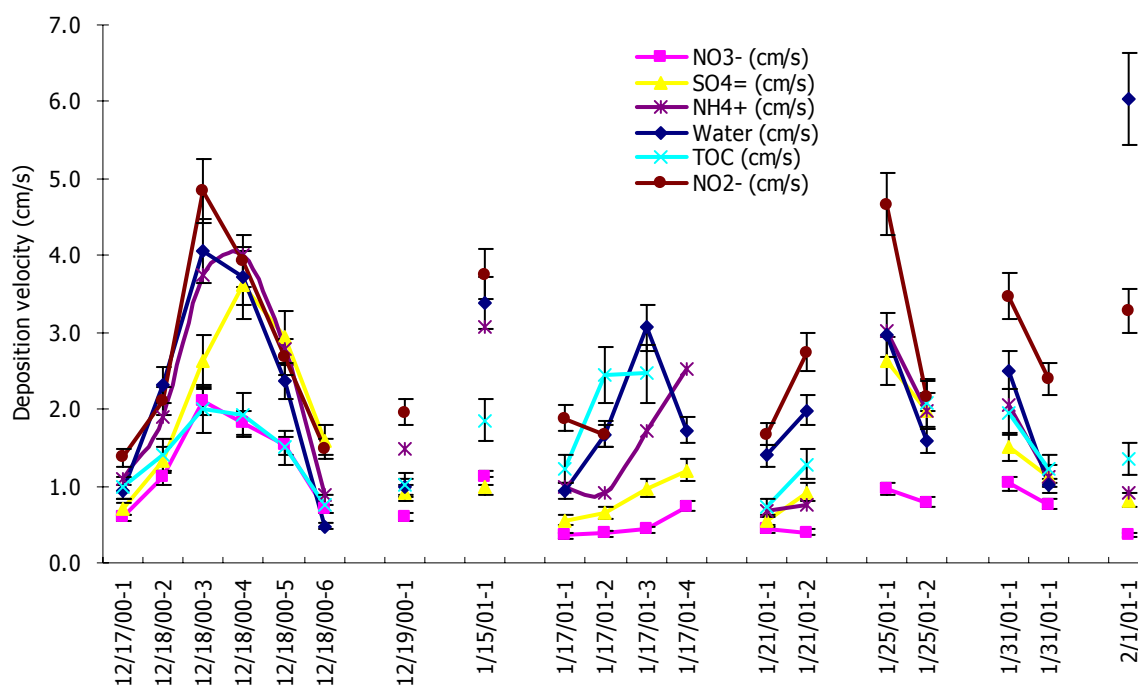


Figure 5-31. Deposition velocities of fogwater, TOC, NH<sub>4</sub><sup>+</sup>, SO<sub>4</sub><sup>2-</sup>, NO<sub>3</sub><sup>-</sup> and NO<sub>2</sub><sup>-</sup>.

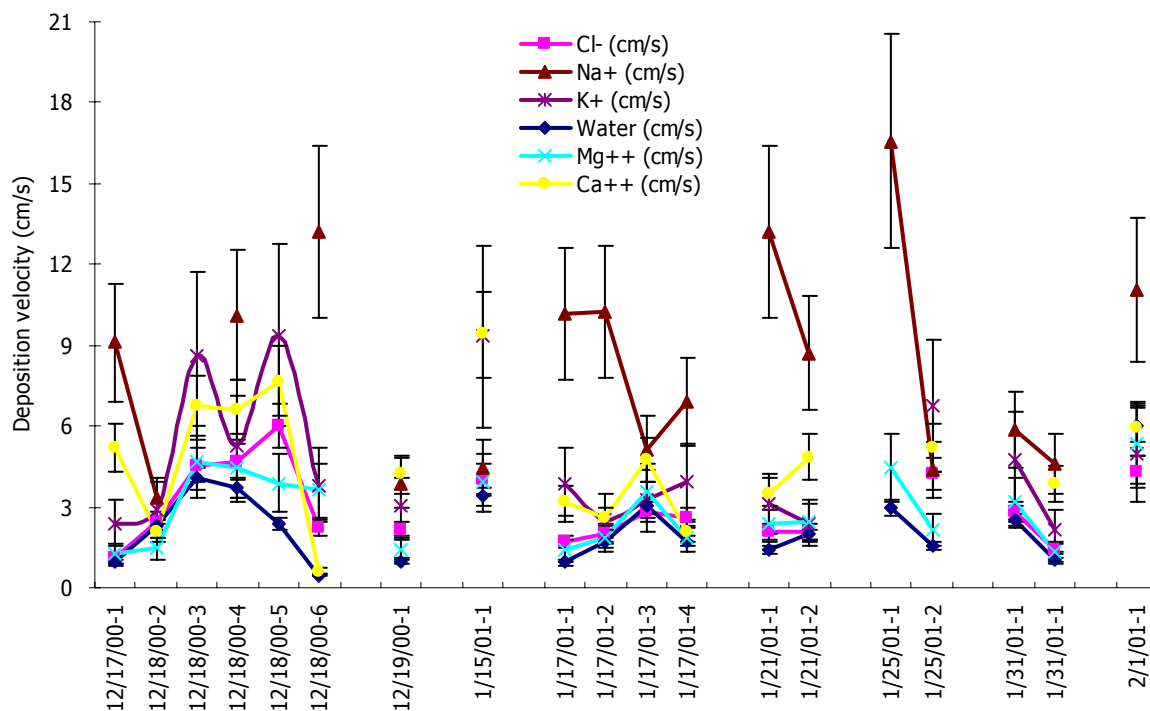


Figure 5-32. Deposition velocities of fogwater,  $\text{Cl}^-$ ,  $\text{Na}^+$ ,  $\text{K}^+$ ,  $\text{Mg}^{2+}$  and  $\text{Ca}^{2+}$ .

To explain these results, Figure 5-33 shows scatter plots of individual species' concentrations in large vs. small fog drops. Any point below the diagonal 1:1 line indicates that the concentration in smaller drops is higher than that in larger drops. It is clear that ammonium, sulfate, nitrate and TOC are enriched in smaller drops, while nitrite is enriched in larger drops. Figure 5-35 shows the trend of deposition velocities of  $\text{NH}_4^+$ ,  $\text{SO}_4^{2-}$ ,  $\text{NO}_3^-$  and  $\text{NO}_2^-$  to their concentration ratios of small / large for fog events on 12/18/00. They were plotted for every sampling period; the lines are trendlines. For each sampling period, the higher the species' small/large drop concentration ratio, the lower deposition velocity is. This is consistent with former study by Moore et al. (2004), who found that fog solute deposition velocities depend on the species distribution across the drop size spectrum. Enrichment of species in small fog drops leads to lower deposition velocities, due to the dependence of settling velocity on drop size. Likewise, species enriched in large drops tend to exhibit higher deposition velocities.

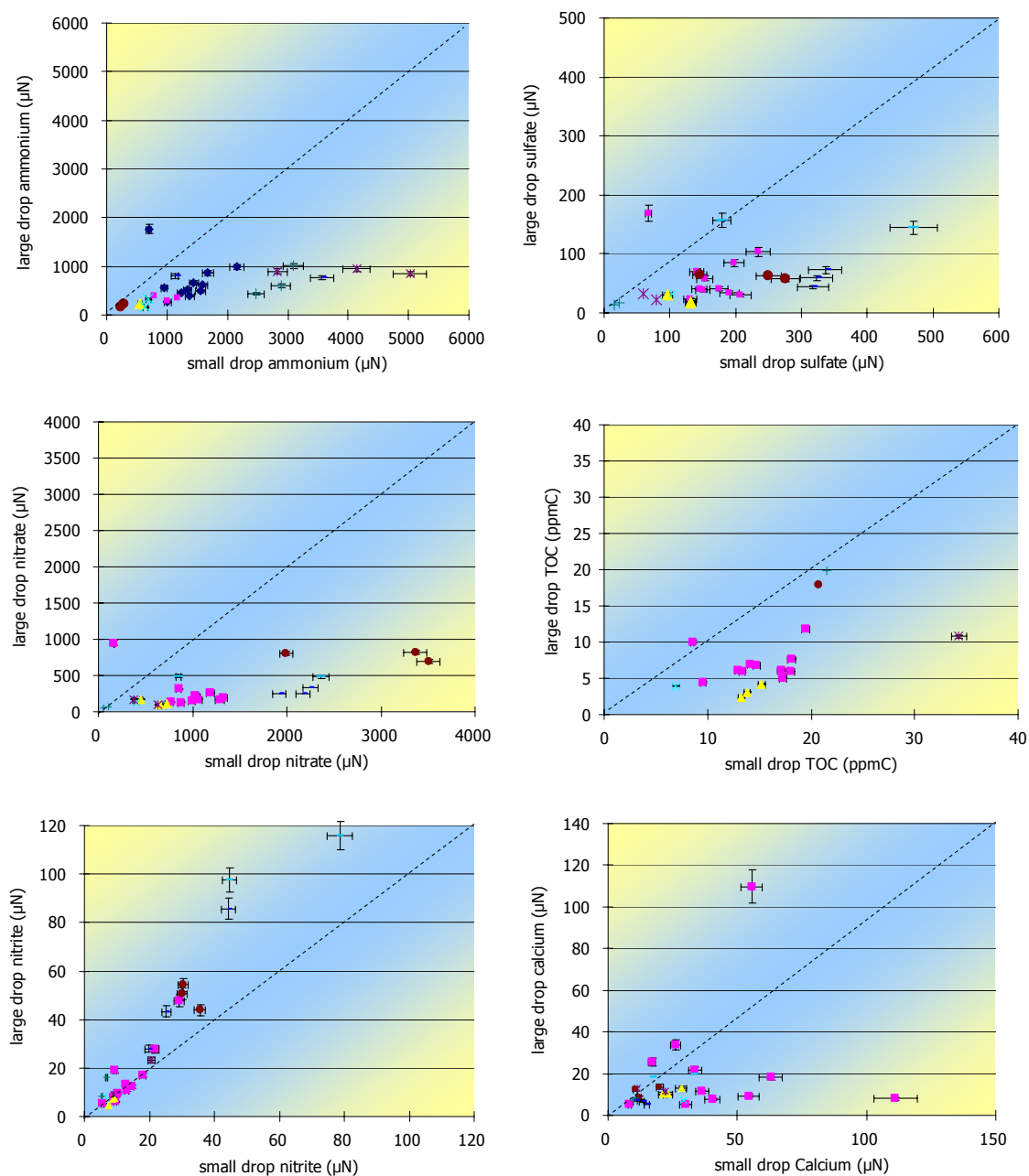


Figure 5-34. Fog drop size distributions (large vs. small drop concentrations from the sf-CASCC or ss-sf-CASCC) of  $\text{NH}_4^+$ ,  $\text{SO}_4^{2-}$ ,  $\text{NO}_3^-$ , TOC,  $\text{NO}_2^-$  and  $\text{Ca}^{2+}$ . Error bars represent one relative standard deviation derived from replicate samples analyzed by ion chromatography.



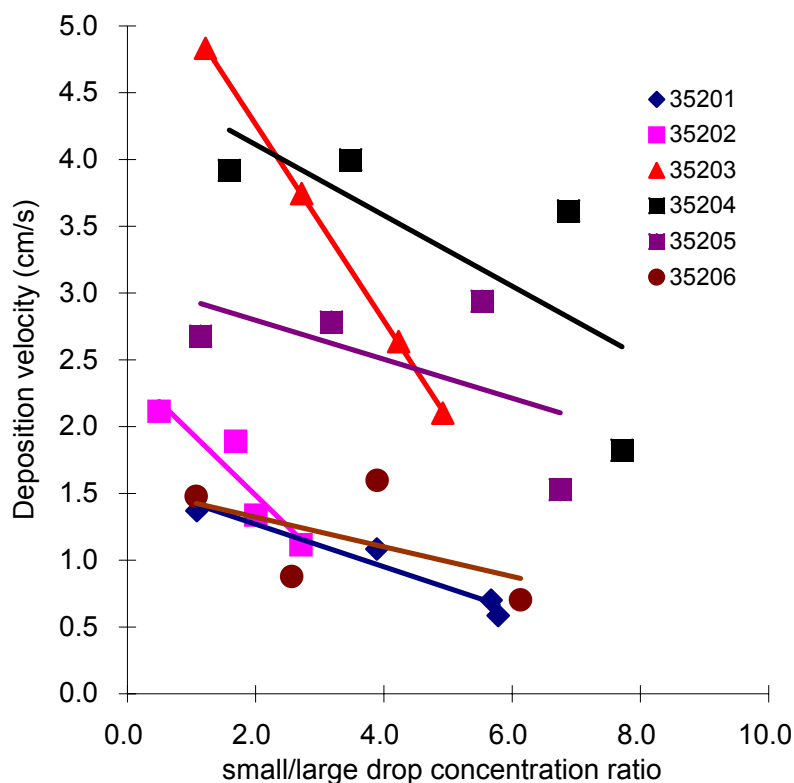


Figure 5-35. Deposition velocity vs. small/large drop concentration ratio for fog samples collected in the 12/18/00 fog event. Each point represents one species (from left to right  $\text{NO}_2^-$ ,  $\text{NH}_4^+$ ,  $\text{SO}_4^{2-}$  and  $\text{NO}_3^-$ ).

Therefore, the tendency for the fog water deposition velocity to exceed the TOC deposition velocity is expected given the enrichment of TOC in smaller fog drops that settle from the atmosphere more slowly. Similarly, the average deposition velocities of sulfate, nitrate, and ammonium were all lower than that of water, since they were enriched in smaller fog drops. Nitrite is, by contrast, enriched in larger drops. Its deposition velocity ranged from 1.5-4.8 cm/s, averaging 2.7 cm/s, higher than the average deposition velocity of fog water. This is also consistent with the dependence of drop settling velocity on drop size.

### 5.3 Sulfur dioxide reaction in fog drops

#### 5.3.1 Theoretical reaction rates

Dissolved sulfur dioxide has three potentially important oxidation reactions (oxidation by ozone, by hydrogen peroxide and by oxygen in the presence of trace metal catalysts) and can also react with HCHO to form HMS. Previous studies have indicated that sulfate production rates can vary with drop size and that various of the S(IV) reaction pathways can be dominant, depending on environmental conditions (e.g., drop pH and concentrations of reactants and catalysts). In order to determine the dominant reaction pathways for S(IV) in various fog drop sizes during CRPAQS, literature expressions of the reaction rates of each relevant pathway were evaluated using the best available measurements or estimates of reactant concentrations and other relevant parameters.

The equations used for S(IV) oxidation rates calculations are as follows, with rate constants computed for a typical fog drop temperature of 283 K.

- For  $H_2O_2$ :

$$-\frac{d[S(IV)]}{dt} = \frac{k[H^+][H_2O_2][HSO_3^-]}{(1+13[H^+])} \quad (5-3)$$

where  $k=3.2 \times 10^7 \text{ M}^{-1}\text{S}^{-1}$  (Seinfeld, 1986).

- For  $O_3$ :

$$-\frac{d[S(IV)]}{dt} = [O_3](k_1[H_2SO_3] + k_2[HSO_3^-] + k_3[SO_3^{2-}]) \quad (5-4)$$

where  $k_1=2.4 \times 10^4 \text{ M}^{-1}\text{S}^{-1}$ ,  $k_2=1.4 \times 10^5 \text{ M}^{-1}\text{S}^{-1}$ , and  $k_3=5.9 \times 10^8 \text{ M}^{-1}\text{S}^{-1}$  (Hoffmann, 1986).

- For  $O_2$ :

$$-\frac{d[S(IV)]}{dt} = k_2[Fe(III)][Mn(II)][S(IV)][H^+]^{-0.74} \quad (\text{when pH} < 4.2) \quad (5-5)$$

$$-\frac{d[S(IV)]}{dt} = k_1[Fe(III)][Mn(II)][S(IV)][H^+]^{0.67} \quad (\text{when } 4.2 < \text{pH} < 6.5) \quad (5-6)$$

where  $k_1 = 6.3 \times 10^{12} \text{ M}^{-1}\text{S}^{-1}$ ,  $k_2 = 9.31 \times 10^6 \text{ M}^{-1}\text{S}^{-1}$  (Ibusuki et al., 1987).

(Note: Only the second rate expression was used in this case since the pH was never low enough for the expression valid at  $\text{pH} < 4.2$  to be relevant. The higher pH expression was used for all computations here, even when pH exceeded 6.5, due to lack of a more suitable published expression).

- For HCHO

$$-\frac{d[S(IV)]}{dt} = k_1[SO_3^{2-}] \left( \frac{k_2}{1 + k_2} \right) [HCHO] \quad (5-7)$$

where  $k_1 = 5.4 \times 10^6 \text{ M}^{-1}\text{S}^{-1}$ ,  $k_2 = 5.5 \times 10^{-4} \text{ M}^{-1}\text{S}^{-1}$  (Seinfeld, 1986).

### 5.3.2 Predicted S(IV) oxidation rates

An aqueous chemistry model (Reilly et al., 2001) was used to predict S(IV) oxidation rates for particular drop sizes during various fog event periods. The model couples gas phase and aqueous phase interactions, based on equations described by Seinfeld et al. (1998).

In the model we assume that temperature is fixed. During drop condensation/evaporation, latent heat will be released/absorbed, and the particle surface temperature will change until the rate of heat transfer balances the rate of heat generation/consumption. The criterion for neglecting this temperature effect can be described as (Seinfeld et al., 1998):

$$\frac{D_g}{\alpha} \left( \frac{M_A}{M_{air}} \right) \ln \left( \frac{1 - x_{As}}{1 - x_{A\infty}} \right) \ll 1 \quad (5-8)$$

where  $D_g$  is the diffusivity of species A in air;  $\alpha = k/\rho c_p$  is the thermal diffusivity of air;  $M_A$  and  $M_{air}$  are the molecular weights of species A and air;  $x_{As}$  and  $x_{A\infty}$  are the mole fractions of A at the particle surface and far away from it. In most applications involving mass and heat transfer to atmospheric particles, this evaporation/condensation effect on temperature can be neglected (Davis, 1983).

Another assumption is that continuum transport properties are valid. If the mean free path of the diffusing vapor molecules becomes comparable to the particle diameter, continuum transport is not valid, and we need to use  $\eta$ , the accommodation coefficient to correct for free molecular effects. This coefficient can be approximated by (Fuchs et al., 1971):

$$\eta = \left\{ 1 + \left[ \frac{1.33 + 0.71 K_n^{-1}}{1 + K_n^{-1}} + \frac{4(1 - a_w)}{3a_w} \right] K_n \right\}^{-1} \quad (5-9)$$

where  $Kn$  is the Knudsen number (ratio of the mean free path of air to droplet radius) and  $a_w$  is a sticking coefficient that describes the probability that a gas molecule reaching the particle surface will adhere to it. This accommodation coefficient was calculated for each species in the model.

Finally, the effective Henry's law coefficient (accounting for ionization reactions in solution) was utilized for species such as dissolved  $SO_2$ , which can deprotonate in solution.

The basic equations we used in the model are (Seinfeld et al., 1998):

$$\frac{dP}{dt} = -k_{mt} w_L P + \frac{1}{H_A} k_{mt} C_{aq} w_L \quad (5-10)$$

$$\frac{dC_{aq}}{dt} = \frac{k_{mt}}{RT} p - \frac{k_{mt}}{H_A RT} C_{aq} - Q R_{aq} \quad (5-11)$$

$$k_{mt} = \left[ \frac{R_p^2 RT}{3D_g} + \frac{R_p (2\pi M_A RT)^{1/2}}{3\alpha} \right]^{-1} \quad (5-12)$$

where  $w_L$  is the cloud liquid water volume fraction,  $p$  is the bulk partial pressure of species A in the fog,  $C_{aq}$  is the corresponding aqueous-phase concentration at the surface of the drop,  $H_A$  is the effective Henry's law coefficient,  $k_{mt}$  is the mass transfer coefficient for gas-phase plus interfacial mass transport,  $R_{aq}$  is the overall rate of aqueous-phase reaction, and  $Q$  is a correction factor for any aqueous-phase mass transport limitations present, defined as:

$$Q = 3 \left( \frac{\coth q}{q} - \frac{1}{q^2} \right), \quad q = R_p \sqrt{\frac{k}{D_{aq}}} \quad (5-13)$$

where  $q$  is a dimensionless parameter,  $D_{aq}$  is the aqueous phase diffusivity and  $k$  is the corresponding rate constant if no mass transport limitations are considered (only consider  $A(aq) \rightarrow B(aq)$  and  $R_{aq} = k[A(aq)] = kH_A P_A$ ).

As stated above potentially important pathways of aqueous phase S(IV) oxidation include oxidation by hydrogen peroxide, by ozone and autooxidation catalyzed by Fe(III) and Mn(II). Previous SJV fog studies (Reilly et al., 2001) found that even if we assume that all Fe and Mn measured in the fog droplets is in a catalytically active form, the autooxidation pathway is still too slow to be an important contributor. So in our modeling, we did not include simulation of the autooxidation pathway; only oxidation of S(IV) by ozone and by hydrogen peroxide and complexation of S(IV) by formaldehyde were included.

One modification is to the aqueous phase mass transport limitation correction factor,  $Q$ . We used the formulation for  $Q$  for a first order reaction given in Seinfeld et al., (1998),

but modified it to account for higher-order reactions. We calculated initial estimates of Q for S(IV), ozone and hydrogen peroxide, then iterated until convergence was reached for each of these species. The Q values for each species were examined as part of the simulation output. A large q (corresponding to a small Q) value indicates significant concentration gradients develop inside the drop.

One parameter which is also in the output file is the partition function of each species, defined as

$$PF = \frac{\text{Real aqueous phase concentration}}{\text{Theoretical aqueous phase concentration}} \quad (5-14)$$

This parameter related the aqueous phase concentration to the Henry's law predicted aqueous phase concentration. Because theoretical aqueous phase concentration is the equilibrium concentration with gas phase, this parameter indicates whether the species has reached equilibrium with the gas phase or not.

### 5.3.3 Experiment approach

The aqueous chemistry model was used to simulate the chemical evolution of large and small drop fog water fractions. Table 5-8 shows the parameters and initial conditions used in the model.

Table 5-8 Parameters and initial conditions in the model

Parameters	Species	Value
Sticking coefficient $\alpha_w$	Default	0.05
	SO <sub>2</sub> (g)	0.035
	O <sub>3</sub> (g)	5.4×10 <sup>-4</sup>
	H <sub>2</sub> O <sub>2</sub> (g)	0.18
	NH <sub>3</sub> (g)	0.06
	HNO <sub>3</sub> (g)	0.2
	HCHO (g)	0.05

Diffusivity $D_g$ ( $\text{cm}^2/\text{s}$ )	S(IV), $\text{O}_3$ and $\text{H}_2\text{O}_2$	$1 \times 10^{-5}$
Initial Q	S(IV), $\text{O}_3$ and $\text{H}_2\text{O}_2$	1.0
Initial PF	S(IV), $\text{O}_3$ and $\text{H}_2\text{O}_2$	1.0
Gas constant (L atm/mol K)		0.082058
Mean free path (cm)		$6.5 \times 10^{-6}$

Table 5-9 shows the input parameters used for simulating fog events at the Angiola main site. Inputs were selected as follows. Temperature and pressure were measured by weather station, averaged to the appropriate sampling time. LWC was measured by the PVM. The pH values of fog water samples (large and small drop fractions) were measured on site. Aqueous concentrations of  $\text{O}_3$  and  $\text{H}_2\text{O}_2$  were calculated according to Henry's law equilibrium from measured gas concentrations averaged over appropriate sampling times. Concentrations of  $\text{SO}_2$ , unfortunately, were not measured in CRPAQS and had to be estimated based on results from previous measurements in the region (Reilly, 2000). Aqueous concentrations of dissolved  $\text{SO}_2$  were then calculated using measured drop pH and assuming equilibrium phase partitioning. HCHO concentrations

Table 5-9. Model input parameters used for fog events at the Angiola main site.

Sample Name	pH	Radius (cm)	Temp (K)	Pressure (p)	$\text{SO}_2$ (ppb)	$\text{SO}_2$ (mol/L)	$\text{O}_3$ (ppb)	$\text{O}_3$ (mol/L)	$\text{H}_2\text{O}_2$ (ppb)	$\text{H}_2\text{O}_2$ (mol/L)	[HCHO] (M)	LWC (L/L)
AGPCL01501	6.08	0.0023	275.80	1015.96	0.94	4.16E-11	5.90	2.61E-10	0.01119	4.96E-13	1.08E-05	1.16E-07
AGPCL01701	6.70	0.0023	273.61	1019.35	0.94	4.21E-11	2.67	1.20E-10	0.19570	8.77E-12	1.79E-05	1.17E-07
AGPCL01702	6.52	0.0023	273.25	1020.09	0.94	4.22E-11	3.22	1.45E-10	0.12810	5.75E-12	1.18E-05	6.70E-08
AGPCL01703	6.35	0.0023	273.46	1020.95	0.94	4.22E-11	1.99	8.94E-11	0.17660	7.93E-12	9.09E-06	7.60E-08
AGPCL02101	6.45	0.0019	275.81	1016.15	0.94	4.17E-11	2.13	9.44E-11	0.00340	1.51E-13	2.35E-05	1.79E-07
AGPCL02102	6.44	0.0019	275.85	1017.33	0.94	4.17E-11	3.50	1.55E-10	0.00260	1.15E-13	1.54E-05	2.32E-07
AGPCL02103	6.58	0.0021	276.05	1017.33	0.94	4.17E-11	5.03	2.23E-10	0.02087	9.25E-13	1.57E-05	1.20E-07
AGPCL02501	6.43	0.0024	276.18	1019.69	0.94	4.17E-11	4.57	2.03E-10	0.05666	2.52E-12	5.22E-06	7.34E-08
AGPCL02502	6.58	0.0023	275.82	1020.68	0.94	4.18E-11	3.10	1.38E-10	0.08144	3.62E-12	7.43E-06	9.28E-08
AGPCL03101	6.50	0.0023	278.16	1019.00	0.94	4.14E-11	4.50	1.98E-10	0.03055	1.35E-12	3.97E-05	2.78E-07
AGPCL03102	6.81	0.0023	277.73	1019.77	0.94	4.15E-11	3.95	1.74E-10	0.04249	1.88E-12	3.74E-05	1.55E-07
AGPCL03103	7.04	0.0023	278.24	1020.77	0.94	4.15E-11	5.87	2.59E-10	0.13870	6.12E-12	4.63E-05	6.70E-08
AGPCL03201	6.61	0.0016	275.45	1021.00	0.94	4.19E-11	2.25	1.00E-10	0.11620	5.18E-12	2.61E-05	3.07E-08
AGPCL03202	6.53	0.0018	274.52	1021.00	0.94	4.20E-11	2.03	9.08E-11	0.11620	5.20E-12	2.78E-05	8.10E-08
AGPCL35201	6.52	0.0027	276.40	1022.54	0.94	4.18E-11	7.44	3.31E-10	0.97890	4.36E-11	1.56E-05	4.50E-07
AGPCL35202	8.02	0.0023	277.43	1022.00	0.94	4.16E-11	6.84	3.03E-10	0.01603	7.10E-13	1.81E-05	2.87E-07
AGPCL35203	7.19	0.0029	278.21	1022.00	0.94	4.15E-11	6.41	2.83E-10	0.05602	2.48E-12	2.05E-05	3.57E-07
AGPCL35204	7.02	0.0027	278.82	1021.50	0.94	4.14E-11	6.31	2.78E-10	0.04186	1.84E-12	2.29E-05	2.40E-07
AGPCL35205	7.31	0.0023	278.84	1021.50	0.94	4.14E-11	8.25	3.63E-10	0.11440	5.04E-12	2.53E-05	2.56E-07
AGPCL35206	7.32	0.0023	278.57	1022.00	0.94	4.15E-11	4.07	1.80E-10	0.16590	7.32E-12	2.77E-05	2.29E-07
AGPCL35207	7.50	0.0021	278.30	1022.42	0.94	4.15E-11	4.32	1.91E-10	0.15960	7.05E-12	3.02E-05	2.31E-07
AGPCL35208	7.42	0.0023	278.52	1022.92	0.94	4.15E-11	6.37	2.81E-10	0.20640	9.12E-12	2.28E-05	2.17E-07
AGPCL35209	7.48	0.0021	279.03	1023.08	0.94	4.15E-11	7.96	3.51E-10	0.03483	1.54E-12	3.00E-05	1.74E-07
AGPCL35210	7.49	0.0021	279.80	1022.83	0.94	4.13E-11	8.55	3.76E-10	0.24030	1.06E-11	2.92E-05	1.57E-07
AGPCL35211	7.47	0.0019	280.47	1022.08	0.94	4.12E-11	9.73	4.26E-10	0.05062	2.22E-12	3.15E-05	1.08E-07
AGPCL35301	6.48	0.0026	276.35	1019.86	0.94	4.17E-11	3.06	1.36E-10	0.02123	9.42E-13	2.27E-05	3.18E-07

AGPCL35302	6.15	0.0029	276.35	1019.12	0.94	4.17E-11	1.95	8.65E-11	0.01234	5.47E-13	2.27E-05	2.63E-07
AGPCL35303	6.41	0.0026	275.85	1020.22	0.94	4.18E-11	1.98	8.81E-11	0.03423	1.52E-12	2.27E-05	1.84E-07
AGPCS01501	6.30	0.0015	275.80	1015.96	0.94	4.16E-11	5.90	2.61E-10	0.01119	4.96E-13	1.08E-05	1.16E-07
AGPCS01701	6.91	0.0015	273.61	1019.35	0.94	4.21E-11	2.67	1.20E-10	0.19570	8.77E-12	1.28E-05	1.17E-07
AGPCS01702	6.91	0.0015	273.25	1020.09	0.94	4.22E-11	3.22	1.45E-10	0.12810	5.75E-12	1.28E-05	6.70E-08
AGPCS01703	6.58	0.0015	273.46	1020.95	0.94	4.22E-11	1.99	8.94E-11	0.17660	7.93E-12	1.28E-05	7.60E-08
AGPCS02101	6.50	0.0014	275.81	1016.15	0.94	4.17E-11	2.13	9.44E-11	0.00340	1.51E-13	2.83E-05	1.79E-07
AGPCS02102	6.68	0.0014	275.85	1017.33	0.94	4.17E-11	3.50	1.55E-10	0.00260	1.15E-13	3.11E-05	2.32E-07
AGPCS02103	6.44	0.0012	276.05	1017.33	0.94	4.17E-11	5.03	2.23E-10	0.02087	9.25E-13	2.94E-05	1.20E-07
AGPCS02501	6.56	0.0016	276.18	1019.69	0.94	4.17E-11	4.57	2.03E-10	0.05666	2.52E-12	1.31E-05	7.34E-08
AGPCS02502	6.60	0.0017	275.82	1020.68	0.94	4.18E-11	3.10	1.38E-10	0.08144	3.62E-12	1.31E-05	9.28E-08
AGPCS03101	6.00	0.0015	278.16	1019.00	0.94	4.14E-11	4.50	1.98E-10	0.03055	1.35E-12	5.58E-05	2.78E-07
AGPCS03102	6.29	0.0015	277.73	1019.77	0.94	4.15E-11	3.95	1.74E-10	0.04249	1.88E-12	5.47E-05	1.55E-07
AGPCS03103	6.73	0.0015	278.24	1020.77	0.94	4.15E-11	5.87	2.59E-10	0.13870	6.12E-12	6.58E-05	6.70E-08
AGPCS03201	6.46	0.0009	275.45	1021.00	0.94	4.19E-11	2.25	1.00E-10	0.11620	5.18E-12	4.69E-05	3.07E-08
AGPCS03202	6.39	0.0013	274.52	1021.00	0.94	4.20E-11	2.03	9.08E-11	0.11620	5.20E-12	4.69E-05	8.10E-08
AGPCS35201	6.75	0.0023	276.40	1022.54	0.94	4.18E-11	7.44	3.31E-10	0.97890	4.36E-11	1.81E-05	4.50E-07
AGPCS35202	6.76	0.0015	277.43	1022.00	0.94	4.16E-11	6.84	3.03E-10	0.01603	7.10E-13	1.93E-05	2.87E-07
AGPCS35203	7.10	0.0015	278.21	1022.00	0.94	4.15E-11	6.41	2.83E-10	0.05602	2.48E-12	2.05E-05	3.57E-07
AGPCS35204	6.85	0.0015	278.82	1021.50	0.94	4.14E-11	6.31	2.78E-10	0.04186	1.84E-12	2.16E-05	2.40E-07
AGPCS35205	6.91	0.0015	278.84	1021.50	0.94	4.14E-11	8.25	3.63E-10	0.11440	5.04E-12	2.28E-05	2.56E-07
AGPCS35206	6.89	0.0015	278.57	1022.00	0.94	4.15E-11	4.07	1.80E-10	0.16590	7.32E-12	2.40E-05	2.29E-07
AGPCS35207	7.25	0.0013	278.30	1022.42	0.94	4.15E-11	4.32	1.91E-10	0.15960	7.05E-12	2.51E-05	2.31E-07
AGPCS35208	7.21	0.0013	278.52	1022.92	0.94	4.15E-11	6.37	2.81E-10	0.20640	9.12E-12	2.68E-05	2.17E-07
AGPCS35209	7.32	0.0013	279.03	1023.08	0.94	4.15E-11	7.96	3.51E-10	0.03483	1.54E-12	2.15E-05	1.74E-07
AGPCS35210	7.25	0.0013	279.80	1022.83	0.94	4.13E-11	8.55	3.76E-10	0.24030	1.06E-11	3.65E-05	1.57E-07
AGPCS35211	7.12	0.0011	280.47	1022.08	0.94	4.12E-11	9.73	4.26E-10	0.05062	2.22E-12	4.13E-05	1.08E-07
AGPCS35301	6.54	0.0022	276.35	1019.86	0.94	4.17E-11	3.06	1.36E-10	0.02123	9.42E-13	3.38E-05	3.18E-07
AGPCS35302	6.37	0.0021	276.35	1019.12	0.94	4.17E-11	1.95	8.65E-11	0.01234	5.47E-13	3.38E-05	2.63E-07
AGPCS35303	6.60	0.0019	275.85	1020.22	0.94	4.18E-11	1.98	8.81E-11	0.03423	1.52E-12	3.38E-05	1.84E-07

taken from measured aqueous concentrations. The average radius of large and small fog drop fractions were computed by combining information about the drop size distribution (from the CSASP) with sf-CASCC drop size dependent collection efficiencies. This approach yields the expected size distributions of drops collected during each sample period in the two sf-CASCC collection stages. The average volume weighted drop size was then computed for each “collected” distribution. When some input data were unavailable, concentrations from preceding or subsequent time periods were used.

### 5.3.4 Results and discussion

#### 5.3.4.1 Model results

Table 5-10 shows key output parameters from the model simulations. Included are the partition function and correction factor,  $Q$ , for each species and the reaction rates for oxidation by hydrogen peroxide and by ozone and the HMS formation rate. Sample names with an “L” indicate they represent the large drop fraction from the sf-CASCC;



those with an “S” represent the small drop fraction. From the partition functions of each species, we can see that partition function of ozone is nearly equal to one for all the fog samples. This is expected since ozone has low solubility in water and can quickly reach phase equilibrium. For S(IV) and  $\text{H}_2\text{O}_2$ , there are very small partition functions for some fog samples, implying the gas-aqueous phase partitioning has not had adequate time to reach equilibrium. Correction factors,  $Q$ , for  $\text{O}_3$  are not very large for all the fog samples, indicating significant concentration gradients inside the drops. For most samples, the correction factors for  $\text{H}_2\text{O}_2$  and S(IV) are close to one, implying concentration gradients inside the drops exist, but are not serious.

Table 5-10. Partition function, Q, and rates for S(IV) oxidation by hydrogen peroxide and ozone and HMS formation.

Samples	S(IV) (mol/L)	HCHO (mol/L)	S(VI) (mol/L)	Partition function_S (IV)	Partition function_O 3	Partition function_H 2O2	Q_O3	Q_H2O2	Q_SIV	r_O3ox (mol s <sup>-1</sup> )	r_H2O2ox (mol s <sup>-1</sup> )	r_HMS (mol s <sup>-1</sup> )	r_totS(IV) (mol s <sup>-1</sup> )
AGPCL0150	6.18E-05	1.08E-05	3.16E-05	7.84E-01	9.84E-01	8.53E-01	8.44E-02	1.00E+00	1.00E+00	2.32E-08	4.03E-09	4.11E-07	4.38E-07
AGPCL0170	5.33E-05	1.79E-05	3.37E-05	1.04E-01	9.74E-01	9.69E-01	5.52E-02	1.00E+00	9.99E-01	1.75E-08	1.31E-08	1.81E-06	1.84E-06
AGPCL0170	8.65E-05	1.18E-05	4.99E-05	2.80E-01	9.71E-01	9.25E-01	5.08E-02	1.00E+00	9.99E-01	2.32E-08	2.28E-08	1.43E-06	1.48E-06
AGPCL0170	9.82E-05	9.09E-06	6.96E-05	5.18E-01	9.74E-01	8.75E-01	5.52E-02	1.00E+00	1.00E+00	1.31E-08	5.41E-08	9.23E-07	9.90E-07
AGPCL0210	6.60E-05	2.35E-05	1.84E-05	3.13E-01	9.77E-01	9.55E-01	6.93E-02	1.00E+00	9.99E-01	1.51E-08	5.51E-10	1.97E-06	1.98E-06
AGPCL0210	8.58E-05	1.54E-05	3.36E-05	4.20E-01	9.74E-01	9.41E-01	6.14E-02	1.00E+00	1.00E+00	2.79E-08	5.52E-10	1.65E-06	1.68E-06
AGPCL0210	7.13E-05	1.57E-05	4.70E-05	2.38E-01	9.73E-01	9.59E-01	5.37E-02	1.00E+00	9.99E-01	3.76E-08	2.52E-09	1.79E-06	1.83E-06
AGPCL0250	1.14E-04	5.22E-06	5.41E-05	5.86E-01	9.69E-01	8.80E-01	4.25E-02	1.00E+00	1.00E+00	3.31E-08	1.53E-08	7.30E-07	7.78E-07
AGPCL0250	1.08E-04	7.43E-06	4.51E-05	3.53E-01	9.66E-01	9.27E-01	4.04E-02	1.00E+00	1.00E+00	2.60E-08	1.44E-08	1.28E-06	1.32E-06
AGPCL0310	3.02E-05	3.97E-05	2.41E-05	1.47E-01	9.83E-01	9.74E-01	7.57E-02	1.00E+00	9.98E-01	1.86E-08	1.92E-09	1.70E-06	1.72E-06
AGPCL0310	2.20E-05	3.74E-05	2.22E-05	4.12E-02	9.82E-01	9.92E-01	6.99E-02	1.00E+00	9.97E-01	1.79E-08	7.94E-10	1.93E-06	1.94E-06
AGPCL0310	1.35E-05	4.63E-05	2.98E-05	1.22E-02	9.83E-01	9.98E-01	7.56E-02	1.00E+00	9.95E-01	2.43E-08	7.40E-10	1.98E-06	2.00E-06
AGPCL0320	7.12E-05	2.61E-05	4.15E-05	2.08E-01	9.73E-01	9.77E-01	6.96E-02	1.00E+00	9.99E-01	2.25E-08	1.33E-08	3.11E-06	3.15E-06
AGPCL0320	6.20E-05	2.78E-05	3.47E-05	2.14E-01	9.76E-01	9.68E-01	7.27E-02	1.00E+00	9.99E-01	1.59E-08	1.47E-08	2.50E-06	2.53E-06
AGPCL3520	4.82E-05	1.56E-05	1.32E-04	1.95E-01	9.78E-01	9.42E-01	5.30E-02	1.00E+00	9.99E-01	3.40E-08	9.32E-08	1.09E-06	1.22E-06
AGPCL3520	1.93E-05	1.81E-05	5.44E-05	3.28E-04	9.73E-01	9.99E-01	4.86E-02	1.00E+00	9.96E-01	4.55E-08	2.47E-12	1.99E-06	2.03E-06
AGPCL3520	1.67E-05	2.05E-05	3.06E-05	8.91E-03	9.79E-01	9.91E-01	5.02E-02	1.00E+00	9.96E-01	2.55E-08	2.18E-10	1.28E-06	1.30E-06
AGPCL3520	2.01E-05	2.29E-05	3.25E-05	2.04E-02	9.79E-01	9.93E-01	5.29E-02	1.00E+00	9.97E-01	2.70E-08	3.52E-10	1.44E-06	1.47E-06
AGPCL3520	1.85E-05	2.53E-05	5.50E-05	6.64E-03	9.77E-01	9.99E-01	5.58E-02	1.00E+00	9.96E-01	4.58E-08	3.14E-10	1.97E-06	2.00E-06
AGPCL3520	1.71E-05	2.77E-05	2.66E-05	5.78E-03	9.78E-01	9.99E-01	5.82E-02	1.00E+00	9.96E-01	2.19E-08	4.07E-10	2.00E-06	2.01E-06
AGPCL3520	1.65E-05	3.02E-05	3.19E-05	2.71E-03	9.77E-01	1.00E+00	6.14E-02	1.00E+00	9.96E-01	2.65E-08	1.88E-10	2.37E-06	2.39E-06
AGPCL3520	1.92E-05	2.28E-05	4.52E-05	4.39E-03	9.76E-01	9.99E-01	5.32E-02	1.00E+00	9.96E-01	3.75E-08	3.87E-10	1.98E-06	2.01E-06
AGPCL3520	1.65E-05	3.00E-05	5.81E-05	3.08E-03	9.78E-01	1.00E+00	6.05E-02	1.00E+00	9.96E-01	4.85E-08	4.40E-11	2.35E-06	2.39E-06
AGPCL3521	1.65E-05	2.92E-05	6.30E-05	3.16E-03	9.77E-01	1.00E+00	5.89E-02	1.00E+00	9.96E-01	5.24E-08	2.90E-10	2.33E-06	2.38E-06
AGPCL3521	1.83E-05	3.15E-05	8.24E-05	3.99E-03	9.77E-01	1.00E+00	6.09E-02	1.00E+00	9.96E-01	6.88E-08	7.26E-11	2.79E-06	2.85E-06
AGPCL3530	4.23E-05	2.27E-05	1.75E-05	1.91E-01	9.80E-01	9.48E-01	6.09E-02	1.00E+00	9.99E-01	1.31E-08	1.99E-09	1.29E-06	1.31E-06
AGPCL3530	4.27E-05	2.27E-05	8.94E-06	4.68E-01	9.85E-01	8.60E-01	7.42E-02	1.00E+00	9.99E-01	5.48E-09	2.56E-09	6.92E-07	7.00E-07
AGPCL3530	4.54E-05	2.27E-05	1.39E-05	2.41E-01	9.81E-01	9.33E-01	6.34E-02	1.00E+00	9.99E-01	8.26E-09	4.16E-09	1.22E-06	1.23E-06

Table 5-10 (Continued). Partition function, Q, and rates for S(IV) oxidation by hydrogen peroxide and ozone and HMS formation.

Samples	S(IV) (mol/L)	HCHO (mol/L)	S(VI) (mol/L)	Partition function_S (IV)	Partition function_O 3	Partition function_H 2O2	Q_O3	Q_H2O2	Q_SIV	r_O3ox (mol s <sup>-1</sup> )	r_H2O2ox (mol s <sup>-1</sup> )	r_HMS (mol s <sup>-1</sup> )	r_totS(IV) (mol s <sup>-1</sup> )
AGPCS0150	1.04E-04	1.08E-05	7.24E-05	7.44E-01	9.75E-01	9.34E-01	8.03E-02	1.00E+00	1.00E+00	5.71E-08	4.19E-09	1.08E-06	1.14E-06
AGPCS0170	1.19E-04	1.28E-05	7.11E-05	1.19E-01	9.56E-01	9.87E-01	4.89E-02	1.00E+00	1.00E+00	4.59E-08	1.52E-08	3.89E-06	3.95E-06
AGPCS0170	1.20E-04	1.28E-05	7.69E-05	1.17E-01	9.56E-01	9.86E-01	4.92E-02	1.00E+00	1.00E+00	5.56E-08	1.01E-08	3.90E-06	3.97E-06
AGPCS0170	1.37E-04	1.28E-05	8.14E-05	3.77E-01	9.63E-01	9.58E-01	5.84E-02	1.00E+00	1.00E+00	2.88E-08	4.31E-08	2.73E-06	2.80E-06
AGPCS0210	8.33E-05	2.83E-05	2.90E-05	3.44E-01	9.73E-01	9.72E-01	7.97E-02	1.00E+00	1.00E+00	2.38E-08	6.15E-10	3.28E-06	3.30E-06
AGPCS0210	7.04E-05	3.11E-05	5.01E-05	1.72E-01	9.72E-01	9.86E-01	7.46E-02	1.00E+00	9.99E-01	4.18E-08	2.37E-10	4.12E-06	4.16E-06
AGPCS0210	9.40E-05	2.94E-05	8.42E-05	4.67E-01	9.74E-01	9.73E-01	9.14E-02	1.00E+00	1.00E+00	6.58E-08	5.01E-09	3.46E-06	3.52E-06
AGPCS0250	1.13E-04	1.31E-05	7.80E-05	4.03E-01	9.67E-01	9.60E-01	5.67E-02	1.00E+00	1.00E+00	5.52E-08	1.15E-08	2.29E-06	2.36E-06
AGPCS0250	1.07E-04	1.31E-05	5.75E-05	3.32E-01	9.67E-01	9.61E-01	5.35E-02	1.00E+00	1.00E+00	3.56E-08	1.41E-08	2.32E-06	2.37E-06
AGPCS0310	4.00E-05	5.58E-05	3.38E-05	7.26E-01	9.89E-01	9.47E-01	1.60E-01	1.00E+00	1.00E+00	1.95E-08	9.22E-09	1.18E-06	1.21E-06
AGPCS0310	4.92E-05	5.47E-05	3.97E-05	4.12E-01	9.83E-01	9.68E-01	1.11E-01	1.00E+00	9.99E-01	2.59E-08	7.74E-09	2.57E-06	2.60E-06
AGPCS0310	2.95E-05	6.58E-05	5.79E-05	7.34E-02	9.81E-01	9.94E-01	9.59E-02	1.00E+00	9.98E-01	4.42E-08	4.43E-09	4.06E-06	4.10E-06
AGPCS0320	9.91E-05	4.69E-05	8.21E-05	4.45E-01	9.73E-01	9.84E-01	1.17E-01	1.00E+00	1.00E+00	4.07E-08	2.86E-08	6.00E-06	6.06E-06
AGPCS0320	6.97E-05	4.69E-05	5.21E-05	3.56E-01	9.78E-01	9.72E-01	1.06E-01	1.00E+00	9.99E-01	2.03E-08	2.46E-08	3.68E-06	3.72E-06
AGPCS3520	4.59E-05	1.81E-05	1.04E-04	9.40E-02	9.74E-01	9.80E-01	5.29E-02	1.00E+00	9.99E-01	4.69E-08	4.66E-08	1.75E-06	1.85E-06
AGPCS3520	8.46E-05	1.93E-05	1.08E-04	1.81E-01	9.67E-01	9.85E-01	5.74E-02	1.00E+00	9.99E-01	8.94E-08	1.35E-09	3.54E-06	3.63E-06
AGPCS3520	5.94E-05	2.05E-05	1.05E-04	4.37E-02	9.65E-01	9.97E-01	5.38E-02	1.00E+00	9.99E-01	8.74E-08	1.07E-09	4.15E-06	4.23E-06
AGPCS3520	6.97E-05	2.16E-05	9.75E-05	1.24E-01	9.68E-01	9.91E-01	5.70E-02	1.00E+00	9.99E-01	7.98E-08	2.14E-09	3.79E-06	3.86E-06
AGPCS3520	6.27E-05	2.28E-05	1.28E-04	9.23E-02	9.68E-01	9.93E-01	5.76E-02	1.00E+00	9.99E-01	1.03E-07	4.34E-09	3.90E-06	4.01E-06
AGPCS3520	6.21E-05	2.40E-05	6.73E-05	9.55E-02	9.69E-01	9.93E-01	5.91E-02	1.00E+00	9.99E-01	5.01E-08	6.69E-09	3.95E-06	4.00E-06
AGPCS3520	5.56E-05	2.51E-05	8.63E-05	2.39E-02	9.64E-01	9.99E-01	5.94E-02	1.00E+00	9.99E-01	7.07E-08	1.66E-09	5.51E-06	5.58E-06
AGPCS3520	5.33E-05	2.68E-05	1.22E-04	2.70E-02	9.65E-01	9.99E-01	6.13E-02	1.00E+00	9.99E-01	1.00E-07	2.38E-09	5.46E-06	5.56E-06
AGPCS3520	5.99E-05	2.15E-05	1.66E-04	2.09E-02	9.62E-01	9.99E-01	5.44E-02	1.00E+00	9.99E-01	1.39E-07	2.98E-10	5.46E-06	5.59E-06
AGPCS3521	3.71E-05	3.65E-05	1.39E-04	1.79E-02	9.70E-01	9.99E-01	6.92E-02	1.00E+00	9.98E-01	1.15E-07	1.64E-09	5.48E-06	5.59E-06
AGPCS3521	4.82E-05	4.13E-05	1.97E-04	3.92E-02	9.69E-01	9.99E-01	7.48E-02	1.00E+00	9.99E-01	1.64E-07	7.11E-10	7.16E-06	7.32E-06
AGPCS3530	3.71E-05	3.38E-05	1.97E-05	1.42E-01	9.81E-01	9.73E-01	7.25E-02	1.00E+00	9.98E-01	1.53E-08	1.51E-09	1.88E-06	1.89E-06
AGPCS3530	4.61E-05	3.38E-05	1.33E-05	2.83E-01	9.82E-01	9.53E-01	7.93E-02	1.00E+00	9.99E-01	9.70E-09	1.72E-09	1.71E-06	1.72E-06
AGPCS3530	4.45E-05	3.38E-05	1.83E-05	1.38E-01	9.78E-01	9.80E-01	7.38E-02	1.00E+00	9.99E-01	1.32E-08	2.50E-09	2.49E-06	2.50E-06

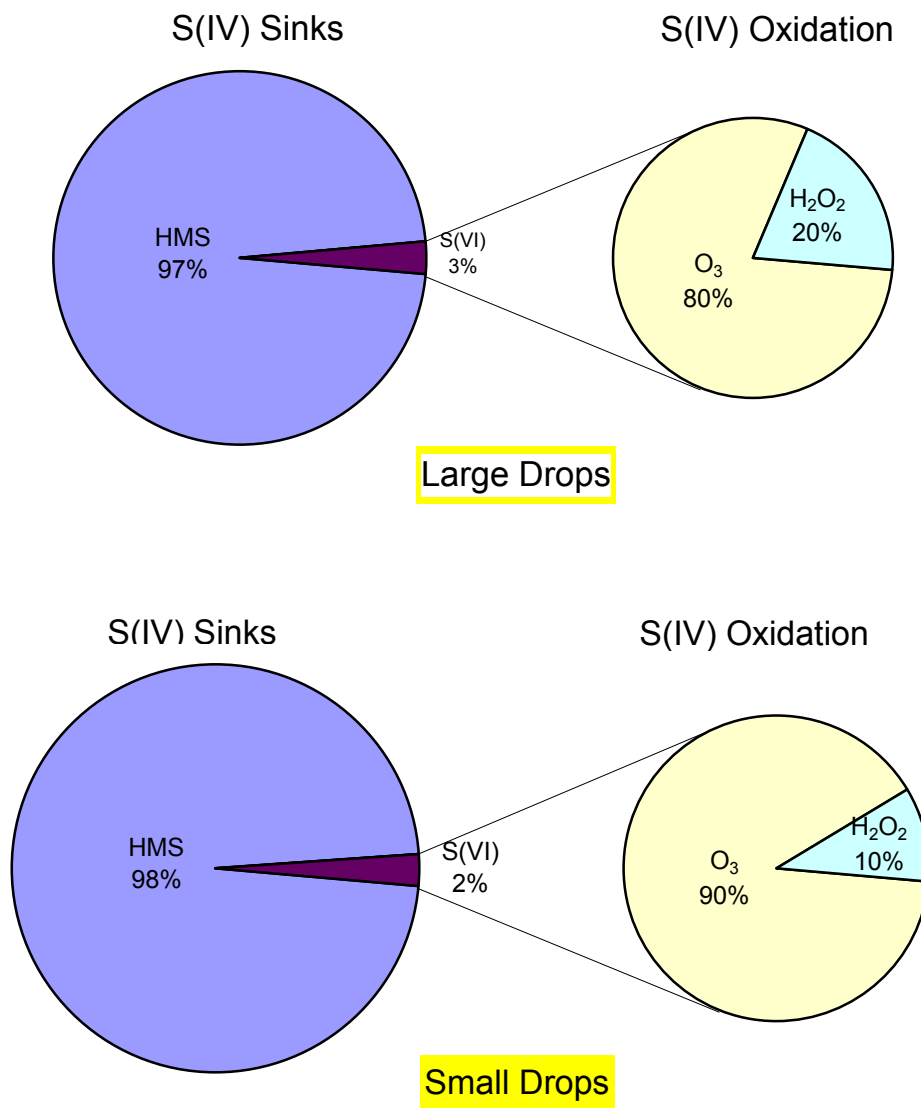


Figure 5-35. S(IV) sinks as calculated by the aqueous phase chemistry model for both the large (upper panel) and small (lower panel) drop fractions from the sf-CASCC.

Figure 5-35 summarizes model predicted average fates of S(IV) during the fog episodes for the large and small drop classes collected with the sf-CASCC. The largest sink of S(IV), based on the model prediction, is complexation with formaldehyde to form HMS. For the large drops, the HMS formation accounts for about 97% of the total S(IV) sink, while in the small drops, HMS formation accounts for 98%. Since the HCHO we

input into the model was the total HCHO we measured, including both “free” HCHO as well as HMS itself, the importance of this pathway may be slightly overestimated.

Figure 5-36 shows a sensitivity test of the dependence of the HMS formation rates on the HCHO concentration. Doubling the HCHO concentration has only a modest effect on the overall HMS formation rate because the rate is controlled primarily by the availability of S(IV) species brought into the drop.

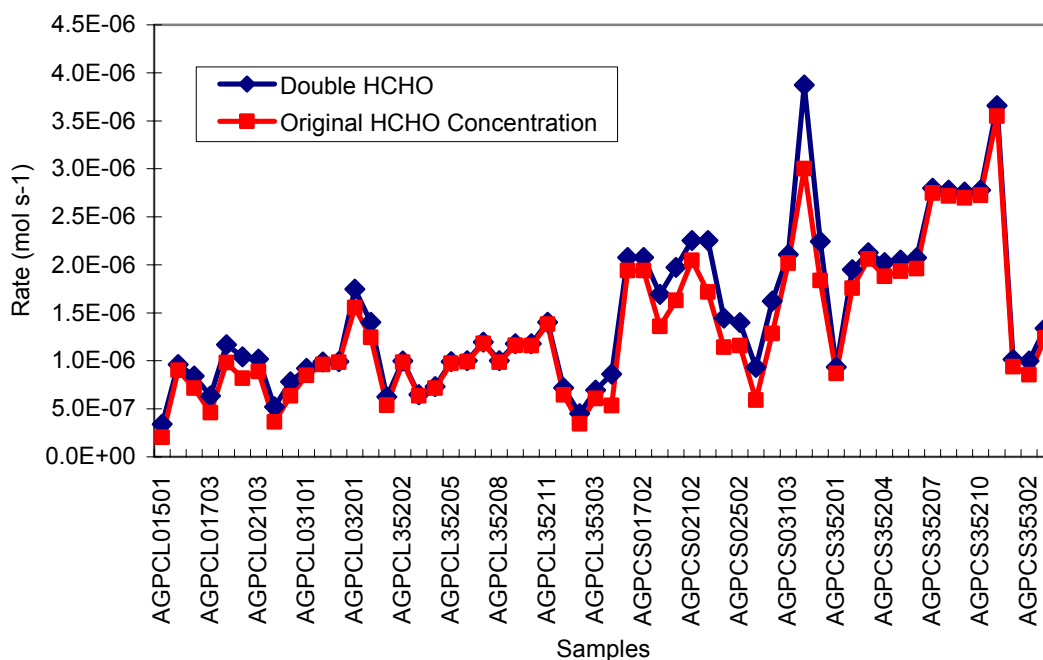


Figure 5-36. Sensitivity test of the rate of HMS formation to changes in the HCHO concentration.

For S(IV) oxidation rates, Figure 5-35 shows that oxidation by ozone accounts for approximately 80% of the oxidation in the large drops, and approximately 90% in the small drops. Oxidation by hydrogen peroxide accounted for 20% in the large drops and 10% in the small drops. Figure 5-37 shows the sensitivity of the rate of the hydrogen peroxide S(IV) oxidation pathway to the hydrogen peroxide concentration. Doubling the H<sub>2</sub>O<sub>2</sub> concentration almost doubles the oxidation rate. Similarly, Figure 5-38 shows sensitivity test results for ozone. Doubling ozone concentrations also almost doubles ozone oxidation rates.

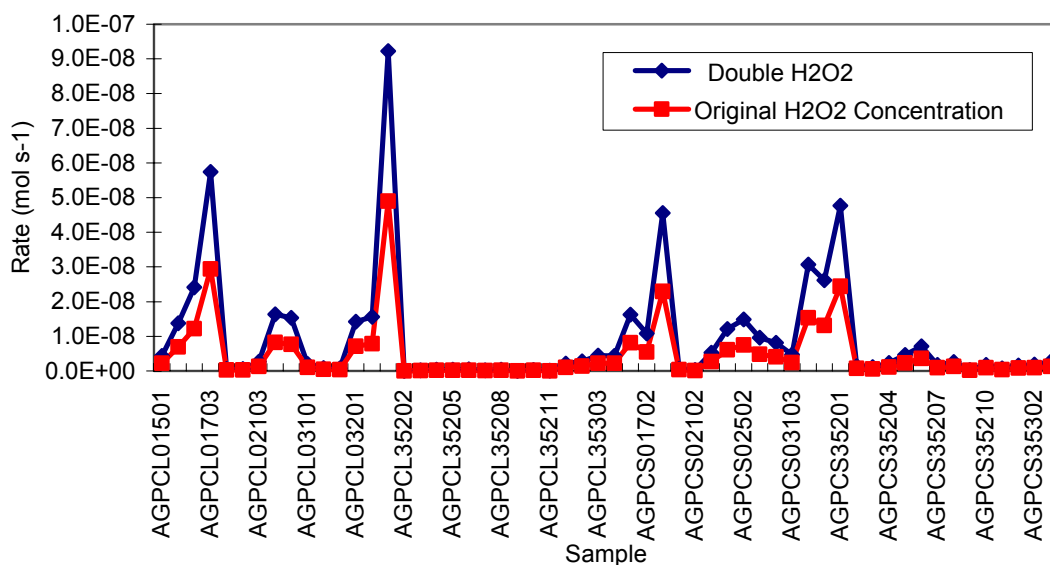


Figure 5-37. Sensitivity test of rate of the  $\text{H}_2\text{O}_2$ -S(IV) oxidation pathway to  $\text{H}_2\text{O}_2$  concentrations.

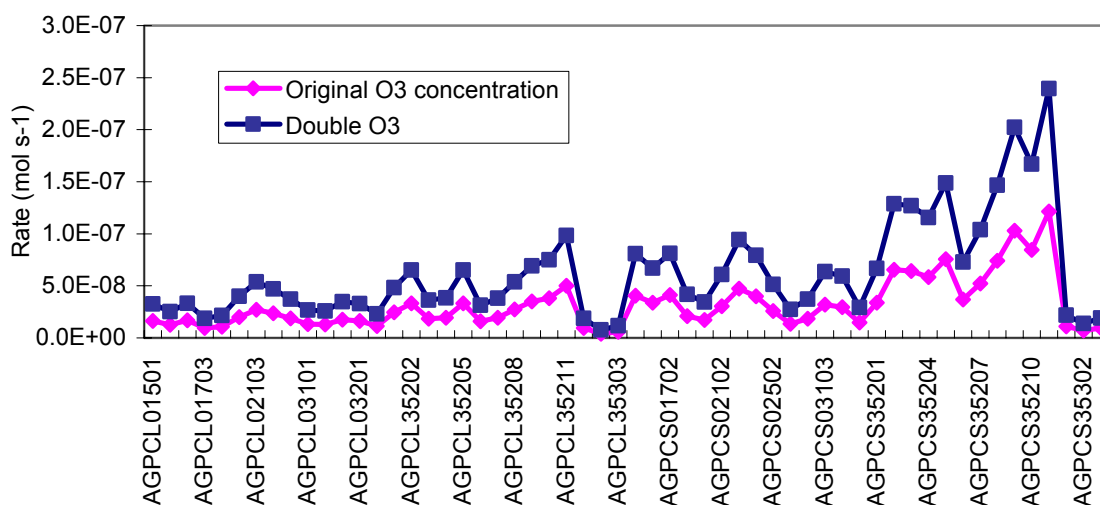


Figure 5-38. Sensitivity test of the rate of the  $\text{O}_3$ -S(IV) oxidation pathway to  $\text{O}_3$  concentrations.

### 5.3.4.2 Theoretical S(IV) reaction rates

Table 5-11. Theoretical S(IV) oxidation rate and HMS formation rate for all fog samples.

Sample Name	Oxidation by H <sub>2</sub> O <sub>2</sub> (M s <sup>-1</sup> )	Oxidation by O <sub>3</sub> (M s <sup>-1</sup> )	HMSA prod. (M s <sup>-1</sup> )	Sample Name	Oxidation by H <sub>2</sub> O <sub>2</sub> (M s <sup>-1</sup> )	Oxidation by O <sub>3</sub> (M s <sup>-1</sup> )	HMSA prod. (M s <sup>-1</sup> )
AGPCL01501	5.97E-09	3.73E-07	2.56E-07	AGPCS01501	5.97E-09	1.03E-06	7.06E-07
AGPCL01701	1.28E-07	3.27E-06	8.92E-06	AGPCS01701	1.28E-07	8.61E-06	1.68E-05
AGPCL01702	8.66E-08	1.76E-06	2.65E-06	AGPCS01702	8.66E-08	1.06E-05	1.73E-05
AGPCL01703	1.17E-07	4.91E-07	9.14E-07	AGPCS01703	1.17E-07	1.42E-06	3.72E-06
AGPCL02101	1.81E-09	7.39E-07	3.05E-06	AGPCS02101	1.81E-09	9.30E-07	4.62E-06
AGPCL02102	1.38E-09	1.16E-06	1.90E-06	AGPCS02102	1.38E-09	3.49E-06	1.16E-05
AGPCL02103	1.09E-08	3.06E-06	3.55E-06	AGPCS02103	1.09E-08	1.65E-06	3.57E-06
AGPCL02501	2.92E-08	1.42E-06	5.99E-07	AGPCS02501	2.92E-08	2.58E-06	2.74E-06
AGPCL02502	4.34E-08	1.96E-06	1.75E-06	AGPCS02502	4.34E-08	2.14E-06	3.40E-06
AGPCL03101	1.32E-08	1.75E-06	5.32E-06	AGPCS03101	1.32E-08	1.75E-07	7.46E-07
AGPCL03102	1.90E-08	6.53E-06	2.16E-05	AGPCS03102	1.90E-08	5.96E-07	2.88E-06
AGPCL03103	5.93E-08	2.73E-05	7.39E-05	AGPCS03103	5.93E-08	6.54E-06	2.52E-05
AGPCL03201	6.41E-08	1.66E-06	7.31E-06	AGPCS03201	6.41E-08	8.32E-07	6.57E-06
AGPCL03202	6.98E-08	1.09E-06	5.82E-06	AGPCS03202	6.98E-08	5.70E-07	5.16E-06
AGPCL35201	4.95E-07	3.46E-06	2.66E-06	AGPCS35201	4.95E-07	9.97E-06	8.91E-06
AGPCL35202	7.37E-09	3.02E-03	2.82E-03	AGPCS35202	7.37E-09	9.11E-06	9.10E-06
AGPCL35203	2.40E-08	5.95E-05	6.54E-05	AGPCS35203	2.40E-08	3.93E-05	4.32E-05
AGPCL35204	1.70E-08	2.60E-05	3.17E-05	AGPCS35204	1.70E-08	1.19E-05	1.37E-05
AGPCL35205	4.63E-08	1.29E-04	1.33E-04	AGPCS35205	4.63E-08	2.05E-05	1.90E-05
AGPCL35206	6.88E-08	6.75E-05	1.56E-04	AGPCS35206	6.88E-08	9.33E-06	1.87E-05
AGPCL35207	6.78E-08	1.66E-04	3.99E-04	AGPCS35207	6.78E-08	5.26E-05	1.05E-04
AGPCL35208	8.60E-08	1.68E-04	2.05E-04	AGPCS35208	8.60E-08	6.39E-05	9.13E-05
AGPCL35209	1.39E-08	2.70E-04	3.40E-04	AGPCS35209	1.39E-08	1.29E-04	1.17E-04
AGPCL35210	8.93E-08	2.92E-04	3.25E-04	AGPCS35210	8.93E-08	9.67E-05	1.34E-04
AGPCL35211	1.77E-08	2.93E-04	3.03E-04	AGPCS35211	1.77E-08	5.86E-05	7.90E-05
AGPCL35301	1.08E-08	1.19E-06	3.23E-06	AGPCS35301	1.08E-08	1.56E-06	6.34E-06
AGPCL35302	6.26E-09	1.65E-07	7.06E-07	AGPCS35302	6.26E-09	4.55E-07	2.90E-06
AGPCL35303	1.82E-08	5.70E-07	2.44E-06	AGPCS35303	1.82E-08	1.37E-06	8.73E-06

Rates of S(IV) reaction were also computed directly using the rate expressions for oxidation by ozone and by hydrogen peroxide, as well as for HMS formation, given above. These calculations assume all species attain phase equilibrium and that, consequently, there is no reactant limitation due to finite rates of mass transport inside or

outside of the droplets. Results of these calculations, termed here to be “theoretical” reaction rates, are shown in Table 5-11.

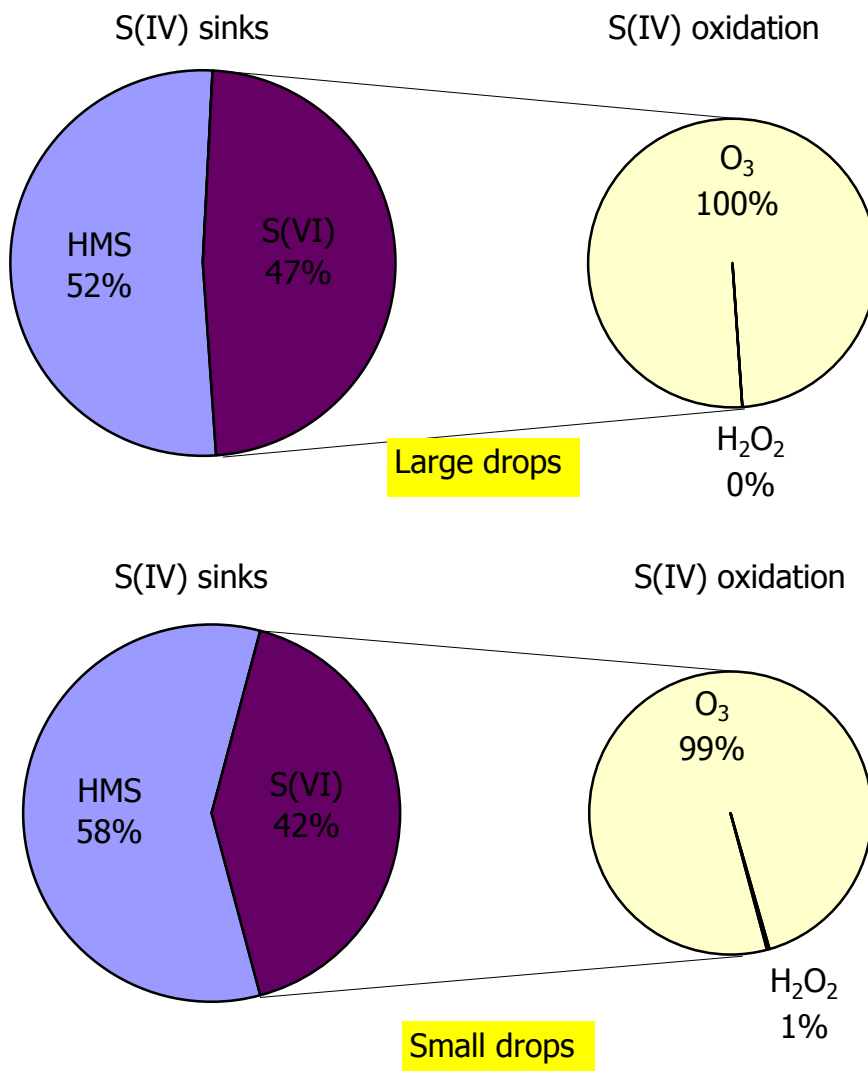


Figure 5-39. Theoretical rates of ozone and hydrogen peroxide oxidation of S(IV) and HMS formation averaged for all the large drop and small drop fog samples.

Based on Table 5-10, Figure 5-39 shows the average rates for the large and small drop classes as pie diagrams. In these calculations, both HMS formation and S(IV) oxidation by ozone are important components of dissolved sulfur dioxide. For small droplets, HMS



formation accounts for about 58%, which is slightly higher than in large droplets.  $O_3$  oxidation pathway is still the dominant pathway for all large and small drops.

#### 5.3.4.3 Comparison of theoretical and modeled rates

Comparing Figure 5-35 and Figure 5-39, we see a very large difference between modeled and theoretical rates. The modeled rates predicted that over 97% of the S(IV) reacts with HCHO to form HMS; while the theoretical rate calculations suggest this value to be somewhat below 60%. Further, S(IV) oxidation is clearly dominated by ozone in the theoretical rate calculations.

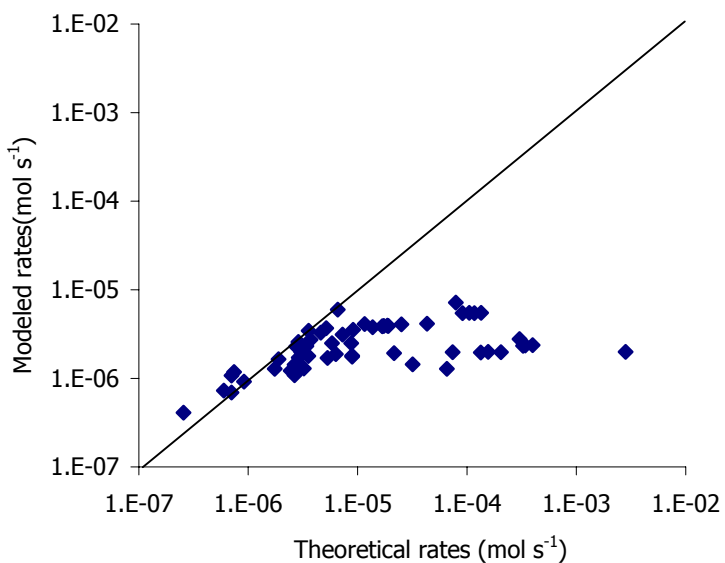


Figure 5-40. Comparison of HMS formation modeled rates and theoretical rates.

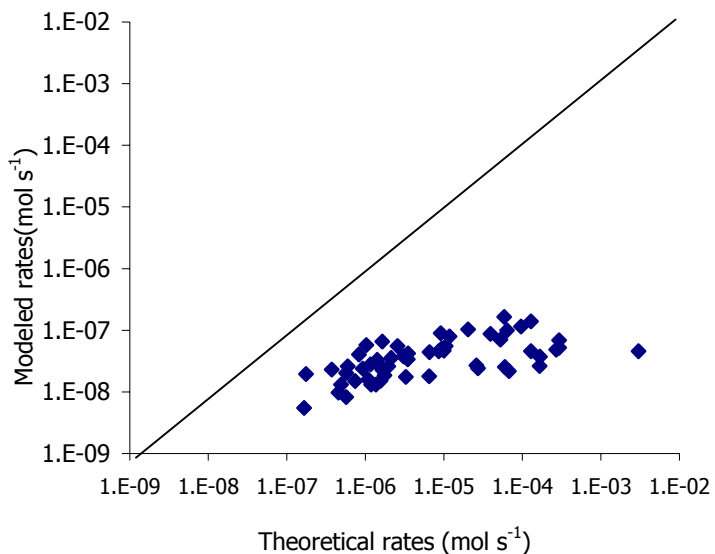


Figure 5-41. Comparison of ozone oxidation modeled rates and theoretical rates.

Figures 5-40 and 5-41 show scatter plots of modeled vs. theoretical rates for HMS formation and ozone oxidation. We can see again quite clearly that theoretical rates are nearly always much higher than modeled rates. Together, these analyses clearly indicate the importance of considering mass transport limitations to rates of reaction in these highly reactive systems.

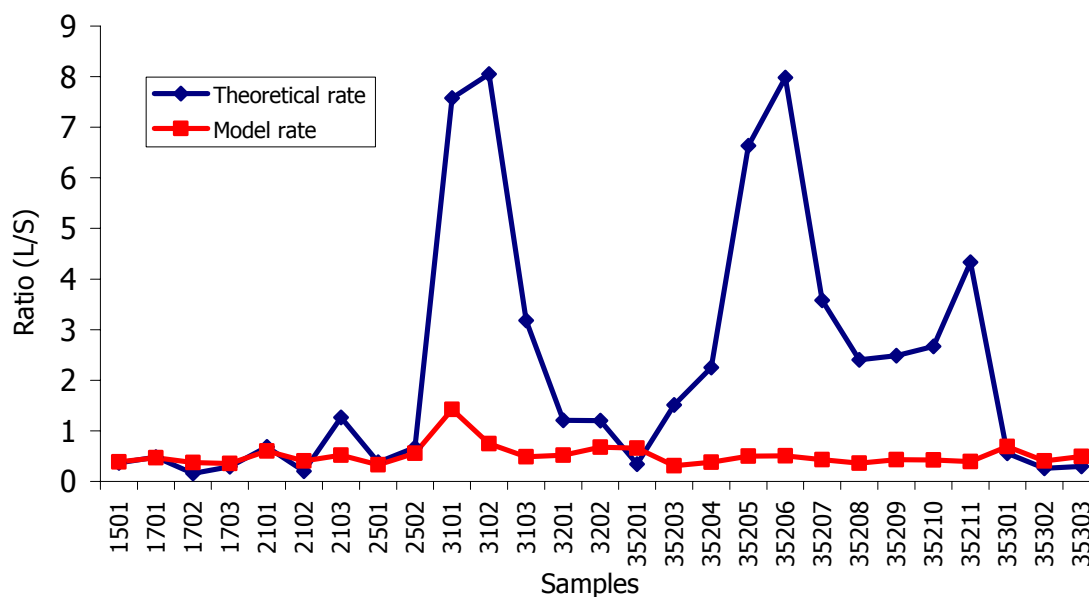


Figure 5-42. Theoretical and model rate comparison to large/small ratios for all fog sample periods.

Figure 5-42 shows large drop/small drop S(IV) total reaction rate (S(IV) oxidation plus HMS formation) ratios for CRPAQS fog sample periods. Rate ratios are shown both for the model results and the direct theoretical rate calculations. Nearly all model predicted ratios are below one, indicating that the total rate of reaction of dissolved  $\text{SO}_2$  is higher in small drops. This is a consequence of the reduced mass transport limitations for smaller drops. The theoretical rate ratios, by contrast, vary widely. Again, the difference between these two sets of results illustrates the importance of considering mass transport limitations to aqueous phase reaction rates.

#### 5.4 Overall effects of fog on atmospheric species concentrations

Based on Table 5-2, the deposition removal rates of each species for all fog events are listed in Table 5-12. Figure 5-43 plots the removal rates for the fog events on 12/17 and 12/18/00.

Table 5-12. Deposition removal rates of each species for all fog events.

Sample Start Date	Start Time	End Time	Cl <sup>-</sup> (µg/m <sup>2</sup> /h)	NO <sub>3</sub> <sup>-</sup> (µg/m <sup>2</sup> /h)	NO <sub>2</sub> <sup>-</sup> (µg/m <sup>2</sup> /h)	SO <sub>4</sub> <sup>2-</sup> (µg/m <sup>2</sup> /h)	Na <sup>+</sup> (µg/m <sup>2</sup> /h)	NH <sub>4</sub> <sup>+</sup> (µg/m <sup>2</sup> /h)	K <sup>+</sup> (µg/m <sup>2</sup> /h)	Mg <sup>2+</sup> (µg/m <sup>2</sup> /h)	Ca <sup>2+</sup> (µg/m <sup>2</sup> /h)	TOC (µg/m <sup>2</sup> /h)
12/17/2000	11:00 PM	1:00 AM	8.56	144.65	5.67	47.13	2.74	113.69	3.10	2.18	19.96	66.61
12/18/2000	1:00 AM	3:10 AM	16.66	281.89	14.11	100.67	6.06	233.67	8.35	5.83	57.29	119.05
12/18/2000	3:10 AM	6:10 AM	20.21	360.69	14.46	110.76	4.20	344.17	8.78	5.28	27.60	117.12
12/18/2000	6:10 AM	8:15 AM	22.35	255.74	17.31	192.67	16.41	425.29	6.21	4.37	27.61	115.90
12/18/2000	8:15 AM	10:00 AM	21.00	157.75	13.48	134.79	14.25	261.14	10.04	3.19	26.12	94.22
12/18/2000	10:00 AM	12:00 PM	5.94	70.59	9.19	77.12	8.70	73.81	5.05	3.03	3.45	45.45
12/19/2000	5:15 AM	7:35 AM	6.15	54.59	5.72	21.54	3.50	86.92	3.18	1.48	10.61	30.91
1/15/2001	1:00 AM	3:00 AM	6.49	25.68	4.12	10.88	2.78	35.45	2.99	1.07	5.54	37.31
1/17/2001	12:15 AM	2:00 AM	7.57	55.39	17.16	21.25	3.28	69.60	5.49	1.42	13.18	56.51
1/17/2001	2:00 AM	3:55 AM	8.98	76.01	23.85	28.92	2.60	95.32	4.60	1.84	10.44	87.57
1/17/2001	4:00 AM	6:00 AM	5.31	32.87	22.61	18.07	1.68	51.01	2.43	1.24	7.58	52.95
1/17/2001	6:00 AM	8:00 AM	8.07	48.70	32.04	24.96	2.76	67.48	3.33	1.60	7.93	--
1/21/2001	6:15 AM	7:15 AM	7.56	247.33	20.17	39.44	4.99	131.22	7.39	1.59	9.37	82.05
1/21/2001	7:15 AM	9:15 AM	8.66	263.16	32.20	66.83	6.36	158.40	5.94	2.51	19.78	135.47
1/25/2001	5:00 AM	6:00 AM	16.88	14.78	3.78	11.86	10.02	27.67	6.23	1.56	19.98	67.42
1/25/2001	6:00 AM	7:30 AM	13.00	14.93	5.42	9.55	6.57	28.51	2.09	1.08	4.85	43.00
1/31/2001	5:15 AM	7:00 AM	22.91	338.56	43.69	143.36	13.77	264.68	7.76	3.99	42.31	258.10
1/31/2001	7:00 AM	9:05 AM	5.17	139.53	30.04	52.97	4.33	119.44	3.21	0.87	5.82	110.56
2/1/2001	2:15 AM	3:55 AM	10.06	57.38	23.63	42.63	5.47	60.38	4.72	1.50	12.00	67.66

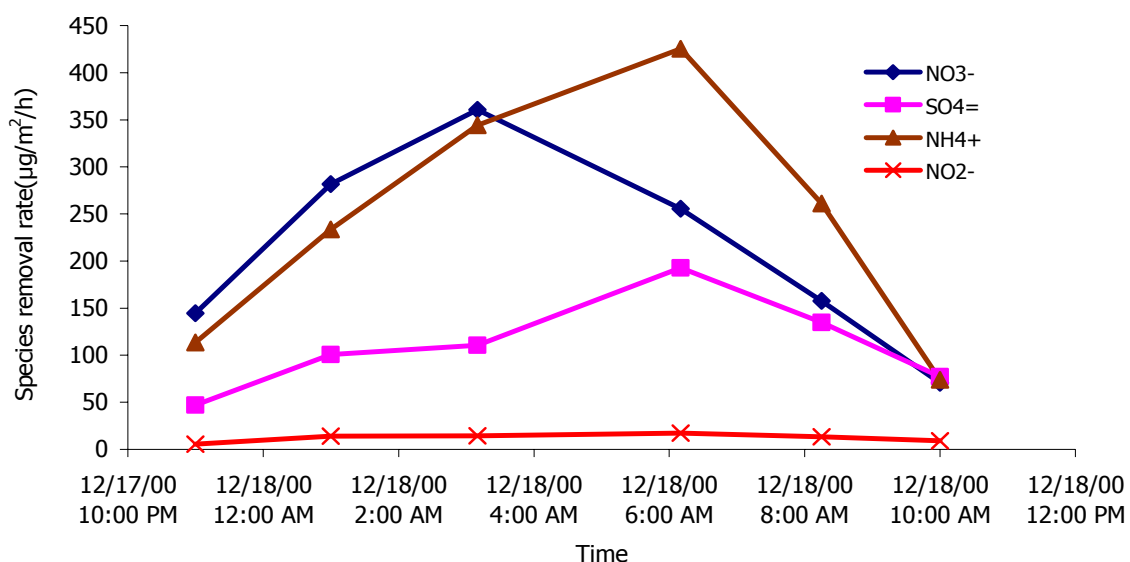


Figure 5-43. Timelines of deposition removal rates of four major ions in the 12/17/00 - 12/18/00 fog event.

Figure 5-43 clearly shows that during an extended fog episode, fog can remove significant quantities of atmospheric pollutant species by occult deposition. The overall removal rate also can vary with time and depends on the species' concentration in the fog, its enrichment in different size fog droplets, and its replenishment via emission or atmospheric production.

Table 5-13. Total mass removal of species by fog episodes during CRPAQS.

Sample Start Date	Sample Time (hour)	NO <sub>3</sub> <sup>-</sup> (µg/m <sup>2</sup> )	SO <sub>4</sub> <sup>2-</sup> (µg/m <sup>2</sup> )	NH <sub>4</sub> <sup>+</sup> (µg/m <sup>2</sup> )	TOC (µgC/m <sup>2</sup> )
12/18/2000	9.0	2246	1223	2627	952
12/19/2000	2.3	127	50	203	72
1/15/2001	2.0	51	22	71	75
1/17/2001	7.8	393	174	526	309
1/21/2001	3.0	774	173	448	312
1/25/2001	2.5	37	26	70	66
1/31/2001	3.8	592	251	463	452
2/1/2001	1.7	96	71	101	113

Table 5-13 shows computed species mass removals for each CRPAQS fog event. Longer fog events tend to produce greater mass removal amounts. Taking into account fog duration and measured fluxes, a typical fog episode in CRPAQS removed approximately

- Sulfate: 46  $\mu\text{g}/\text{m}^2/\text{hour}$
- Nitrate: 108  $\mu\text{g}/\text{m}^2/\text{hour}$
- Ammonium: 105  $\mu\text{g}/\text{m}^2/\text{hour}$
- TOC: 66  $\mu\text{gC}/\text{m}^2/\text{hour}$

Table 5-14. Estimated reduction in ground level ambient concentrations by fog episodes during CRPAQS assuming a 100 m fog depth.

Sample Start Date	Sample Time (hour)	$\text{NO}_3^-$ ( $\mu\text{g}/\text{m}^3/\text{h}$ )	$\text{SO}_4^{2-}$ ( $\mu\text{g}/\text{m}^3/\text{h}$ )	$\text{NH}_4^+$ ( $\mu\text{g}/\text{m}^3/\text{h}$ )	TOC ( $\mu\text{gC}/\text{m}^3/\text{h}$ )
12/18/2000	9.00	22.46	12.23	26.27	9.52
12/19/2000	2.30	1.27	0.50	2.03	0.72
1/15/2001	2.00	0.51	0.22	0.71	0.75
1/17/2001	7.75	3.93	1.74	5.26	3.09
1/21/2001	3.00	7.74	1.73	4.48	3.12
1/25/2001	2.50	0.37	0.26	0.70	0.66
1/31/2001	3.80	5.92	2.51	4.63	4.52
2/1/2001	1.70	0.96	0.71	1.01	1.13

In CRPAQS the typical fog layer was less than 50m high. If we consider a conservative case where the measured fluxes of material are removed from a column 100m deep, we can estimate the effects of CRPAQS fog episodes on boundary layer pollutant concentrations. The results are shown, by fog episode, in Table 5-14. For a typical CRPAQS fog episode, we estimate ambient concentration reductions of approximately:

- Sulfate: 0.46  $\mu\text{g}/\text{m}^3/\text{hour}$

- Nitrate:  $1.08 \mu\text{g}/\text{m}^3/\text{hour}$
- Ammonium:  $1.05 \mu\text{g}/\text{m}^3/\text{hour}$
- TOC:  $0.66 \mu\text{gC}/\text{m}^3/\text{hour}$

These numbers are quite significant and indicate the effective role these fogs can play as atmospheric cleansers. It is important to keep in mind, however, that some of the deposited material may be volatile (but water soluble) and subject to emission back into the atmosphere as the wetted ground dries off following fog evaporation. Removal of scavenged particulate species can also be offset by aqueous phase conversion of volatile precursors to non-volatile products (e.g.,  $\text{SO}_2$  reaction to sulfate or HMS). The competing effects of the fog on new particle mass production and particle scavenging and deposition are best dealt with using a more complex radiation fog model. An approach of this type is described in the following chapter.

## Chapter 6

### Modeling the Influence of Size-Dependent Droplet Composition on Pollutant Processing

by San Joaquin Valley Fogs

#### 6.1. Introduction

Often associated with severe pollution episodes, fogs typically form under conditions that promote pollutant build-up in the fog layer (stable conditions, low wind speeds). Fogs can be considered physicochemical processors of atmospheric species. Under the conditions favoring fog formation, water condenses on pre-existing aerosol particles to form droplets. This condensed water then offers the medium for aqueous phase reactions where atmospheric species, like  $\text{SO}_2$ , are rapidly oxidized. The simultaneous gas dissolution, aqueous phase reactions, and deposition of fog drops change both the amount and distribution of atmospheric species.

Experimental observations of clouds from many locations have indicated a variation of composition across the droplet spectrum (Collett et al., 1994; Gieray et al., 1997; Bator and Collett, 1997; Herckes et al., 2002). This has also been shown for San Joaquin Valley fogs (Collett et al., 1999). This heterogeneity stems, in part, from the size-dependent composition of the preexisting aerosol particles that serve as Cloud Condensation Nuclei (CCN) and the preferential dissolution of highly soluble gas-phase species into smaller droplets. Size-dependent deposition of droplets and size-dependent

reaction rates for S(IV) oxidation serve to further enhance this composition variation across the droplet spectrum.

Many species follow distinct trends in their droplet size-dependence. Some species are enriched in small droplets, others in large droplets (Noone et al., 1988; Hoag et al., 1999). Due to the fact that larger droplets deposit faster than smaller droplets, the species that are more concentrated in the larger droplets will be removed from the atmosphere faster. Observations of deposition velocities in the San Joaquin Valley (SJV) have indicated a difference in deposition between species (Waldman, 1986; Collett et al., 2001), as also illustrated in Chapter 5 of this report. During IMS95 deposition velocities for different species were observed. Nitrate deposited slowest, due to its existence in smaller fog droplets, and ammonium had the highest deposition velocity. Sulfate had a deposition velocity in between the two due to the fact that most of it was produced in 20  $\mu\text{m}$  droplets where there was a heavy weighting of liquid water (Hoag et al., 1999).

For these reasons, knowledge of the size-dependence in fog drop composition may be required to develop a full understanding of fog processing. However, because making size-resolved measurements is challenging, optimizing when and where to make size-resolved measurements would be beneficial. If numerical models can accurately predict the evolution of the size-dependent droplet composition, then the design (frequency, size-resolution, etc.) of measurements may be optimized.

Current three-dimensional chemical transport models typically include a bulk description of aqueous-phase atmospheric chemistry (Chang et al., 1987; Hass et al., 1993; Kumar and Lurmann, 1997; Matthijsen et al., 1997; Roselle and Binkowski, 1999). A chemically homogeneous cloud droplet population is assumed, and pH-dependent aqueous-phase chemical reaction rates are calculated using the pH of the bulk droplet mixture. As previously mentioned, however, clouds and fogs consist of a heterogeneous population of droplets (Collett et al., 1993; Noone et al., 1988; Pandis et al., 1990a). Composition varies across the droplet spectrum, with larger droplets typically being more alkaline than smaller droplets for a given cloud or fog (Collett et al., 1994). While there



are instances when aqueous-phase sulfate production can be modeled effectively using the bulk aqueous-phase chemistry description, there are many cases for which the averaging of the nonconservative  $\text{H}^+$  ion does not adequately describe the pH of a mixture of heterogeneous droplets (Liljestrand, 1985; Gurciullo and Pandis, 1997).

It was shown during the 1995 Integrated Monitoring Study (IMS95) that a model could match the drop size dependence when based on two drop size categories (Collett et al., 1998). There has been only one previous effort to evaluate a size-resolved fog processing model with size-resolved measurements, and this was limited by the availability of only 2 size-sections. In this chapter we predict the size dependent evolution of a number of species and compare the predictions of a size-resolved fog model with measurements of depositional fluxes, liquid water content, and aqueous-phase concentrations measured using Colorado State University's bulk and five-stage cloud collectors (Demos et al., 1996; Moore et al., 2002; Straub and Collett, 2002). Sulfate concentrations predicted by the highly size resolved fog model with the Variable Size Resolution Model (Fahey and Pandis, 2001) are also compared in an effort to further examine the effectiveness of employing the VSRM in three dimensional chemical transport models.

## 6.2. Model Description

The mathematical model employed here describes aqueous-phase chemistry, fog droplet microphysics, wet deposition, ionization, and mass transfer between the gas and aqueous phases in a closed system (Pandis et al., 1990a; Pandis and Seinfeld, 1989). The initial gas-phase concentrations, aerosol size/composition distribution, and temperature profile are inputs to the model. As the temperature drops, the relative humidity of the air parcel rises and water begins to condense on the pre-existing aerosol particles. When critical supersaturation is reached, the wet particles are activated to form droplets. During this phase, rapid aqueous phase reactions take place between the gas phase species transferred to the droplets and the species already dissolved in the water from the initial aerosol core. Aqueous-phase species are depleted from the fog layer via droplet

settling to the ground. When the temperature rises again, usually in the following morning, the droplets evaporate and a new aerosol size/composition distribution remains.

The aerosol distribution is divided into fourteen logarithmically spaced sections. The initial size range is between 0.1 and 8  $\mu\text{m}$ , and the average diameter of the droplet sections change as water condenses onto the particles. As diameters change, the boundaries of these fourteen sections move such that droplets do not cross between sections.

The change in concentration of species  $i$  in droplet section  $j$  ( $q_{ij}$ ) is given by Equation 6-1.

$$\frac{dq_{ij}}{dt} = \left[ \frac{\partial q_{ij}}{\partial t} \right]_{\text{cond / evap}} + R_{ij}^a(q_{1j}, q_{2j}, \dots, q_{nj}) - \frac{v_j}{H} q_{ij} \quad (6-1)$$

Here  $[dq_{ij}/dt]_{\text{cond/evap}}$  is the mass transfer rate of species  $i$  from the gas phase to droplet section  $j$ ,  $R_{ij}^a$  is the rate of change of species  $i$  in section  $j$  due to aqueous-phase chemical reactions,  $v_j$  is the deposition velocity of the droplets in section  $j$ , and  $H$  is the fog height.

The mass rate of change of water is given by the water growth equation derived by Pruppacher and Klett (1980). The other volatile species are represented by the expression used by Pandis and Seinfeld (1989). The chemical mechanism is similar to that of Pandis and Seinfeld (1989) and treats 50 aqueous-phase and 21 gas-phase species and includes 17 aqueous-phase ionic equilibria and 109 aqueous-phase chemical reactions. The change in section diameter,  $D_j$ , is given by:

$$\frac{dD_j}{dt} = \frac{2}{N_j \rho_j \pi D_j^2} \sum_{i=1}^{N_v} \left[ \frac{\partial q_{ij}}{\partial t} \right]_{\text{cond / evap}} \quad (6-2)$$

where  $\rho_j$  is the density of the droplets in section  $j$  and  $N_v$  is the number of species inside the fog droplets (water and solutes).

Under the typical conditions for a radiation fog (wind speeds less than  $2 \text{ m s}^{-1}$ ), droplet sedimentation is responsible for most of the droplet flux to the ground (Dollard and Unsworth, 1983; Lovett, 1984). Recent measurements by Thalmann et al. (2002) showed an average of 81% of droplet flux was associated with sedimentation for radiation fogs at an agricultural site in Switzerland. At these low wind speeds, the deposition velocity of the fog drops can be approximated by Stokes' Law. The turbulence induced by radiative cooling at the fog top and entrainment of air into the fog have been neglected here.

### 6.3. Available Measurements During the Fog Episode

The data used in this study were collected during the California Regional Particulate Air Quality Study (CRPAQS). CRPAQS was an extensive field study meant to improve the understanding of airborne particulates in central California (California Air Resources Board, 2002). Beyond providing an improved understanding of emissions,  $\text{PM}_{10}$  and  $\text{PM}_{2.5}$  composition, and the physicochemical processes affecting PM, the study was also meant to lead to the development of methods to identify the most efficient and cost-effective control strategies in order to meet national  $\text{PM}_{10}$  and  $\text{PM}_{2.5}$  standards traditionally exceeded in Central California (California Air Resources Board, 2002).

A fog episode monitored at Angiola, California, on December 18-19, 2000, was chosen for simulation. Bulk fog samples were collected using the Caltech Active Strand Cloudwater Collector Version 2 (Demoz et al., 1996), and size-resolved fog samples were collected with the Colorado State University (CSU) 5-Stage collector (Moore et al., 2002; Straub and Collett, 2002). The time and size-dependent aqueous-phase concentrations of many important species were measured (e.g.,  $\text{SO}_4^{2-}$ ,  $\text{NO}_3^-$ ,  $\text{NH}_4^+$ ,  $\text{Na}^+$ ,  $\text{Ca}^{2+}$ ,  $\text{Cl}^-$ , Iron, and Manganese). Deposition fluxes for water and major ions were also measured. Descriptions of these measurements are provided in Chapter 2.

Available measurements to determine appropriate inputs for the model included gas phase concentrations of  $\text{H}_2\text{O}_2$ ,  $\text{NH}_3$ ,  $\text{HNO}_3$ ,  $\text{O}_3$ ,  $\text{NO}_y$ ,  $\text{NO}_x$  and the pre-fog aerosol

size/composition distribution collected using a Micro-Orifice Uniform Deposit Impactor. Pre-fog measurements of the aerosol size/composition distribution were made two hours before the fog first appeared. Liquid water content was measured by a Gerber PVM 100 (Borrmann et al., 1994). Measurements of the meteorological conditions (wind speed/direction, temperature, and relative humidity) were also collected at Angiola. The SO<sub>2</sub> levels were estimated from those observed at the Kern Wildlife Refuge during IMS95 which is located only a few miles from the Angiola site. Input conditions are given in Table 6-1.

Table 6-1. Gas phase and aerosol inputs for the simulation of the fog event at Angiola, California on December 18-19, 2000.

Species	Value
Sulfate ( $\mu\text{g}/\text{m}^3$ )	1.9
Ammonium ( $\mu\text{g}/\text{m}^3$ )	3.5
Nitrate ( $\mu\text{g}/\text{m}^3$ )	6.9
Chloride ( $\mu\text{g}/\text{m}^3$ )	1.7
Calcium ( $\mu\text{g}/\text{m}^3$ )	0.6
Sodium ( $\mu\text{g}/\text{m}^3$ )	0.2
Iron ( $\mu\text{g}/\text{m}^3$ )	1.1
Manganese ( $\mu\text{g}/\text{m}^3$ )	0.08
SO <sub>2</sub> (ppb)	0.5
H <sub>2</sub> O <sub>2</sub> (ppb)	0.05
O <sub>3</sub> (ppb)	7.7
NH <sub>3</sub> (ppb)	23
HNO <sub>3</sub> (ppb)	9.6
NO <sub>x</sub> (ppb)	8.8

(Source, CRPAQS database <http://www.arb.ca.gov/airways/Datamaintenance/default.asp> except where otherwise specified in the text)

#### 6.4. Results

A 14-section fog model with explicit microphysics was applied to a winter fog event at Angiola, California. The liquid water content evolution and evolution of key atmospheric species was modeled. In the following sections, the predictions and observations for bulk and size-resolved aqueous-phase concentrations and depositional fluxes are discussed. The evolution of the size-distribution of certain key species is

shown, and finally a comparison is made between the highly size-resolved fog model and the Variable Size Resolution Model (VSRM).

#### 6.4.1 Liquid Water Content and Droplet Diameters

Figure 6-1 shows predicted and observed liquid water content for the fog event. The simulation begins at 6:00 p.m. on December 18, 2000. Around 7:00 p.m. there is a sharp increase in liquid water content. Observations show the fog dissipates for an hour around 11:00 p.m. and reappears by 1:00 a.m. on December 19. This change was likely due to a dry air mass passing over the sampling location and suggests that the fog was not completely homogeneous spatially. The current model cannot reproduce such spatial differences. However, the model predictions correspond to the supersaturated environment observed from 1:00 a.m. on.

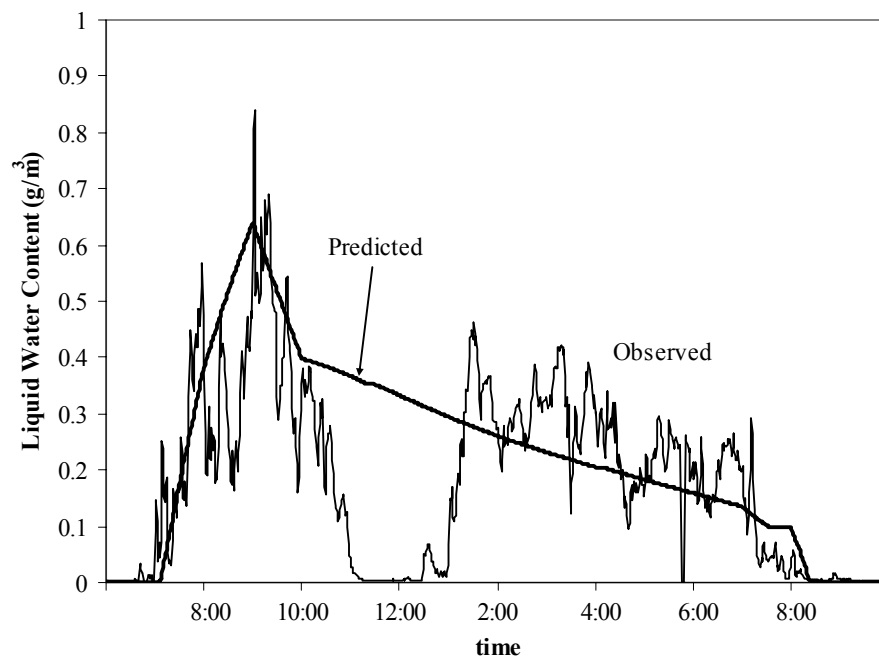


Figure 6-1. Predicted and observed liquid water content for the simulated fog event. The initial time corresponds to 6:00 p.m. on December 18, 2000.

Figure 6-2 shows the predicted evolution of droplet diameters. For the sampling period after hour 7 (1:00 a.m.), there is a gap between droplet diameters in the 7<sup>th</sup> and 8<sup>th</sup> droplet sections (5-15  $\mu\text{m}$  size range). The final 7 sections are thus considered fog droplets, and it is the composition of these sections that will be used in the comparisons

with aqueous-phase concentration measurements. These correspond to aerosol particles with average pre-fog diameters higher than 1  $\mu\text{m}$ .

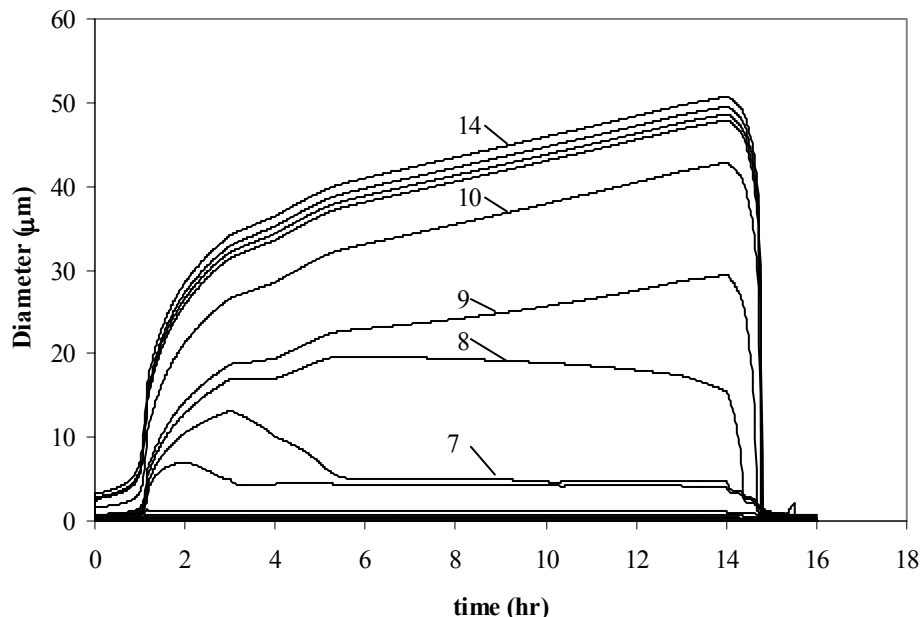
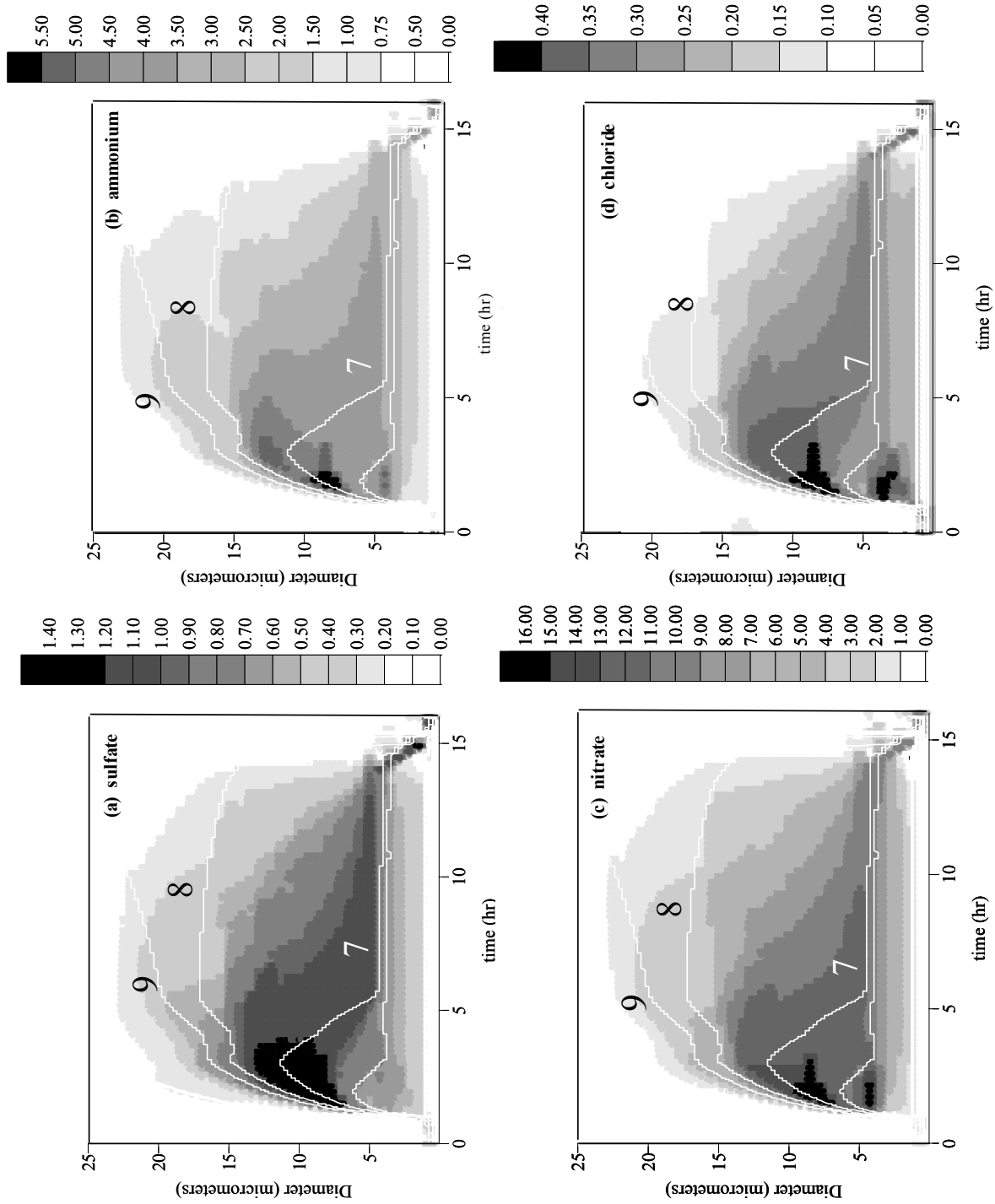


Figure 6-2. Evolution of diameters for the 14 modeled sections.

#### 6.4.2 Evolution of the aerosol size distribution

Figure 6-3 shows the evolution of the size distribution for the duration of the simulated fog. It is evident in these figures that the size distribution of these species changes drastically during the fog lifetime. During the initial stages, particles are activated, larger first, and grow via water condensation. The original distribution shifts towards larger diameters as the particles grow into drops. Following activation, early in the fog, soluble gas phase species dissolve into the newly formed fog droplets. It is during this early period of fog processing (hours 1 – 4) the peak values in sulfate, nitrate, ammonium, and chloride are seen. In addition to the dissolution of soluble gas phase species, sulfate's peak in 7-13  $\mu\text{m}$  droplets is the result of rapid aqueous phase reactions of  $\text{S(IV)}$ . The bimodal peak in nitrate corresponds to the mode in the pre-fog aerosol distribution of nitrate and the dissolution of gas-phase  $\text{HNO}_3$  in the smaller droplets. The ammonium peaks correspond to an effort to neutralize the nitrate and sulfate in the same

regions. The chloride distribution in the droplets is directly related to the shape of the pre-fog chloride distribution.



**Figure 3.** Predicted size distribution evolution for (a) sulfate, (b) ammonium, (c) nitrate, and (d) chloride. The concentration units are  $\mu\text{g}/\text{m}^3$ . The white lines indicate the changing diameters for sections 7-9.

Following the early peaks in mass concentration due to the initial dissolution of gas phase species and fast aqueous phase reactions, the peaks begin to shift towards the lower diameters. This is due to the fact that the larger droplets deposit faster than smaller droplets. Early in fog processing the size distribution is controlled by the dissolution of soluble gases and rapid aqueous-phase chemistry. As the fog continues, deposition takes the largest role in determining the size distribution. As the fog begins to evaporate, depositional fluxes quickly drop off, and the diameters quickly decrease to a size approaching that of their original. While the behavior of sulfate would likely look different in an area where there was a larger amount of  $\text{SO}_2$  before the fog developed, deposition effects can surpass those of aqueous-phase chemistry in the cases of very long-lived fogs in low  $\text{SO}_2$  environments (Collett et al., 1998).

#### *6.4.3 Predicted vs. Observed Mass Concentrations*

Figure 6-4 shows the predicted and observed (bulk measurements) temporal variation of eight key species in the fog. Measurements are available for six hours in the second half of the fog. The predicted and measured concentrations represent only that portion of the aerosol distribution that has been activated. In this case, the predicted concentrations are calculated from sections 8 – 14 (diameters above  $5\text{ }\mu\text{m}$ ). All species remain fairly constant for the first hour of simulation, because the fog has not formed yet. The evolution of each individual species after the first hour, however, depends on their solubility, reactivity, and concentrations across the droplet distribution.

In the case of sulfate, the high liquid water content that is seen before hour 2 (7:00 p.m.) and presence of reactive species ( $\text{H}_2\text{O}_2$ ,  $\text{O}_3$ ) dissolved in the fog water accounts for the rapid aqueous phase oxidation of  $\text{SO}_2$  during the initial hours of the fog. The pH remains above 6 for the duration of fog processing, and therefore the pH-dependent  $\text{O}_3$  production pathway remains important until the  $\text{SO}_2$  is fully depleted. Sulfate reaches its maximum concentration of nearly  $1.4\text{ }\mu\text{g}/\text{m}^3$  in the fog droplets by hour 2 (7:00 p.m.). After most of the  $\text{SO}_2$  is oxidized to sulfate, the deposition process begins to dominate and is responsible for the decline of sulfate in the droplets (Figure 6-4a). Both the rate of



sulfate depletion and absolute values of sulfate concentrations in the aqueous phase agree well with observations.

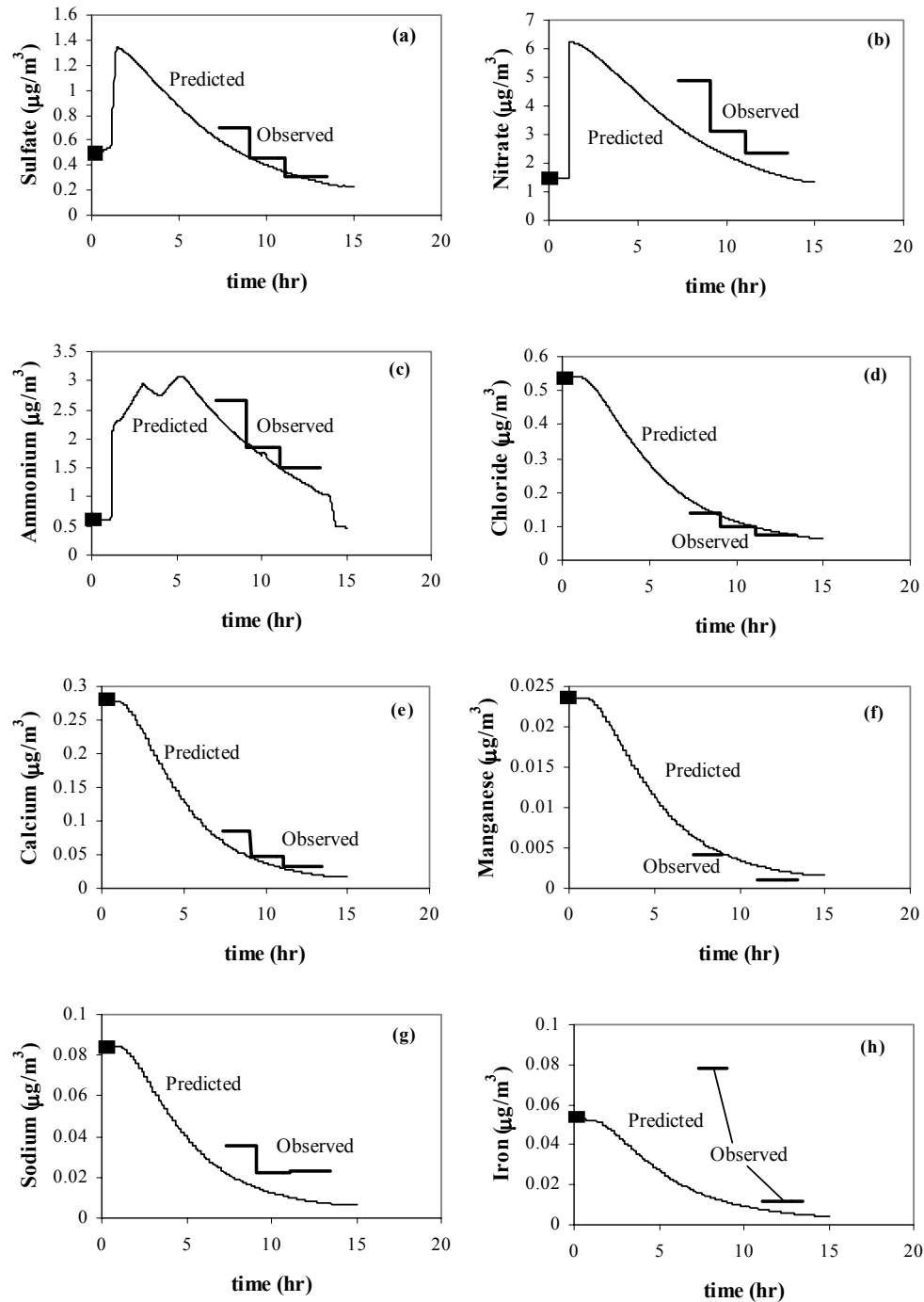


Figure 6-4. Predicted and observed (a) sulfate, (b) nitrate, (c) ammonium, (d) chloride, (e) calcium, (f) manganese, (g) sodium, and (h) iron concentrations in the fog droplets (sections 8-14). The aqueous-phase concentrations are expressed per  $\text{m}^3$  of air. The darkened square at time 0 corresponds to the observed initial concentration.

Nitric acid is highly soluble in water. Once a large amount of liquid water has amassed, the gas phase  $\text{HNO}_3$  is rapidly dissolved. Following the peak in nitrate before hour 2, the deposition process begins to dominate, and nitrate is slowly depleted from the fog layer (Figure 6-4b). The rate of decrease of nitrate fog concentrations agrees well with observations, but the nitrate concentration is underpredicted by the model. Collected drops with diameter less than  $5\text{ }\mu\text{m}$  may account for higher observed nitrate concentrations.

After the initial dissolution of gas phase species like  $\text{SO}_2$  and  $\text{HNO}_3$  and rapid aqueous-phase reactions, the deposition process begins to dominate. For fogs of longer duration, deposition dominates in determining how the total mass and distribution of mass of atmospheric species evolve. Ammonia, which is never fully exhausted in the gas phase, has a different temporal evolution from the other species (Figure 6-4c). Due to its high initial gas phase concentration,  $\text{NH}_3$  is gradually dissolved into the water and tracks the water evolution. This is in contrast to the fast initial dissolution of other gas phase species, like  $\text{SO}_2$  and  $\text{HNO}_3$ , which are dissolved completely, contribute early to the aerosol mass, and then have a quicker decline due to fog droplet deposition.

Chloride, calcium, manganese, sodium, and iron are completely in the aerosol phase at the beginning of the fog and thus monotonically decrease during the fog lifetime. For chloride, it was assumed that the initial gas-phase concentration was zero. Once the fog forms, these species begin to deposit out of the fog layer. The observed rates of removal and absolute aqueous concentrations for chloride, calcium, and manganese are matched by the model (Figures 6-4 d, e, f). For sodium and iron, however, the agreement is weak (Figures 6-4 g, h). The evolution of these species is determined in large part by their initial mass distribution. The difference that is seen between measured and predicted sodium concentrations may be due to inaccurate input conditions, as there were differences between the sodium observations made by the CRPAQS MOUDI and the CSU MOUDI also used. This may be in part due to the fact that the instruments were operated during slightly different sampling periods before the fog. Another item to note, especially in the case of species whose evolution depends heavily on their initial size distribution, is the fact that the pre-fog measurements of aerosol size/composition

distribution were made two hours before the fog first appeared. This may also explain the discrepancies. A change in the distribution of sodium or iron during those two hours between measurement and fog formation may have occurred. Furthermore, the failure of the model to predict the evolution of iron may also be explained by an injection of crustal material into the air during the fog event.

#### *6.4.4 Size-resolved aqueous-phase concentrations*

Figure 6-5 shows the predicted and the observed size-resolved concentrations for hours 11 through 13. The observed trends for all these species show a general decrease in aqueous concentration with increasing diameter. The model also predicts a decrease in aqueous concentration with increasing diameter in the cases of ammonia (6-5a), sulfate (6-5b), chloride (6-5c), and nitrate (6-5d). In the cases of calcium (6-5e) and sodium (6-5f), the model predictions are somewhat more variable. All the aqueous phase concentrations have the appropriate magnitude.

These measurements are taken during the last couple hours of the fog. The low mass concentrations and liquid water content for individual droplet sections used to calculate aqueous-phase concentrations will magnify small differences between predictions and observations. While ammonium, sulfate, and chloride show good agreement between the absolute values of predictions and observations, in the case of nitrate, there is a tendency to underpredict the concentrations in the larger droplet sections. Nitrate concentrations were measured to range from over 400  $\mu\text{M}$  in the small droplets to 120  $\mu\text{M}$  in the largest droplets. While the predictions for nitrate concentrations in the smallest drop section are similar to the observed, the predicted nitrate concentration drops off much more rapidly with increasing drop size than is observed.

Due to the low liquid water content and mass concentrations in these larger sections, a small absolute discrepancy in either of the two will result in a noticeable difference in the predicted aqueous-phase concentration. The average discrepancy between predicted and observed liquid water content during these final stages of fog processing approaches 50% and the average underprediction of bulk nitrate is around 25%. These two factors will serve to make the model underpredict nitrate

concentrations. If there were just an average of an extra  $0.04 \mu\text{g}/\text{m}^3$  in the droplets with diameters above  $30 \mu\text{m}$  during the sampling period, the average nitrate concentration for that collection of droplets would be around  $110 \mu\text{M}$ . This is an example of how small absolute differences in mass may noticeably impact aqueous phase concentrations in these larger fog drops.

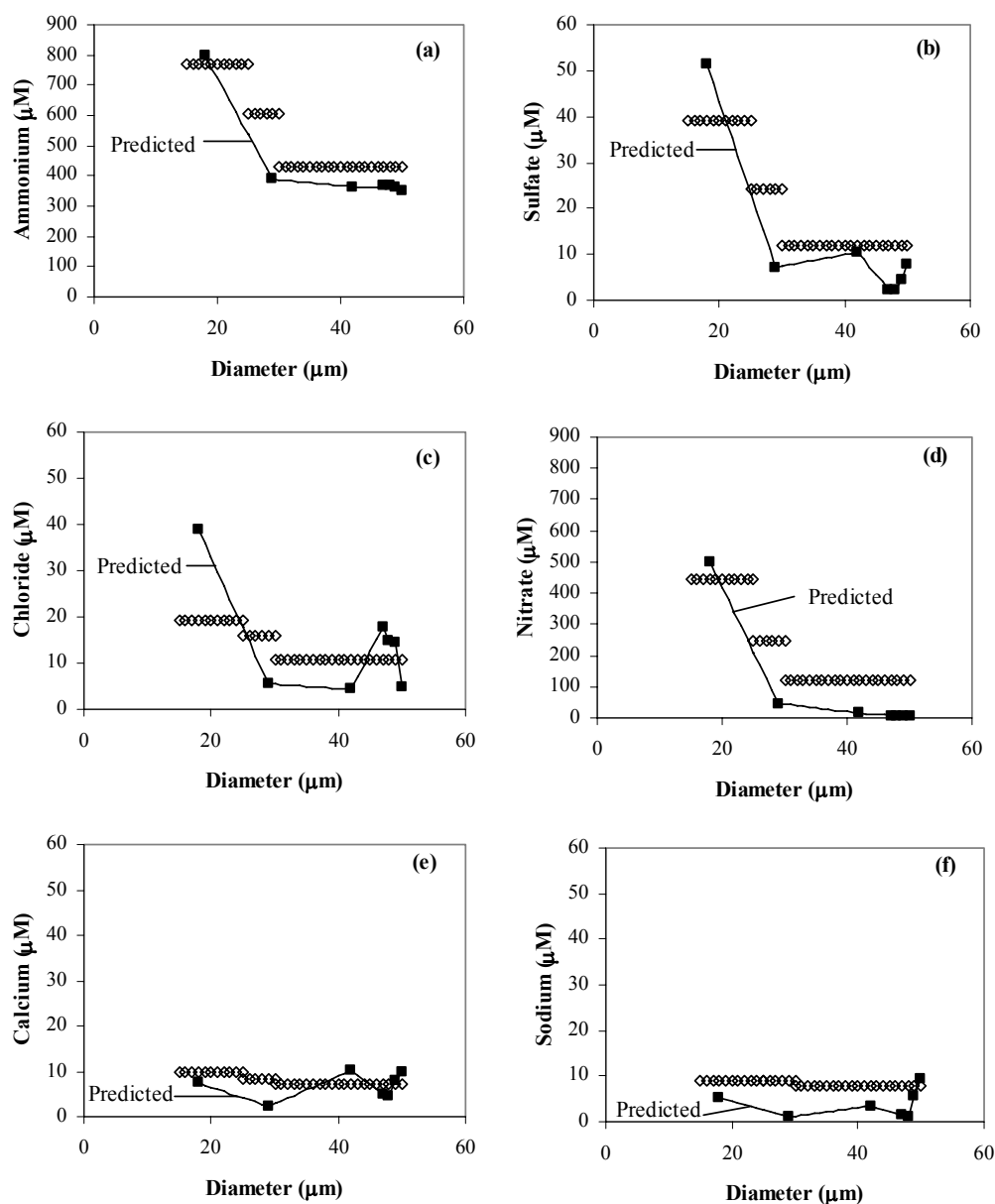


Figure 6-5. Comparison of predicted and observed size-resolved aqueous-phase concentrations of (a) ammonium, (b) sulfate, (c) chloride, (d) nitrate, (e) calcium, and (f) sodium.

In the cases of sodium and calcium, while the differences are relatively large, they are only on the order of a few  $\mu\text{M}$ . In both the predicted and observed values for sodium and calcium, there does not seem to be a very distinct size dependence.

#### *6.4.5 Deposition Fluxes*

Due to the fact that there is a dependence of concentration and deposition on droplet size, different species are deposited to the ground at different rates. The observed and predicted depositional fluxes for different species are given in Figure 6-6. The error bars are calculated from the average of the relative standard deviations for past measurements for each species when the two plates were employed simultaneously. While in the cases of ammonium and chloride (Figures 6-6 a and b), the agreement between observed and predicted depositional fluxes is satisfactory, in other cases the predictions deviate somewhat from the observations. In the case of sulfate (6-6c) and nitrate (6-6d), the model overpredicts the depositional flux. For calcium (6-6e) and sodium (6-6f), the model underpredicts the depositional flux. There are a number of possible explanations for this.

The deposition measurements are made during a period when the deposition flux is changing rapidly. As the fog dissipates and the droplet diameters decrease, the deposition flux of all species rapidly drops off as well. The overprediction in sulfate and nitrate flux to the ground may come from the error in our predicted liquid water content. Figure 6-1 shows that the predicted drop off in liquid water content is shifted slightly later and sharper than the observed. This might explain why the value measured for the sulfate and nitrate deposition flux is not predicted until an hour later. The sulfate and nitrate might be more sensitive to this discrepancy in predicted and observed fog evolution than other species due to their concentration in the smaller droplets. Since smaller droplets evaporate first, species enriched in the smaller droplets should see an earlier drop off in deposition flux than larger droplets during the dissipation stage of the fog.

The low deposition estimates for calcium and sodium could be due to particles above  $8\ \mu\text{m}$  (dry diameter) that were not included in the initialization of the model. Sodium is removed more slowly by the model than observed because there is not much

available inside the domain (Figure 6-4g). Calcium also is slightly underpredicted by the model for the period when deposition flux was measured. The underprediction for calcium and sodium may indicate an inaccurate weighting of our initial distribution of sodium and calcium towards smaller diameters.

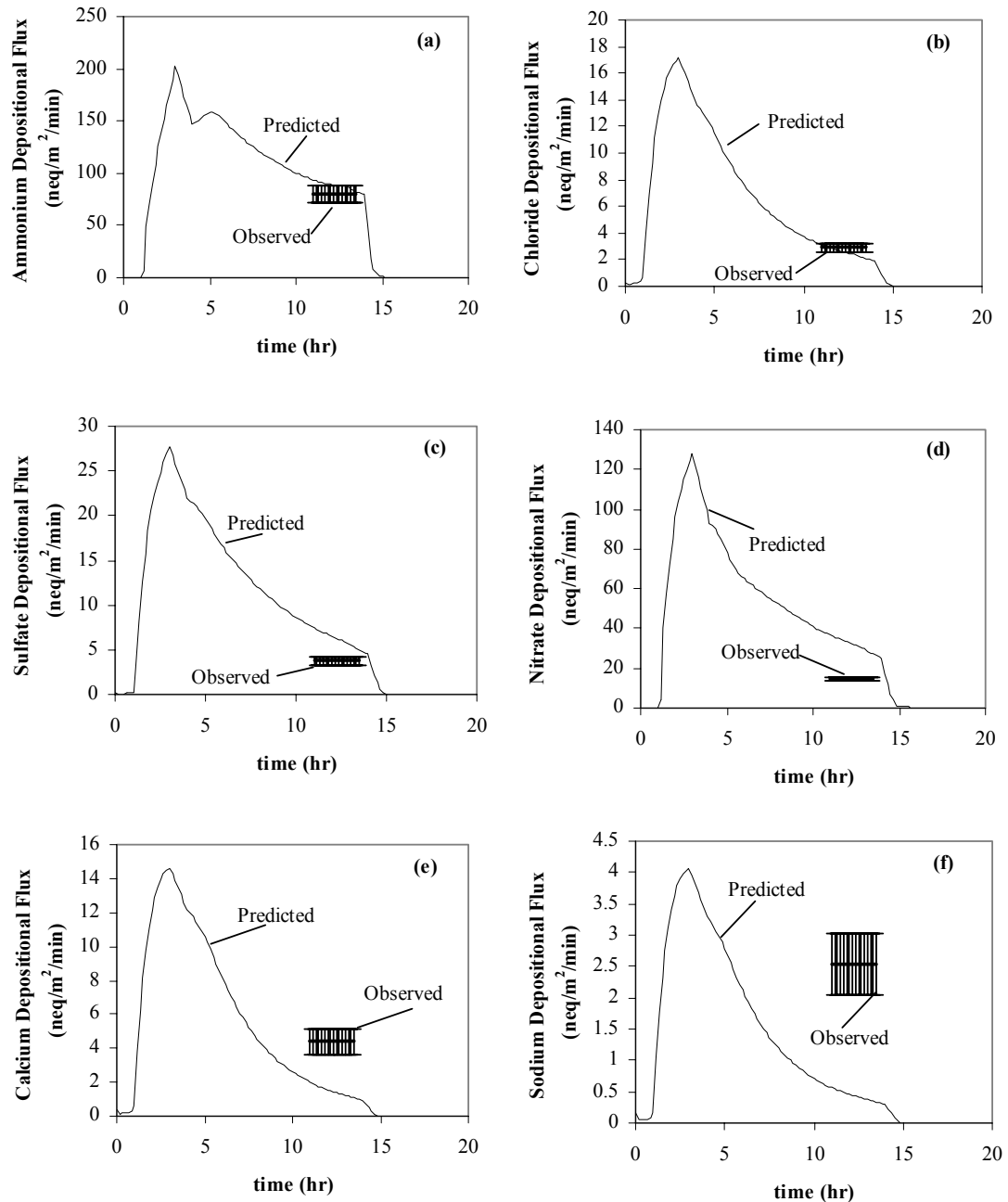


Figure 6-6. Predicted and observed depositional fluxes for (a) ammonium, (b) chloride, (c) sulfate, (d) nitrate, (e) calcium, and (f) sodium in neq/m<sup>2</sup>/min. One deposition sample was collected from 5:15 to 7:35 a.m. on December 19, 2000.

Average deposition fluxes for the major species ( $\text{SO}_4^{2-}$ ,  $\text{NH}_4^+$ ,  $\text{NO}_3^-$ ,  $\text{Cl}^-$ ,  $\text{Ca}^{2+}$ , and  $\text{Na}^+$ ) are given in Figure 6-7. Though larger droplets deposit faster, the sectional depositional flux show a maximum deposition in the middle droplets. This is a result of two competing effects: faster deposition of larger droplets and larger concentrations in smaller droplets. For species that are weighted in the larger size particles, the size range for maximum deposition shifts towards the larger diameter droplets.

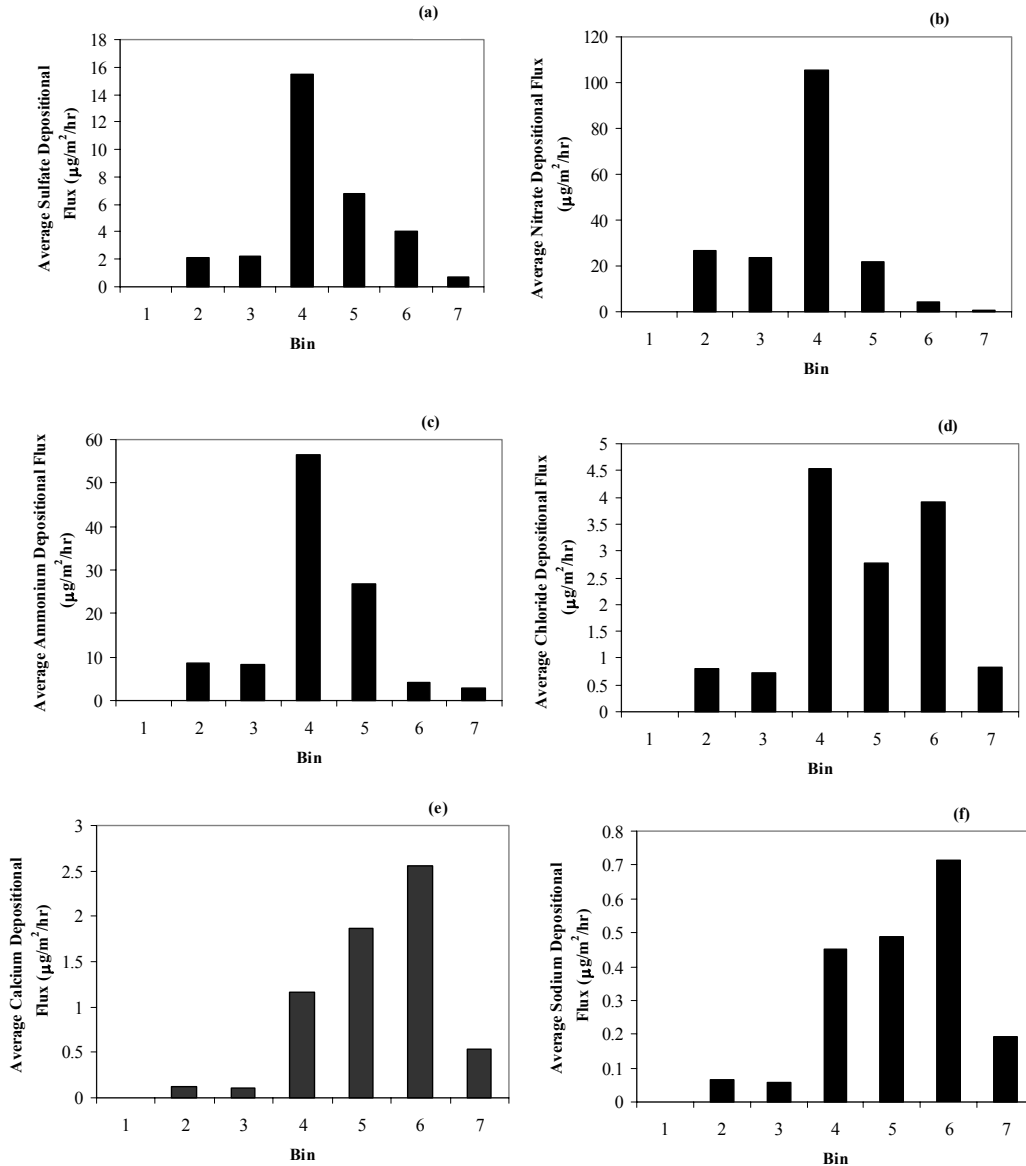


Figure 6-7. Average depositional flux for (a) sulfate, (b) nitrate, (c) ammonium, (d) chloride, (e) calcium, and (f) sodium for different diameter ranges. Bin 1 includes diameters 0 – 1 µm. Bin 2 includes diameters 1 – 5 µm. Bin 3 includes diameters 5 – 10 µm. Bin 4 includes diameters 10 – 20 µm. Bin 5 includes diameters 20 – 30 µm. Bin 6 includes diameters 30 – 40 µm. Bin 7 includes diameters 40 – 50 µm.

## 6.5 Comparison with the VSRM

The fog chemistry model employed here would be infeasible for use in a three-dimensional chemical transport model due to its large computational requirements. Typically cloud modules with parameterizations of cloud and fog microphysics and chemistry with much lower size-resolution are employed in three-dimensional models. With these parameterizations and simplifying assumptions, oftentimes the bulk cloud modules typically employed in three-dimensional chemical transport models can lead to underpredictions in sulfate production. It has been shown that droplet size-resolved aqueous-phase chemistry models predict higher sulfate production rates than comparable bulk models (Gurciullo and Pandis, 1997).

In a previous paper, bulk and size-resolved approaches were combined into a single aqueous-phase chemistry model called the Variable Size Resolution Model or VSRM (Fahey and Pandis, 2001). The motivation for this work was based on the premise that the less computationally intensive bulk model can sometimes match the sulfate predictions of a comparable size-resolved model. The VSRM executes the bulk or size-resolved calculations based on critical inputs and serves to combine the accuracy of a size-resolved model with the efficiency of the bulk.

The VSRM has the same aqueous-phase chemistry mechanism employed in the dynamic fog model described earlier. However, only one or two chemistry size sections are used and the fog microphysics is parameterized. Droplets are formed instantaneously on particles exceeding a given critical diameter, while the remainder serves as interstitial aerosol. In past studies, for a wide range of atmospheric conditions, it has been shown that the VSRM predicts secondary sulfate concentrations within 3% of a six-section size-resolved aqueous-phase chemistry model (Fahey and Pandis, 2001).

In this section, the sulfate concentrations predicted by the VSRM and the dynamic fog module described above are compared.

### 6.5.1 Base Case - Same Deposition

Figure 6-8 shows the total sulfate evolution for the duration of fog processing for the dynamic fog module and the VSRM. The time and size dependent deposition rates



are provided as inputs to the VSRM so that the focus here will be mainly on the effect of size-resolved chemistry between the two modules. The predictions agree within 6% of one another for the duration of fog processing.

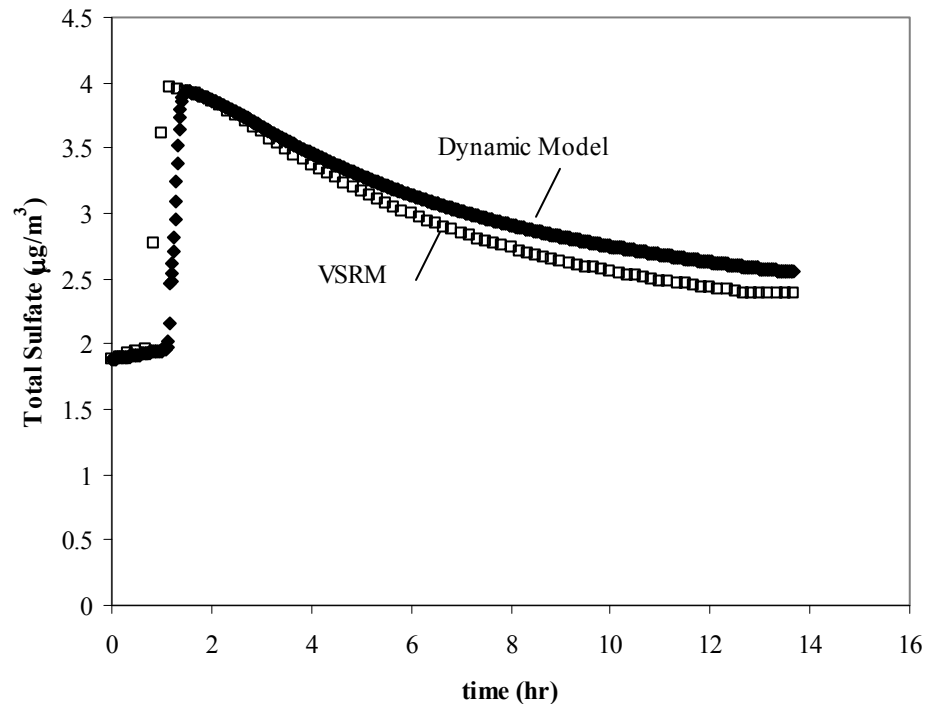


Figure 6-8. Total sulfate predictions for the 14-section dynamic fog model and the VSRM. The deposition coefficients, liquid water content, and temperature calculated in the dynamic fog model were inputs to the VSRM. The difference in sulfate predictions was never more than 6% between the two models.

Figure 9 shows the final size distribution predicted by the VSRM and dynamic fog model. For the significant increase in computational efficiency introduced by the VSRM (the dynamic fog module requires hours and the VSRM takes seconds to run), the agreement between predictions of the final sulfate distribution for the two models is strong.

#### 6.5.2 Parameterized Deposition

As there is no explicit treatment of fog microphysics in the VSRM, the settling of fog droplets is typically parameterized as a function of the fog liquid water content ( $w$ ,  $\text{g m}^{-3}$ ). Pandis et al. (1990b) suggested that two different expressions be used to describe

the gravitational flux of liquid water,  $G$  ( $\text{g m}^{-2} \text{s}^{-1}$ ) for a typical fog depending on whether the fog is in the growth or dissipation stage. This is due to the fact that during droplet growth small droplets have access to more liquid water as a result of their being better able to follow the changes of relative humidity. This results in slower deposition rates than are seen during the fog dissipation stage when small droplets are first to evaporate and most of the liquid water remains in the larger droplets (Pandis et al., 1990b). Here we use the average of the two to describe fog droplet settling.

$$G = 0.014w^{1.67} + 0.009w^{1.08} \quad (6-3)$$

The removal rate coefficient of the fog droplets,  $k_{\text{dep}}$ , is given by the following expression:

$$k_{\text{dep}} = G / (w H) \quad (6-4)$$

where  $H$  equals the fog height.

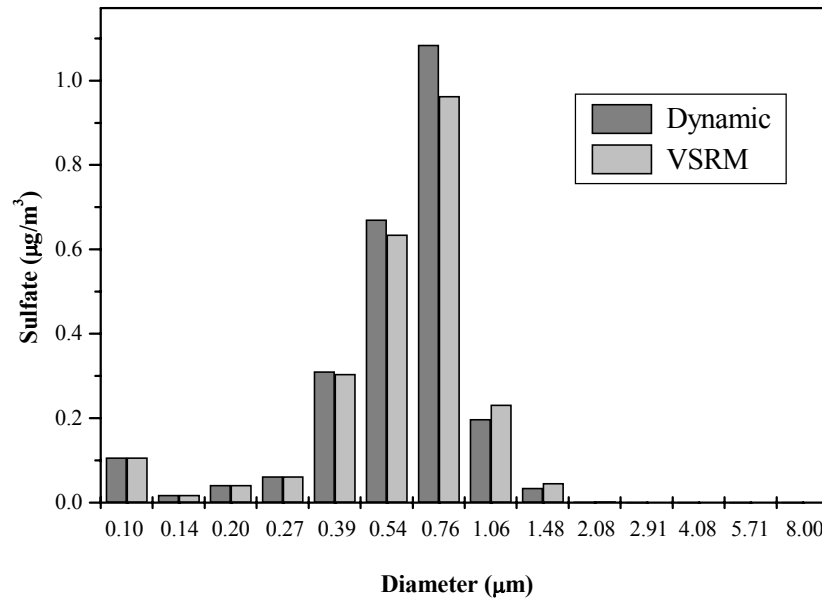


Figure 6-9. The final size distributions of sulfate predicted by the VSRM and dynamic fog model. With a good estimate of deposition rates, the VSRM approaches the predicted size distribution of a much more highly size-resolved model at a much lower computational cost.

Figure 6-10a shows the sulfate predictions of the VSRM with the above relation to describe deposition. The results differ significantly from those given in Figure 6-8 where the removal rate coefficients for each size section are given by those calculated explicitly by the dynamic fog model. The sulfate predictions deviate substantially from the sulfate predicted by the dynamic fog model. When the depositional flux is decreased by 60%, the VSRM predicts sulfate very similar to that of the dynamic fog model (Figure 6-10b). A better understanding of the fogwater deposition rates and their dependence on the pre-existing aerosol size-distribution would be valuable.

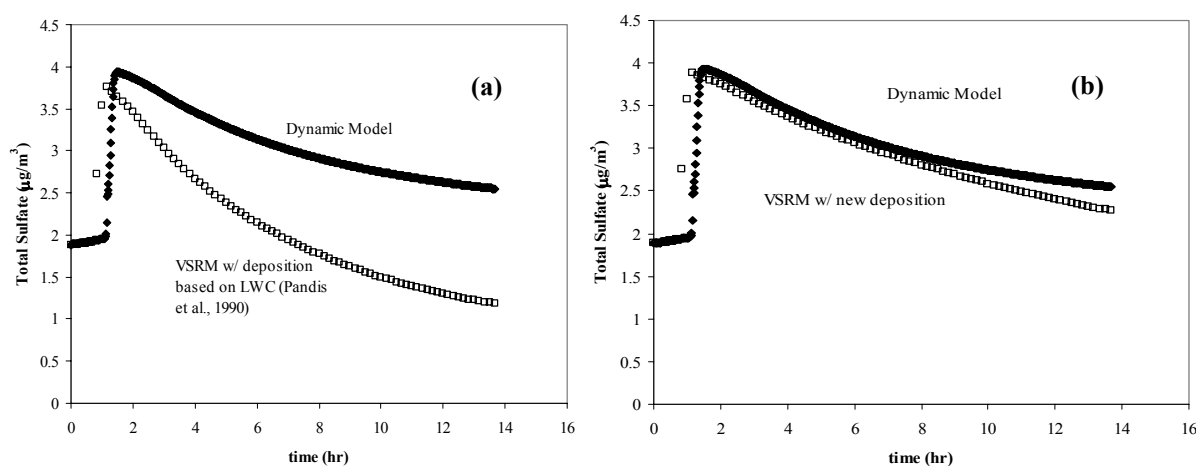


Figure 6-10. Predicted sulfate concentrations for the VSRM and the dynamic fog model (a) using the equation for depositional flux as a function of liquid water content derived by Pandis et al., 1990b and (b) reducing by 60% the depositional flux used in Figure 10a.

## 6.6. Conclusions

The effects of size-dependent fog chemistry and physics on the pre-fog aerosol size/composition distribution were examined for a fog event in the San Joaquin Valley. Measurements were made of initial aerosol and gas phase concentrations, meteorological conditions, and bulk and size-resolved aqueous phase concentrations. A 14-section size-resolved fog model with explicit fog microphysics was able to predict the liquid water evolution, bulk aqueous-phase concentration measurements, size-resolved trends, and deposition fluxes for a number of species in close agreement with observed values.

The predicted evolution of the distribution of aerosol species like sulfate, nitrate, ammonium, and chloride indicated significant differences over the course of fog processing. For this event, different size-dependent processes controlled the size-distribution development at different stages of fog processing. Early in processing, the dissolution of soluble gases and rapid aqueous phase reactions control the development of the size distribution. At later times, the effects of deposition begin to dominate, and push the peak of the distribution towards smaller diameters.

The model predictions of the evolution of most key species approached bulk aqueous-phase concentration measurements. During the early stages of the fog, the behavior of species originating partially in the gas phase ( $\text{NO}_3^-$ ,  $\text{SO}_4^{2-}$ ) was heavily influenced by dissolution into the droplets and rapid aqueous phase reactions. Following these initial peaks in aqueous phase concentrations, deposition began to dominate, and the species were gradually depleted from the fog layer. In an area where there is low initial  $\text{SO}_2$ , the model indicates that size-dependent deposition plays the largest role in the evolution of the sulfate distribution.

Observed and predicted values for the size-dependence of key species indicate a tendency of most species to be more concentrated in smaller droplets than larger droplets during the final hours of the fog. In the cases of calcium and sodium, while there exists a similar size-dependence, it is less distinct. Since the measurements were taken during the last couple hours of the fog, the low mass concentrations and liquid water content for individual droplet sections used to calculate aqueous-phase concentrations will magnify small differences between predictions and observations.

In an effort to further show the accuracy of our Variable Size Resolution Model (VSRM), sulfate concentrations predicted by the highly size resolved fog model were compared with the VSRM (Fahey and Pandis, 2001). While the VSRM approached the sulfate predictions of the dynamic fog model when the size dependent deposition is given as an input, the model failed to predict a similar evolution when using a simplified deposition calculation published for another fog. This indicates that it might be worthwhile to ascertain the appropriate deposition dependence before running the VSRM for lengthy fog applications. It was shown that for lengthy fog events in clean environments the deposition of fog droplets may account for the largest influence on the

evolution of the size composition distribution of aerosols over the course of fog processing. It was predicted that though larger droplets deposit faster, the maximum depositional flux occurs in the mid-sized droplets. This is a result of two competing effects: the faster deposition of larger droplets and the larger concentrations in smaller droplets. These results indicate a need for a larger number of measurements of deposition fluxes for individual species. The rapid change in the size/composition distribution predicted here also indicates the need for aqueous-phase concentration measurements to be made from the early fog formation stage.

## **Chapter 7**

### **Summary and Conclusions**

Colorado State University conducted measurements of fog properties, both physical and chemical, at several Valley sites as part of the CRPAQS winter intensive. Measurements began in mid-December and extended through early February. The most extensive measurements were made at the Angiola core site, where we made both ground and tower-based measurements of fog composition. Additional measurements at this site were made of the fog drop size distribution, fog liquid water content (LWC), fog deposition, and drop size-resolved fog composition. Core site measurements were complemented by additional fog occurrence and fog composition measurements at three satellite sites: Helm, Bakersfield, and McKittrick.

Several fog episodes were successfully sampled in December, January, and early February. In sum, more than 200 fog samples were collected from a variety of fog collector types. Measurements of the composition of collected fog samples included characterization of a wide range of inorganic and organic solutes. Deposition measurements included determination of fog borne fluxes of several major ion species as well as total organic carbon (TOC).

CRPAQS fog observations were explored in the data analysis phase of the project in order to improve our understanding of the interactions between CRPAQS fogs and airborne fine particles and soluble trace gases. Particular emphasis was placed on examining how these fogs process organic pollutants and how variations in fog composition across the fog drop size spectrum influence both particle deposition and production of new particle mass. Results from this and other recent SJV fog campaigns

were also compared to observations made in the early 1980s, to ascertain whether significant changes in fog composition have occurred over this twenty year period.

In order to test the ability of current fog models to accurately simulate the chemical and physical properties of fogs, as well as the influence of radiation fogs on particle scavenging and removal, observations from the CRPAQS fog study were compared to a numerical simulation of a CRPAQS fog episode using the Carnegie Mellon University fog model. Particular attention was paid to the ability of the model to accurately capture key features of the fogs, including fog LWC, bulk and drop size-resolved fog composition, and deposition fluxes of fog borne solutes. The ability of a more heavily parameterized, and computationally practical, version of the model to accurately capture key features was also examined.

The fog measurement campaign and subsequent data analysis phase produced a number of significant findings. These include the following major observations and conclusions:

- Several fog episodes were characterized during CRPAQS. Most of the fog episodes were relatively shallow and featured very large droplets. Rarely did the top of the fog layer reach even 100 m, in contrast to much deeper fogs observed during IMS95 and other studies in the San Joaquin Valley (SJV). The very large drops formed during CRPAQS probably result from strong radiative cooling directly from the drops themselves, through the shallow fog layer, driving rapid condensational growth. These large drops settle from the fog relatively quickly, enhancing the ability of the fogs to rapidly remove scavenged airborne particulate matter.
- The chemical composition of the fogs during CRPAQS was dominated by nitrogen species, with important contributions also from organic compounds and sulfate. Ammonium and nitrate were the most abundant individual compounds; nitrite and sulfate were also found to be present at significant concentrations as were several organic compounds, including formate, acetate, and formaldehyde.

Abundant gas phase ammonia absorbed by fog drops helps keep the fog pH relatively high, with pH values typically well above 6. Material present in fog drops is derived from a combination of aerosol particle scavenging, gas absorption, and aqueous phase reactions.

- Comparison of Bakersfield fog composition measurements in CRPAQS and other recent SJV fog studies with measurements made in the 1980s reveals a statistically significant decrease in fog concentrations of sulfate and an increase in fog pH. These changes are consistent with intervening declines in SO<sub>2</sub> emissions in the southern SJV, which would translate into less production of sulfate and greater availability of ammonia to raise fog pH.
- Comparison of fog composition during CRPAQS at Bakersfield, Angiola, and Helm reveals that Angiola and Helm, both rural sites, have generally similar compositions. Urban Bakersfield fog contained greater concentrations of sulfate and nitrite.
- The high pH droplets present in CRPAQS fogs make them effective atmospheric reactors for dissolved sulfur dioxide. Both oxidation to sulfate and reaction with dissolved formaldehyde to produce hydroxymethanesulfonic acid (HMS) are important reaction pathways. Numerical simulations using a single drop fog chemistry model reveal the importance of considering effects of mass transport limitations on aqueous sulfur chemistry in the large fog drops observed in CRPAQS fogs. Measurement of HMS in individual aerosol particles in the SJV, as suggested by the group of Kim Prather, should provide an effective way for monitoring the fraction of ambient particles that have undergone fog processing.
- Previous studies have documented the important role SJV fogs play in cleansing the atmosphere via particle scavenging followed by drop deposition. The importance of this mechanism was again observed during CRPAQS, with fog deposition fluxes capable of reducing boundary layer fine particle concentrations of major species (e.g., nitrate and ammonium) at a rate on the order of 1 µg/m<sup>3</sup> hr. The fogs are also effective at scavenging and removing sulfate, but this



removal is often offset by similar rates of sulfate production via aqueous phase oxidation of sulfur dioxide.

- Preferential enrichment of major ion species in small fog drops reduces most species' deposition velocities below the deposition velocity for fog water. Nitrite, which was often enriched in large fog drops, exhibited deposition velocities higher than fog water. Accounting for drop size-dependent species concentrations is essential to accurately modeling rates of pollutant deposition in SJV fogs.
- Results obtained during CRPAQS also indicate the important role that SJV fogs play in scavenging and deposition of organic carbon. SJV fogs contain a rich mix of organic compounds, with major constituents including formaldehyde, formate, and acetate. Many larger organic molecules are also observed, including both polar and non-polar compounds. Approximately 25% of the fog organic carbon, on average, is present as undissolved, suspended material in the droplets. As much as half of the fog organic matter may be comprised of high molecular weight compounds, with molecular masses exceeding several hundred Daltons. Future studies are needed to better characterize this high molecular weight material and determine whether it comes mainly from aerosol scavenging or is produced by aqueous phase reactions of lower molecular weight precursors.
- The wide variety of organic compounds observed in the fogs indicates that carbonaceous aerosol particles from many source types undergo active fog processing. Observations of fog scavenging of organic and elemental carbon also indicate the importance of fog processing of carbonaceous aerosol species. Organic carbon was observed to be more actively processed by CRPAQS fogs than elemental carbon. Differences were observed between the efficiency of CRPAQS fogs in scavenging different types of fine particle organic carbon. Wood smoke particles were scavenged more efficiently and particles containing polycyclic aromatic hydrocarbons (PAH) less efficiently than fine particle OC as a whole. CRPAQS fogs were also observed to efficiently scavenge and remove the pesticide Diazinon. Together, these observations suggest that fogs may be

more effective cleansing the boundary layer of OC from some source types than others, a topic deserving further attention in future studies.

- Deposition fluxes of organic carbon in fog water were significant, yielding atmospheric removal rates on the order of  $66 \mu\text{gC}/\text{m}^2 \text{ hr}$ . Because some of the fog burden of organic carbon is comprised of soluble, volatile organic compounds (VOC), a portion of the deposited carbon may be released back to the atmosphere when deposited fog water evaporates following a fog episode.
- Comparisons of fine particle organic carbon concentrations before and after fog episodes also suggests that aqueous phase reactions of dissolved VOCs may be important in producing new, secondary organic aerosol matter. Much more work is needed to examine this hypothesis in future investigations.
- Measurements of the stability of carbonyl compounds in actual fog water reveal the importance of stabilizing these species as soon as possible following sample collection. Analysis of field-stabilized samples collected in Fresno fog episodes after CRPAQS reveal significant contributions of several carbonyl and dicarbonyl compounds to SJV fog organic carbon burdens. Glyoxal and methylglyoxal, in particular, were observed at substantial concentrations nearly equivalent to formaldehyde.
- The CMU fog model, a 14-section size-resolved fog model with explicit fog microphysics, was used to simulate a CRPAQS fog episode and was able to predict the liquid water evolution, bulk aqueous-phase concentration measurements, size-resolved trends, and deposition fluxes for a number of species in close agreement with observed values. The predicted evolution of the distribution of aerosol species like sulfate, nitrate, ammonium, and chloride indicated significant differences over the course of fog processing. For this event, different size-dependent processes controlled the size-distribution development at different stages of fog processing. Early in processing, the dissolution of soluble gases and rapid aqueous phase reactions control the development of the size distribution. At later times, the effects of deposition begin to dominate, and push the peak of the distribution towards smaller

diameters. Model predictions of the evolution of most key species approached bulk aqueous-phase concentration measurements. During the early stages of the fog, the behavior of species originating partially in the gas phase ( $\text{NO}_3^-$ ,  $\text{SO}_4^{2-}$ ) was heavily influenced by dissolution into the droplets and rapid aqueous phase reactions. Following these initial peaks in aqueous phase concentrations, deposition began to dominate, and the species were gradually depleted from the fog layer.

- In an effort to test the accuracy of a computationally less expensive Variable Size Resolution Model (VSRM), sulfate concentrations predicted by the highly size resolved fog model were compared with the VSRM (Fahey and Pandis, 2001). While the VSRM approached the sulfate predictions of the dynamic fog model when the size dependent deposition is given as an input, the model failed to predict a similar evolution when using a simplified deposition calculation published for another fog. This indicates that it might be worthwhile to ascertain the appropriate deposition dependence before running the VSRM for lengthy fog applications.

While the CRPAQS fog study and subsequent data analysis have greatly aided our understanding of the importance of fog processing of both inorganic and organic aerosol species, a significant need remains to continue studies of this type. In particular, our understanding of the production and removal of fine particle organic carbon remains in its infancy. Much more work is needed to elucidate the relative efficiencies with which fogs scavenge and deposit carbonaceous particles from different source types and to determine the extent of secondary organic aerosol formation occurring via aqueous phase reaction pathways that convert soluble VOCs to nonvolatile products that are released back to the aerosol when a fog evaporates.

## Bibliography

- Anastasio, C. and McGregor, K.G., 2000. Photodestruction of dissolved organic nitrogen species in fog waters. *Aerosol Science and Technology*, 32(2): 106 - 119.
- Anastasio, C. and McGregor, K.G., 2001. Chemistry of fog water in California's central valley: 1. in situ photoformation of hydroxyl radical and singlet molecular oxygen. *Atmospheric Environment*, 35: 1079 - 1089.
- Aumont, B., Madronich, S., Bey, I. and Tyndall, G.S., 2000. Contribution of secondary VOC to the composition of aqueous atmospheric particles: A modeling approach. *Journal of Atmospheric Chemistry*, 35(1): 59-75.
- Bator A. and Collett J. L. (1997) Cloud chemistry varies with drop size. *Journal of Geophysical Research-Atmospheres*. 102, 28071-28078.
- Bauer, S.E. and Langmann, B., 2002. An atmosphere-chemistry model on the meso-gamma scale: model description and evaluation. *Atmospheric Environment*, 36(13): 2187-2199.
- Blando, J. D., R. J. Procja, T.-H. Li, D. Bowman, P. J. Liroy, B. J. Turpin, 1998. Secondary formation and the Smoky Mountain organic aerosol: An examination of aerosol polarity and functional group composition during SEAVS. *Environ. Sci. Technol.*, 32: 604-613.
- Blando, J.D. and Turpin, B.J., 2000. Secondary organic aerosol formation in cloud and fog droplets: a literature evaluation of plausibility. *Atmospheric Environment*, 34: 1623 - 1632.
- Bizjak, M. and Divjak, B., 1999. The Great Dun Fell experiment 1995: an overview. *Atmospheric Research*, 50: 151 - 184.
- Borrmann S., Jaenicke R., Maser R., and Arends B. (1994) Instrument intercomparison study on cloud droplet size distribution measurements: Holography vs. laser optical particle counter. *Journal of Atmospheric Chemistry*. 19, 253-258.
- Boyce, S.D. and Hoffmann, M.R., 1984. Kinetics and mechanism of the formation of hydroxymethanesulfonic acid at low pH. *Journal of Physical Chemistry*, 88: 4740-4746.
- Burkhard, R., Eugster, W. and Thalmann, E., 2000. A direct method for fog and cloud droplet deposition flux measurements. *EOS* 81(48): F64 - F65.
- California Air Resources Board (2002). Study Overview. [www.arb.ca.gov/airways/crpaqs/overview.htm](http://www.arb.ca.gov/airways/crpaqs/overview.htm)
- Calvert, J. G., Lazrus, A. L., Kok, G., Heikes, B., Walega, J., Lind, J. and Cantrell, C. A., 1985. Chemical mechanisms of acid generation in the troposphere. *Nature*, 317(6032): 27-35.
- Capel, P.D., Gunde, R., Zürcher, F. and Giger, W., 1990. Carbon speciation and surface tension of fog. *Environmental Science and Technology*, 24(5): 722 - 727.
- Carpenter, A. and Provorse, C., 1998. The World almanac of the U.S.A. Copyright 1998.

- Carrillo, J.H., Emert, S.E., Sherman, D.E. and Collett, J.L.J., 2004. An Economical Optical Fog Detector. in preparation.
- Cereceda, P. and Schemenauer, R.S., 1991. The occurrence of fog in Chile. *J. Appl. Meteor.*, 30: 1095-1105.
- Chameides, W.L. and Davis, D.D., 1983. Aqueous-phase source of formic acid in clouds. *Nature*, 304: 427 - 429.
- Chang J. S., Brost R. A., Isaksen I. S. A., Madronich S., Middleton P., Stockwell W. R., and Walcek C. J. (1987). A three-dimensional eulerian acid deposition model: physical concepts and formulation. *Journal of Geophysical Research* 92, 14681-14700.
- Choularton, T. W., Colville, R. N., Bower, K. N., Gallagher, M. W., Wells, M., Beswick, K. M., Arends, B. G., Mols, J. J., Kos, G. P. A., Fuzzi, S., Lind, J. A., Orsi, G., Facchini, M. C., Laj, P., Gieray, R., Wieser, P., Engelhardt, T., Berner, A., Kruisz, C., Moller, D., Acker, K., Wieprecht, W., Luttke, J., Levsen, K., Bizjak, M., Hansson, H. C., Cederfelt, S. I., Frank, G., Menten, B., Martinsson, B., Orsini, D., Svenningsson, B., Swietlicki, E., Wiedensohler, A., Noone, K. J., Pahl, S., Winkler, P., Seyffer, E., Helas, G., Jaeschke, W., Georgii, H. W., Wobrock, W., Preiss, M., Maser, R., Schell, D., Dollard, G., Jones, B., Davies, T., Sedlak, D. L., David, M. M., Wendisch, M., Cape, J. N., Hargreaves, K. J., Sutton, M. A., StoretonWest, R. L., Fowler, D., Hallberg, A., Harrison, R. M. and Peak, J. D., 1997. The Great Dun Fell cloud experiment 1993: An overview. *Atmospheric Environment*, 31(16): 2393-2405.
- Collett, J.L., Daube, B.C., Gunz, D. and Hoffmann, M.R., 1990. Intensive studies of Sierra-Nevada cloudwater chemistry and its relationship to precursor aerosol and gas concentrations. *Atmospheric Environment*, 24(7): 1741-1757.
- Collett, J., Oberholzer, B. and Staehelin, J., 1993. Cloud chemistry at Mt Rigi, Switzerland - dependence on drop size and relationship to precipitation chemistry. *Atmospheric Environment*, 27(1): 33-42.
- Collett, J.L., Bator, A., Rao, X. and Demoz, B.B., 1994a. Acidity variations across the cloud drop size spectrum and their influence on rates of atmospheric sulfate production. *Geophysical Research Letters*, 21(22): 2393-2396.
- Collett, J.L.J., Bator, A., Demoz, B.B. and Rao, X., 1994b. Cloud chemistry varies with drop size. Proc. Air & Waste Management Association (94-RA105.02).
- Collett, J.L.J., Iovinelli, R.J. and Demoz, B.B., 1995. A three-stage cloud impactor for size-resolved measurement of cloud drop chemistry. *Atmospheric Environment*, 29(10): 1145 - 1154.
- Collett, J.L.J., Hoag, K.J. and Pandis, S.N., 1998. The influence of drop size-dependent fog chemistry on aerosol production and deposition in San Joaquin Valley fogs, Department of Atmospheric Science, Colorado State University, Fort Collins, CO.
- Collett, J.L.J., Hoag, K.J., Rao, X. and Pandis, S.N., 1999a. Internal acid buffering in San Joaquin Valley fog drops and its influence on aerosol processing. *Atmospheric Environment*, 33: 4833 - 4847.

- Collett, J.L.J., Hoag, K.J., Sherman, D.E., Bator, A. and Richards, L.W., 1999b. Spatial and temporal variations in San Joaquin Valley fog chemistry. *Atmospheric Environment*, 33: 129 - 140.
- Collett J. L., Sherman D. E., Moore K. F., Hannigan M. P., and Lee T. (2001) Aerosol particle processing and removal by fogs: observations in chemically heterogeneous central California radiation fogs. *Water, Air, Soil Poll: Focus. 1*, 303-312.
- Dasgupta, P.K., DeCesare, K. and Ullrey, J.C., 1980. Determination of atmospheric sulfur dioxide without tetrachloromercurate(II) and the mechanism of the Schiff reaction. *Analytical Chemistry*, 52: 1912 - 1922.
- Dasgupta, P. K., 1981. Determination of atmospheric sulfur dioxide without tetrachloromercurate (II): further refinements of a pararosaniline method and a field application. *J Air Poll. Control Assoc.* 31: 779-782.
- Daum, P.H., Schwartz, S.E. and Newman, L., 1984. Acidic and related constituents in liquid water stratiform clouds. *Journal of Geophysical Research*, 89(D1): 1447 - 1458.
- Davis, E.J., 1983. Transport phenomena with single aerosol particles. *Aerosol and Science & Technology*, 2: 121-144.
- Decesari, S., Facchini, M.C., Fuzzi, S. and Tagliarini, E., 2000. Characterization of water-soluble organic compounds in atmospheric aerosol: a new approach. *Journal of Geophysical Research*, 105(D1): 1481 - 1489.
- Demoz B., Collett J. L., and Daube B. C. (1996) On the Caltech active strand cloudwater collectors. *Atmospheric Research.* 41, 47-62.
- Dollard G. J. and Unsworth M. H. (1983) Field measurements of turbulent fluxes of wind-driven fog drops to a grass surface. *Atmospheric Environment.* 17, 775-780.
- Dlugi, R., 1989. Chemistry and deposition of soot particles in moist air and fog. *Aerosol Science and Technology*, 10: 93 - 105.
- Dong, S. and Dasgupta, P.K., 1987. Fast fluorometric flow injection analysis of formaldehyde in atmospheric water. *Environmental Science and Technology*, 21: 581 - 588.
- Elbert, W., Hoffmann, M.R., Kramer, M., Schmitt, G. and Andreae, M.O., 2000. Control of solute concentrations in cloud and fog water by liquid water content. *Atmospheric Environment*, 34(7): 1109-1122.
- Emert, S.E., 2001. Design, construction, and evaluation of the CSU optical fog detector. MS Thesis, Colorado State University.
- Erel, Y., Pehkonen, S.O. and Hoffmann, M.R., 1993. Redox chemistry of iron in fog and stratus clouds. *Journal of Geophysical Research*, 98(D10): 18423 - 18434.
- Ervens, B., P. Herckes, G. Feingold, T. Lee, J. L. Collett, Jr. and S. M. Kreidenweis, 2003. On the drop-size dependence of organic acid and formaldehyde concentrations in fog,. *Journal of Atmospheric Chemistry*, 46: 239-269.

- Eugster, W., Burkhard, R., Klemm, O. and Wrzesinsky, T., 2001. Fog deposition measurements with the eddy covariance method. In: R.S. Schemenauer and H. Puxbaum (Editors), 2nd International Conference on Fog and Fog Collection, St. John's, Newfoundland, Canada, pp. 193 - 196.
- Facchini, M.C., Fuzzi, S., Lind, J. A., Fierlinger, H., Kalina, M., Puxbaum, H., Winiwarter, W., Arends, B. G., Wobrock, W., Jaeschke, Wolfgang, Berner, A. and Kruisz, Christian, 1992. Phase-partitioning and chemical reactions of low molecular weight organic compounds in fog. *Tellus*, 44B: 533 - 544.
- Facchini, M.C., Fuzzi, S., Zappoli, Sergio, Andracchio, Antonella, Gelencsér, A., Kiss, Gyula, Krivácsy, Z., Mészáros, E., Hansson, H.C., Alsberg, T. and Zebühr, Y., 1999a. Partitioning of the organic aerosol component between fog droplets and interstitial air. *Journal of Geophysical Research*, 104(D21): 26821 - 26832.
- Facchini, M.C., Mircea, M., Fuzzi, S. and Charlson, R.J., 1999b. Cloud albedo enhancement by surface-active organic solutes in growing drops. *Nature*, 401: 257 - 259.
- Facchini, M.C., Decesari, S., Mircea, M., Fuzzi, S. and Loglio, G., 2000. Surface tension of atmospheric wet aerosol and cloud/fog droplets in relation to their organic carbon content and chemical composition. *Atmospheric Environment*, 34: 4853 - 4857.
- Facchini, M. C., Mircea, M., Fuzzi, S. and Charlson, R.J., 2001. Comments on "Influence of soluble surface properties on the activation of aerosol particles containing inorganic solute". *Journal of the Atmospheric Sciences*, 58: 1465 - 1467.
- Fahey K. M. and Pandis S. N. (2001) Optimizing model performance: variable size resolution in cloud chemistry modeling. *Atmospheric Environment* 35, 4471-4478.
- Finlayson-Pitts, B.J. and Pitts, J.N.J., 2000. Chemistry of the upper and lower Atmosphere: theory, experiments, and applications. Academic Press, San Diego, CA, 969 pp.
- Fitzjarrald, D.R. and Lala, G.G., 1986. Observed fine structure in radiation fog, 23rd conference on radiation meteorology and conference on cloud physics. American Meteorological Society, Snowmass, CO, pp. P226 - P228.
- Forkel, R., Seidl, W., Dlugi, R. and Deigele, E., 1990. A one dimensional numerical model to simulate formation and balance of sulfate during radiation fog events. *Journal of Geophysical Research* 95(D11): 18501 - 18515.
- Fuchs, N.A. and Sutugin, A.G., 1971. High-dispersed aerosols. *Int. Rev. Aerosol Phys. Chem*, 2: 1-60.
- Fung and D, Grosjean., 1981. Determination of nanogram amounts of carbonyls as 2,4-dinitrophenylhydrazones by high-performance liquid-chromatography. *Analytical Chemistry*, 53(2): 168-171.

- Fuzzi, S., 1988. Fog chemistry and deposition in the Po Valley, Italy. In: M.H. Unsworth and D. Fowler (Editors), *Acid deposition at high elevations*. Kluwer Academic Publishers, Dordrecht, pp. 443 - 452.
- Fuzzi S, Facchini M.C., Orsi G, Lind Ja, Wobrock W., Kessel M., Maser R., Jaeschke W., Enderle K.H., Arends B.G., Berner A, Solly I, Kruisz C, Reischl G, Pahl S, Kaminski U, Winkler P, Ogren Ja, Noone K.J., Hallberg A., Fierlingeroberlinninger H., Puxbaum H., Marzorati A., Hansson H.C., Wiedensohler A., Svenningsson Ib, Martinsson B.G., Schell D. and Georgii H.W., 1992. The Po Valley fog experiment 1989- an overview. *Tellus*, 44B: 448-468.
- Fuzzi, S., Facchini, M.C., Schell, D., Wobrock, W., Winkler, Peter, Arends, B. G., Kessel, M., Möls, J. J., Pahl, S., Schneider, T., Berner, A., Solly, I., Kruisz, Christian, Kalina, M., Fierlinger, H., Hallberg, A., Vitali, P., Santoli, L. and Tigli, G., 1994. Multiphase chemistry and acidity of clouds at Kleiner-Feldberg. *Journal of Atmospheric Chemistry*, 19(1-2): 87-106.
- Fuzzi, S., 1995. The multiphase chemistry of clouds in the atmosphere. *Life chemistry reports*, 13: 29-38.
- Fuzzi, Sandro, Laj, Paolo, Ricci, Loretta, Orsi, Giordano, Heintzenberg, Jost, Wendisch, Manfred, Yuskiewicz, Brett, Mertes, Stephan, Orsini, Douglas, Schwanz, Marina, Wiedensohler, Alfred, Stratmann, Frank, Berg, Olle H., Swietlicki, Erik, Frank, Goran, Martinsson, Bengt G., Günther, Armin, Dierssen, Jens Peter, Schell, Dieter, Jaeschke, Wolfgang, Berner, Axel, Dusek, Ulrike, Galambos, Zsuzsanna, Kruisz, Christian, Mesfin, Nigatu S., Wobrock, Wolfram, Arends, Beate and Ten Brink, H., 1998. Overview of the Po Valley fog experiment 1994 (CHEMDROP). *Contributions to Atmospheric Physics*, 71(1): 3-19.
- Fuzzi, S., Decesari, S., Facchini, M.C., Matta, E., Mircea, M. and Tagliavini, E., 2001. A simplified model of the water soluble organic component of atmospheric aerosols. *Geophysical Research Letters*, 28(21): 4079-4082.
- Gerber, H., 1991. Direct measurement of suspended particulate volume concentration and far-infrared extinction coefficient with a laser-diffraction instrument. *Applied Optics*, 30(33): 4824 - 4831.
- Gerber, H., B. G. Arends, and A. S. Ackerman, 1994: New microphysics sensor for aircraft use. *Atmos. Res.*, 31, 235–252.
- Gerber, H., Frick, G. and Rodi, A.R., 1999. Ground-based FSSP and PVM measurements of liquid water content. *Journal of Atmospheric and Oceanic Technology*, 16: 1143-1149.
- Geshen, Z., 2000. Modern weather measurement and detection. Beijing University Publication, Beijing: 114-115.
- Gieray R., Wieser P., Engelhardt T., Swietlicki E., Hansson H. C., Menten B., Orsini D., Martinsson B., Svenningsson B., Noone K. J., and Heintzenberg J. (1997) Phase partitioning of aerosol constituents in cloud based on single-particle and bulk analysis, *Atmospheric Environment*. 31, 2491-2502.



- Guiang, S.F., Sagar, I., Krupa, V. and Pratt, G.C., 1984. Measurements of S(IV) and organic anions in Minnesota rain. *Atmospheric Environment*, 18(8): 1677-1682.
- Gundel, L.A., Dalsey, J.M., Carvalho, L.R.F.d., Kado, N.Y. and Schuetzle, D., 1993. Polar organic matter in airborne particles: chemical characterization and mutagenic activity. *Environ. Sci. Technol.*, 27: 2112-2119.
- Gundel, L.A., Benner, W.H. and Hansen, A.D.A., 1994. Chemical-composition of fog water and interstitial aerosol in Berkeley, California. *Atmospheric Environment*, 28(16): 2715-2725.
- Gurciullo C. S. and Pandis S. N. (1997) Effect of composition variations in cloud droplet populations on aqueous-phase chemistry. *J. Geophysical Research* 102, 9375-9385.
- Hanel, G., 1976. The properties of atmospheric aerosol particles as functions of relative humidity at thermodynamic equilibrium with the surrounding moist air. *Adv. Geoph.*, 19: 73-188.
- Hass H., Ebel A., Feldmann H., Jakobs H. J., and Memmesheimer M. (1993) Evaluation studies with a regional chemical transport model (EURAD) using air quality data from the EMEP monitoring network. *Atmospheric Environment* 27A, 867-887.
- Havers, N., Burba, P., Lambert, J. and Klockow, D., 1998. Spectroscopic characterization of humic-like substances in airborne particulate matter. *Journal of Atmospheric Chemistry*, 29(1): 45-54.
- Heintzenberg, J., Ogren, J.A., Noone, K.J. and Gärdneus, L., 1989. The size distribution of submicrometer particles within and about stratocumulus cloud droplets on Mt. Åreskutan, Sweden. *Atmospheric Research*, 24: 89 - 101.
- Herckes, P., Trenary, L., Hannigan, M.P., Lee, T. and Collett, J.L.J., 2001. Cloud and fog processing of atmospheric organic compounds. In: R.S. Schemenauer and H. Puxbaum (Editors), 2nd International Conference on Fog and Fog Collection, St. John's, Newfoundland, Canada, pp. 13 - 16.
- Herckes, P., Hannigan, M.P., Trenary, L., Lee, T. and Collett, J., J.L., 2002a. Organic compounds in radiation fogs in Davis (California). *Atmos. Res.*, 64: 99-108.
- Herckes, P., Lee, T., Trenary, L., Kang, G. G., Chang, H., Collett, J. L., 2002b. Organic matter in central California radiation fogs. *Environmental Science & Technology*, 36(22): 4777-4782.
- Herckes P., Wendling R., Sauret N., Mirabel P., and Wortham H. (2002) Cloudwater studies at a high elevation site in the Vosges Mountains (France). *Environmental Pollution*. 117, 169-177.
- Hitzenberger, R. and Berner, A., 2002. Surface tension of Rax cloud water and its relation to the concentration of organic material. *Journal of Geophysical Research*, 107: No. D24, 4752.
- Hoag K. J., Collett J. L., and Pandis S. N. (1999) The influence of drop size-dependent fog chemistry on aerosol processing by San Joaquin Valley fogs. *Atmospheric Environment*. 33, 4817-4832.

- Hoffmann, M.R., 1984. Comment on "acid fog". *Environmental Science and Technology*, 18(1): 61 - 64.
- Hoffmann, M.R. and Calvert, J.G., 1985. Chemical transformation modules for eulerian acid deposition models, vol. 2, The aqueous-phase chemistry. EPA/600/3-85/017, U.S. Environ. Prot. Agency, Research Triangle Park, N. C.
- Hoffmann, M.R., 1986. On the kinetics and mechanism of oxidation of aquated Sulfur Dioxide by Ozone. *Atmos. Environ.*, 10: 1145-1154.
- Holets, S. and Swanson, R.N., 1981. High inversion fog episodes in central California. *Journal of Applied Meteorology*, 20: 890 - 899.
- Husain, L., 1989. A technique for determining in-cloud formation of SO<sub>4</sub>. *Geophysical Research Letters*, 16(1): 57 - 60.
- Ibusuki, T. and Takeuchi, A., 1987. Sulfur dioxide oxidation by oxygen catalyzed by mixtures of manganese (II) and iron (III) in aqueous solutions at environmental reaction conditions. *Atmos. Environ.*, 21: 1555-1560.
- Jacob, D.J., Waldman, J.M., Munger, J.W. and Hoffmann, M.R., 1984. A field investigation of physical and chemical mechanisms affecting pollutant concentrations in fog droplets. *Tellus*, 36B: 272 - 285.
- Jacob, D.J., 1986. Chemistry of OH in remote clouds and its role in the production of formic acid and peroxymonosulfate. *Journal of Geophysical Research*, 91(D9): 9807 - 9826.
- Jacob, D.J., Munger, J.W., Waldman, J.M. and Hoffmann, M.R., 1986a. The H<sub>2</sub>SO<sub>4</sub>-HNO<sub>3</sub>-NH<sub>3</sub> system at high humidities and in fogs 1. spatial and temporal patterns in the San Joaquin Valley of California. *Journal of Geophysical Research*, 91(D1): 1073 - 1088.
- Jacob, D.J., Waldman, J.M., Munger, J.W. and Hoffmann, M.R., 1986b. The H<sub>2</sub>SO<sub>4</sub>-HNO<sub>3</sub>-NH<sub>3</sub> system at high humidities and in fogs 2. comparisons of field data with thermodynamic calculations. *Journal of Geophysical Research*, 91(D1): 1089 - 1096.
- Jacob, D.J., F.H., S., J.M., W., Munger, J.W. and Hoffmann, M.R., 1987. Transport and oxidation of SO<sub>2</sub> in a stagnant foggy valley. *Atmos. Environ.*, 21: 1305-1314.
- Kulmala, M., Laaksonen, A., J. Charlson, R. and Korhonen, P., 1997. Clouds without supersaturation. *Nature*, 388(336-337).
- Kumar N. and Lurmann F. W. (1997) Application of the UAM-Aero model to two 1995 PM10 episodes in the south coast air basin. *STI Final Report* STI-95390-1725-FR.
- Laaksonen, A., Korhonen, P., Kulmala, M. and Charlson, R.J., 1998. Modification of the Kohler equation to include soluble trace gases and slightly soluble substances. *Journal of the Atmospheric Sciences*, 55: 853 - 862.
- Laj, P. et al., 1997. Cloud processing of soluble gases. *Atmospheric Environment*, 31(16): 2589 - 2598.

- Lazrus, A.L., Kok, G.L., Gitlin, S.N. and Lind, J.A., 1985. Automated fluorometric method for hydrogen peroxide in atmospheric precipitation. *Analytical Chemistry*, 57: 917 - 922.
- Lazrus, A. L., Kok, G. L., Lind, J. A., Gitlin, S. N., Heikes, B. G., Shetter, R. E., 1986. Automated fluorometric method for H<sub>2</sub>O<sub>2</sub> in air. *Analytical Chemistry*, 58: 594 - 597.
- Lee, T.F., 1987. Urban clear islands in California Central Valley. *Monthly Weather Review*, 115: 1794-1796.
- Lee, T., 2002. M.S. Thesis, Department of Atmospheric Science, Colorado State University, Fort Collins, Colorado.
- Lee, T., Kreidenweis, S. M. and Collett, Jr., J. L. (2004) Aerosol ion characteristics during the Big Bend Regional Aerosol and Visibility Observational study. *J. Air and Waste Management Assoc.* 54: 585-592.
- Li, Z.D., Williams, A.L. and Rood, M.J., 1998. Influence of soluble surfactant properties on the activation of aerosol particles containing inorganic solute. *Journal of the Atmospheric Sciences*, 55(10): 1859-1866.
- Likens, G.E., Edgerton, E.S. and Galloway, J.N., 1983. The composition and deposition of organic-carbon in precipitation. *Tellus*, 35: 16-24
- Liljestrand H. M. (1985) Average rainwater pH, concepts of atmospheric acidity, and buffering in open systems. *Atmospheric Environment* 19, 487-489.
- Lillis, D., Cruz, C.N., Collett, J., Richards, L.W. and Pandis, S.N., 1999. Production and removal of aerosol in a polluted fog layer: model evaluation and fog effect on PM. *Atmospheric Environment*, 33(29): 4797-4816.
- Limbeck, A. and Puxbaum, H., 2000. Dependence of in-cloud scavenging of polar organic aerosol compounds on the water solubility. *Journal of Geophysical Research*, 105(D15): 19857 - 19867.
- Lovett G. M. (1984) Rates and mechanisms of cloud water deposition to a subalpine balsam fir forest. *Atmospheric Environment*. 18, 361-371.
- Luttke, J. and Levsen, K., 1997. Phase partitioning of phenol and nitrophenols in clouds. *Atmospheric Environment*, 31(16): 2649-2655.
- Luttke, J. et al., 1997. Occurrence and formation of nitrated phenols in and out of cloud. *Atmospheric Environment*, 31(16): 2637-2648.
- Maahs, H.G., 1983. Kinetics and mechanism of the oxidation of S(IV) by ozone in aqueous solution with particular reference to SO<sub>2</sub> conversion in non-urban tropospheric clouds. *Journal of Geophysical Research*, 88: 10721-10732.
- Martin, L., 1994. Aqueous sulfur(IV) oxidation revisited. *Environmental Oxidants* ( J. O. Nriagu and M. S. Simmons, Eds.): 221-268.
- Martin, L.R., 1984. Kinetic studies of sulfite oxidation in aqueous solution in SO<sub>2</sub>, NO and NO<sub>2</sub> oxidation mechanism: atmospheric considerations, edited by J. G. Calvert. (Butterworth-Heinemann, Woburn, Mass): 63-100.

- Matthijssen J., Builtjes P. J. H., Meijer E. W., and Boersen G. (1997) Modeling cloud effects on ozone on a regional scale: A case study. *Atmospheric Environment* 31, 3227-3238.
- McArdle, J.V. and Hoffmann, M.R., 1983. Kinetics and mechanism of the oxidation of aquated sulfur dioxide by hydrogen peroxide at low pH. *Journal of Physical Chemistry*, 87: 5425-5429.
- McGregor, K.G. and Anastasio, C., 2001. Chemistry of fog waters in California's central valley: 2. photochemical transformations of amino acids and alkyl amines. *Atmospheric Environment*, 35: 1091 - 1104.
- Mircea, M., Facchini, M.C., Decesari, S., Fuzzi, S. and Charlson, R.J., 2002. The influence of the organic aerosol component on CCN supersaturation spectra for different aerosol types. *Tellus*, 54B: 74-81.
- Moller, D., Acker, K. and Wiprecht, W., 1996. A relationship between liquid water content and chemical composition in clouds. *Atmospheric Research*, 41(3-4): 321-335.
- Moore, K.F., 2001. Ph.D. dissertation Thesis, Colorado State University, Fort Collins, CO.
- Moore K. F., Sherman D. E., Reilly J. E. and Collett J. L. (2002) Development of a multi-stage cloud water collector: 1. Design and field performance evaluation. *Atmospheric Environment*. 36, 31-44.
- Moore, K. F., Sherman, D. E., Reilly, J. E., Hannigan, M. P. Lee, T. and Collett, Jr., J. L. (2004a) Drop size-dependent chemical composition in clouds and fogs. I. Observations. *Atmos. Environ.* **38**, 1389-1402.
- Moore, K. F., Sherman, D. E., Reilly, J. E. and Collett, Jr., J. L. (2004b) Drop size-dependent chemical composition of clouds and fogs. II. Relevance to interpreting the aerosol/trace gas/fog system. *Atmos. Environ.* **38**, 1403-1415.
- Munger, J.W., Jacob, D.J. and Hoffmann, M.R., 1984. The occurrence of bisulfite-aldehyde addition products in fog- and cloudwater. *Journal of Atmospheric Chemistry*, 1: 335 - 380.
- Munger, J.W., Jacob, D.J., Waldman, J.M. and Hoffmann, M.R., 1983a. Fogwater chemistry in an urban atmosphere. *Journal of Geophysical Research*, 88(C9): 5109 - 5121.
- Munger, J.W., Waldman, J.M., Jacob, D.J. and Hoffmann, M.R., 1983b. Vertical variability and short-term temporal trends in precipitation chemistry. In: H.R. Pruppacher, R.G. Semonin and W.G.N. Slinn (Editors), *Precipitation Scavenging, Dry Deposition, and Resuspension*. Elsevier, New York, pp. 275 - 282.
- Munger, J.W., Tiller, C. and Hoffmann, M.R., 1986. Identification of hydroxymethanesulfonate in fog water. *Science*, 231: 247 - 249.
- Munger, J.W., Collett, J.L., Jr., Daube, B.C., Jr. and Hoffmann, M.R., 1989a. Carboxylic acids and carbonyl compounds in southern California clouds and fogs. *Tellus*, 41B: 230 - 242.

- Munger, J.W., Collett, J.L.J., Daube, B.C.J. and Hoffmann, M.R., 1989b. Chemical composition of coastal stratus clouds: dependence on drop size and distance from the coast. *Atmospheric Environment*, 23(10): 2305 - 2320.
- Munger, J.W., Collett, J., Daube, B. and Hoffmann, M.R., 1990. Fogwater chemistry at Riverside, California. *Atmospheric Environment*, 24(2): 185-205.
- Noone K. J., Charlson R. J., Covert D. S., Ogren J. A., and Heintzenberg J. (1988) Cloud droplets: Solute concentration is size dependent. *J. Geophysical Research* 93, 9477-9482.
- Ogren, J.A., Heintzenberg, J., Zuber, Z., Noone, K.J. and Charlson, R.J., 1989. Measurements of the size-dependence of solute concentrations in cloud droplets. *Tellus*, 41B: 24 - 31.
- Pandis, S.N. and Seinfeld, J.H., 1989a. Mathematical modeling of acid deposition due to radiation fog. *Journal of Geophysical Research*, 94(D10): 12911 - 12923.
- Pandis S. N. and Seinfeld J. H. (1989b) Sensitivity analysis of a chemical mechanism for aqueous-phase atmospheric chemistry. *J. Geophysical Research* 94, 1105-1126.
- Pandis S. N., Seinfeld J. H., and Pilinis C. (1990a) Chemical composition differences in fog and cloud droplets of different sizes. *Atmospheric Environment* 24A, 1957-1969.
- Pandis S. N., Seinfeld J. H., and Pilinis C. (1990b) The smog-fog-smog cycle and acid deposition. *J. Geophysical Research* 95, 18489-18500.
- Pandis, S.N., Seinfeld, J.H. and Pilinis, C., 1992. Heterogeneous sulfate production in an urban fog. *Atmospheric Environment*, 26A(14): 2509 - 2522.
- Pinnick, R.G. and Auvermann, H.J., 1979. Response characteristics of Knollenberg light-scattering aerosol counters. *Journal of Aerosol Science*, 10: 55-74.
- Pruppacher H. R. and Klett J. D. (1980) *Microphysics of Clouds and Precipitation*. Reidel Publishing. Netherlands.
- Rao, X. and Collett, J.L.J., 1995. Behavior of S(IV) and formaldehyde in a chemically heterogeneous cloud. *Environmental Science and Technology*, 29: 1023-1031.
- Rao, X., 1997. Cloud chemical heterogeneity and its influence on aqueous sulfur(IV) oxidation. Ph.D. Thesis, University of Illinois at Urbana-Champaign, Urbana-Champaign, IL, 231 pp.
- Rao, X. and Collett, J.L.J., 1998. The Drop size-dependence of iron and manganese concentrations in clouds and fogs: implications of sulfate production. *Journal of Atmospheric Chemistry*, 30: 273-289.
- Rattigan, O. V., Reilly, J., Judd, C. D., Moore, K. F., Das, M., Sherman, D. E., Dutkiewicz, V. A., Collett, J. L. and Husain, L., 2001. Sulfur dioxide oxidation in clouds at Whiteface mountain as a function of drop size. *Journal of Geophysical Research*, 106(D15): 17347-17358.
- Raymond, T.M. and pandis, S.N., 2002. Cloud activation of single-component organic aerosol. *Journal of Geophysical Research*, 107: NO.D24, 4787.

- Reible, D.D., 1982. Investigation of transport in complex atmospheric flow systems. Ph.D. Dissertation, California Institute of Technology.
- Reilly, J.E., 2000. Application of a tracer technique to study sulfur dioxide oxidation in cloud drops as a function of drop size. M.S. Thesis, Colorado State University, Fort Collins, CO.
- Reilly, J. E., Rattigan, O. V., Moore, K. F., Judd, C., Sherman, D. E., Dutkiewicz, V. A., Kreidenweis, S. M., Husain, L. and Collett, J. L., Jr., 2001. Drop size-dependent S(IV) oxidation in chemically heterogeneous radiation fogs. *Atmospheric Environment*, 35(33): 5717-5728.
- Roach, W.T., 1976. On the effect of radiative exchange on the growth by condensation of a cloud or fog droplet. *Quarterly Journal of the Royal Meteorological Society*, 102: 361 - 372.
- Rodhe, H., 1999. Clouds and climate. *Nature*, 401: 223-225.
- Rood, M.J. and Williams, A.L., 2001. Comments on "Influence of soluble surfactant properties on the activation of aerosol particles containing inorganic solute" - Reply. *Journal of the Atmospheric Sciences*, 58: 1468 - 1473.
- Roselle S. J. and Binkowski F. S. (1999) Cloud dynamics and chemistry. Science algorithms of the EPA models-3 community multiscale air quality (CMAQ) modeling system. EPA/600/R-99/030.
- Saxena, P., Hildemann, L.M., McMurry, P.H. and Seinfeld, J.H., 1995. Organics alter hygroscopic behavior of atmospheric particles. *Journal of Geophysical Research*, 100(D9): 18755 - 18770.
- Saxena, P. and Hildemann, L.M., 1996. Water-soluble organics in atmospheric particles: a critical review of the literature and application of thermodynamics to identify candidate compounds. *Journal of Atmospheric Chemistry*, 24: 57 - 109.
- Seinfeld, J.H., 1986. Atmospheric chemistry and physics of air pollution. (Wiley, New York).
- Seinfeld, J.H. and Pandis, S.N., 1998. Atmospheric chemistry and physics. John Wiley and Son, Inc, New York.
- Shulman, M.L., Jacobson, M.C., Carlson, R.J., Synovec, R.E. and Young, T.E., 1996. Dissolution behavior and surface tension effects of organic compounds in nucleating cloud droplets. *Geophysical Research Letters*, 23(3).
- Silva, P.J., Liu, D.Y., Noble, C.A. and Prather, K.A., 1999. Size and chemical characterization of individual particles resulting from biomass burning of local southern California species. *Environ Sci Technol*, 33: 3068-3076.
- Straub D. J. and Collett J. L. (2002) Development of a multi-stage cloud water collector. Part 2: Numerical and experimental calibration. *Atmospheric Environment*. 36, 45-56.
- Suzuki, Y., Imai, S., Kawakami, M., Masuda, Y. and Akasaka, K., 1998. Identification and determination of low-molecular weight organic compounds in contaminated

- fog water using proton nuclear magnetic resonance spectroscopy. *Environ. Contam. Toxicol.*, 60: 355-362.
- Thalmann E., Burkard R., Wrzesinsky T., Eugster W. and Klemm O. (2002) Ion fluxes from fog and rain to an agricultural and a forest ecosystem in Europe. *Atmospheric Research*. 64, 147-158.
- Waldman, J.M., Munger, J.W., Jacob, D.J. and Hoffmann, M.R., 1983. Fogwater composition in Southern California. In: H.R. Pruppacher, R.G. Semonin and W.G.N. Slinn (Editors), *Precipitation Scavenging, Dry Deposition, and Resuspension*. Elsevier, New York, NY, pp. 137 - 145.
- Waldman J. M. (1986) Depositional aspects of pollutant behavior in a fog. Ph.D. Thesis, Caltech. Pasadena, California
- Waldman, J.M. and Hoffmann, M.R., 1987. Depositional aspects of pollutant behaviour in fog and intercepted clouds. In: R.A. Hites and S.J. Eisenreich (Editors), *Sources and Fates of Aquatic Pollutants*. Advances in Chemistry Series #216. American Chemical Society, pp. 79 - 129.
- Wark, K., Warner, C.F. and Davis, W.T., 1998. *Air Pollution: Its Origin and Control*. Addison-Wesley, Menlo Park, CA, 573 pp.
- Welch, R.M. and Wielicki, B.A., 1986. The stratocululus nature of fog. *J. Clim. Appl.*, 25: 101-111.
- Wendisch, M., 1998. A quantitative comparison of ground-based FSSP and PVM measurements. *Journal of Atmospheric and Oceanic Technology*, 15: 887-900.
- Whitby, K.T., 1978. The physical characteristics of sulfur aerosols. *Atmos. Environ*, 12: 135-159.
- Whiteaker, J.R. and Prather, K.A., 2003. Hydroxymethanesulfonate as a tracer for fog processing of individual aerosol particles. *Atmospheric Environment*, 37(8): 1033-1043.
- Wobrock, W., Schell, D., Maser, R., Jaeschke, W., Georgii, H. W., Wieprecht, W., Arends, B. G., Mols, J. J., Kos, G. P. A., Fuzzi, S., Facchini, M. C., Orsi, G., Berner, A., Solly, I., Kruisz, C., Svenningsson, I. B., Wiedensohler, A., Hansson, H. C., Ogren, J. A., Noone, K. J., Hallberg, A., Pahl, S., Schneider, T., Winkler, P., Winiwarter, W., Colvile, R. N., Choularton, T. W., Flossmann, A. I. and Borrmann, S., 1994. The Kleiner-Feldberg cloud experiment 1990 - an overview. *Journal of Atmospheric Chemistry*, 19(1-2): 3-35.
- Wrzesinsky, T., Thalmann, E., Burkhard, R., Eugster, W. and Klemm, O., 2001. Fog deposition of nutrients and pollutants to a montane forest site. In: R.S. Schemenauer and H. Puxbaum (Editors), *2nd International Conference on Fog and Fog Collection*, St. John's, Newfoundland, Canada, pp. 169 - 172.
- Xu, G., Sherman, D. E., Andrews, E., Moore, K., Straub, D., Hoag, K. and Collett, J. L. Jr., 1999. The influence of chemical heterogeneity among cloud drop populations on processing of chemical species in winter clouds. *Atmospheric Research*(51): 119-140.

- Zappoli, S., Andracchio, A., Fuzzi, S., Facchini, M. C., Gelencser, A., Kiss, G., Krivacsy, Z., Molnar, A., Meszaros, E., Hansson, H. C., Rosman, K. and Zebuhr, Y., 1999. Inorganic, organic and macromolecular components of fine aerosol in different areas of Europe in relation to their water solubility. *Atmospheric Environment*, 33(17): 2733-2743.
- Zhang, Q. and Anastasio, C., 2001. Chemistry of fog waters in California's central valley - Part 3: concentrations and speciation of organic and inorganic nitrogen. *Atmospheric Environment*, 35(32): 5629-5643.
- Zhou, X. and Lee, Y.N., 1992. Aqueous solubility and reaction kinetics of hydroxymethyl hydroperoxide. *J. Phys. Chem.*, 96: 265-272.



## **APPENDIX A**

### **An Economical Optical Fog Detector**

Jacqueline H. Carrillo, Scott E. Emert, D. Eli Sherman, and Jeffrey L. Collett, Jr.\*

Colorado State University, Department of Atmospheric Science  
Fort Collins, CO 80523

\* Corresponding Author: Colorado State University, Department of Atmospheric Science,  
Fort Collins, CO 80523, Ph. 970-491-8697, Fax 970-491-8449,  
e-mail: [collett@lamar.colostate.edu](mailto:collett@lamar.colostate.edu)

## **Abstract**

A new, relatively low cost instrument has been developed to detect the presence of fog/cloud for fog/cloud sampling applications. The instrument uses attenuation of an 880 nm light emitting diode signal to detect cloud/fog drops in the optical path between a sending and receiving arm. Laboratory and field testing under a variety of conditions and fog types were carried out to determine the ability of the optical fog detector (OFD) to accurately detect cloud/fog presence as well as to provide some measure of liquid water content. Results indicated that the OFD provided a reliable estimate of fog presence as well as a reasonable estimate of LWC under several different conditions. The OFD does appear to have an interference from rain, resulting in an overestimation of LWC during rainfall. This may occasionally give a false positive indication of fog presence.

**Keywords:** cloud detection, fog detection, liquid water content, optical attenuation, automated sampling

## Introduction

A basic need in cloud and fog sampling applications is a reliable indicator of cloud/fog presence in order to automatically start and stop sample collection. For more complete characterization of fog and ground level clouds, it is often desirable to have an accurate measure of the integrated cloud drop volume, or liquid water content (LWC). Such information is critical to understanding cloud/fog timing within an individual event (onset, development, and dissipation of the cloud), the frequency of cloud presence at a given location, and for mass balance calculations. A commercial instrument commonly used in research applications is the Gerber Scientific Particulate Volume Monitor (PVM) which continuously measures cloud LWC and particle surface area (PSA) by measuring the forward scattering of light from an infrared (780 nm) laser (Arends, et al., 1992, Gerber, 1991). The PVM requires little routine maintenance aside from occasional calibrations, and so is easily deployed for extended periods of time. The relatively high cost of the PVM, however, makes it prohibitively expensive for some network studies or for intensive studies at one location where, for example, measurements at varying heights may be desired.

Several low cost fog detectors have been described in the literature. The Caltech visibility sensor (Collett, et al., 1990) uses a modulated light emitting diode (LED) at 940 nm to measure backscatter from fog drops, while the Poor Man's optical fog detector (Mallant, 1988) uses a pulsed LED at 880 nm to measure forward scattering using a dump spot. Fuzzi et al. (1990) describe a backscatter detector with an unspecified light source. While all were proficient at detecting fog, the Caltech visibility sensor has not been evaluated for measurements of LWC and the electronic components of this device

are no longer commercially available. The Poor Man's optical fog detector has demonstrated poor performance in measuring LWC and Fuzzi et al. specifically state that their detector does not measure LWC.

We describe here the construction and initial laboratory and field testing of the Colorado State University Optical Fog Detector (OFD). The OFD is a new instrument designed to detect fog presence. It may also be capable of making continuous measurements of LWC under certain conditions. It measures light attenuation between a sending and receiving arm from which cloud/fog presence and an estimate of LWC are inferred. Like the PVM, the OFD requires little maintenance aside from regular calibrations and cleaning of the optics. It costs around \$400 for materials, making the deployment of multiple, spatially separated instruments economical.

### **Instrument Description**

The OFD (Figure 1) consists of a weatherproof NEMA enclosure that contains the instrument electronics and a metal arm that extends on either side of the enclosure. The arm is directly above the optical path and serves as a support for the opposing fiber optic cables. An approximately 5 inch wide piece of aluminum sheet, that has been angled to form a roof, extends the length of the arm and acts as a rain shield for the optical path when the instrument is installed with the optical path perpendicular to the wind direction. The critical component of the OFD is the OASBFX Analog Omni-Beam infrared LED, which is housed inside the NEMA box. It consists of a modulated infrared (880 nm) LED light source and a photoelectric detector, tuned to detect light only at the modulated frequency, thereby reducing interference from ambient light. The response time of the

detector is 15 ms. The OASBFX is powered by an OPBA3 power block and light is delivered via 2 opposed mode glass fiber optic cables. All of these optical components are supplied by Banner Engineering Corp., Minneapolis, MN.

The two fiber optic lenses are positioned 53.3 cm apart and facing each other (0° offset) on either end of the instrument arm. Cloud LWC is estimated from attenuation of the beam signal between the two lenses. While most commercial fog sensors infer LWC from scattered rather than attenuated (a result of scattered plus absorbed) light, it was determined that the OASBFX was not sensitive enough to detect backscattered light. When configured with a dump spot or angular offset to detect forward scattered light, the agreement with PVM LWC measurements was significantly worse than in attenuation mode. Details of these experiments are presented in Emert (2001). To reduce the accumulation of dirt and condensation on the fiber optic lenses, a small aquarium pump (Profile 1500) with an inline filter is used to continuously blow clean air past the lenses. Resistors are mounted above each lens housing to further reduce condensation, as well as freezing of any moisture on the lenses through heat dissipation. Once calibrated against a PVM, the signal output from the OFD is 0-5 V, with 1 mV nominally equivalent to 1 mg m<sup>-3</sup> LWC.

## **Experimental**

Initial calibration of the instrument was performed by adjusting the OFD output signal to match that of a well-calibrated PVM within a glovebox containing an artificial fog. This fog was made using a standard home humidifier. After the OFD had been

calibrated to the PVM, fog onset and dissipation were repeatedly simulated to test the ability of the OFD to rapidly respond to changing LWC conditions.

After the initial lab testing phase, several OFDs were constructed and deployed at a variety of field locations along with a PVM. Field locations were Mt. Werner, CO, Angiola, CA, and Volcano, HI. The OFDs and PVM calibrations were checked and, if necessary, adjusted every 3-7 days at each site. After the first field test in Colorado, where it was discovered that dirt accumulating on the lenses was interfering with the OFD signal, OFD lenses were periodically cleaned with isopropyl alcohol as well. The lenses are firmly secured in their housings and cleaning does not disrupt the instrument's optical alignment.

#### *Storm Peak Laboratory*

Storm Peak Laboratory (SPL) is located on Mt. Werner, near Steamboat Springs, CO. The lab is at 3220 m elevation and is operated by the Desert Research Institute Atmospheric Sciences Center (Borys and Wetzol, 1997). During the late summer, monsoonal flow typically results in frequent intercepted clouds at this site. Sampling took place during August 2000. Two OFDs and one PVM were mounted on a railing on the edge of the SPL roof, all at the same height.

#### *Angiola*

Angiola, CA is a small, agricultural town at approximately 60 m elevation and located in the California's San Joaquin Valley. This region frequently experiences radiation fog during the winter months. Sampling was performed near Angiola (ANG)

from December 2000- January 2001 as part of the California Regional Particulate Air Quality Study (CRPAQS) (Herckes, et al., 2002). An OFD was co-located with a PVM atop a 3 m pole in a clear, flat location.

### *Thurston Lava Tube*

The Thurston Lava Tube (TLT) site is at 1190 m elevation and located within the Hawaii Volcanoes National Park on the Island of Hawaii. This site experiences frequent ground level orographic clouds year round, often accompanied by heavy rainfall (Carrillo, et al., 2002). Sampling was performed during April-May 2003. An OFD was mounted on a 19 m sampling tower, along with a PVM operated by the University of Hawaii. The PVM was located on the top level of the tower while the OFD was one level lower (approximately 1.5 m lower).

## **Results and Discussion**

During the initial glovebox testing, the OFD signal was calibrated by adjusting the zero and span on the OASBFX so that the output matched the PVM LWC signal. After this initial calibration adjustment, the OFD signal closely tracked that of the PVM during the artificial fog onset and dissipation (Figure 2). In subsequent tests when LWC was changed rapidly, results were equally promising, with high correlations between the OFD and PVM signals ( $R^2 = 0.99$ ).

In order to be able to calibrate the OFD in the field without the use of a glovebox and artificial fog, a calibration filter was made using Avery 5177 Ink Jet Transparency. It was found that this filter consistently produces a voltage of 330 mV when placed in front

of the receiving lens of an OFD calibrated against a PVM in our glove box setup. Several sheets and batches of the Avery transparency were tested with identical results. These filters were subsequently used in the field for routine calibration adjustments.

Three intercepted cloud events were sampled at SPL, 1 radiation fog event was sampled at ANG, and 12 orographic cloud events were sampled at TLT. The OFDs showed the highest degree of correlation with the PVM for the intercepted cloud events experienced at SPL (Figure 3). Both OFDs showed a nearly 1 to 1 relationship with the measured PVM LWC, with only a slight offset. Correlation was worst for the third sampled event ( $R^2 = 0.8$ ), most likely due to the accumulation of dirt on the OFD fiber optic lenses over the course of the 4 week study. It was this observation that prompted the implementation of a lens cleaning procedure and the addition of the filtered air pump to keep the lenses clean. Despite the lower correlation with the PVM LWC for the third event, the OFD detected cloud presence at the same time as the PVM.

The stability of the baseline signals at SPL was examined to investigate the possibility that changes in temperature or other conditions might affect the OFD baseline over the course of the day. Figure 4 shows the PVM and OFD signals for a 3 day period of time with no clouds. The baselines for both OFDs were stable, varying by less than  $\pm 5 \text{ mg m}^{-3}$ .

At ANG instrument failure resulted in only one sampled event for which the PVM and OFD could be compared. Nonetheless, the signals from the two instruments correlate well, with an overall  $R^2$  value of 0.93. While agreement between the OFD and PVM was very good for the first part of the sampled fog event, the OFD tended to overestimate LWC somewhat compared with the PVM for the latter 3 hours of the event



(Figure 5). This discrepancy may be related to the size of the cloud drops present. Emert (2001) showed that light transmission is dependent upon particle size, according to the following version of the Beer-Lambert equation for a monodisperse drop population:

$$\frac{I}{I_o} = \exp(-\sigma_e L) = \exp\left(-\frac{3C_m Q_e L}{2\rho_p d}\right) \quad \text{Eq. 1}$$

Here  $\frac{I}{I_o}$  is the light transmission, or the ratio of the light traversing the fog to the incident light,  $\sigma_e$  is the extinction coefficient,  $L$  is the path length through the fog,  $C_m$  is the particle mass concentration (LWC),  $Q_e$  is the drop extinction efficiency,  $\rho_p$  is the particle density and  $d$  is the drop diameter. While this simple equation does not capture effects associated with polydisperse drop distributions, we can see that fogs with smaller drops will have a lower transmission (and higher attenuation) for the same LWC. Notice also that transmission is dependent upon  $Q_e$ , which will change for drops of different solute concentrations and compositions.

The effective radius of the fog drops ( $R_{eff}$ ) was calculated from the PVM LWC and PSA and is also shown in Figure 5. For the large drops at the beginning of the event, the agreement in LWC signal is quite good. When  $R_{eff}$  drops below about 15-20  $\mu\text{m}$  however, the OFD indicates a higher LWC than the PVM. The ratio between the OFD and PVM LWC is plotted versus  $R_{eff}$  in Figure 6. Note that below about 15-20  $\mu\text{m}$  the OFD is more likely to over-predict LWC compared to the PVM. Above about 15  $\mu\text{m}$  the agreement between the two instruments is much better, with the ratio near 1.

Although particle surface area (PSA) observations were not available for the initial glovebox calibrations and  $R_{eff}$  is therefore unknown, it is likely that the drops created by the humidifier were relatively large. With calibration under these large-drop conditions, at small drop sizes the OFD may overestimate LWC relative to the PVM according to the relationship in Equation 1. The PVM PSA data are not available at SPL either; however, the consistently good correlation between the OFD and PVM LWC at that site suggests that the drops were large (i.e.  $R_{eff} > 15 \mu\text{m}$ ). Nonetheless, although some differences in signal were observed at ANG, the overall agreement between the OFD and PVM LWC was still quite good and the OFD and PVM determination of cloud presence match well.

At TLT, the overall agreement between the PVM and OFD LWC estimates was significantly worse than at the other 2 sampling locations. For the 12 orographic events sampled, the OFD and PVM showed a low degree of correlation ( $R^2 = 0.33$ , Figure 7), with the OFD generally measuring higher LWC than the PVM. In this figure, data have been averaged over 30 minutes to minimize the effects of a 1 minute time difference and different integrating times for the OFD and the University of Hawaii PVM.

Three factors that might contribute to the discrepancy between the PVM and OFD1 LWC are (1) differences in instrument location (height), (2) effects of cloud drop size and (3) interference by precipitation. Since the OFD LWC estimate generally exceeds the PVM LWC, it is unlikely that instrument position is the main contributor to the observed discrepancy. The PVM, mounted higher than the OFD, would be expected to experience a slightly higher LWC in these orographic clouds.

In order to determine the possible contribution of drop size, the ratio of OFD to PVM LWC was plotted against the effective radius obtained from the PVM. The comparison was restricted to PVM LWC values exceeding  $10 \text{ mg m}^{-3}$ . As shown in Figure 8, there is no apparent relation, suggesting that changes in effective diameter cannot explain the variability observed in the responses of the OFD and PVM. Note however, that the drop sizes observed at TLT were generally smaller than at ANG. At ANG the OFD/PVM ratio approached 1 for data points with  $R_{\text{eff}}$  above about  $15\text{-}20 \text{ }\mu\text{m}$ . Few data points in this size range were observed at TLT.

Data from an on-site tipping bucket rain gauge operated by the University of Hawaii were used to explore whether the occurrence of rain contributed to the enhanced response of the OFD. Each tip of the gauge corresponded to  $0.1''$  ( $0.254 \text{ cm}$ ) of rain. Figure 9 depicts the occurrence of measurable rain along with the OFD and PVM LWC timeline from April 21 to May 2, 2003. As is typical for the site, cloud interception was nearly always accompanied by significant rainfall.

There were several periods of time (April 25, April 27, and April 28) with measured rainfall when the PVM LWC indicated that no cloud was present, but the OFD had a positive response (Figure 9). These false positive signals generally occurred just before or after the occurrence of clouds, as measured by the PVM. While the false OFD signals were generally below  $50 \text{ mg m}^{-3}$ , an exception is the afternoon of April 25, when the OFD indicated over  $100 \text{ mg m}^{-3}$  LWC. This suggests that much of the time, false indicators of fog presence due to rain might be avoided by setting the fog detection threshold to greater than  $50 \text{ mg m}^{-3}$ , but that errors may still occasionally occur during periods of rainfall.

While the OFD signal generally exceeds that of the PVM, an exception is the night of April 29, when cloud was present but no measurable rain fell. Figure 10 shows 10 minute data for the OFD signal plotted versus the PVM LWC for this event. While there is still some scatter, the agreement is generally good ( $R^2 = 0.94$ ). The fog event of May 1 also shows no measurable rainfall, although the agreement between the OFD and PVM is significantly worse than on April 29 ( $R^2 = 0.30$ ). It is possible however that there was drizzle or light rain that was below the detection limit of the rain gauge and which may have interfered with the OFD signal. The improved agreement for the event of April 29 over other events at TLT suggests that although no rain was ever visually observed in the OFD optical path under the rain shield and no wetting of the optics was apparent, the presence of precipitation does interfere with the OFD signal.

## **Conclusions**

The CSU OFD was successful in reliably indicating the presence of cloud/fog in several environments, however, the OFD response had an apparent interference from rain. The enhanced response during rainy conditions resulted in either a false indication of fog or an overestimation of LWC. In locations where rain is expected to coincide with fog, the OFD should be deployed with a rain gauge so that potentially false or inaccurate readings may be flagged.

During rain-free periods of intercepted clouds and radiation fogs with larger drop sizes, the OFD appeared to also provide a reasonable estimate of LWC. When smaller ( $R_{eff} < 15 \mu\text{m}$ ) drops were present, however, the OFD tended to overestimate LWC compared with the PVM, most likely due to the large drop size conditions under which it

was initially calibrated. Future comparisons of OFD and PVM response under a variety of conditions might permit better calibration of the OFD response for varying cloud/fog types and drop size distributions.

## **Acknowledgements**

The authors gratefully acknowledge Professor Barry Huebert and Ms. Karin Schlappa from the University of Hawaii for hosting the Hawaiian portion of this work and for providing their PVM data, as well as Prof. Randy Borys at Storm Peak Laboratory for providing access to the Storm Peak Laboratory site. Major support for this work was provided by NSF grant ATM-9980540. Additional support was provided by the San Joaquin Valleywide Air Pollution Study Agency and NSF grant ATM-0222607. The statements and conclusions in this paper are those of the contractor and are not necessarily those of the California Air Resources Board, the San Joaquin Valleywide Air Pollution Study Agency, or its policy committee, their employees or members. The mention of commercial products, their source, or their use in connection with material reported herein is not to be construed as actual or implied endorsements of said products.

## **References**

- Arends, B. G., Kos, G. P. A., Wobrock, W., Schell, D., Noone, K. J., Fuzzi, S. and Pahl, S., 1992. Comparison of techniques for measurements of fog liquid water content. *Tellus* 44B 604-611.
- Borys, R. D. and Wetzel, M. A., 1997. Storm peak laboratory: A research, teaching, and service facility for the atmospheric sciences. *Bulletin of the American Meteorological Society* 78 (10), 2115-2123.
- Carrillo, J. H., Hastings, M. G., Sigman, D. M. and Huebert, B. J., 2002. Atmospheric deposition of inorganic and organic nitrogen and base cations in Hawaii. *Global Biogeochemical Cycles* 16 (4), doi:10.1029/2002GB001892.

- Collett, J. L., Daube, B. C. and Hoffmann, M. R., 1990. The chemical composition of intercepted cloudwater in the Sierra Nevada. *Atmospheric Environment Part a-General Topics* 24 (4), 959-972.
- Emert, S. (2001) Design, construction, and evaluation of the CSU Optical Fog Detector. MS Thesis, Colorado State University.
- Fuzzi, S., Cesari, G., Evangelisti, F., Facchini, M. C. and Orsi, G., 1990. An automatic station for fog water collection. *Atmospheric Environment* 24A (10), 2609-2614.
- Gerber, H., 1991. Direct measurement of suspended particulate volume concentration and far-infrared extinction coefficient with a laser-diffraction instrument. *Applied Optics* 30 (33), 4824 - 4831.
- Herckes, P., Lee, T., Trenary, L., Kang, G. G., Chang, H. and Collett, J. L., 2002. Organic matter in Central California radiation fogs. *Environmental Science & Technology* 36 (22), 4777-4782.
- Mallant, R. K. A. M., 1988. Poor man's optical fog detector. *Annalen der Meteorologie* 25 (1), 333-334.

## Figure Captions

**Figure 1.** CSU OFD with the weatherproof NEMA box in the open position to show the internal components.

**Figure 2.** OFD and PVM signals during glovebox testing with artificial fog. Signal differences may partially be due to spatial inhomogeneities in fog LWC within the glovebox.

**Figure 3.** Five minute averaged OFD versus PVM response for the 3 cloud interception events sampled at SPL. Both OFDs showed a high degree of correlation with the PVM.

**Figure 4.** PVM and OFD baselines for a 3 day period with no cloud at SPL.

**Figure 5.** OFD versus PVM response for the 1 radiation fog event sampled at ANG.  $R_{eff}$  is calculated from the PVM LWC and PSA signals.

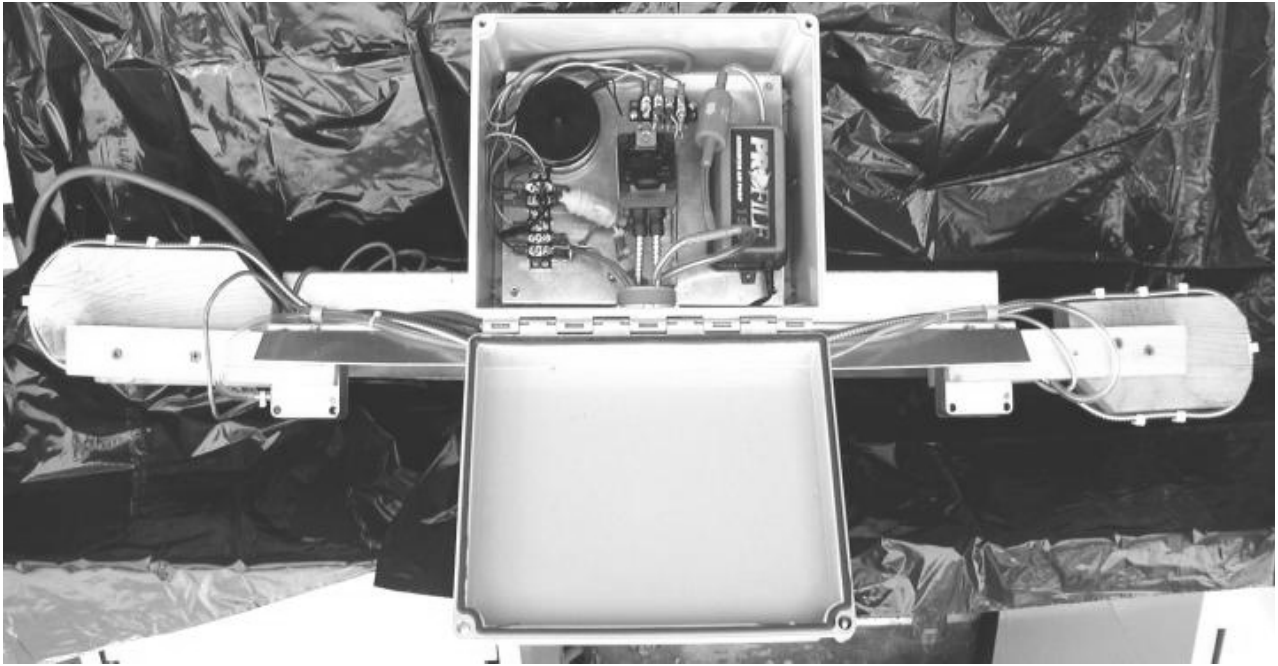
**Figure 6.** The OFD/PVM LWC versus the effective radius of cloud drops at ANG.

**Figure 7.** The OFD and PVM LWC plotted for all events at TLT.

**Figure 8.** The OFD/PVM LWC ratio versus  $R_{eff}$  for sampled clouds at TLT.

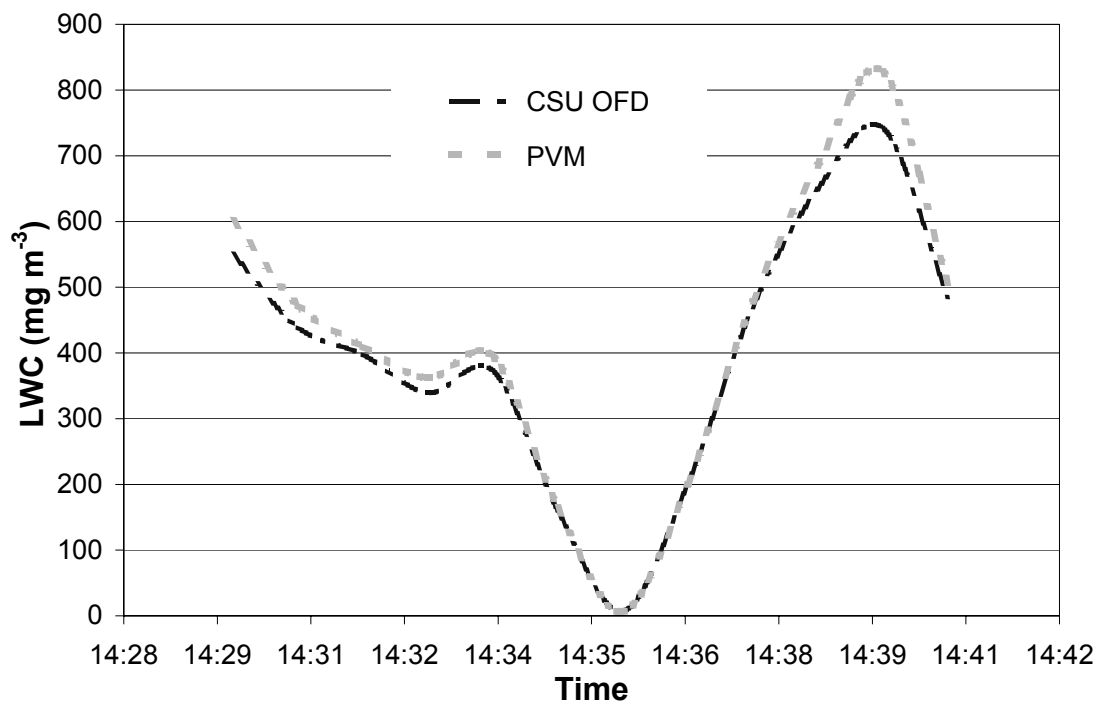
**Figure 9.** LWC and rain signals at TLT. The dates on the x-axis mark the beginning of each day at midnight.

**Figure 10.** OFD versus PVM LWC for the rain-free event of April 29 at TLT.

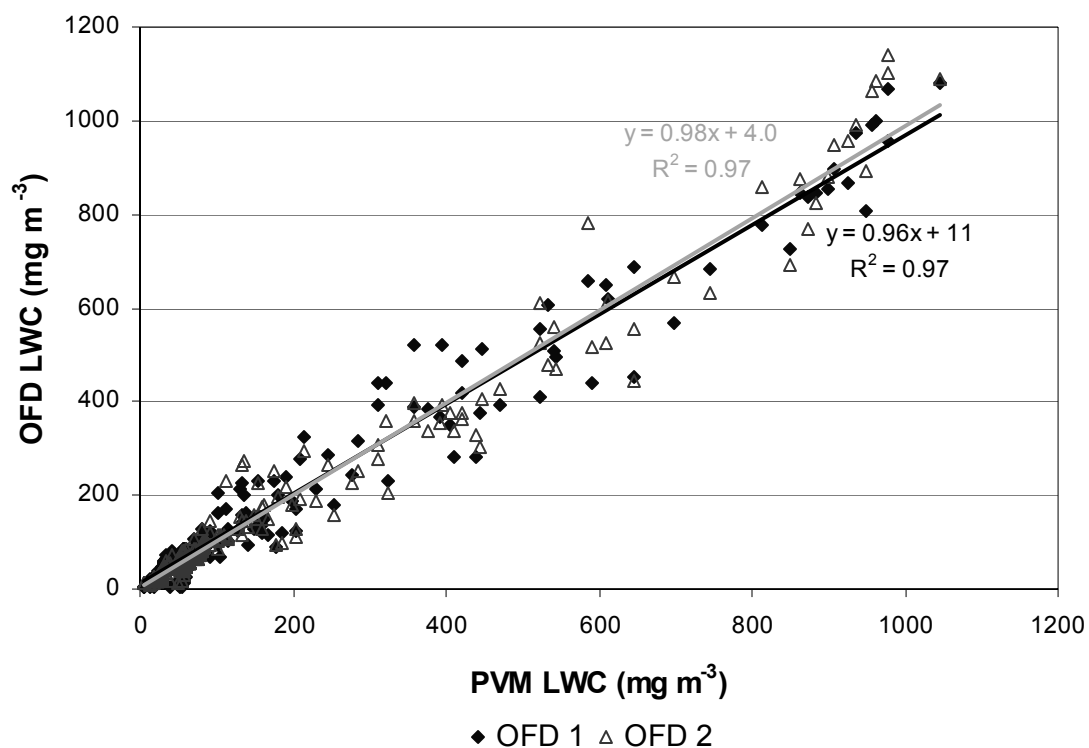


**Figure 1.** CSU OFD with the weatherproof NEMA box in the open position to show the internal components.

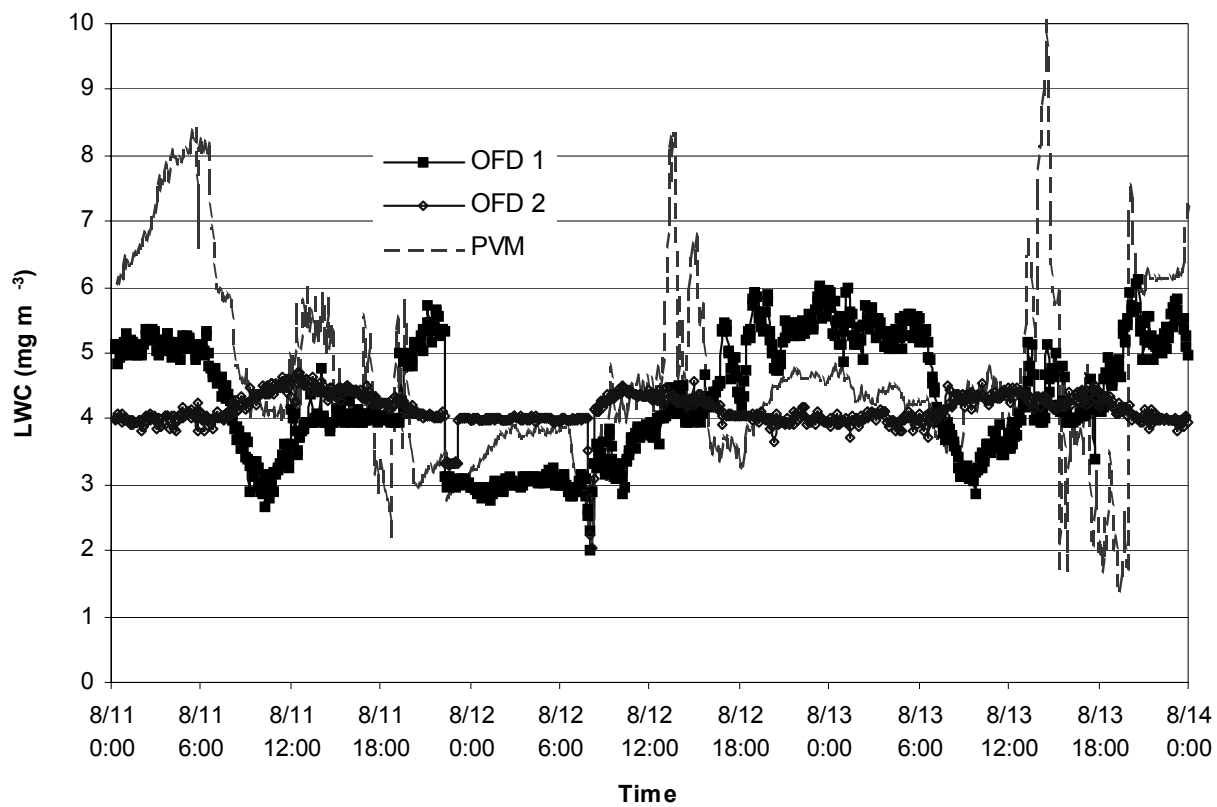




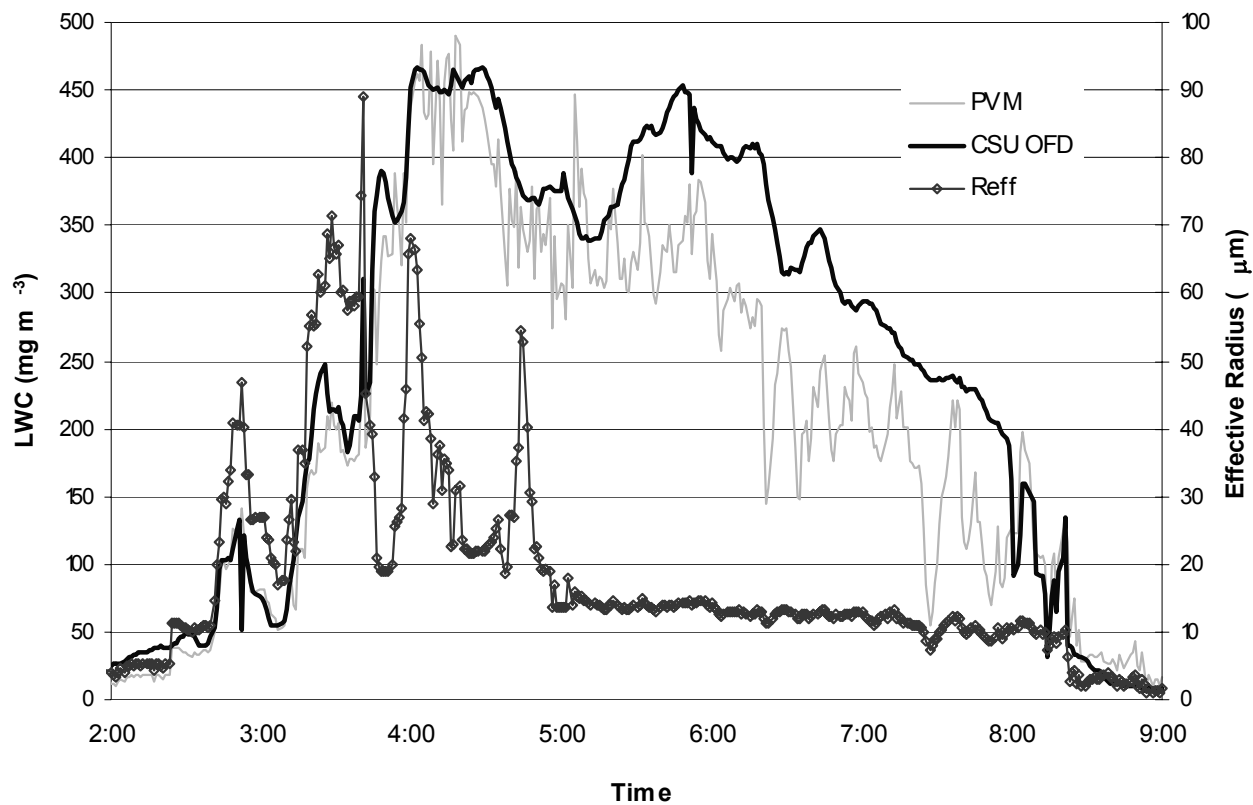
**Figure 2.** OFD and PVM signals during glovebox testing with artificial fog. Signal differences may partially be due to spatial inhomogeneities in fog LWC within the glovebox.



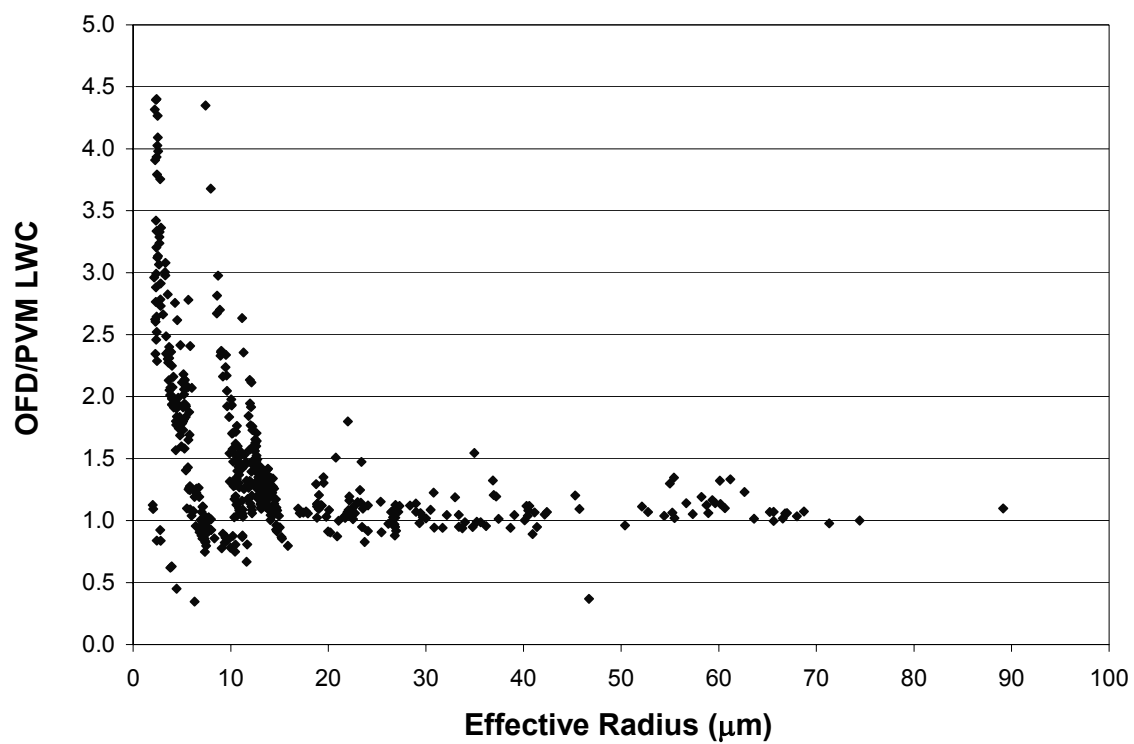
**Figure 3.** Five minute averaged OFD versus PVM response for the 3 cloud interception events sampled at SPL. Both OFDs showed a high degree of correlation with the PVM.



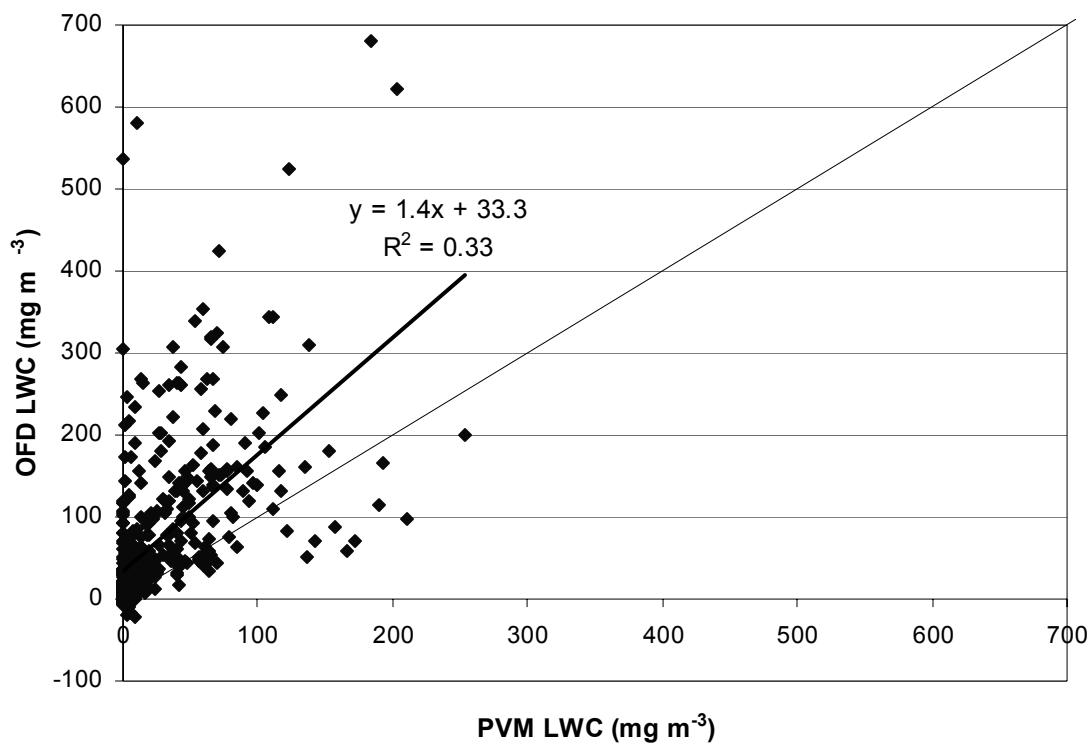
**Figure 4.** PVM and OFD baselines for a 3 day period with no cloud at SPL.



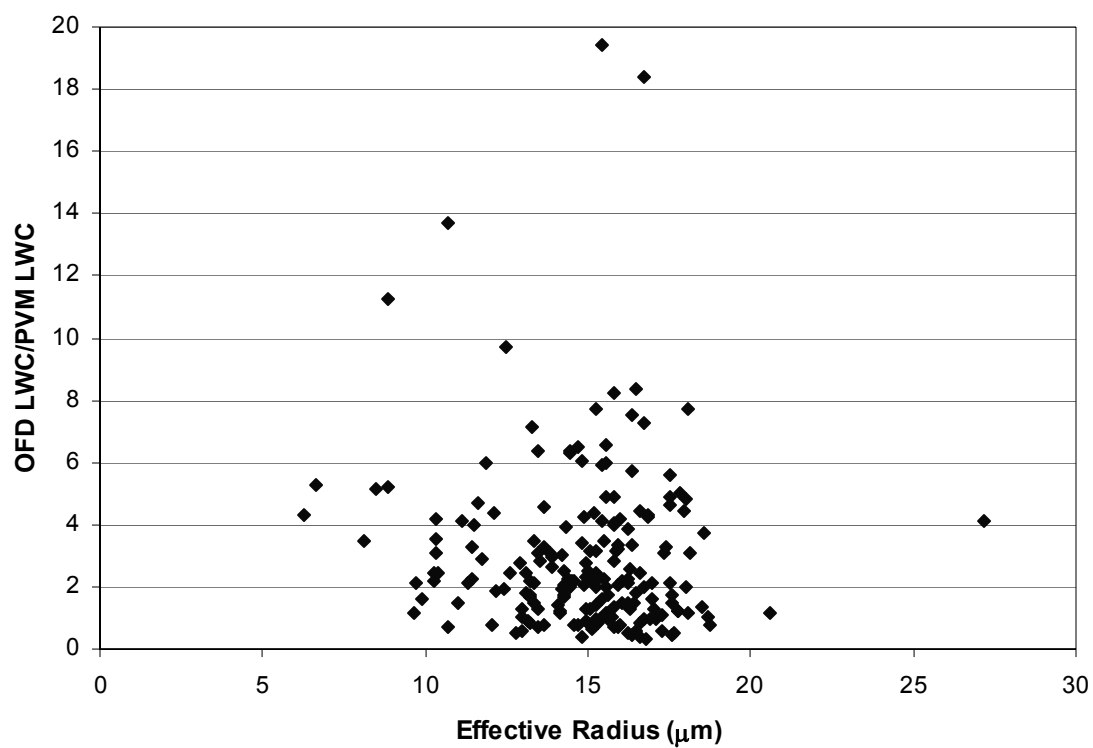
**Figure 5.** OFD versus PVM response for the 1 radiation fog event sampled at ANG. Reff is calculated from the PVM LWC and PSA signals.



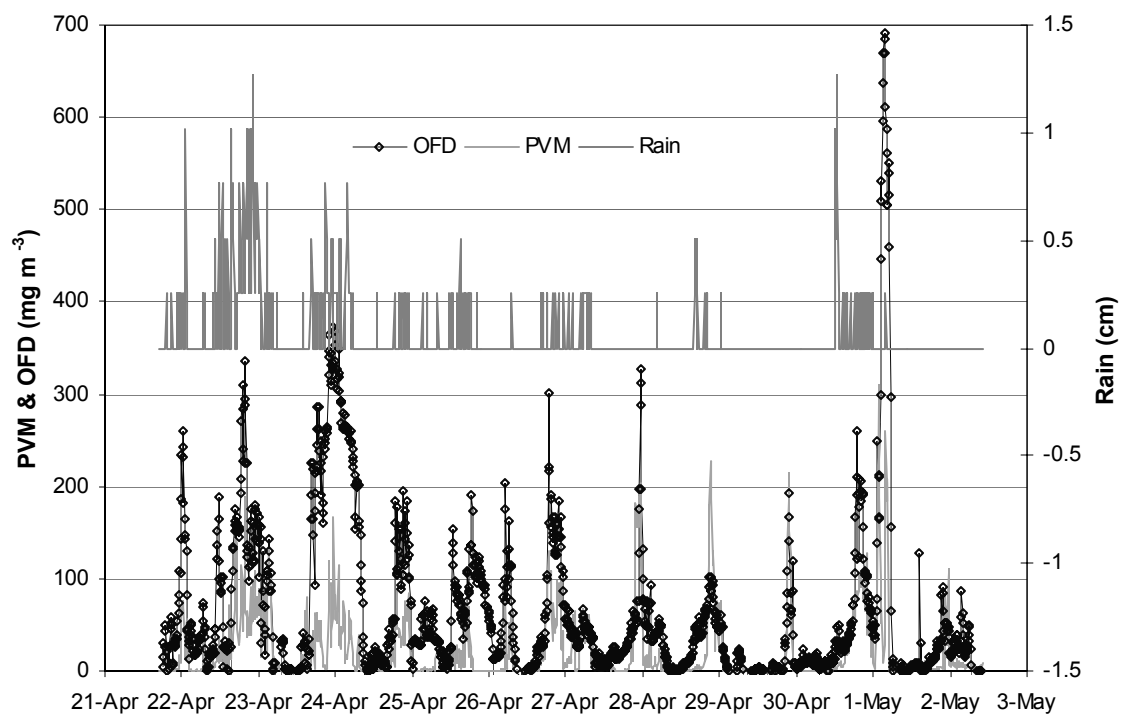
**Figure 6.** The OFD/PVM LWC versus the effective radius of cloud drops at ANG.



**Figure 7.** The OFD and PVM LWC plotted for all events at TLT.

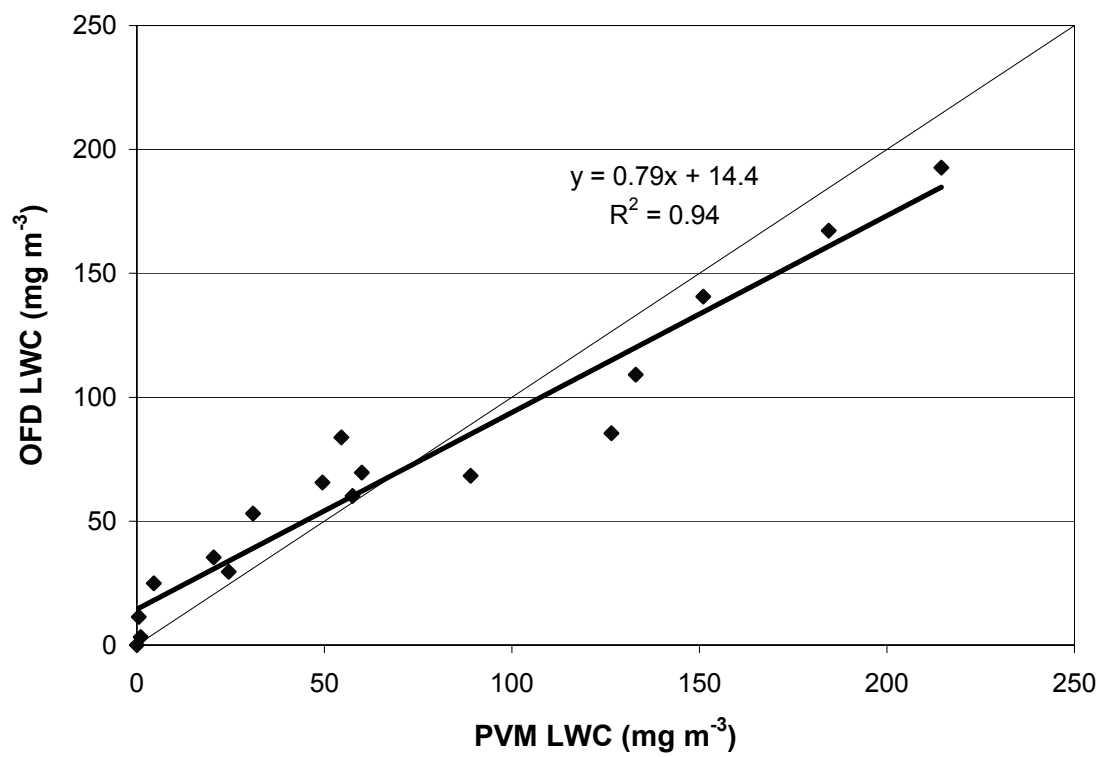


**Figure 8.** The OFD/PVM LWC ratio versus Reff for sampled clouds at TLT.



**Figure 9.** LWC and rain signals at TLT. The dates on the x-axis mark the beginning of each day at midnight.





**Figure 10.** OFD versus PVM LWC for the rain-free event of April 29 at TLT.

# Organic Matter in Central California Radiation Fogs

PIERRE HERCKES,<sup>†</sup> TAEHYOUNG LEE,<sup>†</sup>  
LAURIE TRENARY,<sup>†</sup> GONGUNN KANG,<sup>‡</sup>  
HUI CHANG,<sup>†</sup> AND  
JEFFREY L. COLLETT, JR.\*<sup>†</sup>

*Atmospheric Science Department, Colorado State University,  
Fort Collins, Colorado 80523, and Department of  
Environmental Industry, Wonkwang Health Science College,  
Chonbuk, Korea*

Organic matter was studied in radiation fogs in the San Joaquin Valley of California during the California Regional Particulate Air Quality Study (CRPAQS). Total organic carbon (TOC) concentrations ranged from 2 to 40 ppm of C. While most organic carbon was found in solution as dissolved organic carbon (DOC), 23% on average was not dissolved inside the fog drops. We observe a clear variation of organic matter concentration with droplet size. TOC concentrations in small fog drops ( $<17\ \mu\text{m}$ ) were a factor of 3, on average, higher than TOC concentrations in larger drops. As much as half of the dissolved organic matter was determined to have a molecular weight higher than 500 Da. Deposition fluxes of organic matter in fog drops were high ( $0.5\text{--}4.3\ \mu\text{g of C m}^{-2}\text{ min}^{-1}$ ), indicating the importance of fog processing as a vector for removal of organic matter from the atmosphere. Deposition velocities of organic matter, however, were usually found to be lower than deposition velocities for fogwater, consistent with the enrichment of the organic matter in smaller fog drops with lower terminal settling velocities.

## Introduction

Over the last 20 years, many investigators have examined the chemical compositions of clouds and fogs and studied cloud/fog processing of atmospheric particles (1–4). Some studies have shown the ability of fogs to create new particulate material through gas scavenging, in-cloud reactions to form low volatility products, and subsequent drop evaporation. Fogs have also been shown to remove particles through particle scavenging followed by drop deposition. Most studies, however, have focused on processing of inorganic compounds. Little is known about the organic composition of cloud and fog drops or the processing of organic compounds by fogs and clouds.

Understanding interactions between fogs or clouds and carbonaceous aerosol particles is important for several reasons. First, it is known that organic matter comprises a large fraction of total fine particulate matter in many environments (5). Second, it is also known that interactions with precipitating clouds are a principal determinant of accumulation mode particle lifetimes. Third, activation of carbonaceous aerosol particles to form cloud drops may significantly alter optical properties of clouds and fogs with

associated effects on cloud optical depth and climate. Fourth, it is possible that aqueous reactions occurring in cloud or fog drops are important sources of secondary organic aerosol formation (6). At present, our lack of knowledge regarding interactions between carbonaceous aerosol particles and clouds (or fogs) greatly limits our ability to understand or model atmospheric processing and effects of this important class of particles.

Capel and co-workers (7) showed that fogwater collected in Duebendorf, Switzerland, contained up to 290 ppm of carbon. Subsequent studies confirmed the importance of organic matter in fog and cloud drops (1, 8). Some of these studies differentiated between total and dissolved organic carbon and found that a very large fraction of the total organic carbon was soluble. Nevertheless, the composition and the physical and chemical properties of this organic matter remain largely unknown. Although several studies have examined fog or cloud drop concentrations of specific organic compound families [e.g., pesticides (9), phenols (10), methoxyphenols (11), polycyclic aromatic hydrocarbons, alkanes (12)], these compounds represent only a small fraction of the total organic matter present. Herckes and co-workers (13) have shown that low molecular weight organic compounds (especially formaldehyde, formate, and acetate) are present at high concentrations in radiation fogs in California's Central Valley, yet they comprise only 10–15% of the total organic matter present.

In more recent studies, investigators have attempted to further characterize the organic composition of fogwater. Kiss and co-workers characterized polar compounds by liquid chromatography with UV and mass spectrometric detection (14). There have also been efforts to characterize more of the higher molecular weight compounds in fogwater, including humic substances (8, 15). Zhang and Anastasio (16) have also demonstrated the presence of high concentrations of organic nitrogen in California's Central Valley fog samples.

Another topic receiving increased attention in recent years is the variation of solute concentrations across the fog/cloud drop size spectrum. Drop size-dependent composition is now well-established for inorganic solutes (17–20); however, little attention has been paid to drop size dependence of TOC concentrations or individual organic solute concentrations, with the exception of formaldehyde (21). Variations in solute concentrations across the fog drop size spectrum exert an important influence on solute deposition fluxes (22) since fog drop deposition velocities increase strongly with drop size, mainly due to the higher terminal settling velocities of larger drops.

In this paper, we present the first observations of the variation of organic matter content with drop size as well as new findings concerning the characteristics of organic matter in fog drops. The fogs sampled in this study were radiation fogs, which form by radiative cooling of the surface during clear sky conditions at night. These differ from advection fogs, which form in conjunction with transport of warm, moist air masses over a colder surface. Samples were collected during winter 2000/2001 as part of the California Regional Particulate Air Quality Study (CRPAQS). We focus on the variations in organic carbon concentrations with drop size, the partitioning of organic carbon between soluble and insoluble phases inside fog drops, and the molecular weight distribution of the dissolved organic carbon. Fog-borne deposition fluxes of organic matter are determined and compared to fluxes of inorganic species.

\* Corresponding author e-mail: collett@lamar.colostate.edu; telephone: (970)491-8697; fax: (970)491-8449.

<sup>†</sup> Colorado State University.

<sup>‡</sup> Wonkwang Health Science College.

## Experimental Section

Fog samples were collected in December 2000 and January 2001 in the Central Valley of California as part of CRPAQS. The core sampling site for the fog study was located close to the small town of Angiola [35°35' N, 119°32' W, 60 m above sea level (asl)]. Satellite collection sites were established in Bakersfield (35°21' N, 119°3' W, 119 m asl) and close to the town of Helm (36°5' N, 120°10' W, 55 m asl). The Angiola and Helm sites were located in agricultural areas, whereas the Bakersfield site was located in the city next to a small shopping mall.

Fog samples were collected with various collectors, including the Caltech Active Strand Cloudwater Collector (CASCC), the two-stage version of that collector known as the size-fractionating CASCC (sf-CASCC), and the compact version of the CASCC known as CASCC2. These samplers collect fog/cloud drops by inertial impaction on banks of Teflon strands (CASCC, CASCC2, or second stage of sf-CASCC) or rods (first stage of sf-CASCC). The CASCC2 was used for fog collection at the Helm and Bakersfield sites. Detailed descriptions of the CASCC, CASCC2, and sf-CASCC are given by Demoz et al. (23). In addition, newly developed stainless steel (ss) versions of the CASCC and sf-CASCC, known as the ss-CASCC and ss-sf-CASCC, were utilized in order to provide samples more suitable for analysis of organic compounds. The size cuts of the ss-sf-CASCC are estimated as approximately 6 and 17  $\mu\text{m}$ . The metal collectors were cleaned with solvents and baked in order to reduce contamination by organic compounds.

Fog liquid water content (LWC) was measured using a Gerber Scientific particulate volume monitor (model PVM-100) that was calibrated using a manufacturer-supplied disk. Fog deposition was sampled using two square Teflon deposition plates (0.30 m<sup>2</sup>) placed on top of a large plastic sheet on the ground. This technique proved to be efficient in the California radiation fogs where sedimentation is the major deposition pathway (22). Collected fogwater was sampled from the interior of the plates; a trough is milled near the perimeter of the plate to provide a defined collection area.

Immediately after sample collection, the pH of the samples was measured. Right after collection, aliquots were taken for measurement of total organic carbon (TOC). The samples were then filtered through pre-fired quartz filters (Pallflex Tissuquartz), and an aliquot of the filtrate was created for a dissolved organic carbon (DOC) measurement. The TOC and DOC aliquots were stored, refrigerated and in the dark, in prebaked glass vials until analysis. Contamination of the collectors, of the deionized water (prepared on-site using a Barnstead EasyPure system) used for cleaning, and by the filtration procedure was checked regularly by means of field blanks.

Organic carbon concentrations (TOC and DOC) were determined using a commercial TOC analyzer (Shimadzu TOC 5000A), which oxidizes organic carbon in an injected sample on a catalyst bed at 680 °C, followed by measurement of the evolved carbon dioxide. The TOC analyzer was calibrated using a series of aqueous potassium hydrogen phthalate standards; measurement precision was evaluated through replicate sample analyses.

In some samples, the organic matter was further characterized by ultrafiltration of the DOC fraction. Physical separation of DOC into molecular size ranges was completed in a pressurized and stirred ultrafiltration cell (Amicon model 8050), using the following Millipore ultrafiltration membranes: YM1 (nominal size cut of 1000 Da) and YC05 (nominal size cut of 500 Da). The filtrates were analyzed for TOC as described above. The separation efficiency of the two membranes was tested with tannic acid (MW = 1700) and

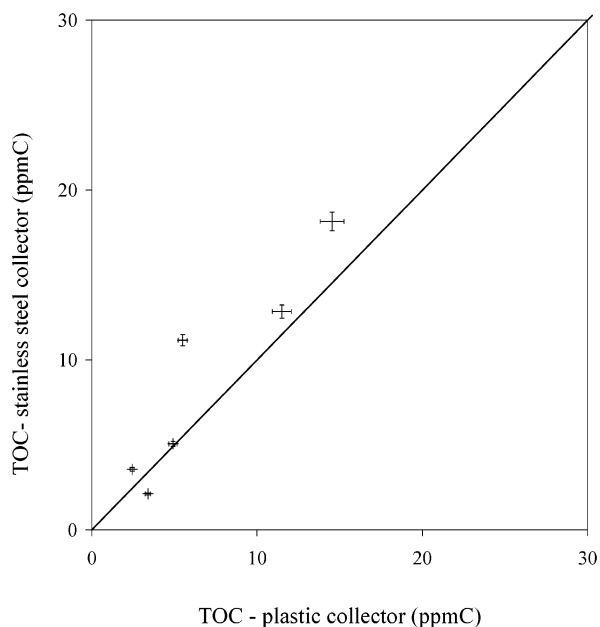


FIGURE 1. TOC concentrations in Angiola fog samples collected using stainless (ss-CASCC) and Teflon (CASCC) fog collectors. Error bars represent the TOC measurement precision (one relative standard deviation) of 5%.

naringin hydrate (MW = 581) for the 1000 MW and 500 MW cut-sizes, respectively. The YM1 membrane showed a separation efficiency of 48% relative to tannic acid, whereas the YM05 showed a 71% efficiency relative to naringin hydrate. These results show that the nominal membrane size-cuts provide only an approximate indication of the size of the organic matter retained. The effective separation depends on the structure of the solute molecule in addition to its molecular weight. DOC fractionation using the membranes will be used to provide an approximate indication of the molecular weight distribution of the organic solutes in the fogwater, although a systematic tendency to underestimate the higher molecular weight fractions appears to exist.

## Results and Discussion

**Comparison between Plastic and Metal Fog Collector Samples.** Previous studies focusing on the inorganic composition of fog mainly used plastic collectors to sample fogwater. Teflon is often considered a material of choice for collection surfaces. TOC concentrations have sometimes been reported in samples collected with plastic collectors (1, 16, 24). To test whether the use of Teflon versus stainless steel sampling surfaces yields a difference in measured sample TOC, concentrations were compared in fog samples obtained simultaneously with two CASCC collectors: one plastic (CASCC) and the other stainless steel (ss-CASCC). The results are illustrated in Figure 1.

Higher TOC concentrations were typically observed in samples collected with the stainless steel collector. This is probably the result of a modest adsorption loss on the plastic collector surfaces rather than contamination by the metal collector surfaces. Field blanks from both types of collector are in the same range and very low (<MDL to 0.5 ppm C for the stainless steel collector and 0.1–0.4 ppm C for the plastic collector). Adsorption of black material was observed visually on the Teflon collection surfaces and could only be removed by cleaning with a surfactant. This blackening of plastic collection surfaces is commonly observed when sampling fogwater in polluted environments. The apparent adsorption of carbonaceous material on plastic collector surfaces suggests that use of these collector types for fog/cloud TOC

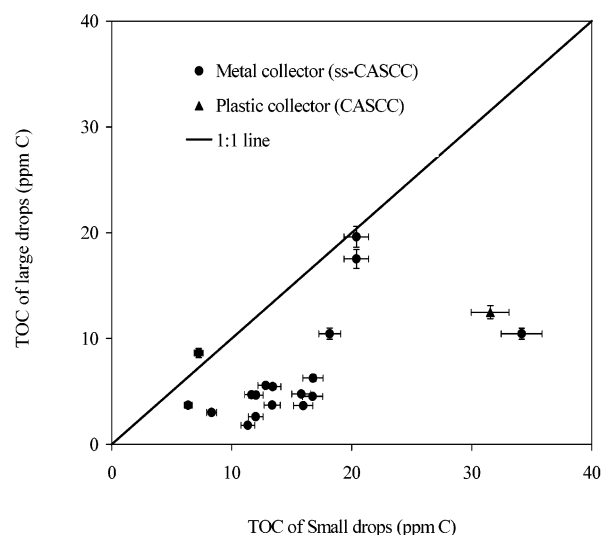


FIGURE 2. TOC concentrations in small (approximately  $4 < D < 17 \mu\text{m}$ ) vs large (approximately  $D > 17 \mu\text{m}$ ) fog drops. Error bars represent the TOC measurement precision (one relative standard deviation) of 5%.

measurements produces a modest negative bias in reported concentrations.

**TOC Variation with Droplet Size.** TOC concentrations were measured in large (approximately  $D > 17 \mu\text{m}$ ) and small (approximately  $6 < D < 17 \mu\text{m}$ ) fog drops collected simultaneously by the two stages of the stainless steel size-fractionating CASCC at the Angiola site. The results, presented in Figure 2, reveal that the TOC concentrations are usually much higher in the small drops with an average enrichment factor (small drop/large drop concentration ratio) of 2.8 (range: 0.8–6.3). A similar enrichment in small drops of most inorganic ions has been previously reported and modeled for San Joaquin Valley fogs (1, 18, 25). Higher TOC concentrations in small drops may result from several possible factors, including formation of small fog drops on smaller aerosol particles that are more likely to contain a significant carbonaceous fraction. Nonequilibrium enrichment of highly soluble gases in small drops is also possible because of their preferential uptake by smaller drops with their higher surface-to-volume ratios and long time scales to reequilibrate across the drop size spectrum. Enrichment of formaldehyde in small drops in San Joaquin Valley radiation fogs has been previously reported (21).

**Comparison of TOC and DOC.** Only a portion of atmospheric organic matter is water soluble (26). Many organic compounds found in carbonaceous aerosol particles are strongly hydrophobic and insoluble. Carbonaceous aerosol particles scavenged by fog drops may contain a mixture of organic compounds that is entirely, or only partially, soluble. Insoluble organic compounds may, for example, represent a small portion of an otherwise hygroscopic cloud condensation nucleus that is activated to grow into a fog drop or a larger fraction of a hydrophobic, nonactivated particle scavenged by a fog drop through a mechanism other than nucleation.

Fog samples collected at the Angiola site were filtered to determine the fraction of TOC dissolved inside fog drops. Figure 3 compares TOC and DOC concentrations in bulk cloudwater (ss-CASCC) as well small and large fog droplets collected by the ss-sf-CASCC. The average DOC/TOC ratio was 0.77, indicating that while most of the organic material was typically in solution, a significant fraction was often present as insoluble material inside the drops. The average organic carbon soluble fraction measured here (77%) is lower than observed by Capel and co-workers in Duebendorf,

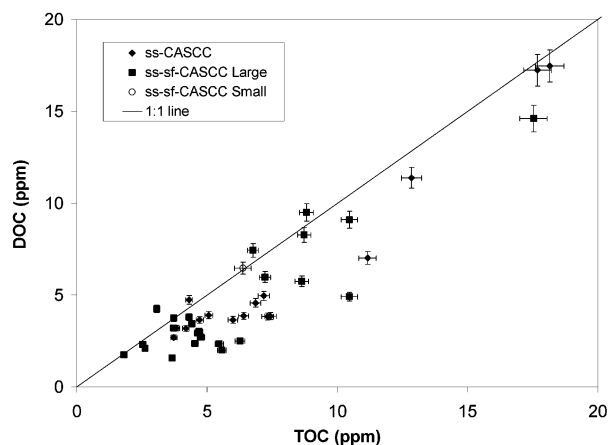


FIGURE 3. TOC vs DOC concentrations in Angiola, CA, radiation fogs. Error bars represent the TOC measurement precision (one relative standard deviation) of 5%.

Switzerland (93–97%) (7). The difference in soluble fraction probably reflects a difference in the composition of organic matter in fogs collected at the two sites but could also be influenced by any difference in filtration efficiency between the studies. TOC concentrations observed in the Duebendorf fogs were much higher (78–281 mg/L) than those found in this study (2–40 mg/L). The presence of a significant insoluble organic fraction highlights the need to consider both soluble and insoluble phases in fog droplets when evaluating carbonaceous aerosol scavenging efficiencies.

**Comparison of TOC Concentrations.** Table 1 compares organic carbon concentrations measured in fog and cloud TOC and DOC concentrations previously reported in the literature. Note that a significant fraction of fog/cloud organic carbon concentrations reported in the literature come from various sites in California.

TOC concentrations in fog samples collected at the rural Angiola site in this study range from 2 to 41 ppm C. Fog samples collected at the second rural site (Helm) also fall within this range. Only one fog sample was collected at the more urban Bakersfield site; its TOC concentration was 27 ppm C, relatively high but within the range measured at Angiola. The concentrations found in this study are similar to the concentration ranges observed in previous investigations of radiation fogs in California's Central Valley (see Table 1 for San Joaquin Valley, Bakersfield, and Davis). Studies of stratiform clouds in southern California (see Henninger Flats and San Pedro in Table 1) have also reported roughly similar concentrations (24). The TOC concentrations observed in this study are somewhat lower than reported in northern Italy's Po Valley (7, 30), where concentrations as high as 108 ppm C have been observed. Even higher organic carbon concentrations have been measured in Duebendorf, Switzerland (outside Zurich), and in Alaska, while much lower concentrations were reported by Hadi and co-workers (31) for cloudwater collected in rural Scotland. Concentrations reported for intercepted cloud samples collected at mountain sites in the eastern (Whiteface Mt., Mt. Mitchell, and Shenandoah) and western (Stampede Pass) United States all fall in the lower half of the range observed at Angiola.

Some concentration differences may result from differences in liquid water content, a parameter that is often not measured or reported. As liquid water content increases in a fog or cloud, solute concentrations typically decrease (33, 34) because of dilution. This trend is apparent for TOC concentrations in the fog samples collected at Angiola. Figure 4 shows that the highest TOC concentrations are observed for the lowest liquid water contents and vice-versa. The anti-



TABLE 1. TOC Concentrations Observed in Fog and Cloud Samples Collected in Different Locations

location	TOC (ppm of C) avg (min–max)	comments	ref
Angiola (20 samples)	10.1 (2.1–41)	ss-CASCC	this study
Helm (6 samples)	6.2–16.2	CASCC2	this study
Bakersfield (1 sample)	26.6	CASCC2	this study
San Joaquin Valley (CA)	5–41	TOC	1
Bakersfield (CA)	8.5–276		27
San Pedro (CA)	12.1 (7.1–19.5)	CASCC	24
Henninger Flats (CA)	14	1 sample	24
Davis (CA)	4–45	TOC	13
Davis (CA)	32.5 (5–111)	DOC	16
Mount Mitchell (NC)	2–6.4	DOC	28
Whiteface Mountain (NY)	11.7 (3.2–18)	DOC	28
Shenandoah Park (VA)	6.7–10.7	DOC	28
Stampede Pass (WA)	7.2 (3.8–10.6)	DOC	28
Tenerife (Canary Islands, Spain)	4.6–5.3	DOC, 2 samples	16
Po Valley (Italy)	15–108	stainless steel active collector	8
Po Valley (Italy)	50 (30–100)	DOC	29
Alaska (USA)	200	water-soluble org carbon/ice fog	30
Scotland	0.7–14	DOC, "harp-wire collector"	31
Duebendorf (Switzerland)	78–281	passive Teflon collector	7
Austria	4.81 (1–14)	organic carbon	32

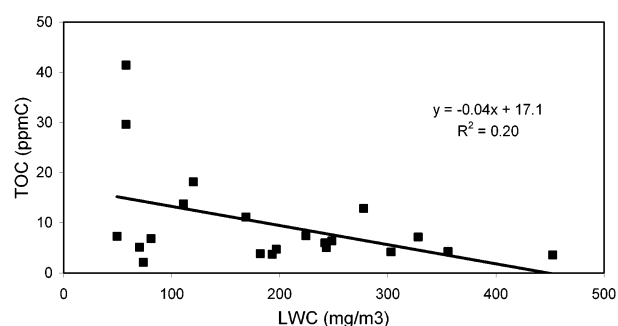


FIGURE 4. TOC vs liquid water content for Angiola fog samples collected with the ss-CASCC during the CRPAQS campaign.

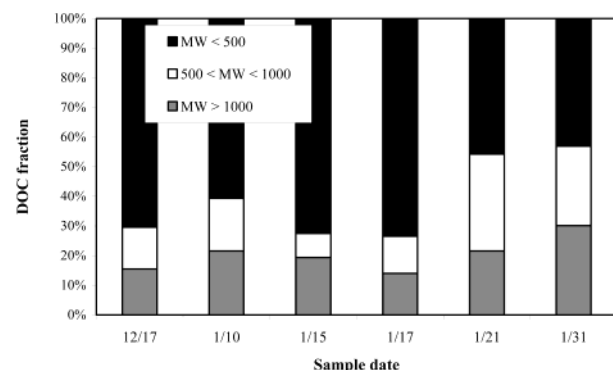


FIGURE 5. Molecular weight (MW) distribution of the dissolved organic matter in several Angiola bulk fogwater samples.

correlation of LWC and TOC yields a correlation coefficient of 20% and is significant at the 95% level; however, it is clear that a simple linear solute dilution model does not explain most of the concentration variability present. Differences in precursor atmospheric concentrations of carbonaceous aerosol particles and soluble organic gases are also important determinants of fog/cloud TOC concentrations.

**Molecular Weight Fractionation of the Organic Matter.** Figure 5 shows the molecular weight (MW) distributions of the organic matter in bulk fog samples collected by the CASCC during six Angiola fog events. These distributions were measured on sample fractions treated by ultrafiltration as described above. The fraction of compounds with MW > 500 is significant, varying from 27% to 57% in these samples. These results are somewhat surprising, as higher MW organic

compounds are often thought to be relatively hydrophobic, but they are consistent with observations that low MW compounds such as formaldehyde, acetate, and formate account generally for less than 20% of the organic matter in fog and cloud drops (13, 32). The importance of high MW material is also supported by previous work that revealed significant concentrations of humic material in fog drops (14).

High molecular weight organic material has also been found to be an important contributor to precipitation composition. Likens and co-workers, using ultrafiltration to characterize organic matter in precipitation (35), found that 42% of the DOC in precipitation collected at a rural site (Hubbard Brook, NH) and 54% of the DOC in precipitation collected at an urban location (Ithaca, NY) had a molecular weight higher than 1000. These percentages are slightly higher than in the Angiola fogs, perhaps reflecting the high efficiency of precipitation scavenging of coarse soil dust particles, but confirm the importance of high molecular weight organic compounds in atmospheric water droplets.

**Deposition Fluxes of Organic Carbon.** Previous studies have shown the importance of fog deposition as a removal process for inorganic aerosol species. To evaluate fog deposition fluxes of organic matter, TOC concentrations of deposited fogwater collected from deposition plates in this study were multiplied by the corresponding fogwater fluxes. Sedimentation is believed to dominate the fog deposition flux to these plates. It is possible that additional turbulent fluxes may occur to rougher natural surfaces, but this effect is expected to be minor because of low wind speeds (<1 m/s) and low surface roughness typical of the study region. Resulting TOC deposition fluxes range from 0.5 to 4.3  $\mu\text{g}$  of C  $\text{m}^{-2} \text{min}^{-1}$  and averaged 1.5  $\mu\text{g}$  of C  $\text{m}^{-2} \text{min}^{-1}$ . To our knowledge, these represent the first reported measurements of organic carbon deposition by radiation fogs. The fluxes are comparable to fogwater deposition fluxes of major inorganic species, including ammonium (average of 1.7  $\mu\text{g}$   $\text{m}^{-2} \text{min}^{-1}$ ) and nitrate (2.2  $\mu\text{g}$   $\text{m}^{-2} \text{min}^{-1}$ ) observed in the study. Similar fluxes were also reported for radiation fogs in Davis (California) (22), with average values of 2.2  $\mu\text{g}$   $\text{m}^{-2} \text{min}^{-1}$  (ammonium) and 4.3  $\mu\text{g}$   $\text{m}^{-2} \text{min}^{-1}$  (nitrate).

The high fog deposition fluxes of organic carbon observed here support the important role fogs play as processors of carbonaceous aerosol in the boundary layer. We highlight this role further with one example. During the night of December 17–18, 2000, a fog event occurred that lasted more than 13 h. Total fogwater deposition in this event exceeded

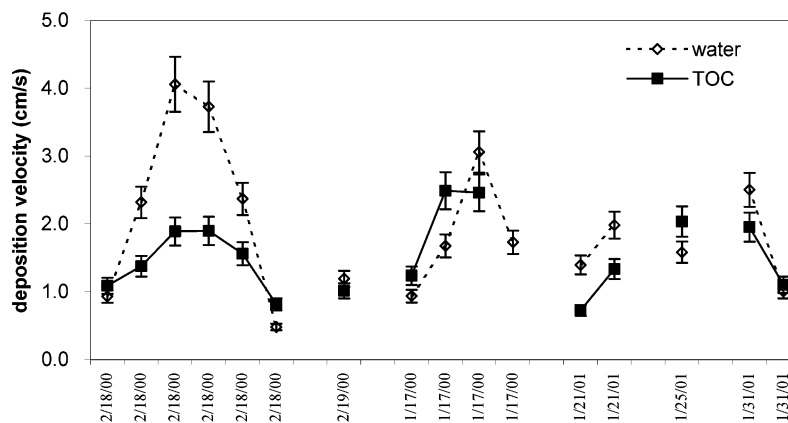


FIGURE 6. Fogwater and fog TOC deposition velocities. Multiple listings of the same date correspond to multiple samples collected during that fog event. Error bars represent the average standard deviation of replicate samples from two collocated deposition plates.

294 g/m<sup>2</sup> while organic carbon deposition in fog drops exceeded 1.2 mg of C/m<sup>2</sup>. If we assume an average fog depth of 100 m for this event, this corresponds to an average reduction of more than 12 µg of C/m<sup>3</sup> over the fog depth, a considerable amount in an environment with typical aerosol concentrations in the range of tens of micrograms of C per cubic meter. Of course some of the organic carbon removed by the fog is associated with volatile species, like formaldehyde, that may return to the gas phase once the deposited fog evaporates.

**Deposition Velocities.** Deposition velocities were determined for fogwater and fog-borne organic carbon. The TOC deposition velocity was calculated according to the following equation:

$$v_{\text{TOC}} = \frac{\text{Flux}_{\text{TOC}}}{\text{LWC} \times [\text{TOC}]_{\text{aq}}}$$

where  $v_{\text{TOC}}$  is the TOC deposition velocity,  $\text{flux}_{\text{TOC}}$  is the measured flux of TOC to the deposition plates, LWC is the fog liquid water content, and  $[\text{TOC}]$  is the aqueous concentration in the simultaneously collected fog sample.

Calculated deposition velocities are presented in Figure 6. Fogwater deposition velocities ranged from 0.5 to 6 cm/s, comparable to previous observations (22) in central California radiation fogs. The TOC deposition velocity is generally similar to or smaller than the fogwater deposition velocity. The tendency for the fogwater deposition velocity to exceed the TOC deposition velocity is expected given the enrichment of TOC in small fog drops that settle from the atmosphere more slowly. Measurements of inorganic species during the present study show similar deposition velocities for sulfate (1.5 cm/s on average). Larger differences between solute and fogwater deposition velocities were reported in earlier radiation fog studies at Davis, CA (22), consistent with stronger enrichments of inorganic solutes in small fog drops (concentrations up to 20 times as high as observed in large drops) in those fogs.

## Acknowledgments

We are grateful to E. Sherman for his contributions to the design of the new stainless steel collectors and for assistance in the preparation of the field project. We are grateful to J. Reilly and S. Emert for assistance during the field experiment. This work was funded by the National Science Foundation (ATM-9980540) and the San Joaquin Valleywide Air Pollution Study Agency. The statements and conclusions in this paper are those of the Contractor and not necessarily those of the California Air Resources Board, the San Joaquin Valleywide Air Pollution Study Agency, or its Policy Committee, their

employees, or their members. The mention of commercial products, their source, or their use in connection with material reported herein is not to be construed as actual or implied endorsement of such products.

## Literature Cited

- (1) Collett, J. L.; Hoag, K. J.; Sherman, D. E.; Bator, A.; Richards, L. W. *Atmos. Environ.* **1999**, *33*, 129–140.
- (2) Collett, J. L.; Daube, B. C.; Gunz, D.; Hoffmann, M. R. *Atmos. Environ.* **1990**, *24*, 1741–1757.
- (3) Fuzzi, S.; Facchini, M. C.; Orsi, G.; Bonforte, G.; Martinotti, W.; Ziliani, G.; Mazzali, P.; Rossi, P.; Natale, P.; Grosa, M. M.; Rampado, E.; Vitali, P.; Raffaelli, R.; Azzini, G.; Grotti, S. *Atmos. Environ.* **1996**, *30*, 201–213.
- (4) Fuzzi, S. *J. Atmos. Chem.* **1994**, *19*, 1–2.
- (5) Heintzenberg, J. *Tellus B* **1989**, *41*, 149–160.
- (6) Blando, J. D.; Turpin, B. J. *Atmos. Environ.* **2000**, *34*, 1623–1632.
- (7) Capel, P. D.; Gunde, R.; Zurcher, F.; Giger, W. *Environ. Sci. Technol.* **1990**, *24*, 722–727.
- (8) Gelencser, A.; Sallai, M.; Krivacsy, Z.; Kiss, G.; Meszaros, E. *Atmos. Res.* **2000**, *54*, 157–165.
- (9) Millet, M.; Wortham, H.; Sanusi, A.; Mirabel, P. *Environ. Sci. Pollut. Res.* **1997**, *4*, 172–180.
- (10) Luttke, J.; Levsen, K. *Atmos. Environ.* **1997**, *31*, 2649–2655.
- (11) Sagebiel, J. C.; Seiber, J. N. *Environ. Toxicol. Chem.* **1993**, *12*, 813–822.
- (12) Capel, P. D.; Leuenberger, C.; Giger, W. *Atmos. Environ.* **1991**, *25*, 1335–1346.
- (13) Herckes, P.; Hannigan, M. P.; Trenary, L.; Lee, T. Y.; Collett, J. L. *Atmos. Res.* **2002**, *64*, 99–108.
- (14) Kiss, G.; Varga, B.; Gelencser, A.; Krivacsy, Z.; Molnar, A.; Alsberg, T.; Persson, L.; Hansson, H. C.; Facchini, M. C. *Atmos. Environ.* **2001**, *35*, 2193–2200.
- (15) Krivacsy, Z.; Kiss, G.; Varga, B.; Galambos, I.; Sarvari, Z.; Gelencser, A.; Molnar, A.; Fuzzi, S.; Facchini, M. C.; Zappoli, S.; Andrachio, A.; Alsberg, T.; Hansson, H. C.; Persson, L. *Atmos. Environ.* **2000**, *34*, 4273–4281.
- (16) Zhang, Q.; Anastasio, C. *Atmos. Environ.* **2001**, *35*, 5629–5643.
- (17) Millet, M.; Sanusi, A.; Wortham, H. *Environ. Pollut.* **1996**, *94*, 345–354.
- (18) Bator, A.; Collett, J. L. *J. Geophys. Res. [Atmos.]* **1997**, *102*, 28071–28078.
- (19) Laj, P.; Fuzzi, S.; Lazzari, A.; Ricci, L.; Orsi, G.; Berner, A.; Dusek, U.; Schell, D.; Guenther, A.; Wendisch, M.; Wobrock, W.; Frank, G.; Martinsson, B.; Hillamo, R. *Contrib. Atmos. Phys.* **1998**, *71*, 115–130.
- (20) Gieray, R.; Wieser, P.; Engelhardt, T.; Swietlicki, E.; Hansson, H. C.; Montes, B.; Orsini, D.; Martinsson, B.; Svenningsson, B.; Noone, K. J.; Heintzenberg, J. *Atmos. Environ.* **1997**, *31*, 2491–2502.
- (21) Rao, X.; Collett, J. L. *Environ. Sci. Technol.* **1995**, *29*, 1023–1031.
- (22) Collett, J.; Sherman, D. E.; Moore, K.; Hannigan, M. P.; Lee, T. Y. *Water Air Soil Pollut.: Focus* **2001**, *1*, 303–312.
- (23) Demoz, B. B.; Collett, J. L.; Daube, B. C. *Atmos. Res.* **1996**, *41*, 47–62.

- (24) Erel, Y.; Pehkonen, S. O.; Hoffmann, M. R. *J. Geophys. Res. [Atmos.]* **1993**, *98*, 18423–18434.
- (25) Hoag, K. J.; Collett, J. L.; Pandis, S. N. *Atmos. Environ.* **1999**, *33*, 4817–4832.
- (26) Decesari, S.; Facchini, M. C.; Fuzzi, S.; Tagliavini, E. *J. Geophys. Res. [Atmos.]* **2000**, *105*, 1481–1489.
- (27) Jacob, D. J.; Waldman, J. M.; Munger, J. W.; Hoffmann, M. R. *Tellus B* **1984**, *36*, 272–285.
- (28) Anastasio, C.; Faust, B. C.; Allen, J. M. *J. Geophys. Res. [Atmos.]* **1994**, *99*, 8231–8248.
- (29) Fuzzi S.; Zappoli S. *12th International Conference on Clouds and Precipitation*; International Commission on Clouds and Precipitation of the International Association of Meteorology and Atmospheric Sciences: Zurich, Switzerland, 1996; pp 1077–1079.
- (30) Grosjean, D.; Wright, B. *Atmos. Environ.* **1983**, *17*, 2093–2096.
- (31) Hadi, D. A.; Crossley, A.; Cape, J. N. *Environ. Pollut.* **1995**, *88*, 299–306.
- (32) Loflund, M.; Kasper-Giebl, A.; Schuster, B.; Giebl, H.; Hitzinger, R.; Puxbaum, H. *Atmos. Environ.* **2002**, *36*, 1553–1558.
- (33) Elbert, W.; Hoffmann, M. R.; Kramer, M.; Schmitt, G.; Andreae, M. O. *Atmos. Environ.* **2000**, *34*, 1109–1122.
- (34) Moller, D.; Acker, K.; Wieprecht, W. *Atmos. Res.* **1996**, *41*, 321–335.
- (35) Likens, G. E.; Edgerton, E. S.; Galloway, J. N. *Tellus B* **1983**, *35*, 16–24.

*Received for review June 17, 2002. Revised manuscript received August 30, 2002. Accepted September 10, 2002.*

ES025889T

# On the use of anion exchange chromatography for the characterization of water soluble organic carbon

Hui Chang, Pierre Herckes, and Jeffrey L. Collett Jr.

Department of Atmospheric Science, Colorado State University, Fort Collins, Colorado, USA

Received 23 August 2004; revised 12 November 2004; accepted 10 December 2004; published 14 January 2005.

[1] An increasingly popular anion exchange chromatography method [Decesari *et al.*, 2000] was used to separate organic matter in fog samples and water soluble organic carbon (WSOC) extracted from aerosol samples according to acidity. Analysis of both fog and aerosol WSOC samples showed results similar to previous studies, with peaks typically identified as corresponding to neutral/basic compounds, mono- and dicarboxylic acids and polyacids. In one example this approach was shown to classify a total of 82% of the WSOC into these three chromatographic fractions. Challenges to the classification scheme were made by injection of single compound solutions. Compounds were chosen to be representative of compounds observed in atmospheric samples. In many cases test compounds eluted in fractions other than expected based on classifying compound structure according to the three classes outlined above. The impact of classification errors is impossible to quantify without understanding the complete organic speciation of a sample, but is serious enough that researchers relying on this method to provide a suitable model for organic aerosol composition should interpret results with caution. The most severe problems are likely for fog samples, due to a prevalence of low molecular weight carboxylic acid and carbonyl compounds which exhibit greater tendency to be misclassified. **Citation:** Chang, H., P. Herckes, and J. L. Collett Jr. (2005), On the use of anion exchange chromatography for the characterization of water soluble organic carbon, *Geophys. Res. Lett.*, 32, L01810, doi:10.1029/2004GL021322.

## 1. Introduction

[2] A large part of the organic matter in fogs, clouds and aerosol particles remains unspcated and poorly characterized [e.g., Fuzzi *et al.*, 2002; Herckes *et al.*, 2002a; Loflund *et al.*, 2002]. Recently various attempts have been made to characterize water soluble atmospheric organic matter by different chromatographic and spectroscopic techniques [e.g., Krivacsy *et al.*, 2000; Decesari *et al.*, 2000, 2001; Krivacsy *et al.*, 2001; Fuzzi *et al.*, 2002]. Decesari *et al.* [2000] proposed anion exchange chromatography to fractionate fog samples and water-soluble organic carbon (WSOC) into three fractions: neutral/basic compounds, mono- and dicarboxylic acids and polyacidic compounds. This methodology was sometimes accompanied by further classification using <sup>1</sup>H-NMR. The developed separation protocol was initially applied to fog and aerosol samples from northern Italy, but has been subsequently applied in

other locations as well [Mayol-Bracero *et al.*, 2002]. Results from these promising efforts, which separate a majority of the water soluble organic carbon (WSOC) into three distinct, chromatographic fractions, are widely used to justify choices of representative organic aerosol model compounds [Fuzzi *et al.*, 2001; Brooks *et al.*, 2004].

[3] In the present study the same anion exchange chromatography approach is applied to fog and aerosol samples. Method challenges utilizing individual compound solutions are also used to evaluate the peak classification scheme.

## 2. Experimental

[4] Fog samples were collected in Fresno, California in winter 2003/4 with stainless steel versions of the Caltech Active Strand Cloudwater Collector [Herckes *et al.*, 2002b]. Aerosol samples were collected in Yosemite National Park, California and in Fort Collins, Colorado using a Hi-volume aerosol sampler (ThermoAndersen, Smyrna, GA) loaded with pre-fired quartz fiber filters. WSOC extracts of the aerosol samples were obtained by sonicating twice a portion of a quartz fiber filter for 20 minutes and refiltering the extract through a pre-fired quartz fiber filter. Typical total filter extraction volumes and resulting WSOC extract concentrations were on the order of 50 ml and 50 ppmC, respectively. Test organic compound solutions were prepared from commercially available high purity chemicals.

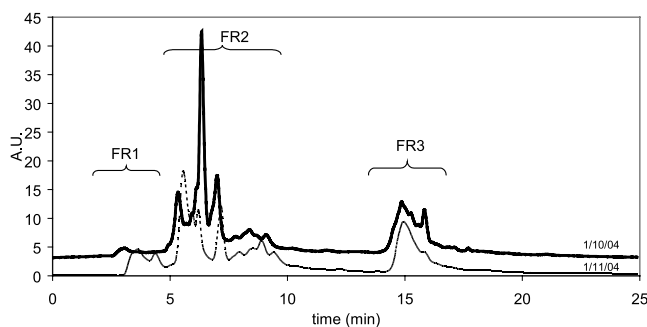
### 2.1. Analytical Separation

[5] WSOC aerosol extracts and fog samples were separated according to the procedure described by Decesari *et al.* [2000]. The method has been reported by these investigators to yield three WSOC fractions which have been characterized as containing neutral/basic compounds, mono- and dicarboxylic acids and polyacidic compounds. Samples were separated on a Tosoh TSK DEAE-5PW gel column (7.5 mm ID, 7.5 cm length). The initial mobile phase was deionized water. From 0.2 minutes to 2 minutes, the solvent composition was linearly increased to 0.02M NaClO<sub>4</sub>, 0.02M TRIS, 10% methanol. This eluent was kept constant until 10 minutes, then linearly changed to the final composition at 15 minutes of 0.4M NaClO<sub>4</sub>, 0.02M TRIS and 10% methanol. The pH was constant at 8. Separation and detection were performed on an HP Model 1050 HPLC equipped with a diode array detector. Absorbance was monitored at 254 nm.

### 2.2. Semi-preparative Scale Fractionation

[6] In a second step we performed separations of larger quantities of sample using a semi-preparative scale column packed with a DEAE-cellulose gel (Amersham HiPrep 16/10 DEAE). We performed a step-wise elution,





**Figure 1.** DEAE separation chromatograms of two Fresno (CA) fog samples collected on January 10th and January 11th 2004 (baseline shifted for sample 1/10/04 for clarity).

identical to *Decesari et al.* [2000], collecting the unretained sample (fraction 0), then eluting with de-ionized water (fraction 1), a 0.05 M  $\text{NaHCO}_3$  buffer (fraction 2 –FR2) and finally a 1.0 M  $\text{NaHCO}_3$  buffer (fraction 3–FR3). Fraction 0 and fraction 1 were combined to form “FR1”. The eluting fractions were collected in 10–25 ml subfractions and analyzed for total organic carbon (TOC) after acidifying the solutions to pH 2 and purging with high purity nitrogen for a minimum of 15 minutes to remove carbonate and bicarbonate. TOC analysis was performed using a Shimadzu TOC analyzer (model 5000A) calibrated with potassium hydrogen phthalate standards.

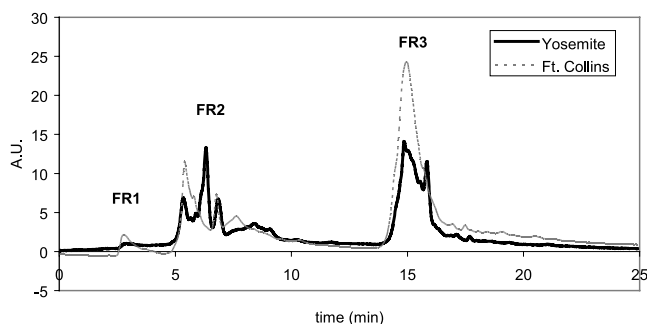
### 3. Results and Discussion

#### 3.1. Analytical Separation of Authentic Samples

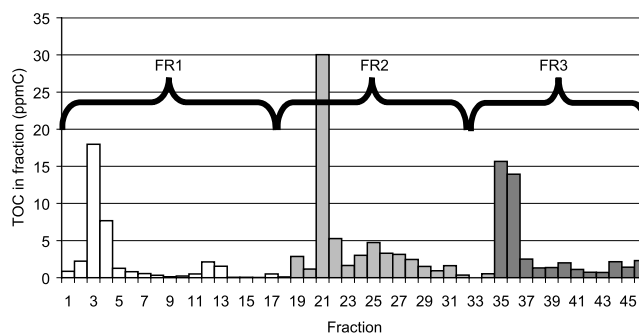
[7] The anion exchange chromatograms obtained for fog samples (Figure 1) and WSOC aerosol extracts (Figure 2) are similar to results published by *Decesari et al.* [2000]. One can distinguish 3 peak zones, previously attributed as FR1 (corresponding to *neutrals*), FR2 (corresponding to *mono and dicarboxylic acids plus nitrate*) and FR3 (*polyacidic compounds*). In WSOC aerosol extracts from Yosemite National Park and Fort Collins, the peaks in the third fraction are the largest; in the fog samples fraction 2 peaks are largest.

#### 3.2. Semi-preparative Scale Separation of Authentic Samples

[8] The semi-preparative scale separation method was applied to a WSOC aerosol extract from Fort Collins



**Figure 2.** DEAE chromatogram of one Yosemite National Park (CA) aerosol WSOC samples, collected on August 14th 2002 and one Fort Collins (CO) aerosol WSOC sample collected on June 28, 2002.



**Figure 3.** Organic carbon elution off the column for a Fort Collins (CO) aerosol WSOC sample from June 28, 2002.

(Figure 3). The most abundant fraction, measured by TOC content, is the second, typically assigned as mono and dicarboxylic acids. FR2 accounts for 44% of the WSOC; FR1 and FR3 account for 17 and 21%, respectively. Total organic carbon recovery for this sample was 82%. These results are consistent with similar studies in the Po Valley of Italy and in the Amazon (Table 1). The ability of this approach to classify >80% of the aerosol WSOC into three distinct chromatographic fractions indicates its utility as a simple way to classify WSOC from aerosols or clouds. It is not surprising, therefore, that results obtained using this methodology appeal to aerosol scientists struggling to devise relevant descriptions of the complex composition of organic atmospheric aerosols.

#### 3.3. Test Separations of Model Compound Solutions

[9] We tested peak classification for the analytical separation by analyzing single compound solutions. As target compounds we tested species reported in previous studies of fog, cloud or WSOC aerosol extracts [*Sagebiel and Seiber*, 1993; *Aneja*, 1993; *Herckes et al.*, 2002a; *Loflund et al.*, 2002], that are suspected of being present [*Blando and Turpin*, 2000] or that have been proposed as model organic aerosol compounds [*Fuzzi et al.*, 2001]. These include various carbonyls, acids, phenolic compounds and aromatics. Results in Table 2 demonstrate that many model compounds elute in fractions other than expected from the *Decesari et al.* [2000] classification system.

[10] Methylglyoxal is a main organic component of fog in polluted environments [*Munger et al.*, 1995]. Recent measurements in urban California fogs indicate that methylglyoxal can comprise several percent of fog TOC. We expected methylglyoxal to elute in the “neutral” fraction. It was observed, however, to yield four different peaks in FR1 and FR2. The multi-peak response may result from methylglyoxal reaction at the high elution pH, possibly forming pyruvic acid and other products. Separate tests of methylglyoxal stability in the eluent matrix did not reveal rapid degradation; however, degradation reactions might be accelerated on column.

[11] Formic and acetic acids are commonly observed in fog samples [*Ervens et al.*, 2003], frequently comprising 10–20% of fog dissolved organic carbon (DOC). We expected these low molecular weight carboxylic acids to elute in the “mono and dicarboxylic acid” fraction; however, they eluted in FR1, typically attributed to neutral compounds.

**Table 1.** Importance of the Different Fractions as Observed in Various Studies

Location	FR1 neutral	FR2 – mono and di-acids	FR3 - polyacids	Reference
Amazonia	21%	51%		Mayol-Bracero <i>et al.</i> [2002]
Po Valley, Italy	25%	35%	17%	Decesari <i>et al.</i> [2000]
Fort Collins, USA	17%	44%	21%	This study

[12] Most tested compounds were observed to elute in FR2, attributed to mono and dicarboxylic acids. However, only a few of these test compounds actually contain carboxylic acid groups. For example, phenol and many other compounds containing an OH group elute in FR2 or even in FR3. Many of these compounds feature phenolic groups with  $pK_a$  values around 8 and are partly dissociated at the eluent pH of 8. The negative charges produced by deprotonation of the hydroxy groups allows these compounds to interact with the anion exchange column, slowing their elution from the column as a carboxylic acid might be expected to behave.

[13] The charge interaction effect is probably not the only property impacting the separation. Benzene, for example, elutes in FR3 and not with the “neutral” compounds in FR1. Ethylguaiacol and cresol also elute in this later part of the chromatogram, commonly attributed to polyacidic compounds. The classification of zones in the DEAE separation chromatograms into neutral, mono and dicarboxylic and polyacidic fractions appears to be oversimplified.

[14] Phenolic compounds can be an important part of atmospheric organic matter. They have been speciated in studies looking at fog [Sagebiel and Seiber, 1993; Herckes *et al.*, 2002a] and at aerosol particles emitted by biomass burning [Schauer *et al.*, 1996, 2001; Simoneit, 2002]. We have also found that carbonyl compounds and carboxylic acids can comprise a large fraction (up to 30%) of the organic content of fogwater.

**Table 2.** Expected and Observed Elution Fractions for Selected Organic Compounds

Compound	Retention Time (min)	Expected Fraction <sup>a</sup>	Observed Fraction
Methyl glyoxal	2.8, 5.5, 7.4, 14.8	1	1, 2
Acetone	2.9	1	1
Acetic acid	3.0	2	1
Formic acid	3.0	2	1
Acridine	4.5	1	1
Pyruvic acid	5.5	2	2
Pinonic acid	5.6	2	2
Syringaldehyde	7.5	1	2
Vanillin	7.8	1	2
Oxalic acid	7.8	2	2
Succinic acid	8.7	2	2
Phthalic acid	8.7	2	2
3-hydroxybenzoic acid	8.8	2	2
Syringol	9.0	1	2
Aniline	9.4	1	2
Catechol	10.0	1	2
Guaiacol	10.6	1	2
o-Nitrophenol	11.7	1	2
Benzaldehyde	11.9	1	2
Phenol	12.9	1	2
Humic Acid (Fluka)	15.5	3	3
Tannic Acid	16.3	3	3
Benzene	17.0	1	3
4-Ethylguaiacol	17.4	1	3
m-Cresol	17.9	1	3

<sup>a</sup>Based on the compound structure and the peak attribution by Decesari *et al.* [2000].

[15] We should emphasize that use of UV detection provides only a qualitative overview of sample composition, due to the large range of organic compound absorbance efficiencies at 254 nm. As an example, molar absorptivities of formic and acetic acids are much smaller than those of methoxyphenols or aromatic compounds. Because of this limitation, the analytical fractionation has not been used quantitatively in previous work.

[16] A quantitative assessment of the different fractions is usually performed after separation on a semi-preparative scale column, followed by TOC measurement. Accordingly we evaluated the separation at the semi-preparative scale level by challenging the method with individual compounds (Table 3). We chose acetic and oxalic acid (typically the most abundant mono and dicarboxylic acids, respectively, in fog [Ervens *et al.*, 2003]); vanillin, an abundant methoxyphenol [Sagebiel and Seiber, 1993]; a model humic acid; levoglucosan, frequently the most abundant individual organic species determined in aerosol particles; catechol and hydroxybenzoic acid, two compounds proposed as model organics [Fuzzi *et al.*, 2001]; and glyoxal and methylglyoxal, two dicarbonyls, abundant in fog samples.

[17] Acetic acid eluted in the second fraction as expected, indicating that the analytical scale and semi-preparative scale methods do not produce identical separations. In the analytical separation the acetic acid appears to elute at a very weak eluent concentration (less than 0.02 M salt). Because FR1 is eluted only with water in the semi-preparative method, acetic acid ends up eluting in FR2. Oxalic acid and hydroxybenzoic acid elute in the “correct” fraction, FR2. Vanillin and catechol, as in the analytical separation, elute in FR2 rather than FR1; their behavior can be explained by deprotonation at the high eluent pH and interaction with the anion exchange column. The dicarbonyls elute in FR2 rather than FR1. The model humic acid eluted in the polyacidic fraction but part of it is so strongly retained that it never elutes off the column. Levoglucosan, as expected from its structure, elutes in the neutral fraction, FR1.

[18] The preparative-scale separation with step elution appears to produce results more consistent with expectations than the analytical separation. Nevertheless we cannot exclude a significant bias of the results due to incorrect elution of model phenolic compounds. Our lack of understanding of the complete speciation of organic matter in

**Table 3.** Elution of Single Compounds From the DEAE Prep Scale Column

Compound	Expected Fraction	Observed Fraction
Levoglucosan	1	1
Vanillin	1	2
Catechol	1	2
Glyoxal	1	2
Methylglyoxal	1	2
4-hydroxybenzoic acid	2	2
Oxalic acid	2	2
Acetic acid	2	2
Humic acid	3	3

fogs and aerosol particles (typically no more than 20% of the OC is speciated) makes it impossible to accurately evaluate impacts of peak misclassification. For fog and cloud samples, there might be a significant bias due to apparent reactivity of dicarbonyls on the column. These issues might be less problematic for ambient aerosol samples if the concentration of phenolic compounds is small, but still significant for biomass burning aerosol with its large content of lignin derived, phenolic type structures.

#### 4. Conclusions

[19] Anion exchange chromatography was used for the fractionation of organic matter in fog samples and WSOC aerosol extracts. Analysis of authentic fog samples and aqueous aerosol extracts gave similar results to previous studies from other regions. In one example 82% of the WSOC in an aerosol extract was successfully separated into three distinct chromatographic fractions. The ability to classify a large fraction of aerosol organic carbon into three distinct fractions is a real advantage of this approach for aerosol scientists struggling to develop realistic models of organic aerosol composition.

[20] The main limitation of the method as previously applied appears to be an oversimplified description of the composition of the three chromatographic fractions as neutral/basic compounds, mono and dicarboxylic acids and polyacids. Tests with single compound solutions revealed many compound types are misclassified by this assignment of peak characteristics. Misclassified compounds analyzed in an analytical scale application of the separation include low molecular weight carboxylic acids (classified as neutral/basic) and several compounds without carboxyl groups, including phenols, carbonyls, and aromatics (classified as mono/dicarboxylic acids and/or polyacids). Some misclassifications can be explained by deprotonation of compound hydroxyl groups at the high pH present in the eluent, resulting in significant interactions with the anion exchange column. Misclassification problems appear to be somewhat less for the preparative scale separation, with carboxylic acids in particular being better characterized.

[21] Misclassification problems are probably most severe for fog samples, due to the abundance of low molecular weight carbonyls and carboxylic acids. The separation technique should give a more reasonable picture for aerosol extracts when combined with TOC quantification of the eluted fractions. Caution is warranted, however, in interpretation of quantitative results from DEAE anion exchange chromatography and further testing is recommended to better characterize the compositions of the chromatographic fractions.

[22] **Acknowledgments.** We are grateful to T. Lee, S. Youngster, A. Simpson, G. Engling, B. Ayres, and J. Carrillo of CSU for assistance. This work was supported by the National Science Foundation (ATM-0222607). Some samples were obtained with support from the National Park Service.

#### References

- Aneja, V. P. (1993), Organic-compounds in-cloud water and their deposition at a remote continental site, *J. Air Waste Manage. Assoc.*, **43**, 1239–1244.
- Blando, J. D., and B. J. Turpin (2000), Secondary organic aerosol formation in cloud and fog droplets: A literature evaluation of plausibility, *Atmos. Environ.*, **34**, 1623–1632.
- Brooks, S. D., P. J. DeMott, and S. M. Kreidenweis (2004), Water uptake by particles containing humic materials and mixtures of humic materials with ammonium sulfate, *Atmos. Environ.*, **38**, 1859–1868.
- Decesari, S., M. C. Facchini, S. Fuzzi, and E. Tagliavini (2000), Characterization of water-soluble organic compounds in atmospheric aerosol: A new approach, *J. Geophys. Res.*, **105**, 1481–1489.
- Decesari, S., M. C. Facchini, E. Matta, F. Lettini, M. Mircea, S. Fuzzi, E. Tagliavini, and J. P. Putaud (2001), Chemical features and seasonal variation of fine aerosol water-soluble organic compounds in the Po Valley, Italy, *Atmos. Environ.*, **35**, 3691–3699.
- Ervens, B., P. Herckes, G. Feingold, T. Lee, J. L. Collett, and S. M. Kreidenweis (2003), On the drop-size dependence of organic acid and formaldehyde concentrations in fog, *J. Atmos. Chem.*, **46**, 239–269.
- Fuzzi, S., S. Decesari, M. C. Facchini, E. Matta, M. Mircea, and E. Tagliavini (2001), A simplified model of the water soluble organic component of atmospheric aerosols, *Geophys. Res. Lett.*, **28**, 4079–4082.
- Fuzzi, S., M. C. Facchini, S. Decesari, E. Matta, and M. Mircea (2002), Soluble organic compounds in fog and cloud droplets: What have we learned over the past few years?, *Atmos. Res.*, **64**, 89–98.
- Herckes, P., M. P. Hannigan, L. Trenary, T. Y. Lee, and J. Collett (2002a), Organic compounds in radiation fogs in Davis (California), *Atmos. Res.*, **64**, 99–108.
- Herckes, P., T. Lee, L. Trenary, G. G. Kang, H. Chang, and J. L. Collett (2002b), Organic matter in central California radiation fogs, *Environ. Sci. Technol.*, **36**, 4777–4782.
- Krivacsy, Z., et al. (2000), Study of humic-like substances in fog and interstitial aerosol by size-exclusion chromatography and capillary electrophoresis, *Atmos. Environ.*, **34**, 4273–4281.
- Krivacsy, Z., et al. (2001), Study on the chemical character of water soluble organic compounds in fine atmospheric aerosol at the Jungfraujoch, *J. Atmos. Chem.*, **39**, 235–259.
- Loflund, M., A. Kasper-Giebl, B. Schuster, H. Giebl, R. Hitznerberger, and H. Puxbaum (2002), Formic, acetic, oxalic, malonic and succinic acid concentrations and their contribution to organic carbon in cloud water, *Atmos. Environ.*, **36**, 1553–1558.
- Mayol-Bracero, O. L., P. Guyon, B. Graham, G. Roberts, M. O. Andreae, S. Decesari, M. C. Facchini, S. Fuzzi, and P. Artaxo (2002), Water-soluble organic compounds in biomass burning aerosols over Amazonia: 2. Apportionment of the chemical composition and importance of the polyacidic fraction, *J. Geophys. Res.*, **107**(D20), 8091, doi:10.1029/2001JD000522.
- Munger, J. W., D. J. Jacob, B. C. Daube, L. W. Horowitz, W. C. Keene, and B. G. Heikes (1995), Formaldehyde, glyoxal, and methylglyoxal in air and cloudwater at a rural mountain site in central Virginia, *J. Geophys. Res.*, **100**, 9325–9333.
- Sagebiel, J. C., and J. N. Seiber (1993), Studies on the occurrence and distribution of wood smoke marker compounds in foggy atmospheres, *Environ. Toxicol. Chem.*, **12**, 813–822.
- Schauer, J. J., W. F. Rogge, L. M. Hildemann, M. A. Mazurek, and G. R. Cass (1996), Source apportionment of airborne particulate matter using organic compounds as tracers, *Atmos. Environ.*, **30**, 3837–3855.
- Schauer, J. J., M. J. Kleeman, G. R. Cass, and B. R. T. Simoneit (2001), Measurement of emissions from air pollution sources. 3. C<sub>1</sub>–C<sub>29</sub> organic compounds from fireplace combustion of wood, *Environ. Sci. Technol.*, **35**, 1716–1728.
- Simoneit, B. R. T. (2002), Biomass burning—A review of organic tracers for smoke from incomplete combustion, *Appl. Geochem.*, **17**, 129–162.

H. Chang, P. Herckes, and J. L. Collett Jr., Department of Atmospheric Science, Colorado State University, Fort Collins, CO 80523–1371, USA. (collett@lamar.colostate.edu)



## On the Drop-Size Dependence of Organic Acid and Formaldehyde Concentrations in Fog

B. ERVENS<sup>1\*</sup>, P. HERCKES<sup>2</sup>, G. FEINGOLD<sup>3</sup>, T. LEE<sup>2</sup>, J. L. COLLETT, JR.<sup>2</sup>  
and S. M. KREIDENWEIS<sup>2</sup>

<sup>1</sup>Cooperative Institute for Research in the Atmosphere (CIRA), Colorado State University,  
Fort Collins, Colorado 80523, U.S.A.

<sup>2</sup>Atmospheric Science Department, Colorado State University, Fort Collins, CO 80523, U.S.A.

<sup>3</sup>NOAA, Environmental Technology Laboratory, Boulder, Colorado 80305, U.S.A.

(Received: 15 May 2003; accepted: 28 July 2003)

**Abstract.** Concentration differences between small ( $r < 8.5 \mu\text{m}$ ) and large droplets ( $r > 8.5 \mu\text{m}$ ) were observed for formic acid, acetic acid and formaldehyde in fog droplets collected in California's Central Valley. The concentration ratios (large/small droplets) of these compounds were investigated by a stepwise model approach. Assuming thermodynamic equilibrium ( $K_H^{\text{eff}}$ ) results in an overestimate of the concentration ratios. Considering the time dependence of gas phase diffusion and interfacial mass transport, it appears that the lifetime of fog droplets might be sufficiently long to enable phase equilibrium for formaldehyde and acetic acid, but not for formic acid (at  $\text{pH} \approx 7$ ). Oxidation by the OH radical has no effect on formaldehyde concentrations but reduces formic acid concentrations uniformly in all drop size classes. The corresponding reaction for acetic acid is less efficient so that only in large droplets, where replenishment is slowed because the uptake rate of acid from the gas phase is slower, is the acid concentration reduced leading to a smaller concentration ratio. Formaldehyde concentrations in fog can be higher than predicted by Henry's Law due to the formation of hydroxymethanesulfonate. Its formation is dependent on the sulfur(IV) concentration. At high pH values the uptake rate for sulfur(IV) is drop-size dependent. However, the observed concentration ratios for formaldehyde cannot be fully explained by the adduct formation. Finally, it is estimated that mixing effects, i.e., the combination of individual droplets into a bulk sample, have a minor influence ( $< 15\%$ ) on the measured heterogeneities.

**Key words:** aqueous phase chemistry, fog, formaldehyde, modelling, organic acid, uptake.

### 1. Introduction

Organic acids and formaldehyde have been detected in high concentrations in fog (e.g., Winiwarter *et al.*, 1994; Millet *et al.*, 1997; Collett *et al.*, 1999a) and in cloud droplets (e.g., Keene *et al.*, 1995; Hegg *et al.*, 2002; Löflund *et al.*, 2002). Organic acids in fog droplets may be derived through particle or gas phase scavenging. Species with low vapor pressures (such as dicarboxylic acids), predominately associated with the atmospheric particulate phase, are contributed mainly from cloud

\* Address for correspondence: NOAA/ETL, 325 Broadway, Boulder, Colorado 80305, U.S.A.,  
e-mail: barbara.ervens@noaa.gov

condensation nuclei. Dicarboxylic acids are typically found in submicron particles (Neusüß *et al.*, 2000; Yao *et al.*, 2002).

The partitioning of volatile species (such as HCOOH, CH<sub>3</sub>COOH and HCHO) between gas and aqueous phases depends on their solubility. The available surface area affects the uptake rate but not the equilibrium partitioning. Simultaneous measurements of gas and aqueous phase concentrations are sparse. In a few studies (e.g., Winiwarter *et al.*, 1994; Voisin *et al.*, 2000) it has been shown that equilibrium between the phases is not achieved. A partition coefficient represents the deviation from equilibrium. Partition coefficients greater than unity indicate that the droplets are supersaturated with respect to gas phase concentrations. For HCOOH and CH<sub>3</sub>COOH partition coefficients between 0.001 and 40 have been found (Leriche *et al.*, 2000). In the presence of sulfur(IV), formaldehyde can form the adduct hydroxymethanesulfonate (HMS<sup>-</sup>). Measured concentrations of formaldehyde in droplets usually include the concentration of this adduct. Therefore, the observed partitioning of formaldehyde can exceed significantly that predicted by Henry's Law (Ang *et al.*, 1987; Olson and Hoffmann, 1989). Concentrations of both formaldehyde and sulfur(IV) in droplets have been observed to be higher by factors of up to 100 and 1000, respectively, than predicted by their Henry's Law constants (Klippel and Warneck, 1980; Ang *et al.*, 1987).

Measurements of solute concentrations in cloud and fog droplets have been analyzed in several studies and often show higher solute concentrations in small droplets (Pandis *et al.*, 1990; Ogren *et al.*, 1992; Collett *et al.*, 1994; Bator and Collett, 1997; Reilly *et al.*, 2001). One contribution to such concentration differences might be that the uptake rates of soluble gases vary for droplets of different sizes. Mass transfer from the gas phase can lead to drop size-dependent uptake rates (Audiffren *et al.*, 1998), while fast chemical reactions within the aqueous phase can also prevent attainment of equilibrium. In addition to these effects, mixing of single droplets into a bulk sample might result in a different equilibrium concentration than present originally in the individual droplets (Pandis and Seinfeld, 1991; Khare *et al.*, 1999). Each of these effects has been addressed in the studies mentioned above, but to date there has been no evaluation of the relative contribution of each effect to observed deviations from equilibrium between the aqueous and gas phases.

In the present study observations are presented of low molecular weight organic compounds in fog. Concentrations of mono- and dicarboxylic acids and formaldehyde are found to vary with drop size. Different hypotheses are examined to explain these observations for formic acid, acetic acid and formaldehyde. An uptake/chemistry model is used to interpret differences in the partitioning between the gas and aqueous phases for these three species. Based on these model results, a more general view of the contributions to deviations from phase equilibrium for transport, chemistry and drop mixing effects is developed.

## 2. Experimental

### 2.1. INSTRUMENTATION

Fog samples were collected in December 2000 and January 2001, close to the small town of Angiola (N35°35', W119°32', 60 m asl) in the Central Valley of California, as part of the California Regional Particulate Air Quality Study (CRPAQS). In this study, radiation fogs usually formed at night and evaporated in the early morning hours. Samples were typically collected at one hour intervals. Drop size distribution spectra were recorded by a Classical Scattering Active Spectrometer Probe (CSASP, Particle Measurement Systems Inc.).

Fog Liquid Water Content (LWC) was monitored at the site using a Particle Volume Monitor (Gerber Scientific, PVM-100). Fog samples for Total Organic Carbon (TOC) and organic acid analyses were collected with stainless steel versions of the Caltech Active Strand Cloudwater Collector (ss-CASCC) and a two-stage version of that collector known as the size-fractionating ss-CASCC (sf-ss-CASCC) (Herckes *et al.*, 2002a). The 50% size cuts of the two sf-ss-CASCC stages are estimated as approximately  $r = 3 \mu\text{m}$  and  $r = 8.5 \mu\text{m}$ . Collection efficiency curves for the cloud collector stages have an S-shape. While the size cut of the small drop stage is fairly sharp, the collection efficiency curve for the large drop stage is flatter (Demos *et al.*, 1996), covering a span of several  $\mu\text{m}$  while rising from low to high collection efficiency. These metal collectors can be cleaned with solvents in order to reduce contamination by organic compounds. Samples for formaldehyde analysis were collected with plastic versions of the CASCC and sf-CASCC (Demos *et al.*, 1996), collocated and operated simultaneously with the metal collectors. Possible contamination was checked with field blanks, taken before fog events.

Immediately after sample collection, the pH value of each sample was measured. Organic acid aliquots were stabilized by addition of chloroform as a biocide and kept refrigerated in the dark until analysis (Wortham *et al.*, 1995 and references therein). Analysis was completed within 4 weeks after the end of the field project. Formic, acetic, propionic, oxalic, pyruvic, malonic and succinic acids were determined by ion chromatography using a Dionex DX500 system equipped with a Dionex AS11-HC column and guard column, a Dionex ATC-1 Anion trap column and a Dionex CD20 conductivity detector. Elution was performed with a sodium hydroxide gradient as follows: start to 8 minutes: 4 mM NaOH; then the NaOH concentration was progressively increased: 15 mM at 23 minutes; 30 mM at 28 minutes; 60 mM at 38 minutes.

Formaldehyde was preserved by reaction with buffered sulfur(IV) to form hydroxymethanesulfonate. This was later dissociated and reacted with 2,4-pentanedione to form 3,5-diacetyl-1,2-dihydrolutidine, which was analyzed by fluorescence (Dong and Dasgupta, 1987). The excitation wavelength used was 412 nm and the emission wavelength 510 nm. This technique allows for total formaldehyde measurement but does not allow for a differentiation between free formaldehyde and hydroxymethanesulfonate.



Table I. Concentrations of small mono and dicarboxylic acids and formaldehyde in bulk fog droplets ( $\mu\text{eq/L}$ )

	Monocarboxylic acids/formaldehyde			
	Formaldehyde	Formic	Acetic	Propionic
	HCHO	HCOOH	CH <sub>3</sub> COOH	CH <sub>3</sub> CH <sub>2</sub> COOH
Minimum	<DL	14.9	5	<DL
Median	21.5	31.6	31.4	<DL
Maximum	43.9	121	197	10.4
Average	23.4	42.1	51.4	–
DL = detection limit	3.3	4.2	4.1	3.7

	Dicarboxylic acids			
	Oxalic	Malonic	Succinic	Glutaric
	(COOH) <sub>2</sub>	HO <sub>2</sub> CCH <sub>2</sub> CO <sub>2</sub> H	HO <sub>2</sub> C(CH <sub>2</sub> )CO <sub>2</sub> H	HO <sub>2</sub> C(CH <sub>2</sub> ) <sub>3</sub> CO <sub>2</sub> H
Minimum	<DL	<DL	<DL	<DL
Median	7.19	<DL	<DL	<DL
Maximum	24.8	5.17	<DL	6.92
Average	8.4	–	–	–
DL = detection limit	3.2	5.0	5.8	5.6

Total Organic Carbon (TOC) concentrations were determined using a commercial TOC analyzer (Shimadzu TOC 5000A), which oxidizes organic carbon in an injected sample on a catalyst bed at 680 °C, followed by measurement of the evolved carbon dioxide. The TOC analyzer was calibrated using a series of aqueous potassium hydrogen phthalate standards; measurement precision was evaluated through replicate sample analyses.

## 2.2. BULK FOG WATER CONCENTRATIONS

Table I gives an overview of observed concentrations of mono- and dicarboxylic acids as well as formaldehyde in bulk fog samples. Measured formaldehyde concentrations represent the sum of free formaldehyde, formaldehyde present in solution in its gem-diol form, and hydroxymethanesulfonate. For the monocarboxylic acids, formic acid and acetic acid concentrations are similar while propionic acid concentrations are much lower, sometimes even undetectable. Dicarboxylic acids are frequently undetectable ( $<5 \mu\text{eq/L}$ ), with the exception of oxalic acid, which shows concentrations in the range of half of formic acid concentrations.

Table II. Average (minimum-maximum) concentrations of formic, acetic and oxalic acids and formaldehyde measured in different studies ( $\mu\text{M}$ )

Location	Formic acid	Acetic acid	Oxalic acid	Formaldehyde	Reference
<i>Radiation fogs</i>					
Angiola (SJV, Ca)	42 (15–121)	51 (5–197)	4.2 (<1.6–12)	23 (3–44)	This study
Bakersfield (SJV, Ca)	77 (40–167)	83 (0–244)		168 (27–498)	Munger <i>et al.</i> , 1989a
McKittrick (SJV, Ca)	21 (0–56)	3 (0–28)		26 (6–93)	Munger <i>et al.</i> , 1989a
Visalia (SJV, Ca)	71 (40–187)	86 (35–187)		31 (18–65)	Munger <i>et al.</i> , 1989a
Buttonwillow (SJV, Ca)	145 (133–157)	60 (47–74)		88 (61–115)	Munger <i>et al.</i> , 1989a
San Joaquin Valley (Ca)	63 (6–270)	117 (10–458)	6.2 (<2.7–16.5)	46.4 (2.3–410)	Collett <i>et al.</i> , 1999a
Po Valley (Italy)	9.5–165.5	12.5–91.5			Winiwarter <i>et al.</i> , 1988
Po Valley (Italy)				130 (16–567)	Facchini <i>et al.</i> , 1990
Strasbourg (France)	110 <sup>a</sup> /190 <sup>b</sup>	305 <sup>a</sup> /440 <sup>b</sup>		n.d.	Millet <i>et al.</i> , 1997
<i>Clouds</i>					
Mt. Rax (Austria)	13 (1–34)	16 (11–37)	4.2 (0.7–12.7)		Löflund <i>et al.</i> , 2002
Whiteface Mt. (U.S.A.)	26 (14–40)	9 (5.1–15)	5.25 (1.5–9.5)		Khawaja <i>et al.</i> , 1995
San Pedro Hill (Ca)	20 (12–43)	10 (6–31)		13 (5–38)	Munger <i>et al.</i> , 1989b

<sup>a</sup> 5–8  $\mu\text{m}$  droplets.

<sup>b</sup> 2–6  $\mu\text{m}$  droplets, n.d. not determined.



Table II presents the range of observations for formic and acetic acid as well as formaldehyde in selected studies. While several data sets exist for these three compounds, published data on other mono- and dicarboxylic acids in cloud and fog droplets are sparse. In previous studies in California's San Joaquin Valley (SJV), Munger *et al.* (1989a, b) determined concentrations of organic acids and formaldehyde similar to those found in the current study. The urban Visalia and Bakersfield sites showed higher concentrations than the rural Angiola sampling site, while the remote McKittrick site showed lower values. Observations from 1989 in the small town of Buttonwillow showed much higher values, but these observations are based on only two samples. In a composite of urban and remote San Joaquin Valley sites, with a large number of samples collected in urban areas (Fresno and Bakersfield), Collett *et al.* (1999a) found higher concentrations than observed in the present study. The Angiola concentrations are also of the same order of magnitude as found in Po Valley radiation fogs (Winiwarter *et al.*, 1988). In the urban environment of Strasbourg higher concentrations were observed in very small droplets (2 to 6  $\mu\text{m}$  or 5 to 8  $\mu\text{m}$  in diameter) by Millet *et al.* (1996, 1997). Finally, observations in intercepted clouds in Europe and in the United States usually exhibit lower concentrations of acetic and formic acid and formaldehyde than are observed in fogs. Oxalic acid concentrations measured in intercepted clouds in Austria and the U.S. were similar to those observed in polluted radiation fogs in the San Joaquin Valley.

#### 2.2.1. Contributions of Low Molecular Weight Organic Compounds to the Total Organic Carbon (TOC)

The total organic carbon (TOC) concentrations in this study ranged from 2 to 40 ppmC. Usually more than 50% of the organic matter consisted of low molecular weight compounds ( $<500$  g/mol) (Herckes *et al.*, 2002a). Figure 1 gives an overview of the contributions of low molecular weight carboxylic acids and formaldehyde to TOC. On average these compounds account for 22% of the fog TOC. Monocarboxylic acids contribute the most to the total organic carbon, accounting for an average of 17% of the TOC. Acetic acid is usually the dominant organic species, accounting for up to 22% of the TOC, while formic and propionic acids contribute less (up to 10 and 2%, respectively). The concentration of pyruvic acid is usually less than 0.1% of the TOC. The dicarboxylic acids investigated account for only 1% of the TOC on average. Oxalic acid is most important; concentrations of the higher dicarboxylic acids are one order of magnitude smaller. Formaldehyde accounts for 4% of the TOC on average. Concentrations of other carbonyls (e.g., acetaldehyde or glyoxal) were not determined in this study. Previous studies by Munger *et al.* (1990) revealed that glyoxal and methylglyoxal concentrations were in the same concentration range as formaldehyde and hence may provide similar contributions to TOC.

The results here are consistent with studies of fog samples in Davis, CA (Herckes *et al.*, 2002b) where acetic acid was also the dominant organic species. In the more urban environment of Davis, however, acetic and formic acid accounted

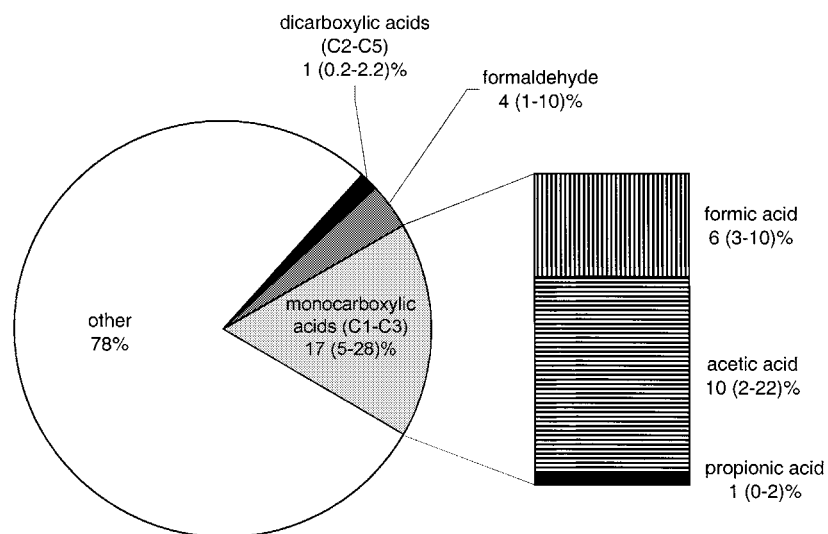


Figure 1. Average (min-max) contributions of formaldehyde, mono- and dicarboxylic acids to the Total Organic Carbon in Angiola fog samples (in % of TOC).

for only 11% of the TOC on average. Similar observations have been made by Löflund (2002) in clouds at Mt. Rax in Austria, where small organic acids accounted for 11% of the OC on average (5–22%) and the dicarboxylic acids only accounted for 1.7% on average.

### 2.3. VARIATION OF CONCENTRATIONS WITH DROPLET SIZE

The collection of size-fractionated samples enables a comparison between concentrations in small droplets ( $3\ \mu\text{m} < r < 8.5\ \mu\text{m}$ ) and large droplets ( $r > 8.5\ \mu\text{m}$ ). Figures 2(a–c) present the observations for low molecular weight acids (formic, acetic, propionic and oxalic acid) and formaldehyde. In general, the small droplets exhibit higher concentrations than the large droplets. Propionic acid does not follow this trend as clearly as the other acids, but few observations are available. Such observations of chemical heterogeneity have already been made for inorganic compounds in radiation fogs (e.g., Millet *et al.*, 1996; Bator and Collett, 1997; Laj *et al.*, 1998) as well as for total organic carbon (Herckes *et al.*, 2002b). Munger and coworkers (1989b) observed little difference in formate, acetate and formaldehyde concentrations between small and large droplets in cloud samples collected at San Pedro Hill (CA). Keene *et al.* (1995) reported making drop size-resolved measurements of organic acid concentrations but did not report results. Millet and coworkers (1997) observed enrichment in smaller droplets in a study investigating two size classes of small droplets (2–6  $\mu\text{m}$  and 5–8  $\mu\text{m}$  in diameter).

Chemical heterogeneity in drop composition has sometimes been explained by the chemical heterogeneity of the aerosol population on which these droplets form

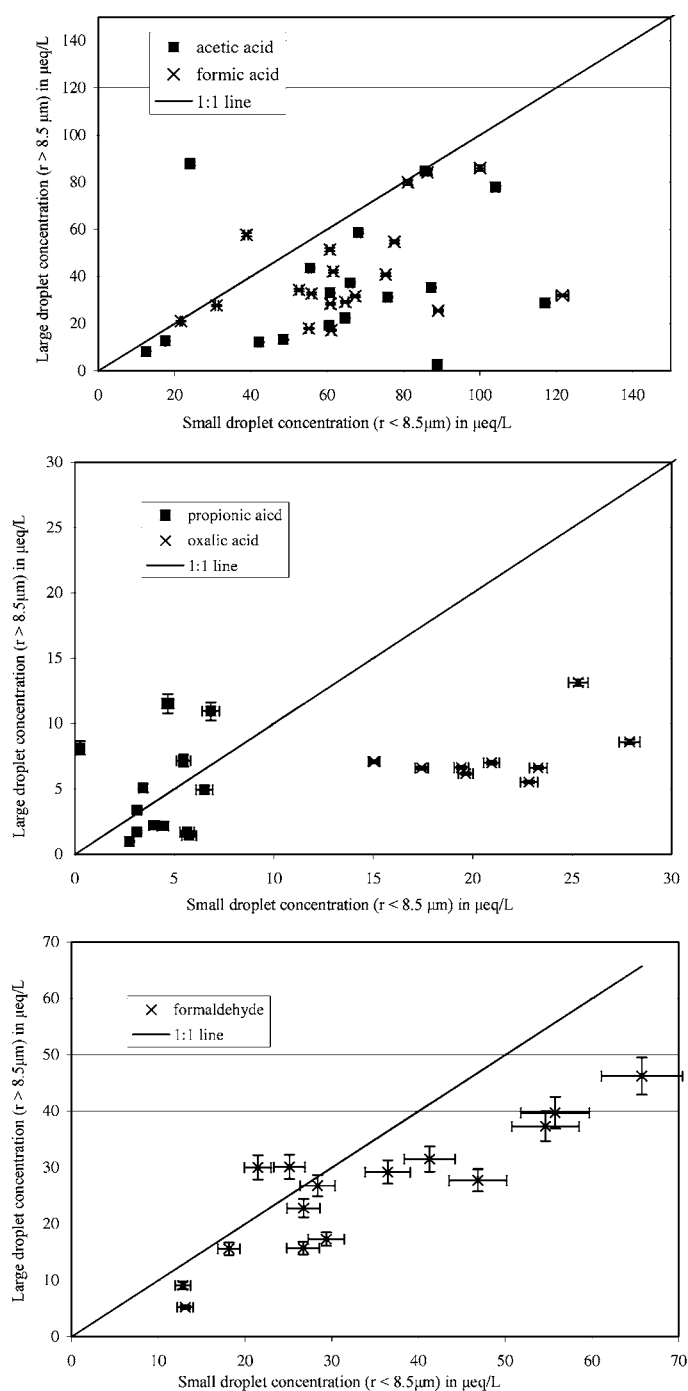


Figure 2. Concentrations in small vs. large droplets in Angiola, California radiation fogs. Error bars represent the measurement precision (one relative standard deviation) associated with sample analysis. (a) Formic and acetic acid; (b) propionic and oxalic acid; (c) formaldehyde.

(Ogren and Charlson, 1992; Bator and Collett, 1997). Smaller cloud condensation nuclei, which typically produce smaller drops, usually show higher concentrations of organic carbon, sulfate and ammonium. Larger fog drops are likely to form on larger condensation nuclei, formed by mechanical processes, which might be relatively enriched in sodium, chloride and calcium.

These relations might not fully explain observed conditions (i) because the dilution of aerosol material in the droplets also influences the concentrations and (ii) because droplet growth depends on aerosol composition. In size resolved aerosol studies, it was shown that oxalic and other dicarboxylic acids are mainly found in the accumulation mode (Ludwig and Klemm, 1988; Neusüß *et al.*, 2000). Hence, the higher concentrations of oxalate (Figure 2(b)) in the smaller droplets can be explained by the enrichment of oxalate in the smaller condensation nuclei.

This explanation, however, cannot account for the observations of formic acid, acetic acid and formaldehyde, as these low molecular weight organic compounds have a high vapor pressure and are found predominately in the gas phase rather than in particles. These compounds are incorporated into fog droplets through gas phase scavenging and, therefore, nucleation scavenging of aerosol particles does not play a significant role in their distribution with drop size. The review by Yu (2000) shows that in most cases roughly 1% of these acids are present in the aerosol phase if no liquid water is present. In a model study by Herrmann *et al.* (2000) it has been shown that under urban conditions ( $\text{pH} < 4$ ) the aqueous phase fractions of these species can increase to about 8% for both acids and more than 90% for formaldehyde. However, the partitioning is strongly dependent on the available liquid water content and the pH value. Under less polluted conditions (i.e., higher pH values) the aqueous phase fractions of the acids will increase significantly. In the following section, possible reasons will be discussed for the observed concentration inhomogeneities of formic acid, acetic acid and formaldehyde in different droplet size classes.

### 3. Modeling

#### 3.1. THERMODYNAMIC EQUILIBRIUM: HENRY'S LAW

The equilibrium phase partitioning of slightly soluble and less reactive gases can be described by the ratio of the aqueous phase concentration  $c_{\text{aq}}$  and the gas phase partial pressure  $p$ , as expressed by the Henry's Law Constant  $K_{\text{H}}$  [ $\text{M atm}^{-1}$ ]

$$K_{\text{H}} = \frac{c_{\text{aq}}[\text{M}]}{p [\text{atm}]} . \quad (1)$$

Dissociation of acids in the aqueous phase increases their effective solubility. For this reason the effective Henry's Law Constant  $K_{\text{H}}^{\text{eff}}$ , including the dissociation constant  $K_{\text{a}}$ , is applied for acids:

$$K_{\text{H}}^{\text{eff}}(\text{acids}) = K_{\text{H}} \cdot \left( 1 + \frac{K_{\text{a}}}{[\text{H}^+]} \right) . \quad (2)$$

For aldehydes, such as formaldehyde, the hydration (hydration constant  $K_{\text{Hydr}}$ ) within the aqueous phase must be taken into account:

$$K_{\text{H}}^{\text{eff}}(\text{aldehydes}) = K_{\text{H}} \cdot (1 + K_{\text{hydr}} \cdot [\text{H}_2\text{O}]) . \quad (3)$$

However, the application of Henry's Law constants might not be appropriate if aqueous solutions with high ionic strengths are present. In addition to organic acids, concentrations of inorganic ions ( $\text{SO}_4^{2-}$ ,  $\text{NO}_3^-$ ,  $\text{Cl}^-$ ,  $\text{NO}_2^-$ ,  $\text{Mg}^{2+}$ ,  $\text{Ca}^{2+}$ ,  $\text{Na}^+$ ,  $\text{K}^+$  and  $\text{NH}_4^+$ ) were determined in the fog droplets. For most of these ions higher concentrations were found in smaller droplets. However, the total ionic strength in both the large and small droplets did not exceed a value of  $I = 0.001 \text{ M}$  so that ionic strength effects on the Henry's Law Constants ('salting out effects') can be neglected here. At equilibrium the monocarboxylic acids and formaldehyde should have the same concentrations in all droplet size classes (assuming the same effective solubility, i.e., the same pH value in the case of the acids).

$$\text{ratio} = \frac{\text{concentration in large droplets [M]}}{\text{concentration in small droplets [M]}} . \quad (4)$$

Observations typically reveal significantly lower pH values in small droplets (e.g., Bator and Collett, 1997); however, in the present study this trend was not clearly observed. Only small differences between the pH values of small droplets (average 7.02, range 6.43–7.75) and large droplets (7.04, 6.2–7.74) were observed. At these high pH values, the ratio  $K_a/[\text{H}^+]$  is always much greater than 1 ( $\text{p}K_a(\text{HCOOH}) = 3.75$ ,  $\text{p}K_a(\text{CH}_3\text{COOH}) = 4.75$ ) and Equations (2) and (4) can be combined to yield

$$\text{ratio} = \frac{[\text{A}^-]_{\text{large}}}{[\text{A}^-]_{\text{small}}} = \frac{[\text{H}^+]_{\text{small}}}{[\text{H}^+]_{\text{large}}} . \quad (5)$$

In Figure 3 the measured concentration ratios of formate and acetate are compared to the values predicted by Equation (5). It is evident that in some cases there is good agreement between the measured and the predicted values; however, in most cases the measured ratio is lower than expected for equilibrium phase partitioning. This result, along with the observations for formaldehyde in Figure 2(c), suggests that the actual partitioning of these three species might not have achieved equilibrium and other effects should be considered.

### 3.2. KINETIC DESCRIPTION OF MASS TRANSFER

Henry's Law describes the equilibrium solubility without any consideration of the time scales of the uptake process. However, as shown by Schwartz (1986) the uptake rate is a time dependent process controlled by several factors, including gas phase diffusion, interfacial mass transfer, aqueous phase diffusion and chemical reactions within the aqueous phase. The reciprocal value of the rate [ $\text{s}^{-1}$ ] of each

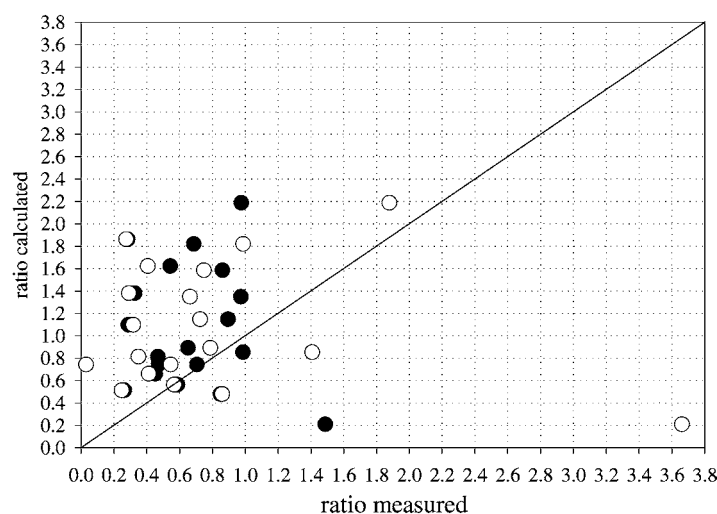


Figure 3. Comparison of measured concentration ratios (large/small drops) and predicted ratios based on the effective Henry's Law Constants for ● formic and ○ acetic acid.

process can be defined as a characteristic time. A comparison of these characteristic times allows the determination of the rate-limiting process. In the following sections each of these factors will be investigated to clarify its possible contribution to the observed concentration inhomogeneities.

### 3.2.1. Gas Phase Diffusion and Interfacial Mass Transfer

The uptake rate is dependent on the rate of transport from the gas phase. Transport slows with decreasing concentration gradients between the bulk gas phase and the droplet surface. The combination of these two factors yield the uptake rate  $[M s^{-1}]$  in terms of the time rate of change of the aqueous phase surface concentrations

$$\frac{d[c]_{aq}}{dt} = k_{mt} \cdot p - \frac{[c]_{aq}}{K_H^{(eff)} \cdot R \cdot T}, \quad (6)$$

where  $k_{mt}$  is the mass transfer coefficient  $[s^{-1}]$ .  $k_{mt}$  can be calculated according to the approach by Schwartz (1986)

$$k_{mt} = \left[ \left( \frac{r^2}{3 \cdot D_g} + \frac{r}{4 \cdot \bar{c} \cdot \alpha} \right) \right]^{-1}, \quad (7)$$

where  $r$  is the drop radius,  $D_g$  the gas phase diffusion coefficient,  $\bar{c}$  the molecular speed  $(8 \cdot R' \cdot T / (\pi \cdot \text{molar mass}))^{0.5}$  (where  $R'$  is the gas constant in  $[J (K \cdot \text{mol})^{-1}]$ ) and

$$\alpha = \frac{\text{No. of molecules entering the liquid phase}}{\text{No. of molecular collisions with the surface}}. \quad (8)$$

The reciprocal value of the mass transfer coefficient (7), multiplied by the (dimensionless) Henry's Law Constant  $K_H^{(\text{eff})} \cdot R \cdot T$ , represents the characteristic time for achieving equilibrium at the drop surface. In the absence of aqueous phase reactions, if further transport through the droplet interior is sufficiently rapid this time scale describes the characteristic time until the whole drop is saturated with the surrounding gas. In the model study by Warneck (1999) it was shown that the uptake rate on droplets of  $r = 5 \mu\text{m}$  is on the order of  $k_{\text{mt}} = 10^5 \text{ s}^{-1}$  for soluble gases ( $K_H^{(\text{eff})} > 30 \text{ M atm}^{-1}$ ). In the present study the concentration ratios of the three species of interest in the aqueous phase were calculated applying Equation (6), combined with Equation (7), using the uptake parameters for formic acid, acetic acid and formaldehyde (Table III). The concentrations in the gas phase were estimated to be 0.1 ppb. They were held constant for the simulation. The choice of the gas phase concentration does not have any influence on the final ratio if a fixed pH value is assumed as done here. The analytical solution of (6) for the fixed-pH, fixed-gas-phase case reveals that the concentration ratio is always independent of the partial pressure, as can be seen from the following

$$c_{\text{aq}}(t) = -(K_H^{(\text{eff})} \cdot R \cdot T) \cdot \exp(-t \cdot k_{\text{mt}} / (K_H^{(\text{eff})} \cdot R \cdot T)) + (K_H^{(\text{eff})} \cdot R \cdot T) \cdot p. \quad (9)$$

Thus, the concentration ratio can be determined as

$$\begin{aligned} \frac{c_{\text{aq}, 1}}{c_{\text{aq}, 2}} &= \frac{-(K_H^{(\text{eff})} \cdot R \cdot T) \cdot p \cdot \exp(-t \cdot k_{\text{mt}, 1} / (K_H^{(\text{eff})} \cdot R \cdot T)) + (K_H^{(\text{eff})} \cdot R \cdot T) \cdot p}{-(K_H^{(\text{eff})} \cdot R \cdot T) \cdot p \cdot \exp(-t \cdot k_{\text{mt}, 2} / (K_H^{(\text{eff})} \cdot R \cdot T)) + (K_H^{(\text{eff})} \cdot R \cdot T) \cdot p} \\ &= \frac{1 - \exp(-t \cdot k_{\text{mt}, 1} / (K_H^{(\text{eff})} \cdot R \cdot T))}{1 - \exp(-t \cdot k_{\text{mt}, 2} / (K_H^{(\text{eff})} \cdot R \cdot T))} \end{aligned} \quad (10)$$

which is independent of the partial pressure. Corresponding measurements of gas phase concentrations are not available from the current study, but the estimate seems to be appropriate leading to aqueous phase concentrations comparable to the measured values. Calculations were performed for pH values between 6 and 8, covering the limits in the present study.

The evolution of the resulting concentration ratios over 30 min, a typical fog drop lifetime, is shown in Figure 4 for formic acid and acetic acid. At the beginning of the simulation time the acid concentrations in the droplets correspond to the ratio of the  $k_{\text{mt}}$  values. Thus, the axis intercept of about 0.45 is due to this ratio. Saturation is achieved for acetic acid after about 30 min at pH = 7. The timescale for formic acid to reach equilibrium is much longer, because due to its higher effective solubility, about ten times more molecules must be transported towards the droplet surface. In previous studies the lifetime of fog droplets was assumed to range from a few minutes to hours (Noone *et al.*, 1992; Winiwarter *et al.*, 1994). This means that within the lifetime of a fog droplet, acetic acid is more likely to reach equilibrium in the droplet than formic acid. The uptake rate for formaldehyde is not shown in the figure as it is almost independent of the pH value and equilibrium is reached after about 10 s. (The more sophisticated approach

Table III. Uptake parameters for formic acid, acetic acid, formaldehyde and OH

	$K_{H, 298\text{ K}}$ [M atm <sup>-1</sup> ]	$\Delta H/R$ [K]	$K_a$ [M]	$\Delta H/R$ [K]	$\alpha_{298\text{ K}}$	$\alpha_{279\text{ K}}$	$D_g$ [m <sup>-2</sup> s <sup>-1</sup> ]
HCOOH	5530	-5630 <sup>a</sup>	$1.77 \cdot 10^{-4}$	-12 <sup>d</sup>	0.012 <sup>f</sup>	0.035 <sup>g</sup>	$1.53 \cdot 10^{-5\text{ h}}$ $1.45 \cdot 10^{-9\text{ j}}$
CH <sub>3</sub> COOH	5500	-5890 <sup>b</sup>	$1.75 \cdot 10^{-5}$	-46 <sup>d</sup>	0.019 <sup>f</sup>	0.05 <sup>g</sup>	$1.24 \cdot 10^{-5\text{ h}}$ $1.29 \cdot 10^{-9\text{ j}}$
HCHO	2.5	-7216 <sup>b</sup>	36	-4030 <sup>e*</sup>	0.02 <sup>**</sup>	0.02	$1.64 \cdot 10^{-5\text{ i}}$ $1.64 \cdot 10^{-9\text{ k}}$
OH	25	-5280 <sup>c</sup>			0.05 <sup>**</sup>	0.05	$1.53 \cdot 10^{-5\text{ j}}$ $1.53 \cdot 10^{-9\text{ k}}$

<sup>a</sup> Khan and Brimblecombe, 1992; <sup>b</sup> Betterton and Hoffmann 1988; <sup>c</sup> Kläning *et al.*, 1985; Harned and Owen, 1958;

\*  $K_{\text{Hydr}}$  [M<sup>-1</sup>]; <sup>d</sup> Olson and Hoffmann, 1989; <sup>e</sup> Davidovits *et al.*, 1995; <sup>f</sup> Nathanson *et al.*, 1996; <sup>g</sup> estimated, therefore

no T dependence available; <sup>h</sup> Schwartz, 1986; <sup>i</sup> estimated based on the method by Fuller, 1986; <sup>j</sup> Hanson *et al.*, 1992;

<sup>k</sup> Lide *et al.*, 2000; <sup>k</sup> estimated  $D_g = 10^4 \cdot D_{\text{aq}}$ .



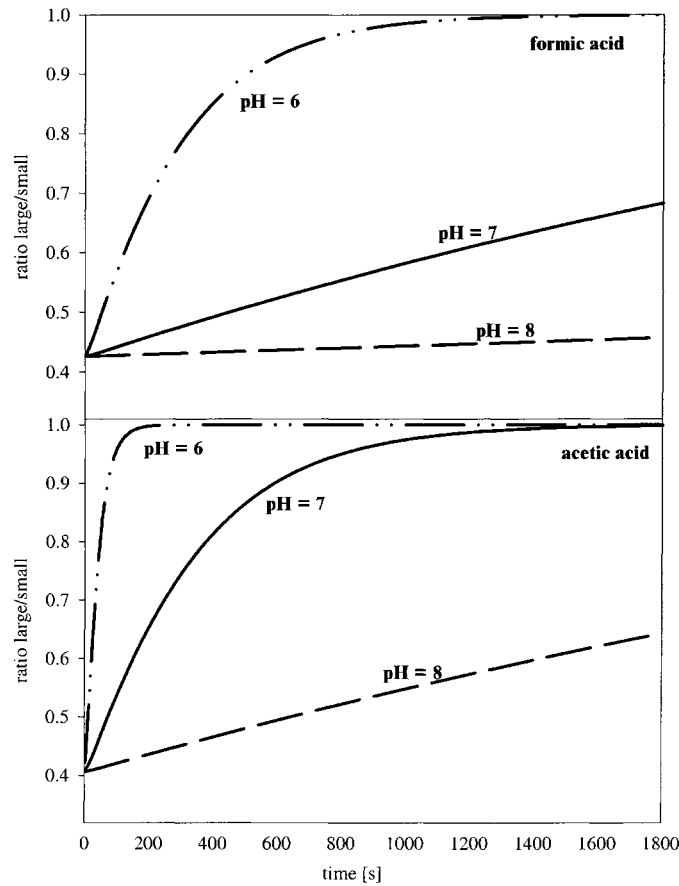


Figure 4. Predicted ratio (concentration in large/small droplets;  $r = 12 \mu\text{m}$ ,  $r = 6 \mu\text{m}$ ) in absence of chemical reactions for formic (upper panel) and acetic acid depending on the time and pH of the aqueous phase — · · · — pH = 6; — pH = 7; - - - - pH = 8.

considering the pH dependence of the formaldehyde uptake as suggested by Swartz *et al.* (1997) is neglected here due to the small variation of the uptake rate between pH = 4 and 10). But if one assumes a lifetime of the fog droplets of several minutes it can be seen (Figure 4) that this simple model, which considers only the uptake kinetics, would not predict for the same time similar concentration ratios for both acids of  $0.6 \pm 0.25$  (mean value of the measured ratios  $\pm$  standard deviation) as found in the measurements.

The characteristic time until achievement of equilibrium ( $k_{\text{mt}}$ )<sup>-1</sup> represents the sum of the characteristic times for the gas phase diffusion  $\tau_{\text{gdiff}}$  and the time for the interfacial transport  $\tau_{\text{interfacial}}$ .

$$\tau_{\text{gdiff}} = \frac{r^2}{3 \cdot D_g} \cdot K_{\text{H}}^{(\text{eff})} \cdot R \cdot T \quad (11)$$

$$\tau_{\text{interfacial}} = \frac{4 \cdot r}{3 \cdot \alpha \cdot \bar{c}} \cdot K_{\text{H}}^{(\text{eff})} \cdot R \cdot T. \quad (12)$$

In addition to the characteristic time associated with the overall mass transfer coefficient these individual characteristic times are shown in Figure 5. In small droplets the interfacial transport processes control the uptake of gases, whereas for larger droplets the transport towards the droplet surface, i.e., the gas phase diffusion, is slower (Figure 5). The radius ( $r_{\text{limit}}$ ) at which the interfacial limitation is surpassed by diffusion limitation is different for the three species ( $r_{\text{limit}}(\text{CH}_3\text{COOH}) \approx 3.5 \mu\text{m}$ ;  $r_{\text{limit}}(\text{HCOOH}) \approx 5.5 \mu\text{m}$ ;  $r_{\text{limit}}(\text{HCHO}) \approx 7.5 \mu\text{m}$ ), but for all of them this crossover fits into the observed ‘small droplets’ category ( $r < 8.5 \mu\text{m}$ ). Therefore, the uptake in the large droplets is always more strongly limited by gas phase diffusion.

One reason for the disagreement between observed and predicted concentration ratios might be the uncertainty in the mass accommodation coefficient. It is known that mass accommodation coefficients show slight temperature dependence due to the decreasing energy barrier to enter the droplet surface with decreasing temperature (Nathanson *et al.*, 1996). This temperature dependence is opposite to that of the Henry’s Law Constant but is much weaker. The average temperature measured during the fog events was approximately 279 ( $\pm 7$ ) K. In this range the mass accommodation coefficients might be enhanced by a factor of 2 compared to the values at 298 K (Nathanson *et al.*, 1996).

The mass accommodation coefficients in Table III are values for pure water surfaces. At enhanced ionic strengths the mass accommodation coefficients are lower. However, the low ionic strengths present in the fog droplets will not significantly change the coefficients applied here.

On small droplets in the atmosphere, the mass accommodation coefficients could be significantly smaller due to organic hydrophobic coatings on the droplet surfaces (Gill *et al.*, 1986). The presence of such films may slow penetration of the surface and therefore increase the limitation of the uptake processes by interfacial transfer. Measurements of film forming compounds such as fatty acids ( $> \text{C}_{12}$ ) in fog droplets are available (e.g., Herckes *et al.*, 2002b). Assuming an average value based on those data it appears that there is insufficient film forming organic material to form a monolayer on the droplets throughout the size distribution from 2 to 47  $\mu\text{m}$  (diameter). However, the presence of organic films in the initial stages of fog droplet formation might lead to a retardation of the droplet growth leading finally to a concentration inhomogeneity in droplets of the same size (Podzimek and Saad, 1975; Feingold and Chuang, 2002). For film forming species, higher concentrations were found in smaller particles (Neusüß *et al.*, 2000), so that smaller droplets within the measured size distribution might be preferentially coated. Due to the lack of more detailed sets of size resolved data a more exact estimate cannot be given here.

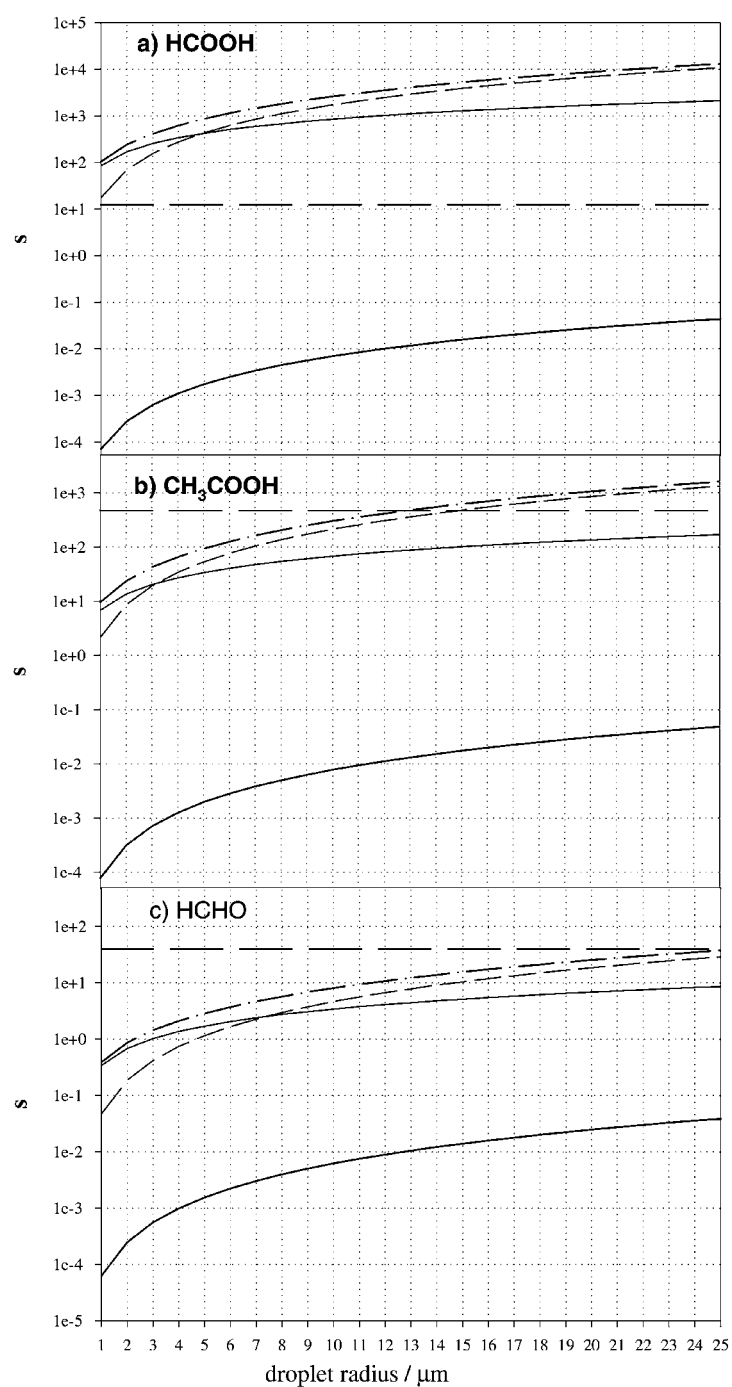


Figure 5. Characteristic times for interfacial mass transfer  $\tau_{\text{interfacial}}$  —; gas phase diffusion  $\tau_{\text{gdiff}}$  - - -; — · —  $\tau_{\text{gdiff}} + \tau_{\text{interfacial}}$  (= time until thermodynamic equilibrium is achieved at drop surface); aqueous phase diffusion  $\tau_{\text{aqdiff}}$  chemical reaction  $\tau_{\text{reac}}$  — and - - -.

### 3.2.2. Aqueous Phase Diffusion

The model equation (6) used in Section 3.2.1 refers to the equilibrium concentration at the droplet surface. In the next step of the model development we investigate if there are concentration gradients between the droplet surface and the droplet interior. Gradients will occur if the diffusion within the droplet is slow compared to the transport from the gas phase. The characteristic time for the aqueous phase diffusion  $\tau_{\text{aqdiff}}$  [s] is given by Equation (13) (Schwartz, 1986).

$$\tau_{\text{aqdiff}} = \frac{r^2}{\pi^2 \cdot D_{\text{aq}}} \cdot \quad (13)$$

The time scale for the aqueous phase diffusion is always significantly shorter than that for the mass transfer from the gas phase ( $\tau_{\text{gdiff}} + \tau_{\text{interfacial}}$ ) (Figure 5). Hence, for the species of interest here the aqueous phase diffusion is fast enough to provide a homogeneous concentration profile through the droplet, in the absence of chemical reaction.

More generally, the crossover between gas phase and aqueous phase mass transport limitations has been derived using different theoretical approaches (Schwartz, 1986; Huthwelker and Peter, 1996). For example, the expression by Schwartz (1986)

$$K_{\text{H}}^{(\text{eff})} > \frac{1}{5 \cdot R \cdot T} \frac{D_{\text{g}}}{D_{\text{aq}}} \quad (14)$$

is based on the assumption that the concentrations in both the gas and aqueous phase might deviate by 10% from their respective equilibrium concentrations. Therefore, for less soluble species aqueous phase diffusion might be the rate limiting process. Using Equation (14), a limit solubility can be estimated at which the limitation by aqueous phase transport gains in importance. Assuming a ratio of  $D_{\text{g}}/D_{\text{aq}} \approx 10^{-4}$  (cf. Table III) at a temperature of 279 K the aqueous phase diffusion is only limiting for species with  $K_{\text{H}}^{(\text{eff})} \leq 90 \text{ M atm}^{-1}$ . However, for the highly soluble species investigated in the present study the effective solubility is greater than this minimum by a few orders of magnitude.

### 3.3. CHEMICAL PROCESSES IN THE AQUEOUS PHASE

The discussion above shows that ( $\tau_{\text{gdiff}} + \tau_{\text{interfacial}}$ ) represents the characteristic time for the droplets to approach saturation with the gases and achieve the concentrations predicted by the Henry's Law constants. But this equilibrium might be disturbed by the consumption of the species of interest by chemical reactions. Schwartz (1986) showed that equilibrium is not reached in the droplets if the timescale for chemical reaction  $\tau_{\text{chem}}$

$$\tau_{\text{chem}} = (k \cdot [\text{reactant}])^{-1} \quad (15)$$

is approximately ten times less than that for aqueous phase diffusion,  $\tau_{\text{aqdiff}}$ . The fastest aqueous phase reactions for the three species considered in this study are the oxidation by radicals. Recently it has been shown that oxidation of organic compounds in the aqueous phase can be adequately described by reactions with the OH radical (Ervens *et al.*, 2003). Even at night the contributions of the  $\text{NO}_3$  radical to oxidation in the aqueous phase are less important due to OH production within the droplets by light-independent sources.

In addition to chemical processes in the bulk aqueous phase, there is evidence that surface processes might take place at the interface between gas and droplet (e.g., Nathanson *et al.*, 1996). But current knowledge of those processes is too limited to implement reliable values into models (Worsnop *et al.*, 2002).

The model was extended to include the uptake of  $\text{OH}_{(\text{g})}$  described in the same way as for the acids, using appropriate uptake parameters (Table III). Gas phase concentrations of  $[\text{OH}]_{\text{g,day}} = 10^7 \text{ cm}^{-3}$  and  $[\text{OH}]_{\text{g,night}} = 10^4 \text{ cm}^{-3}$  were assumed. These concentrations were chosen as reasonable upper limits in order to estimate the maximum likely effect of chemical reactions and give an upper bound for this mechanism. However, if a lower, more moderate, initial gas phase concentration is assumed the characteristic time for chemical reaction in the aqueous phase will be even longer so that at least for acetic acid and formaldehyde the importance of the OH reaction in controlling the aqueous phase concentration is even smaller. The radical concentration was kept constant during the simulation. This is a reasonable simplification for the simulation period of 30 min ( $\approx$  lifetime of fog droplets). Of course, the same considerations for the uptake process made for the acids are also applicable for the OH radical, but its solubility is much lower so that the transport limitation into the droplet is smaller. In addition to the time scales for the transport processes, the characteristic times for the OH reaction are shown in Figure 5. These characteristic times are independent of the drop radius and they are represented by the horizontal (broken) lines in all three figures, respectively. It is assumed that for the short simulation times the OH concentration is constant and the term  $k \cdot [\text{reactant}]$  can be simplified to a first order rate constant  $k^{\text{1st}}$  based on an OH concentration  $[\text{OH}]_{\text{aq}} = 3 \cdot 10^{-11} \text{ M}$  and the rate constants given in Table V. (This OH concentration is based on the 'day time' OH concentration; the corresponding value for 'night time' would be smaller by three orders of magnitude.)

A measure of the effectiveness of aqueous phase diffusion compared to the time scale for the chemical reaction is given by the diffuso-reactive parameter

$$q = r \cdot \sqrt{\frac{k^{\text{1st}}}{D_{\text{aq}}}}. \quad (16)$$

As explained by Schwartz (1986) values of  $q > 1$  correspond to a significant depletion of the species by the chemical processes and lead to a decreasing penetration of the species towards the drop center. The values of  $q$  are shown in Table IV for all three species. They are all significantly smaller than 1 indicating a uniform reaction rate throughout the drop. This result also confirms the applicability of

Table IV. Characteristic times [s] for gas phase diffusion, interfacial mass transfer, aqueous phase diffusion and chemical reactions within the aqueous phase and diffuso-reactive parameter  $q$

	$r/\mu\text{m}$	$\tau_{\text{gdiff}}$	$\tau_{\text{interfac}}$	$(\tau_{\text{gdiff}} + \tau_{\text{interfacial}}) \cdot K_{\text{H}} \cdot R \cdot T$	$\tau_{\text{aqdiff}}$	$\tau_{\text{chem}}$ (OH reaction)	
HCOOH	1	$2 \cdot 10^{-8}$	$1.5 \cdot 10^{-7}$	104	$6.2 \cdot 10^{-5}$	0.08	0.0074
	10	$2 \cdot 10^{-6}$	$1.5 \cdot 10^{-6}$	2633	$6.2 \cdot 10^{-3}$	0.08	0.074
CH <sub>3</sub> COOH	1	$2.2 \cdot 10^{-8}$	$1 \cdot 10^{-7}$	13	$6.6 \cdot 10^{-5}$	0.002	0.0012
	10	$2.2 \cdot 10^{-6}$	$1 \cdot 10^{-6}$	336	$6.6 \cdot 10^{-3}$	0.002	0.012
HCHO	1	$2.7 \cdot 10^{-8}$	$8.5 \cdot 10^{-8}$	0.03	$8.2 \cdot 10^{-5}$	0.025	0.0043
	10	$2.7 \cdot 10^{-6}$	$8.5 \cdot 10^{-7}$	0.8	$8.2 \cdot 10^{-3}$	0.025	0.043

the assumption that aqueous phase diffusion processes are fast enough to ensure a well-mixed drop interior.

### 3.3.1. Formic and Acetic Acid

In Figure 6 the concentration ratios for the acids predicted by the time-dependent reactive transport model approach are presented. It is evident that nighttime chemistry does not significantly influence the concentration ratios in the fog droplets, so that the predictions cannot be differentiated from the results from the ‘pure’ uptake model (Figure 4; pH = 7). On the other hand, it is evident that during daytime, the ratios can be influenced significantly by the oxidation of the acids and values similar to those observed are predicted for a range of droplet lifetimes. The ratios are very sensitive to the assumed OH concentration. Measured concentrations are not available but the OH concentrations assumed here give reasonable lower and upper limits for the possible influence of chemical loss processes.

From Figure 6, one can see that formic acid aqueous phase concentrations will reach steady state, but will never be in equilibrium due to the fast consumption by OH. The difference between  $\tau_{\text{chem}}$  and  $(\tau_{\text{gdiff}} + \tau_{\text{interfacial}})$  is smallest for small droplets (Figure 5). Thus, the concentrations in large droplets will be more affected by chemical processes than those in small ones, leading to a decrease in the ratio. Qualitatively the same argument is valid for acetic acid, but here most of the drops are not significantly affected by reaction so that drops of radius  $< 15 \mu\text{m}$  might approach thermodynamic equilibrium with a timescale of  $(\tau_{\text{gdiff}} + \tau_{\text{interfacial}})$ . In summary, the concentration ratio is more strongly affected by reaction of OH for acetic acid despite a much smaller rate constant. However, the absolute acid concentrations will be decreased more for formic acid.

Jacob (1986) has also discussed implications of the formation of these acids by the oxidation of their corresponding precursors by OH. Formic acid is effec-

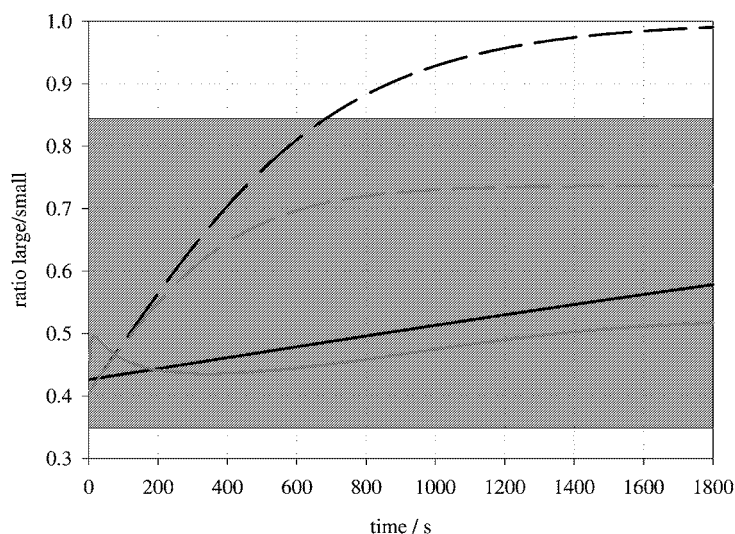


Figure 6. Concentration ratios for formic and acetic acid with chemical loss processes within the aqueous phase ( $\text{pH} = 7$ ); shadowed area: measured ratios (average  $\pm$  standard deviation); grey lines: daytime; black lines: nighttime); solid line:  $\text{HCOOH}$ , broken line:  $\text{CH}_3\text{COOH}$ .

tively produced by the oxidation of formaldehyde, leading to an accumulation or even outgassing of formic acid. However, under the conditions found here ( $\text{pH} \approx 7$ ) formic acid is completely dissociated ( $\text{pK}_a = 3.75$ ). The oxidation of formate by  $\text{OH}$  is about 25 times faster than that of formic acid and formaldehyde ( $k_{\text{HCOO}^-} = 3.2 \cdot 10^9 \text{ M}^{-1} \text{ s}^{-1}$ ;  $k_{\text{HCOOH}} = 1.2 \cdot 10^8 \text{ M}^{-1} \text{ s}^{-1}$ ;  $k_{\text{CH}_2(\text{OH})_2} = 7.7 \cdot 10^8 \text{ M}^{-1} \text{ s}^{-1}$ ). Therefore, the further oxidation of formate is too fast to allow it to accumulate. The corresponding formation process for acetic acid from acetaldehyde is much less important because (1) the gas phase concentration of acetaldehyde is usually found to be lower than formaldehyde (Saxena and Hildemann, 1996) and (2) the effective solubility ( $K_{\text{H}}^{\text{eff}}$ ) is lower due to a smaller hydration constant of acetaldehyde (Betterton and Hoffmann, 1988). Therefore, the main sources of acetic acid are gas phase processes.

### 3.3.2. Formaldehyde

The oxidation of (hydrated) formaldehyde in the aqueous phase represents the main known sink for the  $\text{OH}$  radical within droplets. Formaldehyde can form the sulfur(IV) adduct hydroxymethanesulfonate ( $\text{HMS}^-$ ), which is less reactive with radicals than free formaldehyde and less reactive with other oxidants, such as  $\text{H}_2\text{O}_2$  and  $\text{O}_3$  than sulfite or bisulfite. As pointed out in 2.2.1. the measured formaldehyde concentration includes both free and hydrated formaldehyde as well as  $\text{HMS}^-$ .

The oxidation of  $\text{CH}_2(\text{OH})_2$  by  $\text{OH}$ , the formation of  $\text{HMS}^-$  and the oxidation of this adduct by  $\text{OH}$  were added to the model (Table V). Furthermore, to avoid

Table V. Rate/equilibrium constants of chemical processes of formic and acetic acid and formaldehyde within the aqueous phase

Reaction	$k$ or $K$	$-\Delta H/R$	Reference
$\text{OH} + \text{HCOO}^- \rightarrow \text{products}$	$3.2 \cdot 10^9 \text{ M}^{-1} \text{ s}^{-1}$	1000	Chin and Wine, 1994
$\text{OH} + \text{CH}_3\text{COO}^- \rightarrow \text{products}$	$1 \cdot 10^8 \text{ M}^{-1} \text{ s}^{-1}$	1800	Chin and Wine, 1994
$\text{HCHO}_{(g)} \rightleftharpoons \text{CH}_2(\text{OH})_{2(aq)}$	$4998 \text{ M atm}^{-1}$	4030	Betterton and Hoffmann, 1988
$\text{SO}_{2(g)} \rightleftharpoons \text{SO}_{2(aq)}$	$1.24 \text{ M atm}^{-1}$	3247	Beilke and Gravenhorst, 1978
$\text{SO}_2 + \text{H}_2\text{O} \rightleftharpoons \text{HSO}_3^- + \text{H}^+$	$3.13 \cdot 10^{-4}$	1940	Beilke and Gravenhorst, 1978
$\text{HSO}_3^- \rightleftharpoons \text{SO}_3^{2-} + \text{H}^+$	$6.22 \cdot 10^{-8} \text{ M}$		Beilke and Gravenhorst, 1978
$\text{HSO}_3^- + \text{CH}_2(\text{OH})_{2(aq)} \rightarrow \text{HMS}^-$	$0.436 \text{ M}^{-1} \text{ s}^{-1}$	2990	Boyce and Hoffmann, 1984
$\text{HMS}^- \rightarrow \text{HSO}_3^- + \text{CH}_2(\text{OH})_{2(aq)}$	$1.22 \cdot 10^{-7} \text{ s}^{-1}$		<sup>a</sup>
$\text{SO}_3^{2-} + \text{CH}_2(\text{OH})_{2(aq)} \rightarrow \text{HMS}^-$	$1.23 \cdot 10^5 \text{ M}^{-1} \text{ s}^{-1}$	2450	Boyce and Hoffmann, 1984
$\text{HMS}^- \rightarrow \text{SO}_3^{2-} + \text{CH}_2(\text{OH})_{2(aq)}$	$3.8 \cdot 10^{-6} \text{ s}^{-1}$	5530	<sup>b</sup>
$\text{CH}_2(\text{OH})_{2(aq)} + \text{OH} \rightarrow \text{products}$	$1 \cdot 10^9 \text{ M}^{-1} \text{ s}^{-1}$	1020	Chin and Wine, 1994
$\text{HSO}_3^- + \text{H}_2\text{O}_2 + \text{H}^+ \rightarrow \text{products}$	$7.2 \cdot 10^7 \text{ M}^{-2} \text{ s}^{-1}$	4000	Betterton and Hoffmann, 1988
$\text{HSO}_3^- + \text{O}_3 \rightarrow \text{products}$	$3.7 \cdot 10^5 \text{ M}^{-1} \text{ s}^{-1}$	5530	Hoffmann, 1986
$\text{SO}_3^{2-} + \text{O}_3 \rightarrow \text{products}$	$1.5 \cdot 10^9 \text{ M}^{-1} \text{ s}^{-1}$	5280	Hoffmann, 1986
$\text{HMS}^- + \text{OH} \rightarrow \text{HSO}_3^- + \text{HCOOH}$	$3 \cdot 10^8 \text{ M}^{-1} \text{ s}^{-1}$		Barlow <i>et al.</i> , 1997

<sup>a</sup> Calculated based on the rate constant for the forward reaction and the equilibrium constant given by Olson and Hoffmann.

<sup>b</sup>  $k^{1st}$  at pH = 7, extrapolated from the data by Kok *et al.*, 1986.

overestimation of the  $\text{HMS}^-$  concentration, other sinks for sulfur(IV), i.e., the oxidation by  $\text{H}_2\text{O}_2$  and  $\text{O}_3$ , were considered in the model.

As can be seen in Figure 4 OH reaction with formaldehyde will not influence the equilibrium formaldehyde concentration in the droplet since the timescale for the chemical reaction is longer than those for the other processes. But the ratio might be affected by  $\text{HMS}^-$  formation, since  $\text{HMS}^-$  formation leads to a higher apparent solubility of formaldehyde in the aqueous phase. As mentioned above, the pure uptake model applied to formaldehyde predicts the same concentration in both droplet classes after a few seconds (ratio = 1).

The effective solubility for formaldehyde is increased if  $\text{HMS}^-$  is formed. The partitioning at equilibrium can be described as

$$\begin{aligned}
 K_{\text{H}}^{\text{eff, HMS}}(\text{HCHO}) &= \frac{\text{HCHO}_{\text{aq}} + \text{HMS}^-}{\text{HCHO}_g} \\
 &= K_{\text{H}}^{\text{eff}}(\text{HCHO}) \cdot (1 + K^{\text{HMS}} \cdot [\text{S(IV)}]_{\text{aq}}) [\text{M atm}^{-1}]
 \end{aligned} \tag{17}$$

with  $K^{\text{HMS}} = [\text{HMS}^-]/([\text{S(IV)}]_{\text{aq}} \cdot [\text{HCHO}]_{\text{aq}})$ . Therefore, the solubility of formaldehyde depends on the concentration of sulfur(IV). As shown in Figure 4 the time scale for the uptake of acids depends on the pH. The effective Henry's Law Constant for  $\text{SO}_2$  at pH = 7 is  $K_{\text{H}}^{\text{eff}}(\text{S(IV)}) = 10^6 \text{ M atm}^{-1}$  being comparable to that of acetic acid. It implies that  $\text{SO}_2$  might show a similar uptake time scale as this acid. The  $\text{HMS}^-$  formation and finally the increase of the total formaldehyde



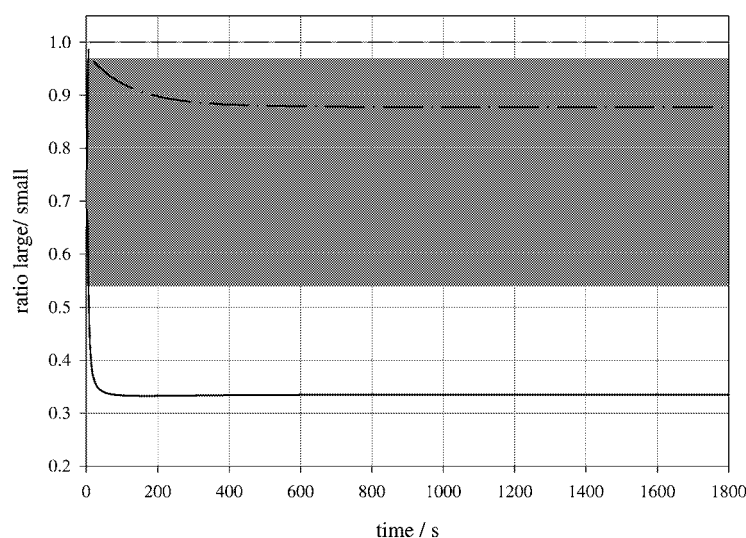


Figure 7. Concentration ratios for formaldehyde — — — no HMS-formation, — · — · : with  $\text{HMS}^-$  formation ( $\text{pH} = 7$ ), shadowed area: measured ratios (average  $\pm$  standard deviation);  $[\text{S(IV)}]_{\text{aq}}/[\text{HCHO}_{\text{tot}}]_{\text{aq}} = 0.2$  (small droplets),  $[\text{S(IV)}]_{\text{aq}}/[\text{HCHO}_{\text{tot}}]_{\text{aq}} = 0.1$  large droplets; — with  $\text{HMS}^-$  formation at high concentration of  $\text{SO}_2$  (= lower limit for concentration ratio for formaldehyde).

concentration in the droplet are correlated with the concentration and the mass transfer rate of  $\text{SO}_2$ .

A few concentration values are available from the observations for sulfur(IV) concentrations in large and small droplets, respectively ( $\approx 3 \mu\text{eq/L}$  in large droplets and  $\approx 10 \mu\text{eq/L}$  in small droplets). Hence, the concentration ratio of  $[\text{S(IV)}]_{\text{aq}}/[\text{HCHO}_{\text{tot}}]_{\text{aq}}$  in the droplets (referring to the total concentrations, i.e. considering the  $\text{HMS}^-$  concentration for both species, respectively) is about 0.2 in the small and 0.1 in the large droplets. At the high pH values found in the fog drops the formation of  $\text{HMS}^-$  is fairly rapid, about six orders of magnitude faster than at low pH (Table V). Therefore, at low total sulfur(IV) concentrations  $\text{HMS}^-$  formation is limited by the available sulfur(IV). In order to estimate the extent to which  $\text{HMS}^-$  formation might influence the concentration ratio of formaldehyde in the droplets under such conditions, an initial  $\text{SO}_{2(g)}$  concentration was chosen leading to a sulfur(IV)/HCHO ratio in the aqueous phase comparable to the observed ratios. Figure 7 shows that the concentration ratio for formaldehyde is decreased to about 0.88. Comparison with the measured values shows that concentration ratios of formaldehyde between 0.45 and 0.95 were observed. Hence, the model approach confirms a decreased concentration ratio for formaldehyde due to  $\text{HMS}^-$  formation but predicts a smaller effect than observed in the fog drops.

More generally, it can be estimated under which conditions the  $\text{HMS}^-$  formation might have the largest influence on the concentration ratio of formaldehyde: if the  $\text{SO}_2$  aqueous phase concentration is completely controlled by transport

processes, i.e., if the deviation from the equilibrium concentration ( $p_A - c_{aq}/K_H^{\text{eff}}$ ) (Equation (6)) is about the same in both drop size classes, the change in the aqueous phase concentrations is determined only by the mass transfer coefficient  $k_{\text{mt}}$  of  $\text{SO}_2$ . Thus, the aqueous phase concentration ratio of formaldehyde corresponds then to the ratio of  $k_{\text{mt}}$  for small and large droplets, respectively. Assuming values for  $\text{SO}_2$  of  $D_g = 10^{-5} \text{ m}^2 \text{ s}^{-1}$ ,  $\alpha = 0.05$ ,  $c = 500 \text{ m s}^{-1}$  we can calculate a ratio of  $k_{\text{mt}}(\text{SO}_2)_{\text{large}}/k_{\text{mt}}(\text{SO}_2)_{\text{small}} = 0.3$ .

Hence, this value represents the lower limit for the concentration ratio for formaldehyde but it can only be achieved if the  $\text{SO}_2$  concentration is sufficiently high and the  $\text{HMS}^-$  formation is not controlled by the concentration ratio of  $[\text{S(IV)}]/[\text{HCHO}]$  in the drops.

Improved input data sets, not only of sulfur(IV) concentrations, but also for other species as considered in the chemistry model, such as  $\text{SO}_2$  and  $\text{OH}$ , might produce better agreement between the measured and modeled values.

### 3.4. MIXING EFFECTS

#### 3.4.1. Definition

As discussed in previous studies (e.g., Pandis and Seinfeld, 1991) the mixing of individual droplets into a bulk sample can lead to a different concentration than the average value present in the original droplets. It was shown that the concentrations of solutes ( $\text{NH}_3$ ,  $\text{SO}_2$ ) in a bulk sample always exceed the concentrations predicted by thermodynamic equilibrium, even if individual drops are in equilibrium. This effect is caused by the change in the average pH value that occurs when single droplets are combined into a bulk sample. The situation becomes more complicated if buffering effects occur due to interactions of different acidic or basic species within the bulk samples. In several studies buffering effects were explained by inorganics such as ammonia, nitrate, carbonate and sulfate. Additionally significant contributions to buffering, perhaps by organics, were found at  $4 < \text{pH} < 7$  in California fogs (Collett *et al.*, 1999b). In the following discussion such buffering effects will not be considered. This assumption represents an oversimplification but it allows an estimate of the potential impact of mixing effects.

In order to estimate the extent to which mixing effects can explain the observed concentration patterns, one of the measured droplet number distributions was chosen (Figure 8(a)). Because there is no clear trend regarding the pH values within the droplet distribution, three different extreme pH distributions were assumed, differing between  $\text{pH} = 6.5$  and  $7.5$  in both the small and large droplets (Figure 8(b), bottom). The first distribution (I) assumes a monotonically increasing pH value from the smallest to largest drop size in each class; the second distribution (II) describes a monotonically decreasing pH value. The third distribution contains a maximum pH value in the middle drop size class. These pH distributions cover the limits of the pH variability determined in the study. Furthermore it is assumed that

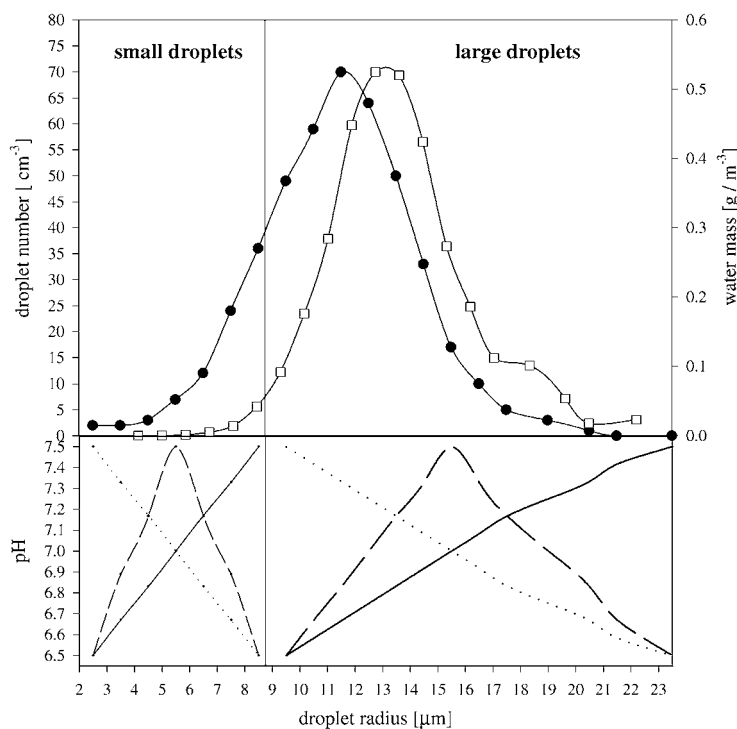


Figure 8. Droplet number distribution (●), water mass distribution (□) and pH values (bottom part) used for Equations (18)–(20), solid line: I; dotted line: II, broken line: III.

– despite the previous discussion – the individual droplets were in thermodynamic equilibrium.

### 3.4.2. Calculation of the Acid Concentration in Individual Droplets and the Bulk Sample

The theoretical equilibrium acid concentrations  $c_{aq,i}$  in all individual droplets can be derived from the corresponding effective Henry's Law constants for the  $H^+$  concentrations  $[H^+]_i$  (Figure 8(b))

$$c_{aq,i} = c_g \cdot \left[ K_H \cdot \left( 1 + \frac{K_a}{[H^+]_i} \right) \right] \quad (18a)$$

with  $K_H$  and  $K_a$  given in Table III. For the calculations gas phase concentrations of  $c_g = 0.1$  ppb for both formic and acetic acid were assumed. The sum of the concentrations  $c_{aq,i}$  multiplied by the corresponding volume fraction of the liquid water gives the total acid concentration  $c_{aq,i,sum}$ .

$$c_{aq,i,sum} = \frac{c_{aq,i} \cdot V_i}{\Sigma(V_i)}. \quad (19)$$

The concentration obtained by (19) represents the sum of all moles of the species in all droplets. This approach is adequate for pH independent species but neglects the pH dependence of the acid solubility.

The average pH in the bulk sample is calculated as a volume weighted average (analogous to Equation (18a)). This average  $H^+$  concentration is used to calculate the equilibrium acid concentration in the bulk sample ( $c_{aq, sample}$ )

$$c_{aq, sample} = c_g \cdot \left[ K_H \cdot \left( 1 + \frac{K_a}{[H^+]_{sample}} \right) \right]. \quad (18b)$$

The ratio  $S$  of the concentrations obtained by Equations (18a) and (18b) shows whether the collected samples should be sub- or supersaturated with regards to the acid concentrations assuming equilibrium in the individual droplets.

$$S = \frac{c_{aq, i, sum}}{c_{aq, sample}}. \quad (20)$$

Table VI shows these  $S$  values calculated from (20) for all three assumed pH distributions and both acids. According to (20) a value of  $S$  greater than 1 shows that the total amount of acid in the individual droplets ( $c_{aq, i, sum}$ ) was larger than that in the corresponding combined sample ( $c_{aq, sample}$ ). In fact, all values of  $S$  are greater than 1; this means that by combining the individual droplets into bulk samples, some of the acid might evaporate. The comparison of the values for large and small droplets in Table VI shows a slight tendency to higher concentration deviations between  $c_{aq, sample}$  and  $c_{aq, i, sum}$  in large droplets. Therefore, the evaporation rate from these samples might be higher and thus the large/small drop ratio measured based on the acid concentration in the bulk samples might be too small. These deviations are roughly <15% for all cases assumed here as can be seen from the comparison of the different ratios in Table VI ( $c_{aq, sample}^{large}/c_{aq, sample}^{small}$  vs.  $c_{aq, i, sum}^{large}/c_{aq, i, sum}^{small}$ ). It is likely that this artifact is even smaller than estimated here because the evaporation rate from the collected sample will be delayed after a certain collection period due to the saturation of the gas phase with acid vapor above the collection bottle. Furthermore, the surface area/volume ratio decreases once the drops are combined also causing outgassing to be slowed from the bulk sample. Internal buffering in drop mixtures will also reduce this effect.

The above calculation represents a rough estimate of the possible influence of mixing effects. To give a more general picture more detailed size resolved measurements are necessary. The correlation between solubility and pH dependence is most sensitive at high pH, i.e., in that regime where the factor  $K_a/[H^+]$  is greater than unity and determines  $K_H^{eff}$  (2). Therefore, it can be concluded that in droplets with lower pH values, i.e., closer to the  $K_a$  values of the acids, the mixing effects will have an even smaller impact than estimated here.

Table VI. Calculated supersaturations  $S$  (Equation (20)) for small ( $<8.5 \mu\text{m}$ ) and large droplets ( $>8.5 \mu\text{m}$ ) and concentration ratios in individual droplets (Equation (18a)) and combined bulk samples (Equation (18b)), corresponding to assumed pH distributions I–III (Figure 8)

pH	I		II		III	
	S					
distribution	Large droplets	Small droplets	Large droplets	Small droplets	Large droplets	Small droplets
HCOOH	1.25	1.12	1.28	1.13	1.48	1.44
CH <sub>3</sub> COOH	1.2	1.13	1.28	1.12	1.48	1.44
	Ratio					
	Bulk sample	Individual droplets	Bulk sample	Individual droplets	Bulk sample	Individual droplets
HCOOH	0.27	0.3	3.29	3.76	2.12	2.17
CH <sub>3</sub> COOH	0.28	0.3	3.28	3.73	2.11	2.09

#### 4. Conclusions

Small chain carboxylic acids and formaldehyde are major components of the total organic carbon in fog droplets. While acetic acid, the single most abundant organic compound, may account for up to 22% of the TOC, dicarboxylic acids (mostly oxalic acid) were only minor components of the TOC ( $\leq 2\%$ ). Size-resolved measurements of organic acids showed a clear heterogeneity in concentrations between small ( $r < 8.5 \mu\text{m}$ ) and large ( $r > 8.5 \mu\text{m}$ ) droplets, with the small droplets typically being more concentrated. For non-volatile species like oxalic acid this result is consistent with preferential enrichment in small cloud condensation nuclei. For volatile species like formaldehyde and formic and acetic acid, the origin of the heterogeneity has been investigated using an uptake model.

In some cases application of Henry's Law to predict the partitioning of the acids is sufficient, if the pH dependence of the acid solubility or hydration of formaldehyde is considered. For example, formaldehyde might achieve thermodynamic equilibrium in the droplet after a few seconds. Comparing time scales for the transport towards the droplet it becomes evident that the time until saturation for formic acid is about a factor of 10 greater than the corresponding time for acetic acid. This implies that, for sufficiently long drop life times, the ratio of acetic acid concentrations is likely to be closer to 1, i.e., closer to equilibrium.

The possible impact of chemical reactions, in particular oxidation by OH, on the species concentrations in small and large droplets was investigated. These effects are highly sensitive to the assumed OH concentration. It is expected that at low OH concentrations ('nighttime') this impact will be negligible but at high OH

concentrations ('daytime') the concentrations can be influenced significantly. The departure from equilibrium will be larger in large droplets so that the large/small droplet concentration ratio will decrease. Considering the formation of hydroxymethanesulfonate, uptake of formaldehyde can be enhanced. Depending on the sulfur(IV) concentration the measured formaldehyde concentrations (including hydroxymethanesulfonate) can be higher than predicted by Henry's Law. Due to the high solubility of S(IV) at high pH values its uptake rate will be different for different droplet size classes. Thus, HMS formation leads to a decrease in the concentration ratio for formaldehyde in the cases considered here.

The influence of possible artifacts by mixing effects was investigated. It has been shown that these effects might lead to an underestimation of the ratio of large-to-small drop concentrations because potential supersaturation and evaporation are larger in the large droplet sizes. It was estimated that in total such effects will lead to deviations of <15% from the ratio present originally in the individual droplets.

With the current model study it is concluded that concentration heterogeneities in fog droplets are produced by the high effective solubility of the species and correspondingly long times to achieve phase equilibrium, due to the limited lifetime of the fog droplets. Concentration heterogeneities can also be affected by concentrations of reactants (e.g., OH) in the aqueous phase. These findings are in agreement with conclusions of other studies. In several studies it was assumed that drop size dependent concentrations in fog and cloud droplets might be caused by kinetic inhibition of mass transfer (e.g., Winiwarter *et al.*, 1994). While in these previous studies these effects were not investigated numerically in the present study bounds are given for each of the possible limitations. Thus, the model applied here enables a prediction of the partitioning of the volatile species investigated in this study (formic acid, acetic acid, and formaldehyde) and might even be extended to other compounds. In the future, more complete datasets, including measurements with high temporal resolution of gas phase concentrations of low molecular weight organic compounds, should enhance our understanding of the drop-size dependent concentrations of volatile species.

### Acknowledgements

We are grateful to E. Sherman for his contributions to the design of the new stainless steel collectors and for assistance in the preparation of the field project. We are grateful to J. Reilly, G. Kang, H. Chang, and S. Emert for assistance during the field experiment. This work was supported in part by the NOAA Office of Global Programs. This work was also funded in part by the National Science Foundation (ATM-9980540, ATM-0222607) and the San Joaquin Valleywide Air Pollution Study Agency. The statements and conclusions in this report are those of the Contractor and not necessarily those of the California Air Resources Board, the San Joaquin Valleywide Air Pollution Study Agency, or its Policy Committee, their employees or their members. The mention of commercial products, their source, or

their use in connection with material reported herein is not to be construed as actual or implied endorsement of such products.

## References

- Ang, C. C., Lipari, F., and Swarin, S., 1987: Determination of hydroxymethanesulfonate in wet deposition samples, *Environ. Sci. Technol.* **21**, 102–105.
- Audiffren, N., Renard, M., Buisson, E., and Chaumerliac, N., 1998: Deviations from the Henry's Law equilibrium during cloud events: A numerical approach of the mass transfer between phases and its specific numerical effects, *Atmos. Res.* **49**, 139–161.
- Barlow, S., Buxton, G. V., Murray, S. A., and Salmon, G. A., 1997: Free-radical-induced oxidation of hydroxymethanesulfonate in aqueous solution, Part 1: A pulse radiolysis study of the reactions of OH and  $\text{SO}_4^-$ , *J. Chem. Soc. Faraday Trans.* **93** (20), 3637–3640.
- Bator, A. and Collett Jr., J. L., 1997: Cloud chemistry varies with drop size, *J. Geophys. Res.* **102**, 28071–28078.
- Beilke, S. and Gravenhorst, G., 1978: Heterogeneous  $\text{SO}_2$ -oxidation in the droplet phase, *Atmos. Environ.* **12**, 231–239.
- Betterton, E. A. and Hoffmann, M. R., 1988: Oxidation of aqueous  $\text{SO}_2$  by peroxy monosulfate, *J. Phys. Chem.* **92**, 5962–5965.
- Boyce, S. D. and Hoffmann, M. R., 1984: Kinetics and mechanism of the formation of hydroxymethane-sulfonic acid at low pH, *J. Phys. Chem.* **88**, 4740–4746.
- Chin, M. and Wine, P. H., 1994: A temperature-dependent competitive kinetics study of the aqueous-phase reactions of OH radicals with formate, formic acid, acetate, acetic acid and hydrated formaldehyde, in G. R. Helz, R. G. Zepp, and D. G. Crosby (ed.), *Aquatic and Surface Photochemistry*, Lewis Publishers, Boca Raton, pp. 85–96.
- Collett Jr., J. L., Bator, A., Rao, X., and Demoz, B. B., 1994: Acidity variations across the cloud drop size spectrum and their influence on rates of atmospheric sulfate production, *Geophys. Res. Lett.* **21**, 2393–2396.
- Collett Jr., J. L., Hoag, K. J., Sherman, D. E., Bator, A., and Richards, L. W., 1999a: Spatial and temporal variations in San Joaquin Valley fog chemistry, *Atmos. Environ.* **33**, 129–140.
- Collett Jr., J. L., Hoag, K. J., Rao, X., and Pandis, S. N., 1999b: Internal buffering in San Joaquin Valley fog drops and its influence on aerosol processing, *Atmos. Environ.* **33**, 4833–4847.
- Davidovits, M., Hu, J. H., Worsnop, D. R., Zahniser, M. S., and Kolb, C. E., 1995: Entry of gas molecules into liquids, *Faraday Discuss.* **100**, 65–82.
- Demoz, B. B., Collett Jr., J. L., and Daube Jr., B. C., 1996: On the design and performance of the California institute of technology cloudwater collector, *Atmos. Res.* **41**, 47–62.
- Dong, S. and Dasgupta, P. K., 1987: Fast fluorimetric flow-injection analysis of formaldehyde in atmospheric water, *Environ. Sci. Technol.* **21**, 581–588.
- Ervens, B., Williams, J., Buxton, G. V., Salmon, G. A., Bydder, M., Dentener, F., George, C., Mirabel, P., Wolke, R., and Herrmann, H., 2003: CAPRAM2.4 (MODAC mechanism): An extended and condensed tropospheric aqueous phase mechanism and its application, *J. Geophys. Res.* **108**, D14 4426 doi: 10.1029/2002 JD002202.
- Facchini, M. C., Lind, J., Orsi, G., and Fuzzi, S., 1990: The chemistry of carbonyl compounds in the Po Valley fog water, *Sci. Total Environ.* **91**, 79–86.
- Feingold, G. and Chuang, P. Y., 2002: Analysis of the influence of film-forming compounds on droplet growth: Implications for cloud microphysical processes and climate, *J. Atmos. Sci.* **59**, 2006–2018.
- Fuller, E. N., 1986: Diffusion coefficients for binary gas systems at low pressures: Empirical correlations, in C. Reid *et al.* (eds), *Properties of Gases and Liquids*, McGraw Hill, New York, p. 587.

- Gill, P. S., Graedel, T. E., and Weschler, C. J., 1983: Organic films on atmospheric aerosol particles, fog droplets, cloud droplets, raindrops, and snow flakes, *Rev. Geophys. Space Phys.* **21**, 903–920.
- Hanson, D., Burkholder, J. B., Howard, C. J., and Ravishankara, A. R., 1992: Measurement of OH and HO<sub>2</sub> radical uptake coefficients on water and sulfuric acid surfaces, *J. Phys. Chem.* **96**, 4979–4985.
- Harned, H. S. and Owen, B. B., 1958, *The Physical Chemistry of Electrolytic Solutions* (3rd edn), Reinhold, New York.
- Hegg, D. A., Gao, S., and H. Jonsson, 2002: Measurements of selected dicarboxylic acids in marine cloud water, *Atmos. Res.* **62**, 1–10.
- Herckes, P., Lee, T., Trenary, L., Kang, G., Chang, H., and Collett Jr., J. L., 2002a: Organic matter in San Joaquin Valley radiation fogs, *Environ. Sci. Technol.* **36**, 4777–4782.
- Herckes, P., Hannigan, M. P., Trenary, L., Lee, T., and Collett Jr., J. L., 2002b: Organic compounds in radiation fogs in Davis (California), *Atmos. Res.* **64**, 99–108.
- Herrmann, H., Ervens, B., Jacobi, H.-W., Wolke, R., Nowacki, P., and Zellner, R., 2000: CAPRAM2.3: A chemical aqueous phase radical mechanism for tropospheric chemistry, *J. Atmos. Chem.* **36**, 231–284.
- Hoffmann, M. R., 1986: On the kinetics and mechanism of oxidation of aquated sulfur dioxide by ozone, *Atmos. Environ.* **20**, 1145–1154.
- Huthwelker, T. and Peter, T., 1996: Analytical description of gas transport across an interface with coupled diffusion in two phases, *J. Chem. Phys.* **105**, 1661–1667.
- Jacob, D. J., 1986: Chemistry of OH in remote clouds and its role in the production of formic acid and peroxymonosulfate, *J. Geophys. Res.* **91**, 9807–9826.
- Keene, W. C., Mosher, B. W., Jacob, D. J., Munger, J. W., Talbot, R. W., Artz, R. S., Maben, J. R., Daube Jr., B. C., and Galloway, J. N., 1995: Carboxylic acids in clouds at a high-elevation forested site in central Virginia, *J. Geophys. Res.* **100**, 9345–9357.
- Khan, I. and Brimblecombe, P., 1992: Henry's Law constants of low molecular weight (<130) organic acids, *J. Aerosol Sci.* **23**, S897–S990.
- Khare, P., Kumar, N., Kumari, K. M., and Srivastava, S. S., 1999: Atmospheric formic and acetic acids: An overview, *Rev. Geophys.* **37**, 227–248.
- Khwaja, H. A., Brudnoy, S., and Husain L., 1995: Chemical characterization of three summer cloud episodes at Whiteface Mountain, *Chemosphere* **31**, 3357–3381.
- Kläning, U. K., Sehested, K., and Holcman, J., 1985: Standard Gibbs energy of formation of the hydroxyl radical in aqueous solution. Rate constants for the reaction  $\text{ClO}_2^- + \text{O}_3 = \text{O}_3^- + \text{ClO}_2$ , *J. Phys. Chem.* **89**, 760–763.
- Klippel, W. and Warneck, P., 1980: The formaldehyde content of the atmospheric aerosol, *Atmos. Environ.* **14**, 809–818.
- Kok, G. L., Gitlen, S. N., and Lazrus, A. L., 1986: Kinetics of the formation and decomposition of hydroxymethanesulfonate, *J. Geophys. Res.* **91**, 2801–2804.
- Laj, P., Fuzzi, S., Lazzari, A., Ricci, L., Orsi, G., Berner, A., Dusek, U., Schell, D., Guenther, A., Wendisch, M., Wobrock, W., Frank, G., Martinsson, B., and Hillamo, R., 1998: The size-dependent chemistry of fog droplets, *Contrib. Atmos. Phys.* **71**, 115–130.
- Leriche, M., Voisin, D., Chaumerliac, N., Monod, A., and Aumont, B., 2000: A model for tropospheric multiphase chemistry: Application to one cloudy event during the CIME experiment, *Atmos. Environ.* **34**, 5015–5036.
- Lide, D. R. (ed.), 2000: *Handbook of Chemistry and Physics* (81st edn), CRC Press, New York.
- Löflund, M., Kasper-Giebl, A., Schuster, B., Giebl, H., Hitzemberger, R., and Puxbaum, H., 2002: Formic, acetic, oxalic, malonic and succinic acid concentrations and their contribution to organic carbon in cloud water, *Atmos. Environ.* **36**, 1553–1558.
- Ludwig, J., and Klemm, O., 1988: Organic acids in different size classes of atmospheric particulate material, *Tellus* **40B**, 340–347.



- Millet, M., Sanusi, A., and Wortham, H., 1996: Chemical composition of fogwater in an urban area: Strasbourg (France), *Environ. Poll.* **94**, 345–354.
- Millet, M., Wortham, H., Sanusi, A., and Mirabel, P., 1997: Low-molecular-weight organic-acids in fogwater in an urban area – Strasbourg (France), *Sci. Total Environ.* **206**, 57–65.
- Munger, J. W., Collett, Jr., J. L., Daube Jr., B., and Hoffmann, M. R., 1989a: Carboxylic acids and carbonyl compounds in southern California clouds and fogs, *Tellus* **41B**, 230–242.
- Munger, J. W., Collett Jr., J. L., Daube Jr., B., and Hoffmann, M. R., 1989b: Chemical composition of coastal stratus clouds: Dependence on droplet size and distance from the coast, *Atmos. Environ.* **23**, 2305–2320.
- Munger, J. W., Collett Jr., J. L., Daube Jr., B., and Hoffmann, M. R., 1990: Fogwater chemistry at Riverside, California. *Atmos. Environ.* **24B**, 185–205.
- Nathanson, G. M., Davidovits, P., Worsnop, D. R., and Kolb, C. E., 1996: Dynamics and kinetics at the gas-liquid interface, *J. Phys. Chem.* **100**, 13007–13020.
- Neusüß, C., Pelzing, M., Plewka, A., and Herrmann, H., 2000: A new analytical approach for size-resolved speciation of organic compounds in atmospheric aerosol particles: Methods and first results, *J. Geophys. Res.* **105**, 4513–4527.
- Noone, K. J., Ogren, J. A., Hallberg, A., Heintzenberg, J., Hansson, H.-C., Svenigsson, I. B., Wiedensohler, A., Fuzzi, S., Facchini, M. C., Arends, B. G., and Berner, A., 1992: Changes in aerosol size- and phase distributions due to physical and chemical processes in fog, *Tellus* **44B**, 489–504.
- Ogren, J. A. and Charlson, R. J., 1992: Implications for models and measurements of chemical inhomogeneities among cloud droplets, *Tellus* **44B**, 208–225.
- Ogren, J. A., Noone, K. J., Hallberg, A., Heintzenberg, J., Schell, D., Berner, A., Solly, I., Kruisz, C., Reischl, G., Arends, B. G., and Wobrock, W., 1992: Measurements of the size dependence of the concentration of non-volatile material in fog droplets, *Tellus* **44B**, 570–580.
- Olson, T. M. and Hoffmann, M. R., 1989: Hydroxyalkylsulfonate formation: Its role as a S(IV) reservoir in atmospheric water droplets, *Atmos. Environ.* **23**, 985–997.
- Pandis, S. N., Seinfeld, J. H., and Pilinis, C., 1990: Chemical composition differences in fog and cloud droplets of different sizes, *Atmos. Environ.* **24A**, 1957–1969.
- Pandis, S. N. and Seinfeld, J. H., 1991: Should bulk cloudwater or fogwater samples obey Henry's Law?, *J. Geophys. Res.* **96**, 10791–10798.
- Podzimek, J. and Saad, A. N., 1975: Retardation of condensation nuclei growth by surfactant, *J. Geophys. Res.* **80**, 3386–3392.
- Reilly, J. E., Rattigan, O. V., Moore, K. F., Judd, C., Sherman, D. E., Dutkiewicz, V. A., Kreidenweis, S. M., Husain, L., and Collett Jr., J. L., 2001: Drop size dependent S(IV) oxidation in chemically heterogeneous radiation fogs, *Atmos. Environ.* **35**, 5717–5728.
- Saxena, P. and Hildemann, L. M., 1996: Water-soluble organics in atmospheric particles: A critical review of the literature and application of thermodynamics to identify candidate compounds, *J. Atmos. Chem.* **24**, 57–109.
- Schwartz, S., 1986: Mass transport considerations pertinent to aqueous phase reactions of gases in liquid water clouds, in Jaeschke, W. (ed.), *Chemistry of Multiphase Atmospheric Systems*, NATO ASI Series, Springer, Berlin, pp. 415–471.
- Swartz, E., Boniface, J., Tchertkov, I., Rattigan, O. V., Robinson, D. V., Davidovits, P., Worsnop, D. R., Jayne, J. T., and Kolb, C. E., 1997: Horizontal bubble train apparatus for heterogeneous chemistry studies: Uptake of gas phase formaldehyde, *Environ. Sci. Technol.* **37**, 2634–2641.
- Voisin, D., Legrand, M., and Chaumerliac, N., 2000: Scavenging of acidic gases (HCOOH, CH<sub>3</sub>COOH, HNO<sub>3</sub>, HCl and SO<sub>2</sub>) and ammonia in mixed liquid-solid water clouds at the Puy de Dôme mountain (France), *J. Geophys. Res.* **105**, 6817–6835.
- Warneck, P., 1999: The relative importance of various pathways for the oxidation of sulfur dioxide and nitrogen dioxide in sunlit continental fair weather clouds, *Phys. Chem. Chem. Phys.* **1**, 5471–5483.

- Winiwarter, W., Puxbaum, H., Facchini, M. C., Orsi, G., Beltz, N., Enderle, K., and Jaeschke, W., 1988: Organic acid gas and liquid-phase measurements in Po Valley fall-winter conditions in the presence of fog, *Tellus* **40B**, 348–357.
- Winiwarter, W., Fierlinger, H., Puxbaum, H., Facchini, M. C., Arends, B. G., Fuzzi, S., Schell, D., Kaminski, U., Pahl, S., Schneider, T., Berner, A., Solly, I., and Kruisz, C., 1994: Henry's Law and the behavior of weak acids and bases in fog and clouds, *J. Atmos. Chem.* **19**, 173–188.
- Worsnop, D. R., Morris, J. W., Shi, Q., Davidovits, P., and Kolb, C. E., 2002: A chemical kinetic model for reactive transformations of aerosol particles, *Geophys. Res. Lett.* **29** (20), 1996.
- Wortham, H., Millet, M., Sanusi, A., and Mirabel, P., 1995: Methods of sampling, preservation and analysis of organic acids in atmospheric samples: A review, *Analysis* **23**, 427–436.
- Yao, X., Fang, M., and Chan, C. K., 2002: Size distributions and formation of dicarboxylic acids in atmospheric particles, *Atmos. Environ.* **36**, 2099–2107.
- Yu, S., 2000: Role of organic acids (formic, acetic, pyruvic and oxalic) in the formation of cloud condensation nuclei (CCN): A review, *Atmos. Res.* **53**, 185–217.